

www.istu.org/istu-2022-toronto

Abstract Book

ISTU 2022

**21st Annual International Symposium
on Therapeutic Ultrasound**

June 07 - 10, 2022
Toronto, Canada



Presented by:



A1-1

Noninvasive and Cell-type-specific Neuromodulation by Integrating Ultrasound with Genetics

Presenter: Hong Chen

Authors in order: Hong Chen, *Washington University in St. Louis*

Established neuromodulation techniques do not satisfy a critical need: the ability to achieve noninvasive cell type-specific neuromodulation.

Focused ultrasound (FUS) can noninvasively deliver ultrasound energy to localized areas in the whole brain with combined depth penetration and spatial focusing that cannot be achieved with other external stimulations. Sonogenetics, integrating focused ultrasound with genetic engineering, can achieve noninvasive control of neurons genetically modified with ultrasound-sensitive ion channels. Crucial to the development of sonogenetics has been the identification of ultrasound-sensitive probes to control neurons.

This talk will present our recent work in the development of sonogenetic tools for neuromodulation. It will show direct evidence that demonstrates cell-type-selective activation of neurons by sonogenetics. It will also show behavior modulation of freely moving mice by targeting the motor control circuits using sonogenetics.

This noninvasive and cell-type-specific neuromodulation technique has the promise to advance the study of the intact nervous system and uncover new ways to treat neurological disorders.

This work was supported by the National Institutes of Health (NIH) BRAIN Initiative (R01MH116981).

Selective Deep Brain Stimulation via Nanobubbles-Mediated Low-intensity Ultrasound

Presenter: Xuandi Hou

Authors in order: Xuandi Hou, *The Hong Kong Polytechnic University*, Jianing Jing, *The Hong Kong Polytechnic University*, Quanxiang Xian, *The Hong Kong Polytechnic University*, ZHIHAI QIU, *Stanford University*, Yizhou Jiang, *The Hong Kong Polytechnic University*, Xiaohui Huang, *The Hong Kong Polytechnic University*, Kin Fung Wong, *The Hong Kong Polytechnic University*, Lei Sun, *The Hong Kong Polytechnic University*

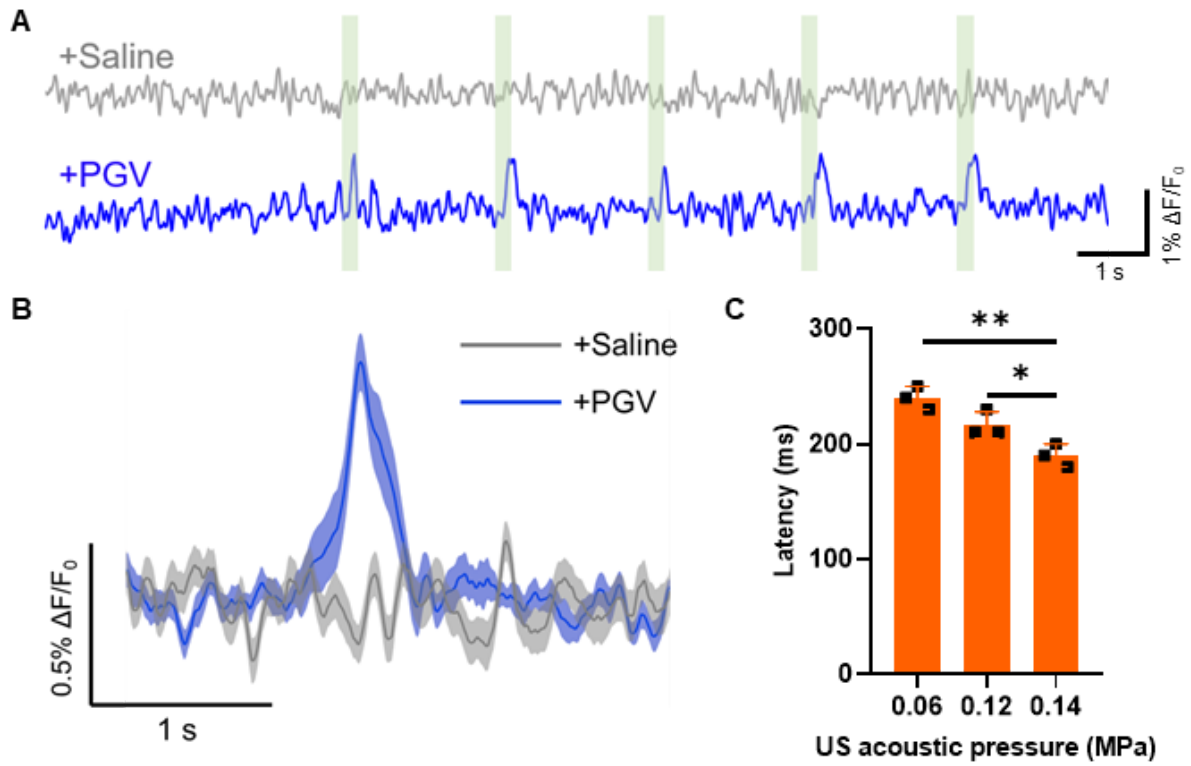
Ultrasound (US) is a promising new modality for non-invasive neuromodulation. This study aimed to develop precise ultrasound deep brain neurostimulation by combining nano-gas vesicles (GVs).

We customized low intensity, low-frequency pulsed ultrasound stimulation system. Grafting poly(ethylene glycol) (PEG) chains onto GV (PGV) improved the colloidal stability and biocompatibility, PGVs acted as ultrasound amplifiers for localized neuron stimulation. Neuronal Ca²⁺ signals were monitored simultaneously as a readout under high-speed fluorescence microscopy. The activation of neurons was further validated in vivo by using c-Fos staining, and fiber photometry measuring. Finally, the mice altering behaviors were recorded to confirm the stimulating effects.

We found that the presence of PGVs can lower the threshold for ultrasound neuron stimulation. Sonicated neurons display reversible Ca²⁺ response within 250 ms latency and increased c-Fos expression in the presence of PGVs in deep-seated brain regions. Moreover, PGVs show chronic utility in vivo with minimal cytotoxicity and remain intact over 10 days for chronic stimulation. Especially, our approach induced-neuronal activation was through the mechanosensitive ion channels. Finally, PGV+US stimulation was confirmed in freely moving mice presenting valid control of specific behaviors. In addition, our treatment scheme was found not to generate significant cytotoxicity, apoptosis, inflammation, and temperature change.

Altogether, our findings provide repeatable, spatially selective, and temporarily precise activation of deep brain neurons, through the use of non-toxic PGVs as localized actuators. Combined with ultrasound imaging, the PGV+US could be developed to have a more theranostic role in the brain in the future.

The authors would like to thank the facility and technical support from the Hong Kong Polytechnic University, and Research grants from the governmental funding agents.



A) GCaMP6s fluorescence traces in mouse brain in the presence of saline or PGVs, before and after US stimulation. Light green rectangle bars indicate ultrasound pulses. B) Averaged GCaMP6s fluorescence traces. C) The latency between ultrasonic stimulation of specified intensity and detection of an above-threshold response.

tFUS Induced Epilepsy Control with Real-time ECoG Monitoring on the Awake Rodent Seizure Model

Presenter: Jeungeun Kum

Authors in order: Jeungeun Kum, *Korea institute of science and technology (KIST)*, Sungjun Lee, *KIST*, Hyungmin Kim, *Korea Institute of Science and Technology (KIST)*,

We aim to demonstrate the online effect of ultrasonic seizure suppression by a transcranial focused ultrasound(tFUS) system with real-time electrocorticography(ECoG) monitoring on an awake animal.

The 16-ch ECoG electrodes were attached to the rat dura for brain monitoring. After recovering from the surgery, a transducer with a fundamental frequency of 300 kHz was fixed on the scalp. Intraperitoneal injection of kainic acid (5mg/kg) was performed on a Sprague-Dawley rat for the temporal lobe epilepsy model generation.

The seizure spike-wave and high-frequency oscillations (HFO) were diminished during and after the tFUS stimulation with pulse-repetition frequency (PRF) of 40 Hz and 5% duty cycle, while the sham stimulated period showed longer seizure spike-wave generation in the same animal. In addition, the suppressive effect of the tFUS stimulation on the seizure activity was observed from the bilateral hemisphere, while acoustic stimulation was delivered to the right hippocampus.

The tFUS stimulation-ECoG recording system built in this study provides to measure the effect of the ultrasound stimulation on the cortex of the stimulation site and near brain regions on an awake animal. This system can be useful to monitor tFUS-induced epilepsy control and other neuromodulation effects in realistic conditions.

This research was supported by SMC-KIST Collaborative Research Program and Basic Science Research Program through the National Research Foundation of Korea (NRF) (Grant no. 2021R1A2C2008829).

A1-12

Piezo1 Mediates Ultrasonic Neuromodulation in Mouse Brain

Presenter: Jiejun ZHU

Authors in order: Jiejun ZHU, *The Hong Kong Polytechnic University*, ZHIHAI QIU, *Stanford University*, Kin Fung Wong, *The Hong Kong Polytechnic University*, Shashwati Kala, Jianing Jing, *The Hong Kong Polytechnic University*, Yong Wu, *The Hong Kong Polytechnic University*, Xinyi Zhao, *The Hong Kong Polytechnic University*, Jinghui Guo, *The Hong Kong Polytechnic University*, Lei Sun, *The Hong Kong Polytechnic University*

We aim to investigate the role of mechanosensitive ion channels Piezo1 plays in mediating the ex vivo and in vivo effects in ultrasonic neuromodulation.

Conditional knockout of Piezo1 (P1KO) neurons in mice brain was generated through Cre-LoxP system. Geno-typing, immunostaining, and calcium imaging under Piezo1 against/antagonist were applied testing Piezo1's functional expression in mice brain and the success of Piezo1 knockout in it. Ex vivo calcium imaging in acute brain slice and in vivo experiment including the motor behavior, electromyography, fiber photometry, and c-Fos expression were adopted testing the neuronal response to ultrasound stimuli in Ctrl and P1KO mice.

The neuronal calcium response to ultrasound is found significantly reduced in P1KO mouse brain slice comparing with that in the Ctrl animal. In addition, under ultrasound stimulation to the motor cortex, P1KO mice exhibited a reduced limb movement, muscle electromyography, local neuronal calcium influx, and c-Fos expression compared to the Ctrl animals. When central amygdala (CEA), one of the brain areas found with high Piezo1 expression in our research, is stimulated by ultrasound, high ultrasound intensity dependency of calcium signaling in vivo is found. Finally, the possible contribution by auditory confound is also excluded through adopting normal and deafened mice.

Thus, we demonstrate that Piezo1 is functionally expressed in different brain regions, and that it is a pivotal factor mediating ultrasonic neuromodulation ex vivo and in vivo, laying the ground for further application of ultrasound in in both neuroscience research and brain disease treatment.

A1-13

Calcium Signaling Dynamics evoked by FUS Stimulation in a Human Neural Cell Model

Presenter: Tom Aubier

Authors in order: Tom Aubier, *INSERM*, Ivan Suarez-Castellanos, *LabTAU - INSERM - Université de Lyon*, Magali Perier, Alexandre Carpentier, *France*, W. Apoutou N'DJIN, *LabTAU, INSERM, Université de Lyon*

The spatiotemporal dynamics of calcium signaling in neurons evoked by Focused UltraSound (FUS) was studied to gain insights on the mechanisms underlying ultrasound neurostimulation.

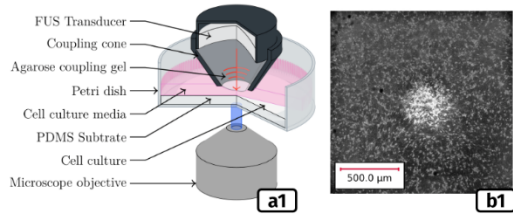
Human neural progenitors (ReNcell-VM) were plated on 35mm Petri dishes and labelled with a Ca²⁺-sensitive fluorescent marker (Fluo-4). The experimental setup was built on an inverted microscope. The calcium signaling activity within the cellular network was evaluated in response to mechanical and ultrasound stimulation. Single-pulse FUS stimulations (duration: 400 μ s, pRMS < 4 MPa) were applied using a custom-made focused transducer (\varnothing :15mm) driven at 8.14MHz (fig a1). Single-cell mechanical stimulations were performed using patch clamp micropipettes (fig a2).

Following FUS, strong and sustained elevations in intracellular Ca²⁺ were immediately observed for a cluster of cells located within the FUS focal spot. An omnidirectional Ca²⁺ flux was subsequently observed extending around the initial response and propagating throughout the neural network (estimated velocity: 7 μ m.s⁻¹) (fig b1 and c1), demonstrating a stimulating effect on neurons located beyond the targeted region. A similar response dynamic was observed after mechanical stimulation of a single neural cell (fig b2 and c2). Velocities of the calcium fluxes propagating along identifiable axons (n=112) were also comparable between FUS and mechanical stimulations (26 μ m.s⁻¹ vs 28 μ m.s⁻¹) (fig d1 and d2).

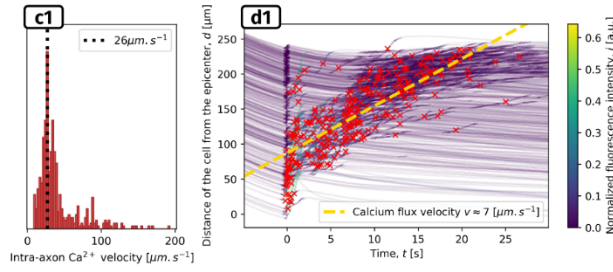
The preliminary results obtained in this study indicate that FUS stimulation can produce network-wide effects following similar dynamics to mechanical stimulation. The different identified velocities by which the FUS-evoked signals propagate indicate that multiple, concurrently-occurring mechanisms are involved in intercellular propagation of FUS-induced neural responses.

This project was supported by the French National Research Agency (ANR-16-TERC-0017 & ANR-21-CE19-0007-01), the Focused Ultrasound Foundation (LabTAU, FUSF Center of Excellence) and LabEx DevWeCan.

FUS Stimulation

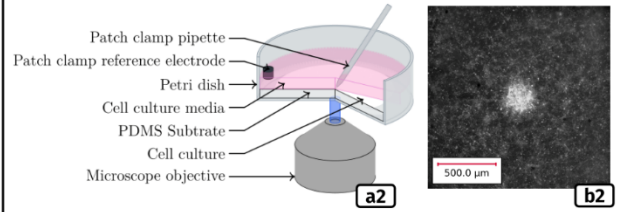


a1: Schematic representation of the setup used for FUS stimulation.
b1: FUS-induced Ca^{2+} in *in-vitro* human neural cells at $t=10\text{s}$.

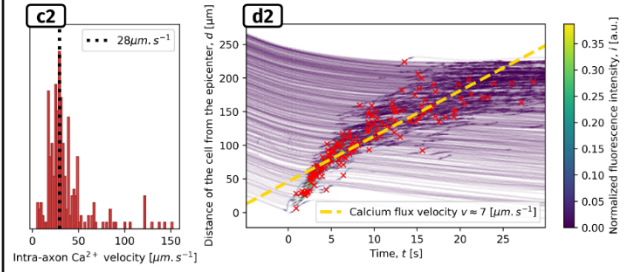


c1: Distribution of Ca^{2+} axon velocities (484 samples over 25mm).
b1: Flux group velocity estimated from cells Ca^{2+} activity (red crosses).

Mechanical Stimulation



a2 Schematic representation of the setup used for mechanical stimulation.
b2: Mechanically-induced Ca^{2+} in *in-vitro* human neural cells at $t=10\text{s}$.



c2: Distribution of Ca^{2+} axon velocities (416 samples over 22mm).
b2: Flux group velocity estimated from cells Ca^{2+} activity (red crosses).

Controlled, Effective Ultrasonic Neuromodulation through the Skull

Presenter: Tom Riis

Authors in order: Tom Riis, *University of Utah*, Jan Kubanek, *University of Utah*

We developed a method to directly measure the ultrasound distortions caused by the skull and correct for them, to deliver a known ultrasound dose for effective neuromodulation.

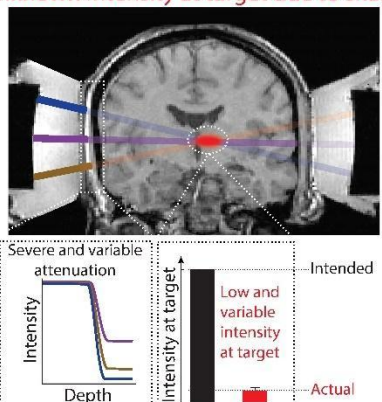
We implemented this correction in hardware and directly measured the delivered intensity field using 3D hydrophone scans in 8 ex-vivo human skulls. We quantified the correction's ability to deliver an intended value of intensity through the skull. We compared this correction to the ground-truth hydrophone correction. Moreover, we show that the correction is crucial for effective ultrasonic neuromodulation. We applied this and other corrections and measured neuromodulation by stimulating nerves in the finger of human subjects placed inside the intact ex-vivo skull.

We found that the ultrasound-based correction method accurately restores the operator's intended intensity at target. With no correction, the intensity was reduced to $10.4 \pm 3.3\%$ (mean \pm s.e.m.) of the intended value. The ultrasound correction delivered intensity $94.8 \pm 8.7\%$ of the intended value and there was no significant difference between this correction and the ideal hydrophone correction. We also found this correction was crucial for effective neuromodulation. Without any correction, no significant neuromodulation was achieved. Following ultrasound correction, we observed a neural stimulation response rate of 62.7%, which was statistically equivalent to the response rate from the ideal hydrophone correction, 66.3%.

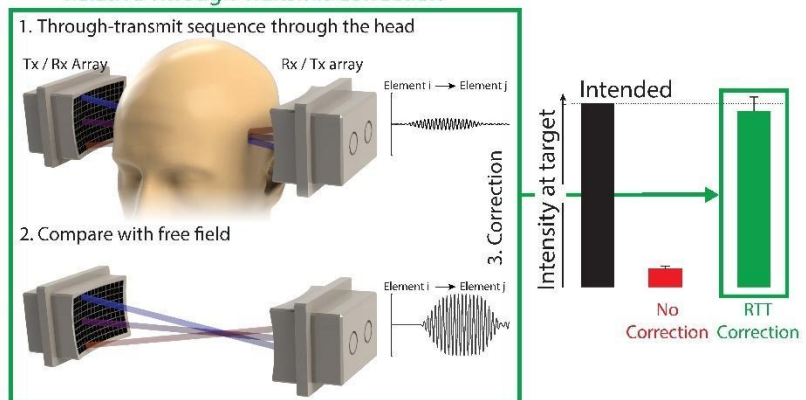
When ultrasound correction is not applied---as in currently used approaches and devices---there is no significant stimulation. This approach and hardware overcome the major barrier of skull aberrations and thus unlock the potential of current and emerging ultrasound-based approaches to provide effective, safe, and reproducible therapies of the brain.

This work was supported by the NIH grant R00NS100986. The method and hardware described herein are subjects of a provisional patent.

Unknown intensity at target due to skull



Relative Through-Transmit Correction



A1-2

High Precision Optically-guided Transcranial Ultrasound Stimulation in the Mouse Brain

Presenter: Daniel Razansky

Authors in order: Daniel Razansky, *University and ETH Zurich*

Precision tools for high-resolution transcranial ultrasound targeting and real-time in vivo tracking of its effects at the mouse brain scale are currently lacking.

We report a versatile bidirectional hybrid fluorescence-ultrasound (FLUS) system. Precise ultrasound emission with a transcranial lateral focus size of 0.35-mm at 3 MHz is achieved with a 512-element spherical-phased array. Cortex-wide fluorescence imaging through a fiberscope inserted in an aperture at the array's zenith was operated at 20 frames per second to provide real-time feedback from the living mouse brain labeled with fluorescent genetically-encoded calcium indicator GCaMP6f.

We show how the marriage between cortex-wide functional imaging and targeted ultrasound delivery can be used to transcranially map previously undocumented localized fluorescence events caused by reversible thermal processes and perform high-speed large-scale recording of neural activity induced by focused ultrasound. The fluoro-thermal tag appears as a fast and localized decrease in fluorescence as the slight temperature increase quenches the fluorescence. We explored the effect of different ultrasound pressure using resting state connectivity analysis, histological analysis, and observed the propagation of cortical spreading depolarization upon high pressure emission.

FLUS naturally harnesses the extensive toolbox of fluorescent tags available in mice and ultrasound's localized bioeffects toward visualizing and causally perturbing a plethora of normal and pathophysiological processes in the living murine brain.

Grant support from the US National Institutes of Health and European Research Council is acknowledged.

A1-3

Low-intensity Focused Ultrasound Mediates Tissue Protection after Stroke

Presenter: Lauren Ruger

Authors in order: Lauren Ruger, *Virginia Polytechnic Institute and State University*, Alexandra Kaloss, *Virginia Polytechnic Institute and State University*, Eman Soliman, *Virginia Polytechnic Institute and State University*, Maya Langman, *Virginia Tech Carilion School of Medicine*, Nathalie Groot, *Virginia Polytechnic Institute and State University*, Eli Vlaisavljevich, *Virginia Tech*, Michelle Theus, *Virginia Polytechnic Institute and State University*

In this study, we examined whether low-intensity focused ultrasound (LIFU) could promote acute neuroprotection in a murine model of permanent middle cerebral artery occlusion (pMCAO).

Adult, male CD1 mice (sham or pMCAO) were exposed to transcranial LIFU for 30 minutes (interstimulus interval, 3s; pulse repetition frequency, 1kHz; duty cycle, 50%; sonication duration, 300ms) using a 1.1MHz single element transducer and peak negative pressures (p-) of 1.8 to 3.5MPa. Then, mice were euthanized and evaluated for infarct volume, blood-brain barrier disruption, and pial collateral remodeling 24 hours after pMCAO. Control mice were collected by applying mock ultrasound to the targeted region.

Pilot experiments comparing p- 1.8MPa to 3.5MPa revealed hemorrhage and mortality in mice treated at 3.5MPa, with no mortality or hemorrhage noted at 1.8MPa. Neuroprotection experiments conducted at p- 2.0MPa identified significant reductions in infarct volume ($7.51 \pm 1.14 \text{ mm}^3$ vs. $19.62 \pm 3.68 \text{ mm}^3$) and immunoglobulin G deposition ($7.29 \pm 2.56 \text{ mm}^3$ vs. $23.77 \pm 4.43 \text{ mm}^3$) in LIFU-treated mice compared to control mice. Additionally, microvessel diameter in the ipsilateral cortex was significantly increased following LIFU compared to mock treatment ($7.07 \pm 0.17 \mu\text{m}$ vs. $4.06 \pm 0.11 \mu\text{m}$). Significant decreases in pial collateral vessel number and size were measured in all pMCAO mice, but no differences were observed between LIFU-treated and mock LIFU pMCAO groups.

This study demonstrates the safety and neuroprotective properties of LIFU in a pMCAO murine model and suggests that LIFU therapy may induce tissue protection through microvascular remodeling. Further investigation is needed to determine LIFU's role as a therapeutic for ischemic stroke and the exact mechanisms underlying the measured protection.

The authors thank the Institute for Critical Technology and Applied Science, Center for Engineered Health, and National Institutes of Health (R01NS112541) for their financial support.

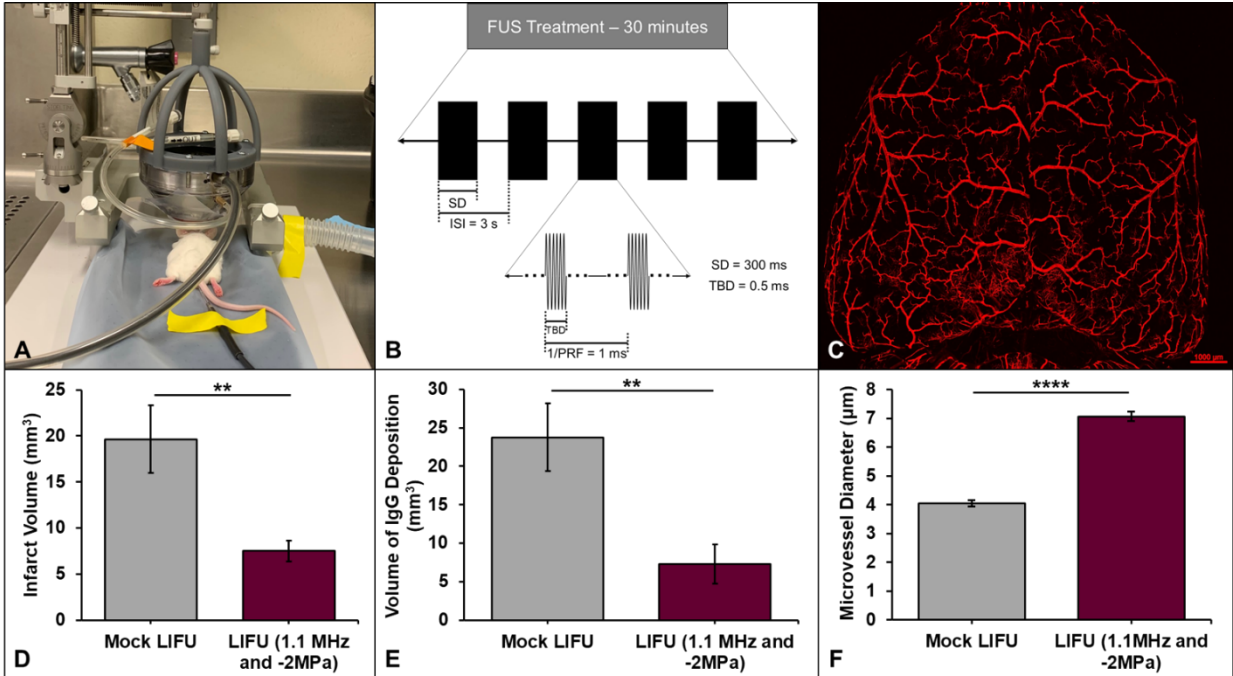


Figure 1: (A) Experimental set-up for focused ultrasound treatment following ischemic stroke. (B) Employed pulsing regime with treatment pressures between -1.8 and -3.5MPa. (C) Vessel painting technique used to evaluate pial collateral vessel changes. (D-E) Significant neuroprotection was measured after LIFU treatment at -2.0MPa with decreases in (D) infarct volume and (E) immunoglobulin G deposition (** $p < 0.01$). (F) Microvessel diameter was significantly increased following LIFU treatment at -2.0MPa (**** $p < 0.0001$).

A1-4

Durable Ultrasonic Neuromodulation for Targeted Treatments of Deep Brain Circuits

Presenter: Taylor Webb

Authors in order: Taylor Webb, *University of Utah*, Matthew Wilson, *University of Utah*, Jan Kubanek, *University of Utah*

We tested the effects of protocols that apply sustained ultrasonic stimulation, and quantified effects on behavior that persist beyond the ultrasonic stimulation.

We delivered ultrasound into the lateral geniculate nucleus (LGN) of nonhuman primates (NHPs) performing a visual discrimination task. Each session consists of a single sonication of 30 seconds. The subjects' choice behavior was measured before, during, and after each sonication. The sonications complied with the FDA 510(k) Track 3 recommendations.

Data of 7 sessions in two NHPs show a substantial and significant increase in the subject's choice of the ipsilateral target following a 30s sonication of the left/right LGN. This effect was observed on average for about two minutes following each sonication. The effects were fully reversible.

This study shows that low-intensity ultrasound can be applied non-invasively to modulate deep brain circuits in NHPs in a durable, artifact-free, and safe manner. These findings unlock the potential of the method for remote, flexible modulation of deep brain circuits in humans.

This work was supported by NIH Grants 5R00NS100986 and F32MH123019.

A1-5

Low Intensity Pulsed Ultrasound excites Synaptic Transmission in Hippocampal Neuron Networks

Presenter: Fenfang Li

Authors in order: Fenfang Li, *Shenzhen Bay Laboratory*, George Augustine, *Lee Kong Chian School of Medicine, Nanyang Technological University*

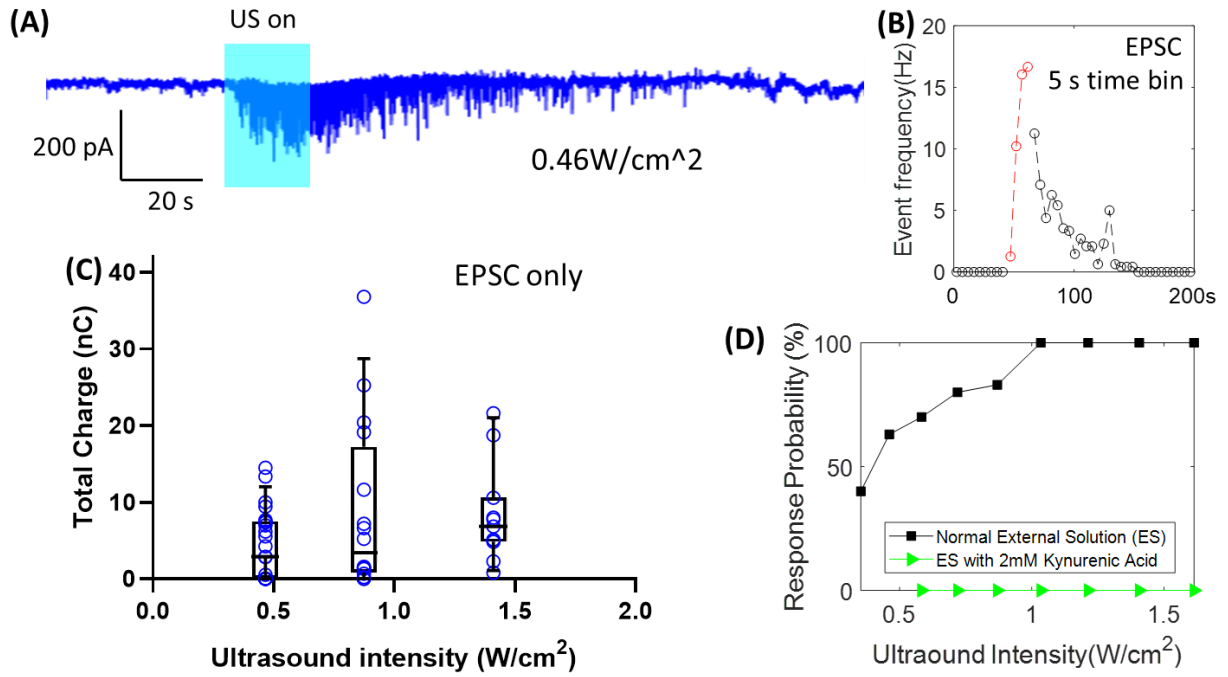
To investigate the effect of ultrasound on synaptic transmission in cultured hippocampal neurons, and understand the underlying cellular mechanisms.

Low-intensity pulsed ultrasound (25MHz, 5% duty cycle, 0.4 - 1.6W/cm²) was used to stimulate hippocampal neuron culture. Action potential firing and excitatory postsynaptic current was recorded with patch-clamp in individual cells in the culture. We also performed simultaneous calcium imaging and electrophysiological recordings to resolve the dynamics of neuron network firing relative to the response of individual cells in the network.

Excitatory postsynaptic currents (EPSCs) were evoked by low-intensity pulsed ultrasound in hippocampal neuron culture. Both the frequency and amplitude of EPSCs increased, indicating enhanced glutamatergic synaptic transmission. The probability of evoking responses, as well as the total charge of EPSCs evoked by ultrasound, increased with ultrasound intensity. Mechanistic analysis reveals that extracellular calcium influx, action potential (AP) firing and synaptic transmission are necessary for the responses to ultrasound. Simultaneous calcium imaging of neuronal network activity indicated that recurrent excitatory network activity is recruited during ultrasound stimulation.

Ultrasound can activate neuronal network activity and synaptic transmission, over tens to hundreds of seconds in individual cells within the network. Synaptic dysfunction is involved in various neurological disorders including Parkinson's and Alzheimer's diseases. Our study provides mechanistic insights for using ultrasound as potential therapy for these disease.

We thank Prof. Yufeng Zhou for the help measuring the acoustic pressure of ultrasound transducers. This work was supported by a LKCMedicine Dean's Postdoctoral Fellowship.



Low intensity ultrasound evokes EPSC through synaptic transmission in network

A1-6

Sonogenetics for Locomotor Behavior Modulation in Freely Moving Mice

Presenter: Kevin Xu

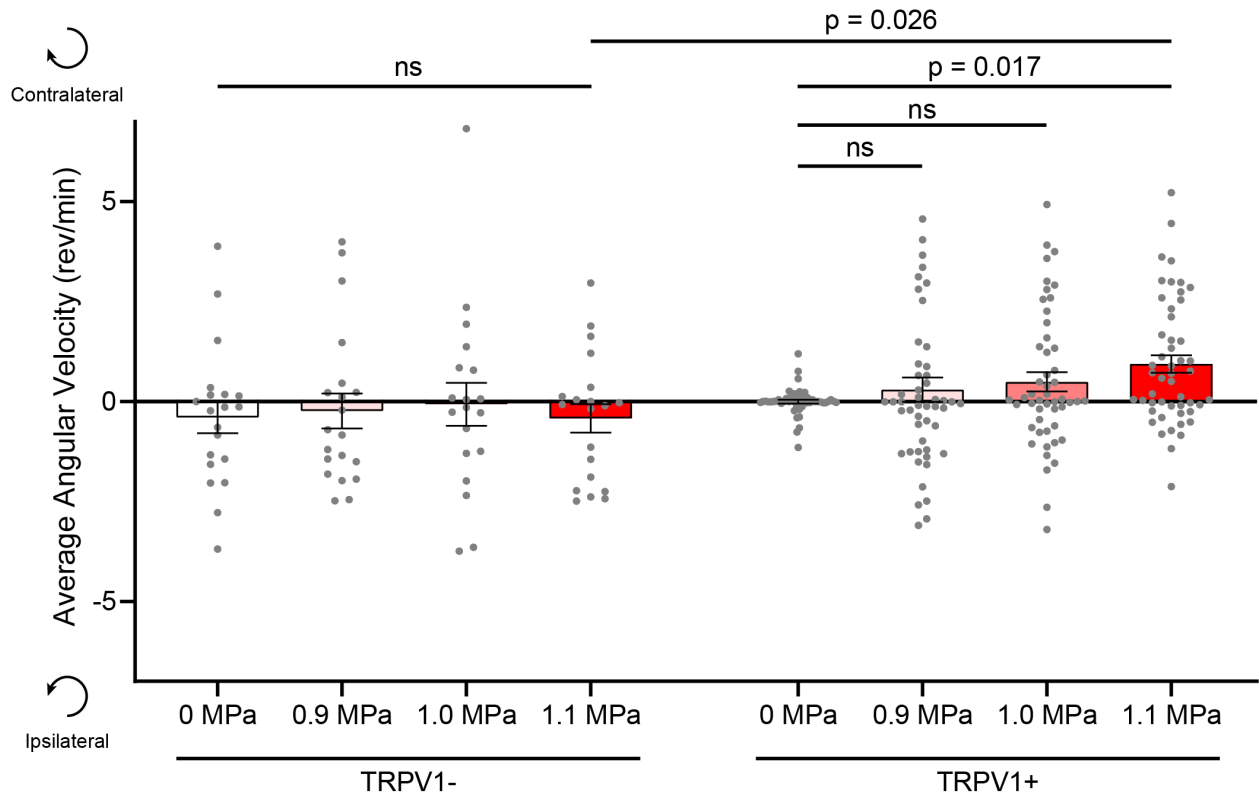
Authors in order: Kevin Xu, *Washington University in St. Louis*, Yaoheng Yang, *Washington University in St. Louis*, Yimei Yue, Hong Chen, *Washington University in St. Louis*

We evaluated the feasibility and safety of TRPV1-mediated sonogenetics to modulate the locomotor behavior of freely moving mice by targeting the motor cortex.

Adeno-associated virus was delivered to the mouse motor cortex via intracranial injection to express TRPV1 (TRPV1+) in excitatory neurons. After a month, a wearable focused ultrasound (FUS) transducer targeting the motor cortex was installed to control neuronal activity by activating TRPV1 through FUS sonication at different pressures. The mouse motor behavior was quantified using angular velocities to characterize the efficacy of sonogenetics. Control mice were injected with TRPV1- virus. Immunohistochemistry was performed for safety evaluation.

Sonogenetic stimulation of TRPV1+ mice at different acoustic pressures evoked rotational behavior in the direction contralateral to the stimulation site. The average angular velocities of TRPV1+ mice increased as acoustic pressure increased, while those of TRPV1- mice did not show such a trend (see figure). At 1.1 MPa, the average angular velocity of TRPV1+ mice was significantly higher compared to that of the sham (0 MPa), indicating that this is the minimum pressure needed for sonogenetic control of motor cortex. Sonogenetics did not induce significant changes in inflammatory or apoptotic markers (GFAP, Iba1, Caspase-3, and TUNEL).

This study demonstrated the feasibility and safety of sonogenetics to modulate locomotor behaviors by targeting the motor cortex.



A1-7

Motor Responses Induced by LIFU Neuromodulation and Piezoelectric Vibration in Mice

Presenter: Jake Hesselink

Authors in order: Jake Hesselink, *University of Calgary*, Siyun Li, *University of Calgary*, Zelma Kiss, *University of Calgary*, Samuel Pichardo, *University of Calgary*

We aimed to compare the motor responses produced by low intensity focused ultrasound (LIFU) neuromodulation to those caused by piezoelectric-induced skull vibrations.

C57Bl/6 mice were stimulated with 477 kHz LIFU with 1.5 kHz pulse repetition frequency (PRF). To obtain motor responses, isoflurane concentration was reduced below 0.5%. Motor activity was recorded via video and electromyography. A piezoelectric actuator was used to produce skull vibrations at the PRF, the parameter that is associated with indirect auditory activation, and a higher-frequency PRF harmonic. Response rates were compared between fixed and random PRF LIFU, sham, piezoelectric vibration, and air-puff stimulations.

Results from 10 mice suggest LIFU treatment with fixed PRF ($68.33 \pm 19.26\%$) and random PRF ($68.33 \pm 26.16\%$) both produced consistent motor responses at rates comparable to a physical air-puff stimulus ($83.19 \pm 21.14\%$). These rates were significantly higher than response rates to piezoelectric-induced skull vibrations and sham treatments ($p < 0.01$). While response rates to 4.5 kHz skull vibrations ($26.11 \pm 24.86\%$) were greater than 1.5 kHz vibrations ($5.05 \pm 5.51\%$), both piezoelectric vibration treatments yielded motor responses comparable to movement during sham treatment ($9.67 \pm 9.87\%$; Figure 1).

The high rate of motor responses to air-puff stimuli showed that arousing physical stimuli can induce motor activity under LIFU neuromodulation experimental conditions. However, as neither piezoelectric vibration treatment produced significant motor response rates, these results suggest that skull vibrations do not contribute significantly to motor responses in LIFU neuromodulation.

I would like to acknowledge the support of Dr. Pichardo and the NeuroFUS Lab, the University of Calgary, NSERC and the Brain Create program.

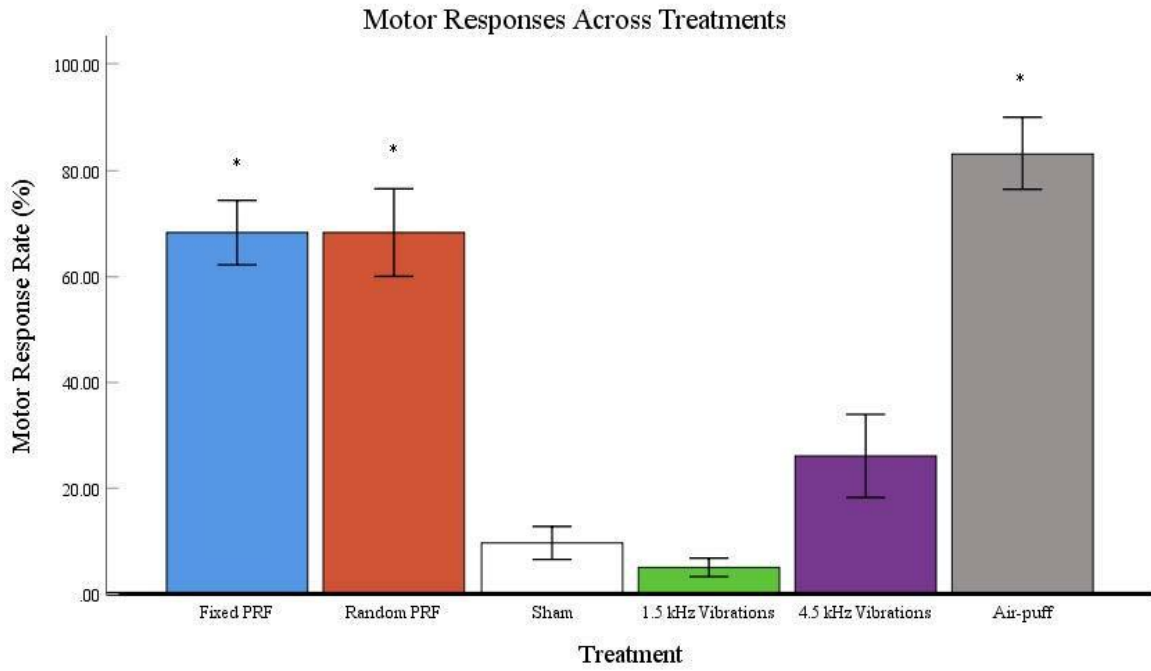


Figure 1. Motor response rates to various treatments including LIFU neuromodulation and piezoelectric-induced skull vibrations. n=10

Transcranial Ultrasound Stimulation Safety in Humans: Personalized Simulation Pipeline of Ultrasound Induced Thermal Rises

Presenter: David Attali

Authors in order: David Attali, *Physics for Medicine Paris, Inserm U1273, ESPCI Paris, PSL University, CNRS UMR 8063, Paris, France* ; Department of Psychiatry, Service Hospitalo-Universitaire, Centre Hospitalier Sainte-Anne, Paris Descartes University, Paris, France, Thomas Tiennot, *Physics for Medicine Paris, Inserm U1273, ESPCI Paris, PSL University, CNRS UMR 8063, Paris, France*, Maxime Daniel, *Physics for Medicine Paris, Inserm U1273, ESPCI Paris, PSL University, CNRS UMR 8063, Paris, France*, Alexandre Houdouin, *Physics for Medicine Paris, Inserm U1273, ESPCI Paris, PSL University, CNRS UMR 8063, Paris, France*, Philippe Annic, *Physics for Medicine Paris, Inserm U1273, ESPCI Paris, PSL University, CNRS UMR 8063, Paris, France*, Mickael Tanter, *Physics for Medicine Paris, Inserm U1273, ESPCI Paris, PSL University, CNRS UMR 8063, Paris, France*, Jean-Francois Aubry, *Physics for Medicine Paris, Inserm U1273, ESPCI Paris, PSL University, CNRS UMR 8063, Paris, France*

The objective of this study is to experimentally validate a personalized pipeline of ultrasound-induced thermal rise simulation to ensure the safety of Transcranial Ultrasound Stimulation.

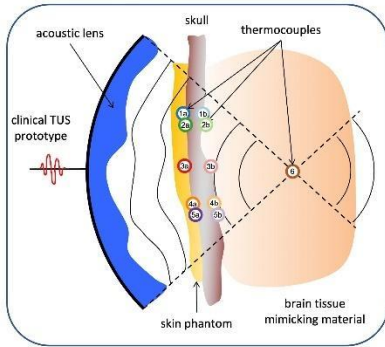
Thermal rises were recorded over time on five human skulls with the Transcranial Ultrasound Stimulation (TUS) parameters used on non-human primates in previous work: 30% duty cycle during 40s (500kHz frequency) and a pic negative pressure at focus of 0.7MPa. On each skull, calibrated thermocouples were placed to cover the entire ultrasound beam passing through the skull and at the acoustic focus. CT-based numerical simulations of the thermal rises were performed on the five skulls.

The ratio "experimental data / simulated data" was 1.02 ± 0.39 for the outer table and 1.11 ± 0.19 for the acoustic focus (mean \pm SD). In the experimental data, the highest thermal rises were on thermocouples located along the axis of symmetry of the spherical transducer, on the outer table of the skull, with a maximum value of 5.3°C. The simulated data have a higher spatial resolution and show hotter spots located between the thermocouples.

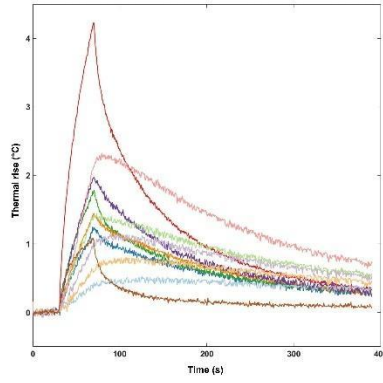
This work shows a good agreement between numerical and experimental thermal rises and lays the ground for estimating the safety of TUS. It also highlights that the parameters used on primates need to be adjusted for human as the thermal rise ($>5.3^\circ\text{C}$) is higher than previously simulated on monkeys (3°C).

Supported by the Bettencourt Schueller Foundation, the Agence Nationale de la Recherche (ANR-10-EQPX-15) and the Focused Ultrasound Foundation.

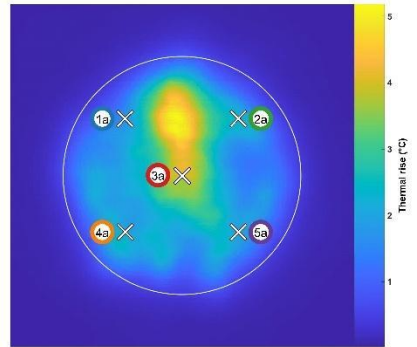
A. Experimental setup



B. Experimental data (skull #485)



C. Simulated data (skull #485, outer table)



A1-9

Focused Ultrasound Stimulation enhances Neural Excitability and Mobility in Awake Mice

Presenter: Chen-Syuan Huang

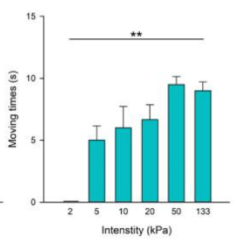
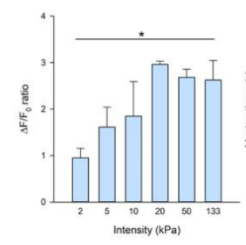
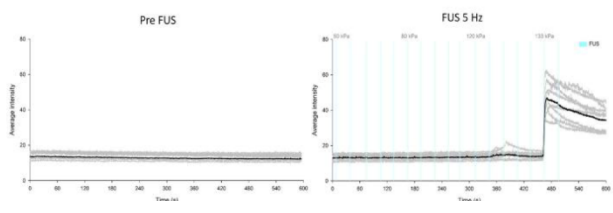
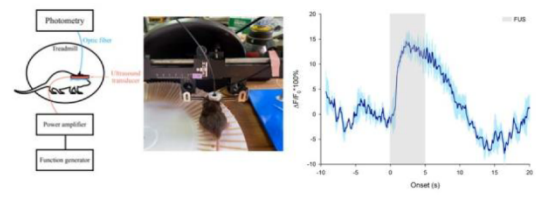
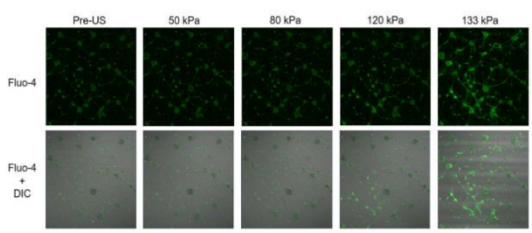
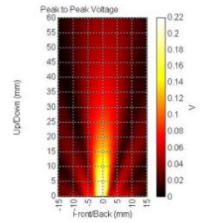
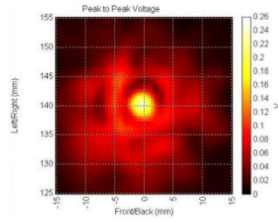
Authors in order: Chen-Syuan Huang, *National Taiwan University*, PO-CHUN CHU, *National Taiwan University*, Hao-Li Liu, *National Taiwan University*, Yi-Chun Yeh, *National Taiwan University*, CHI-HSIANG CHUANG, *National Taiwan University*

To propose a ring-shaped ultrasound setup and verify its utility in the neural modulation effects integrated with the microscope and fiber photometric concurrent stimulation observation.

A ring-shaped interfered FUS transducer (300 kHz) was utilized. The ultrasound parameters were designed with the test pressure range of 2-133 kPa (duty cycle = 20% and pulsed repetition frequency (PRF) = 5 Hz. Primary cortical neurons (in-vitro) and C57BL/6 mice (in-vivo) with AAV9-syn-jGCaMP7s infection into the hippocampus were used for ultrasound stimulation. The calcium fluorescence levels and running times of mice were acquired and analyzed with the fiber photometry system.

The ring-shape ultrasound apparatus generates a constructive ultrasound interference with the focused region of 10 mm in axial direction and 4 mm in cross-section. In in-vitro experiments, the calcium fluorescence levels were increased by focus ultrasound intensity (133 kPa; from 12.7 ± 0.6 to 49.5 ± 3). In in-vivo experiments, the calcium fluorescence levels in the hippocampus were also enhanced while ultrasound. The increased calcium fluorescence ratio is from ~ 0.9 to ~ 2.5 by ultrasound exposure ($p \pm 0.7$ s) by FUS increasing intensity stimulation ($p < 0.01$).

We successfully applied the customized FUS transducer to the confocal microscope setup and the fiber photometry device to real-time observe neural activities under ultrasound stimulation. The neural calcium fluorescence levels and neural activities were enhanced while the intensity of FUS stimulation. Such FUS stimulations were compatible with the locomotion of awake mice.



A2-1

Clinical Trial Design for Musculoskeletal Applications of Focused Ultrasound

Presenter: Matthew Bucknor

Authors in order: Matthew Bucknor, *UCSF*

Provide an overview of clinical trial development in magnetic resonance-guided focused ultrasound (MRgFUS) for musculoskeletal applications.

The key stages of clinical trial development in MRgFUS can be divided into the following four categories: feasibility, pivotal, post-market, and quality/cost/access. Feasibility studies are the most common in the field of MRgFUS, as this technology is developed for an ever-increasing spectrum of indications. This presentation will briefly discuss three trial designs for undifferentiated pleomorphic sarcomas, osteoid osteomas, and bone metastases, along with trial updates.

1. A feasibility study of MRgFUS to promote immune response effects in patients with undifferentiated pleomorphic sarcoma (trial in progress)
2. A randomized controlled trial of MRgFUS versus CT-guided radiofrequency ablation (non-inferiority) (trial in progress)
3. A cost-effectiveness analysis of MRgFUS for ablation of bone metastases (study completed)

Many clinical studies of MRgFUS focus on development of this technology for new indications. Having a broader perspective of the full spectrum of stages of technology development and key obstacles at each stage is critical for sustainable and impactful growth for the field of MRgFUS.

Focused Ultrasound Foundation, AUR GERRAF Program, and all members of the UCSF MRgFUS Team

A2-2

Applications of HIFU in Women's Health

Presenter: Lian Zhang

Authors in order: Lian Zhang, *Chongqing Medical University*, Zhibiao Wang, *Chongqing Medical University*

To retrospectively analyze the safety and efficacy of high-intensity focused ultrasound (HIFU) in management of benign uterine diseases.

From March 2011 to December 2021, 7252 patients with benign uterine diseases and breast tumors were treated with HIFU in Chongqing Haifu Hospital. Among them, 6926 patients had uterine fibroids, 2039 patients had adenomyosis, 190 patients had abdominal wall endometriosis, 86 patients had breast fibroadenomas, 10 patients had breast cancer, 3 patients had caesarean scar pregnancies, and 6 patients had placenta accreta.

All patients completed HIFU in one session. A median non-perfused volume (NPV) ratio of 83.3% was achieved in uterine fibroids. The average NPV ratio of 60.5%±13.1% was achieved in adenomyosis. Compared with baseline data, the menorrhagia severity score and the dysmenorrhea severity pain score decreased significantly after HIFU in patients with uterine fibroids or adenomyosis. The incidence of major adverse effects was 0.31%. No significant difference was observed in the rates of major adverse effects between patients with uterine fibroids, adenomyosis, breast, abdominal wall adenomyosis, and placenta accreta. Over the last 10 years, more than 300 patients with uterine fibroids or adenomyosis have delivered babies after HIFU without HIFU related complications.

Based on the results from our center, we concluded that HIFU is safe in treating patients with benign uterine diseases and breast tumors. As a non-surgical treatment, HIFU is a promising alternative treatment with the advantages of precision, non-invasiveness, rapid recovery and readiness for pregnancy.

A2-3

Non-invasive Ultrasound Therapy of Calcific Aortic Valve Stenosis: From Basic Concept to First-in-Human Study

Presenter: mathieu pernot

Authors in order: mathieu pernot, *Physics for Medicine, INSERM*

The development of non-invasive ultrasound therapy of calcific aortic valve stenosis is presented from basic in vitro experiments to the clinical proof of concept.

Calcific aortic stenosis (CAS) is the most common heart valve disease. To date, surgical or transcatheter aortic valve replacement is the only effective treatment. We proposed recently a novel non-invasive therapeutic approach based on the use of pulsed cavitation focused ultrasound to improve the function of calcified valves. An ultrasound image-guided therapeutic device (Valvosoft, Cardiawave, France) was designed based on this concept for transthoracic treatment of aortic valve stenosis.

This concept was validated in vitro using degenerative and bioprosthetic valves and in vivo on a large animal model. The transthoracic feasibility and safety was demonstrated on 15 swine. On the basis of preclinical results, a prospective first-in-human study was conducted in 2 centers (Hôpital Georges-Pompidou, France; Amphia Hospital, Breda, The Netherlands) in 10 patients (84.1±6.5 years) with symptomatic severe CAS who were not eligible for AV replacement. The procedure was feasible in 10 patients with severe CAS and six patients were responders with an increase in AV area of 27.6% associated with a decrease in mean pressure gradient of 23.5%.

Non-invasive ultrasound therapy of CAS is a promising therapeutic approach. We demonstrated the feasibility of a cohort of 10 patients with severe CAS. Ongoing clinical studies are assessing its safety, dose effect relation and durability.

We acknowledge Cardiawave and the Inserm ART for funding support

A2-4

First-in-man Study using HIFU to Occlude Placental Blood Vessels as a Method of Treating Twin-twin Transfusion Syndrome -TTTS

Presenter: Ian Rivens

Authors in order: Ian Rivens, *Institute of Cancer Research*, Caroline Shaw, *Imperial College London*, Richard Symonds-Taylor, Gail ter Haar, *The Institute of Cancer Research*, Christoph Lees

Early stage clinical trial of HIFU vascular occlusion for treating Twin-Twin Transfusion Syndrome (TTTS) in monochorionic twins to avoid poor outcomes for both babies.

A purpose-built system consisting of an US-image guided HIFU head (Sonic Concepts) on a (collaborative) robotic arm (Universal Robots UR15e) with sealed couplant bag, was tested in vivo prior to clinical use. Up to 13 mothers with anterior placentas who develop TTTS at < 18 weeks' gestation will be treated non-invasively with to establish tolerability, safety and preliminary efficacy information. Eligible patients are those for whom colour Doppler ultrasound identifies one or more placental vascular anastomoses.

Vessels were successfully targeted using advanced Doppler ultrasound (Canon Aplio 900), and were exposed using 3-5 adjacent exposures at focal peak intensities of 2-3 kWcm⁻². The first patient experienced painful abdominal wall heating during an exposure. Lower intensities used subsequently produced no or mild discomfort. No severe adverse effects occurred, with fetal development being unremarkable on follow up scans of up to 2 weeks post procedure. Vascular occlusion of 2 of 3 anastomoses identified resulted in down-staging of TTTS from stage 2 to stage 1 in 1-2 h.. Full resolution of TTTS was achieved within 7 days.

Initial indications are that treatment is well tolerated without analgesia, sedation or anaesthetic. Vascular occlusion can be achieved and persists for at least 2 weeks, without serious adverse effects. Preliminary efficacy data are encouraging. Longer term and additional patient data will be presented at the meeting.

This work was supported by the Medical Research Council [MR/R015384/1]

Transrectal High-intensity Focused Ultrasound (TR-HIFU) for the Management of Rectal Deep Infiltrating Endometriosis: Results of Phase I Clinical Trials

Presenter: Gil Dubernard

Authors in order: Gil Dubernard, *Hospices Civils de Lyon*, Françoise Chavier, *Labtau Inserm U1032*, Laurie Brunel, *EDAP-TMS*, Charles-André Philip, *Hospices Civils de Lyon*, Morgane Dairien, *Hospices Civils de Lyon*, Claire Jossan, *EDAP-TMS*, Cyril Lafon, *INSERM*, Claire Jossan, *EDAP-TMS*

The objectives of this study were to confirm the feasibility of transrectal HIFU treatment for patients with symptomatic rectal endometriosis and to assess its safety and clinical efficiencies.

We are conducting a multicentric prospective safety study. We plan to include 60 patients. To date, 50 symptomatic patients with an indication of surgery after failure of medical treatment have been included. All lesions were assessed using transvaginal sonography and MRI prior and 6 months after treatment. Patients also filled questionnaires on gynecologic, digestive symptoms and quality of life prior to the HIFU and post-treatment at one, three and six months.

For 37 first patients, all the lesions were visualized. The mean duration of the procedure was 33 minutes. The preliminary results demonstrated a significant improvement in visual analogic scales at one, three and six months for dysmenorrhea (-3.6, p=0.004), dyspareunia (-2.4, p=0.006), diarrhea (-3.0, p=0.006), constipation (-3, p=0.002), dyschezia (-3.2, p=0.003), false urges to defecate (-3.3, p=0.007), posterior pelvic pain (-3.8, p=0.002), and asthenia (-4.3, p=0.002). There was also a significant improvement of the MOS-SF36 with an increase of both Physical Composite Score (+9.3%, p=0.002) and Mental Composite Score (+10.9%, p=0.017). No recto-vaginal fistulae occurred during and after the procedure.

In this prospective study we confirm the feasibility of HIFU therapy for rectal endometriosis. It could be an interesting minimally invasive alternative to surgery for the treatment of rectosigmoid endometriosis if its efficacy and safety are confirmed. The inclusion of the 10 remaining patients is scheduled for the end of March 2022.

EDAP-TMS for its financial and methodological supports

A fully-populated MR-guided Focused Ultrasound Phased Array for the Treatment of Uterine Fibroids: A Feasibility Study

Presenter: Ryan Jones

Authors in order: Ryan Jones, *Sunnybrook Research Institute*, Yuexi Huang, *Sunnybrook Research Institute*, Benjamin Lucht, *Arrayus Technologies*, Samuel Gunaseelan, *Sunnybrook Research Institute*, Tyler Portelli, *Arrayus Technologies*, Elizabeth David, *Sunnybrook Research Institute*, Kullervo Hynynen, *Sunnybrook Research Institute/ University of Toronto*

To evaluate the feasibility of using a flat fully-populated MR-guided focused ultrasound (MRgFUS) phased array system for thermal ablation in patients with symptomatic uterine fibroids.

Between 11/2017-02/2022, 40 patients underwent MRgFUS thermoablation with a clinical-prototype system (Symphony, Arrayus Technologies) as part of an ongoing clinical trial (NCT03323905). The MRgFUS system comprises a flat 170 mm-diameter 6144-element array with a half-wavelength inter-element spacing at the driving frequency (518 kHz), mounted on the standard bed of a 3T MRI scanner (MAGNETOM Prisma, Siemens Healthcare). Multi-planar MR-thermometry was carried out for intraoperative treatment monitoring. Patients were followed (clinical/MR imaging) up to 12 months post-treatment.

Patients received 22 ± 8 sonications (power = 144 ± 49 W, duration = 43 ± 11 s) during MRgFUS treatment sessions (min/mean/max duration = 28/69/112 min) resulting in thermal dose volumes of 24 ± 21 cm³ (240 cumulative equivalent minutes at 43°C). The mean nonperfused tissue volume measured immediately post-treatment via contrast-enhanced T1-weighted MR imaging was 75 ± 129 cm³. Increases observed in quality of life scores improved throughout the year post-treatment ($50 \pm 16\%$ / $96 \pm 21\%$ / $114 \pm 34\%$ / $130 \pm 44\%$ at 1/3/6/12 mo). Symptom severity scores improved 1 month post-treatment and were durable throughout the year (68 ± 3 / 46 ± 4 / 39 ± 4 / 46 ± 5 / 38 ± 7 at 0/1/3/6/12 mo). There were no serious adverse events related to the use of the MRgFUS ablation device.

Volumetric thermoablation with a fully-populated phased array appears safe and effective for the treatment of uterine fibroids. The MRgFUS system is capable of large volume tissue ablation without the need for mechanical translation, and the high element count provides increased control over the beam geometry for improved ultrasound energy delivery.

We thank A. Minhas, S. Philip, and H. Meirovich for clinical data compilation, and M. Kazem, R. Ramdoyal, P. Wu, R. Endre for technical support.

Comparison of Intraprostatic Calcification Measurements using CT versus MR Susceptibility Weighted Imaging in TULSA Patients

Presenter: Sandeep Arora

Authors in order: Sandeep Arora, *Yale Medicine*, Clifford Shin, *Yale School of Medicine*, Preston Sprenkle, *Yale School of Medicine*, Rajasekhara Ayyagari, *Yale School of Medicine*, Amanda Beserra, *Profound Medical*, Robert Staruch, *Profound Medical*

Men seeking MRI-guided transurethral ultrasound ablation (TULSA) are screened for ultrasound-obstructing calcifications. We compare calcification measurements on susceptibility-weighted MRI (SWI) and computed tomography (CT).

TULSA screening typically includes CT for identifying size and location of intraprostatic calcifications. Large calcifications can block ultrasound propagation, reducing heating of peripheral prostate tissue. Pre-TULSA CT (0.6mm slices) was acquired for 6 men; in men with calcifications, intraprocedural SWI (1.0mm slices) guided positioning of therapeutic ultrasound elements with respect to calcifications was performed. Calcification diameters were measured in three planes on CT and SWI, and their impact on treatment was assessed using MRI thermometry.

All six calcifications (in 5 men) identified on CT were visible on SWI. Mean (range) diameter was 5.6 (2.0-9.8) mm on CT and 6.2 (2.5-10.7) mm using SWI. SWI diameters were larger in at least one plane for all calcifications, 11/18 measurements overall (median 16% larger). Additionally, 4 calcifications were identified exclusively on SWI with mean diameter 3.6 (1.8-5.7) mm. With SWI-guided device placement, TULSA MR thermometry indicated that 4/5 men had adequate thermal dose for over 98% of target volume. One patient with three calcifications (two not seen on CT) had inadequate thermal dose in 4.6% of target volume.

Intraprocedural SWI detected all CT-identified calcifications, tending to overestimate the diameter but guiding effective device positioning. CT remains the gold standard for pre-TULSA calcification screening, and further studies are warranted to optimize SWI protocols, correlate the size of calcifications on CT and SWI, and predict their impact on ablation coverage.

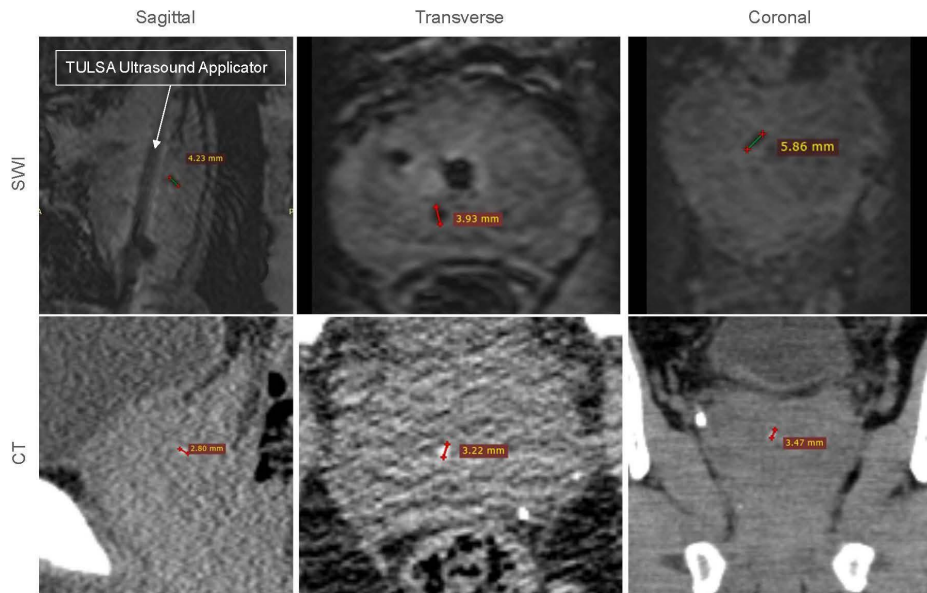


Figure 1. Example where CT detected one calcification, intraoperative SWI detected two.

A New flexible, portable MRI-guided HIFU Device for Treating Musculoskeletal Tumors: Clinical Proof-of-concept

Presenter: Paolo Cabras

Authors in order: Paolo Cabras, *Image Guided Therapy, ICube laboratory*, Pierre Auloge, *Strasbourg University Hospital*, Fabrice Bing, *Hôpital d'Annecy*, Alexandre DURAND, *Axilum Robotics*, Benoît WACH, *CNRS / Laboratoire ICube*, Elodie Breton, *CNRS/University of Strasbourg*, Erik Dumont, *Image Guided Therapy*, Afshin Gangi, *Strasbourg University Hospital*, Jonathan Vappou, *CNRS/University of Strasbourg*

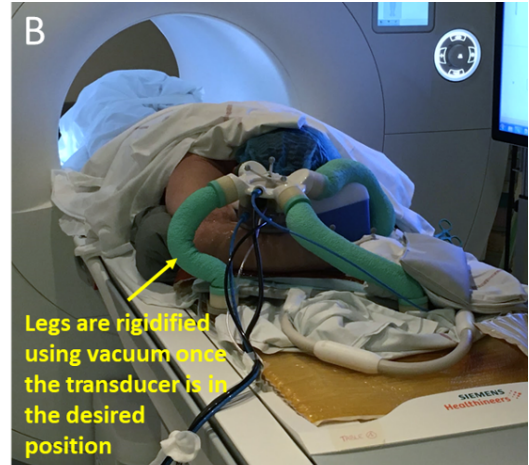
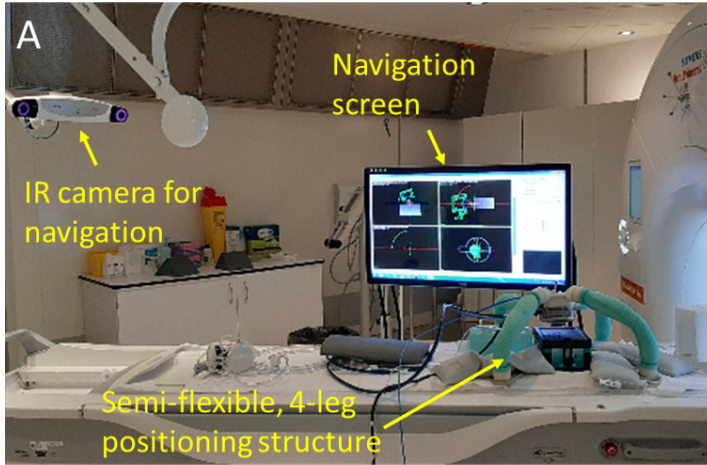
To develop a new MRI-guided HIFU device in which the transducer is directly positioned on the patient, facing the region that needs to be treated.

This system relies on (1) A semi-flexible supporting device that allows free manipulation of the transducer. Once the transducer is in the desired position, the device is rigidified using granular jamming, (2) A navigation software that guides the physician during the transducer positioning process, through a virtual environment displaying the target and the actual transducer position in real time. A first patient suffering from a bone metastasis in the forearm was treated with this system.

Intervention was performed by interventional radiologists of Strasbourg university Hospital, after proper training in phantoms and in swine. For this first patient (clinical trial NCT04803773), the lesion to be treated was an ellipsoid of 8*2*2 cm³. Five different transducer positions were necessary to cover the whole volume, in addition to using electronic steering (using a 128-element, 1MHz transducer of 6cm focal depth) for each transducer pose under MR-Thermometry control. The patient was successfully treated: Pain score decreased from 8/10 to 3/10 four days after treatment, and 85% of the lesion was treated. No adverse effects were reported.

We introduced a versatile HIFU device for treating musculoskeletal tumors. It is not MRI-manufacturer-dependent, and its modularity allows easy targeting of different body parts. Co-developed with interventional radiologists, this system allows easy positioning of the HIFU transducer with 6 degrees-of-freedom thanks to the supporting structure and the navigation software.

Funding was provided by Fonds Unique Interministériel (BPI France-Feder-Région Alsace), UFOGUIDE project



Experimental setup: General (A) and Clinical Case (B)

A3-1

The Impact of Microbubble Cavitation on the Viability, Migration and Cell Cycle Distribution of Melanoma Cells

Presenter: Juan Tu

Authors in order: Juan Tu, *Institute of Acoustics*

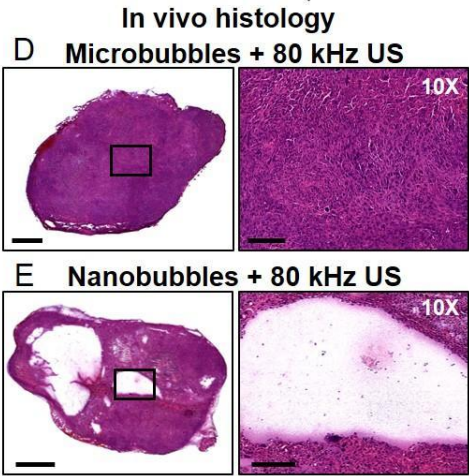
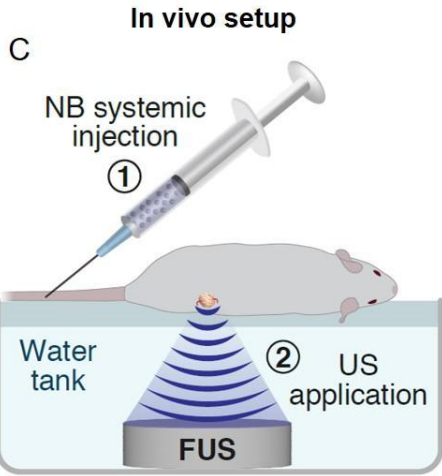
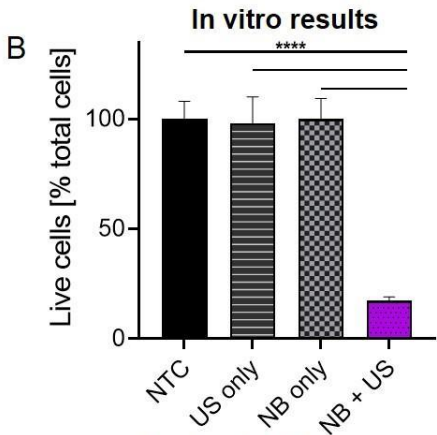
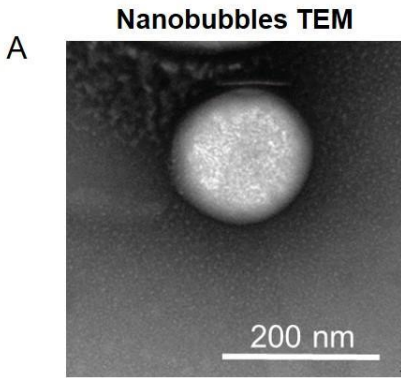
The impact of ultrasound-induced microbubble (MB) cavitation on the viability, migration and cell cycle arrest of A375 melanoma cells was studied.

In vitro experiments were carried out to evaluate the cell viability, migration rate and cell cycle distribution of A375 melanoma after ultrasound irradiation with varied dring parameters (e.g., acoustic pressure and MB concentration). Meanwhile, inertial cavitation dose (ICD) was used as an indicative term to quantitatively evaluate the accumulative IC activities, which could be affected by combined factors, e.g., acoustic parameters and MB properties. Finally, the relationship between ICD and A375 cellular responses, e.g., viability, migration, and cell cycle distribution, were discussed according to the pooled data.

The results showed that: (1) ICD increased with the increasing concentration of MBs at first, but saturated as the MB concentration further increased. (2) A375 cell migration fluctuated until ICD reached a certain threshold (e.g., 3000 $V\text{ms}$) and declined rapidly afterwards. (3) The changes in the proportion of G1 phase of A375 was consistent with the variation trend of cell migration, while the G2/M phase ratio changed oppositely with the cell migration. (4) Significant G2/M cell cycle arrest was found at 8355 $V\text{ms}$.

The results suggested that the cycle distribution, migration, and viability of A375 cells could be influenced by ICD in a dose-dependent manner, which might introduce a promising perspective to the utilization of US in treatment of melanoma.

Nanobubble-mediated low frequency mechanotherapy experimental results



FUS Thermal Ablation and Anti-PD-1 checkpoint Inhibitor Combination Therapy in Murine MMTV-PyMT Breast Cancer

Presenter: Sara Johnson

Authors in order: Sara Johnson, *University of Utah*, Pavitra Viswanath, *Huntsman Cancer Institute*, Nicholas Richards, *University of Utah*, Joshua Hillyard, *University of Utah*, Alana Welm, *Huntsman Cancer Institute*, Jill Shea, *University of Utah*, Allison Payne, *University of Utah*

To assess FUS thermal ablation strategies as mono- and combination immunotherapies in an orthotopic murine breast cancer model.

MMTV-PyMT tumor cells (1×10^4) were injected orthotopically into female mice (FVB-NJ) and grown to a diameter of ~ 1 cm. Mice were assigned to control, α PD-1 only, FUS only, or FUS- α PD-1 combination treatment groups. For a 15-day treatment schedule, α PD-1 checkpoint inhibitor was administered every third day (4 mg/kg/dose). FUS was administered on the third day only, under guidance of MR thermometry. At the study endpoint (day 15), tumor and spleen were harvested for flow cytometry.

Preliminary results are presented for $N=21$ mice ($n=3/4$ per group). Thermal dose maps, saturated at the threshold for cell death ($CEM_{43} = 240$), compare thermal damage between two FUS ablation strategies, “sparse” and “dense” (Fig1). Tumor growth advanced in all treatment groups, with greatest variability in the control- and α PD-1 only groups (Fig2). At the 15-day endpoint, CD45+ and CD3+ T-cell tumor infiltration was greater in FUS- α PD-1 combination groups than control, although not significantly (Fig3a). In the spleen, the CD8+/CD4+ T-Cell ratio was increased above control in all treatment groups (Fig3b). There was no apparent difference in responses between sparse/dense strategies.

Increased T-cell infiltration improves the effectiveness of checkpoint inhibitors in breast cancers. In this preclinical study, there is evidence of prolonged intratumoral immune infiltration following FUS- α PD-1 combination therapy compared to monotherapies. However, long-term outcomes were not assessed. Although initial results are highly variable, these encouraging trends warrant continued investigation.

Research was supported by the Office Of The Director of the NIH (S100D026959) and the Vice President of Research at the University of Utah.

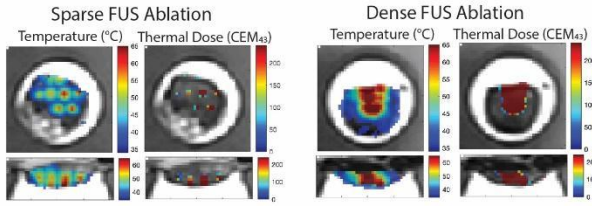


Figure 1. Representative maximum temperature and thermal dose maps (cumulative equivalent minutes at 43°C) of Sparse and Dense tumor ablations, overlaid on T2-weighted MR images.

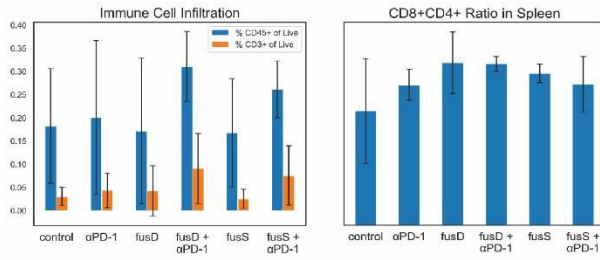


Figure 3. (a) Percent of CD45+ (blue) and CD3+ T Cells (orange) of Live cells in tumor. (b) Ratio of CD8+/CD4+ in spleen. (n=3/4 per group).

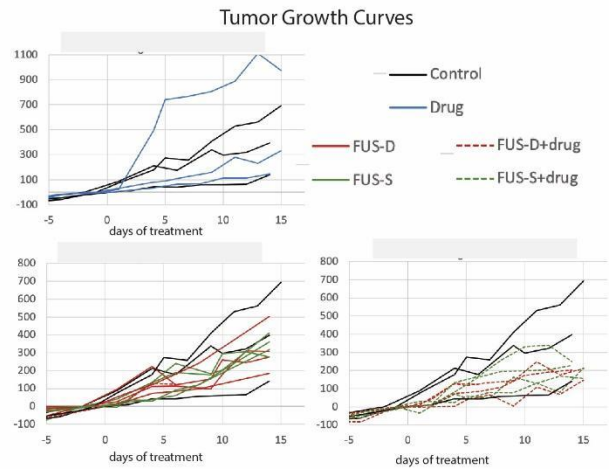


Figure 2. Growth curves calculated as the percent change in tumor volume (as measured by calipers) since Day 0.

A3-11

Assessing Microbubble Mediated Microvascular Disruption Therapy with Two-photon Microscopy and Cavitation Monitoring

Presenter: Xiaoxiao Zhao

Authors in order: Xiaoxiao Zhao, *University of Toronto*, Carly Pellow, *Sunnybrook Research Institute*, David Goertz, *Sunnybrook Research Institute*

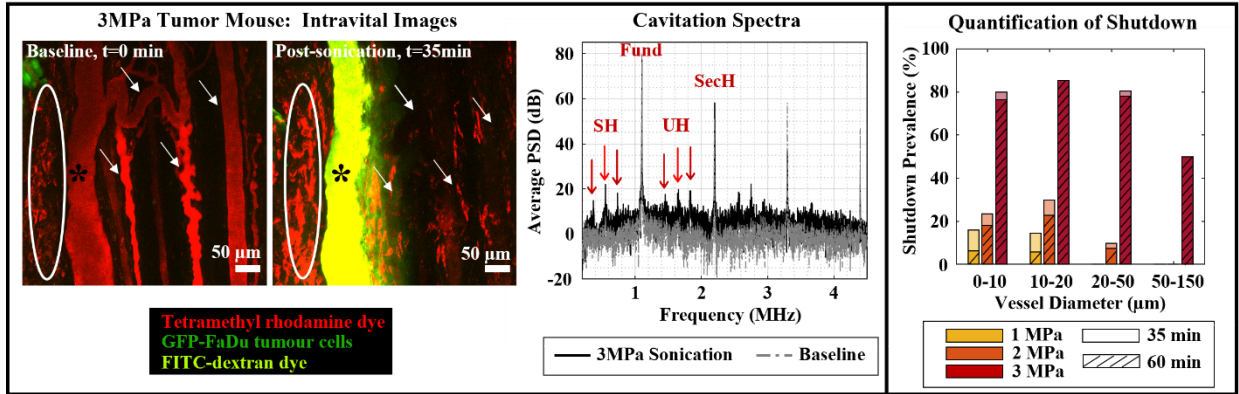
To investigate microbubble mediated microvascular effects at pressure levels associated with mechanical ablation (or vascular disruption therapy -VDT) using real-time multiphoton microscopy and cavitation monitoring.

Ultrasound transmitters and receivers were integrated into a murine dorsal window chamber for simultaneous acoustic monitoring and intravital microscopy. Upon ~1MHz ultrasound exposure (1-3 MPa) of injected microbubbles (MBs), vascular events were monitored with various fluorescent dextrans, and cavitation signatures were linked to biological effects. Vessel type (tumour-affected and healthy), calibre, permeabilization and viability were assessed.

Vascular events (spasms, calibre changes, occlusions, blood flow changes, and permeabilization) were found to occur with increasing incidence with higher pressure, being more pronounced in smaller vessels. Vascular disruptions resulting in focal and diffuse leakage frequently followed spasm and diameter changes, and often preceded occlusion formation, blood flow directionality reversals and shutdown. Vascular shutdown was found to preferentially occur in tumour-affected vessels at higher pressures, with vessel recovery tending to occur at lower pressures and in healthy tissue. Cavitation monitoring indicated broadband emissions, with distinct sub- and ultra-harmonics (1/2, 1/3, 2/3 intervals) appearing with increasing pressure and vascular event incidence.

Despite the recent emergence of VDT into clinical trials, biological effects and associated bubble-vessel interactions at the microvascular scale under VDT exposures remain relatively unexplored. These insights contribute to an improved mechanistic understanding at the microscale of VDT, with implications of establishing an effective VDT-specific treatment protocol and control platform.

S. Bulner, V. Chan, S. Rideout-Gros, M. A. Santos, M. A. O'Reilly, A. Wright, & A. Dorr. Ontario Research Fund, Canadian Institutes for Health Research.



Endobronchial Ultrasound for Lung Cancer Anti-vascular Therapy

Presenter: Yu-Jack Shen

Authors in order: Yu-Jack Shen, *University of Toronto, Yamato Motooka, Division of Thoracic Surgery, Toronto General Hospital, University Health Network, Ontario, Canada*, Alexander Gregor, *Toronto General Hospital, University Health Network, Ontario, Canada*, Yun Xiang, *University of Toronto*, Nicholas Bernards, *Toronto General Hospital, University Health Network*, Sean McGrath, *University of Toronto*, Masato Aragaki, *Toronto General Hospital, University Health Network*, Kazuhiro Yasufuku, *Toronto General Hospital, University Health Network*, Naomi Matsuura, *University of Toronto*

This study investigates the use of nanodroplets (NDs) and microbubbles (MBs) with endobronchial ultrasound (EBUS) for local, anti-vascular therapy of lung tumors in vivo.

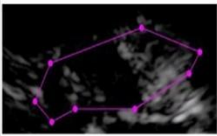
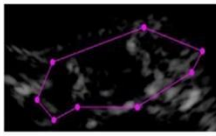
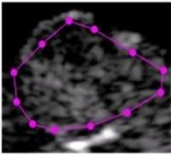
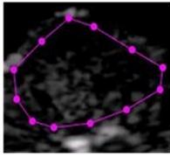
The stability of phospholipid-stabilized, decafluorobutane NDs/MBs was evaluated using a Coulter counter (2×10^6 particles/mL in Isoton, 37°C), for evaluating the treatment window. Vaporization and/or cavitation of NDs/MBs were assessed using a clinical EBUS system (EU-ME2 PREMIER with BF-UC180F bronchoscope, 5MHz, MI=1.2, Olympus, Japan). In vivo antivascular therapy was assessed by measuring the difference in peak signal intensity (PSI) in mouse tumors under contrast ultrasound imaging, before and after the EBUS treatment with NDs/MBs.

NDs were more stable than MBs in 37°C Isoton. A concentration decay to 50% took >5 hrs for NDs (modal diameter: $0.391 \pm 0.049 \mu\text{m}$) and approximately 35min for MBs (modal diameter: $2.17 \pm 0.31 \mu\text{m}$). ND vaporization area (41mm^2) was smaller than MB cavitation area ($>135 \text{mm}^2$). In vivo, both ND and MB treatments with high MI EBUS resulted in a reduction in PSI, with MBs inducing 25% decay in PSI, and NDs inducing 73% decay in PSI.

The NDs had a higher stability and a smaller activation area with EBUS, resulting in an improved treatment window and a more localized treatment ability. Both NDs and MBs reduced the MB contrast signal after exposure to high MI EBUS in vivo. Future work involves verifying the anti-vascular effect histologically.

We appreciate the support of Dr. Brandon Helfield, Mr. Ross Williams, Dr. Marc de Perrot, and Olympus America along with fundings from EMHSeed and NSERC-CRSNG.

a)

Therapy	Before treatment	After treatment
EBUS-MB		
EBUS-ND		

b)

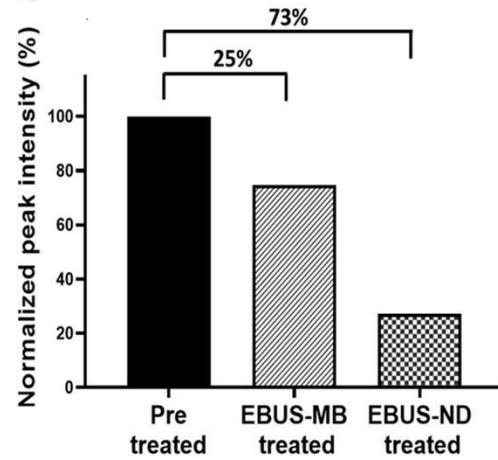


Figure 1: a) Tumor cross sections at peak signal intensity under EBUS contrast mode of C57BL/6 mice, subcutaneously injected with AE 17 OVA mesothelioma. The tumor margin (pink) was drawn based on B-mode images (data not shown). The tumor was treated with microbubbles (MB) and nanodroplets (ND) in combination with endobronchial ultrasound (EBUS) for 6 (for EBUS-MB) and 40 (for EBUS-ND) burst-rest cycles (Burst: MI = 1.2, 5MHz, Rest: MI = 0.06, 3 MHz). The tumors showed reduced peak signal intensity after the treatments were performed. b) Quantification of peak signal reduction in the tumor margin showed a 25% signal reduction post-EBUS-MB treatment and a 73% signal reduction post-EBUS-ND treatment. This is hypothesized to be caused by vascular disruption due to EBUS-MB and EBUS-ND treatment.

Enhancement of 5-ALA Mediated Sonodynamic Therapeutic Effect by MEK Inhibition

Presenter: Kuochen Wei

Authors in order: Chiungyin Huang, *Chang Gung Memorial Hospital*, Chia-Jung Lin, *NaviFUS Corporation*, Hao-Li Liu, *National Taiwan University*, Kuochen Wei, *New Taipei Municipal TuCheng Hospital*

This study aimed to evaluate the effect of MEK inhibitor on accumulation of protoporphyrin IX (PpIX) in 5-aminolevulinic acid (5-ALA) treated animals and sonodynamic therapy.

MEK inhibitor trametinib were systemically administered to animals bearing subcutaneous tumor xenograft 24 hours prior to treatment. Subsequently, the effects of 5-ALA-mediated sonodynamic therapy were determined by measuring the volume of tumor xenografts and the bodyweights animals. Glioma cells and tissue samples were collected, and the effect on MEK signaling pathway were evaluated by immunohistochemistry/PCR/Western blotting. For tumor growth data, comparison across multiple groups was performed with repeated measures two-way analysis of variance (ANOVA).

Animals were divided into 5 groups: control, focused ultrasound (0.35 MPa.duty10%.10min), trametinib (1mg/kg), 5ALA (180mg/Kg) +FUS, trametinib(1mg/Kg)+5ALA(180mg/Kg) +FUS (n=5 for each group). Following treatment, tumor growth was monitored by digital caliper twice a week. As compared with control group, the tumor size of trametinib+5ALA+FUS group is significantly less than control group (p=0.0085, 0.0001 and 0.0255 at day 4, 7 and 11). No significant difference was observed in other groups verse control. The daily mice body weight records revealed no significant change, demonstrated no major toxicity was induced by the MEK inhibitor/5-ALA/sonodynamic combination treatment.

Our study demonstrates that suppression of MEK pathway by MEK inhibitor trametinib significantly increase the accumulation of PpIX. In tumor animal models, mice pretreated with MEK inhibitor presented favorable response to 5-ALA mediated sonodynamic therapy. Our finding may suggest a new strategy to enhance the effect of sonodynamic therapy.

This work is supported by National Health Research Insitiute NHRI-EX111-10502NI and Chang Gung Memoral Hospital.

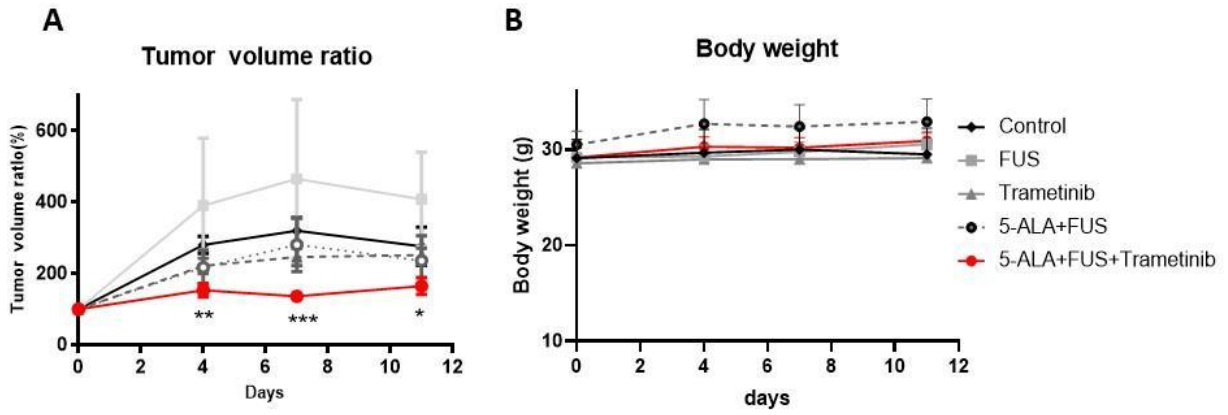


Figure 1: (A) The tumor progression (tumor volume ratio compared with initial tumor volume) and (B) the body weight of mice received sonodynamic therapy.
 * $p < 0.05$, ** $p < 0.05$, *** $p < 0.001$.

Low Frequency Nanobubbles-enhanced Ultrasound Mechanotherapy

Presenter: Mike Bismuth

Authors in order: Mike Bismuth, *Tel Aviv university*, Tali Ilovitsh

Develop a theranostic platform for safe, noninvasive and low energy tumor mechanotherapy, using a combination of nanoscale nanobubbles and 80 kHz low frequency ultrasound

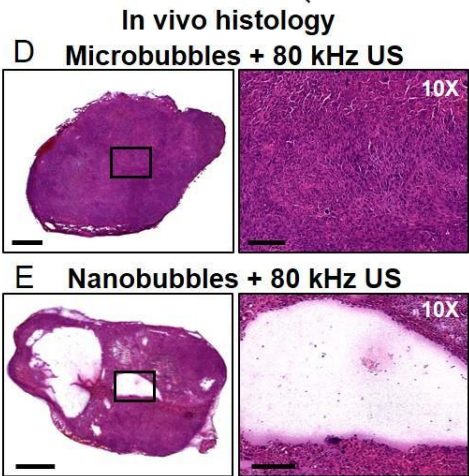
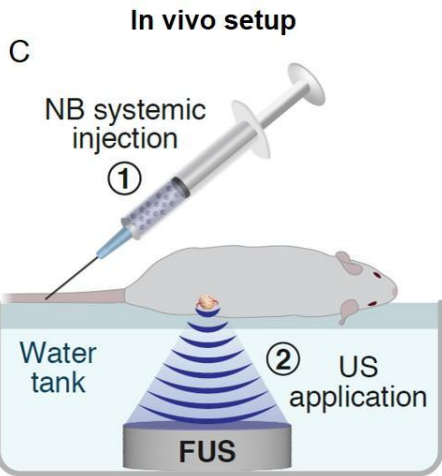
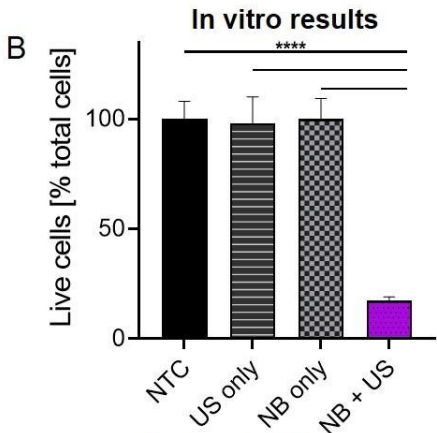
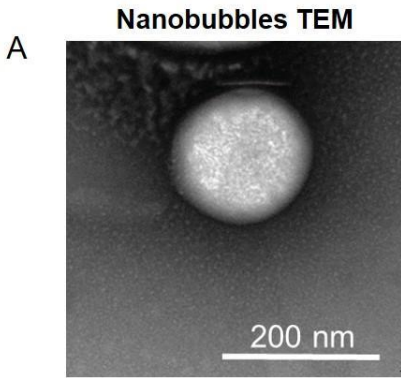
A dual imaging-therapy setup was used to evaluate the nanobubbles acoustical response, while comparing it to microbubbles. In vitro nanobubble-mediated 80kHz low frequency insonation of breast cancer cells was then optimized. In vivo, systemically injected nanobubbles were coupled with 80kHz insonation in a breast cancer mice model. Nanobubbles distribution and tumor accumulation was initially assessed, followed by 80kHz tumor insonation at a mechanical index of 1.3. Histological analysis was performed to evaluate resulting bioeffects.

Complete nanobubbles destruction was achieved at a mechanical index of 2.6 for the 250 kHz insonation, as opposed to 1.2 for the 80 kHz frequency. Thus, the 80 kHz insonation comply with the safety regulations that require operation below a mechanical index of 1.9. In vitro in breast cancer tumor cells, 80 kHz insonation of nanobubbles reduced cell viability to $17.3 \pm 1.7\%$ of live cells, compared to control groups. In vivo, in a breast cancer tumor mice model, the proposed method resulted in effective noninvasive mechanical tumor ablation and tumor tissue debulking, as observed via histology.

Our findings confirm that coupled with 80 kHz ultrasound insonation, nanobubbles can serve as low energy cavitation nuclei for histotripsy, while reducing the energy required for standard ultrasound surgery by over an order of magnitude. nanobubble-mediated ultrasound mechanotherapy was shown to yield effective low energy ultrasound surgery of solid tumors.

This work was supported by the Israel Science Foundation and the Israel Ministry of Science & Technology.

Nanobubble-mediated low frequency mechanotherapy experimental results



Novel Metal–Organic Framework (MOF)-Based Ultrasound-Responsive Sonosensitizer for Bladder Cancer Therapy

Presenter: Zheng Zhu

Authors in order: Zheng Zhu, *Harvard Medical School*, Kaiyuan Ni, *Massachusetts Institute of Technology*, Veera Chandra Sekhar Reddy Chittepu, *Harvard Medical School*, Hizra Farrukh, *Harvard Medical School*, Chun Yang, *Harvard Medical School*, Chong-xian Pan, *Harvard Medical School*

To investigate ethylenediaminetetraacetic acid (EDTA) loaded metal-organic framework (MOF) nanoparticles as novel sonosensitizers (SS) to augment sonodynamic therapy (SDT) in bladder cancer.

A generic SS porphyrin with low solubility is integrated into MOF to increase dispersity and quantum yield of ROS. MOF and SDT conditions on mouse bladder cancer cell line UPPL1541 were tested in vitro. Cytotoxicity and ROS production were quantified for evaluation of SDT efficacy. C57BL/6 mice bearing UPPL1541 subcutaneous tumors were divided into 4 groups receiving PBS, PBS+SDT, MOF, MOF+SDT to test MOF-mediated SDT efficacy in vivo. Mice were monitored for tumor growth and overall survival.

The optimal working concentration for MOF in vitro is 20 μM . HIFU at 3.3mHz, 1W/cm² for 1min had no detectable effects on cells but could activate MOF and generate ROS. In MOF+SDT group, tumor growth was prohibited by SDT 12h and 24h post-MOF intratumor injection. Diagnostic ultrasound showed that the tumor became liquidation on day 3 and shrank during the following week. On day 20, the liquidated tumors in the MOF-SDT group were completely eradicated. By contrast, the tumor growth was not inhibited in all other three groups.

We showed a proof of concept in augmenting SDT with EDTA-loaded MOF in bladder cancer treatment. After activated by HIFU, abundant ROS was produced via MOF-mediated SDT to induce apoptosis and eradicate tumors. Taken together, EDTA-loaded MOF plus SDT might be an alternative for bladder cancer treatment.

Ultrasound-mediated Drug Free Theranostics for Treatment of Prostate Cancer

Presenter: Reshani Perera

Authors in order: Reshani Perera, *Case Western Reserve University*, Eric Abenojar, *Case Western Reserve University*, Youjoung Kim, *Case Western Reserve University*, James Basilion, *Case Western Reserve University*, Agata Exner, *Case Western Reserve University*

This work examines the potential of drug-free targeted nanobubbles (NB) combined with unfocused therapeutic ultrasound (TUS) as a theranostic treatment for prostate cancer (PCa).

Lipid shelled C3F8 NB targeted to the prostate-specific membrane antigen (PSMA-NB), were formulated as described¹. Cellular PSMA-NB internalization was evaluated by confocal imaging before and after TUS application (3MHz, 2.2 W/cm², 10DC, 10min). Mice with dual flank tumors (PSMA+ and -) received PSMA-NB via tail vein injection followed by TUS 1h after injection. Control animals received either PSMA-NB or TUS alone. 24h post-treatment mice were euthanized and tumors were extracted. Apoptosis was assessed via TUNEL staining.

As demonstrated in Figure 1, confocal image analysis showed higher levels of cellular internalization and co-localization with late endosome/ lysosomes of PSMA-NBs with PSMA (+) PC3pip cells. Internalized bubbles and cellular compartments were disrupted after TUS application, indicating endosomal escape resulting from NB cavitation. PSMA-expressing tumors treated with PSMA-NB+TUS demonstrated a significantly greater extent of apoptosis (77.5 ± 17.9 %) compared to all other groups. Tumors treated with either PSMA-NBs or TUS alone showed negligible apoptosis. Survival studies to evaluate the therapeutic efficacy of this approach are ongoing and demonstrate promising early results.

These results support the potential for targeted NBs to be used as effective, highly-specific theranostic agents, even in the absence of a therapeutic agent and without the need for focused US. The approach has the potential to focus the therapy at the target site only without off-target systemic effects.

This work was funded by the NIH (R01EB028144), 1S10OD021635-01, the CWRU Coulter Translational Research Partnership, CCCC P30CA043703 pilot grant, and the NFCR.

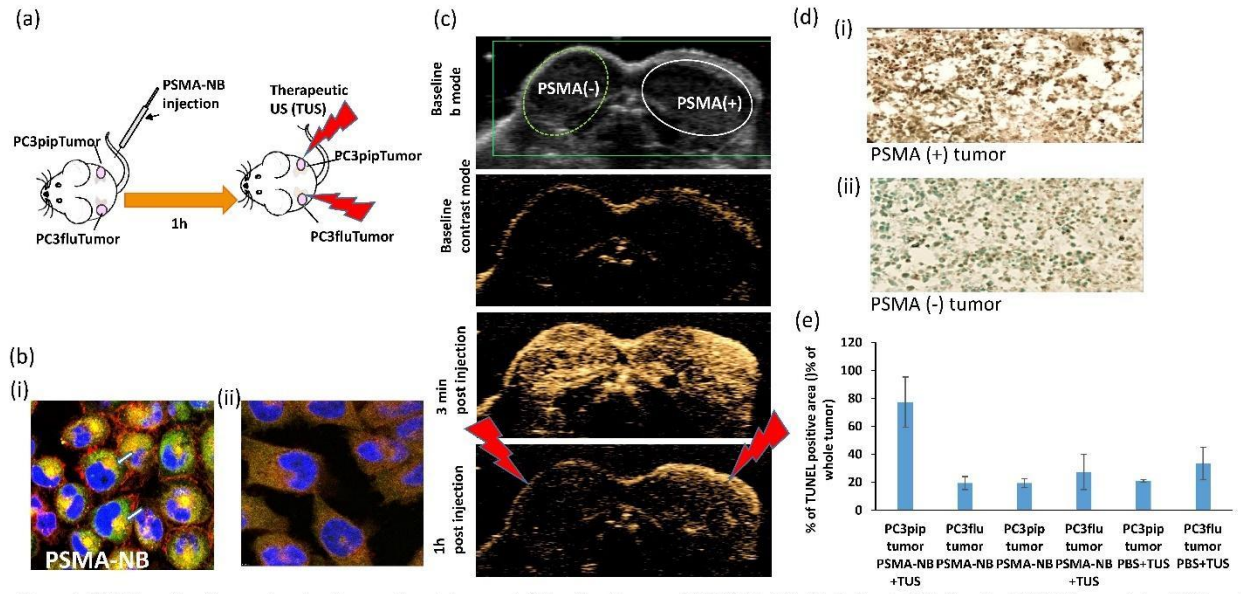


Figure 1. (a) Schematic diagram showing the experimental approach (b) confocal images of (i) PSMA-NB distribution in PC3pip cells; 100X (blue-nuclei, red-NB, and green-late endosome/ lysosomes) (ii) After treatment of TUS for PSMA-NB internalized PC3pip cells (c) US images of PSMA-NB in PSMA(+) and PSMA(-) tumor showing higher retention in PSMA(+) tumor (d) TUNEL stained images of (i) PSMA-NB + TUS treated PC3pip (more brown color, indicating more apoptosis cells) (ii) PSMA-NB + TUS treated PC3flu (more green color, indicating more healthy cells) (e) The % of TUNEL positive area compared to whole tumor area. ¹ Perera, R et al, Nanomedicine, 28 (2020) 102213.

Novel MRI-Guided Focused Ultrasound-Stimulated Microbubble Radiation Enhancement Treatment for Breast Cancer

Presenter: Gregory Czarnota

Authors in order: Murtuza Saifuddin, *Sunnybrook Research Institute*, Archya Dasgupta, *Tata Memorial Centre*, Colleen Bailey, *Sunnybrook Research Institute*, Benjamin Geraghty, *Sunnybrook Health Sciences Centre*, Lin Lu, Gregory Czarnota, *Sunnybrook Research Institute*

This study assessed the efficacy of tumour vasculature perturbation with FUS+MB therapy for radiation therapy (RT) efficacy enhancement.

Nine breast/chest-wall cancer patients were enrolled into a phase 1 study, including one with bilateral disease. All patients were treated with fractionated RT (5 or 10 fractions), with FUS+MB treatment delivered before the 1st and 5th fractions of RT (within 1 hour). Treatments used 800 kHz focussed ultrasound with a peak negative pressure of 570 kPa. Microbubbles were injected at a dose of 10-30 $\mu\text{L}/\text{kg}$ for treatment. Treatment was delivered using a Philips 3T MRI and Profound Medical Sonalleve System.

Seven patients with eight tumours completed three months of follow-up (1 patient had no follow-up, and one succumbed to metastatic disease at three months). All the treatment sessions were well tolerated without any local or systemic complications related to FUS+MB treatment. The maximum grade of acute toxicity was grade-2 radiation dermatitis in one participant at one month. No RT-related late effects were noted. All seven evaluable patients with at least three months follow up treated for eight tumours had a complete response with the absence of contrast-enhancing and clinically palpable disease (three tumours had replacement fibrosis).

This study demonstrated the safety of combined FUS+MB and RT treatment. Promising response rates suggest a strong radioenhancing effect of the investigational modality. The work introduces a new frontier in radiation oncology practice to be explored further for other disease sites and phase 2/3 clinical trials.

This study was funded by Terry Fox Foundation.

A3-4

Partial Thermal Ablation of Melanoma Augments Intratumoral IL-1b Expression, Implicating Pyroptosis as Pro-tumorigenic

Presenter: Richard Price

Authors in order: Eric Thim, *University Of Virginia*, Lydia Petricca, *University of Virginia*, Alexander Mathew, Timothy Bullock, Richard Price, *University of Virginia*,

Investigate IL-1b upregulation in partial thermally ablated (TA) B16 melanoma tumors and determine efficacy of blocking NLRP3, an upstream regulator of IL-1b

C57/Bl6J mice were subcutaneously inoculated with 5×10^4 or 2×10^5 B16F10 cells in the right flank and TA ($f_0 = 3.28$ MHz, PNP = -12 MPa, 10 seconds/treatment point, 2 mm spacing between treatment points) was applied 13 days post inoculation. Post-treatment tumor harvests were performed for RNA sequencing and flow cytometry at 8, 24, 72 and 168 hrs and 24 hrs, respectively. MCC950, an NLRP3 inhibitor, was delivered 1 hr prior to thermal ablation.

TA transiently controlled primary B16F10 melanoma tumor growth (Figure 1A). Bulk RNA sequencing revealed upregulation of IL-1b and NLRP3 transcripts 8 hrs post TA but returns to baseline after 24 hrs (Figure 1B). Pro-IL-1b protein level on a per cell basis increased in the CD45+ cell compartment 24 hrs post TA (Figure 1C), with a striking pro-IL-1b expression redistribution to a predominantly granulocytic myeloid cell population (Figure 1D). Systemically inhibiting NLRP3 (upstream upstream regulator of IL-1b) in combination with TA increased tumor growth control beyond either monotherapy (Figure 1E).

TA shifts IL-1b expression levels and cell sources in the tumor microenvironment. By inhibiting NLRP3 in combination with TA to increase growth control, we have implicated pyroptosis as a pro-tumorigenic mechanism through the NLRP3-IL-1b pathway.

Supported by NIH R01EB030007 to RJP and TNJB

Focused Ultrasound Immunomodulation on the Myeloid Compartment of the Brain in Treating GBM and Alzheimer's Disease

Presenter: Tao Sun

Authors in order: Tao Sun, *Brigham and Women's Hospital, Harvard Medical School*, Nathan McDannold, *Brigham and Women's Hospital, Harvard Medical School*

Focused ultrasound (FUS) effects on the myeloid compartment of the brain are not clear, including the trafficking and functional changes of monocytes/macrophages and resident microglia.

Here, we investigate how FUS modulates the myeloid compartment in murine models of GBM (GL261 and 005) and AD (APP/PS1dE9) in tests with or without passive immunotherapy. In the GBM models, FUS effects were compared with or without anti-PD1 treatment. FUS (690 kHz, 320 kPa, 10-ms pulses at 4-Hz) was applied on Day 14 and Day 20 after the tumor inoculation. In the AD model, we pair FUS with an anti-pGlu3 A β antibody therapy.

In the GBM models, our results demonstrated that FUS enhanced antigen presentation behaviors of tumor-associated macrophages without affecting the microglia. FUS also reprogrammed the macrophages locally towards the anti-cancer phenotype (CD86+CD206-). FUS-anti-PD1 (n = 8) provided significantly increased survival benefits compared to anti-PD1 monotherapy (n = 7, P < 0.05) and the control group (n = 6, P < 0.001). In the AD model, plaque-associated Ly6G+ phagocytes were only present in FUS-treated areas, while microglia activation was found in both antibody-treated groups. Overall, these effects resulted in greater plaque removal, sparing of synapses and improved cognitive function.

Our results offer new evidence in FUS immunomodulation on the myeloid compartment of the brain in GBM and AD-like mouse models. We discover new mechanisms that low-intensity pulsed FUS recruits and activate peripheral monocyte derived macrophages, instead of direct activation of resident microglia.

We thank the funding supports from FUS Foundation, NIH (NIBIB, NCI, and NIA), and Harvard School of Engineering.

FUS-aided ImmunoPET for Quantitative Imaging of PD-L1 Expression in Glioblastoma

Presenter: Céline Chevaleyre

Authors in order: Céline Chevaleyre, *Paris-Saclay University, CEA, CNRS, Inserm*, Anthony Novell, *BioMaps, Université Paris Saclay, CEA, CNRS, Inserm*, Hervé Nozach, *Paris-Saclay University, CEA, INRAE*, Steven Dubois, *Paris-Saclay University, CEA, INRAE*, Dimitri Kereselidze, *Paris-Saclay University, CEA, CNRS, Inserm*, Erwan Selingue, *CEA Saclay*, Bernard Maillère, *Paris-Saclay University, CEA, INRAE*, Nicolas Tournier, *Paris-Saclay University, CEA, CNRS, Inserm*, Benoit Larrat, *CEA*, Charles Truillet, *CEA Saclay*

Evaluate the combination of immunoPET using low FcRn affinity ^{89}Zr -IgG with focused ultrasounds (FUS)-aided brain delivery to estimate programmed-death-ligand 1 (PD-L1) expression in brain tumors.

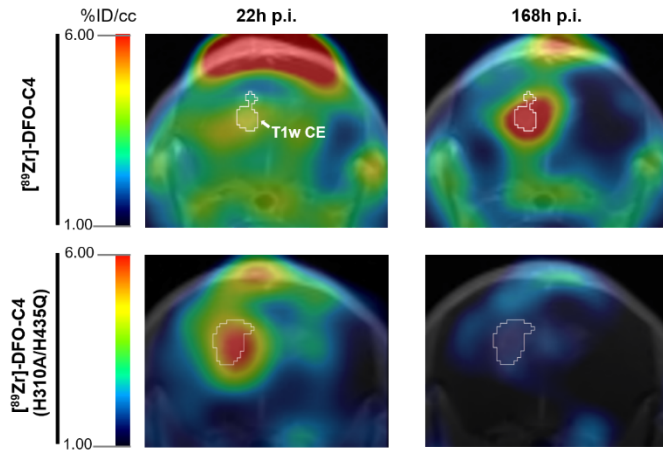
A transcranial FUS protocol (raster scan) was applied shortly before injecting the anti-PD-L1 IgG [^{89}Zr]-DFO-C4 or its low FcRn affinity mutant [^{89}Zr]-DFO-C4(H310A/H435Q) in a syngeneic glioblastoma murine model (GL261). FUS were transmitted at 1.5 MHz (duty cycle: 69%, peak negative pressure: 420kPa, total exposure: 127s) after microbubbles injection (SonoVue®, 50 μL). Brain uptake was measured from PET scans acquired up to 7 days post-injection. Kinetic modeling was performed to compare the brain kinetics of tested IgGs.

Kinetic modeling revealed that the FUS protocol allowed a substantial and comparable entry of both IgGs at a rate of 0.163 ± 0.071 mL/h/g of tissue during 10.4 ± 4.6 min. 1h post-injection, brain uptake of [^{89}Zr]-DFO-C4(H310A/H435Q) reached $3.75 \pm 0.41\%$ ID/cc with FUS versus $1.92 \pm 0.45\%$ ID/cc without FUS. The impaired interaction with FcRn of [^{89}Zr]-DFO-C4(H310A/H435Q) significantly decreased the efflux constant from the healthy brain tissue to plasma (0.015 ± 0.027 h $^{-1}$) compared with [^{89}Zr]-DFO-C4 (0.300 ± 0.218 h $^{-1}$). Due to its fast blood clearance, the highest PET contrast in the tumor was observed at 22h post-injection for [^{89}Zr]-DFO-C4(H310A/H435Q), versus 7 days post-injection for the [^{89}Zr]-DFO-C4.

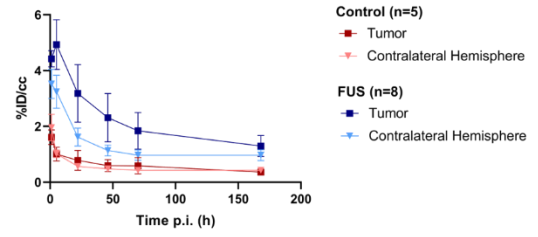
FUS enable sufficient brain delivery of C4 radioligands and therefore provide a robust tool for PD-L1 imaging to predict and monitor response to immunotherapies. Engineered [^{89}Zr]-DFO-C4(H310A/H435Q) moreover offers additional favorable properties compared with [^{89}Zr]-DFO-C4, which enhanced tumor contrast and improved estimation of PD-L1 expression in glioblastoma tumors using immunoPET.

We thank the financial support from the ANR-IM2FUS (grant ANR-20-CE18-0010).

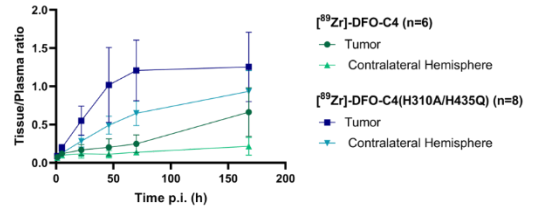
A Representative brain PET- T₁w MRI images of tumor bearing mice.



B $[^{89}\text{Zr}]\text{-DFO-C4(H310A/H435Q)}$ concentrations



C Tissue to plasma ratio of the C4 radioligands after FUS



A3-7

Influence of Biling Histotripsy on Melanoma Growth Control and Acquisition of Tumor Antigen in Tumor-Draining Lymph Nodes

Presenter: Richard Price

Authors in order: Eric Thim, *University Of Virginia*, Lydia Petricca, *University of Virginia*, Fatima Rivera-Escalera, Michael Elliott, Timothy Bullock, Richard Price, *University of Virginia*

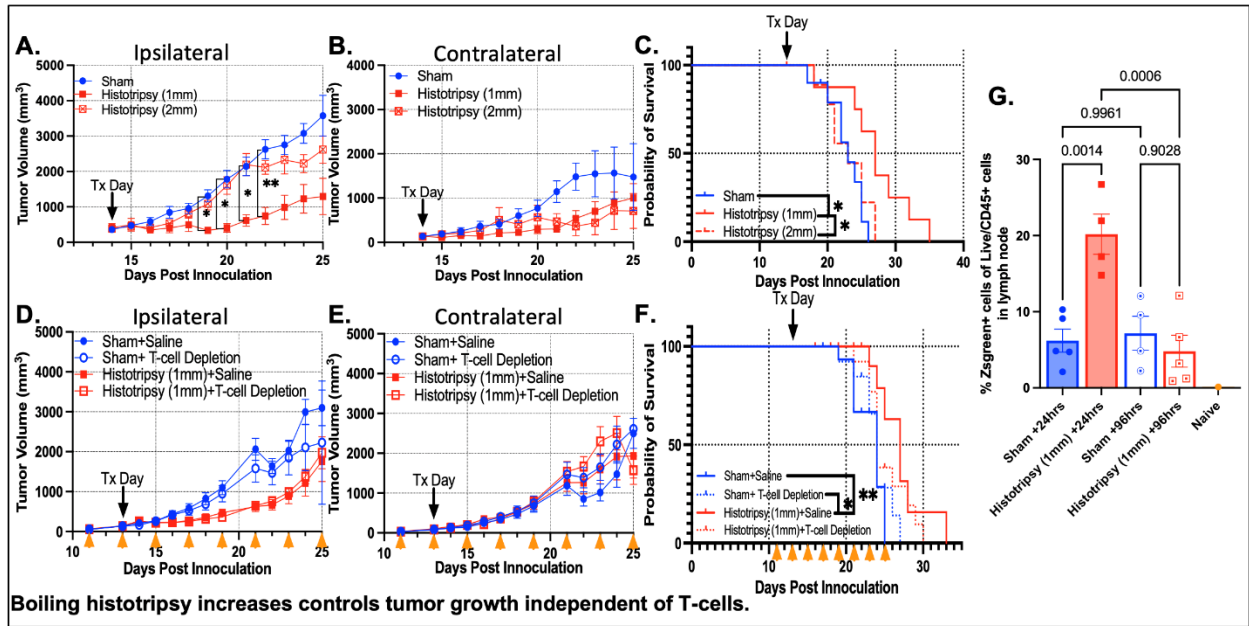
Investigate boiling histotripsy (BH) induced control of tumor growth, survival, and immune response.

C57/Bl6J mice (8-10 wk old) were subcutaneously and bilaterally inoculated with 2×10^5 B16F10 cells or unilaterally inoculated with 4×10^5 B16F1-Zsgreen cells in the flank. BH ($f_0 = 3.28$ MHz, PNP=-21 MPa, 10 seconds/treatment point, 3 ms pulse, PRF=4 Hz, 1/2 mm spacing between treatment points) was applied 13 days post inoculation to primary tumors. CD4 coreceptor blockade and CD8 T-cell depletion were from day 11 to 25. Lymph nodes were harvested 24 and 96 hrs post BH.

BH transiently controlled ipsilateral B16F10 melanoma (Figure 1A) and improved survival (Figure 1C), but contralateral tumor was not controlled (Figure 1B). Ipsilateral tumor growth control was spacing-dependent, as 2 mm spacing did not provide growth control. Growth control elicited by 1 mm spaced BH was not CD8 T-cell and CD4 coreceptor dependent (Figure 1D, "T-cell Depletion" group encompasses both). Zsgreen antigen acquisition in the CD45+ compartment was significantly increased in draining lymph nodes at 24 hrs, but not 96 hrs, post-BH treatment.

BH controls primary melanoma tumor growth. However, in this context, growth control is T-cell independent. Nonetheless, BH does enhance tumor antigen acquisition in the draining lymph node and leads us to hypothesize that antigen presentation and/or T-cell activation could be manipulated to produce systemic adaptive immune mediated tumor control.

Supported by NIH R01EB030007 to RJP and TNJB



Boiling histotripsy increases controls tumor growth independent of T-cells.

Effects of Fluorescein-mediated Sonodynamic Treatment on the Glioma Microenvironment and Immune Landscape

Presenter: Nicoletta Corradino

Authors in order: Nicoletta Corradino, *IRCCS C. Besta Institute, University of Milan*, Matteo Gionso, *IRCCS Istituto Carlo Besta*, Edoardo Porto, *Fondazione IRCCS Istituto Neurologico Carlo Besta - University of Milan*, Luca Raspagliesi, *IRCCS Istituto Carlo Besta, Humanitas University*, Serena Pellegatta, *IRCCS Istituto Carlo Besta*, Francesco DiMeco, *Fondazione IRCCS Istituto Neurologico Carlo Besta, Acoustic Neuroimaging and Therapy Laboratory, Milan, Italy* - *Fondazione IRCCS Istituto Neurologico Carlo Besta, Neurosurgery Department, Milan, Italy* - *Johns Hopkins Medical School, Department of Neurolog*, Francesco Prada, *IRCCS Istituto Carlo Besta, University of Virginia, Focused Ultrasound Foundation*,

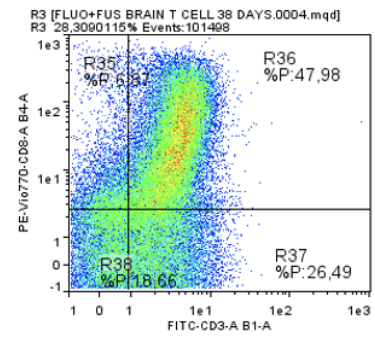
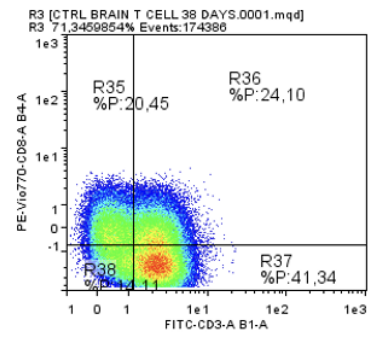
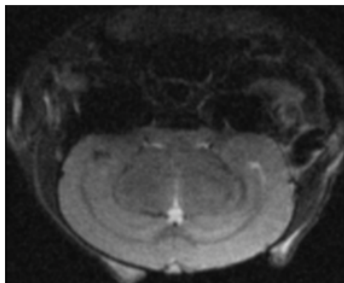
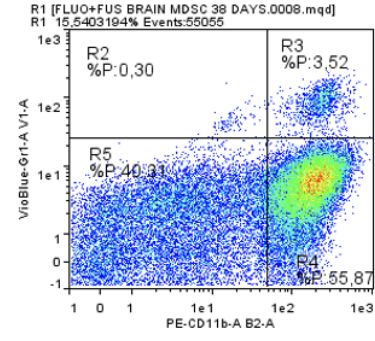
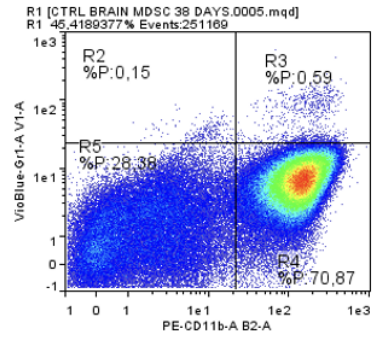
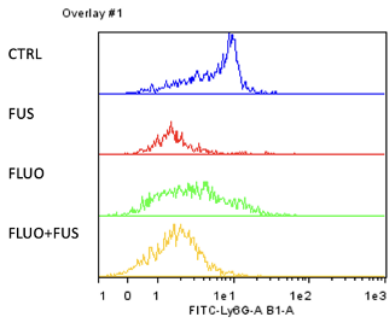
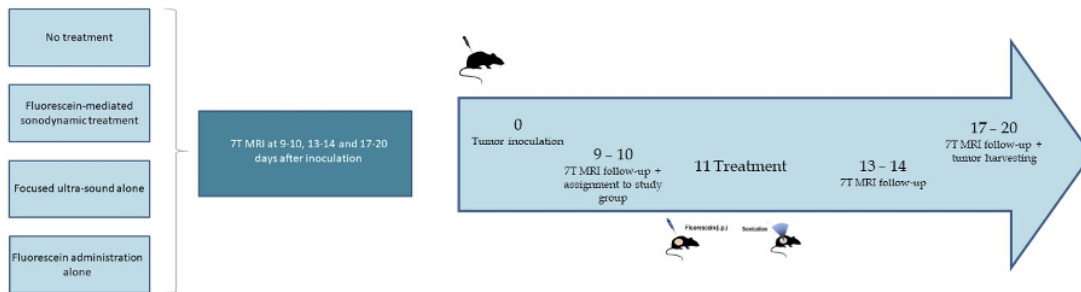
Investigating fluorescein-mediated sonodynamic treatment (FL-SDT) effectiveness and immunological effects in vitro and on an in vivo intracranial mouse model of malignant glioma is our aim.

Both in vitro and in vivo experiments evaluated four conditions: fluorescein; focused ultrasound; FL-SDT, control. In vitro cellular differentiation, antigen response and apoptosis were evaluated on murine glioma cell lines (GL261) through flow-cytometry. In vivo study was conducted on immune competent 6-week-old female C57BL6/N mice that received intracranial injections of GL261 murine glioma cells. In vivo lymphocyte recruitment, microglial activation, MDSCs infiltration were evaluated through flow-cytometry. Afterwards, macroscopical glioma growth was assessed through 7T MRIs.

In vitro study showed that FUS exposure condition induced an immunogenic form of tumor cell death and a relevant increase of immunogenicity by the upregulation of MHC class I, CD80 and CD86 expression. Brain tumor samples from C57BL6/N mice showed increasing CD8+ infiltration and MDSCs reduction in FL-SDT treatment group. In the same group, 7T MRIs showed macroscopical delay or inhibition of tumor growth.

FL-SDT in vitro showed an influence on GL261 immunogenicity and immune activation. In vivo analysis confirmed its influence on tumor microenvironment, also on the immunosuppressive component, consequently FL-SDT could be combined with immunotherapy. Fluorescein is applicable to different types of brain tumors, and it is already used in fluorescence-guided surgery.

The present work was supported by Focused Ultrasound Foundation (Charlottesville, VA), Acoustic NeuroImaging and Therapy Laboratory and Molecular Neuro-oncology Unit of IRCCS Istituto Carlo Besta.



Set-up and SDT impact on tumor microenvironment and immunity

Transcriptomic Effects of Nonablative Focused Ultrasound Treatment on Murine Breast and Melanoma Tumors

Presenter: Scott Burks

Authors in order: Scott Burks, *National Institutes of Health Clinical Center*, Joseph Frank, *NIH*

To investigate varying magnitudes of treatment pulse numbers on the transcriptomic profiles of B16 melanoma and 4T1 breast tumors.

Flanks of C57 BL/6 or BALB/c mice were inoculated with B16 or 4T1 cells, respectively. Tumors (~5mm diameter) were sonicated using 1.15 MHz focused ultrasound. Tumors were treated over their entire volumes with 10 ms pulses, 10 Hz repetition frequency, and 6 MPa peak-negative-pressure. Cohorts were treated for durations of 10, 20, or 50 s per spot. Tumors at 2, 24, and 72 h were harvested and subjected to RNA-seq and compared to time-matched controls.

Global transcriptomic responses diverged significantly between the two tumor types. B16 tumors had substantial responses in pathways relating to innate immune responses and immune cell infiltration. 4T1 cells however, responded major downregulation of basic metabolic pathways (carbohydrate and fatty acid metabolism) and reduction in cell motility pathways. Evaluating different FUS treatment durations within each tumor revealed further changes, where 20 s displayed increased magnitudes of each tumor type's respective transcriptomic changes. However, further increasing treatment time to 50 s in 4T1 did not yield as significant an increase in pathway activation, while 50 s treatments in B16 did.

Nonablative FUS reduces growth of B16 and 4T1 tumors through very different biological mechanisms. However, many treatment parameters in nonablative FUS treatments remain arbitrary and we demonstrate that each changing parameters leads to different biological responses, which in this case are mediated mechanosensitive Ca²⁺ signaling mechanisms.

This work was funded by the Intramural Research Program at the NIH Clinical Center and National Institute of Biomedical Imaging and Bioengineering.

A4-1

Developing Imaging Biomarkers for MR Guided FUS Breast Cancer Treatments

Presenter: Allison Payne

Authors in order: Allison Payne, *University of Utah*, Blake Zimmerman, Sara Johnson, Henrik Odén, *University of Utah*, Sarang Joshi

Increase the potential impact of treating breast cancer with MRgFUS through the development of multiparametric imaging biomarkers that are rigorously registered to volumetric histopathology data.

A comprehensive diffeomorphic registration process has been developed that accurately maps tissue structure between treatment and post treatment MRI images and through all steps of processing to the final histopathology. This pipeline estimates and corrects for deformation at each tissue processing step. These methods have been validated in a VX2 rabbit tumor model and used to train a logistic regressor classifier that utilized non-contrast MRI inputs to predict tissue viability after MRgFUS ablation.

A target registration accuracy of 1.33 ± 0.16 mm was obtained between MR images acquired 3-days post-thermal ablation and MR images acquired during treatment. The landmark-free in vivo MRI-to-histology pipeline achieved <1 mm registration accuracy between the in vivo treatment day MR images and volumetric histology. The non-contrast logistic regressor classifier outperformed cumulative thermal dose as a predictor of treatment outcome (area under curve [AUC] 0.973 vs. 0.875, $n=4$) and was virtually equivalent to the contrast-enhanced MRI derived non-perfused volume prediction (AUC 0.973 vs. 0.986).

This comprehensive registration process will enable development of accurate histology-verified imaging biomarkers to predict treatment outcomes. The promising performance of the presented linear regression classifier demonstrates the potential of success for training supervised classifiers to outperform the predictive powers of current clinically used outcome metrics.

This work was funded by NIH grants R37 CA224141, R01 CA172787 and R03 EB026132.

A4-10

Intraoperative HIFU Treatment at the Hepatic Confluence Preclinical Study

Presenter: Sophie CAMBRONERO

Authors in order: Sophie CAMBRONERO, *LabTAU, INSERM, Centre Léon Bérard, Université Lyon 1, Univ Lyon, F-69003, Lyon, France*, Aurélien DUPRE, Charles MASTIER, David Melodelima, *INSERM*

This preclinical study evaluated, in a porcine model, the feasibility and tolerance of an intraoperative HIFU treatment at the hepato-caval confluence using a toroidal transducer.

The toroidal HIFU transducer operated at 2.5MHz. Its diameter and radius of curvature were both equal to 70mm.

Eleven animals were treated and followed over 7 (P1-9) and 19 (P10-11) days after the HIFU procedure. Ultrasound Doppler images were recorded percutaneously and intraoperatively before and after treatment at day 0 and at day 7 or day 19. 3T MRI images were acquired ex vivo at D7 (P6-9) and in vivo at D15 (P10-11).

HIFU exposures lasted 370s using an applied acoustic power ranging from 80 W to 115 W. HIFU ablations were created at the hepato-caval confluence around the targeted blood vessel and were on average 27.8 ± 4.9 mm large by 42.0 ± 8.6 mm long. The average targeted vessels diameter was 9.1 ± 1.4 mm. HIFU ablations extended to the vessel wall while maintaining normal blood flow at day 7 and day 19 as confirmed by Doppler images. 3T MRI and histological analysis confirmed normal blood flow and no thrombosis.

Tumors located at the hepato-caval confluence are a frequent contra indication for surgery. This preclinical study showed that an intraoperative HIFU treatment of the liver at the hepato-caval confluence is safe and feasible using a toroidal transducer. This treatment modality could represent an alternative for patients not eligible to surgery.

This work was partly funded by the French National Research Agency (ANR-19-CE19-0027-01) and by the FUS Foundation (N° RC17129CC).

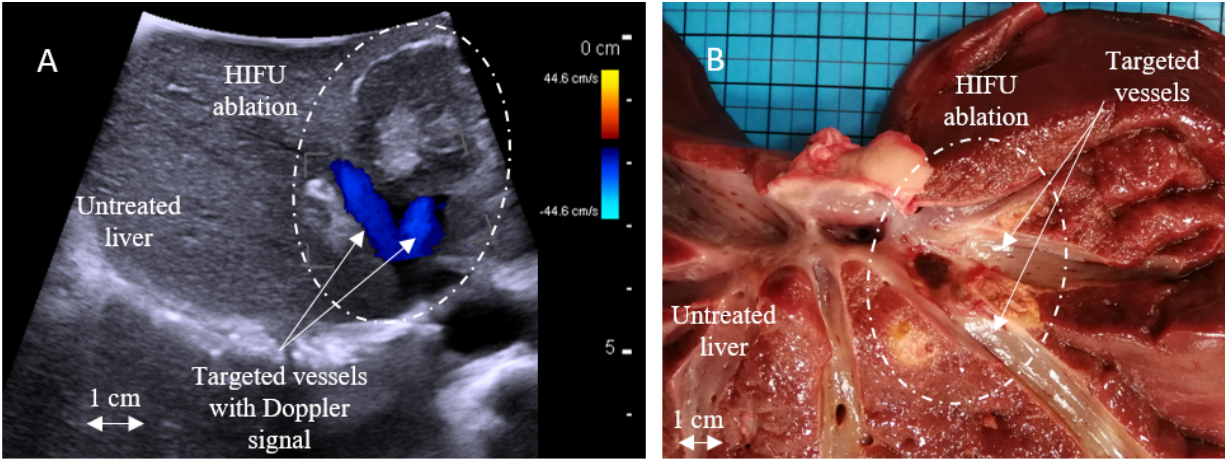


Fig. 1. HIFU ablation at the hepato-caval confluence 7 days after treatment.

Observation of Cavitation Bubbles Generated in Sliced Tissue Phantom for Cavitation-enhanced Heating using High Speed Camera

Presenter: Shin Yoshizawa

Authors in order: Shin Yoshizawa, *Tohoku Univeristy*, Sota Kannoto, *Tohoku Univeristy*

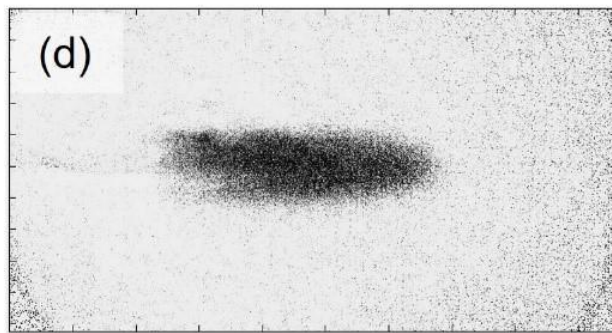
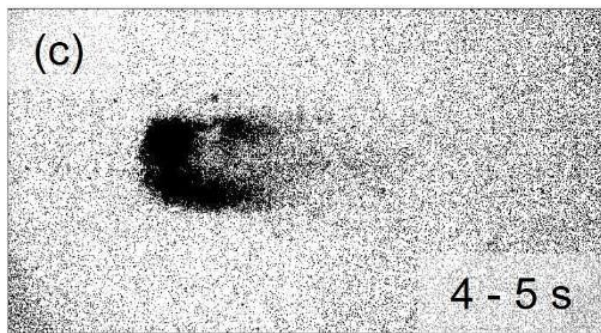
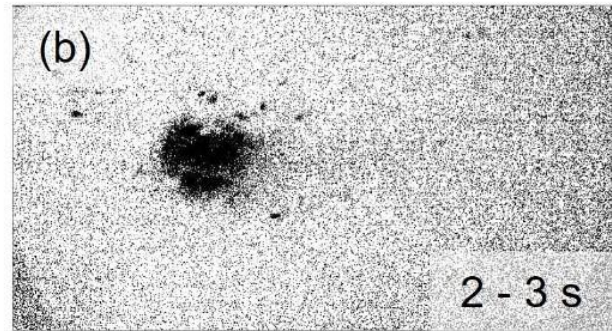
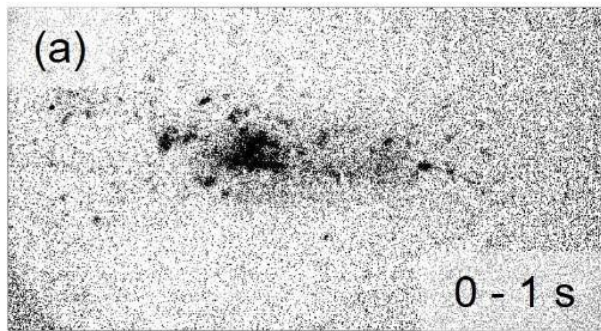
The objective of this study is to experimentally investigate the distribution of cavitation bubbles in a tissue during cavitation-enhanced HIFU heating.

As a HIFU target, a 2 mm slice of chicken breast tissue was embedded in a agarose gel to ensure light penetration. The target was exposed to 1-MHz focused ultrasound generated with a 128-ch array transducer. The sequence consisting of a high intensity pulse at 100 kW/cm² for 0.025 ms followed by continuous waves at 3.5 kW/cm² for 44 ms was repeated for 5 s. During the HIFU exposure, cavitation bubbles were observed by backlight.

Figures (a) – (c) show cavitation bubble images obtained by integrating the high-speed images acquired during the exposure of high intensity pulses. Figure (d) shows the difference image before and after the HIFU exposure, showing the coagulation area. The HIFU focus is located at the center of the images. It was observed that cavitation bubbles generated by the high intensity pulses were distributed upstream of the HIFU as time passed. On the other hand, the center of the coagulation area, observed from 2 s after the start of the HIFU exposure, was kept almost at the focus.

After the first 2 s of the HIFU exposure, the ultrasonic heating might have been enhanced not by not newly generated bubbles by the high intensity pulses but by residual bubbles. The simultaneous observation by ultrasound imaging will help to set the appropriate parameters of high-intensity ultrasound pulses.

5 mm



Cavitation bubbles (a) – (c), and coagulated area (d)

High Intensity Focused Ultrasound (HIFU) Ablation of Fetal Rabbit Umbilicus

Presenter: Ava Danialy

Authors in order: Ava Danialy, *University of Toronto*, Karolina Piorkowska, *Hospital for Sick Children*, Hrishikesh Raghuram, *University of Toronto*, Amanda Headrick, *SickKids Hospital*, Craig Macsemchuk, *University of Toronto*, Nikan Fakhari, *Sickkids*, Jerome Baranger, *The Hospital For Sick Children*, Olivier Villemain, *Translational Medicine, Hospital for Sick Children*, Tim Van Mieghem, *Mount Sinai Hospital*, Adam Waspe, *Hospital for Sick Children*, James Drake, *Hospital for Sick Children*

To demonstrate that magnetic resonance (MR) guided HIFU can effectively ablate and occlude the umbilical cord in fetal rabbits while preserving viability for untreated fetuses.

Five New Zealand white rabbits were used at E25-E26, where fetuses were 6-7 centimeters long. Ultrasound was performed to mark fetuses with Evans-Blue/Gadolinium contrast and to confirm placental blood flow and heart rate. MRI evaluated the size and positioning of the marked fetuses. MRgHIFU ablated the umbilicus in the one marked fetus with a power of 120W for 20s. Post-treatment ultrasound evaluated the cardiac function and viability of targeted fetuses. Necropsy confirmed HIFU lesions.

Injection of Evans Blue and Gadolinium was found to be safe as the viability of the injected control fetuses were confirmed by necropsy. Thermometry confirmed temperatures above 60°C suggesting ablation was achieved. Post-treatment ultrasound confirmed lower cardiac function of the treated fetus in 60% of the cases. Necropsy confirmed termination of the treated fetuses in 60% of cases and showed viability of one adjacent untreated size-matched control fetus in 100% of cases. Ablation marks were visible on the liver or placenta during necropsy in 100% of the cases. No off-heating target in the mother was found during necropsy.

MR-guided HIFU therapy can effectively ablate umbilical artery and vein under the belly button in rabbit fetuses without harming non-targeted fetuses, as a model for a treatment procedure for twin-reversed arterial perfusion (TRAP) sequence. Doppler ultrasound can reliably confirm viability of non-targeted fetuses.

Funding provided by the CIHR-NSERC Collaborative Health Research Project. We thank Lab Animal Services and The Imaging Facility at The Hospital for Sick Children.

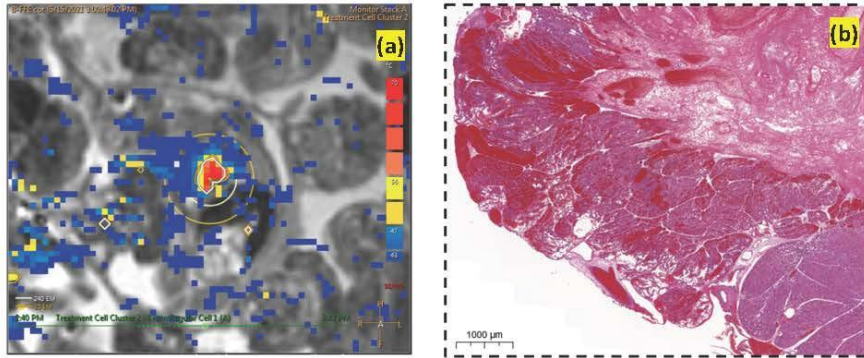


Figure: (a) Temperature map of target fetus. (b) Histology confirming ablation.

Thermal Treatment Planning Module for Clinical Ultrasound Ablation of Prostate Cancer

Presenter: Pragya Gupta

Authors in order: Pragya Gupta, *University of California San Francisco*, Tamas Heffter, *Acoustic MedSystems*, Muhammad Zubair, *University of California, San Francisco*, I-Chow Hsu, *Radiation Oncology, University of California San Francisco*, E. Clif Burdette, *Acoustic MedSystems*, Chris Diederich, *UC San Francisco*

To develop 3D patient-specific FDTD models and pre-treatment planning tools for selective thermal ablation of prostate cancer using FDA 510(k) cleared catheter-based ultrasound interstitial applicators.

A 3D generalized “prostate” model was developed to generate temperature and thermal dose profiles for various applicator operating parameters and anticipated perfusion ranges. A priori planning, based upon pre-calculated lethal thermal dose/temperature clouds, can be used for iterative device selection and positioning. Full 3D patient-specific modeling of actual placement can be applied, with optional integrated pilot-point temperature-based feedback control and urethral/rectum cooling. These numerical models were verified against ex-vivo experimental results obtained in muscle tissues.

For generic prostate tissue, 360 cases were simulated based on the transducers (1-4), power (8-20 W/cm²), heating time (5, 7.5, 10 mins) and blood perfusion (0, 2.5, 5 kg/m³/s) using forward treatment modelling. Selectable ablation zones ranged from 0.8-3.0 cm and 0.8-5.3 cm in radial and axial directions, respectively. 3D patient-specific thermal treatment models for T2/T3 prostate disease demonstrate applicability of workflow and technique within three cases each of focal, quadrant and hemi-gland ablation. A temperature threshold $T=52$ °C at the treatment margin, emulating invasive temperature sensing, can be applied for pilot-point feedback control to improve conformality of thermal ablation.

Prostate-specific simulations of interstitial ultrasound applicators were used to generate a library of thermal dose distributions to visually optimize and set applicator positioning and directivity during pre-procedure planning. Forward treatment planning along with pilot-point control utilized to improve accuracy and control, as shown in patient-specific models to effectively ablate focal disease.

This project work is supported by NIH grant R01CA230323.

Multichannel Matrix-array Based System for Small Animal Hyperthermia and Ablation

Presenter: Steffen Tretbar

Authors in order: Marc Fournelle, *Fraunhofer IBMT*, Christian Degel, *Fraunhofer IBMT*, Christoph Risser, *Fraunhofer IBMT*, Andreas Melzer, *ICCAS - Innovation Center Computer Assisted Surgery*, Steffen Tretbar, *Fraunhofer Institute for Biomedical Engineering IBMT*

Multichannel matrix-array based system for small animal hyperthermia and ablation
Multichannel matrix-array based system for small animal hyperthermia and ablation.

The probe consists of a 128 matrix (1 MHz pitch, $f = 1$ MHz) in a regular grid approximating a circular footprint. The array is water-cooled for sonication at high Duty Cycle (DC). Our high power multichannel electronics system provides up to 16 W per channel (with individual delay and frequency per channel). Temporal sonication patterns can be freely defined within the tri-state pulser module limits with DCs up to 100%.

The probe was integrated into a 3D printed housing and characterized with respect to the acoustic output and thermal effects in tissue. The elements were characterized individually and showed a high array homogeneity with only 19% standard deviation. When driven by our electronics, the acoustic output was assessed and the ISPPA varied from 6,6 W/cm² to 121 W/cm² when focusing to $(x/y/z)=(0/0/15$ mm) for $U_{pp} = 20$ V and 150 V respectively. Lateral -6dB focus size was 2 mm for these settings. Experiments on tissue (chicken breast) showed a temperature increase from 25 °C to more than 50°C within 10

We showed locally-confined hyperthermia generated within seconds in tissue using our multichannel electronics and the matrix-based array. Our system's ability for (dynamic) beam steering allows generation of more complex sonication patterns. Further studies on the system limits (e.g. maximum achievable tissue temperature under in-vivo conditions) will be conducted in the

The authors want to acknowledge the german ministry for education and research BMBF for funding under the project SONORAY.

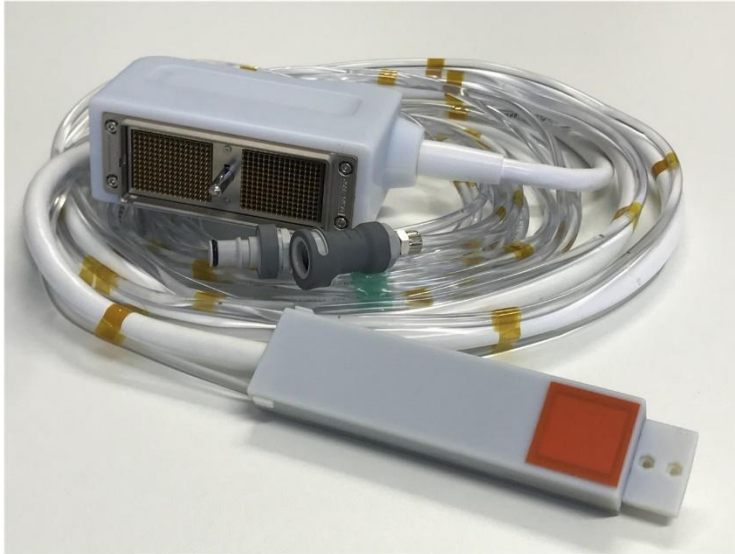


Figure 1: Matrix-array probe after housing integration and multichannel system

Comparison of HIFU Lesion Monitoring Techniques based on B-mode Images

Presenter: Thomas Payen

Authors in order: Thomas Payen, *LabTau*, Sébastien Crouzet, Nicolas Guillen, *EDAP TMS*, Jean-Yves Chapelon, *LabTAU - INSERM*, Cyril Lafon, *INSERM*, Stefan Catheline, *INSERM, University of Lyon*

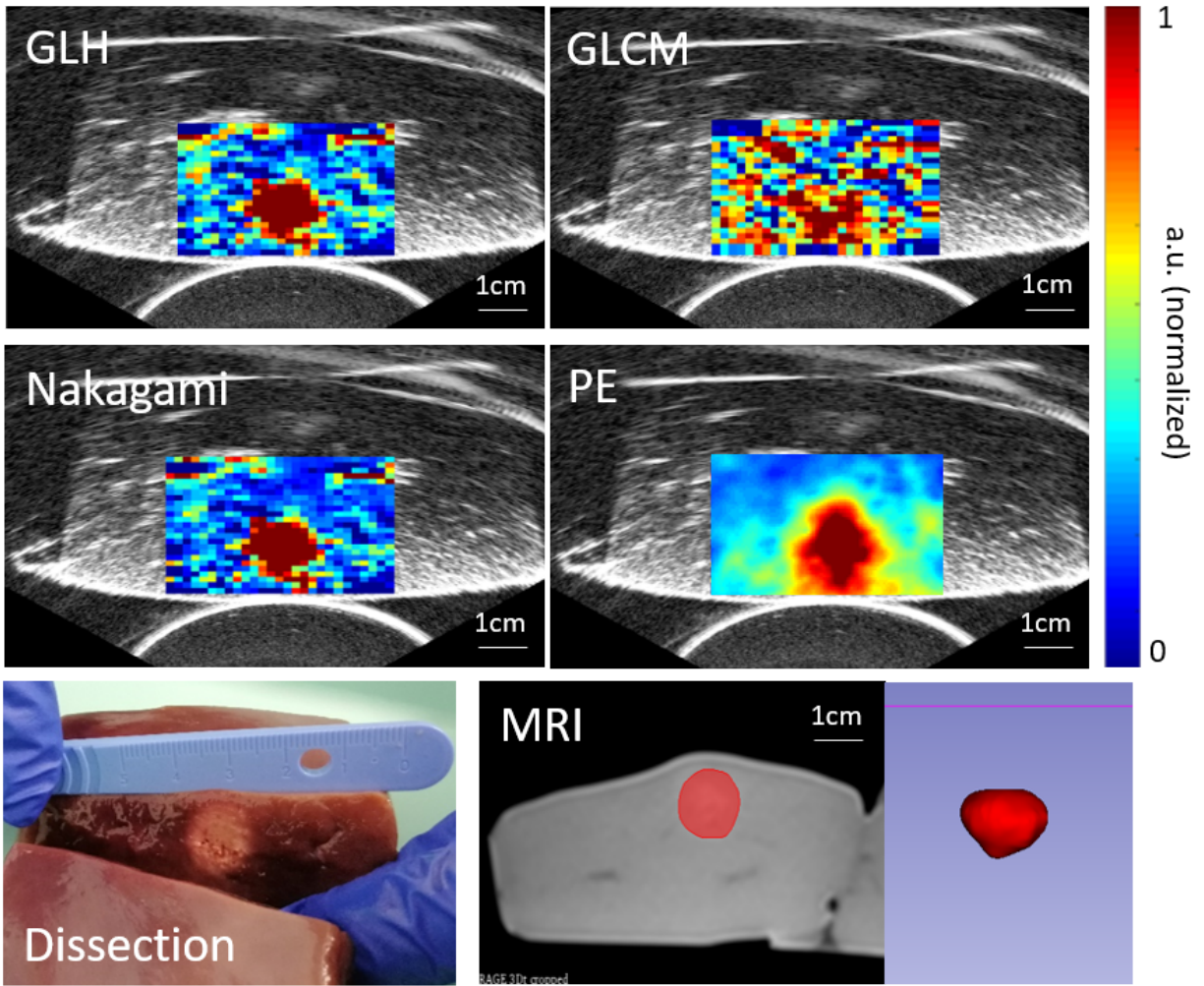
Monitoring techniques based on B-mode images acquired with a clinical system were assessed for HIFU lesion detection and applied in the context of prostate cancer.

Grey-Level Histogram (GLH), Grey-Level Co-Matrices (GLCM), Nakagami and passive elastography (PE) were applied to B-mode images acquired in vitro in 15 bovine livers and in vivo in 10 pigs, before and after HIFU lesions performed with the clinical Focal One® system. Lesion contrast and size were estimated with each parameter extracted to assess their performance and robustness. After validation, the techniques were compared on images acquired in 4 patients with prostate cancer treated with HIFU.

Nakagami demonstrated the highest CNR in vitro (10.2 dB), but size was best correlated to MRI estimates for PE ($r^2 = 0.65$, Figure). Perfusion limits the appearance of bubbles due to HIFU, leading to decreased performances in vivo for pixel intensity-based GLH, GLCM and Nakagami. PE demonstrated higher performances in lesion CNR (4.9 dB) and size ($r^2 = 0.50$). Finally, the clinical proof-of-concept validated the feasibility of all these techniques in prostate cancer setting. PE displayed more sensitive and precise lesion estimation as well as tumor detection than the three other techniques.

Lesion monitoring is crucial to HIFU control in clinical applications. However, open-access, ultrafast US scanners are generally not available in this setting. Four techniques based on B-mode images were developed and compared. PE demonstrated precise lesion detection, independent from uncontrolled bubble appearance.

This work was supported by the RHU PERFUSE (ANR-17-RHUS-0006) within the program “Investissements d’Avenir” operated by the French National Research Agency.



In vitro detection of HIFU lesion

Real-time Lesion Monitoring during HIFU Treatment using Harmonic Motion Imaging Guided FUS (HMIgFUS) Ex Vivo & Human in Vivo

Presenter: Xiaoyue Li

Authors in order: Xiaoyue Li, *Columbia University*, Niloufar Saharkhiz, *Columbia University - UEIL lab*, Yangpei Liu, *Columbia University*, Stephen Lee, *Columbia University*, Murad Hossain, *Columbia university*, M-Sharjeel Ansari, *Columbia University Ultrasound Elasticity and Imaging Laboratory*, Bret Taback, Elisa Konofagou, *Columbia University*

To develop a real time method for lesion monitoring during HIFU treatment using Harmonic Motion Imaging (HMI), an ultrasound elasticity based imaging method.

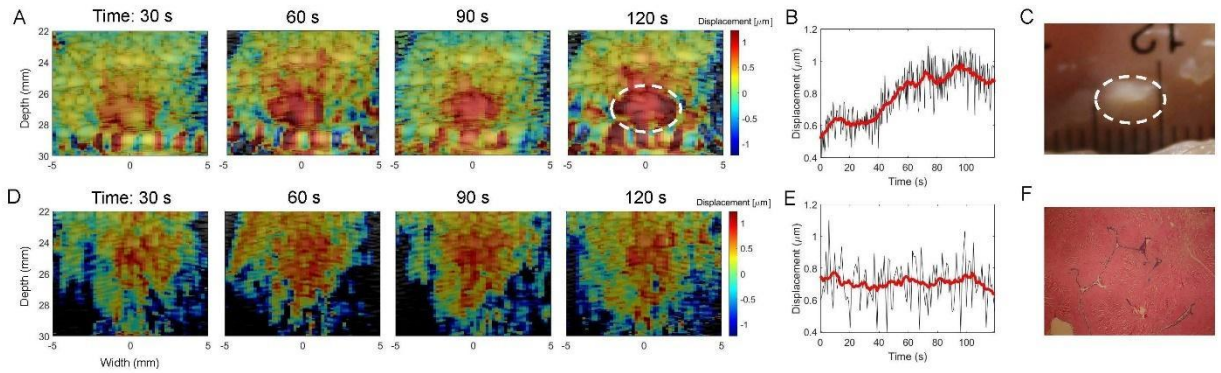
The HMIgFUS system consisted of a coaligned FUS and linear imaging transducer. The FUS transducer was continuously driven (without interruption throughout the ablation duration) with an amplitude-modulated signal, resulting in 100 Hz oscillatory tissue displacement.

At each imaging acquisition during HMIgFUS, 10 frames of RF data at a PRF of 500 Hz were acquired and processed before the next acquisition. Axial displacement was estimated using normalized 1D cross-correlation.

Real-time HMIgFUS was performed in ex vivo chicken breast and an in vivo fibroadenoma patient at 18 MPa peak-positive for 120 seconds. RF data acquisition, beamforming, and displacement estimation lasted 0.5-1s per frameset resulting in HMIgFUS lesion monitoring display rate of 1-2 Hz. The HMI peak positive displacement maps showed increase in both lesion displacement and size in the chicken breast (Fig. 1A-C). The final lesion diameters were found to be 4.2 mm at -18 dB HMI peak-positive displacement in agreement with gross pathology. In the fibroadenoma patient, no lesioning was concluded by HMIgFUS monitoring, which was confirmed in histological examination.

Real-time, continuous HMIgFUS lesion monitoring was shown ex vivo and in clinic in an initial feasibility study. This method would enable real-time (1-2 Hz) localization and lesion growth monitoring, which can significantly improve clinical HIFU ablation treatment. Ongoing clinical investigations aim to determine HMIgFUS lesioning confirmation in breast cancer patients.

This study was supported by the National Institutes of Health (R01CA228275), and the first author is supported by an NSF GRFP fellowship.



Real-time HMIgFUS in an ex vivo chicken breast ($n=1$), where A. Real-time HMI peak positive displacement maps overlaid on b-modes show lesion development over time, with the lesion circled in white at 120 seconds of ablation duration, B. Mean HMI peak positive displacement in a 1.8 mm lateral by 2 mm axial region around the focus (at a depth of 27 mm) over time show displacement increase with ablation progression, and C. Difference in coloration in gross pathology following ablation validates the presence of a lesion (circled in white).

Real-time HMIgFUS in a fibroadenoma subject ($n=1$), where D. Real-time HMI peak positive displacement maps (displacement was bandpass filtered around 100 Hz) overlaid on b-modes do not show large scale changes over time, indicating the lack of lesion formation, and E. Mean HMI peak positive displacement in a 1.8 mm lateral by 2 mm axial region around the focus (at a depth of 25 mm) over time show relatively constant displacement over time, indicating the lack of successful ablation and lesion formation. F. Clinical histology confirmed the lack of lesioning.

Feasibility of Volumetric Hyperthermia using the InSightec ExAblate Body System

Presenter: Kisoo Kim

Authors in order: Kisoo Kim, *University of California, San Francisco*, Muhammad Zubair, *University of California, San Francisco*, Chris Diederich, *UC San Francisco*, Eugene Ozhinsky, *University of California, San Francisco*

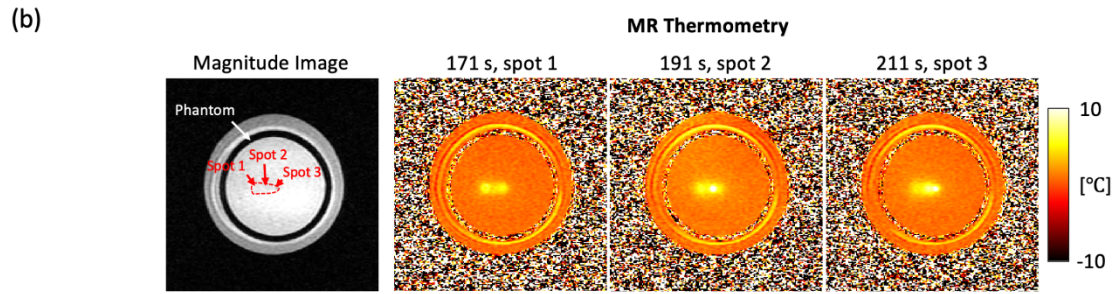
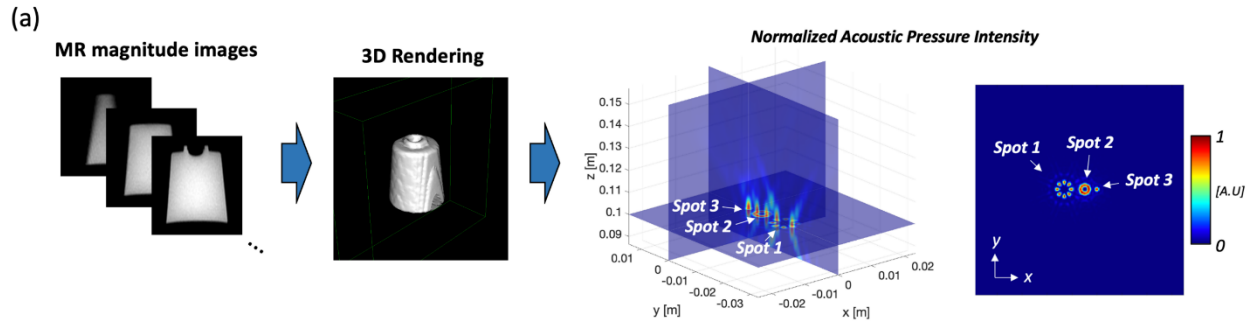
The goal of this study is to develop MR-guided volumetric hyperthermia using the InSightec ExAblate 2000 body array system.

The simulation framework was developed to calculate the 3D acoustic intensity distribution for beamforming and scanning strategies (Fig.1a). System configurations were modified to achieve fast mechanical movement of the transducer and electronic phasing. Based on the acoustic and biothermal simulation, multiple positions were sonicated sequentially using mechanical scanning and multiple beamforming patterns, as selected to best fit the targeted region. We evaluated this approach using the tissue-mimicking phantom with a real-time MR thermometry.

In demonstration of this framework, the sector-vortex concentric-ring array transducer was simulated to generate various beamforming patterns at user-defined positions. Three positions were sequentially sonicated using mechanical scanning and selected beamforming patterns: Spot 1- 12 mm off-axis, Mode 4; Spot 2- on-axis, Mode 2; and Spot 3 - 7 mm off-axis, Mode 0. Interleaved acquisitions were implemented: four images were acquired during the sonication (20 sec) and the transducer was moved to the next spot position (6 sec). Multiple translations and sonication cycles were repeated to reach the targeted temperature elevation (Fig.1b).

Beamforming and scanning strategies could control and increase hyperthermic volume to fit the targeted region within the ExAblate Body system. This study demonstrated the feasibility of volumetric hyperthermia delivery using the InSightec ExAblate 2000 body array system.

The authors would like to thank Noam Maimon at InSightec, Inc. for assistance with developing the techniques. The authors have no conflict of interest. This



Patient Specific Adjuvant Hyperthermia in Prostate, using a Novel Phased-array Applicator of Transperineal Ultrasound

Presenter: Pauline Guillemin

Authors in order: Pauline Guillemin, *Geneva University*, Michael Schwenke, *Fraunhofer Institute for Digital Medicine MEVIS*, David Sinden, *Fraunhofer Institute for Digital Medicine MEVIS*, Giovanna Dipasquale, *Geneva University Hospital*, Orane Lorton, *Geneva University*, Johannes Uiterwijk, *Geneva University*, Jennifer Le Guevelou, *Geneva University*, Juergen Jenne, *Fraunhofer Institute for Digital Medicine MEVIS*, Pierre-Alexandre Poletti, *Geneva University Hospital*, Thomas Zilli, *Geneva University Hospital*, Rares Salomir, *Geneva University Hospital*

Validation and implementation of a new concept of phased array transducer, designed for adjuvant prostate hyperthermia, coupled to a patient-specific immobilization device.

An optimized design of hyperthermia applicator was derived from a numerical model. Performance tests have been conducted on phantom under 3T MRI guidance. From optical surface scans, a patient-specific pelvic immobilization device was computed and 3D-printed to register the hyperthermia applicator. This is interchangeable with a confocal ultrasound imaging probe, to demonstrate a reproducible geometry of the acoustic beam with respect of the patient. Set-up reproducibility was measured using optical surface measurements and MRI.

The optimal specifications were following: frequency 700 kHz, 1D focusing (cylindrical), radius of curvature 140mm, 192 elements pseudo randomly distributed on 6 columns. The experimental focus beam is in good agreement with the simulations. The 3D-printed device demonstrated sub-millimetric production accuracy. The replication of the original targeting position was demonstrated by comparing the US images manually acquired by the radiologist with US images acquired by stand-alone ultrasound probe attached to its 3D printed holder. Pre-positioning accuracy set-up showed sub-millimeter accuracy and small angular rotations less than 2 degrees.

Reported results are considered as a promising step toward rapid and precise positioning of patients and easier integration of radiotherapy and MR-guided ultrasound based local hyperthermia.

The authors wish to thank Imasonic (Voray-sur-l'Ognon, France) and CIBM (Genève, Switzerland).

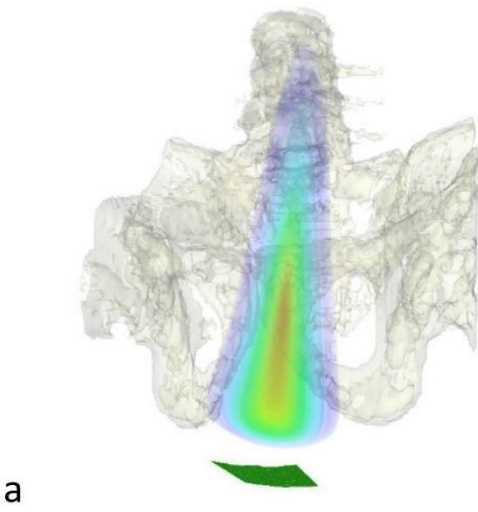


Fig. 1: (a) Numerical model of the acoustic beam in a patient and (b) the manufactured phased array applicator of transperineal ultrasound

A5-1

Investigating Blood-Labyrinth Barrier opening using MRI-guided Focused Ultrasound combined with Microbubbles

Presenter: Neha Chauhan

Authors in order: Neha Chauhan, *Sunnybrook Research Institute*, Dallan McMahon, *Sunnybrook Research Institute*, Emilia Luca, *Sunnybrook Research Institute*, Kullervo Hynnen, *Sunnybrook Research Institute/ University of Toronto*, Alain Dabdoub, *Sunnybrook Research Institute*

We investigated the use of focused ultrasound (FUS) to enhance the permeability of the inner ear's blood-labyrinth barrier (BLB) to achieve minimally invasive therapeutic delivery.

Male Long Evans rats received unilateral sonication with the administration of Definity microbubbles (MBs) and Gadovist, a gadolinium-based contrast agent; contrast enhanced T1-weighted magnetic resonance (CE-T1w MR) images were used as an early indicator of BLB permeability enhancement. Before and after sonication, auditory function was assessed using auditory brainstem response (ABR) and distortion product otoacoustic emissions (DPOAE) tests.

Following FUS+MB exposure, there was a $33\% \pm 2.3\%$ increase in gadolinium contrast in CE-T1w MR images in the sonicated inner ears relative to contralateral control ears. Furthermore, there were no significant changes in auditory function in the sonicated inner ears relative to the contralateral control ears, measured using ABR and DPOAE tests.

This proof-of-principle study shows that FUS+MB exposure can enhance BLB permeability to mediate delivery of large therapeutics to the inner ear. These data support the feasibility of FUS-mediated delivery to treat inner ear disorders; however, further investigation on the safety profile in the inner ear is required for clinical applicability.

The authors would like to thank Shawna Rideout-Gros and Viva Chan for their support as veterinary technicians.

Control of Fibroblast Differentiation using Acoustic Droplet Vaporization

Presenter: Mario Fabiilli

Authors in order: Easton Farrell, *University of Michigan*, Mitra Aliabouzar, *University of Michigan*, Carole Quesada, Brendon Baker, Renny Franceschi, Andrew Putnam, Mario Fabiilli, *University of Michigan*

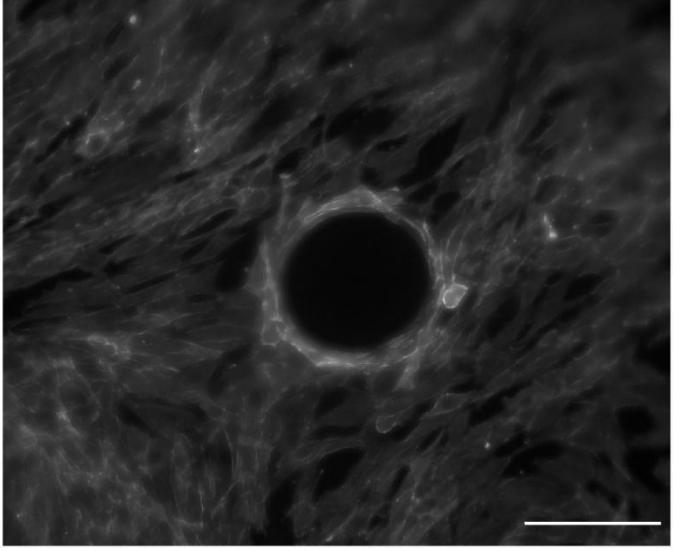
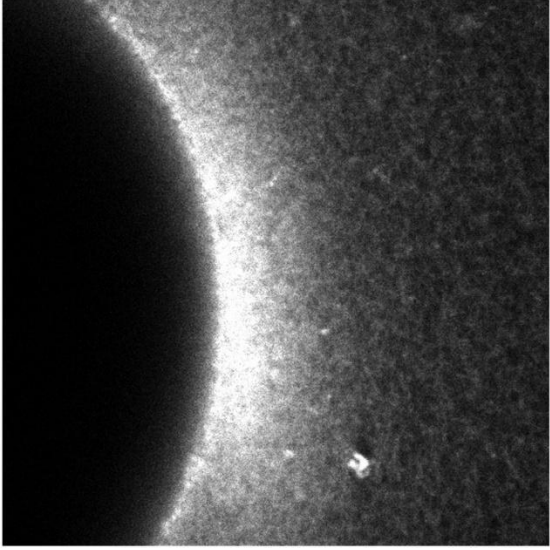
We demonstrate how acoustic droplet vaporization (ADV) causes spatiotemporally controlled stiffening within composite hydrogels. This localized stiffening can induce the differentiation of fibroblasts into myofibroblasts.

Composite hydrogels were fabricated with 4.5 mg/mL fibrin, 2 U/mL thrombin, and 0.01% (v/v) phase-shift emulsion (\emptyset : 13 μ m) containing perfluoroheptane. ADV (2.5 MHz) was generated in the hydrogels, which were analyzed using confocal and atomic force microscopies. Fibroblasts were seeded atop the hydrogels and myofibroblast phenotype was evaluated using α -smooth muscle actin (α -SMA) immunocytochemistry. Studies were conducted in completed media with and without exogenous TGF- β 1, and in starvation media with and without TGF- β 1 inhibitor.

Localized, radial compaction of the fibrin matrix was observed adjacent to ADV-generated bubbles. This compaction was correlated with matrix stiffening. Young's moduli in fibrin regions proximal and distal to the bubble were 6.7 kPa and 0.23 kPa, respectively. α -SMA was significantly elevated in dermal fibroblasts proximal to bubbles compared to distal cells, irrespective of the addition of exogenous TGF- β 1. Control studies in fibrin-only hydrogels revealed that ultrasound exposure in the absence of ADV did not increase α -SMA levels. Proximal enhancement of α -SMA adjacent to ADV-generated bubbles was abrogated with the addition of TGF- β 1 inhibitor.

The volumetric expansion of the phase-shift emulsion after ADV locally compacted and stiffened the strain-stiffening fibrin matrix, thereby increasing α -SMA levels when endogenous TGF- β 1 production was uninhibited. This approach could be applicable to studies of diseases like fibrosis and chronic wounds, which are characterized by dysregulation of myofibroblasts.

This work was supported by NIH grant R01HL139656.



Decorrelation Time Mapping for Analysis of Nanobubble Dynamics in Tumours

Presenter: Dana Wegierak

Authors in order: Dana Wegierak, *Case Western Reserve University*, Michaela Cooley, *Case Western Reserve University*, Reshani Perera, *Case Western Reaserve University*, Michael Kolios, *Ryerson University*, Agata Exner, *Case Western Reserve University*

Nanobubbles (NBs) show potential as an extravascular and therapeutic contrast agent. Here, we propose decorrelation mapping to quantify NB targeting and accumulation in tumours.

NBs and prostate-specific membrane antigen targeted NBs (PSMA-NBs) were formulated as previously described¹. Bubbles were infused via tail vein into mice bearing PSMA-expressing flank tumours and were imaged using nonlinear contrast mode (VisualSonics Vevo 3100, 18 MHz, 5 fps, 4% power). Wash-in and wash-out dynamics were captured for NBs, PSMA-NBs and microbubbles (MB, Lumason). Using intensity data, the 50% decorrelation time (DT) was calculated at each spatial location using MATLAB and decorrelation maps were created.

As shown in Figure 1, DT mapping showed a high degree of sensitivity to tumour versus normal tissue. The average DT in tumour regions was significantly longer (NBs-11.9s; PSMA-NBs-14.5s) than surrounding normal tissue (NBs-1.3s; PSMA-NBs-2.0s). DT was longer for targeted vs. plain NBs, while MBs showed a rapid DT in both regions. Longest DT appears to coincide with NB entrapment in tumours and shortest with areas of flow (blood vessels). NB targeting further extends DT and is linked with greater PSMA-NB retention in tumours. MBs, which typically show a rapid wash-in and wash-out, had the shortest DT without tumour specificity.

Decorrelation mapping of in vivo NBs dynamics presents a sensitive assessment of tumour tissue and may be useful for quantifying extravascular NB kinetics. A comparison of DT mapping vs. mapping of time-intensity curve parameters (time to peak, slope to peak, area under curve) is ongoing.

This work was funded by the National Institutes of Health grants R01EB025741 and R01EB028144 . We thank Dr. James Basilion and group for their contributions.

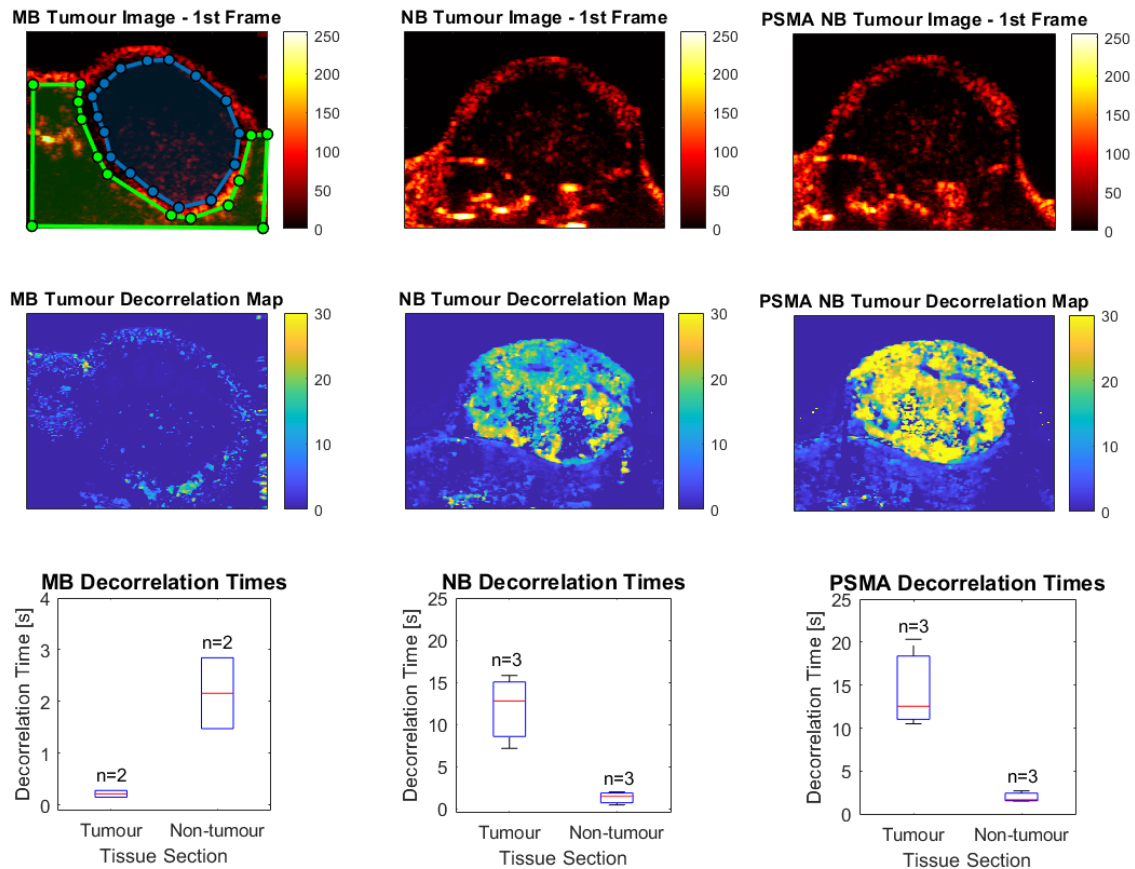


Figure 1. *Top row:* First frame of 1000 frame greyscale wash-in-video collected in nonlinear contrast mode of MBs, NBs or PSMA-targeted NBs. The blue and green polygons represent sectioning of tumour tissue and normal tissue respectively. *Center row:* sample decorrelation maps of tumours after the wash in of MBs, NBs or PSMA-targeted NBs. *Bottom row:* Correlation time comparisons from sectioned ROIs of decorrelation maps after the wash in of MBs, NBs or PSMA-targeted NBs. On each box, the central mark indicates the median, and the bottom and top edges of the box indicate the 25th and 75th percentiles, respectively. The whiskers extend to the most extreme data points not considered outliers, and the outliers are plotted individually using the '+' symbol.¹Perera R et al., *Nanomedicine NBM*, 2020

A Neuronavigation-guided Sonobiopsy Device for the Noninvasive Diagnosis of Brain Diseases

Presenter: Lu Xu

Authors in order: Lu Xu, *Washington University in St. Louis*, Chih-Yen Chien, *Washington University in St. Louis*, Christopher Pacia, *Washington University in St. Louis*, H. Gach, *Washington University School of Medicine*, Yao Hao, *Washington University in St. Louis*, Eric Leuthardt, *Washington University School of Medicine*, Hong Chen, *Washington University in St. Louis*

Develop a neuronavigation-guided sonobiopsy device for noninvasive diagnosis of brain diseases by enhancing the release of disease-specific biomarkers from the brain into the blood circulation.

The sonobiopsy device integrated a neuronavigation system with a single-element, focused-ultrasound (FUS) transducer. The accuracy in targeting specific brain location was characterized in a water tank without and with human skull. It was verified with in vivo pig studies by measuring the offsets between the intended and the actual locations of blood-brain barrier opening. Blood samples were collected post-FUS to analyze the plasma concentration of brain-specific biomarkers (glial fibrillary acidic protein and neurofilament light chain protein).

The targeting accuracy of the neuronavigation-guided sonobiopsy device as measured in the water tank was $1.40\text{mm} \pm 0.70\text{mm}$ without skull (A). It was $11.32\text{mm} \pm 3.42\text{mm}$ with the human skull and the offset was mainly along the FUS beam axis and towards the skull due to the skull aberration (B). This skull aberration caused error can potentially be mitigated with repositioning the transducer deeper. The targeting accuracy evaluated based on in vivo pig study was $0.89\text{mm} \pm 2.24\text{mm}$ (C). The sonobiopsy device successfully enhanced the release of brain-specific protein markers post-sonication compared with pre-sonication.

This study showed that the developed neuronavigation-guided sonobiopsy device had a high spatial targeting accuracy and achieved effective biomarker release in the pig model, paving the foundation for its translation to clinical use.

Preclinical Evaluation of a Dual-Mode CMUT Probe For Ultrasound-Guided HIFU Treatment

Presenter: Ivan Suarez-Castellanos

Authors in order: Ivan Suarez-Castellanos, *LabTAU - INSERM - Université de Lyon*, Geoffroy de Sallmard, *LabTAU - INSERM*, Alice Ganeau, *INSERM*, Guillaume Vanstaevel, *LabTAU - INSERM*, Thomas Payen, *LabTau*, Jean-Yves Chapelon, *LabTAU - INSERM*, Nicolas Guillen, *EDAP TMS*, Nicolas Sénégon, W. Apoutou N'DJIN, *LabTAU, INSERM, Université de Lyon*

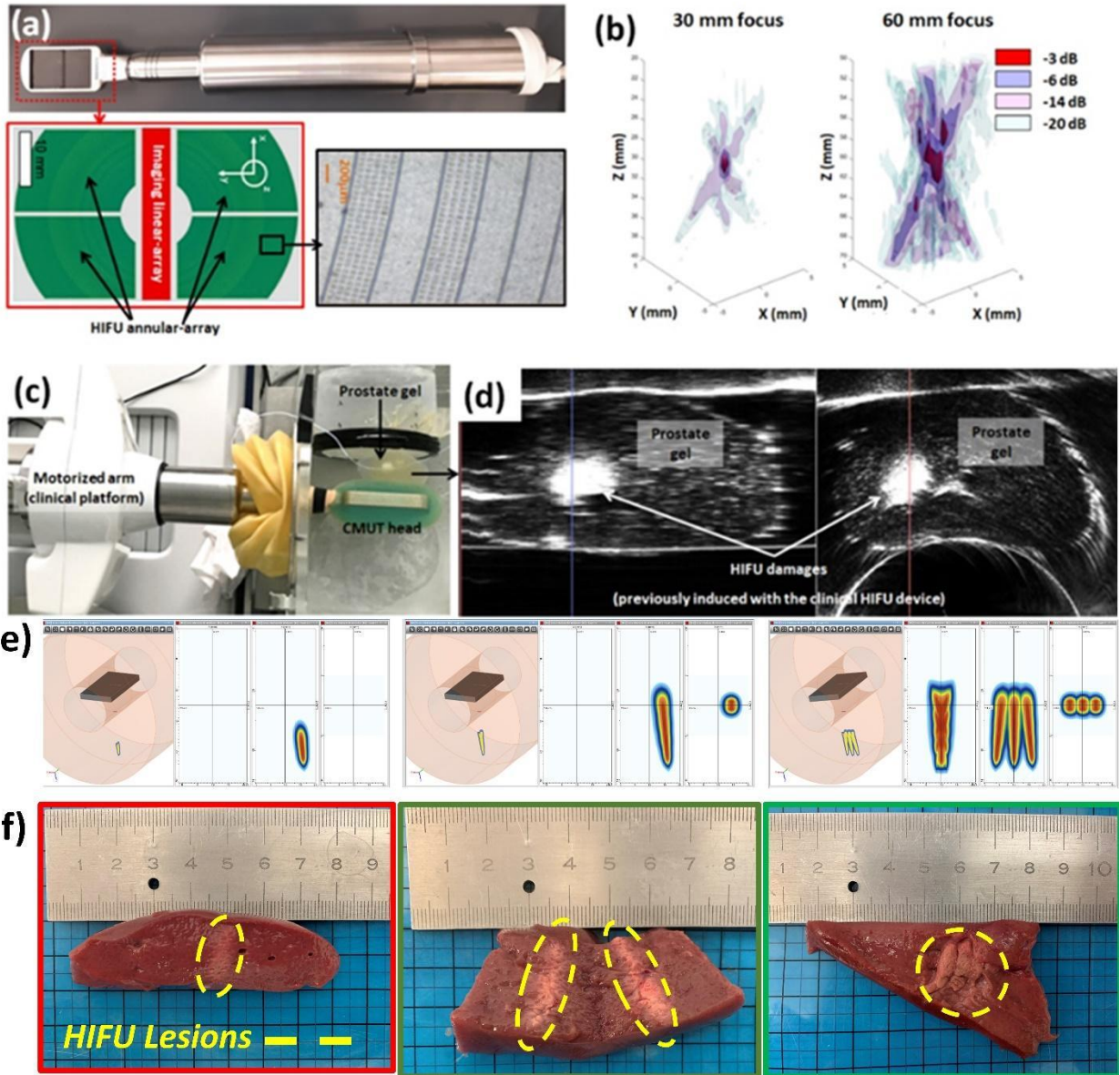
A dual-mode Ultrasound-guided High Intensity Focused Ultrasound (USgHIFU) probe using CMUT technology was investigated as a targeted strategy in the context of cancerous tissue ablation.

The USgHIFU probe included a planar 64-element annular HIFU CMUT array ($f_{\text{HIFU}} = 3\text{MHz}$) surrounding a 256-element linear imaging CMUT array (Fig.a: $f_{\text{img}} = 7\text{MHz}$). Its imaging performance was compared to that of a clinical device via numerical modeling and experimentation using commercial phantoms. Acoustic characterization of the HIFU array included 3D pressure field mapping and radiation force balance measurements. In vitro experiments consisted in generating HIFU sonications with the CMUT probe in 2-3cm thick porcine liver tissues.

The planar CMUT probe enabled HIFU dynamic focusing (Fig.b: 30-70mm) while the imaging component exhibited improved lateral resolutions (0.3-1.5mm, for imaging depths of 10-20mm). The probe was compatible with a routinely-used clinical platform (Fig.c) which allowed for 3D-imaging of gel phantoms and in vivo porcine liver, HIFU treatment planning and visualization of HIFU damages (Fig.d). The HIFU probe provided acoustic surface intensities of $0.9\text{W}/\text{cm}^2$ that allowed producing elementary in vitro lesions in depth of liver tissue ($L \times W \times H \approx 0.5\text{cm} \times 0.5\text{cm} \times 1.0\text{cm}$). Combinations of dynamic focusing and probe rotation produced larger lesions ($L \times W \times H \approx 2.0\text{cm} \times 0.5\text{cm} \times 2.0\text{cm}$) via stacking of multiple elementary lesions (Fig.f), consistent with modelling results (Fig.e).

Technical feasibility of a USgHIFU probe, fully-developed using CMUTs, was demonstrated. The HIFU-CMUT array showed tissue ablation capabilities with volumes compatible with localized cancer targeting, while allowing integration of an imaging array for improved visualization of targeted tissues (versus clinical device), thus providing assets for further development of focal therapies.

This project was supported by BPI (FUI), the Laboratory of Excellence (LabEx) DEVweCAN, and the French National Agency for Research (ANR-RHU).



USgHIFU probe and experimental results of imaging and HIFU performance.

Sonobiopsy Enables Sensitive Detection of Glioblastoma-derived Circulating Tumor DNA

Presenter: Hong Chen

Authors in order: Christopher Pacia, *Washington University in St. Louis*, JINYUN YUAN, *Washington university in st louis*, Yimei Yue, Lu Xu, *Washington University in St.Louis*, Arash Nazeri, *Washington University School of Medicine*, Rupen Desai, *Washington University School of Medicine*, H. Gach, *Washington University School of Medicine*, Xiaowei Wang, *University of Illinois at Chicago*, Michael Talcott, *Washington University School of Medicine*, Aadel Chaudhuri, *Washington University School of Medicine*, Gavin Dunn, *Washington University School of Medicine*, Eric Leuthardt, *Washington University School of Medicine*, Hong Chen, *Washington University in St. Louis*

This study aimed to demonstrate that sonobiopsy could achieve sensitive detection of glioblastoma-derived circulating tumor DNA in mouse and pig models of glioblastoma.

MRI-guided focused ultrasound (FUS) sonication in the presence of intravenously injected microbubbles was targeted at the mouse and pig glioblastoma (GBM) tumors. After sonication, blood was collected via cardiac puncture in mice and via peripheral vein in pigs. Droplet digital PCR was used to quantify the levels of brain tumor-specific genetic mutations, EGFRvIII and TERT C228T, in the circulating tumor DNA (ctDNA). Histological staining was performed to assess off-target tissue damage.

MRI scans confirmed successful FUS-induced BBB disruption. In mice, sonobiopsy significantly increased the plasma levels of EGFRvIII ctDNA (920-fold increase, $p = 0.00089$) and TERT C228T ctDNA (10-fold increase, $p = 0.015$). The detection sensitivities for EGFRvIII and TERT C228T were increased by 57.57% and 31.54% compared with conventional blood-based liquid biopsy, respectively (Fig A). In pigs, sonobiopsy significantly increased the plasma levels of EGFRvIII ctDNA (270-fold increase, $p = 0.016$) and TERT C228T ctDNA (9-fold increase, $p = 0.022$). As a result, sonobiopsy increased the detection sensitivities for EGFRvIII and TERT C228T by 71.43% and 28.57%, respectively (Fig B). No significant off-target damage was observed.

This study demonstrated that sonobiopsy enriched the plasma ctDNA and improved the detection sensitivity of GBM mutations without posing significant safety risks. Sonobiopsy has the potential to advance brain cancer diagnosis, treatment monitoring, and recurrence detection.

Effects of FUS Vasomodulation and Oral Administration of Ginkgo Biloba Extract on Diabetic Peripheral Neuropathy

Presenter: Gin-Shin Chen

Authors in order: Gin-Shin Chen, *National Health Research Institutes*, Gin-Shin Chen, *National Health Research Institutes*

The study aimed to inspect the therapeutic effects of ginkgo biloba oral administration combined with FUS vasomodulation on diabetic distal symmetric polyneuropathy.

Male adult Wistar rats at 4 weeks post-streptozotocin injections were adopted as the diabetic neuropathic model. The medial and lateral plantar arteries of the rat were treated by FUS and blood perfusion in the skin of the pad of the middle toe was measured. FUS or/and Ginkgo Biloba (EGb-761) treatments were carried out once a day for the first 5 days per week for consecutive 2 weeks. Behavioral tests were performed before the weekly treatment.

FUS treatments of the diabetic neuropathic rats (n=6) significantly increased blood perfusion after one-week treatment (323 ± 21 BPU; $p < 0.05$) and further enhanced perfusion post two-week treatments (360 ± 47 BPU; $p < 0.01$), compared with no FUS treatments (266 ± 45 BPU). Furthermore, the paw withdrawal force and latency were significantly increased after two-week FUS treatments (41.13 ± 2.57 g vs. 34.33 ± 4.55 g, & 3.96 ± 0.25 s vs. 5.24 ± 0.86 s; $p < 0.01$). Preliminary results showed that combined treatments of FUS and EGb-761 also increased blood perfusion whereas EGb-761 treatments didn't (n=2). Combined treatments and EGb-761 treatments both increased the paw withdrawal force and latency.

Only FUS treatments enhance peripheral blood microcirculation and improve mechanical allodynia and heat hyperalgesia of the rats with diabetic peripheral neuropathy. The Ginkgo Biloba extract has the anti-inflammatory effect. Combining FUS treatments with oral administration of the extract may halt neuropathic progression more effectively.

This work was partially supported by the National Health Research Institutes (BN-111-PP-10) and the Ministry of Science and Technology (MOST-110-2221-E-400-002), Taiwan.

Bioprinting for super-resolution Acoustic Droplet Vaporization in Hydrogels

Presenter: Mitra Aliabouzar

Authors in order: Mitra Aliabouzar, *University of Michigan*, Adam Ley, Sabine Meurs, *University of Michigan*, Ze Qi Chan, *University of Michigan*, Andrew Putnam, Mario Fabilli, *University of Michigan*

Acoustically responsive scaffolds (ARs) respond to ultrasound via acoustic droplet vaporization (ADV). We demonstrate how 3D-bioprinting impacts spatial resolution and modulation of ADV in ARs.

Bioinks, containing 0.5 % (v/v) phase-shift emulsions (C6F14, ϕ : 13 μm), 20 mg/mL fibrinogen, 7.5 mg/mL hyaluronic acid, and 106 cell/mL fibroblasts were extruded on a 3D-bioprinter using a pneumatic printhead. Printed bioinks were polymerized using 20 U/mL thrombin. ADV (f: 2.5 MHz, P-: 6MPa) was generated in ARs. Rheological properties of the bioinks and bioprinted ARs were characterized. Generated micropatterns were imaged using confocal and epifluorescence microscopies. Non-bioprinted ARs served as controls.

The developed bioinks possessed high zero-shear viscosity and shear thinning characteristics, which are crucial for extrusion-based bioprinting. This resulted in ARs with high print fidelity. Due to low shear rates (90%) along with phase-shift emulsion in distinct patterns. At similar acoustic parameters, the widths of ADV-generated bubbles were $\sim 500 \mu\text{m}$ and $\sim 1100 \mu\text{m}$ in bioprinted and non-bioprinted ARs, respectively. Greater alignment of fibrin fibers was observed in bioprinted versus non-bioprinted ARs. Distinct morphologies of ADV-induced bubbles were also achieved.

Bioprinting enabled micropatterning of (i) multiple phase-shift emulsions within an AR at spatial resolutions unachievable using conventional polymerization techniques and (ii) ADV-induced bubbles at spatial resolutions higher than the ultrasound beam dimensions. This approach can be applied to modulating ADV-induced behaviors in ARs to optimize tissue regeneration.

This work was supported by NIH grant R01HL139656, Basic Radiological Sciences Innovation Award, and Focused Ultrasound Foundation.

A5-6

A Low-intensity Ultrasound Delivery System using Acoustic Holograms

Presenter: Diana Andres

Authors in order: Diana Andres, *Universitat Politècnica de València*, Alicia Carrión, *Universitat Politècnica de València*, Nathalie Lamothe, *Universitat Politècnica de València*, Jose Pineda-Pardo, *HM CINAC (Centro Integral de Neurociencias Abarca Campal)*, *Hospital Universitario HM Puerta del Sur*, *HM Hospitales*, Noe Jimenez, *Universitat Politècnica de València*, Francisco Camarena, *Universitat Politècnica de València*

The aim of this work is create curved holographic lenses to adapt large-aperture transducers' focus to deep-brain structures in primates for localized blood-brain barrier opening.

Acoustic holograms were designed using time-reversal methods to adapt the elongated focus of a 100-mm aperture 140-mm focal transducer to the left posterior putamen of a macaque. Focusing performance was evaluated by simulations and validated by experimental ex-vivo measurements in a degassed water tank using a macaca mulata skull. The field near the skull was reconstructed by holographic projections of the experimental far field. A passive cavitation detector was located confocally to monitor microbubble activity.

Good agreement was found between simulated field, direct experimental and holographic projection data. FWHM on the x-axis was of 3, 3.9 and 3.8 mm for simulation, direct measurement, and reconstructed field, respectively, while it was of 2.8, 3.9 and 3.6 in the y-axis. The system was tuned to experimentally generate 0.5 MPa rarefaction pressure at focus, with a total 84% of the focus volume lying in the target region, while cavitation signals were acquired and processed in real.

Acoustic holograms can adapt the elongated focal spot of large-aperture focused transducers to target small deep-brain structures with great versatility. Results show that this technology can provide the typical values for BBB opening in non-human primates, paving the way to apply this low-cost system for localized preclinical drug screening.

Research supported by the Spanish Ministry of Science, Innovation and Universities through grant PID2019-111436RB-C22, IJC2018-037897-I, FPU19/00601, FJC2019-040453-I. Action co-financed by European Union (IDIFEDER/2021/004).

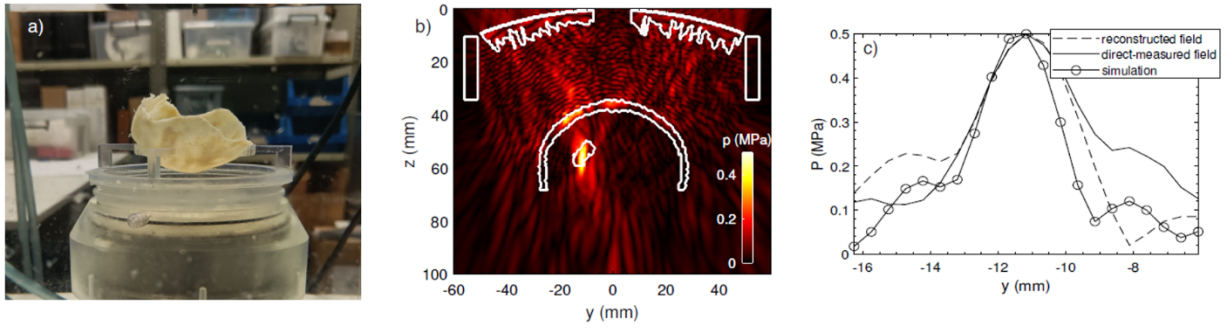


Figure 1. a) Experimental set-up. b) Simulated acoustic field with holographic lens. c) Comparison between simulated and experimental acoustic fields.

Regional Enhancement of Glymphatic Transport by Pulsed Transcranial FUS

Presenter: Seung-Schik Yoo

Authors in order: Seung-Schik Yoo, *The Brigham and Women's Hospital, Harvard Medical School*, Hyun-Chul Kim, *Kyungpook National University*, Jaeho Kim, *Hallym University College of Medicine*, Evgenii Kim, *The Brigham and Women's Hospital, Harvard Medical School*, Kavin Kowsari, *The Brigham and Women's Hospital, Harvard Medical School*, Jared Van Reet, *The Brigham and Women's Hospital, Harvard Medical School*, Kyungho Yoon, *Yonsei University*

We aim to show that acoustic streaming effects of transcranial FUS can regionally enhance convective flow of cerebrospinal fluid, promoting solute transport in the brain.

We applied 200 kHz FUS in both pulsed and continuous modes to induce fluidic flow of soluble dyes (toluidine blue O) to the porous media (melamine foams and agar gels). The pulsing parameter that resulted in the highest dye infiltration was subsequently used in rodent experiments whereby we transcranially applied FUS to a localized brain area and examined the spatial distribution of intracisternally injected fluorescent CSF tracers (2000 kDa FITC-dextran and 45 kDa ovalbumin).

We found that the use of 100 ms pulse duration given at 10% duty cycle and ISPPA of 5 W/cm² generated the greatest dye infiltration at the foam surface. In contrast, sonication did not have any impact on the dye infiltration to agar gel blocks. Fluorescent imaging showed that FUS increased the uptake of ovalbumin at the sonicated brain region, especially around the ventricles (shown in Figure). The spatial distribution of high-molecular weight dextran in the brain was spatially restricted and remained unaffected by the sonication. FUS did not disrupt the blood brain barrier and the animal behavior/histology remained normal.

Regional administration of acoustic pressure waves to the rat brain facilitates cerebrospinal fluid bulk flow into the brain parenchyma, accompanied by the movement of intracisternally injected tracers. Further investigation of the effects of FUS on directly promoting brain solute clearance, as a part of the 'glymphatic' system, is needed.

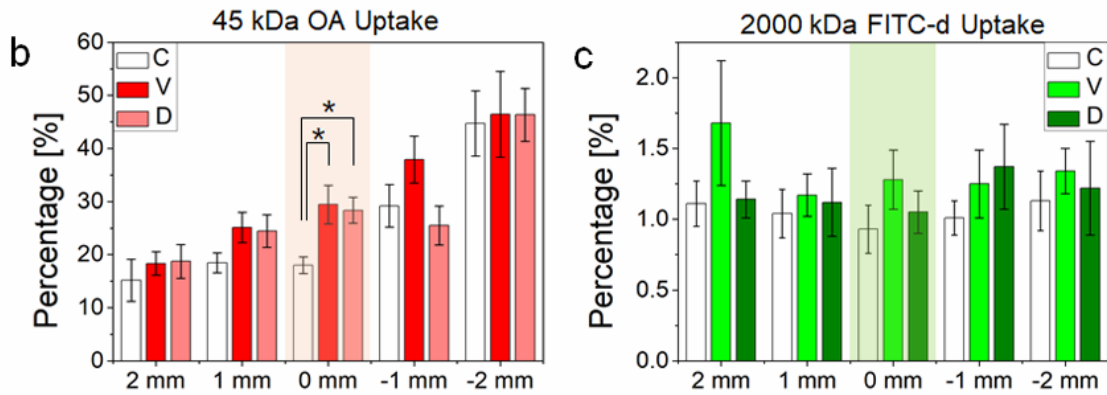
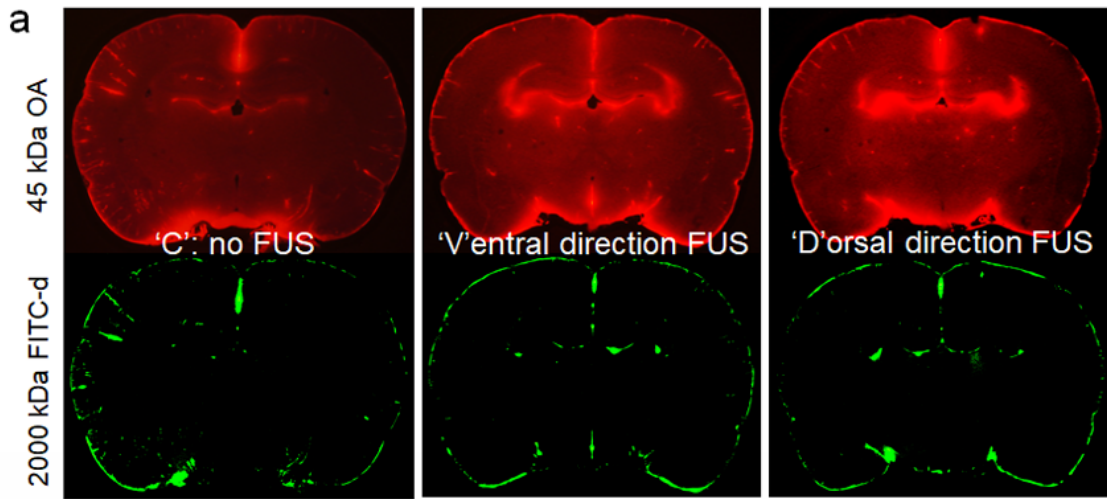


Figure (a) CSF tracer distribution across the experimental condition (b) % uptake of OA and (c) FITC-d (n=6) across the rostral (+) and caudal (-) planes. Colored sections indicate the location of the acoustic focus. *: $p < 0.05$

Machine Learning-based Classification of Focused Ultrasound-stimulated Microbubble Activity in 3D Passive Cavitation Imaging

Presenter: Dallan McMahon

Authors in order: Dallan McMahon, *Sunnybrook Research Institute*, Ryan Jones, *Sunnybrook Research Institute*, Dallas Leavitt, *Sunnybrook Research Institute*, Rohan Ramdoyal, *SRI FUS lab*, Edwin Lee, *Sunnybrook Research Institute*, Wai Meng Kan, *Sunnybrook Health Sciences Centre*, Steven Yang, *Sunnybrook Research Institute*, Yi-Shiuan Chen, *Sunnybrook Research Institute*, Chris Adams, *Sunnybrook Research Institute*, Kullervo Hynynen, *Sunnybrook Research Institute/ University of Toronto*

Compare classification methods for detecting spatially coherent ultraharmonic activity in 3D passive cavitation imaging (PCI) data to calibrate focused ultrasound (FUS) and microbubble-mediated brain therapy.

FUS exposures for increasing blood-brain barrier (BBB) permeability were performed in rabbits (~3 kg) using a 3840-element sparse hemispherical phased array. Following microbubble injection (4 μ l/kg DefinityTM), FUS (258 kHz, 10 ms bursts every 1s) was electronically steered to 8-16 targets, with PCI (128 receiver elements) data collected. Classification of spatially coherent ultraharmonic activity was assessed using fixed imaging parameters (peak sidelobe ratio), logistic regression model, and convolutional neural network (CNN), and compared to manual classification.

Using 3 rabbits (48 targets), fixed imaging parameter thresholds were optimized, and a logistic regression and CNN model were trained to detect manually classified spatially coherent ultraharmonic activity. Each classification method was evaluated retrospectively in 9 rabbits (93 targets) for which the applied acoustic pressure was ramped to levels beyond those required for generating ultraharmonic emissions. CNN-based classification demonstrated the best performance (ie. matching manual classification), with significantly higher F1-scores (F1 = 0.83 \pm 0.09) compared to both fixed imaging parameters (F1 = 0.62 \pm 0.21; $p < 0.05$) and logistic regression model (F1 = 0.70 \pm 0.15; $p < 0.05$).

CNN-based classification can detect spatially coherent ultraharmonic activity with a high degree of precision and recall. These methods may be incorporated within acoustic imaging-based control algorithms designed to calibrate exposure levels for FUS and microbubble-mediated BBB permeability enhancement, and are expected to result in finer control of the induced bioeffects.

We thank S. Rideout-Gros for help with animal care, and S. Gunaseelan, W. Li, K. Leung, J. Zhou, T. Jakaza, A. Rajkumar for technical support.

Array based Focusing to the Human Vertebral Canal using Non-invasive Phase Correction

Presenter: David Martin

Authors in order: David Martin, *University of Toronto*, Rui Xu, *University College London*, Meaghan O'Reilly, *Sunnybrook Research Institute*

The fidelity of two simulation-based phase correction methods for transvertebral focusing applications was explored in ex vivo benchtop experiments.

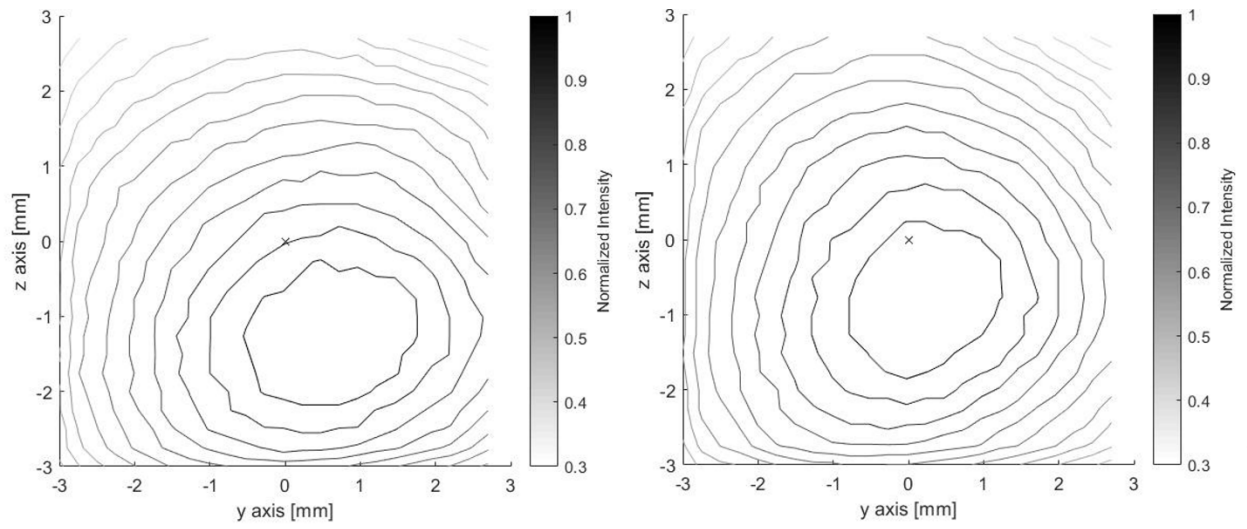
Two simulation models were tested for transvertebral focusing: steady-state ray acoustics (in-house) and a pseudospectral time domain model (kWave). Sound (400 kHz) was propagated in silico from a target location in the vertebral canal to the transducer surfaces of a custom, 64-element phased array. Phase corrections were extracted and applied experimentally for transvertebral focusing in a segment (T7 to T9) of ex vivo human thoracic spine at eight vertical locations (2 mm spacing).

Hydrophone measurements of the focus in the spinal canal were recorded in the transverse and sagittal planes (0.25 mm step size). Geometric (i.e. no correction for bone distortion) focusing and gold-standard hydrophone-based correction were performed for comparison.

Geometric focusing produced mean focal shifts of 1.2 ± 0.4 mm (transverse) and 1.5 ± 0.6 mm (sagittal), while hydrophone correction produced focal shifts of 0.6 ± 0.3 mm (transverse) and 0.7 ± 0.4 mm (sagittal). Simulation-based focusing performed better than geometric but worse than hydrophone correction. Ray acoustics produced foci shifted by 1.1 ± 0.4 mm (transverse) and 1.2 ± 0.5 mm (sagittal), and kWave produced shifts of 1.0 ± 0.5 mm (transverse) and 1.1 ± 0.5 mm (sagittal).

Steady-state ray acoustics and the kWave time domain model produce a comparable partial correction of bone-induced focal shifts in the human vertebral canal. Additional benchtop and in vivo experiments are needed to assess the viability of these methods in therapeutic treatment planning applications.

This work was supported by the Terry Fox Research Institute and NSERC.



Transverse plane of a geometric (left) and kWave-corrected (right) focus.

Focused Ultrasound for Parkinson's Disease: From Evidence to Experience

Presenter: Raul Martinez Fernandez

Authors in order: Raul Martinez Fernandez, *HM CINAC, Hospital HM Puerta del Sur*, Rafael Rodriguez-Rojas, *FUNDACIÓN DE INVESTIGACIÓN HM HOSPITALES. CIF:G83643841*, Marta del Álamo, *HM CINAC (Centro Integral en Neurociencias), University Hospital HM Puerta del- CEU San Pablo University*, Elena Natera-Villalba, *HM CINAC (Centro Integral en Neurociencias), University Hospital HM Puerta del- CEU San Pablo University.*, Carmen Gasca-Salas, *HM CINAC (Centro Integral en Neurociencias), University Hospital HM Puerta del- CEU San Pablo University*, Michele Matarazzo, *HM CINAC (Centro Integral en Neurociencias), University Hospital HM Puerta del- CEU San Pablo University*, Jorge Máñez-Miró, *HM CINAC (Centro Integral en Neurociencias), University Hospital HM Puerta del- CEU San Pablo University.*, Jose Pineda-Pardo, *HM CINAC (Centro Integral de Neurociencias Abarca Campal), Hospital Universitario HM Puerta del Sur, HM Hospitales*, Jose Obeso, *HM CINAC (Centro Integral en Neurociencias), University Hospital HM Puerta del- CEU San Pablo University*

To describe the actual landscape of MRgFUS for the treatment of Parkinson's disease (PD) and, specifically, the evidence on subthalamic nucleus focused ultrasound/thermoablation (MRgFUS-STN)

Two published studies applying unilateral MRgFUS-STN for the treatment of PD included asymmetrical PD patients who were not optimally controlled with medication. The primary outcome was improvement in the motor status of the treated side according to the MDS-UPDRS motor scale. Occurrence of treatment related-adverse events along follow-up was considered the primary outcome of safety. Secondary outcomes included global motor status, motor complications, disability, quality of life, medication use and patient global impression of change.

Two studies have applied unilateral MRgFUS-STN for the treatment of PD. The first, an open-label study including 10 asymmetrical PD patients showed improvements of 52% in the motor features of the treated body side, according to the MDS-UPDRS motor scale. Most secondary outcomes also improved. The second study, a randomized sham-controlled trial enrolling 40 patients demonstrated superiority of MRgFUS-STN as compared to a sham group in terms of motor improvement and in most secondary outcomes. Adverse events in both trials were frequent but mainly mild and were mostly resolved by the last follow-up at 12 months.

MRgFUS ablation is a new therapeutic option for PD. Several targets, including the STN, have shown safety and efficacy and the selection of the most suitable will depend on the clinical phenotype of each patient.

A6-2

Neuromodulation for Drug-resistant Epilepsy by Focused Ultrasound

Presenter: Hsiang-Yu Yu

Authors in order: Hsiang-Yu Yu, *Taipei Veterans General Hospital*, Cheng-chia Lee, Chien-Chen Chou, Hao-Li Liu, *National Taiwan University*, Yen-Cheng Shih

To investigate the safety and efficacy of low intensity focus ultrasound (LIFUS) in patients whose seizure onset zone has been determined in comprehensive presurgical evaluation.

Patients with epilepsy undergoing SEEG for localization of the seizure onset zone (SOZ) were enrolled. FUS was delivered to SOZ using a neuronavigation-guided focused ultrasound system (ceiling ISPTA level = 2.8 Watts/cm², duty = 30%, modulating duration = 10 minutes). Simultaneous SEEG recordings were obtained during sonication and for 3 days after treatment. Seizures, interictal epileptiform discharges, and adverse events after FUS were monitored. A cross-over design was carried out in our phase II study.

In the pilot study, six patients met the eligibility criteria and completed FUS treatment. A decrease in seizure frequency was observed in two patients within the 3-day follow-up; however, one patient presented an increase in the frequency of subclinical seizures. Post-treatment MRI revealed neither lesion nor brain edema. Significant changes in spectral power of SEEG were noted at the targeted electrodes during FUS treatment. One patient reported subjective scalp heating during FUS and one patient developed transient naming and memory impairment which resolved within three weeks after FUS.

The phase II study is now undergoing, and two patients were enrolled.

FUS can be safely delivered to SOZ of patients with DRE, resulting in significant changes in spectral power of SEEG. A larger sample cohort and pursuing optimal sonication parameters will be required to elucidate the neuromodulatory effects of FUS when used for seizure control.

The study was supported in part by NaviFUS Corporations, Taiwan Ministry of Science and Technology (107-2314-B-075-059-MY3 and 109-2314-B-075-053), and National Health Research Institutes (NHRI-EX109-10905NI, NHRI-EX110-11006NC).

A6-3

Focused Ultrasound in Brain Cancer: Early Human Experience and Emerging Applications

Presenter: Nir Lipsman

Authors in order: Nir Lipsman, *Sunnybrook Health Sciences Centre*

Focused ultrasound mediated BBB opening offers important opportunities for the safe, effective and targeted delivery of large molecule therapeutics for a wide range of brain pathologies.

To date, pilot phase I trials in human brain cancer have shown that FUS BBB opening is safe, reversible and well tolerated, with no serious adverse events. To provide the first primary evidence of target engagement across the BBB, we performed a single-arm open-labeled study in four patients with progressive Her2+ breast cancer metastases who underwent infusion of 111-Indium labelled trastuzumab.

Twenty treatments combining transcranial FUS with concomitant intravenous trastuzumab-based therapies were administered as outpatient procedures in four patients. There were no clinical or radiographic serious adverse events. On average FUS-treated lesions saw an SUVR increase of 100% compared to baseline, with 87% of sonicated voxels seeing at least a 20% increase in uptake, with some voxels seeing a 450% increase. Following treatment, unidimensional tumor measurements decreased on average by 19%. While this trial provides the first evidence of target engagement, previous trials in human brain cancer have also provided compelling data supporting the safety, feasibility and tolerability of serial FUS BBB opening.

The first FUS trials in human cancer patients provide strong evidence of noninvasive, spatially targeted large molecule therapeutic delivery across a temporarily permabilized BBB. In doing so, these results demonstrate the promise of this technology for a broad range of CNS diseases.

Harquail Centre for Neuromodulation, Sunnybrook Foundation, Focused Ultrasound Foundation, InSightec, CIHR

Pilot Study of Blood-brain Barrier Disruption in Alzheimer's Disease

Presenter: Michael Canney

Authors in order: Michael Canney, *Carthera*, Stephane Epelbaum, Ninon Burgos, *CNRS - Paris Brain Institute*, Dawn Matthews, Marion Houot, Mathieu Santin, *ICM*, Carole Desseaux, Guillaume Bouchoux, Cyril Martin, Marie-Odile Habert, *Hospital Pitié-Salpêtrière*, Marcel Levy, Karine Martin, *Assistance Public Hopitaux de Paris (AP-HP)*, Benoit Delatour, *Paris Brain Institute*, Maximilien Riche, Bruno Dubois, *APHP*, Lisa Belin, Alexandre Carpentier, *France*

Temporary disruption of the blood-brain barrier (BBB) using pulsed ultrasound leads to the clearance of both amyloid and tau from the brain in preclinical models.

An implantable, 1 MHz ultrasound device (SonoCloud-1) was implanted under local anesthesia in the skull of 10 mild AD patients to target the left supra-marginal gyrus. Over 3.5 months, seven ultrasound sessions in combination with intravenous infusion of microbubbles were performed twice per month to temporarily disrupt the BBB. PET imaging was performed on a combined PET/MRI scanner to monitor brain metabolism and amyloid levels.

A total of 63 BBB opening procedures were performed in nine subjects. The procedure was well-tolerated. A slight decrease in amyloid accumulation at four months of -6.6% (SD=7.2%) on 18F-Florbetapir PET imaging in the sonicated gray matter targeted by the ultrasound transducer was observed compared to baseline in six subjects that completed treatments and who had evaluable imaging scans. No significant effect on cognition evolution was observed.

These results demonstrate the safety of ultrasound-based BBB disruption and potential of this technology to be used as a therapy for AD patients.

This project was realized with the support of BPI France.

Combination of Neuronavigation-guided Focused Ultrasound and Bevacizumab for Patients with recurrent Glioblastoma

Presenter: Ko-Ting Chen

Authors in order: Ko-Ting Chen, *Chang Gung Memorial Hospital*, Hao-Li Liu, *National Taiwan University*, Kuo-Chen Wei, *Chang Gung Memorial Hospital*

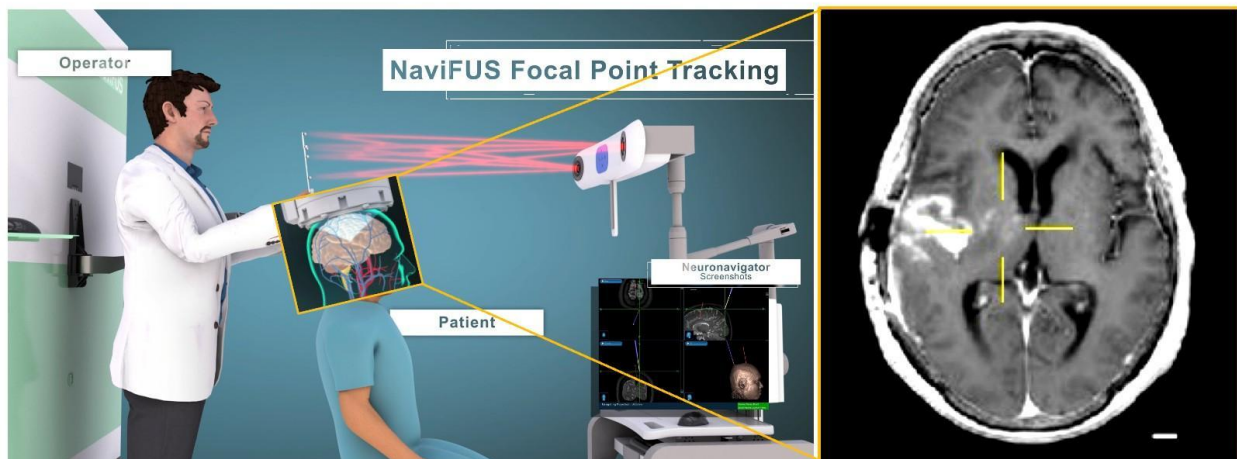
This study aims to evaluate the safety and efficacy of Bevacizumab (BEV) + focused ultrasound with microbubbles (MB-FUS) for treating patients.

This is a phase IIa, open-label, single-arm clinical trial (NCT04446416). We aim to include 10 rGBM patients completing chemoradiation therapy with their first recurrence. The MB-FUS is planned to be an add-on modality to the bi-weekly BEV therapy for up to 18 sessions (34 weeks). The primary endpoint is 6-month progression free survival (PFS) and the secondary endpoints are tumor control and overall survival.

The enrollment is ongoing. Currently, the first 4 patients with their period of treatment >3 months (>6 sessions of BEV-FUS) are summarized. Subject 01 completed 17 sessions of treatment (miss one BEV due to proteinuria) without disease progression (PD); subject 02 had PD with a PFS of 5 months (8 sessions); subject 03 (12 sessions) and 04 (7 sessions) remain in the ongoing trial with a response of complete response and stable disease, respectively. An evaluation of the relation between FUS beampaths and T2 high signal regions revealed a trend of normalizing T2 hyperintensity at beampath-concentrated regions.

We report the preliminary result of combined BEV-FUS for rGBM treatment. Results have demonstrated the safety, feasibility, and a potential to decrease edema or tumor invasion by the mechanism of enhance bevacizumab delivery to the treated site. The preliminary results are encouraging. More data are needed to proof the efficacy.

Neuronavigation-guided focused ultrasound system for BBB opening



Combining Accelerometer and Handwriting Biomarkers towards the Evaluation of the Tremor with MRgFUS Thalamotomy

Presenter: Hongchae Baek

Authors in order: Hongchae Baek, *Cleveland Clinic Foundation*, Daniel Lockwood, *Cleveland Clinic Foundation*, Emmanuel Obusez, *Cleveland Clinic Foundation*, Matthew Poturalski, *Cleveland Clinic Foundation*, Sean Nagel, *Cleveland Clinic Foundation*, Stephen Jones, *Cleveland Clinic Foundation*

To evaluate a quantitative analysis tool measuring tremor reduction in patients' handwriting during and after MRgFUS thalamotomy.

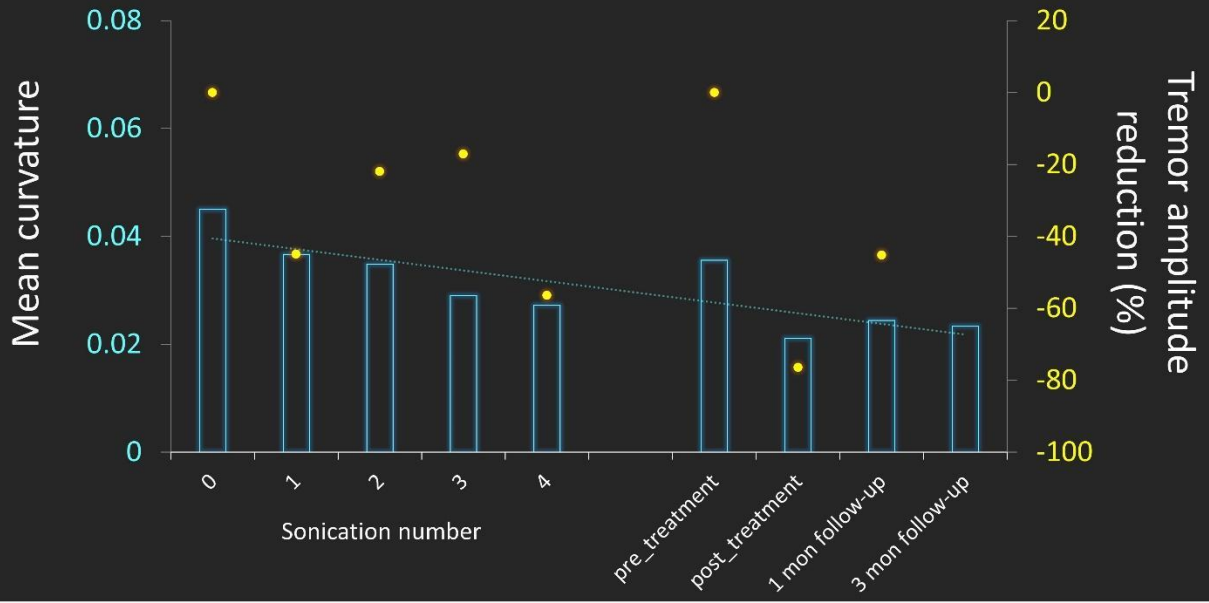
Throughout MRgFUS thalamotomy patients are tested for tremor by writing their name, drawing spirals and lines. During these tests we simultaneously measured the tremor amplitude using MRI compatible accelerometers on finger, forearm, and arm.

Post-treatment analysis of drawings used custom software written using IDL, measuring 7 different features, including line length and curvature, that characterize the severity of tremor. These measurement can be performed remotely long after the procedure to measure the amount of recurrence.

The correlation between RMS amplitude from accelerometer measurements and the biomarkers from handwriting/drawing was calculated in 10 essential tremor (ET) and 5 Parkinson's disease (PD) patients. A high correlation in Archimedes spiral metrics was found in 72% of ET, and a high correlation in a line drawing metrics was found in 60% of PD. These results indicate that biomarkers of Archimedes spiral are effective to detect ET tremor change, whereas biomarkers of line drawing are effective to detect PD tremor change. We estimated 10% tremor recurrence from a patient's 3-month follow-up sheet, where they self-reported their tremor reoccurrence as 15%.

We identified biomarkers of quantitative analysis method that characterize ET and PD tremor in handwriting/drawing. We demonstrated the reliability of the biomarkers by correlating the scores with accelerometer tremor amplitudes. Drawing sheets are being mailed for patients' follow-up and are currently used to estimate treatment durability using the quantitative analysis.

Archimedes spiral drawing in a essential tremor patient



Early Outcomes from First-in-Human Use of Low Intensity Focused Ultrasound in Depressed Patients

Presenter: Amanda Arulpragasam

Authors in order: Amanda Arulpragasam, *Brown University/VA Providence*, Christiana Faucher, *Providence VA Health Care System*, Emily Aiken, *VA Providence Healthcare System*, Mascha van 't Wout-Frank, *VA Providence Healthcare System*, Stephen Mernoff, *VA Providence Healthcare System*, Stephen Correia, *VA Providence Healthcare System*, Ryan Van Patten, *VA Providence Healthcare System*, Jennifer Barredo, *VA Providence Healthcare System*, Benjamin Greenberg, *VA Providence Healthcare System*, NOAH PHILIP, *Alpert Medical School of Brown University & VA Providence*

This report describes preliminary outcomes from our first-in-human study of low intensity focused ultrasound (LIFU) targeting the amygdala in patients with depression (U01MH123427).

Three male patients (ages 53-63) received MRI-guided LIFU (fundamental frequency: 650 kHz, PRF: 10Hz, pulse-width: 5ms, 20 sonications, 30s on/off, ISPTA.3: 719 mW/cm²) targeting the amygdala or control region (S1) separated by ≥ 1 -week in a controlled, crossover design. Participants were assessed at 24-hours and 1-week post-LIFU. Safety assessments included clinical MRIs, psychiatric, neurologic, and neuropsychological evaluation. Arterial spin labeling (ASL) MRI was acquired at baseline and immediately after LIFU to assess regional brain perfusion.

Clinical MRIs revealed no injury, and no clinically significant changes were observed during neurological or neuropsychological assessments. Side effects included reported headache (n=3) and sedation (n=1); all were time-limited and fully resolved. Participants reported meaningful improvements in mood, noticeable 24 hours after amygdala-targeted LIFU. All participants demonstrated reduction in right amygdala relative blood flow on ASL; with a 39%, 25%, or 14% perfusion decrease in patients 1, 2, and 3, respectively. These changes were not observed when LIFU targeted the control S1 region.

The results represent an early indication of LIFU's ability to safely and focally modulate the amygdala in patients with depression, with mild and transient side effects. With further study of neural effects, relationship with clinical symptom change, and safety, LIFU may be a transformative technology in neuropsychiatric research and treatment.

A6-8

Ultrasonic Deep Brain Neuromodulation in Disorders of Consciousness

Presenter: Joshua Cain

Authors in order: Joshua Cain, *UCLA*, Martin Monti

We investigate the impact of magnetic resonance (MR)-guided LIFU applied to the thalamus on brain activity and neurobehavioral measures in disorders of consciousness (n=21).

Acute patients (n=11) underwent 1, 10 minute MRg-LIFU session, while chronic patients (n=10) underwent two, one week apart.

Behavioral responsiveness was assessed at baseline (1 hour, 1 day, 1 week prior) and following (1 hour, 1 day, 1 week following) LIFU.

Concurrent fMRI data was used to assess the biological origins of observed recovery.

Both cohorts show significant improvements in responsiveness following thalamic LIFU. Interestingly, this appears to emerge only after the first (1-hour post LIFU) period.

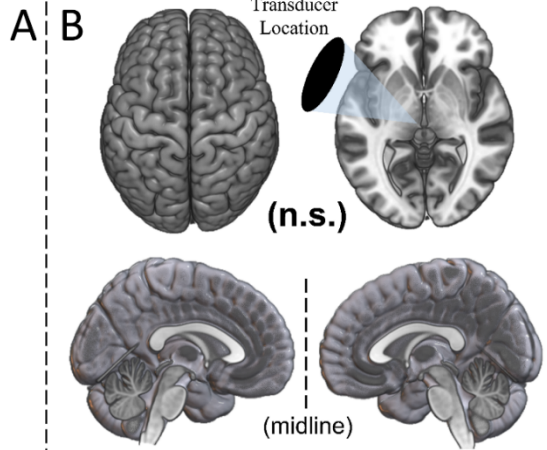
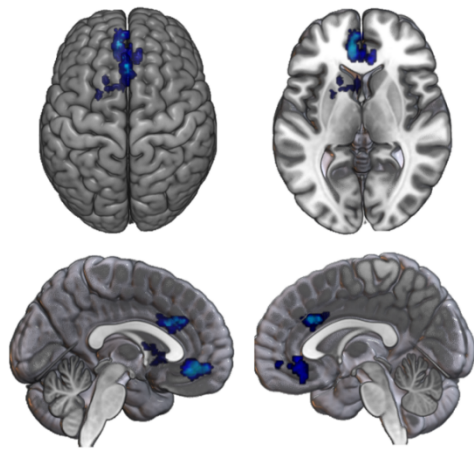
We observe inhibition of BOLD signal in several clusters during LIFU in both cohorts with inhibition of the ventral striatum predicting recovery in chronic patients. Changes in connectivity were found between the targeted thalamus and the rest of the brain for both cohorts but not between the untargeted thalamus and the rest of the brain. Changes in connectivity predicted recovery throughout large areas of association cortex for both cohorts.

We find preliminary evidence for the safety and feasibility of LIFU in DOC. The acute effect of LIFU may be inhibitory at these parameters, in line with prior investigations. However, these data emphasize the role of changes in connectivity with the thalamic target in the behavioral recovery of subjects.

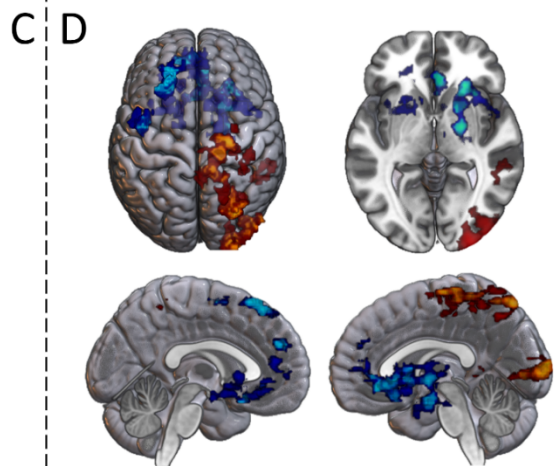
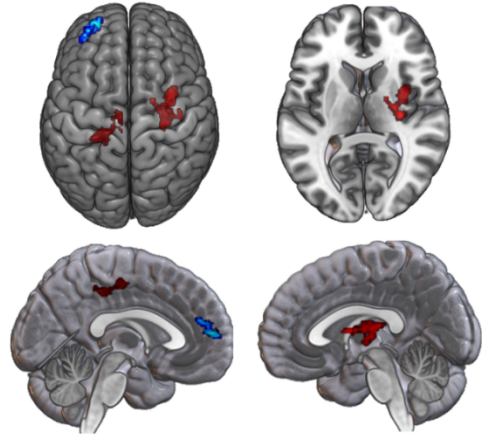
Change During LIFU Blocks

Change Associated with Recovery

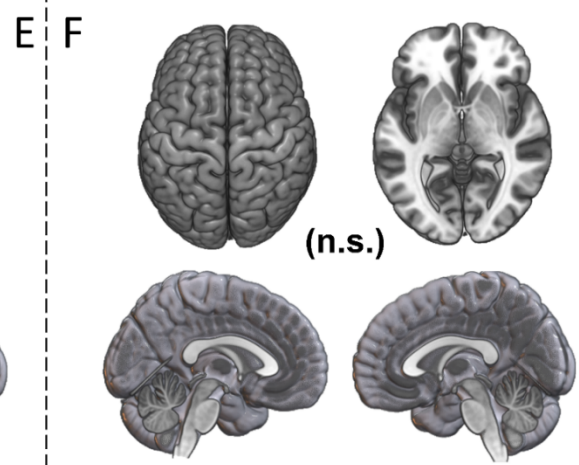
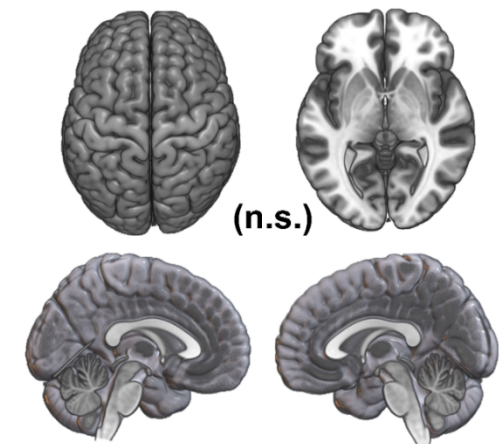
Activity (BOLD Signal)



Connectivity with Target
Thalamus



Connectivity with Control
Thalamus



Ultrasound-based BBB Opening Leads to Drug Penetration in the Human Brain

Presenter: Adam Sonabend

Authors in order: Adam Sonabend, *Northwestern Medicine Malnati Brain Tumor Institute of the Lurie Comprehensive Cancer Center, Feinberg School of Medicine, Northwestern University*, Andrew Gould, *Northwestern University*, Yu Luan, *Northwestern Medicine*, Ye Hou, *Northwestern Medicine*, Li Chen, *Northwestern University*, Mikoto Kobayashi, *Northwestern Medicine*, Brandyn Castro, *Northwestern Medicine*, Daniel Zhang, *Northwestern Medicine*, Farida Korobova, *Northwestern Medicine*, Christina Amidei, *Northwestern Medicine*, Mark Youngblood, *Northwestern Medicine*, John Bebawy, *Northwestern Medicine*, Benjamin Liu, *Northwestern Medicine*, Craig Horbinski, *Northwestern Medicine*, Carole Desseaux, Irene Helenowski, *Northwestern Medicine*, Hui Zhang, *Northwestern Medicine*, Miguel Muzzio, *Illinois Institute of Technology Research Institute (IITRI)*, Feng Yue, *Northwestern Medicine*, Michael Canney, *Carthera*, Roger Stupp, *Northwestern Medicine*

Ultrasound-based BBB opening to deliver drugs to the brain is under investigation. The effect sonication on drug penetration to the human brain remains unknown.

We evaluated the effects of ultrasound-based BBB opening on drug concentrations in the human brain. As part of clinical trials using skull-implantable ultrasound for BBB opening in gliomas, we performed intraoperative pharmacokinetic studies with brain sonication and administration of carboplatin or paclitaxel, where drug was quantified on targeted brain biopsies. For this, ultrasound-based BBB opening in the peri-tumoral brain was visualized and mapped using fluorescein. Electron microscopy and single-cell transcriptomic analyses were performed in the tissue.

Targeted biopsies of peri-tumoral-brain with BBB opening showed a several fold increase in tissue paclitaxel and carboplatin concentrations. BBB opening was associated with ultra-structural alterations in brain capillary endothelial cells, and transcriptional dysregulation of membrane transporters, pathways related to trans-cytosis, cell permeability as well as cell-cell and cell-matrix adhesion in brain endothelial cells.

The BBB opening using skull-implantable ultrasound can enhance the penetration of chemotherapeutic drugs in large regions of the brain, a procedure that can be performed repeatedly and safely. Ultrasound-based BBB opening leads to ultrastructural and transcriptional alterations in brain endothelial cells.

NIH/NCI 1R01CA245969-01A1, Carthera (SC9 devices), Celgene/BMS (Abraxane), Malnati Brain Tumor Institute, Mocerri Family Foundation.

A7-1

Engineering Viral Vectors for Acoustically Targeted Gene Delivery

Presenter: Hongyi Li

Authors in order: Hongyi Li, *California Institute of Technology*, Mikhail Shapiro, *Caltech*

We aim to apply high-throughput in vivo selection to engineer novel AAV vectors specifically for local neuronal transduction at the sites of focused ultrasound blood-brain-barrier opening (FUS-BBBO).

We employ an in vivo viral evolution method: a library of AAVs with mutated capsids based on AAV9 (Fig. 1a) is injected intravenously into hSyn1-Cre mouse and delivered via FUS-BBBO to one hemisphere. When a particular AAV variant transduces Cre-expressing neurons, its viral genome is modified, becomes detectable by a Cre-dependent PCR and Next-generation Sequencing (NGS) (Fig. 1b). Repeated rounds of selection for vectors uniquely appear in the targeted hemisphere lead to desired novel AAV vectors for objectives.

Histological analysis revealed higher efficiency of transduction in the brain for all final 5 viral variants (AAV.FUS.1-5) (Fig. 2a,b; up to 130% improvement over AAV9). Each serotype transduced the liver less strongly (Fig. 2c,d; up to 6.8-fold reduction compared to AAV9). The top AAV.FUS variant (AAV.FUS.3) showed 12.1-fold improvement in overall tissue specificity (Fig. 2e). All candidates show improved neuronal tropism as well: AAV.FUS.3 has a 69.8% likelihood of transducing a neuron, compared to 44.7% for AAV9 (Fig. 2f,g,h). Our screen yielded AAV.FUS.3, the first viral vector expressly engineered to work in conjunction with ultrasound-mediated gene delivery to the brain.

Overall, this study shows that the molecular engineering of AAV capsids can lead to improved noninvasive, site-specific ultrasound-mediated gene delivery to the brain. Our screen yielded AAV.FUS.3, the first viral vector expressly engineered to work in conjunction with the specific physical delivery method (FUS-BBBO).

The authors thank Viviana Gradinaru lab, and the CLOVER center at Caltech for helpful discussions. Thanks to Prof. Mikhail Shapiro and Jerzy Szablowski for extraordinary mentorship.

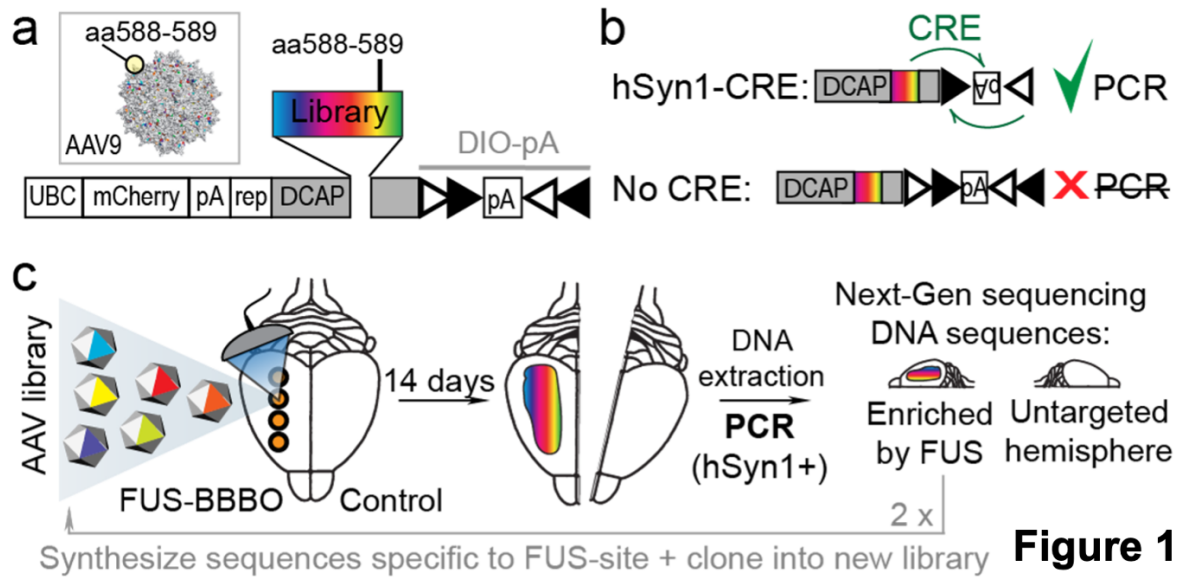


Figure 1

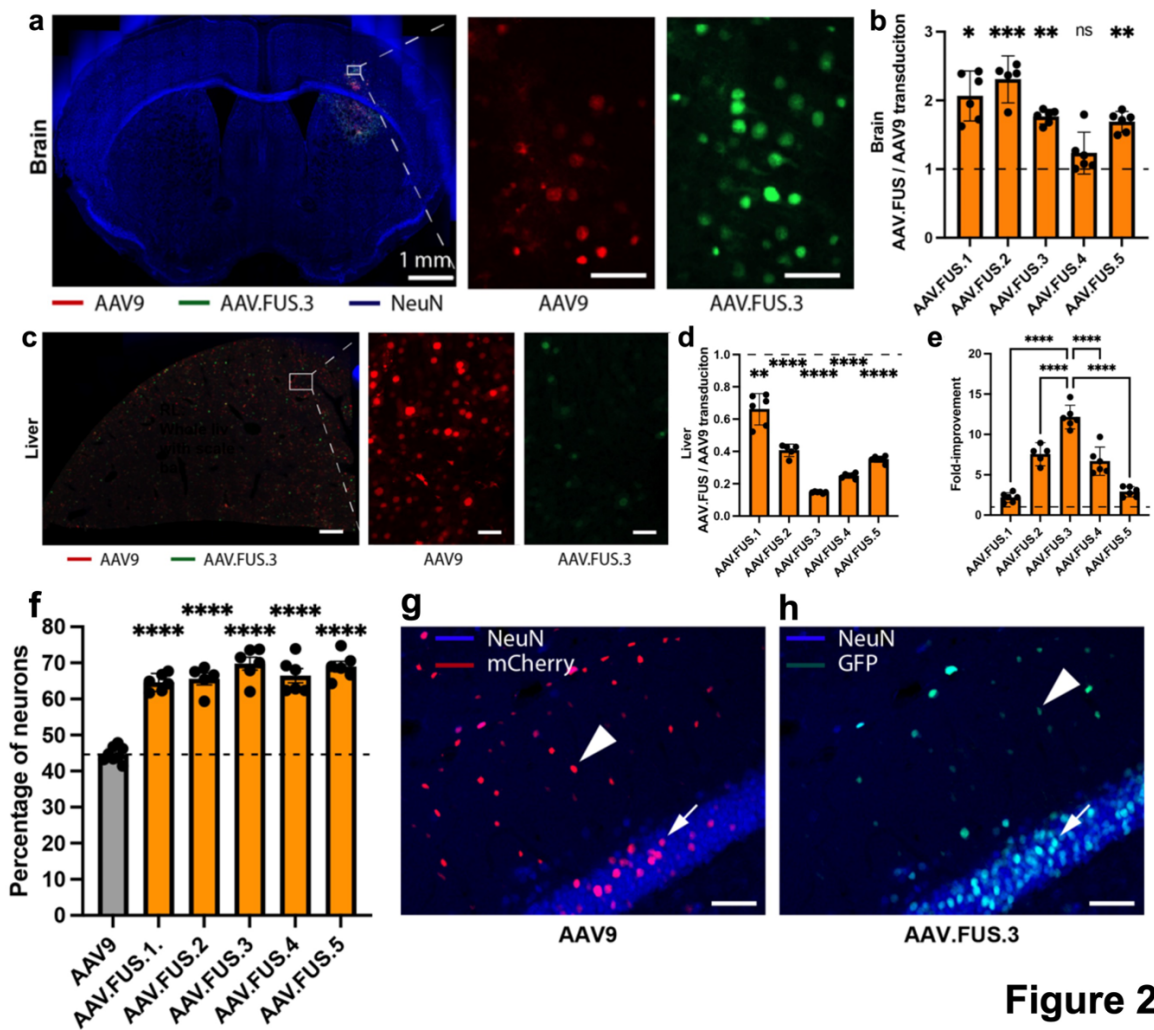


Figure 2

A7-10

Effects of Single and Repeated FUS-mediated BBB Disruption Treatments on Neuroinflammation and Neurovascular Coupling

Presenter: Nick Todd

Authors in order: Cleide Angolano, *Beth Israel Deaconess Medical Center*, Xiaojie Chen, *Boston University*, Emily Martin, *Boston University*, Natalie Fomin Thunemann, *Boston University*, Martin Thunemann, *Boston University*, Christiane Ferran, *Beth Israel Deaconess Medical Center*, Anna Devor, *Boston University*, Nick Todd, *Brigham and Women's Hospital*

To characterize changes in neuroinflammation and the neurovascular response after single and 5x-repeated focused ultrasound blood-brain barrier disruption treatments in mice.

FUS-BBB opening was targeted to left striatum or left barrel field cortex in mice. Mice underwent either single session treatment or five weekly-spaced treatments. For neuroinflammation assessment, groups of N=8 were sacrificed at 1, 6, and 24-hrs post-treatment and a panel of inflammatory markers were obtained from both hemispheres. For neurovascular coupling assessment, mice with cranial windows and expressing the calcium indicator jRGECO1a will undergo optical imaging to quantify neuronal and hemodynamic responses.

BBB disruption was consistently seen in the targeted hemisphere as measured by trypan blue (~67 kDa) and Immunoglobulin G (~150 kDa) (Figure 1A). For single session FUS treatment, the only inflammatory marker with significantly elevated mRNA level was CCL2. For 5x treatments, a trend was observed across several pro-inflammatory markers of decreased levels, and two anti-inflammatory markers, A20 and eNOS, were seen to be elevated (Figure 1B). Measurements of the neurovascular response to a whisker air puff stimulus after BBB disruption are set to be performed (Figure 1C).

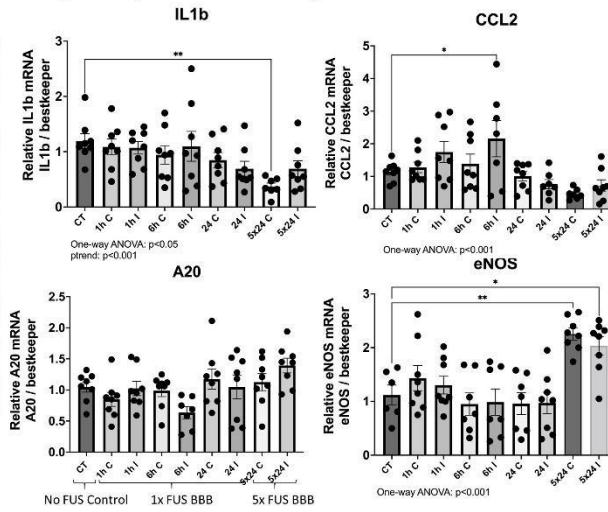
FUS treatments sufficient to deliver kDa size molecules across the BBB can be performed repeatedly (at least 5 times) with minimal inflammatory response, and possibly induce a pre-conditioning anti-inflammatory response. Neuronal and hemodynamic signals will be measured to determine whether or not significant changes are present.

This work is supported by NIH grant 1R21EB030173.

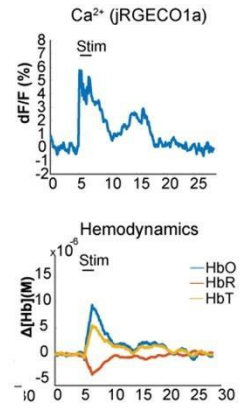
A) Example BBB disruption



B) Example inflammatory markers



C) Example calcium signal and hemodynamic signals



Quantitative Determination of FUS-induced BBB Permeability using PET Imaging

Presenter: Anthony Novell

Authors in order: Gaelle Hugon, *BioMaps*, Sebastien Goutal, *BioMaps*, *Université Paris Saclay*, *CEA*, *CNRS*, *Inserm*, Ambre Dauba, *Université Paris Saclay*, Louise Breuil, *BioMaps*, *Université Paris Saclay*, *CEA*, *CNRS*, *Inserm*, Benoit Larrat, *CEA*, Alexandra Winkeler, *CEA*, Anthony Novell, *BioMaps*, *Université Paris Saclay*, *CEA*, *CNRS*, *Inserm*, Nicolas Tournier, *Paris-Saclay University*, *CEA*, *CNRS*, *Inserm*

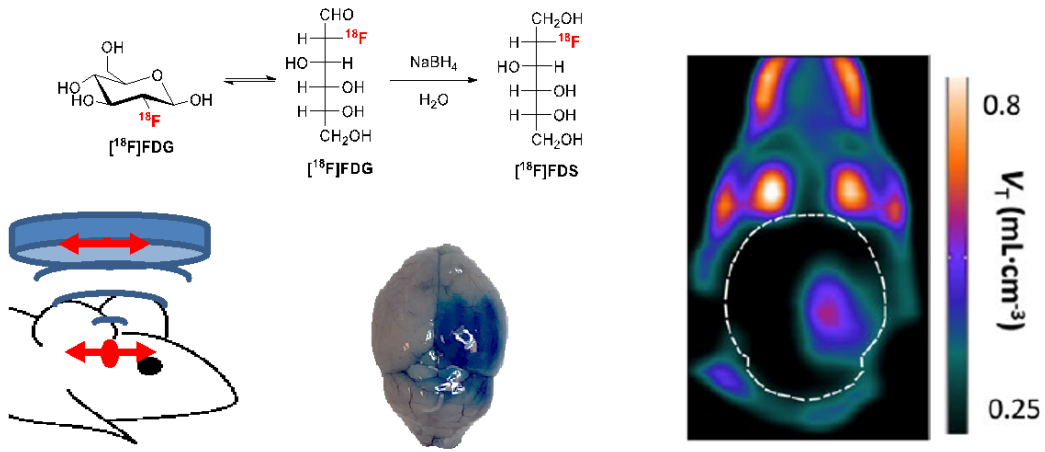
Translational and quantitative imaging techniques are required to monitor the impact of FUS on BBB permeability. [18F]2-fluoro-2-deoxy-sorbitol ([18F]FDS) was evaluated as marker of BBB integrity.

[18F]FDS can be straightforwardly produced from chemical reduction of commercial [18F]FDG. Five mice underwent an optimized FUS method designed to generate spatially controlled BBB disruption (raster scan) in the right hemisphere. The FUS protocol was composed of microbubbles administration (SonoVue®, 50µL) and ultrasonic waves transmitted for 120s at 1.5MHz (duty cycle: 71%; in situ peak negative pressure: 420kPa) synchronized with beam displacement with. Evan's Blue (EB 100µL) and [18F]FDS (4.2±0.76MBq) were intravenously injected before PET imaging.

PET kinetics of [18F]FDS in each brain hemisphere were described by a 1-tissue compartment model using an image-derived input function. BBB disruption resulted in a 2.4±0.8-fold increase in the brain distribution (VT, p [18F]FDS. Low variability (coefficient of variation = 10.1%) of VT in the sonicated hemisphere of the FUS group suggests limited variability of the estimation of BBB permeability and exquisite reproducibility of the FUS method. One hour after FUS, animals were euthanized and brains were removed to visually confirm EB extravasation.

Thanks to the quantitative performance of PET compared with other neuroimaging techniques, [18F]FDS PET provides a readily available, sensitive and reproducible method to non-invasively monitor BBB permeability after FUS in various conditions in vivo.

We thank Maud Goislard for helpful technical assistance.



Focused ultrasound

Evan's Blue

[¹⁸F]FDS PET imaging

Theranostic Ultrasound-mediated Blood-brain Barrier Opening and Viral Delivery with a Novel Pulse Sequence

Presenter: Alec Batts

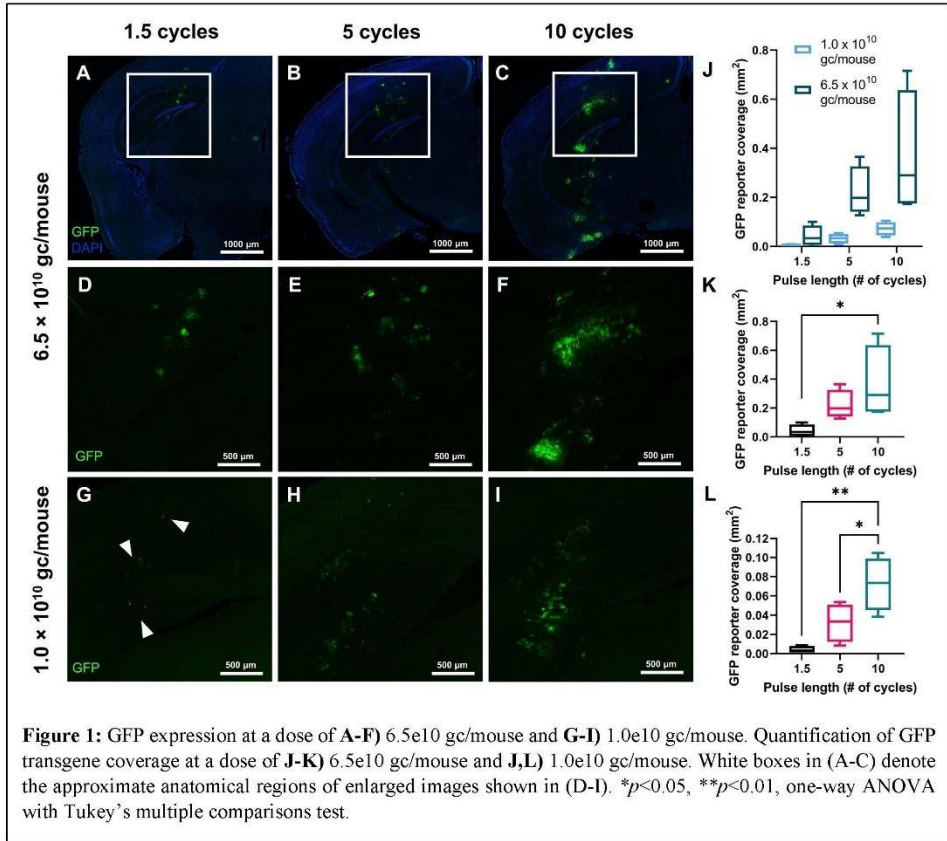
Authors in order: Alec Batts, *Columbia University*, Robin Ji, *Columbia University*, Rebecca Noel, *Columbia University*, Alina Kline-Schoder, *Columbia University*, Nancy Kwon, *Columbia University*, Elisa Konofagou, *Columbia University*

This study aims to characterize the gene delivery potential of theranostic ultrasound-mediated blood-brain barrier opening (BBBO) in mice using a novel bilateral sonication pulse sequence.

A P4-1 (Philips) phased array (1.5 MHz Tx frequency, 1.0 MPa derated peak-negative pressure, $\pm 3.72^\circ$ electronic steering angles), was operated by a custom Verasonics MATLAB script to employ the rapid alternating steering angles (RASTA) pulse sequence for bilateral viral delivery (AAV9-CAG-GFP) at two systemic doses: 6.5×10^{10} gc/mouse and 1.0×10^{10} gc/mouse. RASTA consists of interleaved focused transmits deployed on the right and left hemispheres with hemisphere-specific short pulse lengths (1.5, 5, and 10 cycles).

GFP reporter transgene expression was detectable with fluorescence microscopy on coronally-oriented brain sections 4 weeks after BBBO with TUS RASTA at both AAV9 dose groups, with increasing GFP expression observed with pulse length (Fig. 1A-I). 1.5, 5 and 10-cycle pulse lengths elicited GFP reporter coverage dependent on pulse length ranging from 0.042 mm^3 - 0.367 mm^3 at a dose of 6.5×10^{10} gc/mouse (Fig. 1D-F, K), and 0.004 mm^3 - 0.014 mm^3 at a dose of 1.0×10^{10} gc/mouse (Fig. 1G-I, L). A 6.5-fold increase in AAV dose yielded an average 7.5-fold increase in GFP reporter gene expression across all pulse lengths evaluated (Fig. 1J).

TUS RASTA in conjunction with systemically administered AAV9 presented a novel bilateral gene delivery platform within a single diagnostic imaging array configuration. Such a platform could provide a computationally flexible alternative to existing preclinical ultrasound-guided focused ultrasound (USgFUS) systems currently employed for viral delivery to the brain.



Real-time Intravital Imaging of the Vascular effects induced by Acoustic Cluster Therapy (ACT®) in a Murine Brain

Presenter: Melina Mühlenpfordt

Authors in order: Melina Mühlenpfordt, *NTNU*, Emma Bøe Olsen, *Department of Physics, Norwegian University of Science and Technology, Trondheim, Norway*, Spiros Kotopoulos, *National Centre for Ultrasound in Gastroenterology, Haukeland University Hospital, Bergen, Norway*, Sverre Torp, *Department of Pathology, St. Olavs Hospital, Trondheim University Hospital, Trondheim, Norway*, Sofie Snipstad, *Department of Physics, Norwegian University of Science and Technology; Department of Biotechnology and Nanomedicine, SINTEF Industry; Cancer Clinic, St. Olav's Hospital, Trondheim, Norway*, Catharina Davies, *Department of Physics, Norwegian University of Science and Technology, Trondheim, Norway*, Marieke Olsman, *Department of Physics, Norwegian University of Science and Technology, Trondheim, Norway*

Acoustic Cluster Therapy (ACT®) increased blood brain barrier (BBB) permeability. The aim was to study ACT®-induced changes in BBB permeability using real-time intravital microscopy.

Healthy mice underwent an open skull cranial window surgery to obtain optical access to the brain. Subsequent imaging of the brain during ACT® was achieved by aligning the cranial window with a ring transducer and a 20× objective. Fluorescein isothiocyanate (FITC)-labelled 2 MDa dextran were intravenously injected to study ACT®-induced vascular effects in the murine brain. The safety of the treatment was assessed by histology and immunohistochemistry staining of the vasculature.

The large ACT® bubbles (25 µm in diameter) observed in the brain induced a transient and local increase in FITC-dextran fluorescence intensity inside the blood vessels. Furthermore, a reduction and expansion of blood vessel diameter was observed. Extravasation occurred from ACT®-induced outpouchings in the vessel wall, varying in size and with heterogenous distribution of FITC-dextran in the brain parenchyma. Real-time observations as well as histology showed no haemorrhage. Most blood vessels remained functional.

Real-time intravital imaging of the brain vasculature during ACT® increased our understanding of the mechanism behind ACT®-induced increased BBB permeability. This is the first-time extravasation is reported to occur from outpouchings in the vessel wall. The study gave novel insights for future therapeutic applications of ACT® for neurological diseases.

The project was greatly supported by EXACT Therapeutics AS (Oslo, Norway) and funded by the Research Council of Norway Nano2021 262228.

A7-14

Effects of Aducanumab and Scanning Ultrasound on Amyloid Plaques and Behavior in the APP23 Mouse Model of Alzheimer Disease

Presenter: Gerhard Leinenga

Authors in order: Gerhard Leinenga, *The University of Queensland*, Wee Kiat Koh, Jürgen Götze, *University of Queensland*

We tested how the effects of focused ultrasound blood-brain barrier opening on plaques and behavior compare to aducanumab immunotherapy in APP23 mice and if the combination is effective.

In a study comprising four treatment arms, we tested the efficacy of an Aducanumab analog (Adu) both in comparison to SUS, and as a combination therapy, in APP23 mice (aged 13-22 months), using sham as a control. The active place avoidance (APA) test was used to test spatial memory, and histology and ELISA were used to measure amyloid. Brain Adu levels were also determined

We found that both Adu and SUS reduced the total plaque area in the hippocampus with no additive effect observed with the combination treatment (SUS + Adu). Whereas in the cortex where there was a trend towards reducing the total plaque area from either Adu or SUS, only the combination treatment yielded a statistically significant decrease in total plaque area compared to sham. Only the SUS and SUS + Adu groups included animals that had their plaque load reduced to below 1% from above 10%. There was a robust improvement in spatial memory for the SUS + Adu group only,

These findings suggest that SUS should be considered as a treatment option for AD. Alternatively, a combination trial using Aducanumab together with ultrasound to increase brain levels of the antibody may be warranted.

We acknowledge support by the Estate of Dr. Clem Jones AO, the National Health and Medical Research Council of Australia and the State Government of Queensland.

Oxygen-loaded Nanodroplets Enhance Cerebral Ablation in Sonodynamic Therapy

Presenter: Harriet Lea-Banks

Authors in order: Harriet Lea-Banks, *Sunnybrook Research Institute*, Sheng-Kai Wu, *Sunnybrook Research Institute*, Hannah Lee, *Sunnybrook Research Institute*, Kullervo Hynynen, *Sunnybrook Research Institute/ University of Toronto*

To enhance tissue damage by locally delivering oxygen during sonodynamic therapy using ultrasound-sensitive oxygen-loaded nanodroplets in healthy rat brain.

Oxygen-loaded volatile nanodroplets (250 +/- 8 nm) were formed by condensing lipid-shell decafluorobutane microbubbles, and significantly increased the dissolved oxygen content of the injectate (27 +/- 2 mg/L). The right striatum of 16 healthy rats was sonicated following an intravenous dose of 5-ALA (200 mg/kg), followed by saline, nanodroplets, or oxygen-loaded nanodroplets. MR imaging and histology were performed to assess haemorrhage, edema and cell apoptosis immediately following, 24 hr, and 48 hr after treatment.

Here we show that by locally delivering oxygen during treatment, using oxygen-loaded perfluorocarbon nanodroplets, we can enhance the toxicity of 5-ALA, and monitor the severity of damage by recording acoustic emissions in the brain. The localized volume of damaged tissue was significantly enhanced by the presence of oxygen nanodroplets, compared to ultrasound with unloaded nanodroplets (3-fold increase), and ultrasound alone (40-fold increase). Sonicating 1 hr following 5-ALA injection was found to be more potent than 2 hr following 5-ALA injection (2-fold increase), and the severity of tissue damage corresponded to the cavitation activity from acoustic droplet vaporization.

Enhancing the local toxicity of 5-ALA with monitored cavitation activity and oxygen delivery could have significant implications in the treatment of atherosclerosis and non-invasive ablative surgeries.

Gene Delivery using Ultrasound-mediated Blood-brain Barrier Opening

Presenter: Benoit Larrat

Authors in order: Marie-Solenne Felix, *Aix-Marseille University*, Emilie Borloz, *Aix-Marseille University*, Khaled Metwally, *Aix-Marseille University*, Ambre Dauba, *Université Paris Saclay*, Benoit Larrat, *CEA*, Valerie Matagne, *Aix-Marseille University*, Yann Ehinger, *Aix-Marseille University*, Laurent Villard, *Aix-Marseille University*, Anthony Novell, *BioMaps, Université Paris Saclay, CEA, CNRS, Inserm*, Serge Mensah, *Aix-Marseille University*, Jean-Christophe Roux, *Aix-Marseille University*

Focused ultrasound (FUS) coupled with microbubbles appears as a technological breakthrough to deliver viral vectors into the central nervous system.

The present work proposes to permeabilize the BBB of entire brains of mice (n=30) for gene therapy using an adeno-associated virus (AAV9-CMV-GFP) and SonoVue microbubbles. Concretely, a square surface (6 mm × 6 mm) covering the main part of the brain was scanned iteratively for a total duration of 150 s. FUS were transmitted (1.5 MHz, Imasonic) at 0.57 MPa with a pulse duration of 100 ms and a duty cycle of 99%.

Our results show that the whole brain of mice was strongly and safely infected. An increase in vector DNA (19.8 times), GFP mRNA (16.4 times), and GFP protein levels (17.4 times) was measured in whole brain extracts of FUS-treated GFP injected mice compared to non-FUS GFP injected mice. In addition to this increase in GFP levels, on average, a 7.3-fold increase of infected cells in the cortex, hippocampus, and striatum was observed. No side effects were detected in the brain of transfected mice.

Gene therapy represents a powerful therapeutic tool to provide a durable and effective correction of protein expression. The combination of FUS and intravenous AAV injections is very promising to deliver genes efficiently over large brain volumes in the framework of the treatment of neurological diseases.

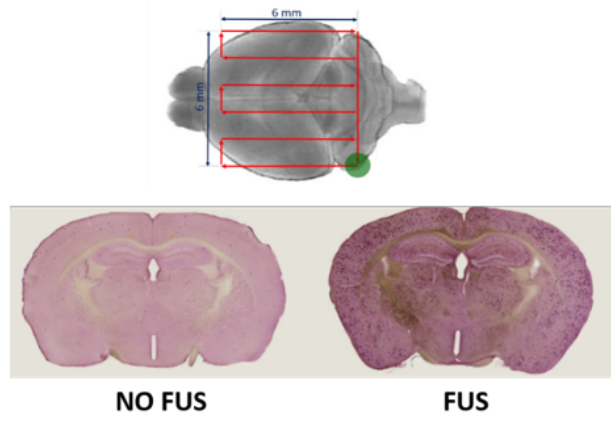


Figure. Scanning trajectory and neurons infection with FUS-mediated gene-therapy

Evaluation of Subharmonic Emissions during Ultrasound-mediated Blood-brain Barrier Disruption in Glioblastoma Patients

Presenter: Nathan McDannold

Authors in order: Nathan McDannold, *Brigham and Women's Hospital, Harvard Medical School*, David Reardon, *Dana Farber Cancer Institute*, Alexandra Golby, *Brigham and Women's Hospital*

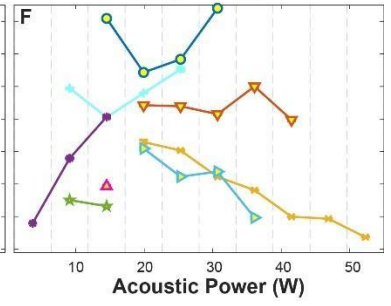
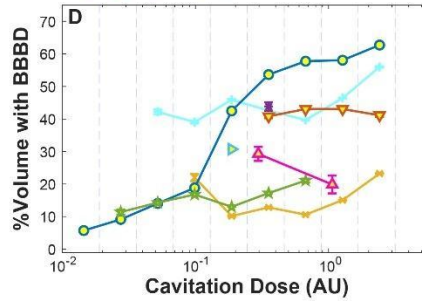
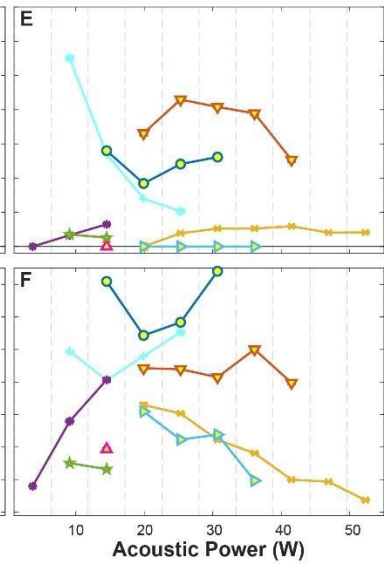
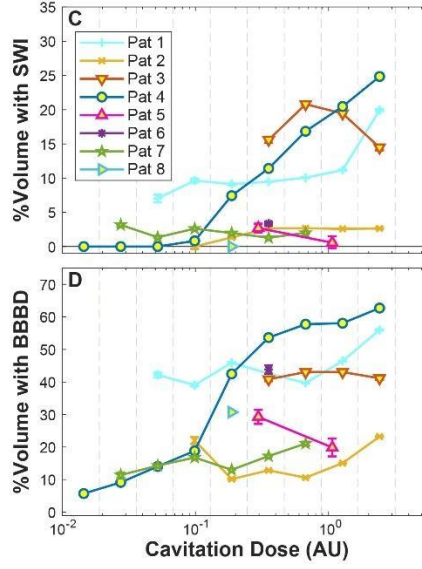
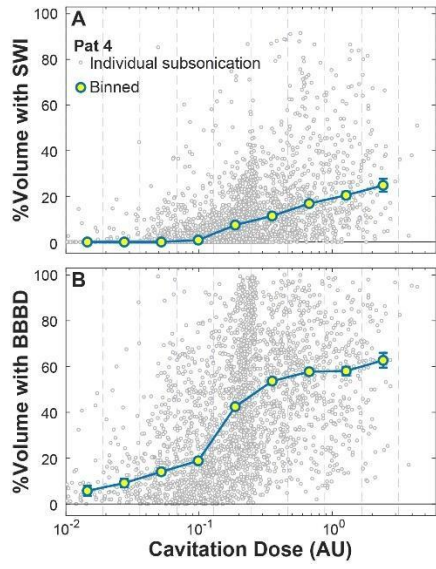
We investigated the relationship between subharmonic emissions, contrast-enhanced MRI, and vascular damage measured in susceptibility-weighted imaging during blood-brain barrier (BBB) disruption in glioma patients.

Blood brain barrier disruption was performed in eight glioblastoma patients receiving temozolomide chemotherapy using the ExAblate Neuro device; patients received up to six monthly treatments. The device actively controlled the exposure level based on the subharmonic emissions. We measured contrast enhancement in T1-weighted MRI in an ellipsoid volume centered on each sonication target using an automated routine in images obtained several days before and immediately after treatment. We manually segmented hypointense regions in susceptibility-weighted imaging.

Over 32 sessions, 7925 targets were sonicated in the eight patients. New contrast enhancement was observed in every patient. Hypointense regions were often observed, but most were resolved by the next treatment. While there was substantial variability, we observed a clear relationship between subharmonic emission and the percentage of the sonicated volume with BBB disruption and vascular damage in individual patients (Figure 1A-B). However, taken together the relationship between acoustic emissions, BBB disruption, and vascular damage varied substantially between patients (Figure 1C-D). The sonication power level varied significantly between patients (Figure 1E-F).

Subharmonic emissions measured by the device can be useful in individual patients to ensure consistent BBB disruption. However, variability between patients suggest that more work is needed. Accounting for skull attenuation, cavitation detector location, microbubble infusion rate, harmonic emissions, and variable vascular density might improve this approach.

The clinical trial was supported by InSightec. Additional support provided by the Jennifer Oppenheimer Cancer Research Initiative



Focused Ultrasound Mediated Intranasal Delivery by Enhancing the Glymphatic Transportation

Presenter: Dezhuang Ye

Authors in order: Dezhuang Ye, *Washington University in St. Louis*, Si Chen, *Harvard Medical School and Massachusetts General Hospital*, Yajie Liu, *Engineering - Biomedical Engineering, Charlotte Weixel, Engineering - Ugrad Student Services*, Zhongtao Hu, *Washington University in St. Louis*, Hong Chen, *Washington University in St. Louis*

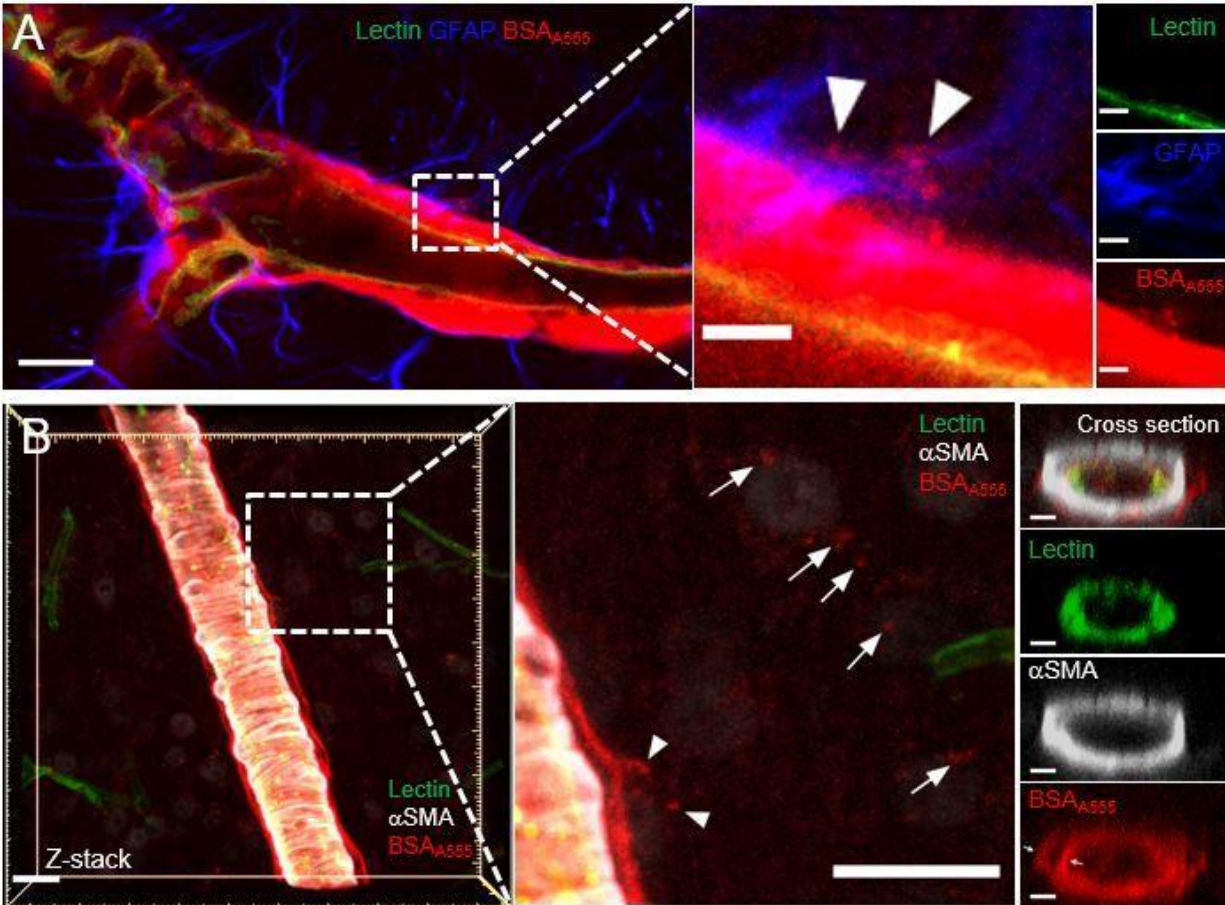
This study aimed to reveal the potential mechanism of focused ultrasound (FUS)- mediated intranasal delivery (FUSIN).

Mice were treated by FUSIN to deliver Alexa Fluor 555-conjugated BSA (BSAA555). BSAA555 was intranasally administered to the mice, followed by intravenous injection of microbubbles and FUS sonication targeting at left thalamus. Mice were transcardially perfused at 15 mins after FUS and sliced into 1-mm coronal slices. Tissue clearing was performed to increase the transparency of brain tissue for fluorescence images. The brain slices were stained with lectin, α SMA and GFAP to identify vessel types and the glymphatic pathway.

After FUSIN delivery, BSAA555 was found in the perivascular space defined by the space between the lectin-stained blood vessel and the GFAP-stained astrocyte (Fig. A). BSAA555 was also found to extravasate to the intestinal space (Fig. B). In contrast, BSAA555 was not clearly observable in the perivascular space and intestinal space in the non-treated contralateral side of the brain. Furthermore, the distribution of the BSAA555 was found mainly along arterioles, not venules.

Findings from this study suggest that FUSIN enhances the delivery of agents through enhancing the glymphatic transportation.

We acknowledge the staffs at WUCCI for their technical support and discussion on tissue clearing and confocal imaging.



(A) FUSIN-enhanced BSA mainly associated with the arterioles (SMA+ vessels) and can extravasate those vessels. **(B)** BSA accumulate to the perivascular space (glymphatic pathway) after FUSIN delivery.

Small Focal Volume Blood Brain Barrier Opening in the Non-human Primate through Intact Skull

Presenter: Thomas Manuel

Authors in order: Thomas Manuel, *Vanderbilt University*, M. Phipps, *Vanderbilt University Medical Center*, Huiwen Luo, *Vanderbilt University*, Jiro Kusunose, *Vanderbilt University Medical Center*, Pai-Feng Yang, *Vanderbilt University Medical Center*, Jamie Reed, *Vanderbilt University Medical Center*, Michelle Sigona, *Vanderbilt University*, Allen Newton, *Vanderbilt University Medical Center*, William Grissom, *Vanderbilt University*, Li Min Chen, *Vanderbilt University Medical Center*, Charles Caskey, *Vanderbilt University Medical Center*

Develop a transducer and cavitation monitoring system for millimeter-scale blood brain barrier opening (BBBO) in non-human primates (NHPS) through the intact skull under image guidance.

Transducer design was performed in k-Wave (81 transcranial simulations in four NHPs varying transducer frequency and geometry). We integrated the transducer into an image-guidance system and developed a custom python application to process cavitation signals and guide transducer output during therapy. The system was validated in the macaque by first targeting the cortex and then performing BBBO on 2 macaques using Gadolinium-based contrast enhancement to quantify BBBO volume and susceptibility-weighted imaging (SWI) to assess safety.

A 1 MHz, 128-element transducer ($f=53.2$ mm, $D=58$ mm) with one central receive element (2 MHz) was identified as the optimal design based on spot size and footprint. When steering inward 10 mm through skull simulations showed an ellipsoidal focus with lateral size of 2.9 ± 0.5 mm by 3.1 ± 0.8 mm and axial 11.6 ± 3.4 mm and transmission of $13 \pm 3.1\%$ ($n=4$ NHPs). In vivo BBBO was demonstrated with a FWHM (evaluated with contrast enhancement) of $3 \times 3 \times 11$ mm. Therapy with stable cavitation showed no hemorrhage signature in SWI, and therapy with inertial cavitation showed hemorrhage.

We designed and evaluated a small footprint transducer capable of BBBO at volumes comparable to functional brain regions in monkeys. The transducer generated a smaller focus steered inward than when steered to the geometric focus. The system will be used to facilitate precise BBBO for neuromodulation via acoustically targeted chemogenetics.

NIH UG3 MH120102 for funding. Vanderbilt University Institute of Imaging Science.

In Vivo Delivery of a Cobalt-based Drug using Rapid Short Pulses Reduces the Amyloid Beta Burden in Alzheimer's Disease Mice

Presenter: Sophie Morse

Authors in order: Sophie Morse, *Imperial College London*, Tiffany Chan, *Imperial College London*, Bibiana Mota, *Imperial College London*, Robertas Aleksynas, *Imperial College London*, Timonthy Kench, *Imperial College London*, Ramon Vilar, *Imperial College London*, Magdalena Sastre, *Imperial College London*, James Choi, *Imperial College London*

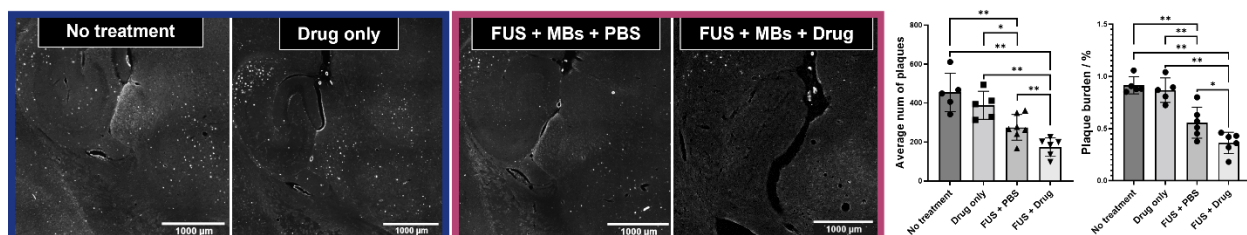
Investigate whether delivering a cobalt-based drug to the brain with rapid-short-pulses of ultrasound can improve cognition and reduce the amyloid-beta burden of Alzheimer's disease.

This study was performed in 5xFAD Alzheimer's mice with 3-weekly treatments (groups: no treatment, drug, ultrasound+vehicle, ultrasound+drug, wild-type; n=8). Focused ultrasound was emitted onto the left hippocampus using a rapid short-pulse sequence, designed for safe and efficient delivery. SonoVue® microbubbles and the cobalt-based drug, designed to prevent amyloid-beta aggregation, were administered intravenously. Hippocampal sections were stained to assess amyloid-beta burden (Thioflavin-S, MOAB-2), whilst improvements in cognition were assessed with behavioural studies (novel object, open field).

The cobalt-based drug was successfully delivered to the brain with rapid short-pulses of ultrasound. The combination of ultrasound with the drug led to a reduction in both the percentage of amyloid-beta plaques and the average number of plaques compared to all control groups ($P < 0.01$). Open field behavioural tests showed no differences between all treated groups, indicating that no treatment negatively affected the locomotory function and anxiety levels of the mice. Novel object recognition tests showed mice treated with both ultrasound and the drug performed closest to the non-Alzheimer's wild type mice.

This cobalt-based drug, normally unable to enter the brain, can be delivered noninvasively to the brain with a rapid short-pulse sequence, preventing the aggregation of amyloid-beta in vivo. These results indicate a promising therapeutic strategy for Alzheimer's disease using a safe and efficient focused ultrasound drug delivery technique.

This work was supported by the Engineering and Physical Sciences Research Council (EP/T51780X/1) and the Alzheimer's Research UK charity (ARUK-IRG2017A-7).



Repeated 5-Aminolevulinic Acid-mediated Sonodynamic Therapy Using MR-guided Focused Ultrasound in 9L Brain Tumour Model

Presenter: Sheng-Kai Wu

Authors in order: Sheng-Kai Wu, *Sunnybrook Research Institute*, Chia-Lin Tsai, *Tri-Service General Hospital, National Defense Medical Center, Taipei, Taiwan*, Aisha Mir, *Sunnybrook Research Institute, Toronto, ON, Canada*, Stuart Marcus, *Sun Pharmaceutical Industries Inc., Princeton, New Jersey, United States*, Kullervo Hynynen, *Sunnybrook Research Institute/ University of Toronto*

To investigate the optimal ultrasound parameters during sonodynamic therapy (SDT), which utilizes ultrasound to activate a sonodynamic agent to treat rodent 9L gliosarcoma brain tumour.

9L tumour cells were implanted into the right striatum. After one week of tumour incubation, thirty rats with brain tumours were treated with SDT on a weekly cadence for three weeks. A dose of 60 mg/kg 5-ALA was intravenously injected six hours before sonication. With a fixed pressure of 0.745 MPa at 0.58 MHz, different burst lengths of 10, 50, and 86 ms were applied in SDT. The therapeutic responses were followed by MRI.

Here we show that we can achieve significant anti-tumour effects by repeatedly conducting SDT, using multiple targets to cover the entire tumour volume. Therapeutic data show 100 percent survival with the destruction of all tumour tissue in all SDT animals with 86 ms burst length, whereas 10 and 50 ms burst lengths do not significantly improve the outcome. In other words, the therapeutic efficacy seems to be proportioned to the burst length.

These promising results indicate that transcranial focused ultrasound can significantly inhibit tumour growth and prolong survival. A longer burst produces a greater therapeutic effect, but a shorter burst reduces the treatment time for larger volume exposures. This tradeoff needs further investigation.

The authors would like to thank Shawna Rideout-Gros for the help with animal preparation and monitoring during experiments.

Acoustic Holograms for Bilateral Blood-brain Barrier Opening in Mice

Presenter: Sergio Jimenez Gambin

Authors in order: Sergio Jimenez Gambin, *Columbia University*, Antonios N. Pouliopoulos, *Columbia University*, Noe Jimenez, *Universitat Politècnica de València*, José M. Benlloch, *Universitat Politècnica de València*, Elisa Konofagou, *Columbia University*, Francisco Camarena, *Universitat Politècnica de València*

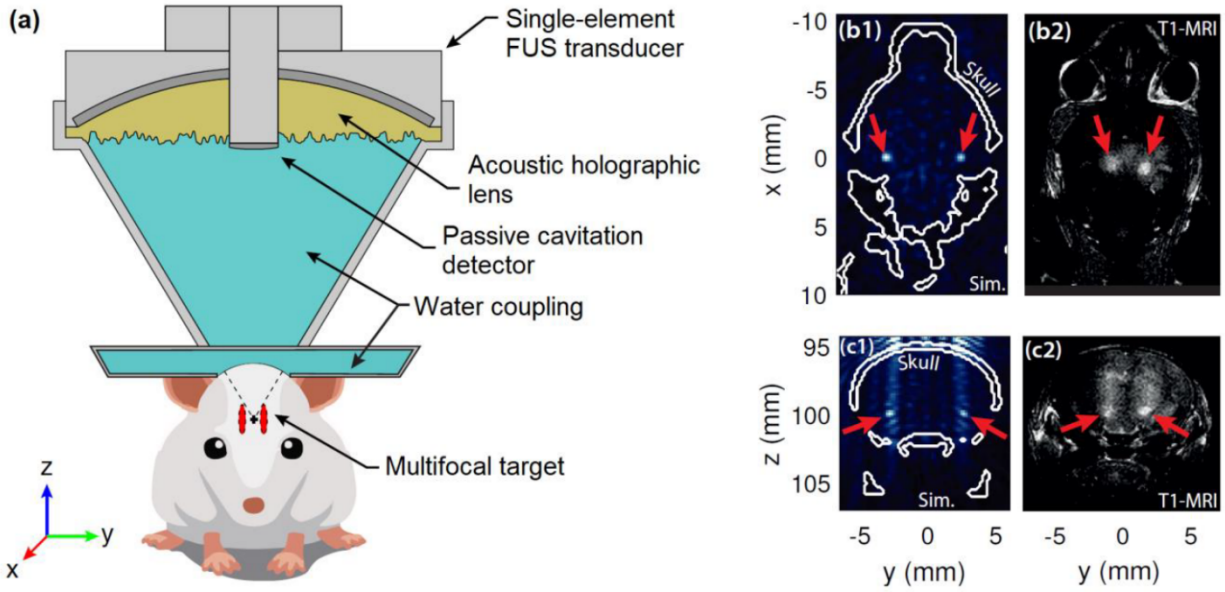
Design and test simple, low-cost acoustic holograms coupled to a single-element FUS transducer for aberration-free, highly-localized, simultaneous, multiple BBB-opening in both brain hemispheres in mice.

Skull geometry and properties were acquired from a micro-CT scan, and target structure from a mouse atlas. The lens was designed from the wavefront generated by the virtual-source target at the design surface using Time-Reversal, and then manufactured by stereolithographic 3D-printing. For in-vivo experiments, 1 μ l/g Definity microbubbles were injected intravenously and 1.68-MHz 400-kPa-PNP FUS was applied for 2 minutes. Then, 0.2 ml gadolinium tracer was injected intraperitoneally, and BBB opening was assessed using T1-MRI.

T1-MRI showed gadolinium extravasation at two symmetric focal spots separated 3.2 \pm 1.0 mm (n=3 mice) compared to 5.3 mm in simulations. In addition, the lens ability to encode time-reversed wavefronts resulted in a focusing performance enhancement, providing quasi-spherical, high-resolution BBB opening locations of 1.0 \pm 0.3 mm size for the higher contrast enhancement regions, considerably reduced as compared to the 19.2 mm axial size for the calibration in water. Note that air nuclei trapped within the irregular lens surface may have contributed to the field distortion. Moreover, using the particular micro-CT scan of each treated subject would improve the pressure-field prediction.

This study demonstrates that acoustic holograms are feasible to produce a high-resolution, simultaneous bilateral BBB opening in mice using a single sonication and injection of microbubbles, as well as in different animals using a separate unique micro-CT scan, defining therefore a time- and cost-efficient therapeutic approach for neurological disease treatments.

This research was supported by the following grants: MICINN (IJC2018-037897-I, PID2019-111436RBC22), AVI (INNCON/2021/8, INNVA1/2020/92), GVA (ACIF/2017/045, BEFPI/2019/075), NIH (5R01EB009041, 5R01AG038961), FEDER (IDIFEDER/2021/004).



CAPTION (10 words):
 (a) In-vivo setup scheme. (b1,c1) Simulated pressure-field. (b2,c2) Experimental T1-MRI.

Investigating the Feasibility of MRgFUS to Target Mesial Temporal Lobe Structures to Treat Temporal Lobe Epilepsy

Presenter: sijia guo

Authors in order: sijia guo, *University of Maryland*, John Snell, *Focused Ultrasound Foundation*, Jiachen Zhuo, *University of Maryland, Baltimor*, Dheeraj Gandhi, *University of Maryland School of Medicine*, Alexander Ksendzovsky, *University of Maryland School of Medicine*, Paul Fishman, *University of Maryland School of Medicine*, Rao Gullapalli, *University of Maryland School of Medicine*

In this study, we explored the feasibility of use of Insightec ExAblate systems for ablating the mesial temporal lobe (MTL) to treat epilepsy.

We performed acoustic and thermal simulations to assess the feasibility of targeting the MTL by estimating peak temperature rise on MTL targets/skull base and the resultant CEM at 43 °C. Furthermore, we validated the simulations on ex-vivo cadaveric skulls by measuring temperature at MTL and at temporal bone where heating is a concern. Treatment efficacy using transducer elements blocking algorithms was also assessed to potentially reduce the ratio of target heating/skull heating.

Simulations suggest the use of lower power and longer sonication duration minimize skull heating (Figure 1). The 50°C-60s sonication led to reasonable lesions with safer skull heating (below 47°C) covering the whole MTL region using six sonications. Experimental validation on cadaver skulls demonstrated that the highest target temperature rise with sonication level of 600W for 60s, which led to 14.2/9.8°C (target/skull), respectively, while the skull temperature rise was 10.2/11.2°C. Simulations suggest the possibility of further reduction in skull heating by 2-3°C by strategically blocking or lowering the power of elements that contribute mainly to skull heating.

We have demonstrated through simulations that targeting the MTL for ablation using MRgFUS is possible with the currently approved clinical neuro system operating at 670 kHz. Furthermore, we have demonstrated experimentally that ablative temperatures can be obtained at the MTL target while avoiding excessive skull heating.

Ultrasound-Stimulated Microbubbles Potentiated Enhancement of Radiation Response of Brain Tumors

Presenter: Deepa Sharma

Authors in order: Deepa Sharma, *Sunnybrook Health Sciences Centre*, Evan McNabb, Colleen Bailey, *Sunnybrook Research Institute*, Anoja Giles, Wenyi Yang, Murtuza Saifuddin, *Sunnybrook Research Institute*, Martin Stanisiz, Arjun Sahgal, Gregory Czarnota, *Sunnybrook Research Institute*

In this study, we tested the effectiveness of MRI-guided focused ultrasound (FUS) combined with microbubbles (MB) and radiation in a rabbit human-metastatic brain tumor model.

Experiments were performed using New Zealand White rabbits bearing prostate cancer tumors (PC-3) in their brain. Treatment conditions consisted of FUS+MB alone, radiation alone (6 Gy), or a combination of FUS+MB and radiation. Animals were divided into two-time cohorts - 24 hours (receiving single treatment) and 3 weeks (receiving multiple treatments). Tumor response was assessed 24 hours and longitudinally after treatment. Histopathology analyses were used to evaluate tumor response.

Hematoxylin and eosin (H&E) staining revealed increased cell death within tumors exposed to combined treatments compared to control tumors or tumors exposed to FUS+MB or radiation alone. Vascular deterioration was determined using factor VIII immunohistochemical labeling. A similar but opposite trend in vascularity was observed in the tumors receiving the combined treatment. The presence of vessels was less prominent in a combined treated group compared to the control, FUS+MB, or radiation alone group. A comparison was made between cell death and vessel damage. A correlation between cell death and vascular remnants was observed in the combined treated group.

Our study suggests radiation enhancement effects using ultrasound-stimulated microbubbles therapy in large tumor models.

This work was supported by the Ontario Research Fund (ORF) and the Terry Fox Foundation.

A8-1

Neuronavigation-guided Transcranial Histotripsy on Human Cadavers: A Feasibility Study

Presenter: Sang Won Choi

Authors in order: Sang Won Choi, *University of Michigan*, Mahmoud Komaiha, *University of Michigan*, Timothy Hall, *University of Michigan*, Zhen Xu, *University of Michigan*, Jonathan Sukovich, *University of Michigan*, Dave Choi, *University of Michigan*, Ning Lu, *University of Michigan*, Aditya Pandey, *University of Michigan*, Sandra Camelo-Piragua, *University of Michigan*, Neeraj Chaudhary, *University of Michigan*, Badih Junior Daou, *University of Michigan*

We aim to demonstrate the feasibility of transcranial histotripsy for non-invasive brain treatment by treating whole-body cadavers (< 96 hours postmortem) guided by a neuronavigation system.

Approximately 1cm³ of the brains of two whole-body cadavers were treated by electronically steering the focus with a 1.1 mm spacing using a 700kHz, 360-element, 15cm focal distance, hemispherical array. 1-cycle pulses, 200Hz PRF, p- of >28 MPa, and 50 pulses per focal location were used. Aberration correction was done with Kranion and pre-treatment CT scans. Prescribed ablation locations on pre-treatment MRI and post-treatment MRI were compared to evaluate the treatment accuracy.

Three lesions were successfully generated in the septum, thalamus, corpus callosum, and identified by the post-treatment MR images. Representative pre and post-treatment MRI images of one of the cadavers treated are shown (Figure 1). Apparent Diffusion Coefficient (ADC) images best showed the histotripsy homogenized region. The targeting accuracy was 4.1, 8.0, and 6.5 mm for the septum, corpus callosum, and thalamus respectively. The low targeting accuracy is attributed to the imperfect co-registration between the cadaver head and the array and the suboptimal setup. On-going improvements to the experimental setup and workflow are expected to increase the targeting accuracy.

The feasibility of neuronavigation-guided transcranial histotripsy was demonstrated on human cadavers. Future improvements to the system are needed to increase accuracy to a clinically acceptable level. We plan to study the full extent of transcranial histotripsy treatment location profile and efficacy in human cadaver brains.

This work was funded by NIH grants (R01 - EB028309, R01 - NS - 108042) and Focused Ultrasound Foundation

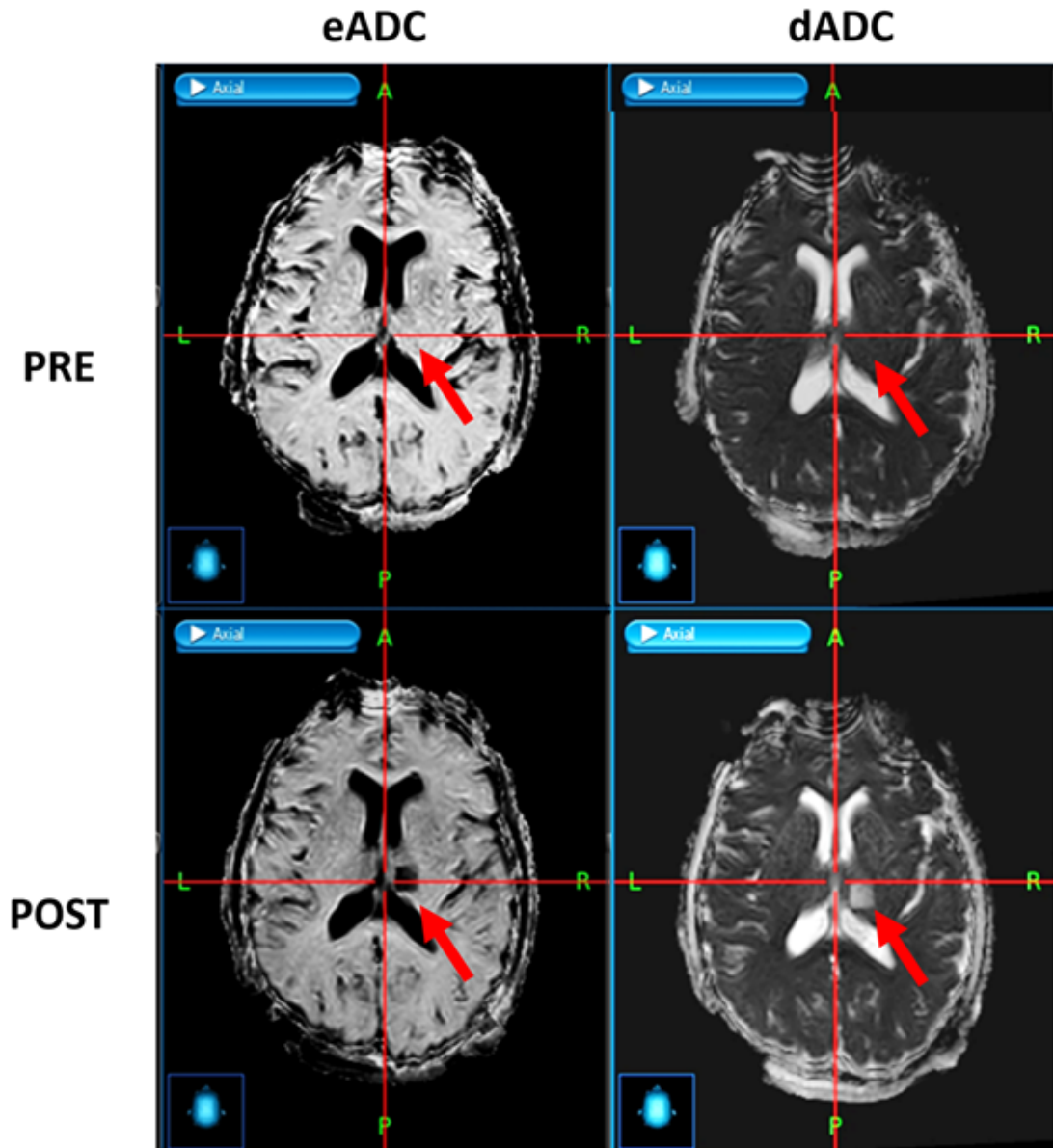


Figure 1. Apparent Diffusion Coefficient (ADC) images of one of the cadavers.

MR-Thermometry Pre-treatment Targeting for MR-guided Histotripsy

Presenter: Dinank Gupta

Authors in order: Dinank Gupta, *University of Michigan*, Dave Choi, *University of Michigan*, Ning Lu, *University of Michigan*, Steven Allen, *Brigham Young University*, Timothy Hall, *University of Michigan*, Douglas Noll, *University of Michigan*, Zhen Xu, *University of Michigan*

The aim of this study is to evaluate the use of MR-thermometry for pre-treatment targeting of MR-guided histotripsy treatments in ex-vivo brain.

A 15-element 750-kHz MR-compatible transducer with specialized drivers was used for both histotripsy and low-temperature heating. The tissues were first heated to 1-2°C using continuous-waves at ~4MPa p- for 15 seconds during simultaneous MR-thermometry acquisition. Target location was estimated by fitting a Gaussian over the heated region. Then histotripsy was delivered with 1-cycle pulses, 54MPa p-, 50Hz PRF, and 100-pulses. Post-treatment MRI of histotripsy lesion was compared with pre-treatment MR-thermometry to evaluate the targeting accuracy.

For targeting accuracy evaluation, the mean/standard-deviation of the difference between the target location estimated by pre-treatment MR-thermometry and the histotripsy lesion location from post-treatment diffusion-weighted MR images was 0.64/0.49 mm and 1.21/0.91 mm in transverse and longitudinal direction, respectively. Targeting error was also estimated by comparing histotripsy lesion location with array geometrical focus estimated using fiducials placed on the array (mean/std difference: 0.24/0.20 and 0.93/0.48 mm in transverse and longitudinal directions). Since the image resolution was 0.5mm, the error accounts for a few voxels.

There is a concern regarding the accuracy of using low-temperature heating and MR-thermometry for histotripsy targeting, because low-temperature heating is a linear process while histotripsy depends on non-linear ultrasound propagation at a high pressure. This is the first study demonstrating good accuracy of MR-thermometry for pre-treatment targeting of MR-guided histotripsy.

This work was funded by NIH grant R01 - EB028309.

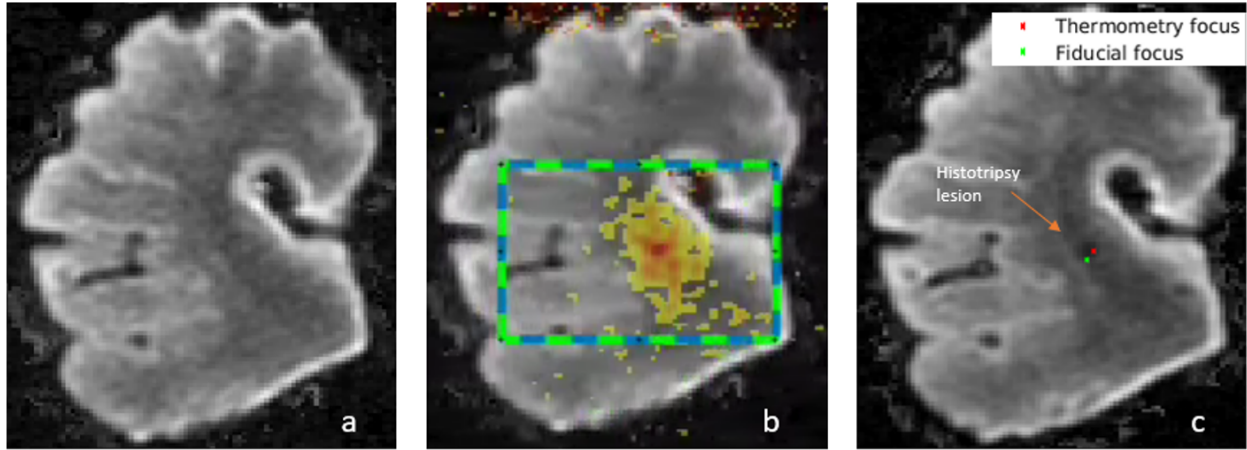


Figure 1: DWI ($b=1000$) for a tissue. a) Pre-treatment. b) MR-thermometry and ROI to fit Gaussian. c) Histotripsy lesion along with estimated foci for thermometry and fiducials

Performance Characterization of a High-Frequency Image-Guided Histotripsy Platform

Presenter: Jeremy Brown

Authors in order: Jeremy Brown, *Dalhousie University*, Jessica Gannon, *Virginia Tech - Wake Forest School of Biomedical Engineering and Sciences*, Eli Vlasisavljevich, *Virginia Tech*, Thomas Landry, *Dalhousie University*

An image guided histotripsy system was developed in an endoscopic form factor for minimally invasive applications. Imaging and therapy performance was characterized.

A 64 element 30 MHz phased imaging array was designed and laser micromachined with an element pitch of 48 μm and wire-bonded to a compact interconnect such that the packaged array was less than 4mm in size. The imaging array was bonded within a central cutout of a 10mm diameter 6.3MHz histotripsy transducer based on an aluminum lens focused to a 7mm depth. Imaging and histotripsy were synchronized using custom hardware.

The performance of the 30 MHz phased imaging array was characterized by measuring bandwidth, beamwidths, and in-vivo rat brain imaging. The pulse bandwidth was measured to be 65%, the beamwidth 40 μm by 130 μm (axial by lateral), and high quality in-vivo images were generated with more than 60dB dynamic range. The performance of the histotripsy transducer was characterized by measuring the pressure/volt sensitivity, the beamwidth, bubble cloud size, and real-time in-vivo ablation in rat brains. The transducer had a sensitivity of 0.25MPa/V, a beamwidth of 150 μm , a bubble cloud diameter of 300 μm , and ablation regions less than 500 μm .

We have demonstrated a completely new and novel image guided surgical platform as a potentially effective system for the resection of brain tumours. The integrated system performance has been characterized and preliminary evaluation was investigated by precisely targeting and ablating shapes and regions in healthy rat brains in vivo.

This study was funded by the Atlantic Canada Opportunities Agency (Atlantic Innovation Fund no.207828) and the Natural Sciences and Engineering Research Council of Canada (NSERC).

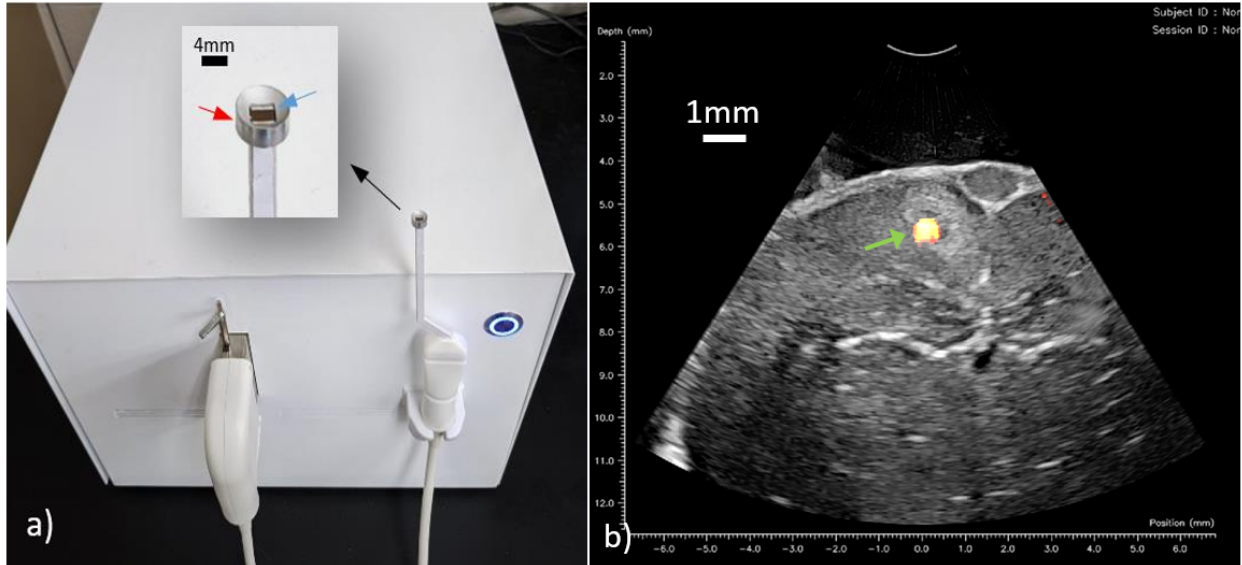


Figure 1: a) photograph of prototype image guided therapy system b) example B-Mode image of in-vivo rat brain with synchronized histotripsy

Safety of Histotripsy in an Anticoagulated Porcine Model

Presenter: Timothy Ziemlewicz

Authors in order: Scott Mauch, *University of Wisconsin Hospital & Clinics*, Annie Zlevor, Emily Knott, *University of Wisconsin - Madison*, Allison Couillard, Sarvesh Periyasamy, Eliot Williams, John Swietlik, Paul Laeseke, Xiaofei Zhang, Zhen Xu, *University of Michigan*, E. Abel, Fred Lee, Timothy Ziemlewicz, *University of Wisconsin*

Determine the risk of mechanical vessel wall damage resulting in hemorrhage during and after hepatic and renal histotripsy in an anticoagulated in vivo porcine model.

Non-tumor-bearing pigs (n=8, weight=55kg) were anticoagulated with warfarin (initial dose 0.08 mg/kg) to a target PT of 30-50% above baseline. A total of 15 histotripsy procedures were performed (kidney n=8, 2.0 cm sphere; liver n=7, 2.5 cm sphere). Treatments were immediately followed by CT imaging. Animals were observed for 7 days while continuing anticoagulation, followed by repeat CT and necropsy.

All animals survived the entire protocol without disability or distress. Three animals had hematuria. Baseline PT values (mean 16.0) were elevated to 22.0 (37.5% above baseline, $p < 0.05$) at treatment, and 28.8 (77.8% above baseline, $p < 0.05$) at necropsy. During treatment 5/8 subjects were at a therapeutic anticoagulation level, and 8/8 reached therapeutic levels prior to necropsy. There were no cases of parenchymal, peritoneal, or retroperitoneal hemorrhage despite 13/15 treatments extending to the organ surface. One liver treatment extended into the adjacent spleen, also without hemorrhage. Small subcapsular hematomas near two renal ablations resolved within one week. No bowel injuries were noted.

Liver and kidney histotripsy appears safe with no elevated bleeding risk in this anticoagulated animal model. If this finding is validated in future studies, the ability to treat liver and kidney tumors while maintaining anticoagulation could decrease the complexity, cost, and morbidity associated with treating liver and kidney cancers.

Transrectal Histotripsy Ablation of the Prostate: Initial Preclinical In Vivo Assessment

Presenter: George Schade

Authors in order: George Schade, *UNIVERSITY OF WASHINGTON*, Rishi Sekar, *University of Washington, School of Medicine*, Zorawar Singh, *University of Washington, School of Medicine*, Tatiana Khokhlova, *University of Washington*, Alex Peek, Yak-Nam Wang, *Center for Industrial and Medical Ultrasound, University of Washington, Seattle, United States of America*, Helena Son, *UNIVERSITY OF WASHINGTON*, Stephanie Totten, *University of Washington*, Wayne Kreider, *University of Washington*, Oleg Sapozhnikov, *University of Washington*, Adam Maxwell, *University of Washington*, Vera Khokhlova, *Physics Faculty, Lomonosov Moscow State University, Moscow, Russian Federation; Center for Industrial and Medical Ultrasound, University of Washington, Seattle, United States of America*

To assess the feasibility of transrectal boiling histotripsy (BH) ablation of the prostate in a canine model with a custom built pre-clinical system

Intact male (N=6) and orthotopic ACE-1 prostate cancer-bearing (N=2) canines underwent transrectal BH using a custom BH transducer (2 MHz, focal length 4 cm) with in-line B-Mode ultrasound guidance. BH was administered with power 10% above bubble threshold, pulse durations of 2-10ms, duty factor of 1%, and 5-60 pulses/focus. Unilateral treatment was performed in ACE-1 subjects with the contralateral side for tumor growth confirmation. Canines were euthanized post-BH and prostates were processed for histologic evaluation.

Boiling threshold (visible hyperechoic bubbles on B-mode) required a shock amplitude of 399 MPa. As BH progressed, a hypoechoic region became apparent (Figure). At necropsy, no evidence of collateral injury to the periprostatic structures was observed. On histology, minimum threshold for cellular damage was observed at 5 pulses/focus while complete homogenization was achieved at 30 pulses/focus with a narrow (μm) ablation boundary. Shorter pulses produced similar ablation in less time, though lesions were smaller. Lesions in ACE-1 subjects, appeared similar to benign dogs without definitive evidence of residual tumor cells while the contralateral prostate demonstrated viable tumor cells.

Transrectal BH ablation of the prostate is feasible in the clinically relevant canine model, producing precise mechanical ablation of benign and malignant prostate tissue. Further studies are needed to characterize the impact of tissue/anatomic properties and optimize future clinical implementations.

Work supported by NIH R01EB007643, R21CA219793, R01DK119310, RFBR 175433034.

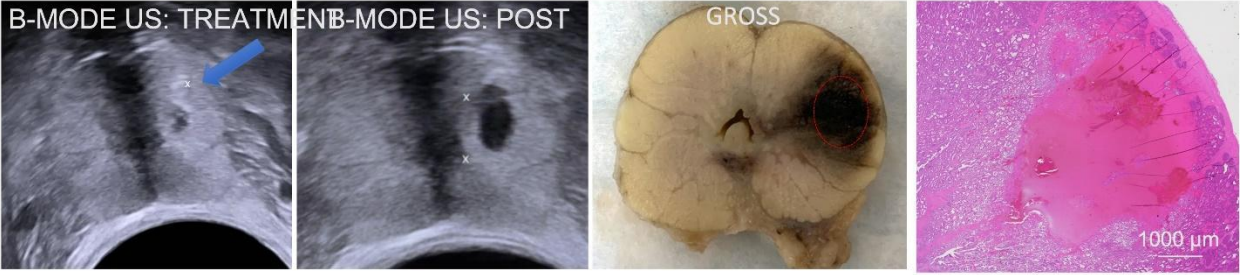


Figure: Ultrasound, gross and histologic appearance transrectal prostate BH

An MRI-guided High-Intensity Focused Ultrasound Platform for Neonatal Neurosurgery: Assessment of Clot Lysis

Presenter: Hrishikesh Raghuram

Authors in order: Hrishikesh Raghuram, *University of Toronto*, Thomas Looi, *Hospital for Sick Children*, Samuel Pichardo, *University of Calgary*, Adam Waspe, *Hospital for Sick Children*, James Drake, *Hospital for Sick Children*

This study quantifies our MRI-guided high-intensity focused ultrasound (MRgHIFU) platform's efficacy at lysing blood clots for the potential non-invasive treatment of intraventricular hemorrhage in neonates.

Brain-mimicking phantoms with ventricular cavities were developed to test the platform's capabilities in a controlled setting (Fig.1). Whole porcine blood was clotted in the cavities and lysed using a boiling histotripsy procedure (500W, 10ms pulse duration, 1.0% duty cycle, and 40s duration). After treatment, the cavities were drained, and the solid clot fragments were collected via vacuum filtration to quantify the percentage of clot lysis (Fig.2). The phantom's cavities were inspected for collateral damage.

A total of 9 phantoms were treated with the MRgHIFU platform, which yielded an average clot lysis of 97.0% with a standard deviation of 2.57%. HIFU sonications resulted in systematic treatment within the brain-mimicking phantom and the progression of clot lysis was distinctly apparent in T2-weighted MR scans (Fig.3). No apparent collateral damage to the phantom was observed after treatment. Results showed the MRgHIFU platform could successfully lyse more than 90% of a blood clot with statistical significance.

The robotic MRgHIFU platform was shown to lyse a large percentage of a given blood clot with no observable collateral damage to the phantom. These results demonstrated the platform's ability to induce clot lysis when targeting through simulated brain matter and show promise towards the final application in a neonatal

Funding was provided by the Natural Sciences and Engineering Research Council (NSERC), the Canadian Institutes of Health Research (CIHR), and the Hydrocephalus Association.

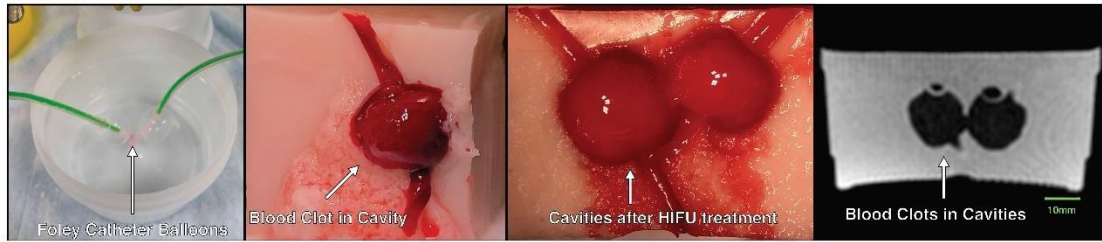


Fig.1: The brain-mimicking phantoms developed to model intraventricular hemorrhage.

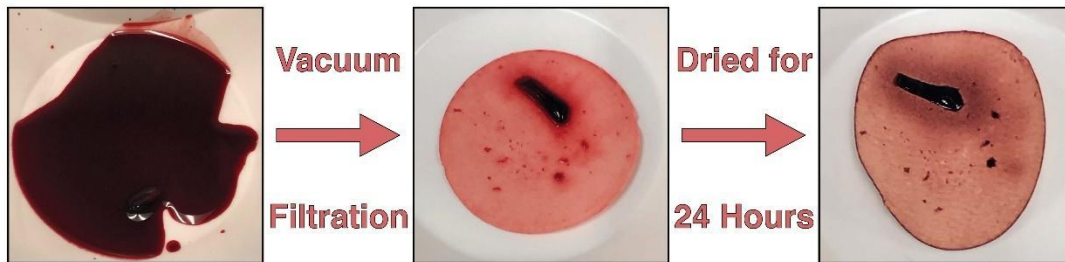


Fig.2: Remaining solid clot fragment and liquid blood after HIFU treatment.

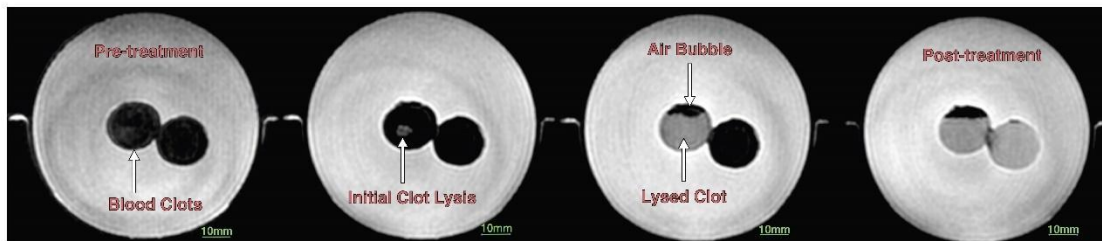


Fig.3: T2-weighted MR scans showing the progression of clot lysis.

Rapid and precise fractionation of embolus using boiling histotripsy with acoustic trapping: A proof-of-concept study

Presenter: Jeongmin Heo

Authors in order: Jeongmin Heo, *Korea Institute of Science and Technology*, Hyo Jun Kim, *Korea Institute of Science and Technology (KIST)*, Jun Hong Park, *Korea Institute of Science and Technology (KIST)*, Sungmin Han, *Korea Institute of Science and Technology*, Ki Joo Park, *Kyung Hee University*

A new strategy for treating thrombus and embolus with boiling histotripsy (BH) and acoustic trapping is proposed and demonstrated in in vitro experiments.

To investigate the feasibility of the proposed method, an experimental setup consisting of two 1-MHz focused ultrasound transducers (dFUS) for acoustic trapping ($P = 1.33$ MPa) and a 2-MHz HIFU transducer for BH was employed (Fig.1a). The dFUS blocked an embolus movement by producing a fringe patterned-acoustic field in a vascular phantom (Fig 1a). A 10-ms long BH pulse ($P+ = 79$ MPa; $P- = -17$ MPa) was then applied to fractionate the captured embolus.

The dFUS fields successfully captured moving blood clot of 3 to 4 mm in size at a flow velocity of up to 6.19 cm/s. After acoustic trapping, the blood clot was fractionated by BH (Fig.1b). Most of the clot debris sizes were less than 60 μm . Furthermore, the debris size was gradually reduced with increasing the pulse repetition frequency used (10, 20 and 30 Hz). No damage on the vessel wall was observed during the experiments.

We demonstrated new method for precise and rapid fragmentation of embolus. Since the proposed method can trap and destroy embolus noninvasively, this could be a valuable therapeutic tool for treating thrombosis and embolisms.

This work was supported by the National Research Foundation of Korea (NRF) and National Research Council of Science & Technology (NST) (No. NRF-2021R1C1C1008240, CAP-18-01-KIST).

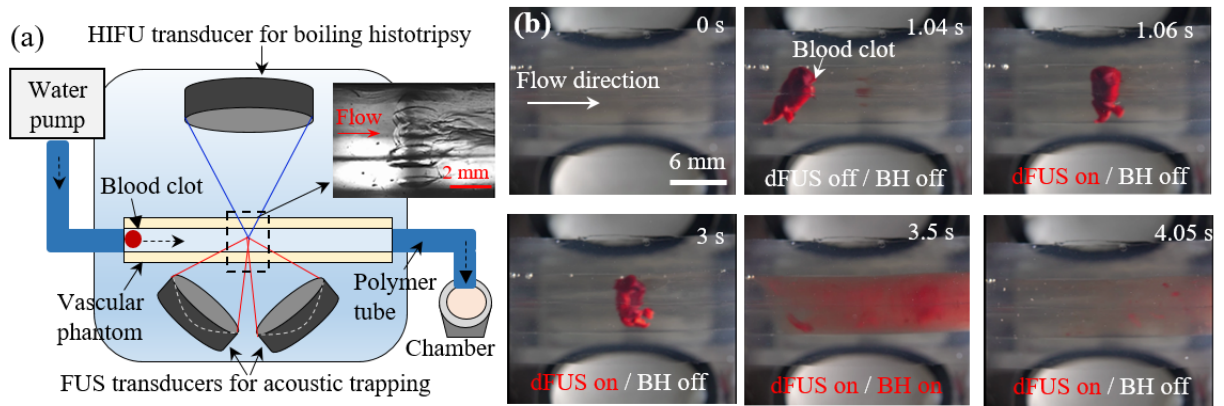


Fig. 1 (a) Experimental setup used for demonstrating the proposed method for treating thrombus and embolus
 (b) Images illustrating the captured blood clot by acoustic trapping and the destroyed blood clot by BH.

Histotripsy for the Treatment of Pancreatic Tumors: Feasibility Study in an in vivo Porcine Model

Presenter: Jessica Gannon

Authors in order: Jessica Gannon, *Virginia Tech - Wake Forest School of Biomedical Engineering and Sciences*, Khan Imran, *Virginia-Maryland College of Veterinary Medicine*, Michael Edwards, *Virginia-Maryland College of Veterinary Medicine*, Neha Singh, *Virginia Tech Carilion School of Medicine*, Alissa Hendricks-Wenger, *Virginia-Maryland College of Veterinary Medicine*, Lauren Ruger, *Virginia Polytechnic Institute and State University*, Margaret Nagai-Singer, *Virginia-Maryland College of Veterinary Medicine*, Hannah Sheppard, *Virginia Polytechnic Institute and State University*, Benjamin Tintera, *Virginia Tech Carilion School of Medicine*, Kristin Eden, *Virginia Tech Carilion School of Medicine*, Joan Vidal-Jove, *Comprehensive Tumor Center Barcelona*, David Luyimbazi, *Department of Surgery at Carilion Clinic*, Mishal Mendiratta-Lala, *University of Michigan*, Martha Larson, *Virginia-Maryland College of Veterinary Medicine*, Sheryl Coutermarsh-Ott, *Virginia Polytechnic Institute and State University*, Irving Allen, *Virginia Polytechnic Institute and State University*, Eli Vlaisavljevich, *Virginia Tech*

This study investigates the preclinical feasibility of using histotripsy for non-invasively targeting and ablating pancreatic tumors in large animal (porcine) models.

A 500 kHz histotripsy system was used to target the pancreas in healthy pigs (n=10) and SCID-like RAG2/IL2RG deficient pigs (n=3) containing orthotopically implanted human Panc01 tumors. Before treatment, pigs were either fasted or fed a custard diet with simethicone (2 mL/pig) and bisacodyl (0.3 mg/kg) to reduce flatulence and improve acoustic access to the pancreas. Treatment was guided by real-time ultrasound imaging. Post-treatment safety and efficacy was characterized by contrast-enhanced CT and histological analysis.

Histotripsy generated bubble clouds in pancreases of pigs that received the custard diet whereas the fasting group was not successfully treated due to gas blockage. Histological analysis showed ablated regions within the pancreas with small regions of bruising on overlying intestines and stomach, particularly in the fasting group. In pigs that survived 1-week, treatments were well-tolerated with no signs of complications/changes in blood markers. CT confirmed successful growth of Panc01 xenografts in the immunocompromised model, with histotripsy successfully applied to one tumor at >35MPa, a 500Hz pulse repetition frequency, and 1.75cm spherical volume. Histopathological analysis of tumor treatments is ongoing.

Results of this study demonstrate the potential of histotripsy as a non-invasive pancreas ablation method and are a first step in developing histotripsy for pancreatic cancer. The results also highlight challenges of US-guidance for histotripsy of the pancreas that warrant further evaluation.

This work was supported by grants from the Focused Ultrasound Foundation (FUF61057) and the National Institutes of Health (EB028429).

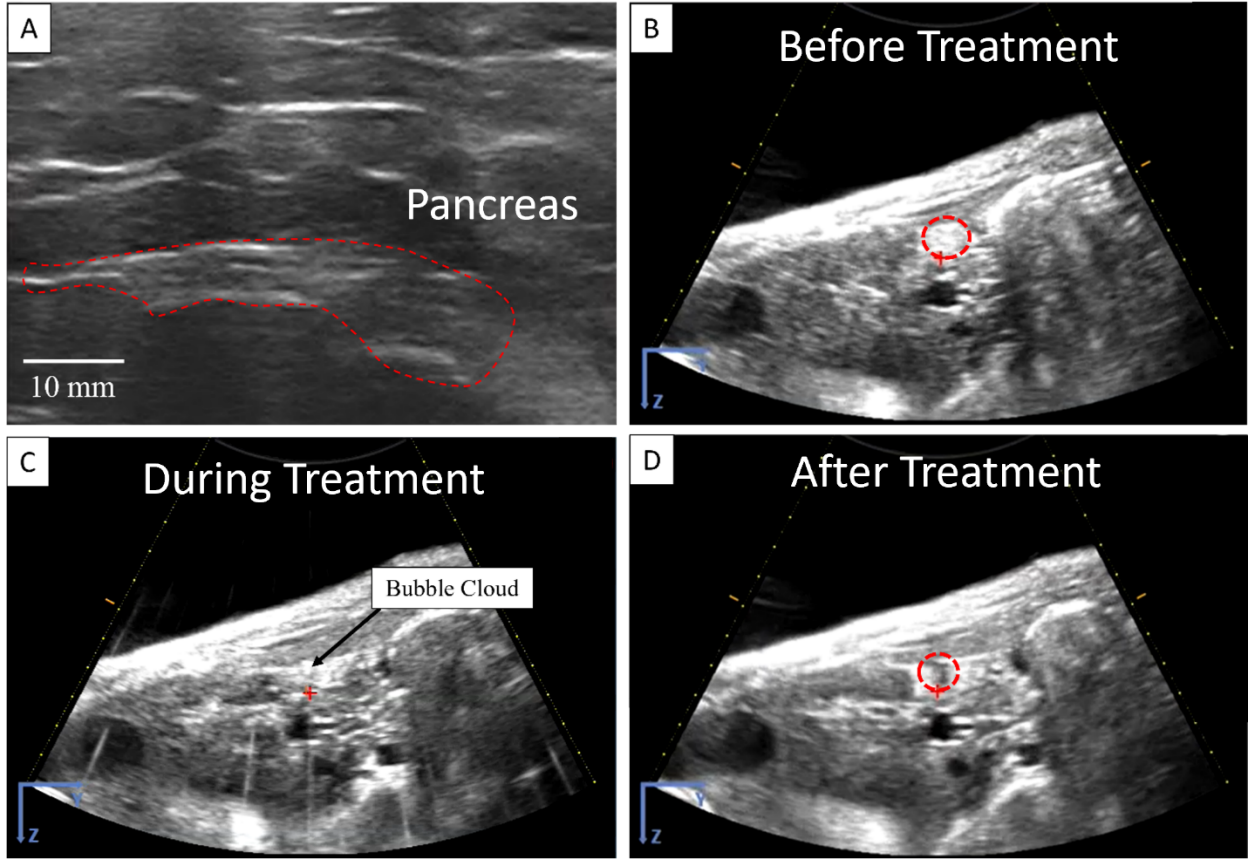


Figure 1. Ultrasound images of histotripsy treatment in porcine pancreas.

Two-step Aberration Correction for Transcranial Histotripsy

Presenter: Ning Lu

Authors in order: Ning Lu, *University of Michigan*, Timothy Hall, *University of Michigan*, Jonathan Sukovich, *University of Michigan*, Sang Won Choi, *University of Michigan*, John Snell, *Focused Ultrasound Foundation*, Nathan McDannold, *Brigham and Women's Hospital, Harvard Medical School*, Zhen Xu, *University of Michigan*

We propose and investigate a two-step aberration correction method for transcranial histotripsy through excised human skulls.

The two-step approach consists of the CT-based raytracing correction followed by a cavitation-based correction using the acoustic cavitation emission (ACE) shockwaves. A 700 kHz, 360-element hemispherical transducer array capable of transmit-and-receive on all channels was used to generate histotripsy-induced cavitation and acquire ACE shockwaves. Skull CT data were co-registered to the histotripsy array using a skull surface map reconstructed from acoustic pulse-echo signals. Cavitation collapse shockwave signals were analyzed to calculate the aberration correction delays.

The performance of the 2-step method was investigated with 3 skulls placed at 2 different locations in the transducer array. The 2-step method achieved 0.90 ± 0.07 peak pressure normalized to the gold standard hydrophone correction and $143.8 \pm 42.6\%$ increase compared to no correction, yielding a focal shift of 0.3 ± 0.2 mm and a focal volume of 3.8 ± 1.2 mm. The CT-based correction and ACE-based correction alone produced 0.51 ± 0.16 and 0.74 ± 0.14 peak pressure normalized to hydrophone correction, respectively. The 2-step aberration correction yielded better refocusing compared to either approach alone and can be implemented in real-time.

The 2-step aberration correction provided comparable performance to hydrophone correction and substantial improvements over the CT-based approach that is currently used for ultrasound brain therapy. These improvements are highly relevant and beneficial for all cavitation-based focused ultrasound brain therapy including transcranial histotripsy.

This work is funded by the Focused Ultrasound Foundation and National Institutes of Health (R01-EB028309 and R01-NS108042).

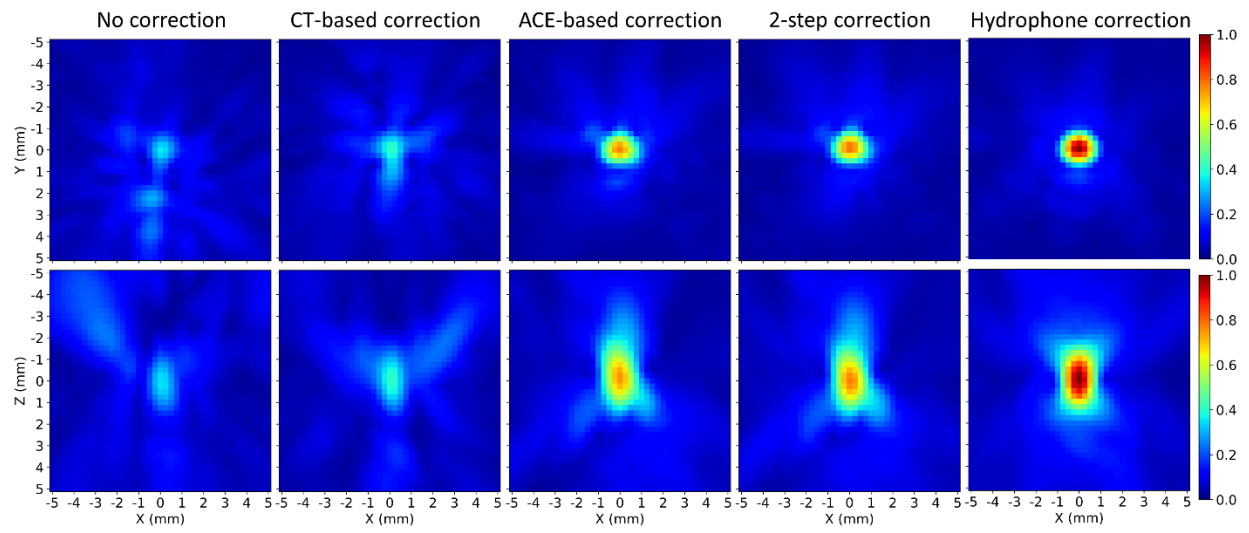


Figure 1. Normalized Pressure field maps centered at the spatial peak locations.

Comparing Focused Ultrasound and Dry Needling Therapies on Healing of Rat Tendinopathy

Presenter: Molly Smallcomb

Authors in order: Molly Smallcomb, *The Pennsylvania State University*, Sujata Khandare, *The Pennsylvania State University*, Jacob Elliott, *The Pennsylvania State University*, Meghan Vidt, *The Pennsylvania State University*, Julianna Simon, *The Pennsylvania State University*

The objective of this study is to compare healing after focused ultrasound (fUS) or dry needling (DN) treatments in a murine tendinopathy model.

Twenty-six rats were subjected to Achilles tenotomy. One week post-surgery, tendons were treated with fUS (1.5MHz, 1-ms pulses @10Hz for 60s, p+ = 89MPa, p- = 26MPa) or DN (30G needle, 5 fenestrations over 20s) and survived for 1 additional week. Blood was collected from the tail vein immediately before and after treatment and before euthanasia. Plasma was assayed for IGF-1, VEGF-A, and TGF- β healing factors. Tendons were harvested for histology or mechanical testing.

No significant differences were found between fUS and DN in the release of IGF-1 and TGF- β healing factors (Fig.1a); VEGF-A concentrations were too low to be detected. For both fUS and DN, IGF-1 concentrations decreased immediately after intervention and increased 1 week post-intervention. Conversely, TGF- β concentrations for both treatments increased after intervention and decreased 1 week after intervention. No differences were found between fUS- or DN-treated tendons and controls in H&E-stained histology (Fig.1b). Stiffness and percent relaxation of DN-treated tendons were lower than controls (p=0.0041, p=0.0441, respectively), whereas stiffness and percent relaxation of fUS-treated tendons were similar to controls.

fUS performed similar to DN in the release of healing factors with no differences noted upon histological analysis. However, fUS better preserved the mechanical integrity of the tendon compared to DN, which suggests fUS may be a viable alternative to DN in the treatment of tendinopathies.

This work was funded by NIH – National Institute of Biomedical Imaging and Bioengineering (R21EB027886), and NSF Graduate Research Fellowship (Smallcomb; DGE1255832).

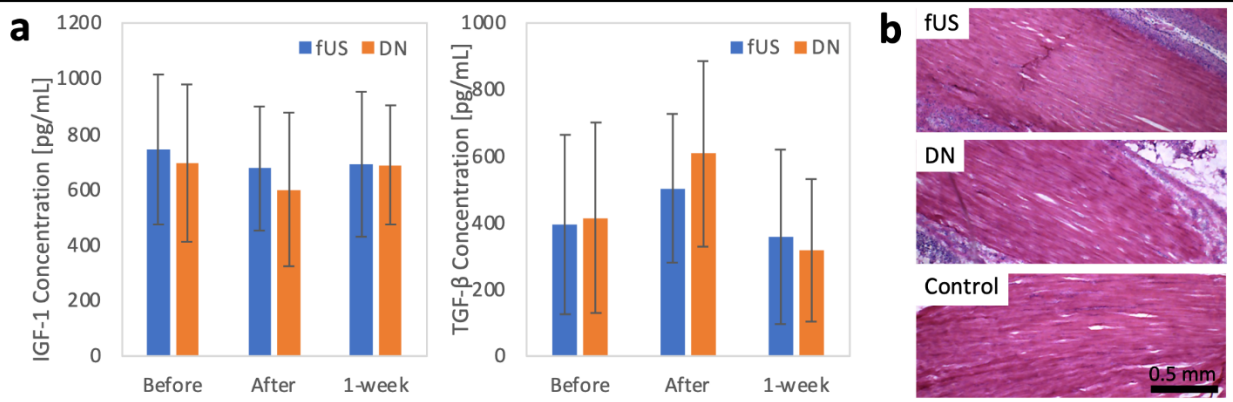


Fig.1 a) Healing factor concentrations for treatments. b) H&E-stained histology for treatments.

Changes in Tumor Viability and Vasculature following Histotripsy Exposure

Presenter: Kenneth Bader

Authors in order: Kenneth Bader, *University of Chicago*, Fernando Flores-Guzman, *The University of Chicago*, Isabella Iwanicki, *University of Chicago*, Sonia Hernandez, *University of Chicago*

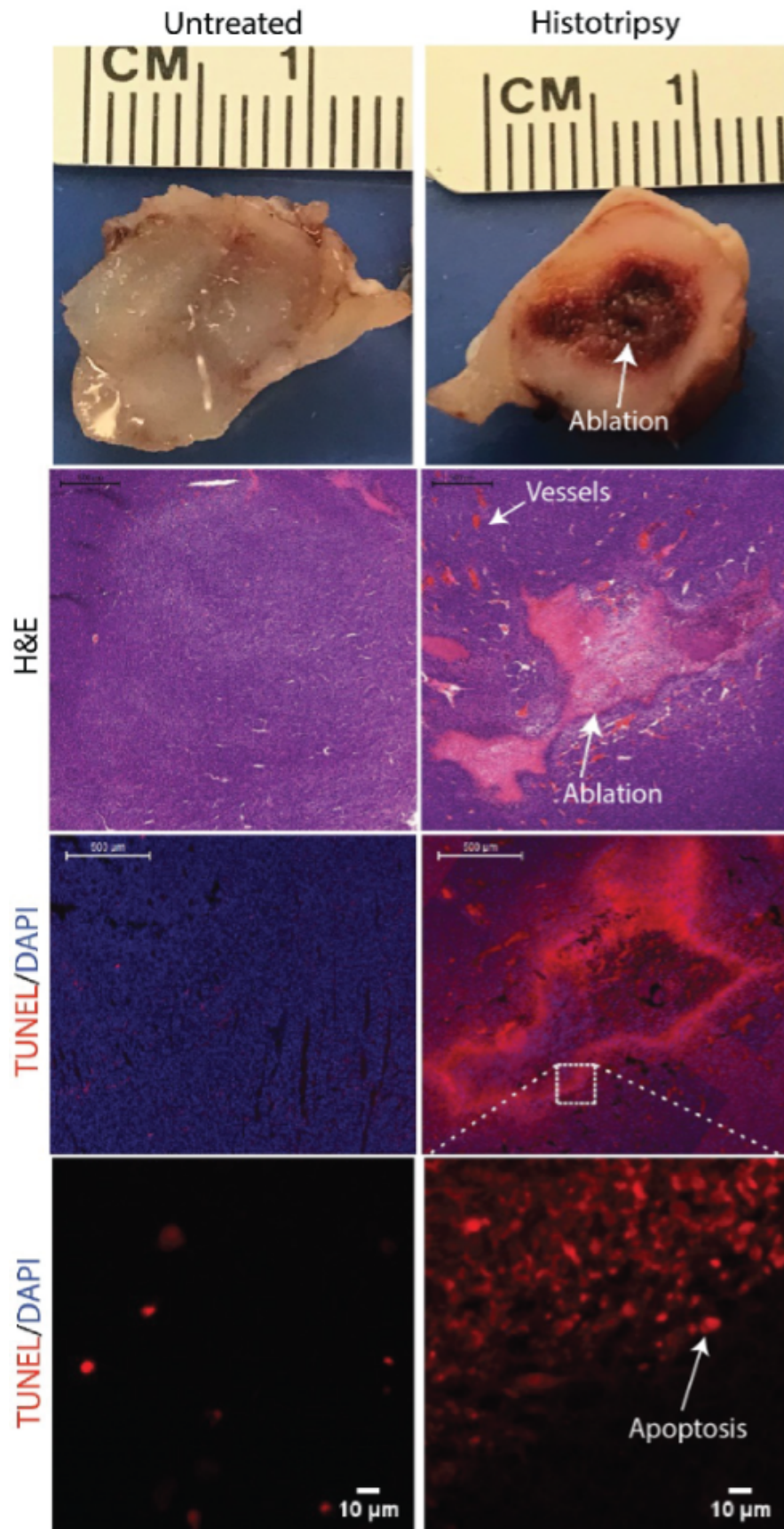
The relationship between histotripsy-induced tumor ablation, changes in tumor vasculature, and the intensity of bubble activity was investigated in pre-clinical murine models.

The effects of histotripsy were tested in subcutaneous squamous cell carcinoma (SCC VII) and orthotopic renal neuroblastoma (NGP-luciferase) murine models. The strength of histotripsy bubble activity generated within tumors was quantified based on acoustic emissions mapped with passive cavitation imaging. The viability of NGP tumor following ablation was quantified with bioluminescent imaging (IVIS). Tumors with and without histotripsy exposure were also analyzed histologically (H&E, endothelial marker isolectin-B4, and apoptosis marker TUNEL).

Robust bubble activity denoted by intense acoustic emission was generated within all tumor types. There was a significant reduction in bioluminescence intensity, indicating a diminished NGP tumor viability. Histological observations were consistent with bioluminescence measurements: treated areas displayed a loss of nuclear (DAPI) and hematoxylin staining. A narrow margin of sporadic apoptotic tumor cells were observed at the edge of the ablation zone, as indicated by large gaps in TUNEL signal. Interestingly, vasculature within 100 μm of the ablation zone appeared dilated in both models. Untreated controls displayed no change in bioluminescence or notable histological features.

The tumor models tested here mimic malignancies resistant to standard interventions. Intense histotripsy bubble activity was found to achieve effective ablation while increasing perfusion in the adjacent tissue. These findings indicate histotripsy is an attractive approach for known resistant disease, and is a promising adjuvant to conventional treatment paradigms.

These studies were funded in part by the American Cancer Society and the University of Chicago Comprehensive Cancer Center.



Nanodroplet-mediated Ultrasound Mechanotherapy for Low Energy Histotripsy

Presenter: Bar Glickstein

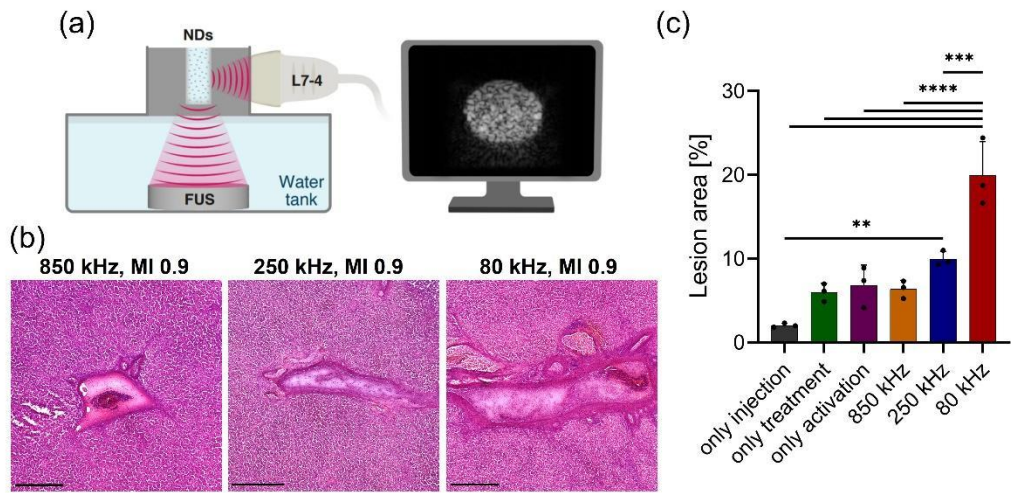
Authors in order: Bar Glickstein, *Tel Aviv University*, Tali Ilovitsh

Develop low energy ultrasound mechanotherapy by coupling low frequency ultrasound (e.g. 80 kHz) with nanoscale nanodroplets to remotely detonate tissues, with minimal off target effects

A dual imaging-therapy setup is used for the concurrent activation and detonation of nanodroplets. Nanodroplet activation was performed with an imaging transducer (L7-4, Philips ATL). Following activation into microbubbles, a spherically focused transducer operating either at 850, 250 or 80 kHz at different peak negative pressures (PNPs) was applied to the sample. Initial optimization was performed in a tissue-mimicking phantom. Next, nanodroplet-mediated histotripsy was tested in ex-vivo samples, where mechanical damage was evaluated via histology.

Nanodroplets with a mean diameter of 300 nm were fabricated. Nanodroplets vaporization into microbubbles was optimized and found to yield maximal contrast for a frequency of 5 MHz and mechanical index of 1.82. In ex-vivo chicken liver samples, comparing the results of vaporized nanodroplets insonation at 850, 250 and 80 kHz, for the same mechanical index of 0.9 revealed significant lesions and tissue debulking for the 250 and 80 kHz, while for 850 kHz the results were similar to that of the control groups. The largest lesions were observed for the 80 kHz frequency, compared to all other groups.

Our findings show that coupled with low frequency ultrasound, nanodroplets can serve as low energy cavitation nuclei for histotripsy, reducing the required energy for standard ultrasound surgery by over an order of magnitude. This method can potentially be used in the future as a low energy ultrasound surgery in tumors.



(a) The dual imaging-therapy setup. (b) Histological photomicrographs of ND-mediated histotripsy at 3 center frequencies. (c) Quantification of the lesion area for each group in (b)

B1-1

Gemcitabine-Loaded Microbubbles Reduce Toxicity of Chemoradiation

Presenter: Eleanor Stride

Authors in order: Jia-Ling Ruan, Richard Browning, Yesna Yildiz, Michael Gray, *University of Oxford*, Luca Bau, Sukanta Kamila, *Ulster University*, Anthony McHale, *Ulster University*, John Callan, *Ulster University*, Boris Vojnovic, Eleanor Stride, *University of Oxford*, Anne Kiltie, *University of Aberdeen*

To target delivery of chemotherapy using microbubbles and ultrasound, to reduce treatment toxicity in chemoradiation treatment in a murine model of muscle-invasive bladder cancer.

CD1-nude mice were injected orthotopically with RT112 bladder tumour cells. Mice were treated with intravenous gemcitabine (10mg/kg) with or without microbubbles, or microbubbles loaded with gemcitabine followed by exposure to ultrasound (1.1MHz, 1MPa peak negative pressure, 1% duty cycle, 0.5Hz pulse repetition frequency) and then irradiation (6Gy). Tumour volumes were measured by 3D ultrasound imaging. Acute normal-tissue toxicity in the lower bowel area was assessed using an intestinal crypt assay.

A significant delay in tumour growth was observed with conventional chemoradiation therapy and both microbubble groups ($P < .05$ compared with the radiation-only group). Transient weight loss was seen in the microbubble groups, which resolved within 10 days post treatment. A positive correlation was found between weight loss on day 3 post treatment and tumour growth delay ($P < .05$; $R^2 = 0.76$). In contrast to conventional chemoradiation therapy, ultrasound-mediated drug delivery methods did not exacerbate the acute intestinal toxicity using the crypt assay.

Ultrasound and microbubbles offer a promising new approach for improving chemoradiation therapy for muscle-invasive bladder cancer, maintaining a delay in tumour growth but with reduced acute intestinal toxicity compared with conventional chemoradiation therapy.

The authors thank Cancer Research UK and the Engineering and Physical Sciences Research Council for funding this work.

B1-10

Microbubble-mediated Mir-1 Delivery to Cardiomyocytes for Treatment of Hypertrophic Cardiomyopathy

Presenter: Davindra Singh

Authors in order: Davindra Singh, *Concordia University*, Stephanie He, *Concordia University*, Brandon Helfield, *Concordia University*

The aim of this study is to demonstrate the feasibility of viable ultrasound-mediated microbubble delivery of miR-1 to hypertrophic cardiomyocytes.

Our hypertrophic cardiomyopathy model was developed by incubating isolated neonatal rat cardiomyocytes (CMs) with phenylperine (100 μ M). Suspensions of healthy or diseased CMs along with homemade microbubbles (1:250 cell to bubble ratio) and free miR-1 (84nM) were placed in a chamber within a 37°C water bath. These samples were insonicated for 2 minutes (1 MHz, 62.5-250 kPa PNP; 20 cycles; 200 μ s PRI) and bubble echoes were simulatenoulsy recorded via a co-aligned 3 MHz transducer.

Two days post-delivery, miR-1 levels and cell viability were quantified with RT-qPCR and MTT assays respectively. These assays demonstrated a trend associating increasing peak-negative pressures with an increase in miR-1 delivery in healthy and diseased CMs. Specifically, treatment using a pressure of 62.5 kPa was determined to be most optimal as it resulted in a 2.79 and 2.44 fold relative increase in miR-1 in healthy and diseased CM respectively ($p=0.02$; $p=0.07$), while also ensuring a high cell viability (98% and 95% respectively). Additionally, passive cavitation data highlights that relative miR-1 expression positively correlates with inertial cavitation dose ($r=0.76$, $p=0.04$).

In this study, we demonstrated miR-1 delivery to both healthy and hypertrophied cardiomyocytes while maintaining cell viability using ultrasound-stimulated microbubbles. These findings provide evidence of the ability for ultrasound and microbubbles to be used as an image-guided delivery method for molecular therapeutics in cardiovascular disease.

This work would not be possible without funding from the Heart and Stroke Foundation of Canada.

B1-11

Enhancing Neoadjuvant Chemotherapy with Ultrasound Stimulated Microbubbles in an Orthotopic Murine Breast Cancer Model

Presenter: Carly Pellow

Authors in order: Carly Pellow, *Sunnybrook Research Institute*, Sharshi Bulner, *Sunnybrook Research Institute*, Alex Wright, *Sunnybrook Research Institute*, Kullervo Hynynen, *Sunnybrook Research Institute/ University of Toronto*, David Goertz, *Sunnybrook Research Institute*

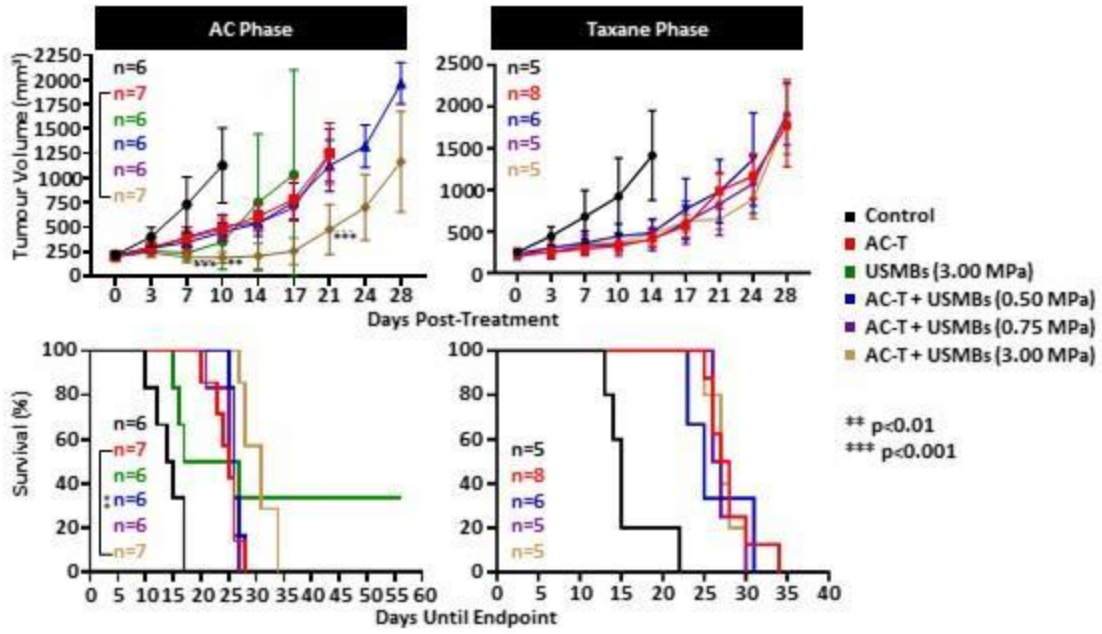
To investigate the ability of ultrasound-stimulated microbubbles (USMBs) to enhance standard-of-care neoadjuvant adriamycin+cyclophosphamide+taxane (AC-T) chemotherapy in a mouse model of locally advanced breast cancer.

Experiments were performed to inform the design of a clinical trial. USMBs treatments were assessed as a function of pressure (0.50, 0.75, 3.00 MPa) and timing (AC-phase or T-phase). Triple-negative orthotopic EMT6 tumours were employed with MRI-guided USMB treatments performed with the LP100 system (FUS Instruments) at 580 kHz. Acute experiments were conducted to permit histologic and perfusion analysis; longitudinal studies investigated tumour growth and survival. Sham, drug-only, USMB-only and combination groups were acquired.

When treating with ultrasound in the T-phase, none of the combination treatments resulted in any difference relative to the drug-only group. When treating earlier in the AC-phase, combination treatments of AC-T and USMBs resulted in tumour vascular shutdown and cell necrosis, with significantly slowed tumour growth and increased survival relative to drug-only controls at 3.00 MPa (mechanical ablation/vascular disruption regime), but not at lower (conventional drug-delivery) pressures. Notably, the USMB-only treatments in the mechanical ablation regime also resulted in 33% complete tumour regression, consistent with our previous results.

USMBs can enhance neoadjuvant AC-T chemotherapy for a triple-negative breast cancer model, but pressure and timing are critical factors. Higher pressures (3.00 MPa) can shutdown tumour perfusion and blunt tumour growth, but this combination approach should be applied in the AC-phase, or possibly prior to the start of neoadjuvant chemotherapy.

Funded by the Terry Fox New Frontiers Program project grant.



Tumour growth and survival upon treatment in the AC- and T-phases

B1-2

Microbubble Mediated Chemo-Sonodynamic Therapy for the Treatment of Prostate Cancer

Presenter: Keiran Logan

Authors in order: Keiran Logan, *Ulster University*, Thomas McKaig, *Ulster University*, Heather Nesbitt, *Ulster University*, John Callan, *Ulster University*, Anthony McHale, *Ulster University*, Sukanta Kamila, *Ulster University*

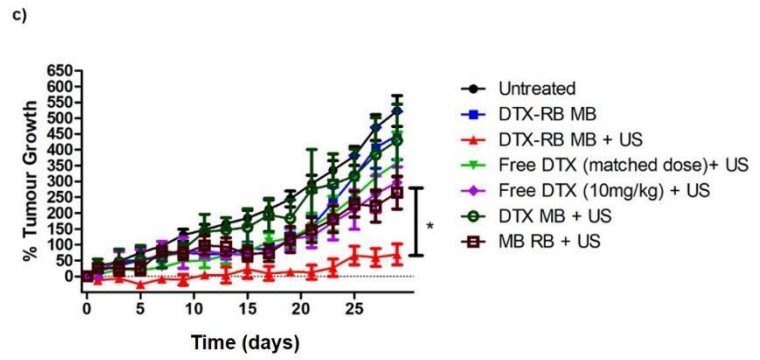
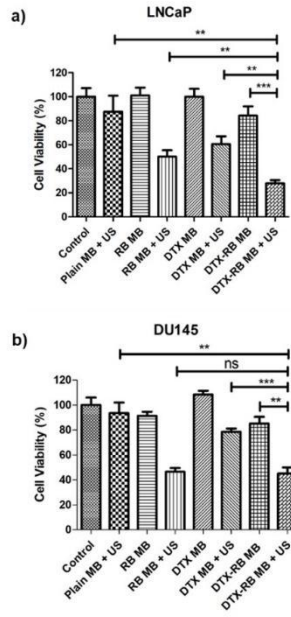
To develop a single MB formulation carrying Docetaxel/Rose-Bengal and determine the chemo-sonodynamic efficacy in spheroid and murine models of androgen sensitive/resistant prostate cancer (PC).

The commercially available phospholipid DSPE was chemically modified to carry the sonodynamic therapy sensitiser Rose Bengal (DSPE-RB). DTX-RB-MBs were prepared using a standard thin-film-hydration technique incorporating DSPE-RB and DTX within the MB-shell. The efficacy of chemo-sonodynamic therapy using the DTX-RB-MBs was determined in androgen sensitive (LNCaP) and androgen-insensitive (DU145) 3D spheroid models of prostate cancer as well as an androgen insensitive (PC3) murine model.

The cell viability (MTT) of spheroids treated with DTX-RB-MB +ultrasound (US) were 28% and 45% for LNCaP and DU145 respectively, which was significantly lower than spheroids treated with blank-MB +US (LNCaP = 87%, DU145 = 93%), DTX-MB +US (LNCaP = 60%, DU145 = 78%) or RB-MB +US (LNCaP = 50%, DU145 = 46%). Ectopic PC3 tumours treated with DTX-RB-MB+US grew only 69% after 30 days compared with 445% for tumours treated with DTX-RB-MB-US and 297% for DTX+US (scaled clinical dose). Animals treated with DTX-RB-MB showed an overall median survival of 37-days compared with free-DTX+US (23-days), DTX-MB+US (27-days) and RB-MB+US (29-days).

The efficacy of DTX-RB-MB-US was established in two clinically-relevant 3D-spheroid models of PC. This was translated into a significant reduction in tumour growth rate, and an increase in overall median survival in an ectopic mouse model. These results demonstrate the therapeutic potential of dual-loaded MBs for chemo-sonodynamic treatment of PC.

Prostate Cancer UK (Grant Ref: RIA18-ST2-003).



a) and b) MTT assay of LNCaP and DU145 spheroids; c) tumour growth delay for ectopic PC3 tumours

B1-3

Sonoporation-mediated DNA Vaccination against Hepatitis B

Presenter: Yuanchao Shi

Authors in order: Yuanchao Shi, *Shenzhen University*, Mengting Chen, *Shenzhen University*, Yaxin Hu, *Shenzhen University*

To increase the antigen expression efficiency of a hepatitis B DNA vaccine, we employed ultrasound and microbubble-mediated sonoporation to facilitate the intracellular delivery of DNA.

Cationic microbubbles loaded with DNA and Polyethylenimine (PEI) complex were first injected into the tibialis muscle of the mouse hind leg. Then, pulsed ultrasound (frequency: 0.5 MHz, pulse duration: 100 cycles, pulse repetition frequency: 1 kHz) of different pressures (0.16, 0.33, 0.52 and 0.70 MPa) and durations (5 seconds and 2 minutes) was applied to trigger sonoporation and to facilitate plasmid delivery. The status of the microbubbles was imaged using high-frequency (40 MHz) ultrasound.

We found that the transfection efficiency of sonoporation in muscle decreased with the increasing N:P ratio of DNA-PEI complex. Obvious cytotoxicity of PEI on muscle cells was found at the N:P ratio of 7. We also found that the highest transfection efficiency was achieved using ultrasound pressure of 0.7 MPa and duration of 2 minutes. Using immunofluorescence labelling, we found that the number of antigen-presenting immune cells increased in muscle treated with sonoporation. Using a plasmid encoding small surface antigen of the hepatitis B virus (HBsAg) as DNA vaccine, we detected anti-HBsAg antibody in mouse serum 4 weeks after sonoporation.

After the optimization of sonoporation parameters for muscle transfection, antigen expression efficiency as well as immune responses of the HBsAg DNA vaccine were improved.

This work was funded by the National Natural Science Foundation of China (Grant No.: 82071947) and the Shenzhen Science and Technology Programme (Grant No.: 20200813152218001).

B1-4

Novel Drug Delivery Platform for Coronary and Peripheral Arteries using Intravascular Lithotripsy

Presenter: James Kwan

Authors in order: James Kwan, *University of Oxford*, Xiaoqian Su, Hui Ying Ang, Khung Keong Yeo

Demonstrate that an intravascular lithotripsy device can facilitate the delivery of drug loaded sound-sensitive microparticles in a porcine model.

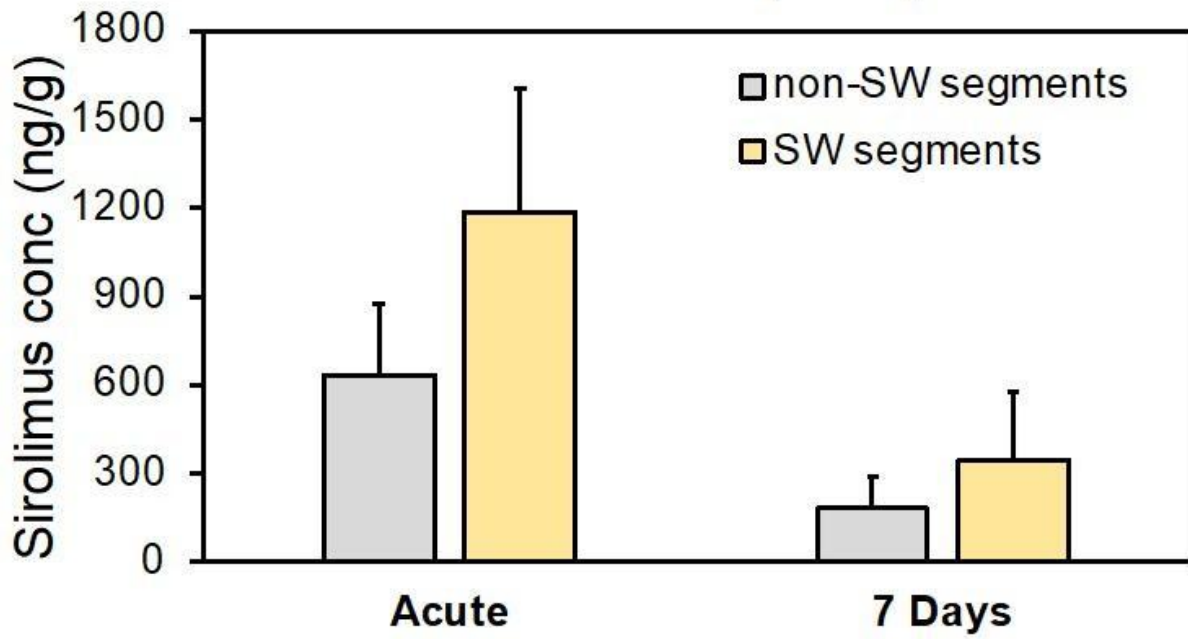
Sirolimus-loaded sound-sensitive microparticles are produced using a double emulsion method. Four pigs were divided into acute and 7 day follow up. The pigs were surgically prepared for the deployment of the Shockwave Medical Intravascular Lithotripsy (IVL) device and an occlusion balloon using two guide wires. After the artery was occluded, sound-sensitive microparticles (SSMPs) loaded with sirolimus was locally administered and shockwaves were delivered. After (immediately or one week later) treatment, arteries were measured for sirolimus.

SSMPs produced by the double emulsion method exhibited the expected multi-cavity shapes with a mean diameter around 2 micrometers. All batches of SSMPs were able to nucleate cavitation in response to ultrasound. The porcine studies were conducted to the standards set by the Institutional Animal Care and Use Committee in Singapore. Resected arteries were homogenised and sirolimus concentrations in the arterial wall was determined using LCMS. Vascular concentrations of sirolimus tended to be higher in arteries exposed to shockwaves and SSMPs compared to those not exposed to shockwaves at 0 and 7 days (Figure 1).

SSMPs in conjunction with IVL demonstrated an improved delivery of sirolimus to the arterial wall compared to arteries exposed to SSMPs but not treated with IVL. This was evident in arteries acutely harvested and those harvested 7 days after treatment, indicating that SSMPs were able to sustain delivery of sirolimus.

The authors wish to acknowledge the National Medical Research Council of Singapore and the Singapore MIT Alliance for Research and Technology for funding this work.

Vessels with SW (n=10)



B1-5

Sononeoperfusion: A New Therapeutic Effect of Enhancing Tumor Blood Perfusion using Diagnostic Ultrasound and Microbubble

Presenter: Zheng Liu

Authors in order: Zheng Liu, *Xinqiao Hospital*, Najiao Tang, Yi Zhang, Jiawei Tang

The study is to explore the blood perfusion enhancement of solid tumor using diagnostic ultrasound stimulated microbubble (USMB) treatment, a possible new therapeutic ultrasound effect.

Fifty-six rats bearing Walker-256 tumor were divided into six experimental groups and one control to explore the blood perfusion effect. USMB treatment were performed with a VINNO 70 ultrasound system and SonoVue® microbubble. The 4 MHz therapeutic ultrasound was operated with the PNP range of 0.26 to 0.32 MPa and the PRF range of 50 Hz to 2 kHz under 10.5 cycles pulse length. Another 25 rats were used to explore drug delivery and mechanism.

The USMB treatment could significantly enhance tumor perfusion and increase perfusion area at a 35% increment when treated with the 0.26 MPa and PRF 1.0 kHz pulses ($P < 0.05$). The sononeoperfusion effect occurred immediately after treatment and could last for more than 4 hours. The treatment also increased the Doxorubicin delivery to tumor about 3.12 times more than the control. ELISA tests showed that cytokines, such as ATP, eNOS, NO, PGF₂, PGI₂, C5a, LTC₄, TNF- α and ROS, increased 4 hours after treatment compared with control ($P < 0.05$).

USMB treatment using diagnostic ultrasound could enhance blood perfusion of Walker 256 tumor and significantly improve drug delivery. The sononeoperfusion effect may be related to the release of vasodilators and inflammatory factors. It might be a novel solution for overcoming therapeutic resistance of hypoperfused and hypoxia tumor.

the National Natural Science Foundation of China (No. 82127804, 82102075, 82102077), the National Key Research and Development Program of China (No. 2017YFC0107300)

B1-6

Focused Ultrasound improves the Penetration of Intrathecally Administered Methotrexate to the Spinal Cord

Presenter: Paige Smith

Authors in order: Paige Smith, *Sunnybrook Research Institute*, Danielle Charron, *Sunnybrook Research Institute*, Meaghan O'Reilly, *Sunnybrook Research Institute*

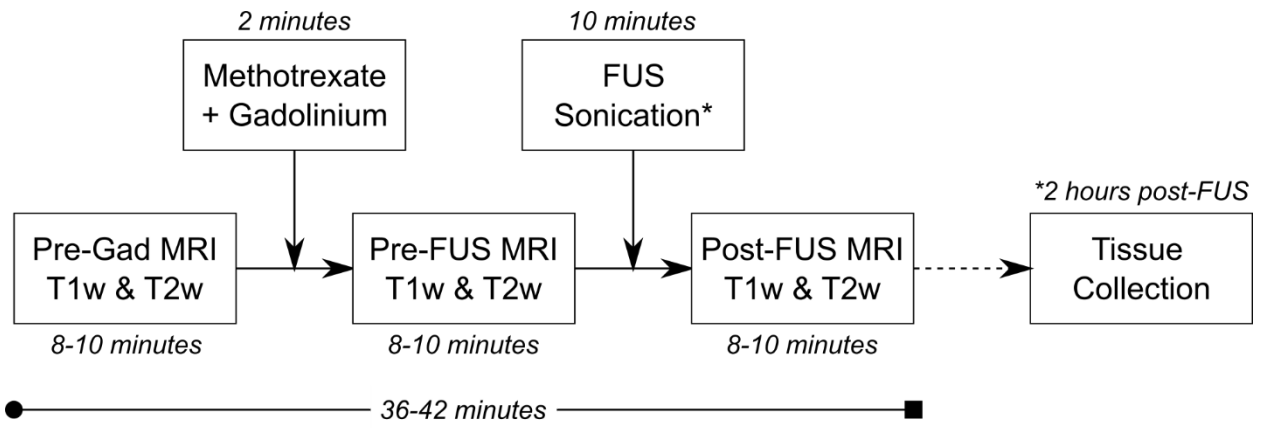
The aim of this study is to determine whether focused ultrasound (FUS) can improve the penetration of intrathecally administered methotrexate to the spinal cord.

Seven Sprague-Dawley rats underwent lumbar catheterization surgery to the subarachnoid space. After 1-week of recovery, rats were anesthetized. Methotrexate(0.05mL/kg) and gadolinium(0.003mL/kg) were injected via the catheter. Rats were sonicated with 514kHz FUS for 10-minutes (500ms sine waves, 5s pulse repetition period, 0.86MPa). Gadolinium-enhanced, 7-Tesla MRI was used to estimate drug distribution. The treatment timeline is outlined in the supporting figure. FUS-targeted and non-targeted cord samples were collected. Methotrexate concentration was measured using liquid chromatography-mass spectrometry(LC-MS).

All seven rats had accessible tubing for injections i.e., not blocked by blood. Intrathecal gadolinium was visible on pre-FUS imaging. Gadolinium enhancement was assessed on both pre- and post-FUS gadolinium-enhanced MRI. At the FUS-targeted location, gadolinium enhancement was $-10.3 \pm 23.9\%$ before sonication, compared to a non-targeted location. Enhancement increased to $27.3 \pm 30.1\%$ following sonication. LC-MS analysis revealed a methotrexate concentration of $11.7 \pm 11.1 \text{ ng/mg}$ at the FUS-targeted location. The concentration at the non-targeted location was $0.64 \pm 0.75 \text{ ng/mg}$. Pairwise analysis of methotrexate concentration in tissue samples within the same animal showed a 19 ± 10 -fold increase from non-targeted to targeted locations.

FUS appears to improve the penetration of drugs from the cerebrospinal fluid to the spinal cord as evidenced by an increase in gadolinium enhancement on MRI and an increased methotrexate concentration following LC-MS analysis. Further studies including sham groups and a rat model of spinal cord leptomeningeal metastases are ongoing.

This work was supported by the Terry Fox Research Institute. Thank you to Shawna Rideout-Gros for performing the catheter surgeries.



B1-7

Focused Ultrasound Stimulated Docetaxel-loaded Nanobubbles for Breast Cancer Therapy

Presenter: Patrick Dong Min Chang

Authors in order: Patrick Dong Min Chang, *University of Toronto*, Yiran Zou, *Department of Materials Science & Engineering*, Yun Xiang, *University of Toronto*, Sharshi Bulner, *Sunnybrook Research Institute*, Alex Wright, *Sunnybrook Research Institute*, David Goertz, *Sunnybrook Research Institute*, Naomi Matsuura, *University of Toronto*

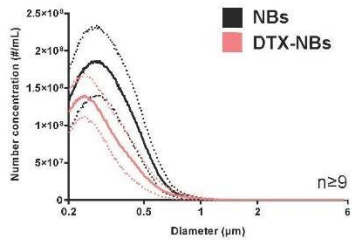
To develop and characterize the in vivo theranostic capabilities of docetaxel (DTX)-loaded nanobubbles (DTX-NBs) in combination with focused ultrasound (FUS).

Perfluorobutane-filled, phospholipid-stabilized DTX-NBs were synthesized. Size distribution was assessed by Coulter counting. DTX loading was quantified by liquid chromatography-mass spectrometry. In vitro cytotoxicity was assessed on EMT-6 cells with samples cavitated using a 1-MHz FUS transducer (0.25-1.36 MPa, 10% duty cycle, 3 min). In vivo bubble (DTX-NBs, Definity™) circulation was assessed by contrast-enhanced ultrasound (CEUS) using the Philips EPIQ7G clinical ultrasound scanner and L12-5 transducer on BALB/c mice model tumours with FUS exposure.

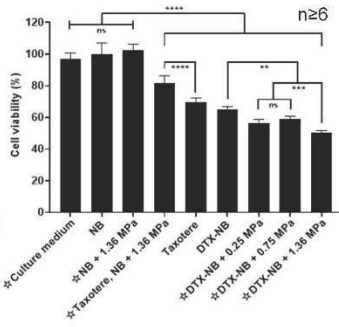
106±16 µg of DTX (n≥6) were loaded onto ~1010 nanobubbles (mode diameter~230nm) per ~0.4 µL of decafluorobutane (n≥9). Using a reported safe-for-injection gas dosage of 9 µL/kg, DTX-NBs can achieve DTX dosages of 1.6 mg/kg; this is comparable to clinical dosages of the commercial DTX formulation, Taxotere®. The greatest in vitro cytotoxic effects were elicited by DTX-NBs post-FUS exposure of 1.36 MPa. DTX-NBs demonstrated in vivo circulation times of ~5 min via CEUS imaging at off-resonant frequencies with 0.5 MPa FUS. Exposing DTX-NBs to 1.65 MPa of FUS elicited acute vascular disruption of tumours using Definity™ for pre-/post-FUS treatment imaging.

DTX-loaded phospholipid-stabilized nanobubbles were synthesized with DTX dosages comparable to Taxotere® and exerted greater cytotoxic effects on EMT-6 cells in vitro post-FUS exposure. FUS-triggered bubble destruction of DTX-NBs can be visualized in real-time via CEUS in vivo. Future work will examine combined drug delivery and vascular disruption capabilities of DTX-NBs.

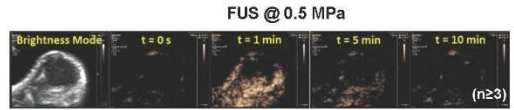
The authors thank the CIHR, NSERC, ORF, Government of Ontario, EMHSeed, SickKids, OCE, CCSRI, PCC, NFRF, OGS, BME and Dr. Carly Pellow, Dr. Cameron Stewart.



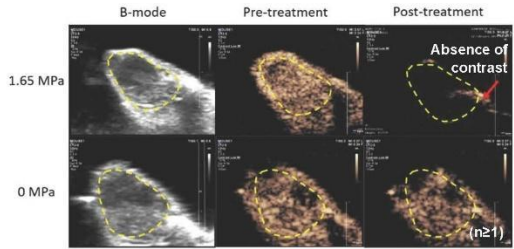
Number size distribution of unloaded nanobubbles (NBs) and DTX-NBs.



EMT-6 cell viability of DTX-NBs, NBs, and Taxotere® *in vitro*.



Brightness mode+minute CEUS images of DTX-NBs *in vivo* tumours.



B-mode/CEUS images of Definity™ *in vivo* pre-/post-FUS exposure of DTX-NBs.

B1-8

A Quantitative Method to Study Ultrasound-Induced Nano-Drug Delivery

Presenter: Tyler Hornsby

Authors in order: Tyler Hornsby, *Ryerson University*, Anshuman Jakhmola, *Ryerson University*, Farshad Moradi Kashkooli, *Ryerson University*, Michael Kolios, *Ryerson University*, Jahangir (Jahan) Tavakkoli, *Ryerson University*

Determine the significance of thermal and non-thermal mechanisms of low-intensity pulsed ultrasound (LIPUS) induced release of anticancer drugs from gold nanoparticle (GNP) drug carriers.

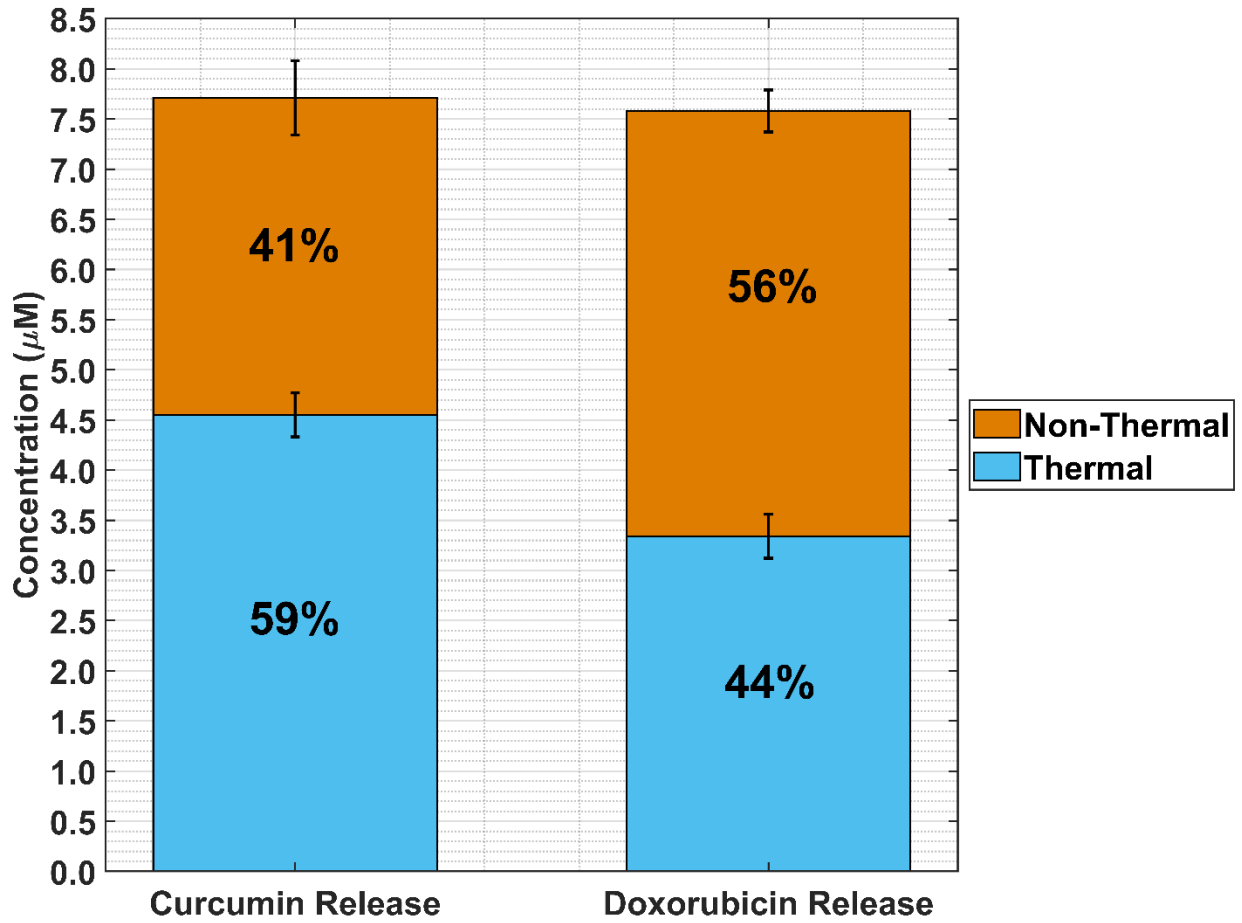
Two types of treatments, with similar temperature profiles, were used to induce drug release: localized tissue heating with a water bath, and LIPUS exposure, both for 5 minutes. Water bath heating was used to measure drug release caused by thermal effects only, while LIPUS exposure was used to achieve a combined thermal and non-thermal drug release. Drug release was compared via fluorescence measurements toward quantifying thermal and non-thermal mechanisms of release.

Drug release was performed for two anticancer drugs bound to the surface of GNP drug carriers, curcumin and doxorubicin, using either a water bath or LIPUS treatment. There was a 69.5% and 127.0% increase in drug release when comparing LIPUS treatment (both thermal and non-thermal mechanisms) to water bath (thermal mechanisms only) heating for curcumin and doxorubicin, respectively. It was determined that thermal and non-thermal mechanisms account for 59% and 41% respectively in curcumin release, and 44% and 56% respectively in doxorubicin release.

Curcumin and doxorubicin release from GNP drug carriers was achieved in an ex vivo tissue model using both water bath heating and LIPUS treatments. By comparing drug release for both treatments, contributions to drug release for thermal and non-thermal mechanisms in LIPUS-induced release were quantified.

The authors wish to thank Dr. Kevin Rod at Toronto Poly Clinic, for their support. Partial funding was provided by NSERC Alliance grant (ALLRP 556270-20).

Thermal vs. Non-Thermal Drug Release In *Ex Vivo* Tissue



Comparing Drug Delivery Efficiency of Lipid-shelled Drug-loaded Nanobubbles versus Microbubbles in Orthotopic Liver Tumors

Presenter: Pinunta Nittayacharn

Authors in order: Pinunta Nittayacharn, *Case Western Reserve University*, Eric Abenojar, *Case Western Reserve University*, Michaela Cooley, *Case Western Reserve University*, Claire COUNIL, *Case Western Reserve University*, Felipe Matsunaga, Celina Yang, *Ryerson University*, Amin Jafarisojahrood, *Sunnybrook Health Science Center*, Muhammad Khan, *Ryerson University*, Agata Exner, *Case Western Reserve University*, Michael Kolios, *Ryerson University*

We report on the pharmacokinetics and biodistribution of sonicated Doxorubicin-loaded C3F8 nanobubbles (hDox-NBs) in orthotopic rat liver tumors compared to microbubbles (hDox-MBs).

hDox-NB/MBs were formulated and purified as previously reported¹. Tumors were initiated in the livers of rats by direct injection of N1-S1 cells. 1mL of bubbles (Dox dose: 327.75 µg/kg) was administered via the tail vein. After 2 min, tumors were exposed transabdominally to unfocused TUS at 3 MHz, 2.2W/cm², 10% duty cycle for 5 min. hDox fluorescence in tumors was measured after 3h using optical imaging (Maestro), and drug distribution was analyzed using ImageJ.

hDox-MBs (diameter 1104 nm) and hDox-NBs (diameter 321 nm) were prepared using size isolation via centrifugation (Fig 1a) and normalized to total Dox dose. Kinetics of purified bubbles (Fig 1b) show higher peak intensity and longer circulation time for MBs. However, treatment with hDox-NB+TUS, resulted in a 30.4% increase in Dox accumulation in tumors compared to hDox-MB+TUS, with higher tumor specificity and less off-target effects in the liver and other major organs (Fig 1e). Treatment with NBs decreased Dox by 1.3, 1.5, 7.5, 5.1-fold in the kidney, spleen, heart, and lung, respectively.

Results demonstrate an increase in delivery efficiency and tumor specificity with hDox-NBs compared to hDox-MBs and TUS, highlighting the potential of this approach as a viable treatment modality for tumors in the liver. Experiments to assess acute damage in tumors and surrounding normal liver and Dox in organs are ongoing.

This work was supported by the National Institutes of Health (RES224345).

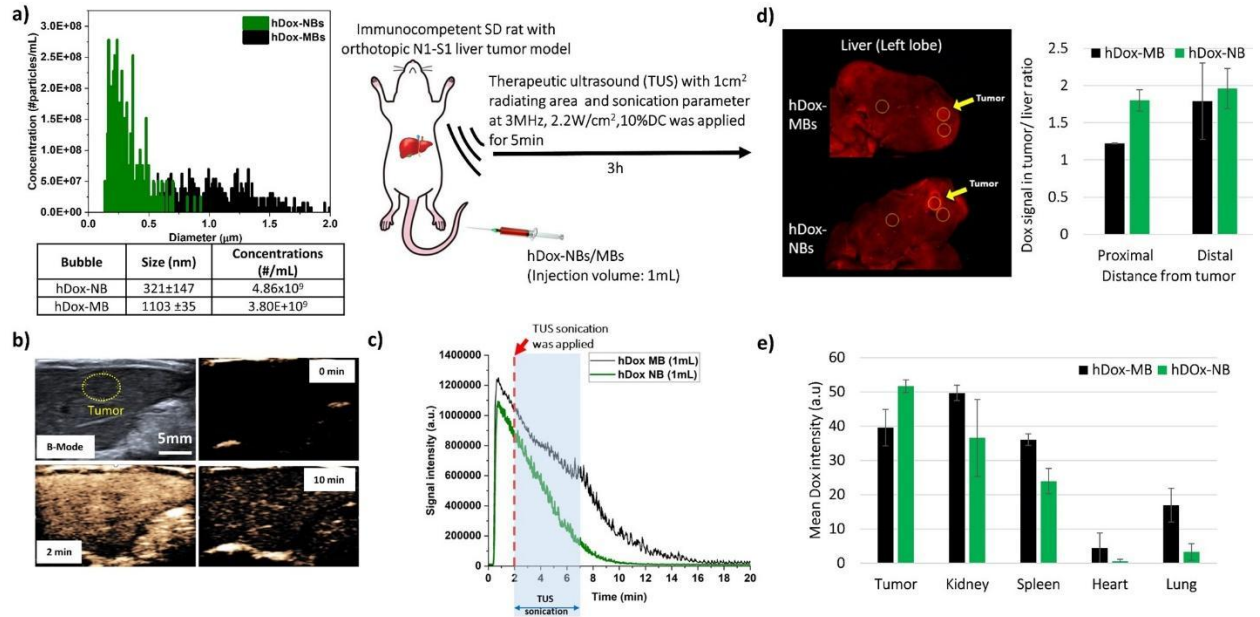


Figure 1. a) Concentration and size distribution of purified hDox-NBs and MBs measured by RMM (Malvern); b) Representative US imaging of tumor in the liver. Prior treatment, location of tumor were imaged using clinical US in B-mode. NB/MB enhancement of tumor in the liver was imaged at 8 MHz with an 18 MHz probe, 0.1 MI; c) Time intensity curves of tumor after bubble administration; d) Representative *ex vivo* fluorescence images of tumors, 3h after rats were i.v. injected with hDox-NBs/MBs and exposed to TUS; e) Average fluorescent intensity of Dox in rat organs. Organs without hDox were used as baseline signal. The analyzed region of interest is shown in yellow dashed line. ¹Nittayacharn P, et.al.2020 Front Phamacol.

B2-1

Therapeutic Applications of Nanobubbles in Cancer

Presenter: Agata Exner

Authors in order: Pinunta Nittayacharn, *Case Western Reserve University*, Eric Abenojar, *Case Western Reserve University*, Reshani Perera, *Case Western Reserve University*, Agata Exner, *Case Western Reserve University*

Nanobubbles offer unique advantages in ultrasound-mediated therapy due to their size, stability and high concentration. This presentation will highlight emerging nanobubble applications in cancer therapy.

Lipid-shelled C3F8 nanobubbles [1] are being examined in a variety of stand-alone or combination therapeutic strategies. These include ultrasound-mediated delivery of doxorubicin for treatment of ovarian [2] and liver cancer, delivery of iridium III complexes for sonodynamic therapy (SDT) [3], sensitization of external beam radiotherapy for prostate cancer treatment [4], and drug-free therapy of prostate cancer using nanobubbles targeted to the prostate specific membrane antigen (PSMA) [5].

Outcomes of nanobubble-based therapies were assessed in cell culture and human cancer xenografts in mice, rats and rabbits. In vitro, nanobubbles show effective intracellular drug delivery and an ability to induce endosomal escape following cavitation. SDT using nanobubbles also showed strong effects and resulted in production of reactive oxygen species. In vivo, ultrasound-mediated drug delivery using nanobubbles shows improved tumor penetration and increased delivery efficiency. Tumor sensitization using nanobubbles results in improved radiation treatment compared to microbubbles and leads to significant tumor regression. Finally, drug-free therapy using PSMA-targeted nanobubbles led to apoptosis and arrested tumor development in flank and prostate.

Nanobubbles can effectively reach target tissues and cells due to prolonged in vivo circulation times of nearly 1 hour, and the ability to extravasate in regions of increased vascular permeability. At concentrations of several orders of magnitude higher than microbubbles, they are ideal for efficient drug delivery and combination therapies.

We acknowledge our exceptional collaborators at CWRU, Ryerson, and Sunnybrook, National Institute of Biomedical Imaging and Bioengineering R01EB025741, National Cancer Institute R01CA260826 and the Case-Coulter Translational Research Partnership.

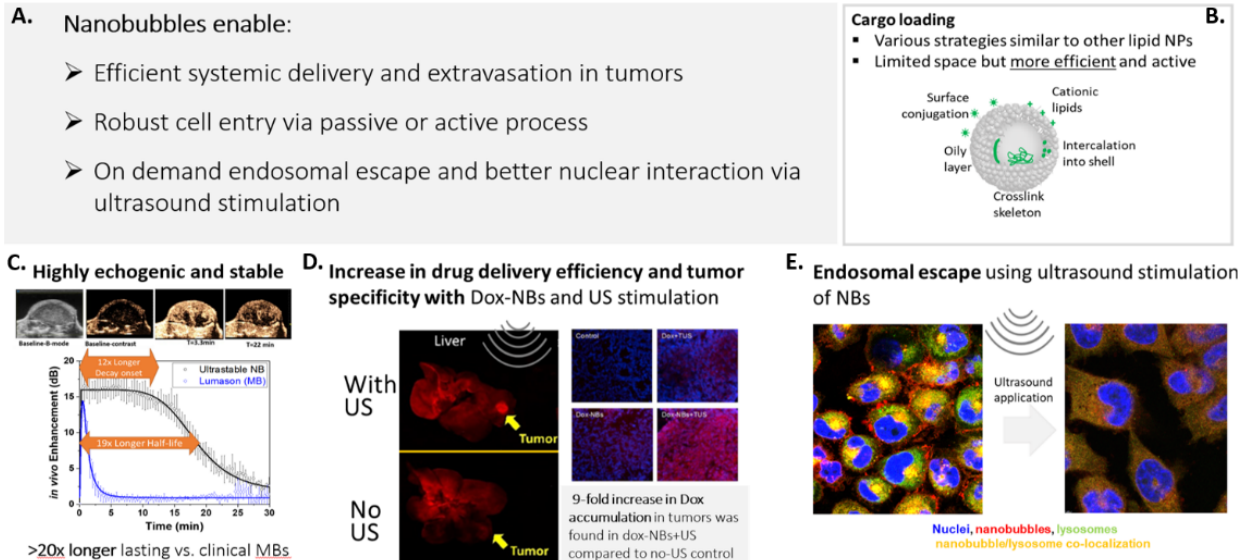


Figure 1: Overcoming barriers to cancer therapy with nanobubbles. **(A)** unique drug delivery processes enabled by the compressible, deformable gas-core, lipid shelled nanobubbles. **(B)** Cargo loading strategies in nanobubbles. **(C)** *In vivo* echogenicity of nanobubbles in flank murine tumor imaged in nonlinear contrast mode (Visualsonics Vevo 3100) and their stability in mouse kidneys compared to MBs [1]. **(D)** Improved drug delivery efficiency with doxorubicin loaded bubbles [2]. **(E)** Nanobubbles internalized via receptor mediated endocytosis are immobilized in vesicles for up to 24 hours, and endosomal escape can be facilitated by low frequency, higher intensity ultrasound (1.5 MHz, 2.2 W/cm²) [3].

[1] De Leon et al, *Nanoscale* 2020; [2] Nittayacharn et al, *J Pharm Sci* 2019; [3] Nittayacharn et al, *Bioconj Chem* 2021; [4] Hysi et al, *Photoacoustics* 2021 ;[5] Perera et al, *Nanotheranostics* 2022.

B2-10

Bubble Nucleation in Polyacrylamide Hydrogels with Varying Stiffness and Impurities

Presenter: Ferdousi Sabera Rawnaque

Authors in order: Ferdousi Sabera Rawnaque, *Pennsylvania State University*, Julianna Simon, *The Pennsylvania State University*

Our objective was to evaluate the effect of varying stiffness and impurities on bubble nucleation in tissue mimicking polyacrylamide (PA) hydrogels.

Acoustic cavitation was induced in 17.5%, 20% and 22.5% v/v PA hydrogels using a 1.5-MHz focused ultrasound transducer with pressures ranging up to $p_+ = 89$ MPa, and $p_- = 26$ MPa and monitored using high-speed photography. The effect of impurities was evaluated by embedding hydrophobic cholesterol crystals at 0.25% w/v (maximum dimension=0.6 mm) in 17.5% v/v PA hydrogels (n=3) or by adding 10% bovine serum albumin (BSA) in separate 17.5% v/v PA hydrogels (n=3).

Bubble nuclei available for acoustic cavitation was found to increase with increasing peak negative pressure and to decrease with increasing hydrogel stiffness. Adding cholesterol crystals decreases the acoustic cavitation threshold (peak negative pressure at which acoustic cavitation probability $\geq 50\%$) from $p_- = 19$ MPa for 17.5% v/v hydrogels with no added impurities to $p_- = 9$ MPa for the same concentration hydrogel with added cholesterol crystals. Increasing the protein concentration in 17.5% v/v PA hydrogels from 1% BSA to 10% shows decrease in acoustic cavitation threshold from $p_- = 19$ MPa to $p_- = 6$ MPa.

These results suggest acoustic cavitation in PA hydrogels depends on the availability of bubble nuclei. The addition of impurities such as hydrophobic cholesterol crystals or BSA proteins introduces inhomogeneities similar to biological tissues and increases the number of trapped bubble nuclei available for acoustic cavitation.

Work supported by NSF CAREER 1943937 and PSU Riess Fellowship.

B2-11

Assessing Tumoral Vascular Permeability and Nanoparticle Extravasation with Nanobubble Contrast-enhanced Ultrasound Imaging

Presenter: Michaela Cooley

Authors in order: Michaela Cooley, *Case Western Reserve University*, Dana Wegierak, *Case Western Reserve University*, Reshani Perera, *Case Western Reaserve University*, Eric Abenojar, *Case Western Reserve University*, Michael Kolios, *Ryerson University*, Agata Exner, *Case Western Reserve University*

This work examined whether multiparametric dynamic contrast-enhanced ultrasound imaging using nanobubbles could help predict tumor vascular permeability and retention of doxorubicin-loaded liposomes.

Athymic nude mice were injected (hind limb) with either LS174T (colorectal adenocarcinoma, n=5; highly permeable) or U87 (glioblastoma, n=5; minimally permeable) cells. Mice were imaged with nonlinear contrast-enhanced ultrasound (VisualSonics Vevo 3100, 18 MHz, 4% power) using nanobubbles¹ injected via tail vein weekly for 2-3 weeks, depending on tumor size. 1 day before euthanasia, doxorubicin-loaded liposomes were injected into the mice. Time-intensity curve (TIC) and decorrelation analysis (created with MATLAB) were performed.

Parameters including peak intensity, area under the curve, area under the rising curve (AUCR), time to peak, and decorrelation time (DT) were extracted from the TIC data. Larger LS174 tumors showed a 4.8-fold larger AUCR and 2.8-fold higher peak intensity compared to U87 tumors (Figure 1a-b). Smaller tumors did not show similar differences. DT maps starting from peak intensity showed a mean DT of 16.5s for LS174T (Figure 1c) compared to 2.5s for U87 (Figure 1d). These parameters may be correlated to nanoparticle extravasation and retention in tumors. Histological analysis of doxorubicin distribution in tumors is ongoing.

Substantial differences in nanobubble-generated TIC parameters AUCR, peak intensity, and decorrelation time were noted between LS174T and U87 tumors. This suggests that nanobubbles may be useful in determining tumor permeability and could potentially be used as a biomarker for patient responsiveness to nanoparticle therapies.

The authors would like to acknowledge funding from NIBIB (R01EB025741 and R01EB028144), CWRU MSTP and NIGMS (T32GM07250), and NHLBI (F30HL160111)

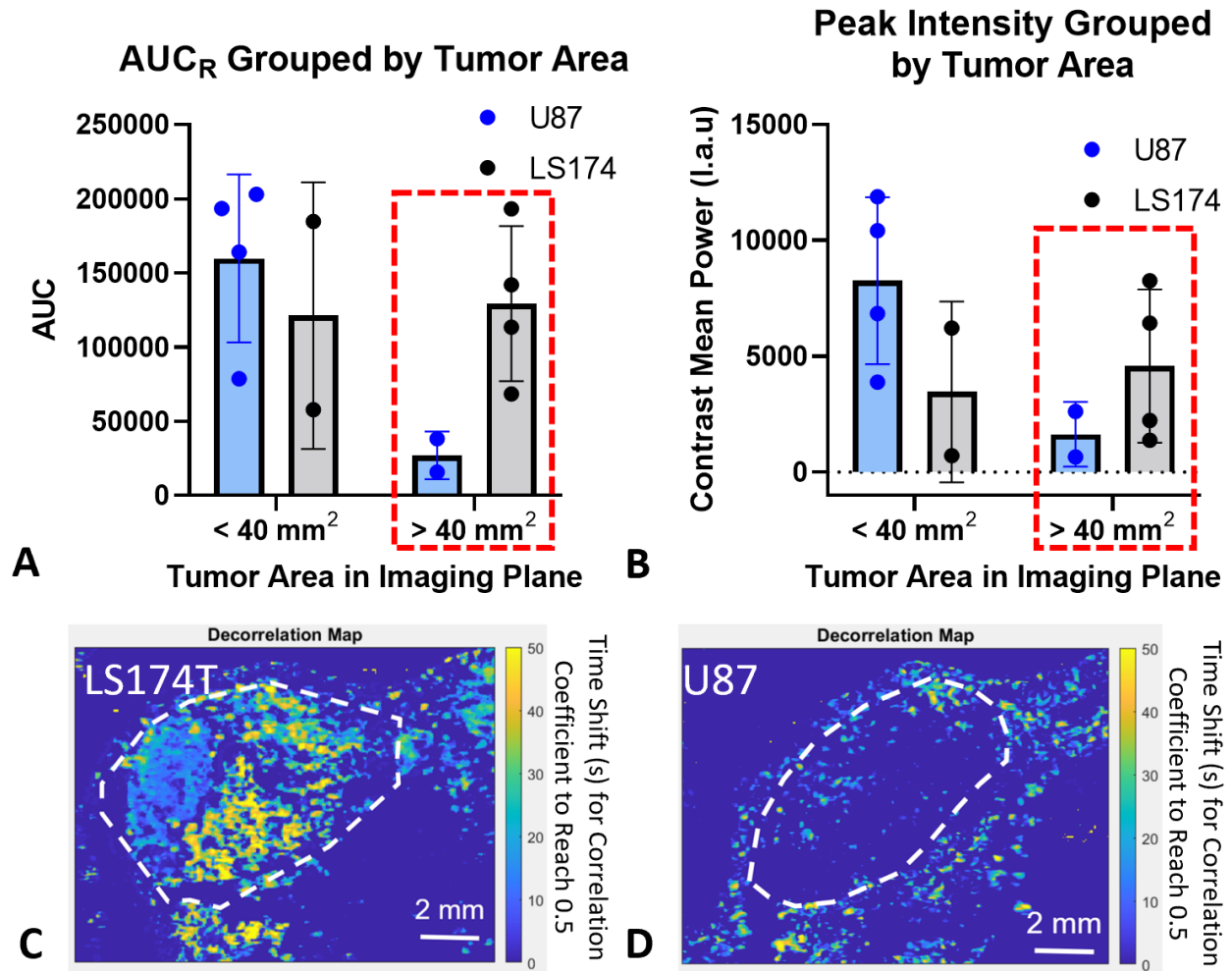


Figure 1. Contender parameters extracted from time-intensity curve data comparing U87 and LS174 tumors. (a) Area under the rising curve (AUC_R) comparing tumors of different sizes. (b) Peak intensity comparing tumors of different sizes. Like the AUC_R, larger tumors tend to show greater differences between tumor type than smaller tumors. (c) Representative decorrelation time maps beginning from the time at peak intensity in LS174T and (d) U87 tumors. The LS174 tumor shows a longer decorrelation time. Tumors are outlined in white.

¹De Leon et al. *Nanoscale*. 2019

B2-2

Cavitation Bubble Cloud Behavior and Tissue Ablation from a 6.3 MHz High Frequency Endoscopic Histotripsy System

Presenter: Jessica Gannon

Authors in order: Jessica Gannon, *Virginia Tech - Wake Forest School of Biomedical Engineering and Sciences*, Thomas Landry, *Dalhousie University*, Jeremy Brown, *Dalhousie University*, Jeffrey Woodacre, *Dalhousie University*, Eli Vlasisavljevich, *Virginia Tech*

This study investigates the cavitation bubble cloud dynamics and ablation capabilities of a 6.3MHz endoscopic histotripsy transducer recently developed for high precision histotripsy ablation.

High-speed optical imaging captured bubble cloud images generated by the high-frequency transducer inside 1% agarose phantoms. Bubble cloud features were characterized for 1-12 cycle pulses applied at pressures ranging from 26-44MPa at 1kHz pulse repetition frequency. Histotripsy was applied to red blood cell (RBC) phantoms to evaluate ablation efficiency, comparing ablation area as a function of pulse number for each pulsing parameter. Results for all experiments were compared to previous histotripsy studies at lower frequencies.

Results showed that the 6.3MHz histotripsy transducer was capable of generating precise, well-defined bubble clouds (< 1 mm in maximum dimension), with no off-target cavitation observed outside the focus. The cavitation threshold decreased as a function of applied cycles, ranging from ~ 34 and ~ 26 MPa for 1 and 12 cycle pulses, respectively. Cloud size increased with cycles, with maximum cloud dimension ranging from $\sim 0.35 \pm 0.08$ mm and $\sim 0.83 \pm 0.24$ mm for 3 and 12 cycle pulses, respectively. Compared with lower frequency histotripsy systems, the 6.3MHz cloud was significantly smaller and well-defined, suggesting this system is ideal for high-precision treatments. Ablation efficiency characterization in RBC phantoms is ongoing.

This study demonstrates the high-precision capabilities of a 6.3MHz endoscopic histotripsy transducer in development for the treatment of brain tumors and other disorders. Results further show the bubble cloud dimensions can be finely tuned by adjusting acoustic parameters, allowing for the generation of sub-millimeter bubble clouds and precise tissue ablation.

This work is supported by a National Science Foundation Graduate Research Fellowship and the Atlantic Canada Opportunities Agency (Atlantic Innovation Fund no.207828).

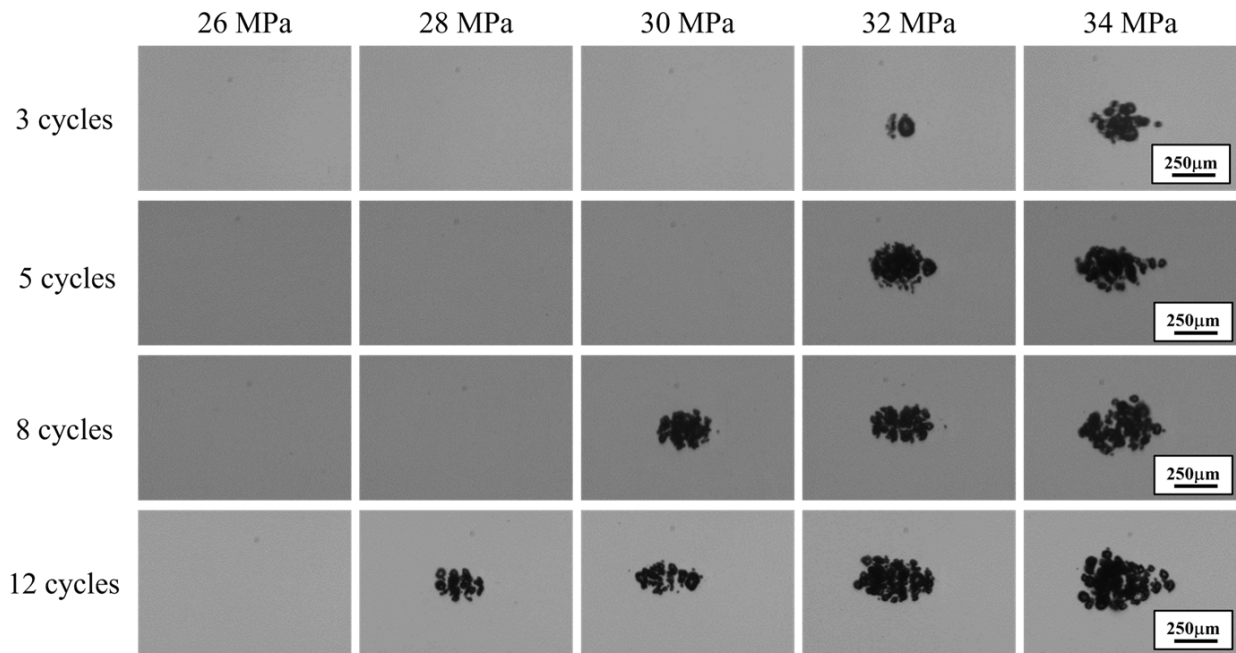


Figure 1. 6.3MHz bubble cloud images in 1% agarose phantoms.

B2-3

High-speed Microscopy of Microbubble-vessel Interactions in an In-vivo Chorioallantoic Membrane Model

Presenter: Rojin Anbarafshan

Authors in order: Rojin Anbarafshan, *University of Toronto, Sunnybrook Research Institute*, Carly Pellow, *Sunnybrook Research Institute*, Alex Wright, *Sunnybrook Research Institute*, Sara Mar, *University of Toronto*, Hon Leong, *Sunnybrook Research Institute*, David Goertz, *Sunnybrook Research Insititute*

To investigate microbubble-microvessel interactions in an in-vivo chorioallantoic membrane (CAM) model using high-speed microscopy and cavitation monitoring at high pressures relevant to mechanical ablation.

A novel high-speed microscopy system (10kfps, 2 μ s shutter speed) was developed to directly visualize the interaction of ultrasound-stimulated microbubbles and vasculature in-vivo in the chorioallantoic membrane of a duck embryo. This enables co-aligned simultaneous optical monitoring (single vessel: 40x, 100 μ s timescale; vascular network: 10x, 0.3ms timescale) and sonication (custom PZT 'ring' transducer) of the CAM with passive cavitation detection during high pressures and therapeutically relevant long exposures (1MHz, 5ms pulse length, 1-4MPa).

Insonated microbubbles were observed to interact with and deform microvessel walls, leading to blood flow alterations and eventual extravasation of intact microbubbles in some cases. At 1MPa, wall deformations were minor (2MPa), local deformations reached as high as 88% and led to vessel wall rupture and erythrocyte leakage, with sustained damage in 48% of cases. Smaller vessels () were preferentially affected whereas larger vessels (>75 μ m) mostly remained intact. Acoustic emissions at higher pressures exhibited broadband noise levels, in addition to distinct 1/3 and 1/2 order sub- and ultraharmonics.

These observations provide the first direct in-vivo evidence of microbubble extravasation along with new insights into the mechanisms of microbubble-microvessel interactions under conditions relevant to mechanical ablation (vascular disruption therapy). Results suggest that the induced effects are highly dependent on vessel size, with smaller vessels being more susceptible to damage.

This work was funded by the Canadian Institutes of Health Research.

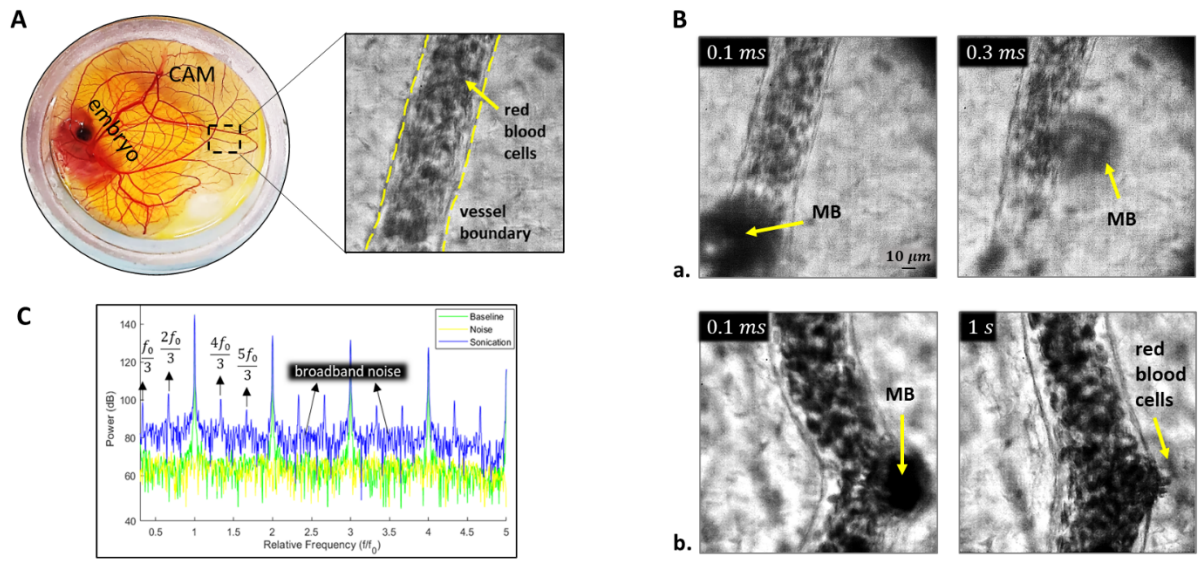


Fig. 1. (A) Duck embryo in custom dish with example image of CAM. **(B)** Microbubble activity and vascular effects (a. MB extravasation b. Blood leakage) **(C)** Frequency spectrum of the acoustic signal associated with bubble activity.

Conditions for the Propagation of Focused Ultrasound through Dense Bubble Clouds with Minimum Loss: A Numerical Study

Presenter: Amin Jafarisojahrood

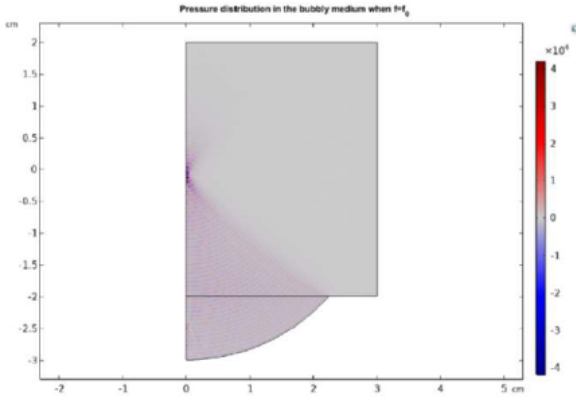
Authors in order: Amin Jafarisojahrood, *Sunnybrook Health Science Center, Raffi Karshafian, Toronto Metropolitan University*, David Goertz, *Sunnybrook Research Institute*, Michael Kolios, *Ryerson University*

Applications of microbubbles (MBs) in biomedical ultrasound (US) require detailed knowledge of the nonlinear pressure-dependent changes of the attenuation and sound speed in bubbly media.

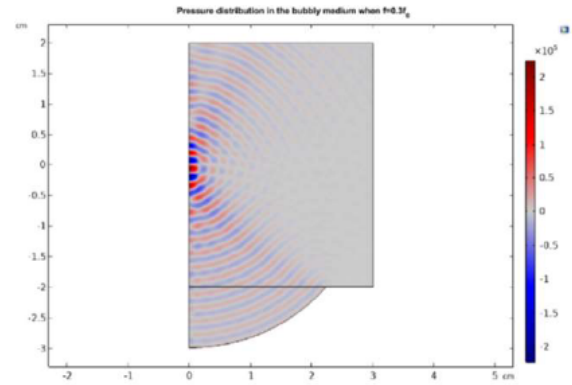
Using our recently developed comprehensive bifurcation analysis, radial oscillations of MBs were studied as a function of pressure at various frequencies, including the linear resonance frequency (f_r), super-harmonic (SuH) and subharmonic (SH) f_r . For each nonlinear oscillation regime, propagation of focused ultrasound through bubbly media is studied using finite element simulations. Accordingly, the pressure-dependent attenuation and sound speed of the bubbly media are classified in each regime and for therapeutically relevant MB concentrations and exposure parameters.

Finite element simulations show that the pre-focal MB activity and attenuation can considerably be suppressed when MBs are sonicated with frequencies sufficiently below their f_r . Figure 1 shows that MBs shield the focus when they are sonicated with their f_r , while sub-resonance sonication can considerably suppress pre-focal MB activity and reconstruct the focus. This suppression of pre-focal activity is due to the pressure dependence of MB SuH f_r where MBs oscillate very weakly for lower pressures; however, they exhibit an abrupt increase in oscillations above a pressure threshold (depending on the US frequency and MB size).

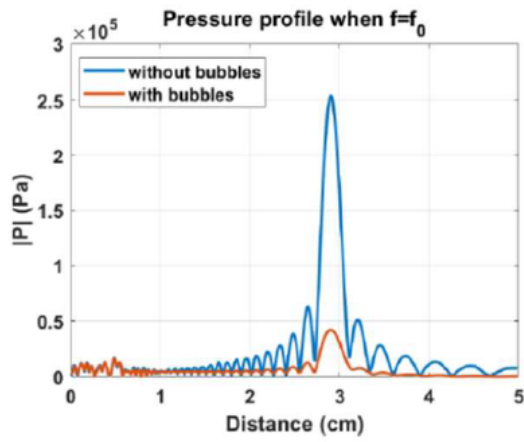
By considering the classified pressure-dependent attenuation regimes, focused ultrasound wave propagation through bubbly media can be optimized. We show that the ultrasonic waves can tunnel through dense MB populations with a minimum loss if the sonication frequency (value depending on the desired focal pressure) is chosen sufficiently below f_r of the MBs population.



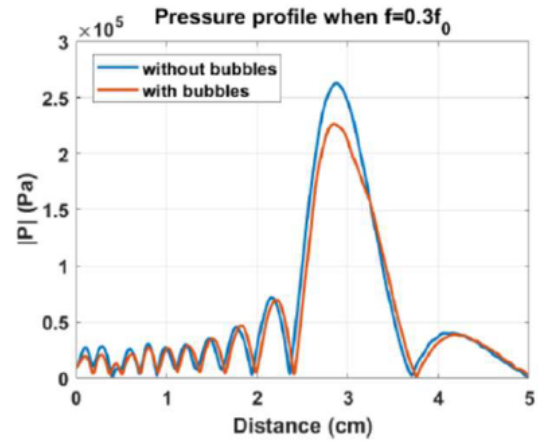
(a)



(b)



(c)



(d)

Figure 1: Spatial pressure profiles when a suspension of $3.6\mu\text{m}$ MBs is sonicated with: a- f_r , b- $0.3f_r$. c-d- the corresponding axial pressure profile

B2-5

Integrin Ligation Mediates Ca²⁺ Response Elicited by Cavitation Microbubble

Presenter: Fenfang Li

Authors in order: Fenfang Li, *Shenzhen Bay Laboratory*, Brenton Hoffman, Pei Zhong

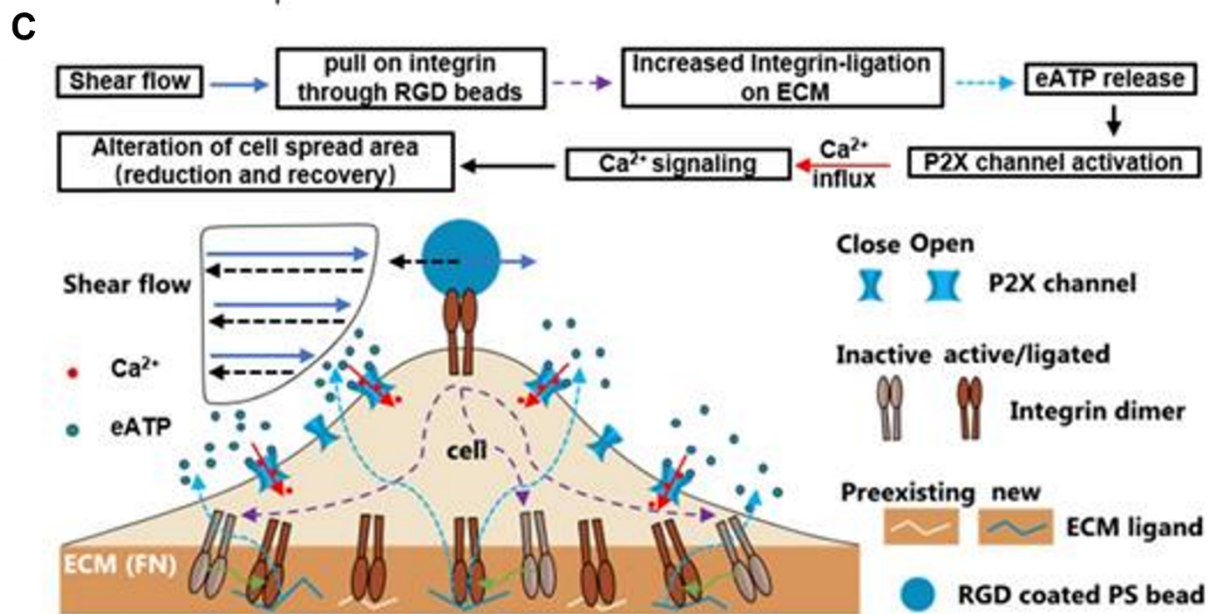
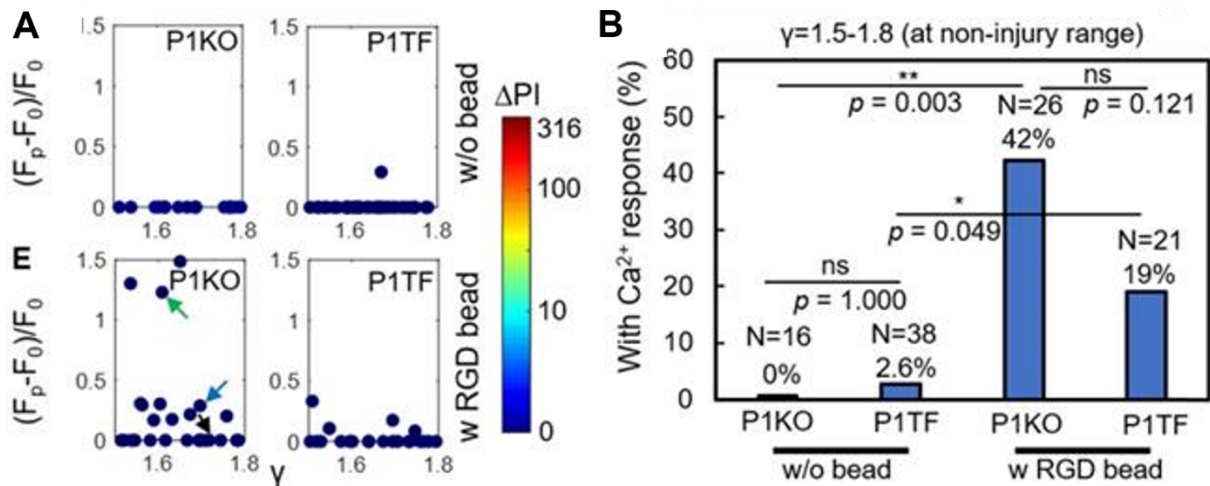
To understand the effect of potential mechanosensitive molecular players for microbubble induced Ca²⁺ signaling, including mechanosensitive ion channels, purinergic signaling and integrin ligation.

Here, laser-induced microbubbles were used to stimulate individual HEK293T cells either genetically knocked out (PIKO) or expressing Piezo1 ion channels (PITF) with different normalized bubble-cell distance. Ca²⁺ signaling and potential membrane poration (indicated by PI) were evaluated with a real-time fluorescence imaging system. Integrin-binding microbeads were attached to the apical surface of the cells under mild cavitation conditions, where the effect of Piezo1, P2X receptors and integrin ligation on single cell intracellular Ca²⁺ signaling was assessed.

Ca²⁺ responses were rare at normalized cell-bubble distances that avoided membrane poration, even with overexpression of Piezo1, but could be increased in frequency up to 42% of the cells by attaching integrin-binding beads. We identified key molecular players in the bead-enhanced Ca²⁺ response: 1) increased integrin ligation by substrate ECM triggered ATP release and 2) activation of P2X-but not Piezo1-ion channels. The resultant Ca²⁺ influx caused dynamic changes in cell spread area.

This approach to safely eliciting a Ca²⁺ response with cavitation microbubbles and the uncovered mechanism by which increased integrin-ligation mediates ATP release and Ca²⁺ signaling may inform new strategies to stimulate tissues with ultrasound and shockwaves.

We thank Prof. Jorg Grandl and Dr. Kenneth Yamada for providing cell lines, plasmids and antibodies. This work was supported by the NIH Grant 5R37-DK052985-23.



Enhancement of Ca^{2+} response requires integrin ligation and eATP release

Characterisation of Cavitation Threshold Properties of Selected Hydrogels as Tissue Mimics for Therapeutic Ultrasound

Presenter: Lisa Braunstein

Authors in order: Lisa Braunstein, *The Institute of Cancer Research*, Sarah Brüningk, *ETH Zurich*, Ian Rivens, *Institute of Cancer Research*, John Civale, *The Institute of Cancer Research*, Gail ter Haar, *The Institute of Cancer Research*

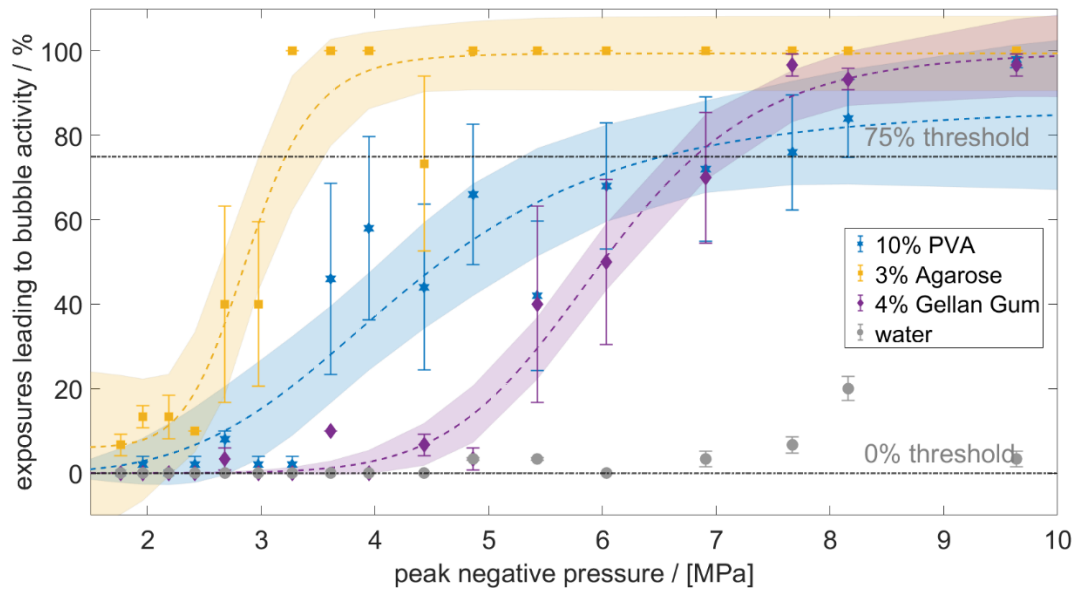
Mechanical effects of ultrasound traversing tissue, specifically ultrasonic cavitation, can be exploited for therapeutic applications. To evaluate its potential, tissue mimicking materials have been characterised.

10% w/w poly(vinyl alcohol) (PVA) hydrogels, with or without cellulose scatterers (5-10% w/w), agarose hydrogels (concentrations 1.25 and 3% w/w \pm 3% cellulose) and gellan gum gels (concentration 4% w/w \pm 2% silicone oxide scatterer) were studied. All hydrogels were acoustically characterised (sound speed (cs), attenuation coefficient (α)), using the finite amplitude insertion substitution method (frequency range 1.8-3MHz). The cavitation thresholds were investigated at peak negative pressures of 1.76-9.64MPa, using a passive cavitation detector.

The measured acoustic parameters were higher in PVA (cs:1532-1590m/s, α :0.08-0.37dB/cmMHz) than in agarose hydrogels (cs:1484-1492m/s, α :0.03-0.05dB/cmMHz). Acoustic gellan gum data will be presented. Cavitation thresholds for all materials followed a sigmoidal trend in probability of occurrence as a function of negative acoustic pressure, with agarose showing the lowest (2.9-3.5MPa for 75% probability). While gellan gum showed cavitation later than the other gels (6.6-7.2MPa), the increase in cavitation was steeper (slope: 8.7 ± 2.9 , Figure 1). Addition of cellulose scatterers lowered the 75% probability cavitation threshold in PVA gels from 5.4-8.2MPa (no cellulose) to 3.8-4.3MPa (10% cellulose w/w).

The acoustic properties of PVA hydrogels were close to those of published tissue data. Cavitation thresholds of gellan gum and PVA gels appear more suitable than agarose gels for mimicking tissues for these applications.

This project has received funding from the European Union's Horizon 2020 research and innovation programme under the Marie Skłodowska-Curie grant agreement No. 813766.



B2-7

Design of Radiosensitizing Pluronic Nanobubbles for Cancer Treatment

Presenter: Claire COUNIL

Authors in order: Claire COUNIL, *Case Western Reserve University*, Dana Wegierak, *Case Western Reserve University*, Pinunta Nittayacharn, *Case Western Reserve University*, Celina Yang, *Ryerson University*, Amin Jafarisojahrood, *Sunnybrook Health Science Center*, Reshani Perera, *Case Western Reaserve University*, Michael Kolios, *Ryerson University*, Agata Exner, *Case Western Reserve University*

This work focuses on developing long-circulating lipid nanobubbles (NB) loaded with a radiation sensitizer, Pluronic, to enhance prostate cancer radiation therapy.

NBs were formulated as previously described¹. The radiosensitizing surfactants² Pluronic L61, L62, and P85 were co-solubilized with lipids at a 1:10 and 1:100 Pluronic:lipid molar ratio. NB size and concentration were characterized. Pluronic NBs were imaged for 500s, using a clinical US system in contrast harmonic imaging mode (12 MHz, MI: 0.1, 1 fps). Pluronic NB responses were evaluated using passive cavitation detection (PCD) (FUS Instrument, RK50 Stereotactic Focused Ultrasound) at 1.51MHz and 515kHz.

Results show that an increased number of poly(ethylene oxide) segments and Pluronic MW reduced bubble size and yield. P85 produced the smallest NB size but reduced yield by tenfold. L61 increased the initial US signal intensity (18 dB) and exhibited a signal decay of only 20%, against 34% for P85 after 8 min of US exposure. Passive cavitation detector analysis showed sub- and ultra-harmonics at both frequencies (1.51MHz and 515kHz) and pressure-dependent activity. At 515 kHz, bubble cavitation activity is first observed at 1 MPa, compared to 0.5 MPa when the 1.51 MHz frequency transducer is used.

The inclusion of Pluronic L61, L62, and P85 in lipid shells results in stable NBs with strong acoustic activity. Based on these data, Pluronic L61 appears to be the best candidate for this theranostic application based on size, yield, and ultrasound response. Studies to test L61 NB radiosensitizing activity are ongoing.

We would like to acknowledge funding support from the National Institutes of Health (1R01EB028144-01A1).

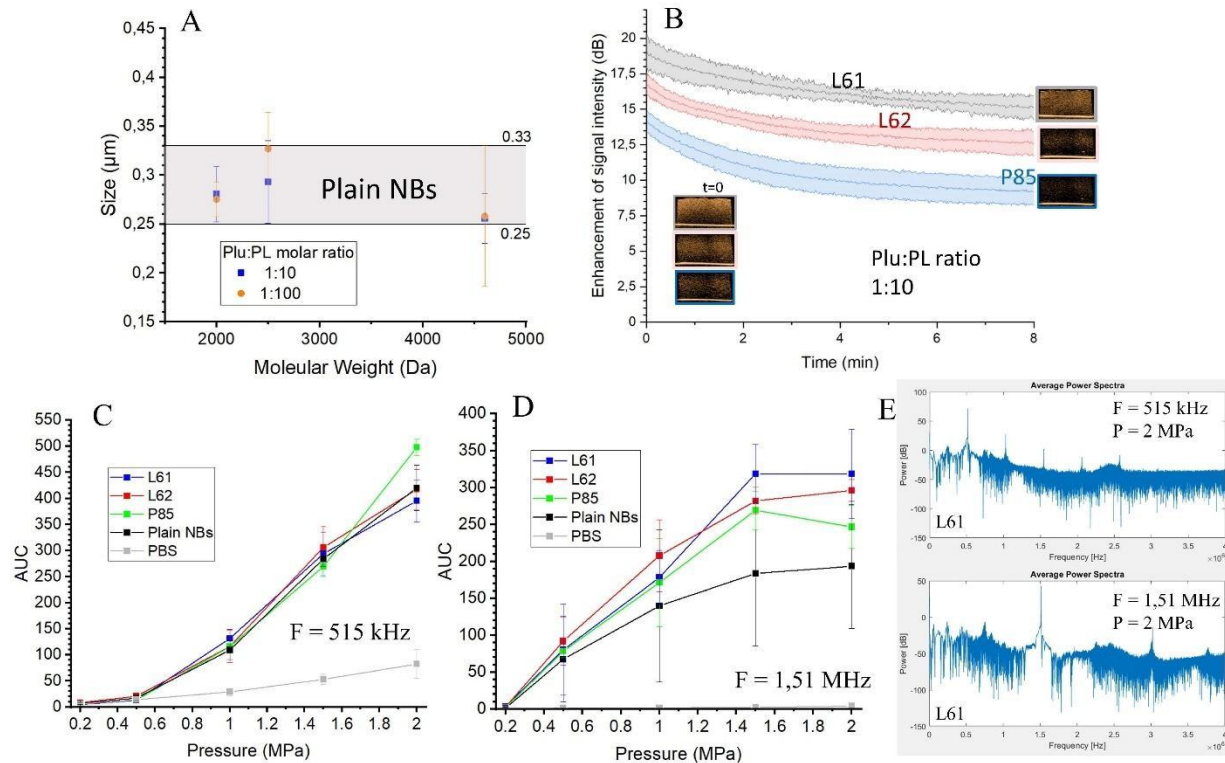


Figure: (A) NB size, (B) Signal intensity over time of Pluronic NBs for 1:10 molar ratio, (C) Area under the curve (AUC) from the frequency spectrum as a function of focal pressure for degas PBS (gray), plain NBs (black), and pluronic NBs: L61 (blue), L62 (red) and P85 (green), at 1:10 molar ratio, plain, error bar correspond to the SD of the average of the triplicate (E) Frequency spectra of L61 NBs for 1:10 molar ratio at 515 kHz and 1.51 MHz at 2 MPa. [1] A. De Leon et al. *Nanoscale*, 2019, 11, 15647. [2] Reshani H. Perera, *Int J Radiat Biol.* 2013 October ; 89, 10, 801–812.

High-speed Imaging of Nanoparticle-loaded Microbubbles for Drug Delivery

Presenter: Sofie Snipstad

Authors in order: Sofie Snipstad, *Department of Physics, Norwegian University of Science and Technology; Department of Biotechnology and Nanomedicine, SINTEF Industry; Cancer Clinic, St. Olav's Hospital, Trondheim, Norway*, Charlotte Nawijn, *Physics of Fluids group, Department of Science and Technology, MESA+ Institute for Nanotechnology and Technical Medical Center, University of Twente, Enschede, The Netherlands*, Tim Segers, *Physics of Fluids group, Department of Science and Technology; BIOS Lab-on-a-Chip group, Max Planck Center Twente for Complex Fluid Dynamics; both at MESA+ Institute for Nanotechnology and Technical Medical Center, University of Twente, Enschede, The Neth*, Guillaume Lajoinie, *Physics of Fluids group, Department of Science and Technology, MESA+ Institute for Nanotechnology and Technical Medical Center, University of Twente, Enschede, The Netherlands*, Sigrid Berg, *Department of Health Research, SINTEF Digital, Trondheim, Norway*, Yrr Mørch, *Department of Biotechnology and Nanomedicine, SINTEF Industry, Trondheim, Norway*, Catharina Davies, *Department of Physics, Norwegian University of Science and Technology, Trondheim, Norway*, Michel Versluis, *Physics of Fluids group, University of Twente*

The aim was to apply high-speed optical characterization of nanoparticle-loaded microbubbles to understand how the ultrasound treatment can be tuned for efficient nanoparticle delivery.

The acoustic response of microbubbles in a CLINicell was characterized using bright field microscopy with a Shimadzu high-speed camera (10 million frames per second, 40-cycle ultrasound pulses, frequencies of 1 - 3 MHz and acoustic pressures of 81 - 1200 kPa). To study bursting bubbles and nanoparticle deposition, fluorescence high-speed imaging was performed at 500 000 frames per second using a 532 nm laser (140-cycle pulses, 1 - 3 MHz and 81 - 1200 kPa).

The microbubbles displayed rigid shell behavior, and non-uniform shell properties across bubbles of the same size and across the shell of single bubbles, resulting in asymmetric oscillations. Large variation in bubble behavior was observed at the same ultrasound parameters. In general, the probability of shell rupture and nanoparticle delivery increased with increasing acoustic pressures, above a frequency-dependent pressure threshold. For each frequency, a clear resonance behavior was observed in the probability of nanoparticle release, leading to an optimum delivery for a relatively narrow range of bubble sizes. In addition, larger pressures were required to release the nanoparticles at higher frequencies.

High-speed imaging elucidated the temporal and spatial behavior of microbubbles during ultrasound exposure, enabling tuning of ultrasound parameters and microbubble size to optimize nanoparticle delivery. Such mechanistic information is useful for understanding ultrasound-mediated drug delivery, and for tailoring future formulations of nanoparticle-loaded microbubbles for therapeutic purposes within oncology and neurology.

B2-9

Characterisation of Gas Vesicles as Cavitation Nuclei for Ultrasound Therapy using Passive Acoustic Mapping

Presenter: Cameron Smith

Authors in order: Avinoam Bar-Zion, *California Institute of Technology*, Cameron Smith, *California Institute of Technology*, Mikhail Shapiro, *Caltech*, Constantin Coussios, *Institute of Biomedical Engineering*

Characterise the performance of Gas Vesicles (GVs) as nuclei for cavitation therapy using Passive Acoustic Mapping, to facilitate their development as genetically encodable therapeutic agents.

GVs suspended in liquid at a range of concentrations were exposed to of between 10 and 5000 cycles of 0.5 or 1.6 MHz ultrasound at pressures ranging from 0.1 to 2.1 MPa at a PRF of 0.25 Hz. Cavitation emissions were monitored using two co-planar L7-4 linear arrays at 90 degrees to each other, and processed using the Passive Acoustic Mapping (PAM) algorithm.

Gas Vesicles cavitate for the duration of the pulse applied to them; however, a significant reduction in cavitation energy is observed between pulses. This suggests that upon collapse of the GV the gas is released, can continue to cavitate throughout the duration of the pulse, and then dissipates. GV exhibit significantly different acoustic behaviours at 0.5 and 1.6 MHz, with far less broadband behaviour in the case of 1.6 MHz, even with comparable mechanical indexes. The acoustic emissions generated by GV also exhibit interesting behaviour as the concentration of GV vary.

GVs are the first genetically encodable cavitation agent with the potential for new applications in the field of ultrasound therapy. In the detailed characterisation of their cavitation behavior in this work will aid in determining optimal parameters and applications of this agent in targeted biomolecular and cellular ultrasound-triggered therapy.

This work was supported by the National Institutes of Health and the David and Lucille Packard Foundation.

B3-1

Real-time Transcranial Cavitation Monitoring for Blood-brain-barrier Opening in Non-human Primates

Presenter: Sua Bae

Authors in order: Sua Bae, *Columbia University*, Keyu Liu, *Columbia University*, Antonios N. Pouliopoulos, *Columbia University*, Robin Ji, *Columbia University*, Omid Yousefian, *Columbia University*, Elisa Konofagou, *Columbia University*

A pilot study was conducted for passive acoustic mapping (PAM) during focused ultrasound (FUS) mediated blood-brain-barrier opening (BBBO) in two non-human primates (NHPs).

A portable neuronavigator-based FUS system was used with a coaxial 2.5-MHz phased array (P4-2) and a Verasonics ultrasound system as in Fig. 1(a). Two NHPs were sedated and sonicated at the right cerebellum and the right hippocampus, respectively. A 10-ms FUS pulse ($f_c=0.25\text{MHz}$) was transmitted at a PRF of 2Hz for 2 min with microbubble injection. Treatment was monitored by cavitation map, spectrum, and cavitation doses over time. BBBO was confirmed by T1 contrast-enhanced MRI.

Cavitation maps were reconstructed by coherence-based PAM with GPU for online processing. During the treatment, a cavitation map for each pulse was reconstructed showing dynamic cavitation activities at the targeted area and also intermittently around the skull and skin. Most of the cavitation energy was detected within the FUS focal zone (Fig. 1(c) and (f)), which were correlated with BBBO regions at the right cerebellum and the right hippocampus, respectively (Fig. 1(d)) and the right (g)).

We demonstrated the feasibility of transcranial cavitation mapping in NHPs with a portable FUS system. The cavitation signal was detectable using the ultrasound imaging probe through human skull and real-time PAM was implementable with GPU. The BBBO regions were well correlated with the cavitation maps in both sessions.

This work was supported by the National Institutes of Health (R01AG038961, R01EB009041) and the Focused Ultrasound Foundation.

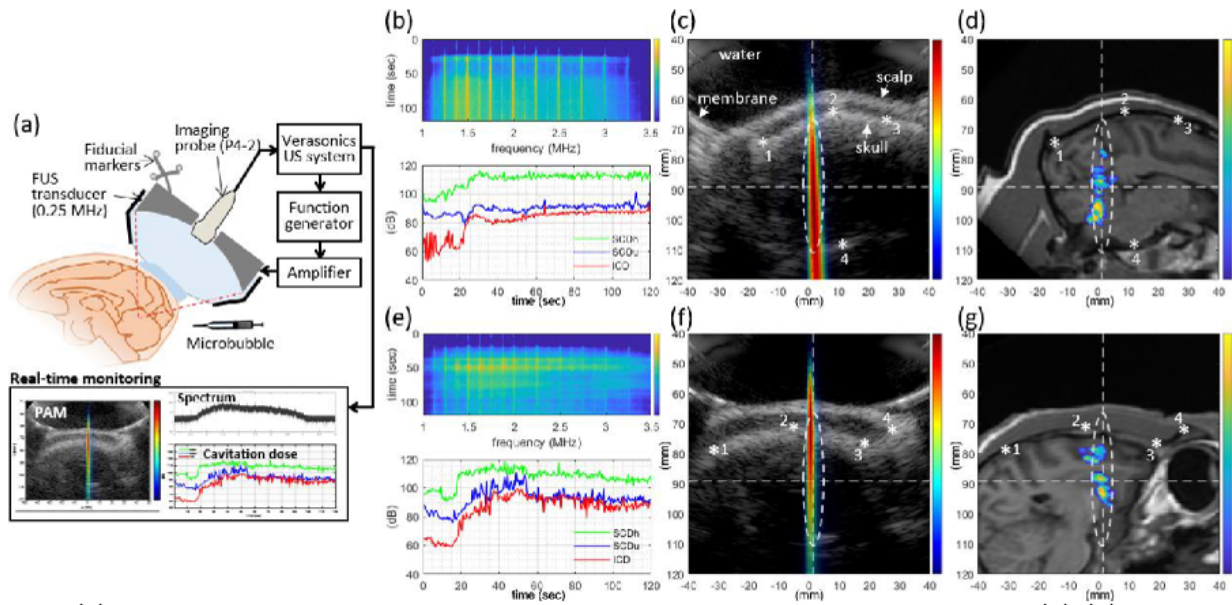


Fig. 1(a) Setup for FUS treatment with PAM monitoring. BBBO treatment results in NHP1 (b)–(d) and NHP2 (e)–(g). (b), (e) Spectrogram (upper panel) and harmonic (green), ultra-harmonics (blue), and inertial (red) cavitation doses (lower panel) over time. (c), (f) Averaged cavitation map across all bursts (color) overlaid on B-mode image (grayscale). (d), (g) BBBO region (color) overlaid on T1-weighted MRI (grayscale). Microbubble was injected and flushed at $t = 10\text{--}20$ s and the cavitation doses increased after $t = 20$ s in (b) and (e). The dashed ellipsoid in (c), (d), (f) and (g) indicates -6 dB contour of FUS. The intensities in PAM and BBBO images were normalized by itself.

B3-10

3D PAM of a Cavitating Source with Adaptive Beamformers

Presenter: Audrey Sivadon

Authors in order: Audrey Sivadon, *Inserm*, Jean-Christophe Béra, Barbara Nicolas, François Varray, Bruno Gilles

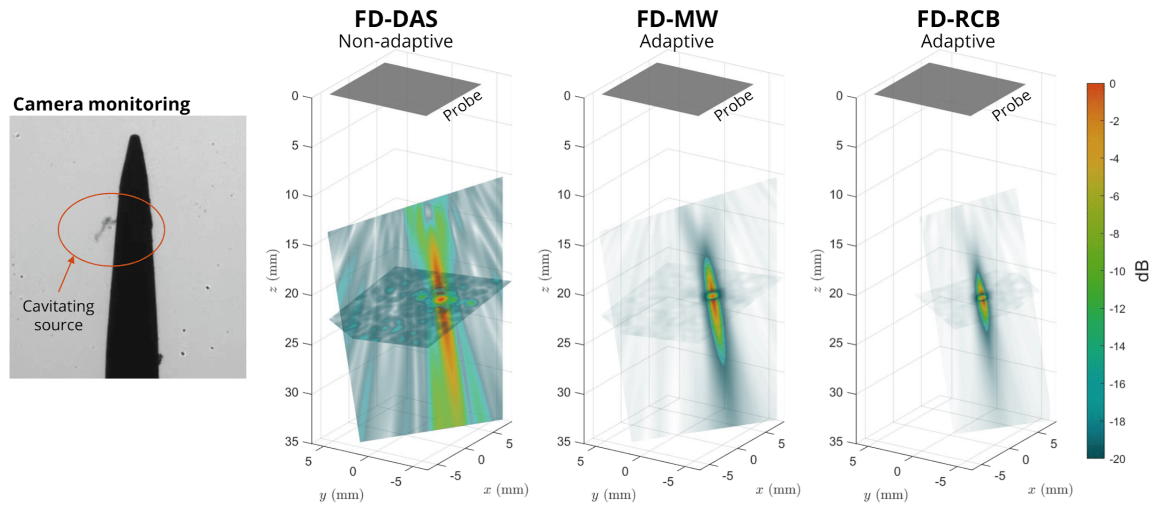
We propose adaptive beamforming in Fourier Domain to enhance the resolution of 3D Passive Acoustic Mapping (3D-PAM) of cavitation using a commercial imaging array.

Performances of Frequency-Domain RCB (FD-RCB) and MidWay Pisarenko (FD-MW) beamformers for 3D Passive Acoustic Mapping of a point-like cavitating source are evaluated in comparison to Delay-And-Sum (DAS) beamforming used in previous 3D-PAM studies. A random sparse array configuration of a multiplexed commercial probe is used to reduce the number of channels used for the reconstruction without degrading its quality, and achieve a versatile well-resolved passive cavitation imaging method.

Cavitation is initiated by a HIFU transducer at the tip of a needle and monitored with a high-speed camera confirming the presence of cavitation on the needle tip. The cavitation signals were acquired using one single Verasonics Vantage system, 256-channels, with a multiplexed Vermon 1024-elements matrix array using a random sparse apodization. The 3D power maps were computed at different frequencies for FD-DAS, FD-MW, and FD-RCB beamformers: at 3.5 MHz, the volume at -3dB is respectively 5.6mm³, 0.6mm³, and 0.2mm³. The position errors along with FWHM lateral and axial are also evaluated.

The presented work shows the feasibility of doing 3D cavitation monitoring on real cavitation signals with a rather simple setup. The use of multiplexing with random apodizations reduces the number of channels to acquire and the parameter-free adaptive beamformer FD-MW drastically enhances the mapping resolution.

This work was carried out thanks to the financial support of the LabEx CeLyA (ANR-10-LABX-0060) of the University of Lyon.



3D-PAM resolution enhancement using adaptive beamformers on a cavitating source

B3-11

A Preclinical Sparse Hemispherical Array for Acoustic Monitoring and Control of Microbubble-mediated Ultrasound Brain Therapy

Presenter: Yi Lin

Authors in order: Yi Lin, *University of Toronto*, Ryan Jones, *Sunnybrook Research Institute*, Kullervo Hynynen, *Sunnybrook Research Institute/ University of Toronto*

A high frequency transmit array capable of acoustic mapping is needed to monitor and calibrate safe exposure levels in preclinical settings of ultrasound brain therapy.

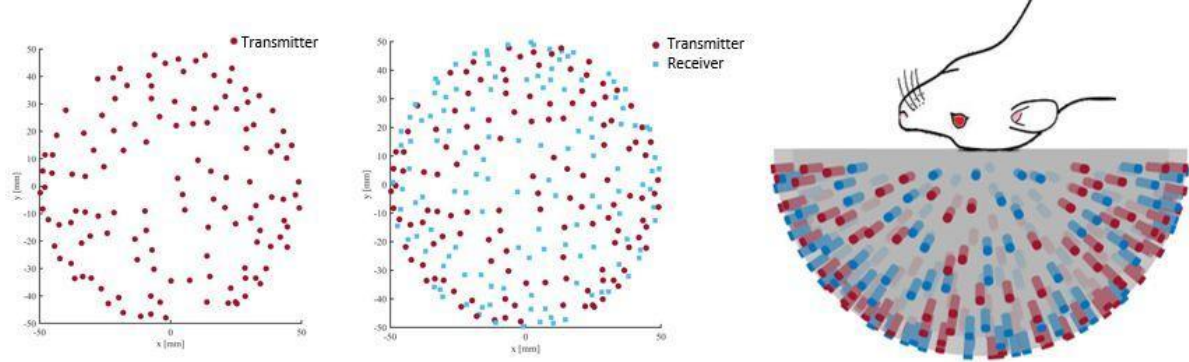
Numerical simulations were performed using a ray-acoustic model. Design considerations included number of elements, array aperture and steering range. The transmit array was optimized from 5,000 distinct configurations based on the peak sidelobe ratio (PSLR). The receive array was then optimized for signal-to-noise ratio from 10,000 configurations at ultra/second harmonic frequencies, utilizing the remaining physical space. The array was assembled with PZT ring transmitters (2.5mm diameter) and PVDF receivers (1mm²) on a 3D printed scaffold.

A 100 mm diameter, 128-element transmit array was optimized to output at least 2.5 MPa pressure with a 30% pressure PSLR and millimeter focal sizes (-3 dB beamwidths: axial = 1.7 mm, lateral = 0.7 mm). A 128-element receiver array was optimized with an 8% intensity PSLR at submillimeter -3 dB beamwidths (ultraharmonic: axial=0.8 mm, lateral=0.7 mm). Future work will involve integration of the individual elements within the scaffold, benchtop characterization of the array with phantom experiments, and in-vivo evaluation of the phased array system's ability to image bubble clouds during ultrasound brain therapy in a rodent model.

A compact hemispherical array with therapeutic delivery and cavitation monitoring capabilities was designed and constructed. Benchtop characterization of the array and in-vivo studies will demonstrate the feasibility of this system in both delivering and

monitoring ultrasound brain therapies with high spatiotemporal resolution in a preclinical setting.

Support was provided by fundings from National Institute of Health, Canadian Institutes of Health Research, and a Natural Sciences and Engineering research Council scholarship.



Acoustic Emission Feedback Based Blood-Brain Barrier Energy Control

Presenter: Hsiang-Ching Lin

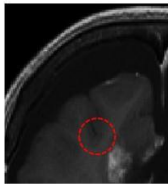
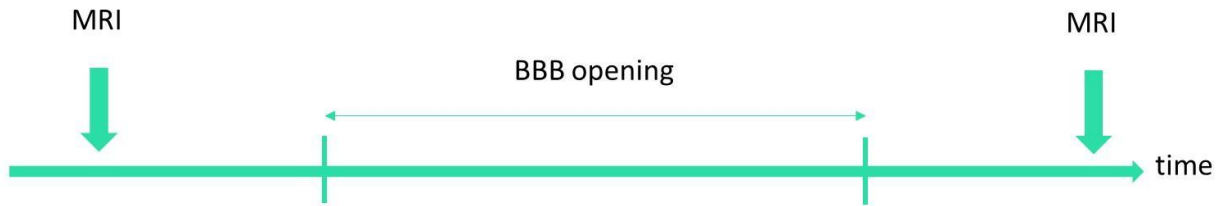
Authors in order: Hsiang-Ching Lin, *NaviFUS Corporation / National Taiwan University*, Chih-Hung Tsai, *NaviFUS Corporation*, Kuo-Chen Wei, *Chang Gung Memorial Hospital*, Ko-Ting Chen, *Chang Gung Memorial Hospital*, Hao-Li Liu, *National Taiwan University*

We propose an acoustic emission feedback (AEF) control and microbubble-free passive beam mapping to monitor the BBB-opening. Assure the procedure safety and gain procedure effectiveness.

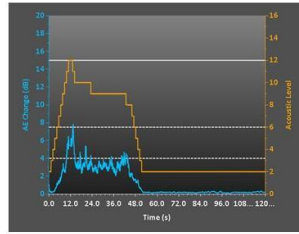
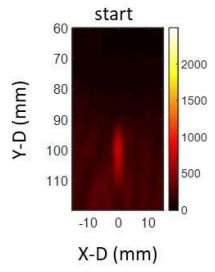
We implement the AEF concept in a dual-mode ultrasound 256-element (32 selected to transmit/received) system (NaviFUS-001, NaviFUS, Taiwan). Long-burst excitation was designated in transmit mode (500 kHz, 5000 cycles, MI= 0.02~0.48, PRF = 20 Hz) and short-cycle excitation was designated in receiving mode (250-1000kHz, 2 cycles, MI = 0.02~0.48). The AEF signals were summed for power level control during the long-burst excitation phase, whereas also proceed the AEF beam mapping to monitor the emission distribution.

The relationship between passive cavitation detection and acoustic emission feedback was estimated in vivo experiment and was applied in clinical trial. The AEF based energy control was implemented in in vivo showing that BBB can be opened effectively and safely. As the results showing in the time flowchart during clinical trial, sonication energy was controlled by AEF and passive beam reconstruction during sonication. MRI image also showed the BBB opening was successful. According to our AEF based energy control algorithm, BBB can be opened effectively and safely in clinical trial.

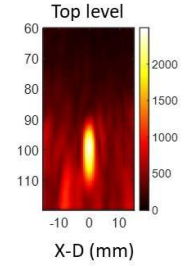
We propose to employ AEF based strategy to control and monitor the BBB opening procedure. Results have demonstrated that the concept can be implemented in a clinical based dual-mode ultrasound apparatus, and demonstrated its feasibility both in the preclinical animals and in humans.



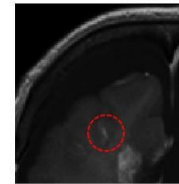
MRI before BBB opening



AEF signal and energy level



X-D (mm)



MRI after BBB opening

3D Ultraharmonic Imaging for Exposure Calibration and Damage Prediction during Microbubble-mediated Ultrasound Brain Therapy

Presenter: Ryan Jones

Authors in order: Ryan Jones, *Sunnybrook Research Institute*, Dallan McMahon, *Sunnybrook Research Institute*, Dallas Leavitt, *Sunnybrook Research Institute*, Rohan Ramdoyal, *SRI FUS lab*, Edwin Lee, *Sunnybrook Research Institute*, Wai Meng Kan, *Sunnybrook Health Sciences Centre*, Steven Yang, *Sunnybrook Research Institute*, Yi-Shiuan Chen, *Sunnybrook Research Institute*, Chris Adams, *Sunnybrook Research Institute*, Kullervo Hynynen, *Sunnybrook Research Institute/ University of Toronto*

Evaluate 3D passive cavitation imaging (PCI) for exposure calibration and treatment monitoring during microbubble-mediated focused ultrasound (FUS) brain therapy using a novel transmit/receive phased array.

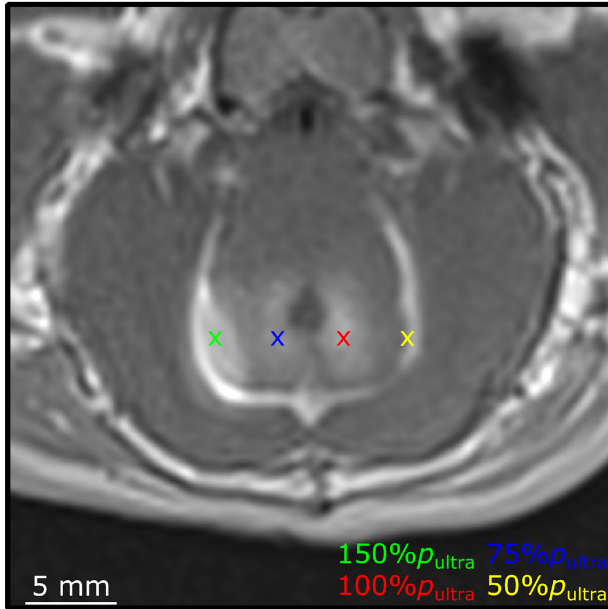
Experiments were performed on rabbits (~3 kg) using a 3840-element simulation-optimized sparse hemispherical phased array (25 cm diameter). Burst-mode FUS (258 kHz, 10 ms bursts every 2 s, 120 s) was steered electronically over 4x4 square grids (3.5 mm spacing) following microbubble injection (4 µl/kg Definity™) via real-time 3D PCI-based exposure calibration (128 receiver elements, whole-burst temporal averaging). Exposures were carried out at 50-150% of the pressure required to detect ultraharmonic activity in vivo (pultra).

Spatially coherent ultraharmonic activity was detected trans-rabbit skull near the intended target locations during pressure ramp sonications (0.7 ± 0.3 MPa, free-field estimate). T2*-weighted MRI revealed signal hypointensities induced by all exposures at $p \geq 100\%$ pultra, occasional exposures at $p = 75\%$ pultra, and no exposures at $p = 50\%$ pultra. The tissue damage volumes assessed via T2*-weighted MRI were found to increase with increasing target level, and were associated with regions of red blood cell extravasations on H&E sections. Sonication-aggregate 3D PCI data generated via delay, sum, and integrate beamforming (burst-wise average) correlated linearly with MRI-assessed tissue damage volumes ($R^2 = 0.82$), and predicted the damage volume centroid locations (error= 1.4 ± 0.7 mm).

3D ultraharmonic imaging can be used to calibrate exposure levels for microbubble-mediated FUS brain therapy, and can predict the tissue damage volumes and their locations resulting from high target level sonications. The spatial information provided by PCI is expected to improve acoustic emissions-based control schemes for cavitation-based FUS therapies.

We thank S. Rideout-Gros for help with animal care, and S. Gunaseelan, W. Li, K. Leung, J. Zhou, T. Jakaza, A. Rajkumar for technical support.

T₁-weighted + Gd



T₂*-weighted

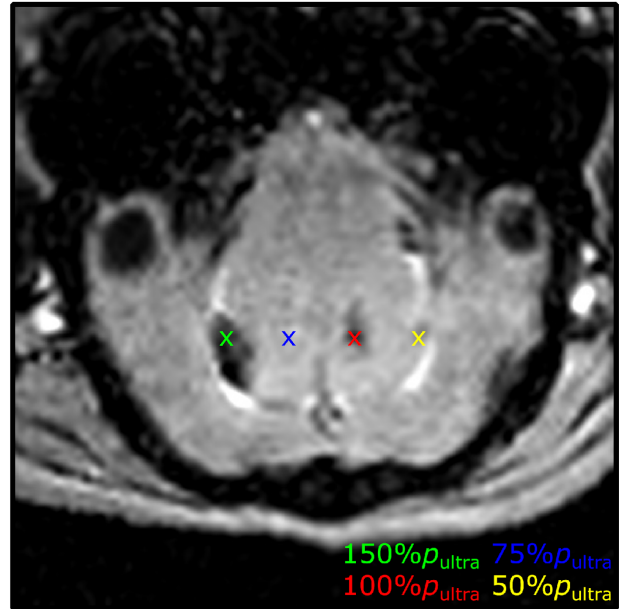


Fig. 1: MRI data (coronal plane) displaying 4 targets in one animal. Gd = gadolinium.

Ultrafast Intrapulse Feedback Control of FUS-induced BBB Disruption

Presenter: Corentin Cornu

Authors in order: Corentin Cornu, *CEA Saclay*, Anthony Novell, *BioMaps, Université Paris Saclay, CEA, CNRS, Inserm*, Erwan Selingue, *CEA Saclay*, Paul Mondou, *CEA Saclay*, Pauline Agou, Sebastien Meriaux, *CEA Saclay*, Benoit Larrat, *CEA*

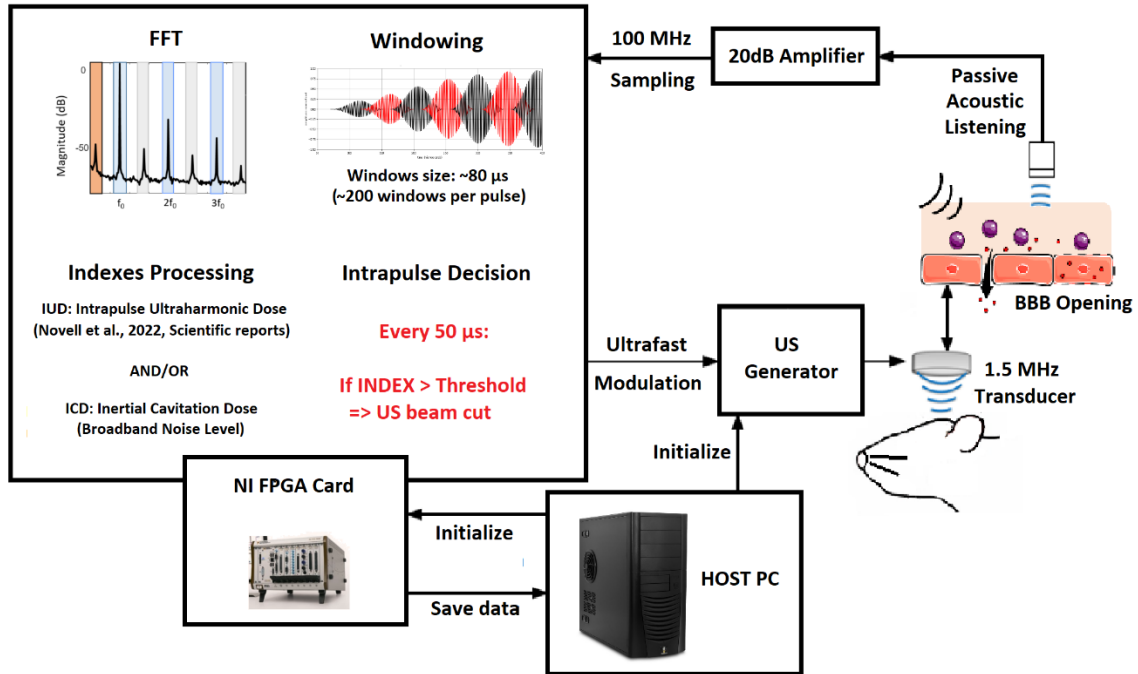
Intrapulse feedback control based on passive cavitation monitoring can be performed (1) to enhance BBB disruption and (2) to guaranty safety.

The approach was validated in vivo for BBB disruption in mice (n= 4). Mice were injected with SonoVue® microbubbles (2mL/kg) and MRI contrast agent Dotarem® (4mL/kg) and then sonicated with FUS pulses (1.5MHz, 10ms, PRF: 10Hz). Backscattered signal from microbubbles was acquired using a FPGA board, and cavitation indexes based on harmonic, ultraharmonic and broadband emissions were calculated every temporal windows (50µs), allowing an ultrafast power output modulation of the FUS amplifier.

BBB disruption at focus and absence of hemorrhages were evaluated by T1 and T2 weighted MRI respectively as well as gross pathology. Each intrapulse-controlled sonication resulted in efficient and safe BBB disruptions while reaching higher pressure levels than usual.

The results highlight that cutting the FUS beam inside the pulse (i.e., few ms) avoids damages, even at high pressure conditions (Peak-Negative-Pressure up to 1MPa in degazed water conditions). Intrapulse feedback was also successful for a lower microbubbles concentration (0.4mL/kg), closer to the clinical dose.

We developed a new strategy based on an ultrafast intra-pulse control avoiding potential harmful FUS conditions. Several tests on mice have demonstrated this strategy to be able to adjust the acoustic pressure in real-time, in a safer and more efficient way.



B3-4

Evaluating Cavitation Mapping During Histotripsy with Electronic Focal Steering

Presenter: Greyson Stocker

Authors in order: Greyson Stocker, *University of Michigan*, Ning Lu, *University of Michigan*, Zhen Xu, *University of Michigan*, Jonathan Sukovich, *University of Michigan*, Timothy Hall, *University of Michigan*

Evaluate TEA-PAM (Time Exposure Acoustics Passive Acoustic Mapping) for monitoring the cavitation memory effect during histotripsy using a transmit-receive capable histotripsy array.

When treating a tissue volume with electronic focal steering, residual cavitation nuclei from a previously steered location can be re-excited by the low pressure field outside the current steered location. To monitor this, a 750 kHz 260-element histotripsy array was used to pulse at adjacent foci within 1% agarose gel at 1000 Hz PRF. TEA-PAM was used to reconstruct a cavitation map and assessed for localization performance and the ability to resolve two cavitation clouds.

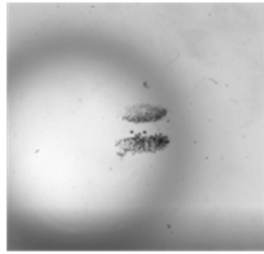
Both cavitation expansion and collapse acoustic emissions could be received by the histotripsy array to create cavitation maps. A TEA-PAM map of a single cavitation cloud had FWHM's of 1.5 (laterally) and 5.5mm (axially). TEA-PAM was able to resolve clouds spaced by as little as 5mm axially (center to center) and 3mm laterally. The method had a median localization error of 1.2 ± 1.04 mm when steering within ± 10 mm in the axial and lateral directions when compared to the optical images, with higher error associated with larger steering distance.

Using signals acquired using the transducer array elements, TEA-PAM performed well at resolving the re-excited, non-focal cavitation events associated with the cavitation memory effect during histotripsy. The results of this study demonstrate the feasibility of using PAM approaches to accurately localize cavitation using narrow bandwidth, large aperture arrays.

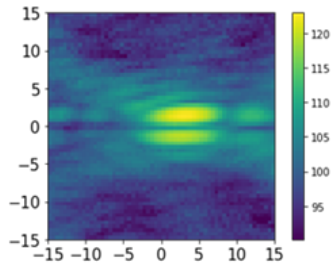
This grant work is funded by NIH grant R01 CA 211217.

3 mm
Lateral
Spacing

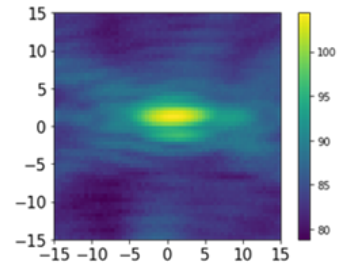
Optical Imaging



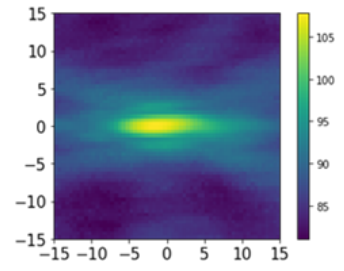
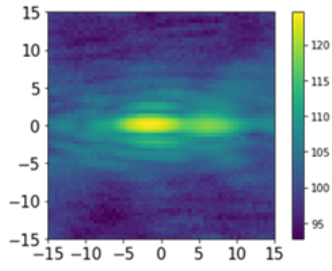
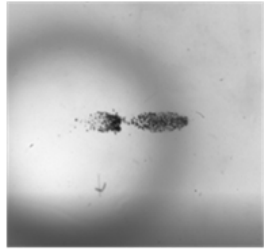
TEA-PAM Expansion



TEA-PAM Collapse



5 mm
Axial
Spacing



Simulation of Transvertebral Passive Acoustic Mapping for Bubble Based Therapy in the Spinal Cord

Presenter: Andrew Frizado

Authors in order: Andrew Frizado, *Sunnybrook Research Institute/University of Toronto*, Meaghan O'Reilly, *Sunnybrook Research Institute*

Passive Acoustic Mapping (PAM) through the intact spine, for BSCB disruption, is required as a means of treatment monitoring during microbubble mediated FUS.

Using CT-derived acoustic property maps of ex-vivo stacked human vertebra, time-domain FUS (forward) and cavitation (inverse) emission simulations were performed using the kWave toolbox in MATLAB. A spine-specific phased array was used in receive mode for trans-vertebral signal detection, Signals were then beamformed using the passive Time Exposure Acoustics (TEA) algorithm and its "gated" or "synchronous" alternative. Considerations for unwanted, pre-focal cavitation and associated acoustic interference were also interrogated.

To investigate the transvertebral detection of intra-canal sources (microbubbles), acoustic emissions from short burst sonications were simulated as single point source locations along the axial, lateral and vertical directions, then sampled across over these 150 locations in 10 vertebrae. Using TEA beamforming, source localization error was 1.3 ± 1.1 mm, with peak side-lobe ratio of 0.43 ± 0.14 which were improved via phase-correction methods to 0.4 ± 0.5 mm and 0.36 ± 0.7 , respectively. In the presence of pre-focal sources, localization of intra-canal sources was disrupted when using TEA and its gated form algorithms.

With the spine-optimized aperture, beamforming through the vertebra presents to be feasible when isolating point sources, though with the introduction of significant pre-focal source interference, TEA and its gated form, proved insufficient for cavitation site localization. Further work regarding pre-focal and focal source interactions, and their suppression, will be required.

This work was supported by the Canadian Institutes of Health Research and the QEII-GSST Scholarship.

B3-6

The Fast and The Spurious: Characterization and Mitigation of Passive Acoustic Mapping and B-Mode Co-registration Errors

Presenter: Michael Gray

Authors in order: Michael Gray, *University of Oxford*, Constantin Coussios, *Institute of Biomedical Engineering*

To characterize and minimize errors in the co-registration of B-mode images and passive acoustic mapping (PAM) of cavitation activity.

PAM and B-mode image co-registration was assessed using simulated and measured data sets for homogeneous and layered soft-tissue media, with the latter intended to represent a range of thoracic soft tissue treatment scenarios. Co-registration errors were quantified as a function of target location, array geometry, and assumed sound speed. The performance of a candidate sound speed optimization method was assessed for its ability to minimize co-registration errors in all evaluated scenarios.

Since PAM does not inherently contain anatomic information, it is critical to co-register PAM with other imaging data for accurate treatment guidance. Target depth co-registration errors ranged from a 1-10 mm depending on the specifics of the imaging scenario and the assumed sound speed. Notably, the use of a sound speed that is optimized for B-mode imaging alone may still lead to non-negligible co-registration errors with PAM, especially when there is substantial refraction in the propagation path. The proposed optimization method reduced co-registration errors to less than 1-mm for all imaging scenarios.

It has been shown that mis-registration errors can be reduced to radiologically negligible levels through a sound speed optimization process. Ongoing efforts are aimed at evaluating the proposed method under clinical conditions for a variety of therapeutic ultrasound applications.

This work was supported by the NIHR, Oxford Biomedical Research Centre.

B3-7

Micro-elastography on Spheroids and the Impact of Ultrasonic Cavitation

Presenter: Gabrielle Laloy Borgna

Authors in order: Gabrielle Laloy Borgna, *University of Lyon*, Thomas Lambin, Gabrielle Lescoat, Litan Wang, Maxime Lafond, *LabTAU, Inserm U1032*, Andrew Drainville, *LabTAU INSERM U1032*, Jacqueline Ngo, Magali Perier, Cyril Lafon, *INSERM*, Stefan Catheline, *INSERM, University of Lyon*

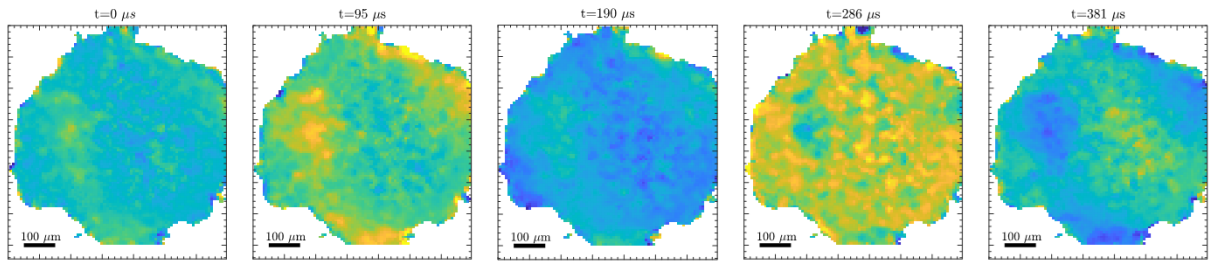
In the context of development of a new treatment against pancreatic adenocarcinoma combining chemotherapy and cavitation, it is of high interest to characterize tumor models.

Spheroids, made of cancerous cells and fibroblasts, were made by linking magnetic nanoparticles to cells placed on magnetic cell culture plates. A pulsed magnetic field was generated, inducing vibrations inside the 500 μm spheroid thanks to the nanoparticles. Spheroids were observed with an ultrafast camera mounted on a microscope. Displacements and local shear wave velocity were determined using phase tracking and noise correlation algorithms, and can be used to calculate the shear elasticity.

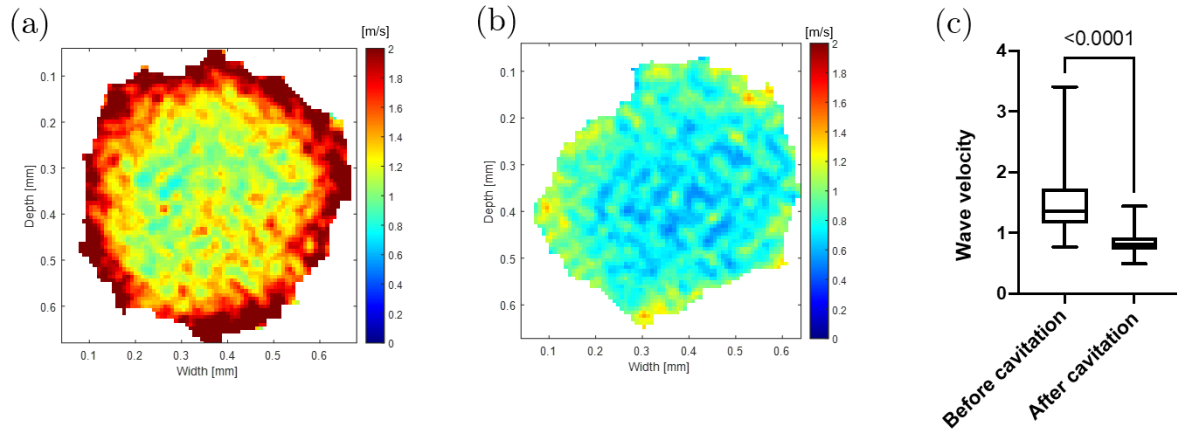
The influence of trypsin, which disrupts the bounds between the cells, on shear wave velocity maps was studied. As expected, a decrease of the wave velocity was observed, confirming that this method is sensitive to elasticity. Furthermore, the impact of cavitation inside the spheroid has been investigated. Cavitation designates the bubble generation using ultrasound. In our experiment, cavitation substantially decreased shear waves velocity. This result suggests an alteration of the stroma of the tumor model, leading to a stiffness decrease.

An original method has been developed to estimate the mechanical properties of cells aggregates called spheroids. Optical micro-elastography was performed using an original shear wave source, constituted of magnetic nanoparticles distributed inside the spheroid, stimulated by a magnetic pulse. Ultrasonic cavitation has been shown to soften the samples.

Work supported by ITMO Cancer through its PCSI 2020 call.



Displacement maps showing waves propagating inside the spheroid



Wave velocity maps (a) before cavitation and (b) after cavitation.
(c) Statistical analysis showing that the difference is significant.

Immune Checkpoint Targeted Therapy in Glioma with Closed Loop Microbubble Enhanced Focused Ultrasound

Presenter: Hohyun Lee

Authors in order: Hohyun Lee, *Georgia Institute of Technology*, Yutong Guo, *Mechanical Engineering, Georgia Institute of Technology*, James Ross, *Emory University, Department of Microbiology and Immunology*, Scott Schoen Jr., *Harvard Medical School and Massachusetts General Hospital*, Levent Degertekin, *Georgia Institute of Technology*, Costas Arvanitis, *Georgia Institute of Technology*

To assess the abilities of a closed-loop microbubble-enhanced FUS system to promote discrete changes in the blood-brain barrier phenotype and facilitate anti-PD1 delivery in glioblastoma.

The system is composed of a focused ultrasound (FUS) transducer and a confocally and coaxially aligned imaging transducer that is operated in passive mode. The system is integrated with closed-loop control algorithm that controls the microbubble (MB) acoustic emission (AE) strength and tracks cerebrovascular MB kinetics, which is used to activate/deactivate the controller. The performance of the system and its impact on BBB/BTB phenotype and anti-PD1 delivery was tested on GL261 glioma-bearing mice brains.

The proposed system was able to safely achieve a target AE level with 3dB tolerance within 6 seconds of risetime, with its operation time safely controlled by tracking the MB kinetics. Post sonication analysis revealed upregulation of the inflammatory marker, ICAM-1, and improvement in anti-PD1 delivery in AE level (i.e., 3rd harmonic) dependent manner. Interestingly, our data also shows that the combined treatment was able to elicit a 2-fold increase in proinflammatory macrophage (M1 - polarized). Finally, we found that closed-loop controlled MB-FUS in combination with anti-PD1 conferred a statistically significant improvement in survival, as compared to control group ($p < 0.05$).

Our findings demonstrate the ability of a closed-loop controlled microbubble-enhanced focused ultrasound system to sharply tune the exposure settings to attain and sustain desirable MB oscillation in tumor-bearing mice brains and promote distinct pro-inflammatory responses in BBB phenotype and facilitate safe and effective anti-PD1 delivery in the glioblastoma tumor microenvironment.

This study was supported by the NIH Grant R37CA239039.

Individualized Closed-loop Feedback Control of Focused Ultrasound for Blood-brain Barrier Opening

Presenter: Chih-Yen Chien

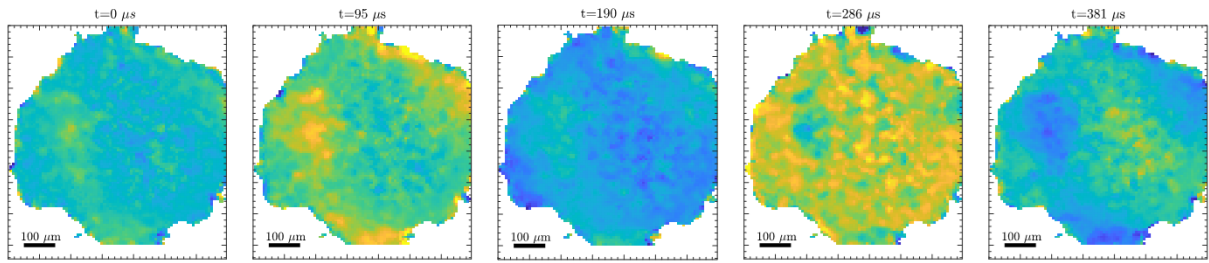
Authors in order: Chih-Yen Chien, *Washington University in St. Louis*, Yaoheng Yang, *Washington University in St. Louis*, Yan Gong, Yimei Yue, Hong Chen, *Washington University in St. Louis*

To develop an individualized closed-loop cavitation-based feedback controller for focused ultrasound combined with microbubble-mediated blood-brain barrier opening (FUS-BBBO).

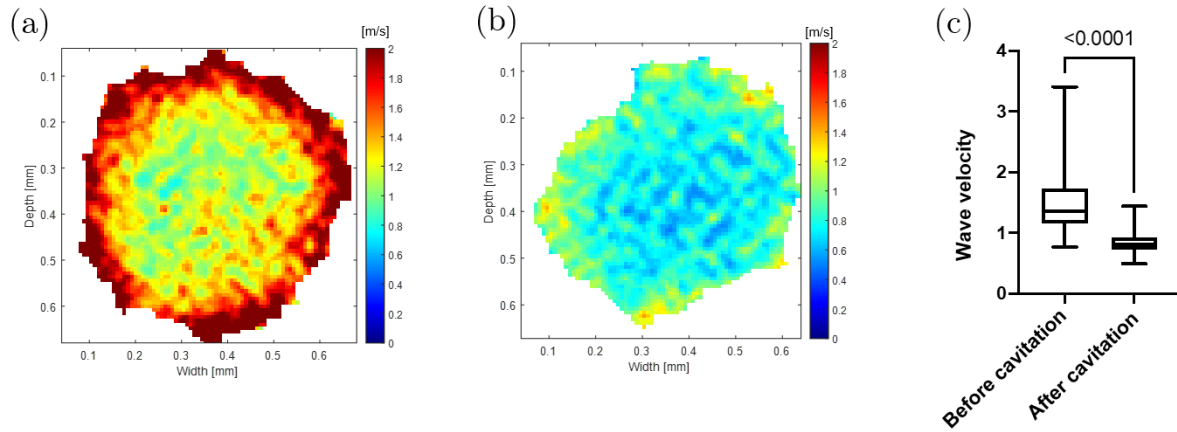
A single-element FUS transducer with a coaxially aligned passive cavitation detector (PCD) was used. PCD signals were acquired before microbubble injection and determined the individual baseline level. During sonication with microbubble infusion, cavitation was monitored and a custom closed-loop feedback controller controlled cavitation level to be at target cavitation level (TCL) defined to be 1-3 dB above the baseline level. After sonication, FUS-BBBO at different TCLs were quantified using fluorescence imaging of Evans blue extravasation.

The proposed feedback control algorithm controlled and maintained the stable cavitation level at the TCL (Fig. A). Consistent delivery of Evans Blue dye by FUS-BBBO was observed in all three TCLs (Fig. B). The fluorescence intensity of the delivered Evans Blue dye increased as the TCL increased, suggesting that the proposed feedback controller can control the FUS-BBBO drug delivery outcome (Fig. C). The good burst rate, which was used to quantify the stability of the controller, was 78.6%, 71.7%, and 65.9% for 1 dB, 2 dB, and 3 dB, respectively.

FUS-BBBO was achieved using an individualized closed-loop feedback control algorithm at selected targeted cavitation levels with high stability.



Displacement maps showing waves propagating inside the spheroid



Wave velocity maps (a) before cavitation and (b) after cavitation.
(c) Statistical analysis showing that the difference is significant.

B4-1

Multi-axial Technology for the Generation and Detection of Ultrasound

Presenter: Samuel Pichardo

Authors in order: Samuel Pichardo, *University of Calgary*

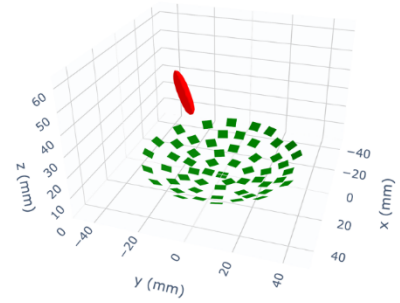
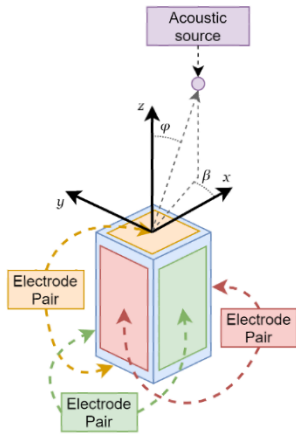
I will present a summary of the multi-axial technology for piezoceramic transducers and the applications explored by our group using this technology.

The multi-axial method consists of the driving/reading-out of simultaneous orthogonal electric fields in piezoceramic materials. In driving mode, a differentiated vibration mode that steers ultrasound in a single transducer element can be produced by modulating the amplitude and phase of the electric signals. In reading-out mode, the processing of the measured orthogonal electric signals can be used to detect the directivity of acoustic sources such as reflectors or cavitation activity or improve the signal-to-noise ratio.

The steering capabilities of the multi-axial method are being tested to develop a new type of ring-shaped transducers to improve the focusing of ultrasound for pre-clinical research and develop a new generation of sparse-type arrays for transcranial ultrasound therapy. In reception mode, we found that a single multi-axial transducer can detect the direction ($\pm 25^\circ$) of the sound generated by a spherical acoustic source. Tests with a simple multi-axial 3-element 6 MHz imaging array and a 0.36mm-diameter wire demonstrated that multi-axial processing in reception improved signal-to-noise ratio by 10dB and axial resolution from 3mm to 0.9mm.

The multi-axial method has a significant potential to help developing a new generation of applicators and detectors that can improve focusing, localization of acoustic events by incorporating detection of ultrasound directivity and enhance imaging quality metrics by applying more advanced signal formation and processing.

Canada Foundation for Innovation. Natural Sciences and Engineering Research Council of Canada. Canada Institutes of Health Research. Mathematics of Information Technology and Complex Systems.



Left) Tri-axial prismatic detector.
 Center) 500 kHz/1500 kHz Bi-axial ring transducer ensemble.
 Right) Simulation of steering of tri-axial, 56-element sparse phase array at 320 kHz.

B4-10

Focalization Improvements in Single-element Ultrasound Ring Transducers by the Application of Biaxial Excitation

Presenter: Sagid Delgado

Authors in order: Sagid Delgado, *University of Calgary*, Siyun Li, *University of Calgary*, Laura Curiel, *University of Calgary*, Samuel Pichardo, *University of Calgary*

We demonstrate with simulation and experimental work the focalization improvements in a single-element PZT ring transducer while applying the biaxial method at higher harmonics.

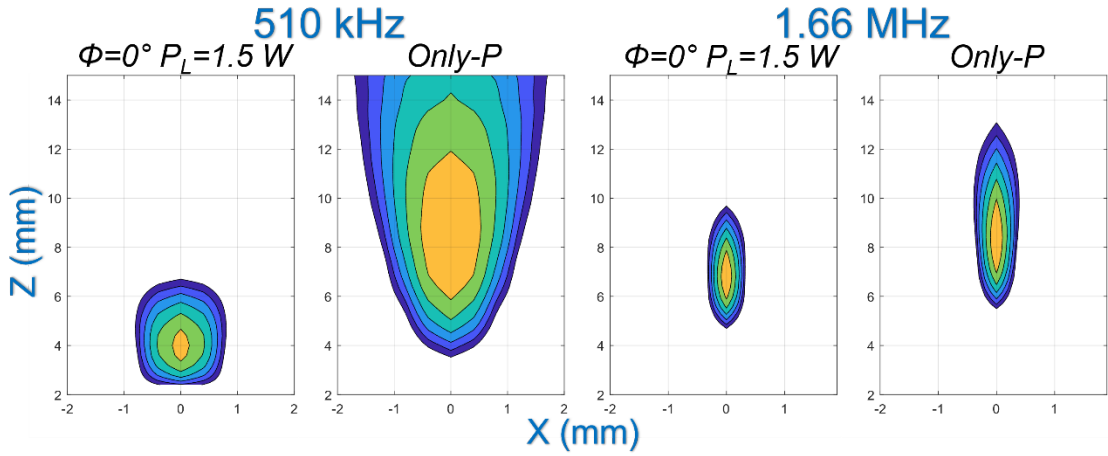
Finite element simulations were used to calculate the -6 dB focal area and distance for a single-element ring shaped biaxial transducer (T=2.95mm, D=11.5mm, W=2.35mm) operating at 510 kHz and 1.66 MHz. Experimental validations were performed (n=2) and the acoustic field measured with a hydrophone system. Different phases ($\phi = 0^\circ$ to 315° , 45° step) and powers (PL = 0.1 W, 1.0 W and 1.5 W) were tested for each acoustic field simulation and characterization.

Simulation and experimental electrical response showed a 2% to 5.5% frequency difference for the 1st and 3rd harmonic. For first resonance, simulations showed that the focal area varied from 51.7 mm² to 5.9 mm² and displaced 5.4 mm to 15.7mm, while experimental validation focal area varied from 30.2 mm² up to 14.9 mm² and displaced 6.9 mm to 9.7 mm. For 3rd harmonic, focal area varied from 4.4 mm² to 2.6 mm² and 3.1 mm² up to 2.6 mm² and displaced 8.0 mm to 16.1 mm and 6.9 mm to 9.3 mm for simulation and experimental, respectively.

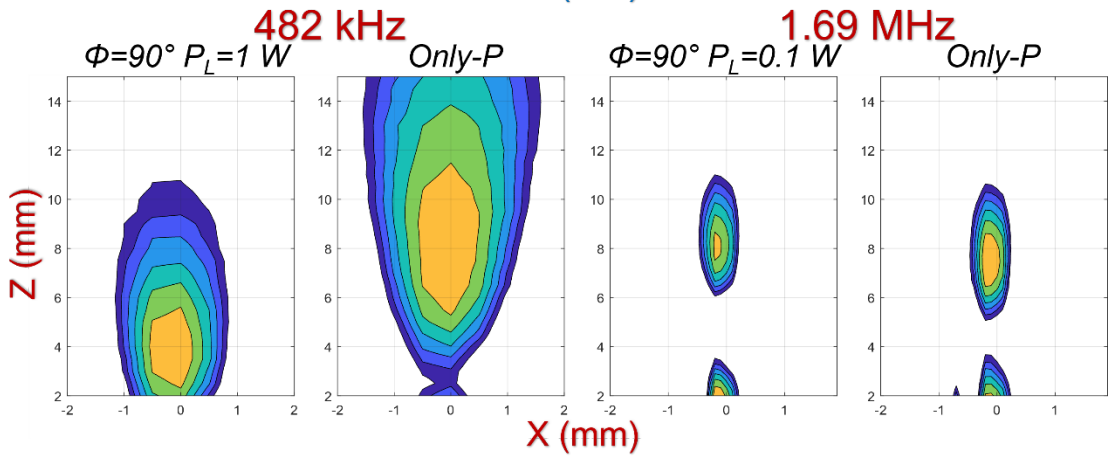
The biaxial driving of single-element ring shaped transducers offers new opportunities to displace and produce small areas of the focal spot without the need of using a transducer array.

Natural Sciences and Engineering Research Council of Canada. Mitacs Accelerate. Canada Foundation for Innovation.

Simulation



Experiment



Computational Simulation Based Investigation of Phase Aberration for Transabdominal Histotripsy

Presenter: Ellen Yeats

Authors in order: Ellen Yeats, *University of Michigan*, Dinank Gupta, *University of Michigan*, Jonathan Sukovich, *University of Michigan*, Zhen Xu, *University of Michigan*, Timothy Hall, *University of Michigan*

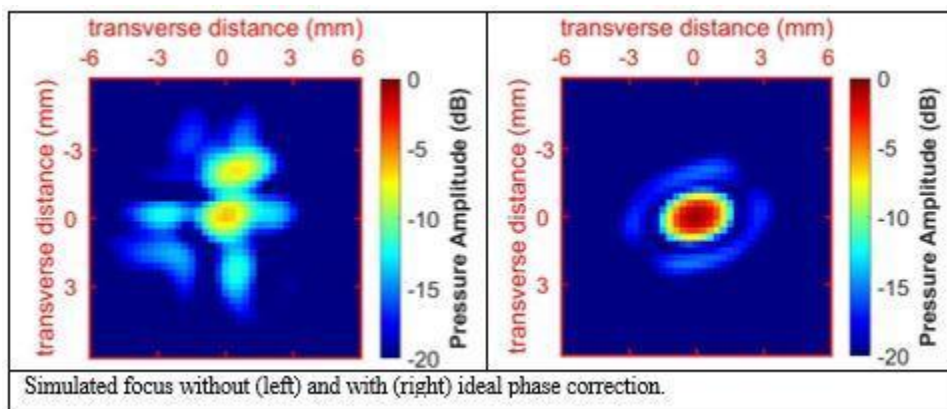
This study aimed to investigate the effects of phase aberration from heterogeneous tissue paths on a large aperture, low f-number transducer used for transabdominal histotripsy.

Abdominal CT images from 10 human subjects were segmented into water, bone, air, fat, skin, and other non-fat soft tissue. A computational model (k-Wave) was experimentally validated and used to simulate focusing a histotripsy transducer (f-number 0.62, central frequency 750 kHz) at 3 targets in the liver of each subject. Simulations were performed with ideal phase correction, without phase correction, and after separately matching the sound speed of water and fat to non-fat soft tissue.

Experimental validation in porcine abdominal tissue showed that simulated and measured arrival time differences agreed well (average error, ~ 0.10 cycles at the central frequency). In simulations of human tissue, aberration created arrival time differences of $0.72 \mu\text{s}$ (~ 0.5 cycles) at the target and shifted the focus from the target by 6.9 mm (6.5 mm pre-focally along depth direction), on average. Phase correction increased maximum pressure amplitude by 89.9%. Matching the sound speed of water and fat to non-fat soft tissue decreased the average pre-focal shift by 4.4 and 0.6 mm and increased pressure amplitude by -1 and 72.8%, respectively.

Soft tissue phase aberration of large aperture, low f-number histotripsy transducers is substantial despite low therapeutic frequencies. Phase correction could potentially recover significant pressure amplitude for transabdominal histotripsy. Different heterogeneity sources distinctly affect focusing quality. The water path causes the focal shift, while irregular tissue boundaries (fat) dominate pressure loss.

This work is funded by NIH grant R01 CA 211217.



A 32-element PZT-PVDF Stacked Transducer Array for Transcranial Focusing and Reception using Short Ultrasound Pulses

Presenter: Zheng Jiang

Authors in order: Zheng Jiang, *Imperial College London*, Javier Cudeiro-Blanco, *Imperial College London*, Betul Ilbilgi Yildiz, *Imperial College London*, Robert Dickinson, *Imperial College London*, Lluís Guasch, *Imperial College London*, MengXing Tang, *Imperial College London*, Timothy Hall, *University of Michigan*, James Choi, *Imperial College London*

We aimed to build a multi-element ultrasound array that could stimulate and monitor microbubble activity across the human skull efficiently and with highly sensitivity.

Many array systems place emitters and receivers at separate locations, creating a trade-off between efficient transmission and reception. Here, we built a 32-element array (radius: 150 mm, F-number: 1.06) with each element composed of a PZT-PVDF stack [PZT for narrowband (500 kHz) emission, PVDF for broadband reception as a front layer]. We evaluated the array's ability to focus, steer, and monitor microbubble activity in water alone and across an ex vivo human skull.

The array was shown to focus ultrasound and receive microbubble signals across the skull. In water alone, the focal dimensions were 4.5*4.5*32 mm and the peak-rarefactional pressure could reach 1.95 MPa. The focus could be steered 30-40 mm and greater than 30 mm in lateral and axial directions, respectively. With aberration correction, ultrasound was focused through the skull with a pressure of 28.8%. The array received acoustic emissions from microbubbles flowing through a 0.6-mm-in-diameter channel exposed to a 3.5-cycle, 0.45-MPa pulse. Microbubble signals were detected with the PVDF and microbubble location was accurately defined using passive acoustic mapping.

By stacking the emitters and receivers, we have overcome the traditional trade-off of efficient transmission and sensitive reception. Such an array design may improve our ability to stimulate and monitor ultrasound methods for delivering drugs across the blood-brain barrier, providing safer and more robust clinical methods.

The authors would like to thank Dr. Matthieu Toulemonde and Dr. Carlos Cueto for their help with the Verasonics. Funding source: Alzheimer's Research U.K (ARUK-IRG2017A-7).

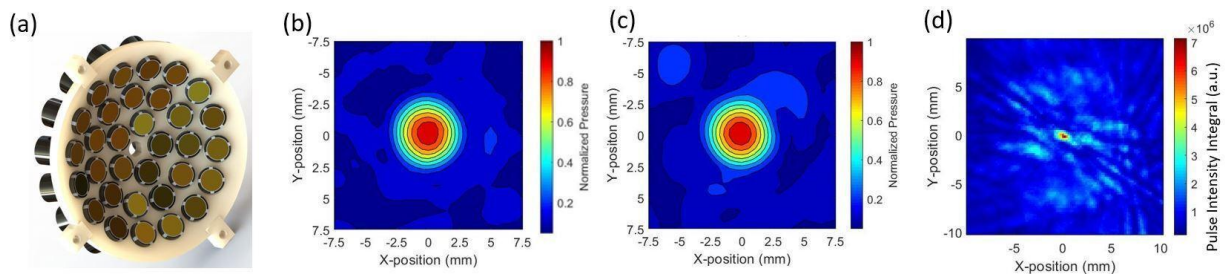


Fig.1. (a)The array. Beam profile (b) in water and (c) through the skull. (d)Transcranial passive acoustic mapping.

B4-3

An Affordable and Easy-to-use Focused Ultrasound Device for High Precision Drug Delivery to the Mouse Brain

Presenter: Zhongtao Hu

Authors in order: Zhongtao Hu, *Washington University in St. Louis*, Si Chen, *Harvard Medical School and Massachusetts General Hospital*, Yaoheng Yang, *Washington University in St. Louis*, Yan Gong, Hong Chen, *Washington University in St. Louis*

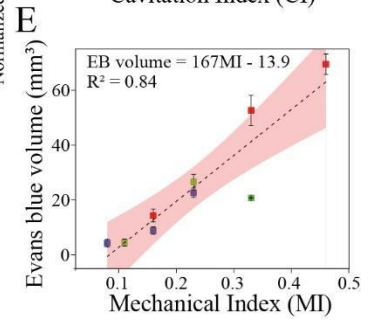
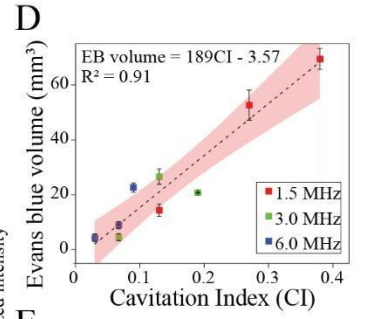
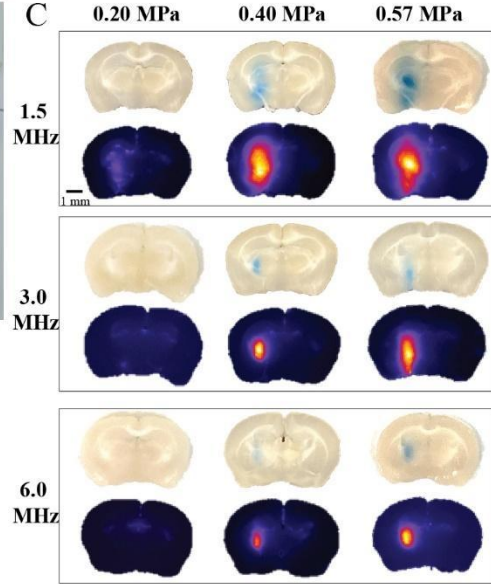
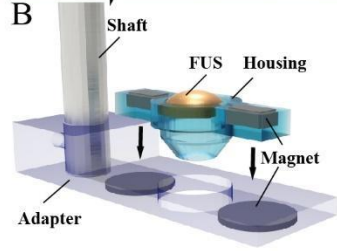
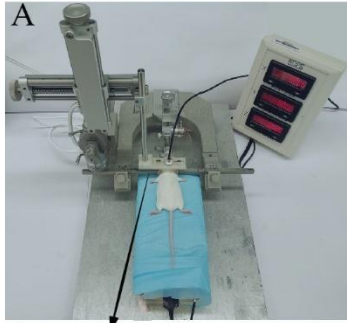
The objective of this study was to design and fabricate an affordable, easy-to-use, high-precision FUS device for preclinical research.

We designed and fabricated in-house mini-FUS transducers (~\$80 each in material cost) with three frequencies (1.5, 3.0, and 6.0 MHz) and integrated them with a stereotactic frame for precise mouse brain targeting using established stereotactic procedures (Fig. A-B). The BBB opening volume by FUS at different acoustic pressures (0.20–0.57 MPa) was quantified using T1-weighted contrast-enhanced magnetic resonance imaging of gadolinium leakage and fluorescence imaging of Evans blue extravasation.

The targeting accuracy of the device as measured by the offset between the desired target location and the centroid of BBBO was 0.63 ± 0.19 mm. The spatial precision of the device in targeting specific brain structures was improved using higher frequency FUS transducers (Fig. C). The BBB opening volume had a higher linear correlations with the cavitation index (defined by the ratio between acoustic pressure and frequency) comparing to mechanical index (defined by the ratio between acoustic pressure and the square root of frequency) (Fig. D-E).

This study demonstrated that spatially accurate and precise BBB opening was achievable using an affordable and easy-to-use FUS device. The BBB opening volume was tunable by modulating the cavitation index. This device is expected to decrease the barriers to the adoption of the FUS-BBBO technique by the broad research community.

This work was supported in part by the National Institutes of Health grants (R01EB027223, R01EB030102, and R01MH116981).



Simulation-guided Navigation System for Transcranial Focused Ultrasound

Presenter: TaeYoung Park

Authors in order: TaeYoung Park, *Bio-Medical Science and Technology, KIST School, Korea Institute of Science and Technology*, Heekyung Koh, *Korea Institute of Science and Technology (KIST)*, Hyungmin Kim, *Korea Institute of Science and Technology (KIST)*

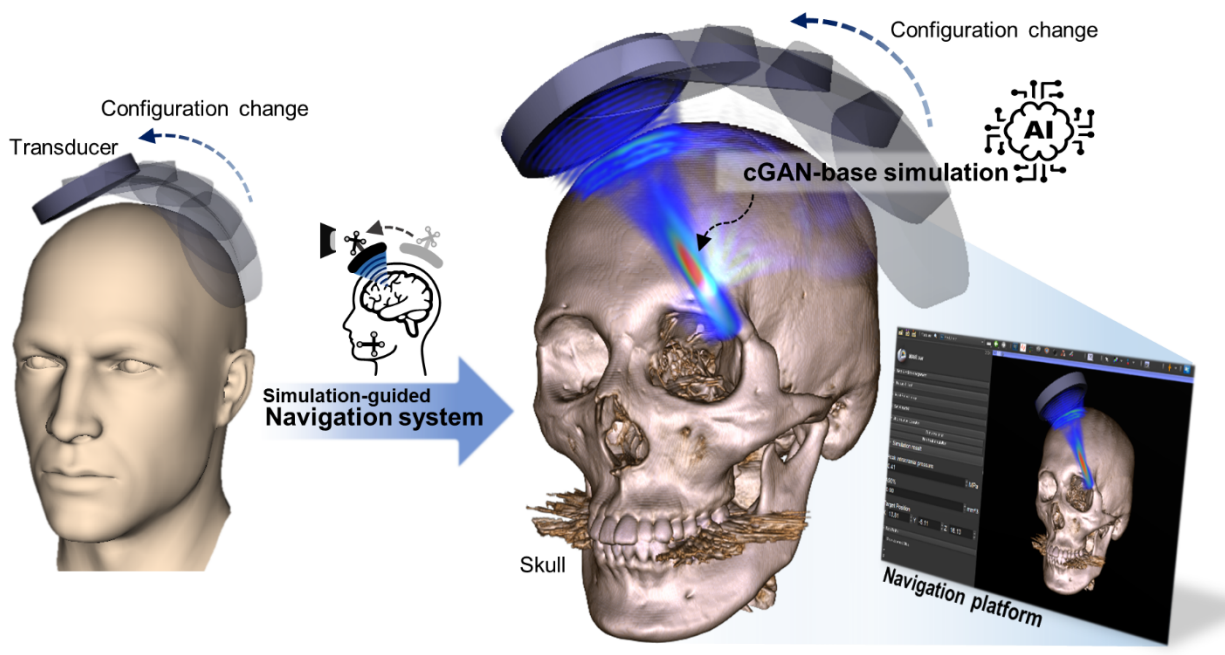
We proposed a simulation-guided navigation system, which can provide an online simulation of the intracranial acoustic field based on a neural network.

For real-time acoustic simulation, the 3D conditional generative adversarial network (cGAN) model featuring residual blocks and multiple loss functions was suggested. The acoustic simulation result, pre-calculated by the conventional numerical solver, was used as training data for the cGAN model. We implemented a simulation-guided navigation system based on 3D Slicer (<https://www.slicer.org/>) by integrating the real-time acoustic simulation. We also validated the accuracy of the simulation-guided navigation system numerically and experimentally.

The figure below shows the overview of the simulation-guided navigation system. The cGAN-based real-time acoustic simulation was performed at the transducer configuration provided by the navigation system. The simulation result was updated with a sampling rate of 4 Hz, including all pre/post-processing time (computed in Intel Core i9-10900K, NVIDIA GeForce RTX 3090, 128 GB RAM). In numerical and experimental validation of cGAN-based acoustic simulation, the intracranial peak pressure error was less than 5.7 %, and the positional error of the acoustic focus was less than 4.2 mm.

We proposed the simulation-guided navigation system using the cGAN-based real-time acoustic simulation. The proposed system can predict intracranial acoustic fields in real-time depending on the transducer's configuration.

This work was supported by the University of Science and Technology (UST) Young Scientist Program and the National Research Council of Science and Technology (NST).



Simulation and Visualization Tool for Subject-specific Transcranial Focused Ultrasound Neuronavigation

Presenter: Mohammad Daneshzand

Authors in order: Mohammad Daneshzand, *Massachusetts General Hospital, Harvard Medical School*, Aapo Nummenmaa, *Massachusetts General Hospital, Harvard Medical School*, Jian Li, *Massachusetts General Hospital, Harvard Medical School*, Livia Vendramini, *Massachusetts General Hospital*, Jason Stockmann, *Massachusetts General Hospital, Harvard Medical School*, Tina Chou, *Massachusetts General Hospital*, Darin Dougherty, *Massachusetts General Hospital*, Brian Edlow, *Massachusetts General Hospital, Harvard Medical School*, Bastien Guerin, *Massachusetts General Hospital, Harvard Medical School*

To provide an open-source, user-friendly MATLAB-based application for simulation and planning of transcranial Focused Ultrasound (tFUS) human studies as well as real-time tFUS neuronavigation.

We use mSOUND, a fast angular spectrum method that models nonlinear ultrasound propagation in heterogeneous media (e.g., skull). The pipeline consists of 1) generation of a pseudo-CT image from a T1w-MRI image; 2) computation of tFUS acoustic beams of the transducer at hundreds of locations on the scalp; 3) a tool for visualization of the beams at the modeled transducer locations, and 4) real-time neuronavigation for visualization of the tFUS beam when moving the transducer.

Pre-processing steps 1) and 2) take ~12 hours for simulation of a 650kHz focused transducer at ~1000 locations on the subject' scalp with mSOUND. For each beam solution, 3D rendered surfaces of the intensity distribution are saved, along with the average acoustic energy deposition for various deep brain nuclei, evaluated using FreeSurfer. These data are accessed for rapid visualization of different beam solutions for tFUS planning (step 3) and real-time neuronavigation (step 4). Using a navigation system with optical tracking, TMS Navigator (Localite, Germany), an overall frame rate of 2 Hz for MATLAB-based beam calculations and visualization was achieved.

The proposed tool allows subject-specific, simulation-based planning and real-time visualization of the acoustic beam created by curved ultrasound transducers at hundreds of locations on the scalp. We are currently evaluating the impact of skull-induced beam deformations on tFUS navigation compared to line of sight targeting approach.

We thank Yun Jing and Juanjuan Gu for their help with mSOUND. This research is supported by NIH R01MH111829, P41EB030006-01 and MGH McCance "Spark" fellowship.

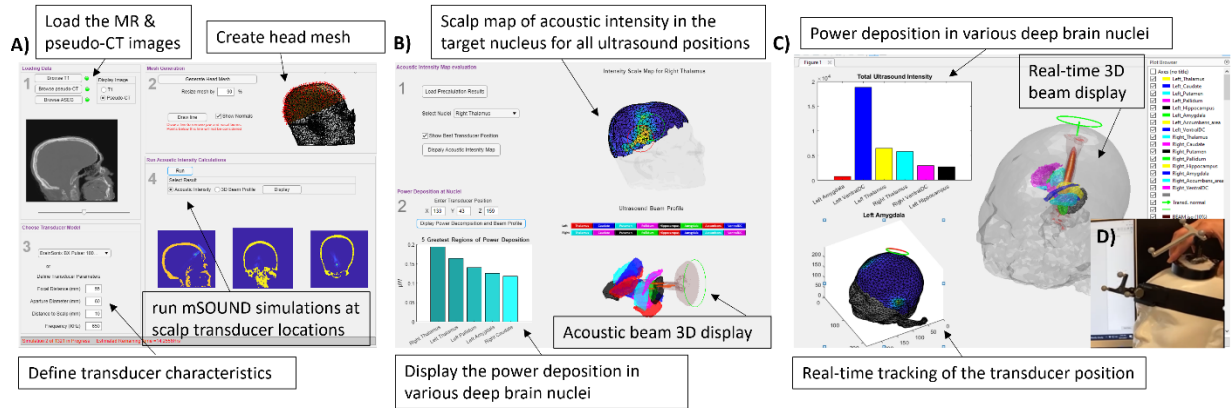


Figure 1. A) Pre-processing GUI (step 2). B) tFUS visit planning GUI (step 3). C) real-time acoustic beam display engine integrated with the Localite navigation system (D, step 4).

Acoustic Evaluation of Synthetic Skulls from Conditional Adversarial Networks

Presenter: Michelle Sigona

Authors in order: Michelle Sigona, *Vanderbilt University*, Han Liu, *Vanderbilt University*, Thomas Manuel, *Vanderbilt University*, Li Min Chen, *Vanderbilt University Medical Center*, Benoit Dawant, *Vanderbilt University*, Charles Caskey, *Vanderbilt University Medical Center*

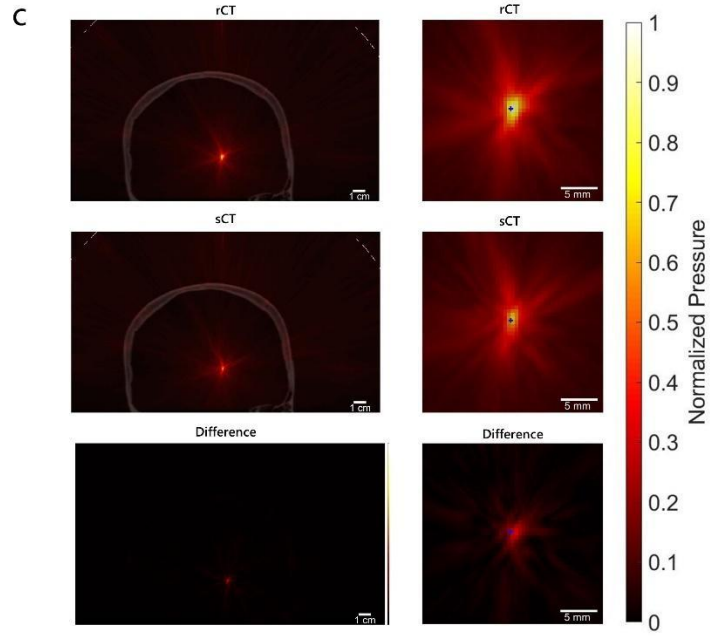
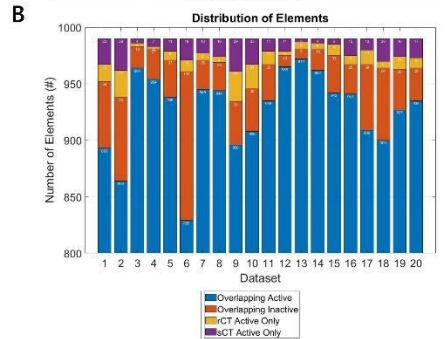
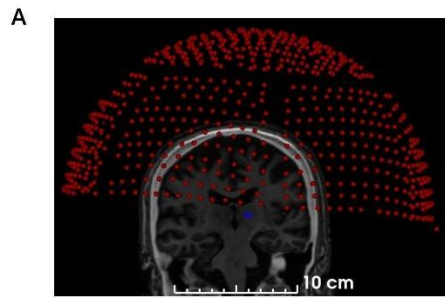
Evaluate synthetic CT (sCT) images generated from a 3D conditional generative adversarial network (cGAN) by comparing clinical metrics and acoustic simulations to real CTs (rCT).

Our network was a 3D patch-based cGAN that enabled paired training to synthesize CT skull images from T1-weighted MRIs. 86 paired datasets were split so that 66 were used for training, 10 for parameter tuning, and 10 for testing. Treatment planning software, Kranion, was used to compare skull density ratio, skull thickness, and the number of active elements for each CT using a hemispherical array. Simulations were performed in k-Wave to evaluate the pressure field.

Skull metrics from Kranion had strong positive linear correlation between rCT and sCTs, demonstrated by Pearson's Correlation Coefficients for the skull density ratio, skull thickness, and the number of active elements (0.915, 0.941, and 0.989). 97.5% of active and inactive elements overlapped between real and synthetic CTs. The pressure fields in simulations of rCT versus sCT contained a lower root-mean-squared pressure (RMS) at the maximum focus of sCTs (23.5 +/- 6.51%). The focal volume of sCTs was 10.9% greater than rCTs. A focal shift of 0.35 +/- 0.40 mm between rCT and sCT maximum RMS pressure location was observed.

Focused ultrasound (FUS) tools were used to compare synthetic CTs generated from deep-learning methods to rCTs. sCTs had strong similarities in skull measurements to rCTs, but simulations revealed subtleties within the skull layers causing differences in the simulated pressure fields. sCTs would be feasible to replace rCTs for FUS planning.

This work was funded by R01 MH111877 and U18EB029351. All simulations were run on a Quadro P6000 GPU donated by NVIDIA Corporation.



A) Hemispherical array positioned at the thalamus target (blue). B) Comparison of overlapping elements between rCT and sCT. C) Simulated pressure fields (enlarged on right) normalized to rCT.

B4-7

An Ultrasound-guided Hemispherical Phased Array for Microbubble-mediated Ultrasound Therapy

Presenter: Lulu Deng

Authors in order: Lulu Deng, *Sunnybrook Research Institute*, Steven Yang, *Sunnybrook Research Institute*, Meaghan O'Reilly, *Sunnybrook Research Institute*, Ryan Jones, *Sunnybrook Research Institute*, Kullervo Hynynen, *Sunnybrook Research Institute/ University of Toronto*

To develop a magnetic resonance imaging-free ultrasound-guided transcranial focused ultrasound (FUS) system and evaluate different transcranial aberration correction methods on both transmit and receive.

A clinical-scale prototype hemispherical FUS brain system was constructed by integrating a 128-element 11 MHz array for skull localization within a 256-module multi-frequency (306/612/1224 kHz) dual-mode phased array. Benchtop experiments were performed with ex-vivo human skullcaps to evaluate the system's transmit and receive performance using transcranial phase aberration corrections calculated via: (1) CT-based simulations via ultrasound-based registration (USCT); (2) CT-based simulations via landmark-based registration (LMCT); and (3) a gold-standard fixed source emitter (FSE)-based method.

Displacement and rotation registration errors of 1.4 ± 0.4 mm and $2.1 \pm 0.2^\circ$ were obtained using USCT, resulting in targeting errors of 0.9 ± 0.2 mm and 0.9 ± 0.3 mm when driven at 306 and 612 kHz, respectively, and source localization errors of 1.0 ± 0.3 mm and 0.6 ± 0.2 mm when receiving at 306 and 612 kHz, respectively. No significant differences were found between USCT and LMCT on either transmit or receive. During volumetric multi-point exposures, ~70% (60%) of the transmit frames in which microbubble activity was detected via FSE were recovered using USCT when imaging at the second- (half-) harmonic, compared to 60% (69%) using LMCT.

An ultrasound-guided transcranial FUS treatment platform has been developed. The system affords ultrasound-based CT skull registration with accuracy comparable to landmark-based registration methods, resulting in sub-millimeter targeting and localization errors. Such systems have great potential to advance the adoption of microbubble-mediated FUS brain therapy by improving access to the technology.

The authors would like to thank K. Leung, T. Portelli, F. Orfanidis, and R. An for their technical assistance.

B4-8

Clinical Transmit-receive High-power Transducer Array System for the Treatment of Deep Vein Thrombosis

Presenter: Maryam Dadgar

Authors in order: Maryam Dadgar, *University of Toronto*, Kullervo Hynynen, *Sunnybrook Research Institute/ University of Toronto*

A phased-array transducer system was designed and fabricated to produce high pressure amplitudes suitable for mechanical clot fragmentation for the treatment of deep vein thrombosis.

To produce high pressures and make the system durable under high power applications, there are challenges such as delamination of layered transducer elements and electrical connections and several other failure modes. A special attention was paid to these challenges and a 258 kHz, high-power system was fabricated. To monitor the bubble activity associated with the cavitation, a second harmonic receiver array was incorporated into the transmit system.

The system was capable of producing a maximum of 34 MPa pressure at 50 mm focal distance (the average distance from the surface of the thigh to the human femoral vein). In-vitro results demonstrated the ability of the system to fragment the thrombus by only half of the maximum pressure. The benchtop experiments on the passive acoustic mapping of the bubble activity showed the consistency with the simulation results. Furthermore, with the special configuration of the array we were able to confine the focus in the human femoral vein (average diameter of 12 mm).

The system was designed to fit on the inner surface of the human thigh and was able to fragment the clot in-vitro and monitor the bubble activity. The results together have opened the path to examine the system in in-vivo studies and expectantly in future clinical settings.

I would like to acknowledge my supervisor Dr. Kullervo Hynynen, supervising committee, and the focused ultrasound lab members for their helps and support.

B4-9

A Novel Catheter-based Ultrasound Device for Treating Vascular occlusions

Presenter: Jingjing Liu

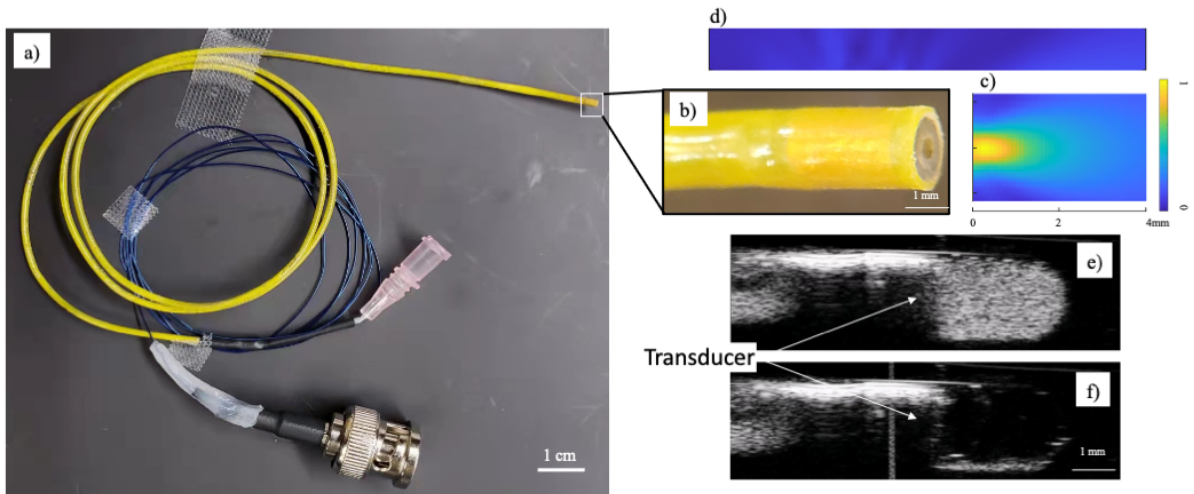
Authors in order: Jingjing Liu, *Sunnybrook research institute*, Alex Wright, *Sunnybrook Research Institute*, Bradley Strauss, *Sunnybrook Research Institute*, Kullervo Hynynen, *Sunnybrook Research Institute/ University of Toronto*, David Goertz, *Sunnybrook Research Institute*

A novel prototype catheter device with forward-looking ultrasound projecting from a hollow cylindrical transducer was developed to perform cavitation seed mediated treatments of vascular occlusions.

Radially-polarized miniature cylindrical PZT transducers were characterized by length and resonant mode with hydrophone scans. OnScale™ simulations guided the design. The constructed catheter (1.55/0.6mm inner/outer diameter currently) had a transducer situated at its tip such that its lumen could accommodate a guidewire and also act as a conduit for administering cavitation agents. Its size and flexible braided shaft permit entry into relevant vessels. Initial testing was conducted in occluded vessel phantoms with microbubbles.

2.5 mm length PZT transducers excited at the 3rd length mode harmonic at 1.89 MHz achieved high forward-looking pressures. An air backing layer and catheter sheath attenuated the backward and lateral pressures by at least 90%, reducing the potential for vascular injury. An epoxy layer at the distal face broadened the forward full width at half maximum, while the catheter structure improved the transducer pressure output compared to bare transducers. The peak pressures of over 2.9 MPa was measured 0.5 mm from the tip. Phantom experiments demonstrated the ability to introduce microbubbles into the vessel then induce cavitation and damage.

This compact catheter-based ultrasound device prototype can project high pressures in the forward -direction and its design is compatible with navigating to vascular occlusions and releasing cavitation seeds and enzymes. This approach is relevant to the treatment of thrombotic and chronic total occlusions in for example cardiology or peripheral vascular.



(a). Constructed catheter-based ultrasound transducer and (b). cylindrical PZT transducer situated at the catheter tip; (c). forward-looking pressure profile, and (d). attenuated backward & lateral pressure map; and (e). vessel phantom after injection of MBs and (f). subsequent MB destruction after sonication

Topography Predicts MRgFUS-subthalamotomy Outcome in Parkinson Disease

Presenter: Rafael Rodriguez-Rojas

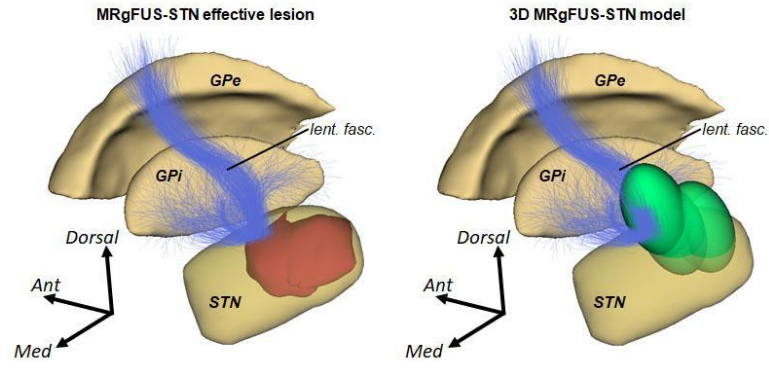
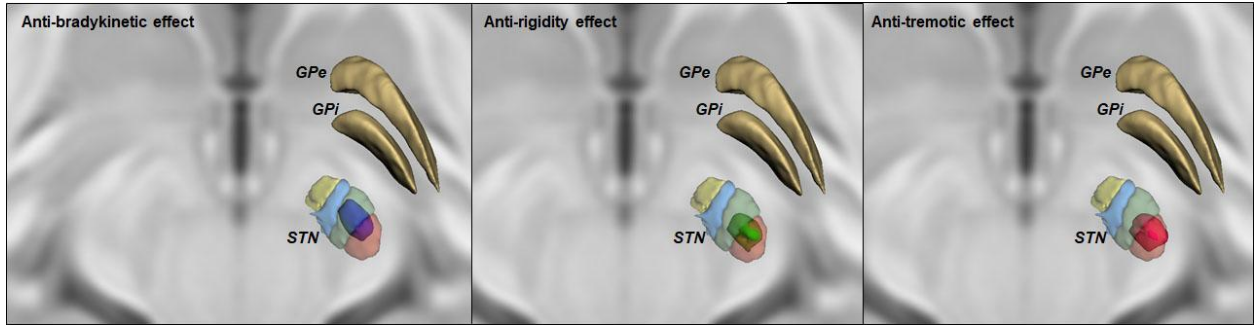
Authors in order: Rafael Rodriguez-Rojas, *FUNDACIÓN DE INVESTIGACIÓN HM HOSPITALES. CIF:G83643841*, Jorge Máñez-Miró, *HM CINAC (Centro Integral en Neurociencias)*, *University Hospital HM Puerta del- CEU San Pablo University.*, Jose Pineda-Pardo, *HM CINAC (Centro Integral de Neurociencias Abarca Campal)*, *Hospital Universitario HM Puerta del Sur, HM Hospitales*, Marta del Álamo, *HM CINAC (Centro Integral en Neurociencias)*, *University Hospital HM Puerta del- CEU San Pablo University*, Raul Martinez Fernandez, *HM CINAC, Hospital HM Puerta del Sur*, Jose Obeso, *HM CINAC (Centro Integral en Neurociencias)*, *University Hospital HM Puerta del- CEU San Pablo University.*

To explore the relation between the topography of MRI-guided Focused Ultrasound subthalamotomy (MRgFUS-STN) and motor outcomes, according to the Unified Parkinson's Disease Rating Scale (UPDRS-III).

Forty-five PD patients undergoing unilateral MRgFUS-STN were included. Scores for bradykinesia, rigidity and tremor were computed at baseline and at 4-month follow-up after the treatment. Lesion topographies were derived from manual segmentation on post-treatment MRI-data, following normalisation into a standard stereotactic space. The effective impacts were calculated by computing the voxels that are common to the lesion and an atlas-defined STN, and hierarchical multiple regression analyses were used to examine the relationship to motor outcome.

The relationship between lesion topography and the STN organization (Figure 1) explains specific improvement in bradykinesia ($r=-0.34$; $p=0.041$), rigidity ($r=0.492$; $p=0.002$), and tremor ($r=0.41$; $p=0.016$). The tremor-effective cluster is located posteriorly, while the bradykinesia-effective cluster appears more medial and anterior. The rigidity effective cluster lay in between. Based on a data-driven analysis of local impact of MRgFUS, we introduce a realistic 3D model of the lesion and surrounding anatomy.

Effective MRgFUS-STN is associated with a specific spatial profile that can predict outcome for each motor feature. Identifying the probabilistic sweet spots will facilitate better definition of the optimal subthalamotomy and improve specific cardinal features in PD.



Effect of Skull Plastination on Ultrasound Transmission for Neuromodulation

Presenter: Maxime Bilodeau

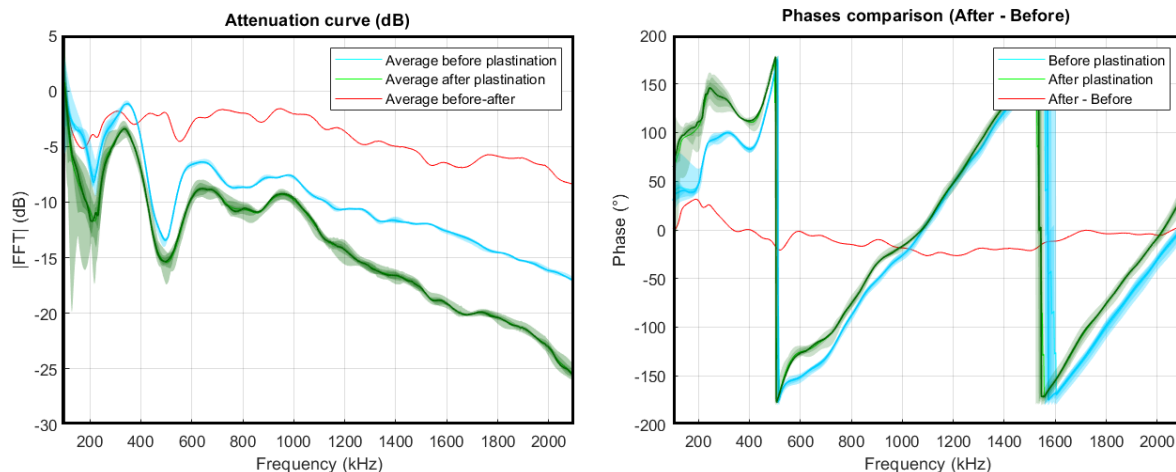
Authors in order: Soline Bernard, *Universite de Sherbrooke*, Maxime Bilodeau, *GAUS - Université de Sherbrooke*, Patrice Masson, *Université de Sherbrooke*, François Moreau, *Université de Sherbrooke*, Philippe Micheau, *Université de Sherbrooke*, Jean-Francois Lepage, *Université de Sherbrooke*, Nicolas Quaegebeur, *Université de Sherbrooke*

Quantify the effects of plastination on ultrasound transmission through temporal and parietal areas of human skulls over a wide frequency range (200 kHz-2 000 kHz)

Three different skulls were installed inside an immersion tank instrumented with a 5 MHz probe and a calibrated hydrophone in order to characterize the transmission curves in terms of attenuation and phase difference. Repeatability of the experimental setup was first demonstrated, allowing transmission characterization up to -60 dB. The same transmission measurements were performed before (i.e. fresh skulls) and after plastination to characterize the changes induced by this conservation method.

Varying attenuation levels are observed after the plastination process with an added absorption between 2 dB and 12 dB for the 24 measurement areas assessed. The increase in attenuation is more important over the parietal area than over the temporal area and, for all skulls, the added absorption remains below 10 dB between 300 kHz and 600 kHz. The porosity of the skulls could influence the increase of absorption after 1 MHz. Concerning phase changes, no significant changes have been observed. The plastination process does not appear to have an effect on the focalization of ultrasound waves through plastinated areas.

An increase in the transmission loss between 2 dB and 12 dB is observed after plastination of different skulls, and between 0 and 5 dB in the frequency band of interest for neuromodulation (200-800 kHz). Plastination does not alter the phase of the transmitted signal which should not affect focalization.



Modular Design for a Hybrid Multichannel TMS-tFUS Device

Presenter: Mohammad Daneshzand

Authors in order: Mohammad Daneshzand, *Massachusetts General Hospital, Harvard Medical School*, Bastien Guerin, *Massachusetts General Hospital, Harvard Medical School*, Aapo Nummenmaa, *Massachusetts General Hospital, Harvard Medical School*

We combine a modular multi-channel TMS array with a focused ultrasound transducer to allow concurrent control of ultrasonic and electromagnetic fields for brain stimulation.

We arrange three of our previously developed 3-axis TMS coils around a Brainsonix focused ultrasound transducer. The distance between the 3-axis TMS coils is 3 cm. The tFUS transducer has a focal length of 80mm and is raised 30mm using a coupling cone from the scalp surface to allow cortical stimulation. We compute TMS E-field and tFUS acoustic profiles using BEM-FMM and mSOUND methods, respectively, in sphere and anatomically realistic head models.

Fig. 1 shows that the total E-field created by the combination of the 9 TMS channels (3x3) that can be shifted across a patch of cortical surface with resolution ~ 5 mm. In particular, the multi-channel TMS device enables suprathreshold stimulation at the center of the array, which also corresponds to the axis of the tFUS transducer, by optimizing the input currents to each coil without altering the ultrasound field. The localization errors map in Fig. 1E shows that TMS E-field minimum norm optimization yields to stimulation hotspot steering error below 10 mm in an area of approximately 20 cm²

Since tFUS is sub-threshold, and may be predominantly inhibitory, it has been difficult to characterize its mechanisms. By providing fine control of the TMS and tFUS excitation field overlap, we hope that our device opens the door for in-depth studies of the mechanisms of action of tFUS neuromodulation in-vivo.

This research is supported by NIH R01MH111829, P41EB030006-01 and an MGH McCance “Spark” fellowship.

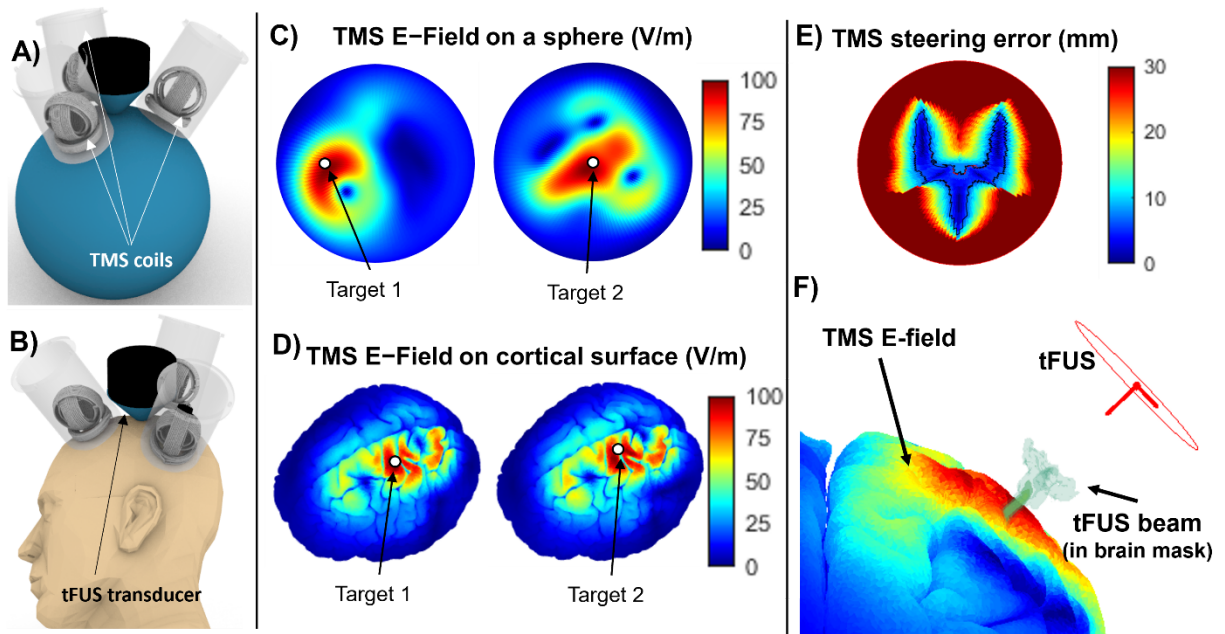


Figure 1. A-B) The 3 by 3 TMS array (shown in grey) paired with the tFUS (shown in black). The E-field can be steered based on the linear combination of all coils in the array which is shown for two different targets on a sphere model (C) as well as cortical surface (D). E) The steering (Localization) error map for the 3 by 3 array. The area with less than 10 mm in steering error is outlined in black. F) The tFUS 3D beam visualization can provide more accurate targeting and dosing of the stimulation.

P1-12

Simulation of Transcranial Ultrasound Transmission Based on Micro-CT Skull Images

Presenter: Milan Fritsche

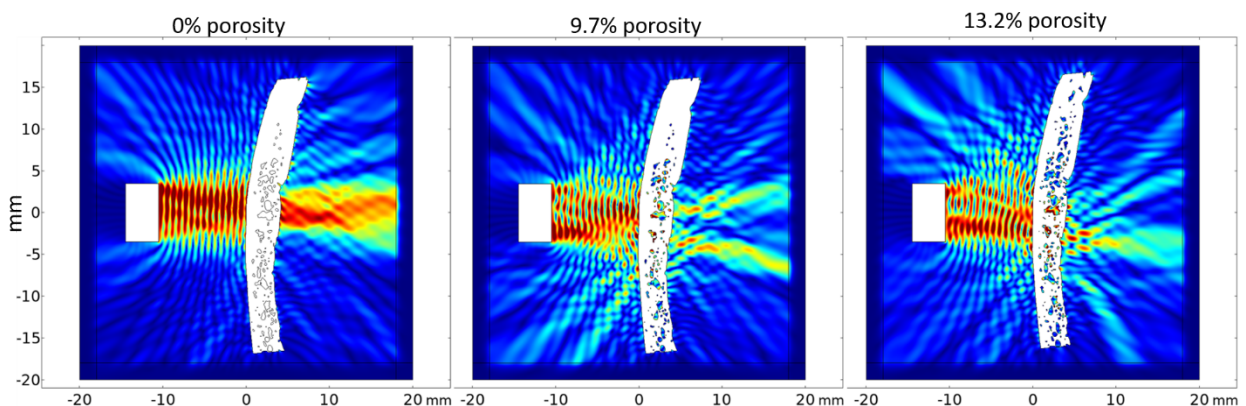
Authors in order: Milan Fritsche, *Nuremberg Institute of Technology*, Florian Steinmeyer, *Technische Hochschule Nürnberg*, Matthias Neugebauer ,

Considering transcranial ablation, neuromodulation and imaging we simulate the influence of the skull fine structure on Ultrasound (US) propagation based on micro-CT skull images.

In order to increase the resolution of the cortical and diploë structure - as compared to clinical CT - ex-vivo occipital skull was scanned by micro-CT (CTportable, Fraunhofer EZRT) with $40.6\mu\text{m}$ resolution. A slice was threshold binarized with regions representing either bone or bone marrow pores. Calculations for a flat 1 MHz transducer were performed in a linear acoustic 2D COMSOL model. Continuous wave and pulse simulations were conducted in frequency and time domain respectively.

We are presenting pressure fields with varying pore fractions (see figure, time averaged in a.u.), incidence angles and wave forms. At 0% porosity the skull shape causes visible distortion. At 9.7% and 13.2% note the pronounced pressure loss along the symmetry axis behind the skull, sensitive to a relatively small porosity variation. Near field interference patterns smooth out during propagation deeper into the skull. Distortion also critically depends on the incidence angle. Short pulse propagation demonstrates that even without inserting an attenuation coefficient significant amount of wave energy is guided into the skull bone and is lost for transmission.

US transmission amplitude and spatial aberration are highly sensitive to detailed skull geometry as well as transducer angular alignment, in particular in the near field close to the skull interior. This will have implications e.g. for neuromodulation targeting cerebral mantle areas.



P1-13

A Computational Method to Predict Peripheral Auditory Activation during Transcranial Ultrasound Stimulation (TUS) in Mice

Presenter: Mi Hyun Choi

Authors in order: Mi Hyun Choi, *Stanford University*, Gerald Popelka, *Stanford University*, Kim Butts Pauly, *Stanford University*

The objective was to develop and experimentally validate a computational ultrasound signal processing approach to assess peripheral auditory activation during TUS in mice.

Ultrasound pulses (500kHz,80ms) with varying amplitudes, pulse repetition frequencies, smoothing profiles, and sinusoidal modulation frequencies were selected. Each pulse's time-varying frequency spectrum was obtained with 1ms segments, equivalent to the mouse gap detection threshold. The spectrum was differentiated across frequencies, weighted by the mouse hearing sensitivity, then summed over frequencies. The resulting time-varying function predicting the peripheral audibility was validated against experimental auditory brainstem responses (ABR) in mice during TUS with the corresponding pulse.

A linear relationship ($R^2 = 0.79$) was found between the predicted audibility and ABR power at TUS onset (0ms) and mid-stimulation (40ms) (Figure 1). The ABR threshold was used as the theoretical hearing threshold. For continuous ultrasound pulses (CW), ABRs were found at the beginning and the end of rectangular envelopes (RE) but not smoothed envelopes (SE). ABR amplitudes diminished with decreasing spatial peak pulse-averaged intensities. Pulsed waves (PW) with 80% duty cycle (DC) had additional auditory activation throughout the signal at pulse repetition frequencies (PRFs) less than 8kHz. These trends were accurately reflected in the prediction model.

The ultrasound pulse frequency spectrum and intrinsic mouse auditory system characteristics can be used to predict peripheral auditory activation in mice subjected to TUS. This approach can be modified and applied to other species. Additional studies are needed to assess the downstream impact of peripheral auditory activation on brain activity.

We would like to acknowledge funding from NIH RF1 MH 116977 and NSF 1828993.

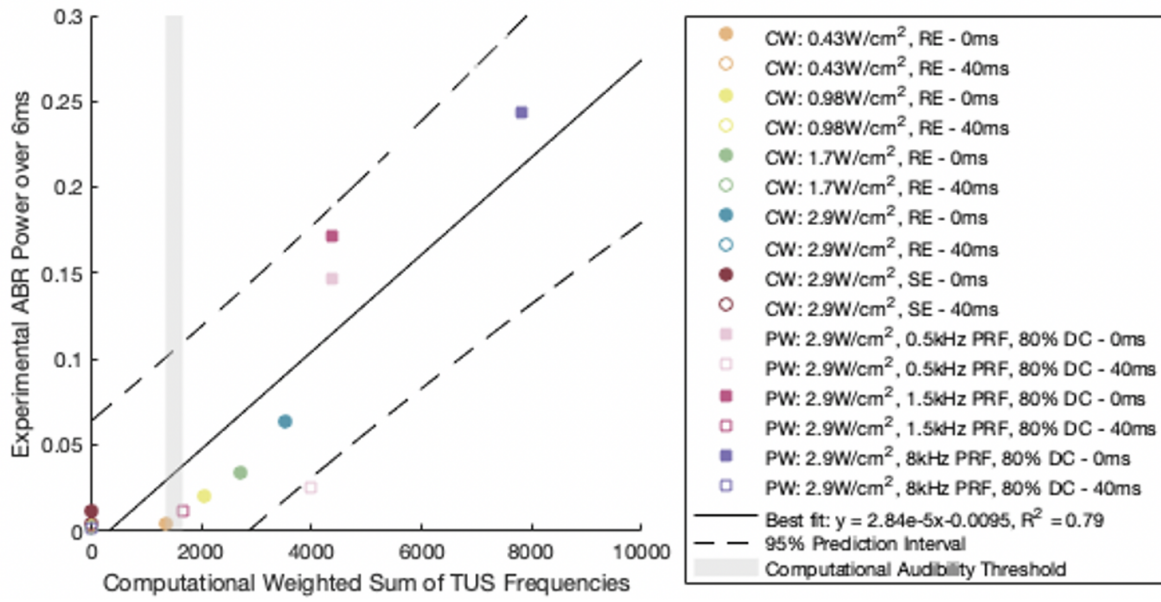


Figure 1. Audibility prediction based on TUS pulse vs. ABR power.

Docetaxel Perfluorocarbon Nanodroplets: A New Glioblastoma Therapeutic Agent

Presenter: Benoit Larrat

Authors in order: Charlotte Berard, *Aix-Marseille University*, Stephane Desgranges, *Avignon Université*, Noé Dumas, Anthony Novell, *BioMaps, Université Paris Saclay, CEA, CNRS, Inserm*, Benoit Larrat, *CEA*, Mourad Hamimed, *Aix-Marseille University*, Nicolas Taulier, *Sorbonne Université, CNRS, INSERM, Laboratoire d'Imagerie Biomédicale*, Marie-Anne Estève, *Aix-Marseille University*, Florian Correard, *Aix-Marseille University*, Christiane Contino-Pepin, *Avignon Université*

Nanoemulsions combined with FUS represent a real opportunity to improve brain tumor treatment. Here, docetaxel was loaded into PFOB nanodroplets (ND-DTX) stabilized with fluorinated surfactants.

Healthy (n=65) and GL261 glioma-bearing (n=40) mice (syngeneic model) were used for pharmacokinetic and FUS-mediated BBB disruption studies. After SonoVue® intravenous injection (50 µL), ultrasonic waves were transmitted at 1.5 MHz with duty cycle of 72%. A raster scan synchronized to the generator induced a hemispheric brain BBB disruption of 6 mm (anterior-posterior) × 3.6 mm (lateral right hemisphere). The sequence was repeated 20 times for a total exposure of 112 s.

After intravenous administration in mice, stabilized PFOB droplets are eliminated from the bloodstream in 24 h (blood half-life = 3.1 h) and they are completely excreted from mice body after 72 h. In addition, intracerebral accumulation of unloaded tagged-droplets is safely and significantly increased after FUS-mediated BBB disruption for each mouse ($p < 0.05$). Glioma-bearing mice were either treated with saline, docetaxel, ND or ND-DTX combined with FUS-mediated BBB disruption (4 sessions). The median survival time of GL261 glioma-bearing mice treated with ND-DTX was significantly longer compared to docetaxel, saline or ND groups (32 days vs. 27 days, $p < 0.05$).

These promising results demonstrate the potential of our ND-DTX combined with FUS-mediated BBB disruption to improve treatment of glioblastoma.

This work was conducted with financial support from ITMO Cancer AVIESAN.

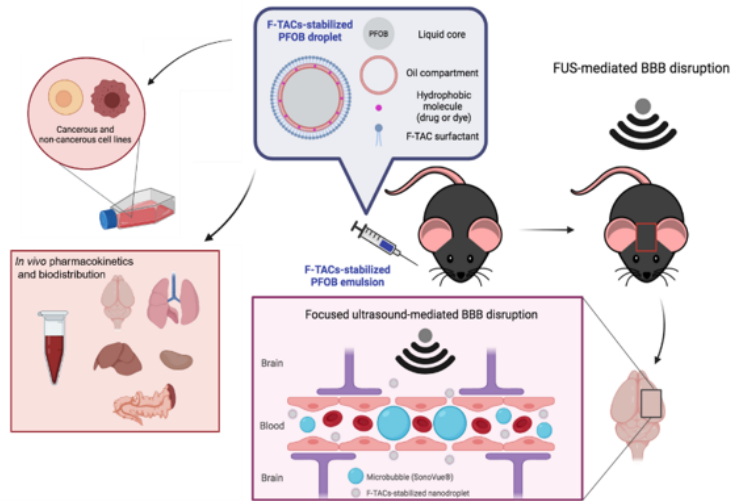


Figure. Stabilized PFOB nanodroplets as suitable nanocarriers for brain drug delivery.

Amplification of Drug Effects at Targeted Brain Regions for Treatment of Chronic Pain

Presenter: Nick Todd

Authors in order: Nick Todd, *Brigham and Women's Hospital*, Nathan McDannold, *Brigham and Women's Hospital, Harvard Medical School*, Yongzhi Zhang, *Brigham and Women's Hospital*, David Borsook, *Massachusetts General Hospital*

To assess focused ultrasound (FUS) blood-brain barrier (BBB) disruption to locally amplify analgesic effects of gabapentin at pain network nodes in the brain.

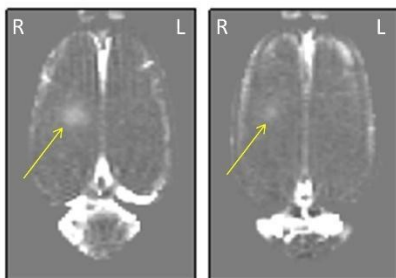
FUS-BBB opening was targeted to right somatosensory cortex in combination with IV injection of 100 mg/kg gabapentin in the rat spared nerve injury (SNI; left leg) model of chronic pain. N=8 rats have been assessed under five experimental conditions: pre-SNI surgery, and post-SNI surgery with +/- FUS and +/- Drug. Post-treatment assessment consists of resting-state fMRI to evaluate changes in brain network connectivity and von Frey behavioral testing to evaluate pain sensitivity.

Treatments combined mild BBB disruption with high dose gabapentin, a clinically used drug that readily crosses the BBB. Significant differences were seen in resting-state fMRI connectivity matrices for all post-surgery groups compared to pre-surgery, indicating network reorganization in this pain model. Behavioral tests showed significantly increased pain sensitivity for both post-surgery groups without gabapentin. Pain sensitivity was not significantly different for FUS + Drug vs. No FUS + Drug groups. Differences in connectivity between several nodes were observed for FUS with Drug versus No FUS with Drug groups, but none that survived correction for multiple comparisons.

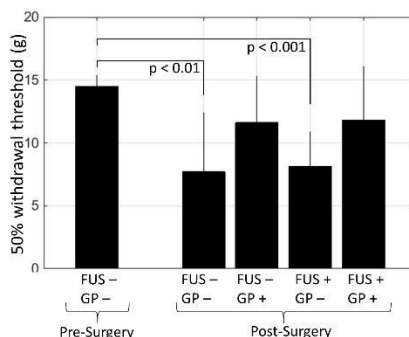
Resting state fMRI and behavioral testing both showed increased pain sensitivity due to the SNI surgery, and the analgesic effects of gabapentin. Under the conditions tested, the combination of FUS + gabapentin did not produce obvious effects over gabapentin alone. We will next try stronger FUS with lower dose gabapentin.

This work is supported by NIH grant 1K01EB023983-01 and The David Borsook Project, supported by the Cathedral Fund

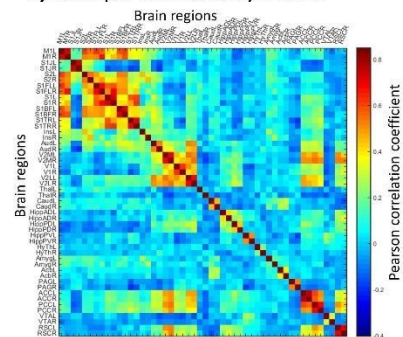
A) Example BBB disruption in right cortex



B) Von Frey Behavioral results (N=8)



C) Example connectivity matrix



Striatal Blood Brain Barrier Opening in Parkinson's Disease

Presenter: Jose Pineda-Pardo

Authors in order: Jose Pineda-Pardo, *HM CINAC (Centro Integral de Neurociencias Abarca Campal), Hospital Universitario HM Puerta del Sur, HM Hospitales, Carmen Gasca-Salas, HM CINAC (Centro Integral en Neurociencias), University Hospital HM Puerta del- CEU San Pablo University, Rafael Rodriguez-Rojas, FUNDACIÓN DE INVESTIGACIÓN HM HOSPITALES. CIF:G83643841, Beatriz Fernández-Rodríguez, HM CINAC (Centro Integral en Neurociencias), University Hospital HM Puerta del Sur., Marta del Álamo, HM CINAC (Centro Integral en Neurociencias), University Hospital HM Puerta del- CEU San Pablo University, Ignacio Obeso, 1. HM CINAC (Centro Integral de Neurociencias Abarca Campal), Fundación Hospitales de Madrid. Hospital Universitario HM Puerta del Sur, HM Hospitales, Madrid, Spain, Frida Hernández-Fernández, HM CINAC (Centro Integral en Neurociencias), University Hospital HM Puerta del Sur., Clara Trompeta, HM CINAC (Centro Integral en Neurociencias), University Hospital HM Puerta del Sur., Raul Martinez Fernandez, HM CINAC, Hospital HM Puerta del Sur, Michele Matarazzo, HM CINAC (Centro Integral en Neurociencias), University Hospital HM Puerta del- CEU San Pablo University, David Mata, HM CINAC (Centro Integral en Neurociencias), University Hospital HM Puerta del Sur., Pasqualina Guida, HM CINAC (Centro Integral en Neurociencias), University Hospital HM Puerta del Sur., José David Albillo Labarra, University Hospital HM Puerta del Sur., Alicia Duque, University Hospital HM Puerta del Sur., Isabel Plaza de las Heras, Juan Montero, University Hospital HM Puerta del Sur., Guglielmo Foffani, HM CINAC (Centro Integral en Neurociencias), University Hospital HM Puerta del Sur., Gabriella Toltsis, Insightec Ltd., Itay Rachmilevitch, Insightec Ltd., Javier Blesa, Fundacion de Investigacion HM Hospitales, Jose Obeso, HM CINAC (Centro Integral en Neurociencias), University Hospital HM Puerta del- CEU San Pablo University.*

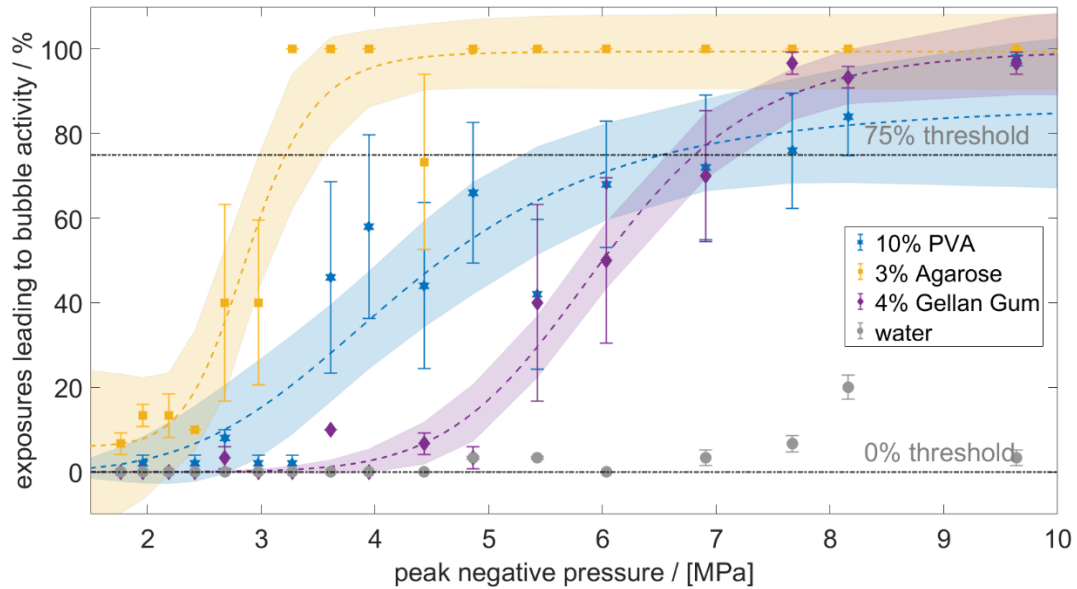
To test safety and feasibility of repeated low-intensity focused ultrasound (FUS) blood brain barrier opening (BBB) in the striatum of Parkinson's disease (PD) patients.

Seven PD patients were treated for BBBO in the posterior putamen as part of a phase I clinical trial (NCT03608553). This was performed in two sessions separated by 2-4 weeks, where the second session included bilateral putamina opening in three patients. Primary outcomes were safety and feasibility of focal striatal BBBO, the latter evaluated by Gadolinium-enhanced MRI. Additional exploratory outcomes included changes in motor and cognitive functions, and PET imaging of 18F-fluorodopa and 18F-florbetaben.

The procedure was feasible, well-tolerated, and with no serious adverse events. BBBO was confirmed in all the procedures (Fig. 1A-B). Three patients received bilateral opening in the second session. BBB closing occurred shortly after treatment and hemorrhagic and ischemic lesions were ruled out. No neurologically relevant change in motor and cognitive functions was recognized upon follow up. There was a significant reduction of 18F-florbetaben uptake in the targeted region (median [interquartile range] = -18.6% [-25.3% - -9.0%], $P = 0.0019$), with no change in 18F-fluorodopa PET (Fig. 1C-D). No significant changes were observed in 18F-fluorodopa PET.

These results indicate that FUS-mediated BBBO could become an effective tool to facilitate safe and repeated delivery of putative neurorestorative molecules to specific brain regions in Parkinson's disease and other neurodegenerative disorders.

The study was supported by Plan Nacional Ministerio de Educación y Ciencias (Government of Spain), MAPFRE Foundation grant, Fundación Hospitales de Madrid and Insightec Ltd.



FUS Mediated Delivery of an AAV9 Gene Therapy for Huntington's Disease

Presenter: Beyza Erdem

Authors in order: Beyza Erdem, *Simmons University*, Tao Sun, *Brigham and Women's Hospital, Harvard Medical School*, Yongzhi Zhang, *Brigham and Women's Hospital*, Jaymin Upadhyay, *Boston Children's Hospital, Harvard Medical School*, Kimberly Kegel-Gleason, *Massachusetts General Hospital*, Nick Todd, *Brigham and Women's Hospital*

To assess the safety and efficacy of an AAV-packaged Huntington's disease gene therapy delivered by FUS-BBB opening to the mouse brain.

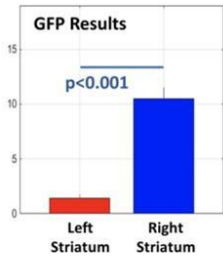
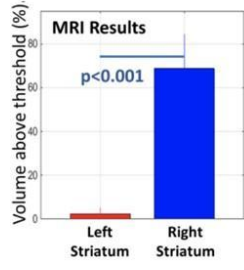
FUS-BBB opening was used to deliver AAV-9-GFP to the right cortex and striatum of wild type (N=3) and Huntington's disease (HD) model (N=4) mice. Delivery efficacy was evaluated based on contrast MRI to quantify BBB opening, immunohistochemistry (IHC) staining to quantify GFP signal, and immunofluorescence (IF) staining for GFP + [NeuN, GFAP, Iba1] for cell type specificity. Safety was assessed based on IHC staining of astrocytes (GFAP) and microglia (Iba1) to determine level of activation.

In HD mice, significant differences were observed between the left and right striatum for MRI signal change ($p < 0.001$) and GFP signal ($p < 0.001$, Figure 1A). Qualitative observations of cell type specificity in WT mice indicate GFP primarily in neurons, secondarily in astrocytes and not at all in microglia (Figure 1B). In HD mice, microglia activation did not show a significant difference between the two sides of the striatum ($p = 0.80$) and cortex ($p = 0.59$) (Figure 1C). Significantly increased activation of astrocytes was observed in the right cortex based on mean GFAP signal ($p = 0.02$) (Figure 1C).

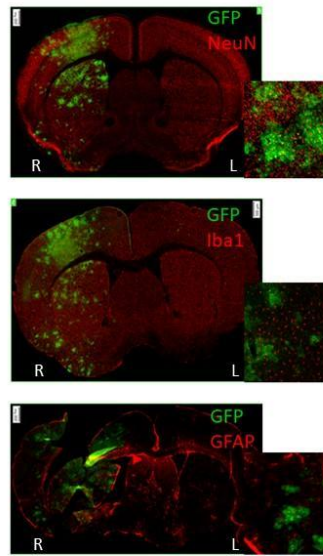
Our results suggest that FUS enables the safe and effective delivery of an AAV9 gene therapy to the brain in HD model mice.

Project supported by the Hereditary Disease Foundation and the Simmons University PLP Grant.

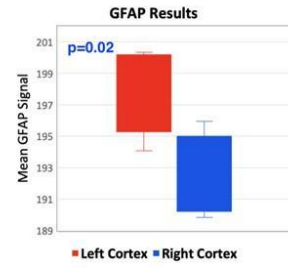
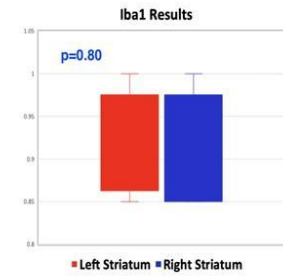
A) Delivery efficacy



B) Cell type specificity examples



C) Microglia and astrocyte activation



Remote Targeted Neurostimulation with Combined Ultrasonic and Magnetic Fields

Presenter: Jan Kubanek

Authors in order: Jan Kubanek, *University of Utah*, Rahul Cheeniyil, *University of Utah*, , , ,

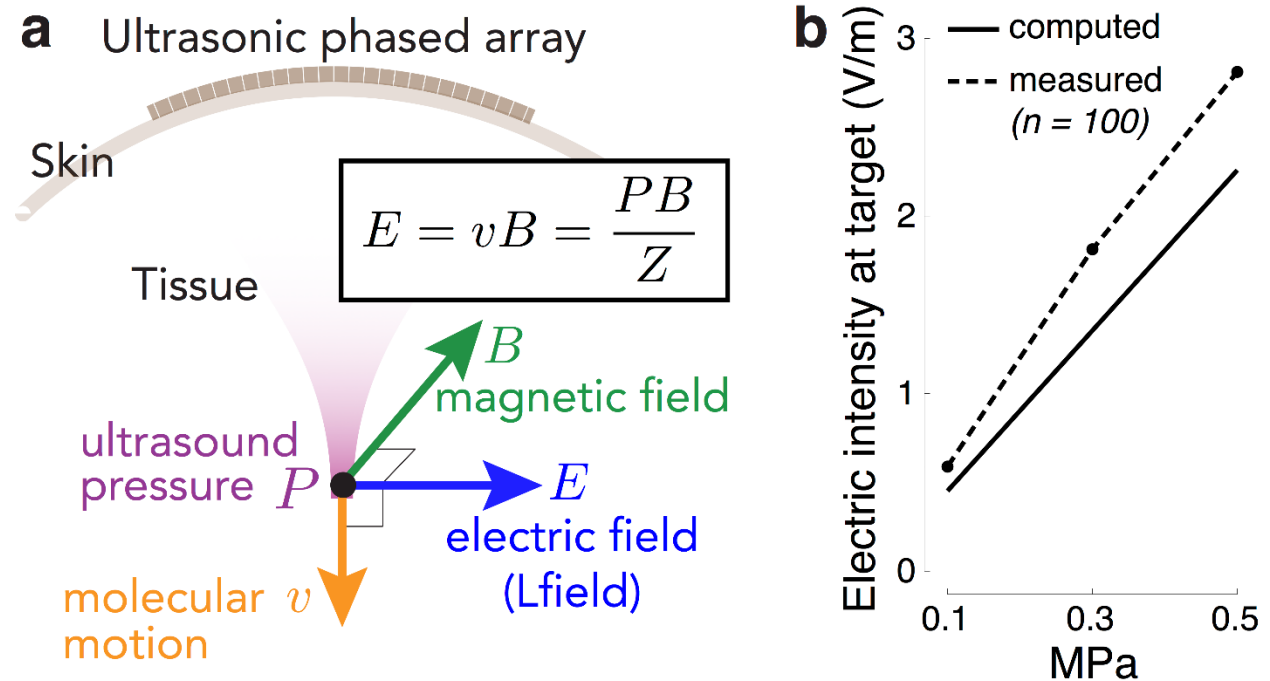
The ability to generate electric fields in deep tissues remotely, without surgically implanting electrodes, could transform our understanding and treatments of the nervous system.

Here, we show that focal electric fields can be generated from distance in specified targets by combining two orthogonal, remotely applied energies---magnetic and focused ultrasonic fields.

We confirmed the generated electric fields through direct electric field measurements. Moreover, we applied the effect to realize remote targeted neuromodulation, safely stimulating peripheral nerves in humans from a distance of more than 5 cm.

The ability to produce localized electric fields remotely opens a new set of applications in which electric fields are generated with high spatiotemporal resolution in intact tissues or materials.

We thank Samer Merchant for technical assistance. This work was supported by the NIH grants R00NS100986 and F32MH123019.



Ultrasound and Cationic Microbubble Assisted Gene Delivery in the Brain for Fragile X Syndrome Therapy

Presenter: Thomas Ador

Authors in order: Thomas Ador, *CNRS - Centre de Biophysique Moléculaire*, Mylène Fournie, *Centre de Biophysique Moléculaire*, Colleen Guillard, *Centre de Biophysique Moléculaire*, Christophe Delehedde, *Centre de Biophysique Moléculaire*, Vasile STUPAR, *INSERM*, Arnaud Menuet, *Immunologie et Neurogénétique Expérimentales et Moléculaires*, Chantal Pichon, *Centre de Biophysique Moléculaire*, Anthony Delalande, *CNRS - University of Orléans*

Develop an efficient, non-invasive, and safe gene transfer method with cationic microbubbles capable to open the blood brain barrier for the fragile X syndrome therapy.

We used pulsed ultrasound (1MHz, 109 or 145kPa, 5% duty cycle, 1sec period) combined with cationic microbubbles bounded to plasmid DNA (luciferase or Fmr1-eGFP). The mix was injected in the tail vein followed by targeted ultrasound stimulation in the left hippocampus area. Blood Brain Barrier (BBB) permeabilization and brain damage were observed through MRI, histology analysis, or in vivo fluorescence with indocyanine green (ICG) uptake. Gene transfer efficiency was analyzed through luciferase activity or immunohistochemistry.

Gadolinium uptake was observed up to 2 hours after sonoporation in T1 MRI showing that we were able to open the BBB transiently. The T2 MRI images did not show any bleeding or damage in the brain after treatment. Histology analysis of the brain 24h after treatment confirms the BBB opening area at the targeted location. In vivo fluorescence showed significant retaining of ICG 24h after treatment. Luciferase activity showed specific gene expression in the targeted area compared to control area. The use of Fmr1-eGFP encoding plasmid on Fmr1KO mouse model showed FMRP expression in neurons and astrocytes by immunohistochemistry.

Our results shows that we can express a transgene in a specific area in the brain without inducing damage, including a transgene expressing FMRP, which absence is the main cause of the fragile X syndrome. It shows the potential of this technique for brain gene therapy for intellectual disability disorders.

This research was conducted thanks to the funding from the “agence nationale de la recherche”.

P1-2

Transcranial Shock Waves: Impact of Skull Bone and Brain Tissue on the Sound Field Parameters

Presenter: Nina Reinhardt

Authors in order: Nina Reinhardt, *Chair of Medical Engineering, RWTH Aachen University*, Christoph Schmitz, Stefan Milz, Matias de la Fuente,

The objective of our work is to determine the impact of human skull and brain tissue on the spatial and temporal characteristics of therapeutic shockwaves.

The sound field of a commercial therapeutic shockwave transducer was investigated after passing human skull bone (n=5) or skull bone combined with brain tissue (n=2) in this ex-vivo study. The maximum and minimum pressure distribution as well as the focal pressure curves were measured at different intensity levels and penetration depths and compared to measurements in water. The characteristic parameters of the pressure curves and the sound field were determined.

The positive peak pressure was attenuated by between 20.85 and 25.39dB/cm by the skull bone and additionally by between 0.29 and 0.83dB/cm by the brain tissue. Peak positive and negative pressures of up to 10.7MPa and -7.3MPa, respectively, were reached behind the skull and brain tissue. Compared to water measurements, the pulse intensity integral in the focal spot was reduced by 84% by the skull bone and by additional 2% due to the brain tissue. While the focal position was shifted up to 8mm, the basic shape of the pressure curves was preserved and focusing was still possible.

The pressures reaching the brain tissue during transcranial shock wave treatment are high enough to possibly cause positive effects but damage cannot be excluded. Thus, further investigation of the mechanisms of action and side effects of transcranial shockwave treatment is necessary.

Research funding: This work was supported by Richard Wolf GmbH, Knittlingen, Germany.

Adapting the Hybrid Angular Spectrum Method to Improve Simulation of Transcranial Ultrasound Propagation

Presenter: Ningrui Li

Authors in order: Ningrui Li, *Stanford University*, Steven Leung, *Stanford University*, Kim Butts Pauly, *Stanford University*

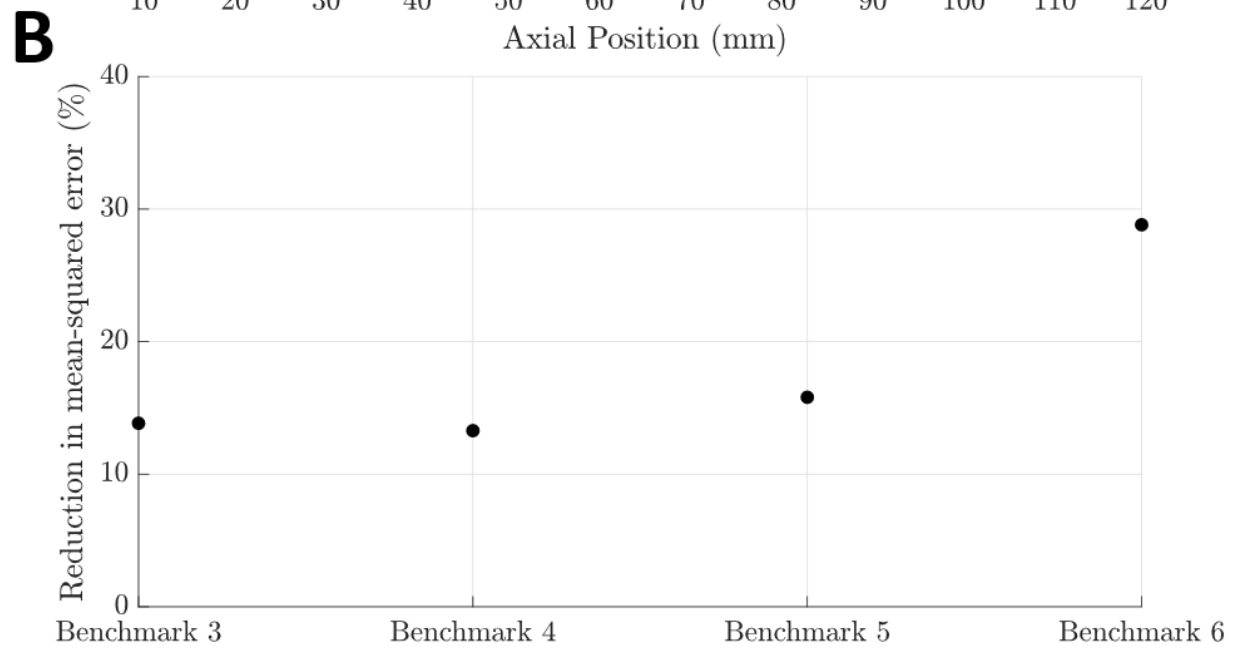
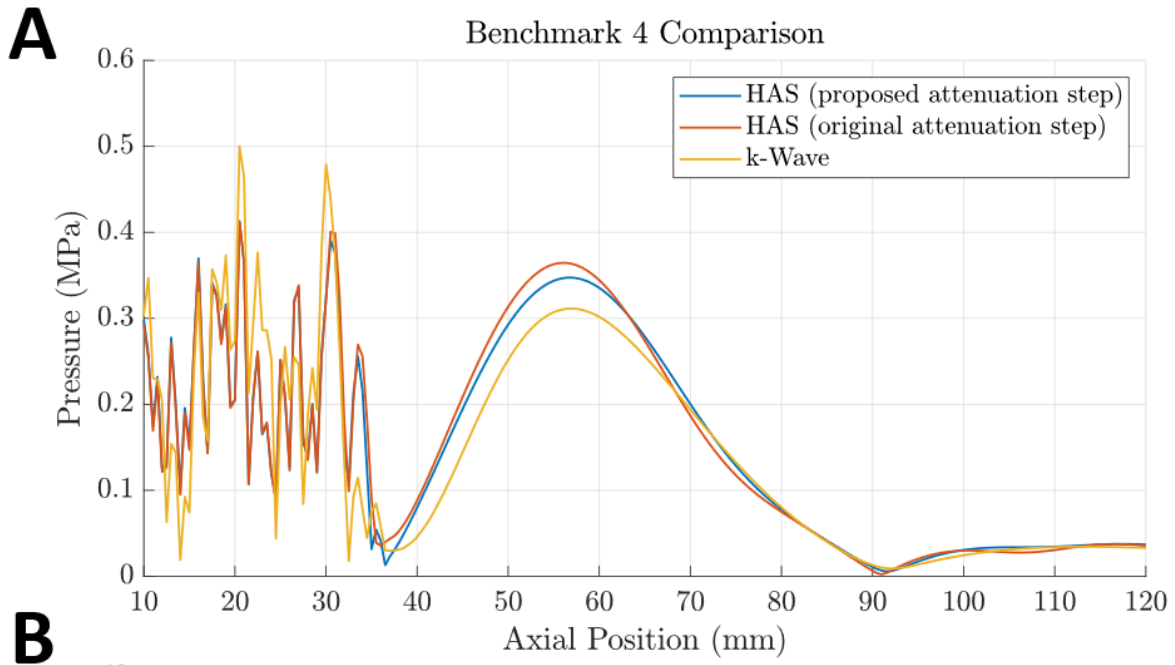
To improve the accuracy of the hybrid angular spectrum (HAS) method for transcranial applications that involve highly focused transducers and extremely heterogeneous media.

The proposed method applies attenuation in a two-step process. Bulk attenuation was applied in the spatial-frequency domain, accounting for the distance traveled by each angled plane wave. Deviations from the bulk attenuation due to medium heterogeneity were applied as an attenuation screen in the spatial domain. The accuracy of the proposed attenuation step was evaluated using benchmarks established by the planning group of the International Transcranial Ultrasonic Stimulation Safety and Standards consortium.

Pressure fields were computed using HAS using both the original and proposed attenuation steps, and an example of simulated pressure fields for Benchmark 4 is provided in Fig. 1A that shows the reduction in error relative to k-Wave when using the proposed attenuation step. The voxel-wise mean-squared error (MSE) was computed relative to the pressure field simulated with k-Wave. Reduction in MSE was observed across all benchmarks with heterogeneous media, with greater reductions of up to 28.8% observed for more complex benchmarks with multiple curved tissue layers (Fig. 1B).

The fidelity of the varying attenuation experienced by plane waves traveling at high incidence angles was preserved by extending attenuation into the spatial-frequency domain without changes in computational complexity. Future work will involve validation of this proposed method using highly heterogeneous CT-derived skull models.

We acknowledge support from the NIH (R01-CA227687, T32-EB009653) and the NSF (DGE-1656518), Bradley Treeby for providing k-Wave benchmarks, and Prof. Douglas Christensen for valuable discussions.



P1-21

A Comparison of Cavitation and Displacement During Non-invasive Peripheral Focused Ultrasound Neuromodulation

Presenter: Erica McCune

Authors in order: Erica McCune, *Columbia University*, Stephen Lee, *Columbia University*, Elisa Konofagou, *Columbia University*

To investigate the levels of both cavitation and nerve displacement during focused ultrasound (FUS) neuromodulation of the peripheral nervous system.

The sciatic nerve in the mouse (n=2) hindlimb was sonicated (3.1MHz, 1ms pulse duration, >10MPa) to induce paw movement (Fig. 1a). Targeting displacement was estimated for pulses that did and did not induce movement. After successful targeting, cavitation was passively recorded for five pulses delivered at a rate of 0.5Hz. Each pulse was categorized as generating a twitch or not using camera recordings. This process was repeated until no more twitches occurred within either leg

Averaged passive acoustic maps (PAM) were processed for the twitch (n=42 pulses) and no twitch (n=78 pulses) conditions. A greater total average cavitation value was found in the twitch condition (75.6dB vs. 75.4dB), but was not significant (Fig. 1b). Time-averaged inertial (ICD) and stable (SCD) cavitation doses showed low but statistically insignificant increases in the twitch condition (SCD: 81.4dB vs. 81.0dB; ICD: 55.7dB vs. 55.4dB). The average interframe displacement estimated for the targeting pulses showed a statistically significant greater average interframe displacement when a twitch occurred (n=21 pulses) compared to no twitch (n=21 pulses) (22.9 μ m vs. 16.2 μ m; p<.05) (Fig. 1c).

This preliminary study demonstrates no significant differences between cavitation occurring during successful and unsuccessful neuromodulation in the mouse hindlimb. Conversely, a significant difference occurred in the average interframe displacement for pulses with and without paw movement. These findings indicate that cavitation may not constitute the primary mechanism for FUS peripheral neuromodulation.

The authors would like to thank the National Institutes of Health (R01EB027576) for funding.

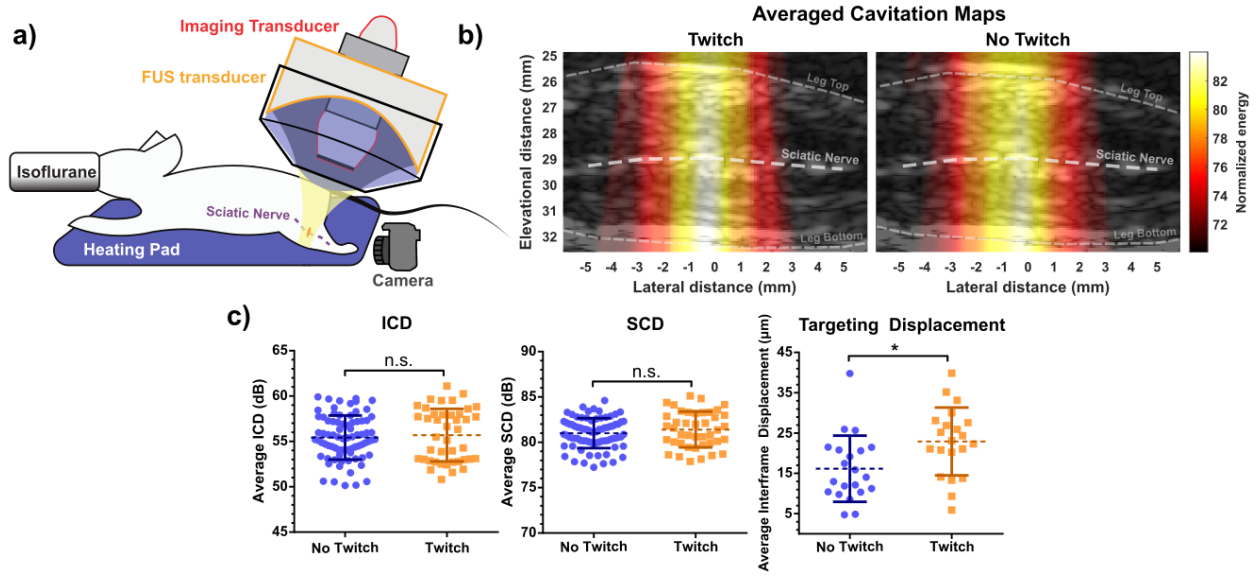


Fig 1. (a) Experimental set-up for mouse hindlimb neuromodulation. (b) Averaged PAM for twitch and no twitch conditions. (c) Averaged ICD, SCD, and targeting displacement for both conditions.

P1-22

Microbubbles for Blood-brain Barrier Opening: From In Vitro to In Vivo

Presenter: Ambre Dauba

Authors in order: Ambre Dauba, *Université Paris Saclay*, Laurène Jourdain, *Université Paris-Saclay*, Thi Hong Van Nguyen, Estelle Porret, *CEA*, Laurence Moine, *Université Paris-Saclay*, Erwan Selingue, *CEA Saclay*, Jean-Luc Gennisson, *Université Paris Saclay - CNRS*, Charles Truillet, *CEA Saclay*, Benoit Larrat, *CEA*, Anthony Delalande, *CNRS - University of Orléans*, Nicolas Tsapis, *CNRS, Université Paris-Saclay*, Anthony Novell, *BioMaps, Université Paris Saclay, CEA, CNRS, Inserm*

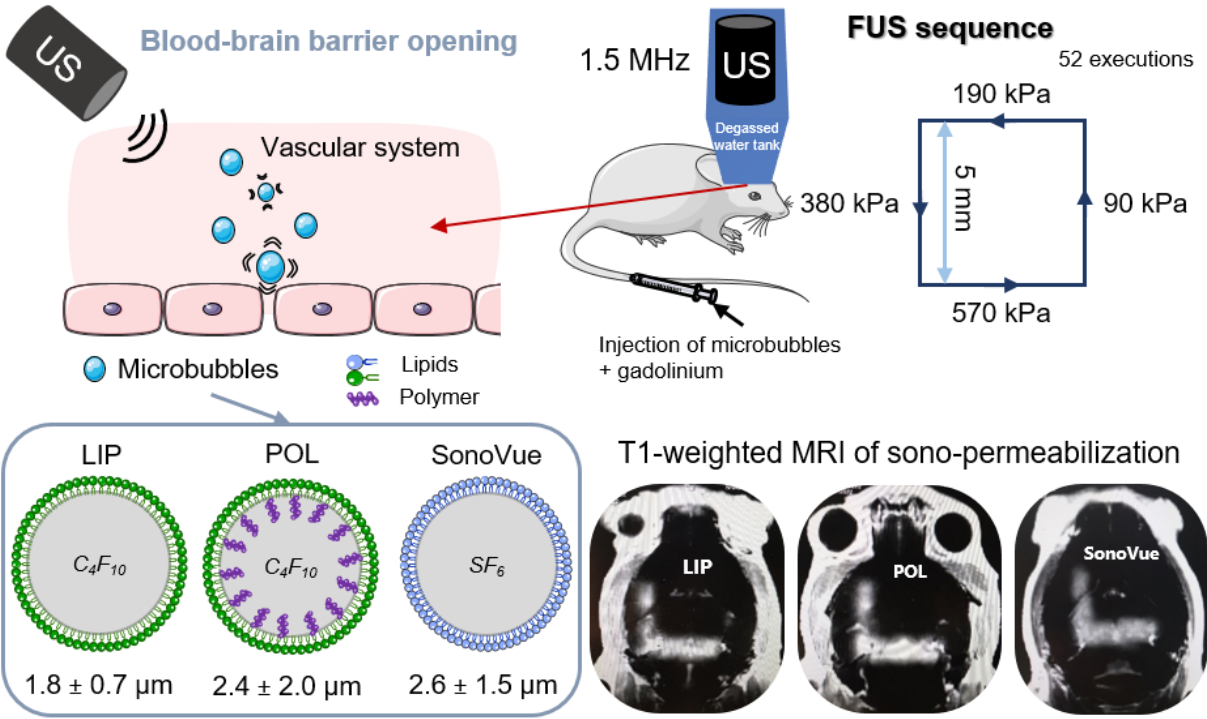
This project aim is to develop innovative sonosensitive agents (microbubbles) in order to disrupt the blood-brain barrier (BBB) under focused ultrasound.

Acoustical behavior, efficiency and safety of microbubbles with lipid (LIP) and lipid-polymer mixture (POL) shells are compared with SonoVue as a function of the Peak-Negative-Pressure (PNP: 50-570kPa). First, non-linear responses of suspended microbubbles into water are analyzed (f_0 : 1MHz). Then, in vitro propidium iodide (PI) uptake is performed on U87-cells at a constant number of bubbles and cells. Finally, in vivo BBB opening on mice is evaluated at different PNP levels and confirmed by MRI.

LIP, POL and SonoVue have respectively a concentration of $1E+10$, $1E+8$, and $2E+8$ particles/mL. The appearance of ultra-harmonic components (destabilization) occurs at 220kPa for SonoVue and 190kPa for LIP and POL. Compared to cells alone, PI uptake at 190 kPa (40 cycles every 100 μ s for 30s) is increased by a factor of 5 ± 1 % for LIP and less than 2% for SonoVue and POL. At 380kPa, PI uptake is increased by 14 ± 3 %, 11 ± 2 and 4 ± 3 for SonoVue, LIP and POL, respectively. BBB disruption was successfully performed at higher pressure (>380kPa) without brain damage observed for all microbubbles (Figure).

The destabilization threshold of LIP bubbles correlates with in vitro sono-permeabilization efficacy while this is not the case for the POL. Although SonoVue has better in vitro sonoporation efficacy at 380 kPa, the in vivo success of BBB opening encourages us to pursue the research on LIP and POL bubbles.

This work was partly funded by the ANR DROPMUT (grant ANR-19-CE19-0011).



P1-23

Phase-shift Nanoemulsions for the Targeted Treatment of Pancreatic Cancer

Presenter: Chloe McClenaghan

Authors in order: Chloe McClenaghan, *Ulster University*, Keiran Logan, *Ulster University*, Sukanta Kamila, *Ulster University*, Heather Nesbitt, *Ulster University*, Bridgeen Callan, *Ulster University*, Anthony McHale, *Ulster University*, John Callan, *Ulster University*

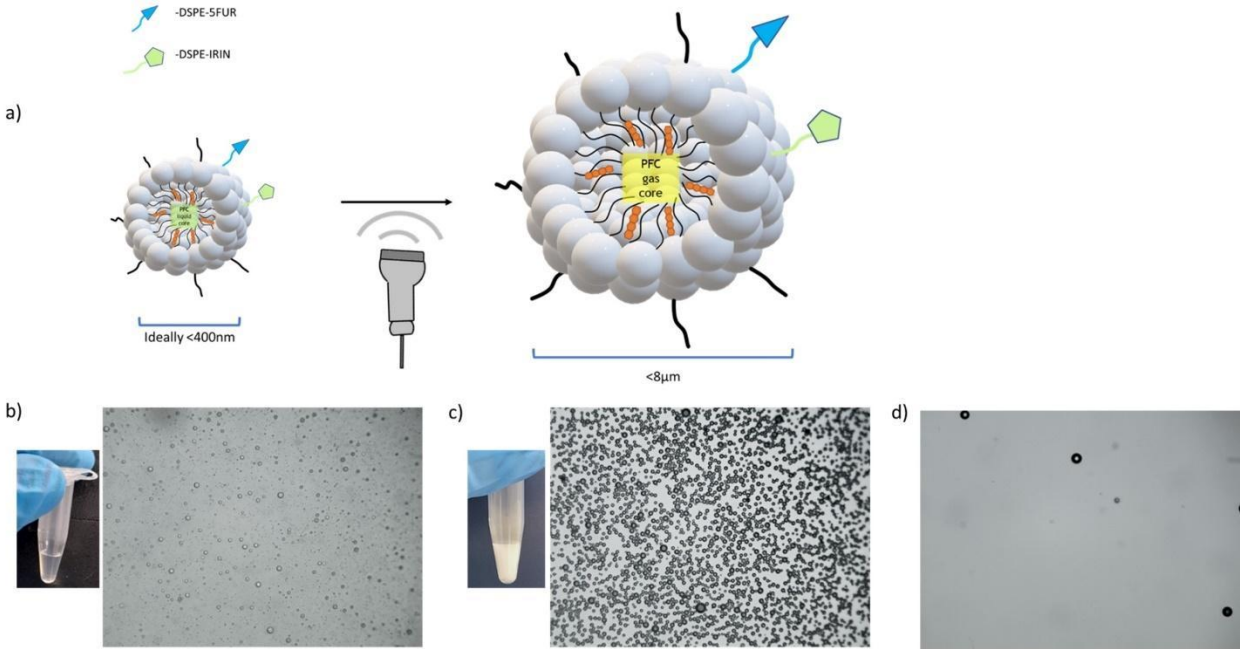
Preparation and characterisation of drug-loaded phase-shift nanoemulsions (PSN's). Initiation of a phase-shift from PSNs-to-microbubbles (MBs) upon the application of ultrasound (US).

FIRINOX PSN's comprised of functionalised phospholipid derivatives of 5-fluorouracil (F) and irinotecan (IRIN) were initially prepared as perfluorobutane (PFB) encapsulated MBs, and subsequently condensed under pressure at -10°C. PSN size was determined using Malvern Nano ZetaSizer. The PSN-to MBs phase-shift was initiated using low-intensity US (Duty cycle=50%, 3.0W/cm², 30seconds, PNP=0.45MPa, frequency= 1MHz). FIRIN-MB size and number were determined using optical microscopy and MATLAB software.

The FIRIN PSN produced had an average hydrodynamic diameter of 432.4nm with a poly dispersity index (PDI) of 0.214. After exposure to US a successful phase-shift was observed with an average MB concentration of 1.56x10¹⁰/ml and mean diameter of 3.40µm. The next step will involve testing the PSN in 3D spheroid and animal models of pancreatic cancer.

Drug-loaded PSNs were successfully prepared and underwent a phase shift when exposed to appropriate ultrasound conditions. The cavitation effects associated with the PSN to MB conversion and subsequent inertial conversion could enhance drug dispersion within the tumour tissue.

C. McClenaghan thanks Department for the Economy in Northern Ireland for a PhD studentship



a) Phase-shift from PSN to MB, b) photograph and micrograph of PSN sample prior to US exposure, c) Photograph and micrograph of PSN-to-MB phase-shift after insonation ($3\text{W}/\text{cm}^2$, 30seconds), d) MBs burst after further insonation

P1-24

Investigating Endothelial Sonoporation under Fluid Flow Conditions

Presenter: Elahe Memari

Authors in order: Elahe Memari, *Concordia University*, Fiona Hui, *Concordia University*, Brandon Helfield, *Concordia University*

This study aimed to elucidate the effect of fluid flow rate on the adjacent endothelial cell perforation in response to ultrasound-stimulated microbubbles.

A confluent monolayer of human umbilical (HUVECs) or brain endothelial cells (HBECs) were cultured in flow chambers, either statically or under unidirectional flow (9 dyn/cm² wall shear stress). Using our acoustically-coupled microscope, flow chambers were perfused with a solution of lipid-encapsulated microbubbles and propidium iodide at either a flow rate of 5 or 30 ml/min and exposed to 1 MHz ultrasound (PNP=305 kPa, N=20, PRI=1ms, duration = 2s). Fluorescence uptake was recorded for 90s post-treatment.

Our findings have demonstrated that under identical acoustic stimulus, microbubble-mediated cell perforation is dependent on the speed of microbubble flow over the adjacent cells. Cell permeabilization was quantified after ultrasound treatment offline with in-house MATLAB software. The results have indicated that a flow rate of 30 ml/min significantly increased cell perforation relative to a flow rate of 5 ml/min in both endothelial cell lines, pre-seeded either under constant flow provided with a fluidic system (8.2-fold and 1.5-fold increase in HUVECs and HBECs, respectively) or static conditions (9.7-fold and 2.3-fold increase in HUVECs and HBECs, respectively).

Our results suggest that fluid flow conditions, independent of cell seeding state, strongly influence the efficacy of ultrasound-mediated cell permeabilization, with implications in anatomical location-specific applications of microbubble-based drug delivery.

This work was partly funded by NSERC and the FRQNT

A Numerical Model of Ultrasound-Induced Nano-Drug Release

Presenter: Tyler Hornsby

Authors in order: Tyler Hornsby, *Ryerson University*, Farshad Moradi Kashkooli, *Ryerson University*, Anshuman Jakhmola, *Ryerson University*, Michael Kolios, *Ryerson University*, Jahangir (Jahan) Tavakkoli, *Ryerson University*

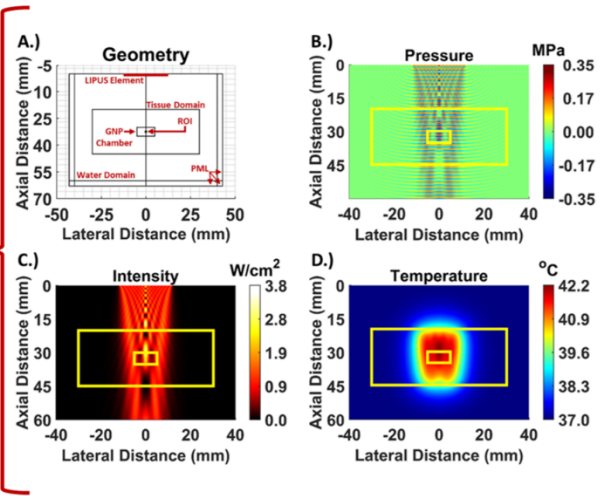
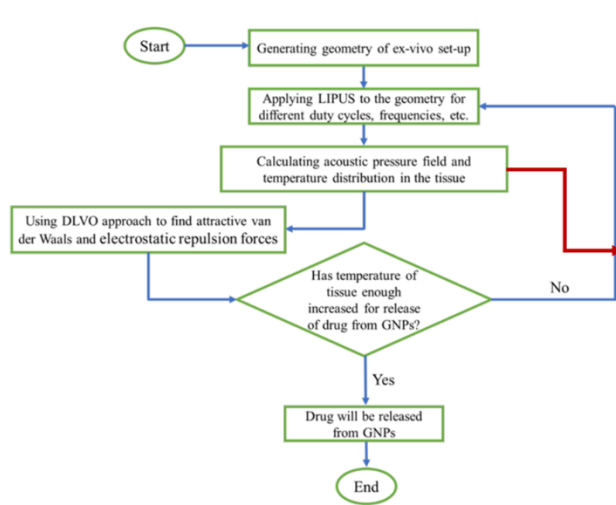
Simulate low-intensity pulsed ultrasound (LIPUS) heating of tissue, and apply Derjaguin, Landau, Verwey, Overbeek (DLVO) theory to predict drug release from gold nanoparticle (GNP) carriers.

The LIPUS acoustic and thermal fields in ex vivo tissue were calculated using COMSOL Multiphysics, then the DLVO model was implemented in Matlab Livelink to calculate the temperature-dependent attractive Van der Waals (Vvdw) and repulsive electrostatic (Velec) potential between two GNP drug carriers. By plotting DLVO potential ($V_{DLVO} = V_{vdw} + V_{elec}$), a threshold temperature for aggregation, and therefore doxorubicin release, was determined when V_{DLVO} was less than the product of the Boltzmann constant and temperature (kBT).

The LIPUS acoustic and thermal fields in ex vivo tissue were simulated, yielding maximum pressure and intensity value of 0.35 MPa and 3.8 W/cm² respectively, and a maximum tissue temperature of 42.2°C after 5 minutes of exposure. Next, the temperature was input into the DLVO model to calculate the DLVO potential between two GNPs. From this, a threshold temperature for aggregation, and therefore doxorubicin release, was determined. This temperature threshold is expected to be in the hyperthermia temperature regime (41-45°C) based on preliminary experimental data.

Temperature-dependent LIPUS-induced doxorubicin release from GNP drug carriers in an ex vivo tissue model was simulated, and the DLVO theory was applied to calculate a threshold temperature for doxorubicin release from the surface of GNP drug carriers.

The authors wish to thank Dr. Kevin Rod at Toronto Poly Clinic, for their support. Partial funding was provided by NSERC Alliance grant (ALLRP 556270-20).



P1-26

New Sensitisers for Antimicrobial Sonodynamic/Photodynamic Therapy

Presenter: Heather Nesbitt

Authors in order: Heather Nesbitt, *Ulster University*, Keiran Logan, *Ulster University*, Sukanta Kamila, *Ulster University*, Anthony McHale, *Ulster Univeristy*, John Callan, *Ulster University*

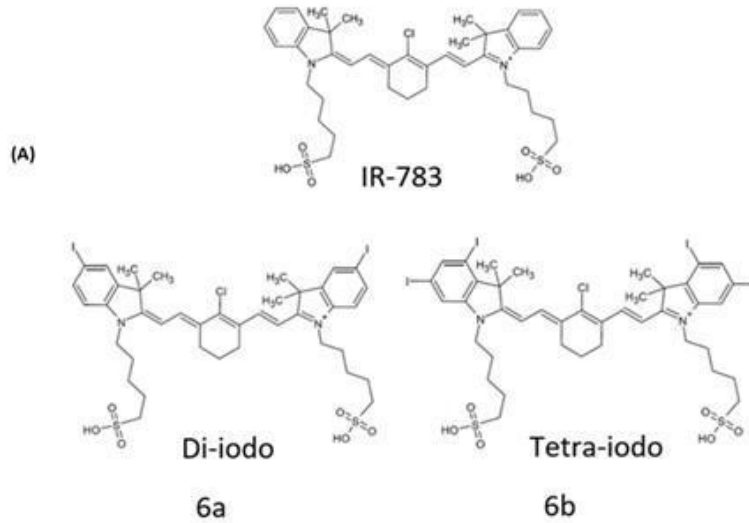
To determine the effectiveness of two iodinated IR-783 derivatives as antimicrobial Photodynamic and Sonodynamic therapy sensitisers.

Two IR-783 derivatives were prepared by substituting hydrogen atoms in each indole ring of IR-783 with either one or two iodine atoms generating the di-iodo (6a) and tetra-iodo(6b) derivatives respectively. The effectiveness of 6a and 6b as NIR light and ultrasound activated sensitisers was examined in *S. aureus* 4330 (gram-positive) bacteria. Bacterial viability was measured using standard spread plate methodology.

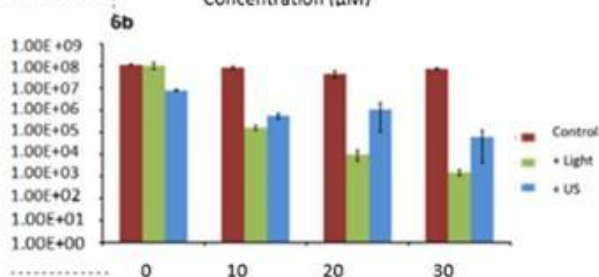
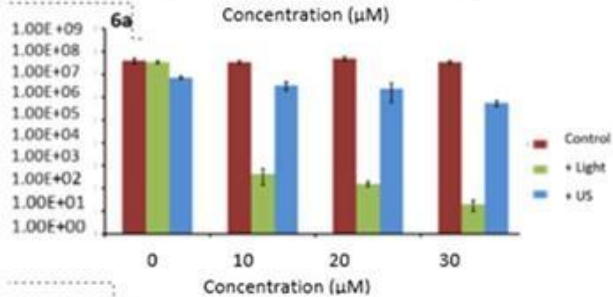
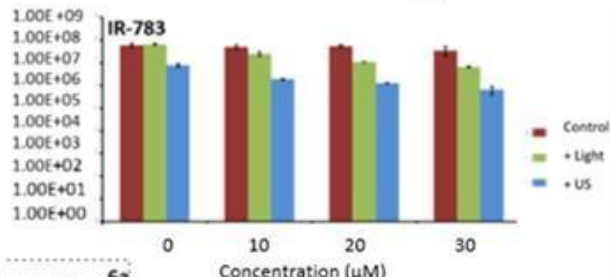
6a and 6b were more effective antimicrobials than IR-783 when activated with NIR light generating 6 and 5 log reductions respectively at 30 μM drug concentration compared to < 1 log for IR-783. However, 6a was more effective 6b than across all the concentrations tested. Ultrasound activation of 6a and 6b produced less dramatic reductions with 3 log reduction observed for 6b at 30 μM drug concentration. Interestingly, when combined light and ultrasound activation was employed, complete bacterial eradication was observed for both 6a and 6b.

Iodination of the NIR dye IR-783 improved its antimicrobial Photo and Sonodynamic therapy efficacy, presumably by increasing spin-orbit coupling through a heavy atom effect. Combining ultrasound and light activation improves efficacy dramatically. More investigations into other bacteria and biofilm forming models are in progress.

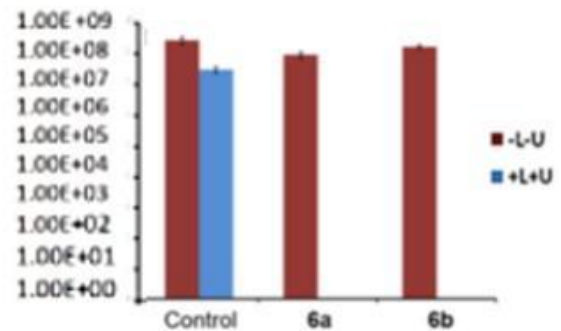
The EPSRC (Engineering and Physical Sciences Research Council) programme grant (1907DF002/CS9)



(B)



(C)



(A) Structure of IR-783, di-iodo (6a) and tetra-iodo (6b) derivatives (B) Cell viability of *S. aureus* after exposure to light and ultrasound in the presence of either 6a or 6b. (C) Cell viability of *S. aureus* after exposure to light and ultrasound in the presence of 30 μM of either 6a or 6b.

P1-27

Optimization of Ultrasound-mediated Microbubble Transfection of MicroRNA-126 to Endothelial Cells

Presenter: Stephanie He

Authors in order: Stephanie He, *Concordia University*, Davindra Singh, *Concordia University*, Hossein Yusefi, *Concordia University*, Brandon Helfield, *Concordia University*

This project aims to develop and characterize a microbubble formulation to deliver proangiogenic microRNA-126 (miR-126) into endothelial cells (HUVEC).

Cationic microbubbles (polyethyleneglycol-40 stearate, distearoylphosphatidylcholine and 1,2-disearoyl-3-trimethylammoniumpropane) with a perfluorobutane gas core were synthesized and characterized in terms of size, surface charge, and stability. MiR-126 loading was quantified by gel electrophoresis. HUVEC were treated at 37°C with suspensions of miR-126-loaded microbubbles at 1 MHz ultrasound (50 kPa, N=1000, duty cycles from 20-40%) for 2 minutes. Quantification of miR-126 delivery was performed by RT-qPCR, downstream protein target expression by Western blotting and cell viability via MTT.

The cationic microbubbles ($1.12-1.27 \times 10^9$ microbubbles/ml) are stable over at least 80 minutes, exhibit a volume-weighted peak size of 3.1-3.4 μm , and a loading capacity of 6 μg of miR-126 per 10^9 microbubbles. Under acoustic conditions that maintain cell viability (>90%), we were able to deliver modest amounts of miR-126 up to 1.7 fold compared to sham treatment controls, with expression levels increasing with duty cycle. For a subset of ultrasound conditions, downstream miR-126 protein targets PIK3R2 and SPRED1 exhibited decreased expression by 46% and 33%, respectively, compared to controls.

Our results indicate the feasibility of our miR-126-loaded microbubbles to modulate key molecules to promote angiogenesis in HUVEC towards the treatment of ischemia.

This work was supported by scholarships from Concordia University and Hydro Québec, as well as funding from the Heart and Stroke Foundation.

Drug-loaded Microbubbles for Image-guided Treatment of Inflammation

Presenter: Yara Ensminger

Authors in order: Yara Ensminger, *University of Toronto*, Haochen Zhang, *University of Toronto*, Una Goncin, *University of Saskatchewan*, Steven Machtaler, *University of Saskatchewan*, Naomi Matsuura, *University of Toronto*

This study investigates methotrexate (MTX)-loaded microbubbles (MBs) for image-guided, local treatment of gastrointestinal inflammation in combination with ultrasound-triggered MB cavitation.

Lipids and MTX were co-dissolved in tetrahydrofuran to form a lipid-MTX complex, which were then used to synthesize perfluorobutane MTX-MBs. Control MBs did not contain MTX.

Size distribution and in vitro stability were determined using a Coulter Counter (37°C for 90 min, 1000x dilution). MTX-MBs were assessed under flow (1.8x10⁶ MB/mL, 0.5 mL/s, 6 MHz transducer) and echogenicity quantified using MATLAB. MTX-loading was assessed using ultraviolet-visible spectroscopy (absorbance at 298 nm) and ultra-performance liquid chromatography.

MTX-MBs were loaded with 37±5 µg MTX onto ~108 MBs (0.0167 mg/mL gas, encapsulation efficiency ~17%). Control MBs and MTX-MBs had similar size distribution (mean sizes of 0.80±0.04 µm). MTX-MBs exhibited higher stability than control MBs, with 40% decrease in number concentration after 110±20 min (20°C) and 80±10 min (37°C) in MTX-MBs, and 70±20 min (20°C) and 35±5 min (37°C) for control MBs. Under flow, MTX-MBs and control MBs could be observed using CEUS for 70±5 min and 60±5 min, respectively.

Acoustically responsive MTX-MBs were synthesized with 0.0167 mg MTX loaded per mL gas. MTX-MBs showed improved stability and were similar in US signal brightness when compared with control MBs. Future work will assess theranostic potential and treatment efficacy in murine inflammatory bowel disease models.

We would like to thank CIHR, NSERC, ORF, OCI, NFRF, and the Government of Ontario for contributing funding to this project.

Drug-loaded microbubbles for image-guided treatment of inflammation

Yara Ensminger¹, Haochen Zhang¹, Una Gonciv², Steven Machtaler² and Naomi Matsuura^{1,3,4}

¹Department of Materials Science & Engineering, University of Toronto, Ontario, Canada, ²Department of Medical Imaging, University of Saskatchewan, Saskatchewan, Canada, ³Institute of Biomedical Engineering, ⁴Department of Medical Imaging, University of Toronto, Ontario, Canada

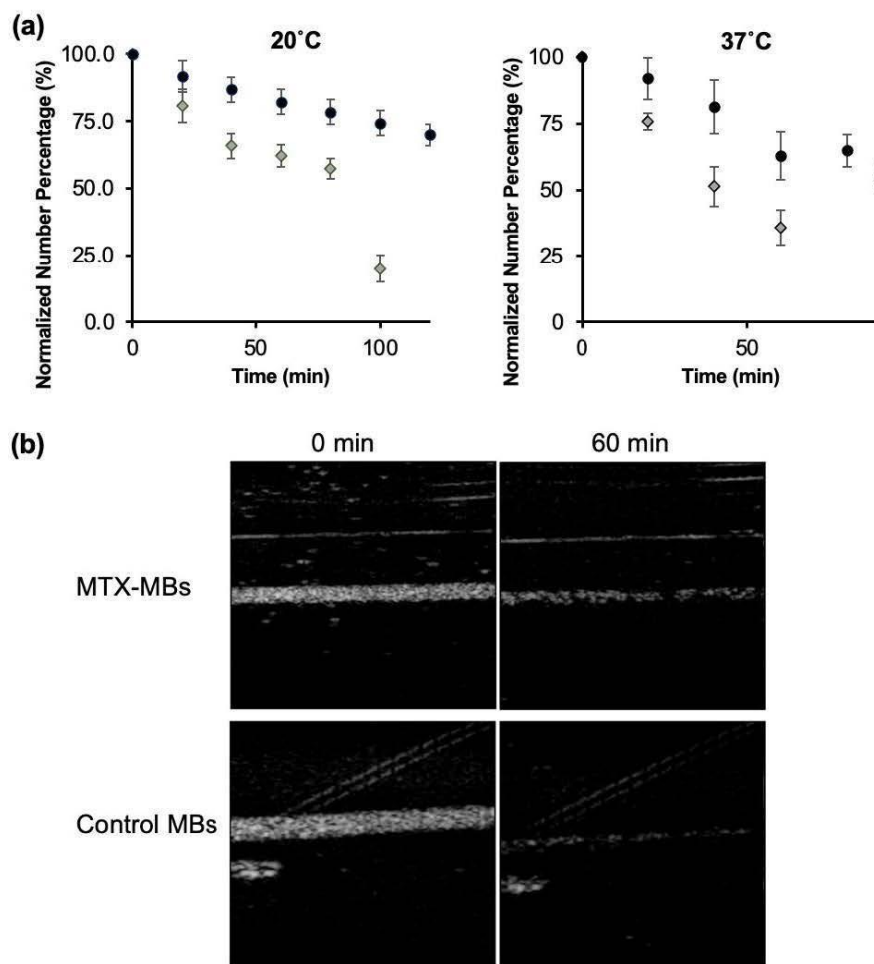


Figure 1: (a) Normalized number concentration of MTX-MBs (black) and control MBs (grey) over time ($n=3$) at 20°C and 37°C; (b) CEUS images of MTX-MBs and control MBs in an agarose flow phantom at 37°C.

Effect of a Combined Immune Checkpoint Inhibitor and Mechanical Focused Ultrasound Treatment in a MC38 Preclinical Model

Presenter: Myleva Dahan

Authors in order: Cécile Fant, *Univ Lyon, Université Claude Bernard Lyon 1, Centre Léon Bérard, INSERM, LabTAU UMR1032*, Chloé Grasselly, *Anticancer Antibodies, CRCL, INSERM U1052, CNRS UMR 5286, CLB, UCBL*, Myleva Dahan, *Inserm U1032*, morgane Denis, *CRCL*, Doriane Mathé, *ANTINEO*, Pierre-Antoine Choffour, *ANTINEO*, Loic Daunizeau, *Univ Lyon, Université Claude Bernard Lyon 1, Centre Léon Bérard, INSERM, LabTAU UMR1032*, Jean-Louis Mestas, *Univ Lyon, Université Claude Bernard Lyon 1, Centre Léon Bérard, INSERM, LabTAU UMR1032*, Cyril Lafon, *INSERM*, Christophe Caux, *Centre de Recherche en Cancérologie de Lyon (CRCL), UMR INSERM U1052 CNRS 5286 Université de Lyon*, Stéphane Depil, *Centre de Recherche en Cancérologie de Lyon (CRCL), UMR INSERM U1052 CNRS 5286 Université de Lyon*, Charles Dumontet, *Anticancer Antibodies, CRCL, INSERM U1052, CNRS UMR 5286, CLB, UCBL*, Frederic Padilla, *Focused Ultrasound Foundation & University of Virginia*

We describe the impact of combinatory treatment between immune checkpoint inhibitor (ICI) and mechanical focused ultrasound (M-FUS) in a MC38 tumor model.

MC38 tumor model were subcutaneously implanted into C57Bl6 mice. Mice were then treated each week by M-FUS using a confocal device generating and monitoring pulsed cavitation ultrasound (Frequency 1.1 MHz, PRF 250 Hz, DC 1%, PNP = 20.5 MPa) and anti-PD1 antibody intraperitoneal administration. Treatment schedules were investigated: simultaneous treatment, ICI three days before or three days after M-FUS. Tumor growth and overall survival was recorded and flow cytometry was performed for monitoring tumor infiltration.

Significant increased survival and tumor growth control were observed when M-FUS was first delivered three days before anti-PD1. Compared to control, survival rate was three-fold higher for combined treatment. No impact was shown with simultaneous treatment compared to combined one. Flow cytometry revealed that combined treatment may lead to increased antigen priming as increased CD11c⁺ CMHII^{high} conventional dendritic cells (DC), activated CD8⁺ and Sirpa-CD24⁻ subpopulations were found. This analysis also showed an increase of PD1 and LAG3 expression levels, higher population of CD8⁺ cells as well as various co-inhibitory molecules at CD4⁺ and tumor cells surface for the combined group.

This study demonstrated that the combination between M-FUS and ICI have an impact on tumor growth control, overall survival and on the changes in the immune response depending on the treatment schedule. This shows that schedule in a combinatory treatment is a very important parameter to be considered.

This work was supported by the LabEx DEVweCAN (ANR-10-LABX-0061) of the University of Lyon and by the Focused Ultrasound Foundation.

Ablation of the Rodent Fornix using MR-guided Focused Ultrasound (MRgFUS)

Presenter: Carena Cornelssen

Authors in order: Carena Cornelssen, *University of Utah*, Henrik Odéen, *University of Utah*, Allison Payne, *University of Utah*, Dennis Parker, *University of Utah*, Matthew Alexander, *University of Utah*, Braden Brown, *University of Utah*, Jacob Christensen, *University of Utah*, Karen Wilcox, *University of Utah*, John Rolston, *University of Utah*

Using a craniectomized rat model and combining a high-precision mechanical positioning system with acoustic radiation force imaging we achieved accurate FUS ablation of the fornix.

Sprague-Dawley rats (n=14) were anesthetized and a midline craniectomy was performed prior to MRgFUS. Rats were head-fixed, mounted in a custom MRgFUS system with a 3 MHz annular transducer array (Image Guided Therapy, IGT) to lesion the fornix. Pre- and post-ablation MRI (3T Siemens Prisma) was performed (T2-weighted SPACE) to identify lesion size and location, and magnetic resonance thermal imaging (MRTI; Thermoguide™, IGT) was used to monitor temperature rise (Figure 1). Lesions were verified histologically.

The rat fornix could be accurately located on high-resolution T2-weighted images on a clinical MRI scanner. A mechanical positioning system with sub-mm accuracy in three directions was used together with 3D volumetric MR acoustic radiation force imaging for accurate targeting without inducing tissue damage. Sonication parameters (power and duration) were optimized to create focal lesions (0.19 +/- 0.22 mm³) of the fornix while minimizing surrounding collateral damage. The craniectomy was necessary to avoid near-field heating and damage. Histology shows 100% targeting of the fornix.

Our method allows for the accurate targeting of small and deep structures, like the fornix, in the rodent brain, enabling MRgFUS investigations of neurological disorders in chronic disease models. Future studies will investigate the ability of precise fornix lesions to prevent seizures in a rat model of temporal lobe epilepsy.

NSF GRFP (CC), Richard L. Stimson Endowed Chair (KSW), University of Utah Research Incentive Seed Grant (JDR), NINDS K23 NS114178 (JDR), S100D018482

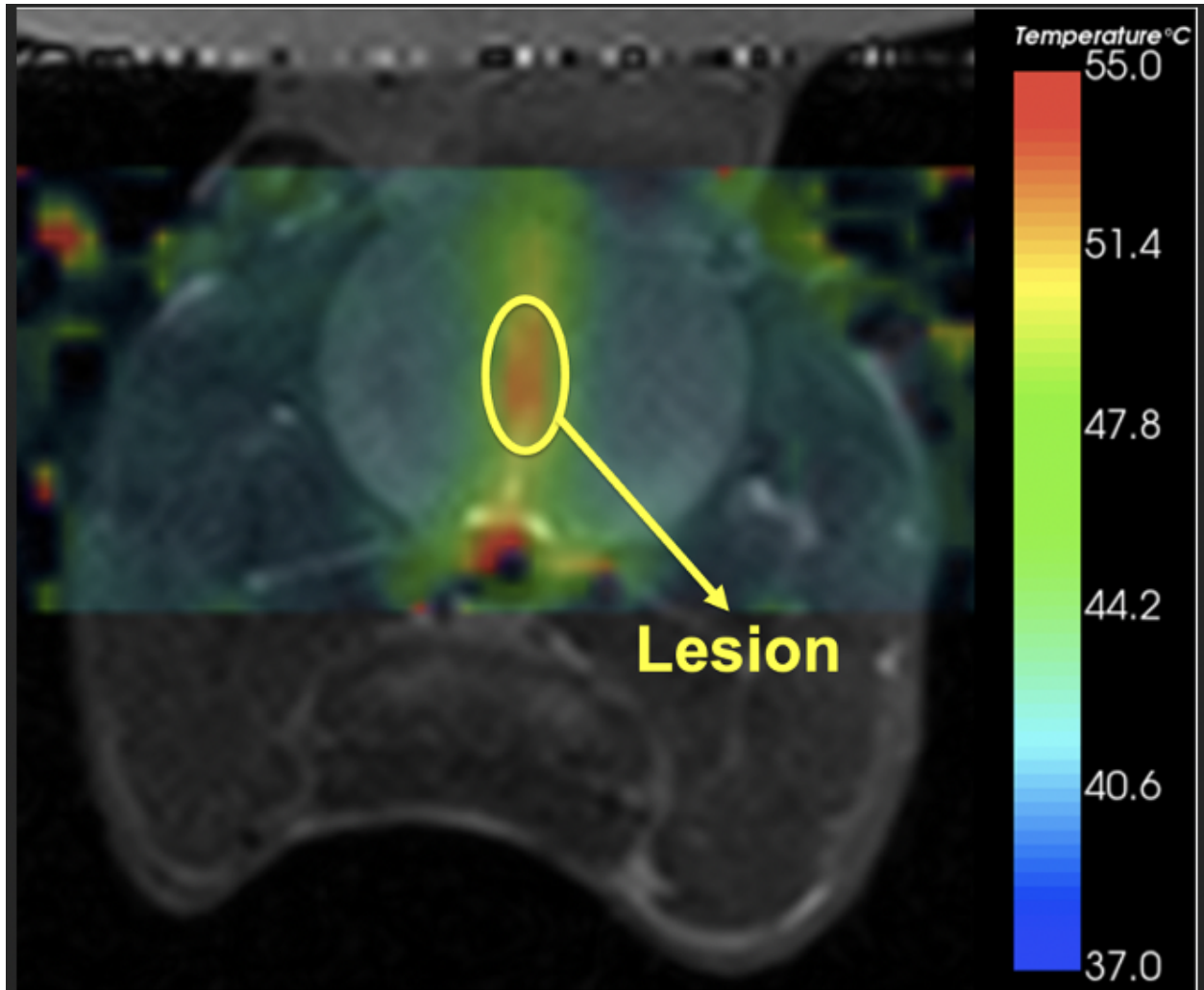


Figure 1: MRTI overlaid with post-treatment T2w shows agreement between heating and lesion.

Ultrasound-Stimulated Microbubble and Radiation Therapy Monitored by Dynamic Contrast Enhanced Magnetic Resonance Imaging

Presenter: Colleen Bailey

Authors in order: Colleen Bailey, *Sunnybrook Research Institute*, Evan McNabb, Deepa Sharma, *Sunnybrook Health Sciences Centre*, Gregory Czarnota, *Sunnybrook Research Institute*

Vascular changes in white rabbit tumours following ultrasound microbubble (USMB) and radiation (XRT) therapies were studied using Dynamic Contrast Enhanced Magnetic Resonance Imaging (DCE-MRI).

Thirty-two rabbits with prostate cancer (PC3) xenografts underwent DCE-MRI before and 24 hours after treatment. There were five treatment groups: control (n=3), XRT (n=3), USMB (n=5), XRT + 7-minute USMB (n=10), XRT + 14-minute USMB. The 14-minute USMB consisted of 7 minutes whole-tumour + 7 minutes low-perfusion (n=5) or high-perfusion (n=6) sub-region treatment, determined from pre-treatment DCE-MRI. Changes in wash-in rate, washout rate and area under the DCE-MRI curve (AUC) (Figure 1) were examined.

The XRT + 14-minute USMB treatment demonstrated a significant decrease (*p < 0.05, t-test) in wash-in rate and area under the curve between pre- and post-treatment (Figure 2). The change in AUC remained significant regardless of whether low-perfusion or high-perfusion areas were the target for the final 7 minutes of treatment. Changes in other treatment groups were not significant, nor were there changes in the washout rate. Normalizing AUC to muscle produced similar results, suggesting that contrast agent administration had little influence.

DCE-MRI measures related to vascular flow and volume decreased following combined XRT + 14-minute USMB. Treatment changes were not detectable for XRT + 7-minute USMB combined treatment, likely due to the sensitivity of DCE-MRI and small group sizes. This method offers promise for monitoring combined USMB therapies.

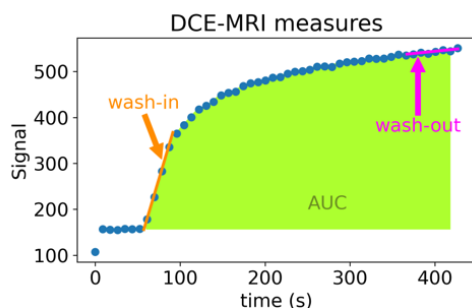


Figure 1 DCE-MRI parameter definitions

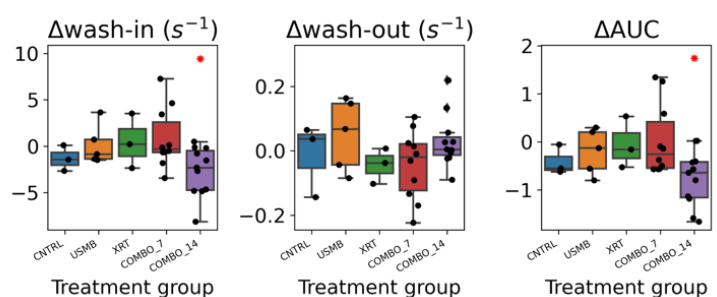


Figure 2 Changes in parameters between pre- and post-treatment

Anatomical Guinea Pig Brain Comparative Atlas: A New Tool for Preclinical Focused Ultrasound Research

Presenter: Francesco Prada

Authors in order: Edoardo Porto, *Fondazione IRCCS Istituto Neurologico Carlo Besta - University of Milan*, Laura Librizzi, *Fondazione IRCCS Istituto Neurologico Carlo Besta, Epilepsy Unit, Milan, Italy*, Laura Uva, *Fondazione IRCCS Istituto Neurologico Carlo Besta, Epilepsy Unit, Milan, Italy*, Nicoletta Corradino, *IRCCS C. Besta Institute, University of Milan*, Riccardo Ciocca, *University of Milan*, Francesco DiMeco, *Fondazione IRCCS Istituto Neurologico Carlo Besta, Acoustic Neuroimaging and Therapy Laboratory, Milan, Italy - Fondazione IRCCS Istituto Neurologico Carlo Besta, Neurosurgery Department, Milan, Italy - Johns Hopkins Medical School, Department of Neurolog*, Marco de Curtis, *Fondazione IRCCS Istituto Neurologico Carlo Besta, Epilepsy Unit, Milan, Italy*, Francesco Prada, *IRCCS Istituto Carlo Besta, University of Virginia, Focused Ultrasound Foundation*

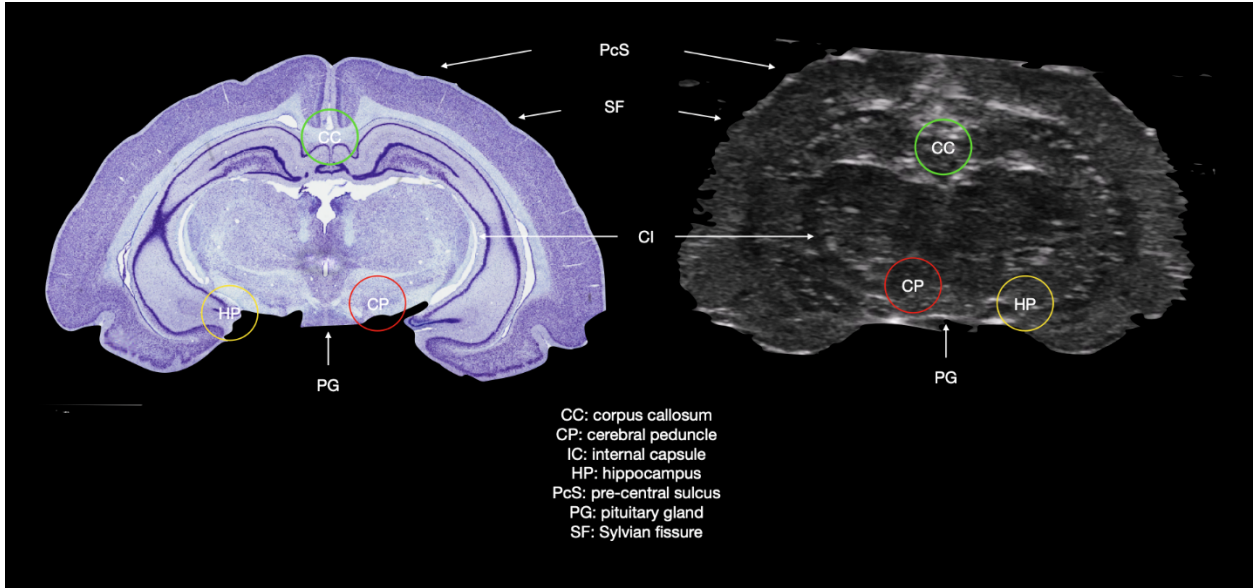
The aim of the present study is to illustrate an anatomical comparative atlas of isolated Guinea pig brains using ultra-high-frequency ultrasound images and histological sections.

Three in vitro perfused and isolated guinea pig brains were employed to perform ultra-high-frequency ultrasound scanning. Sequential B-mode images were acquired through Vevo 3100 (VisualSonics, Fujifilm). B-mode images were selected, properly coupled based on anatomical landmarks, and respectively compared with Guinea pig brain histological sections.

Ten sets of multimodal images were analyzed, and several anatomical structures were labeled in order to make comparisons. Vertebral arteries, basilar artery, internal carotid arteries, hippocampi, basal ganglia (with interthalamic adherence), ventricular system, corpus callosum, cerebellar hemispheres (with vermis and folia), pons, medulla oblongata, olfactory bulb, pyramids, pituitary infundibulum were easily recognizable in both ultrasound and histologic sections. (Fig. 1)

Ultra-high-frequency ultrasound images provide an anatomical image set that is comparable to the 'gold standard' histological data. These can be used for the construction of a digital atlas that will be accessible, searchable, and will represent a valuable resource for preclinical focused ultrasound research.

The authors acknowledge Dr. Dieter Fuchs and Dr. Savino Laceranza (Fujifilm) for providing Vevo 3100.



Amygdala Neuromodulation for Reducing Agitation and Aggressive Behaviour in a Mouse Model of Alzheimer's Disease

Presenter: Flavia Venetucci Gouveia

Authors in order: Flavia Venetucci Gouveia, *The Hospital for Sick Children Research Institute*, Harriet Lea-Banks, *Sunnybrook Research Institute*, Isabelle Aubert, *Sunnybrook Research Institute*, Nir Lipsman, *Sunnybrook Health Sciences Centre*, Kullervo Hynynen, *Sunnybrook Research Institute/ University of Toronto*, Clement Hamani, *Biological Sciences, Sunnybrook Research Institute*

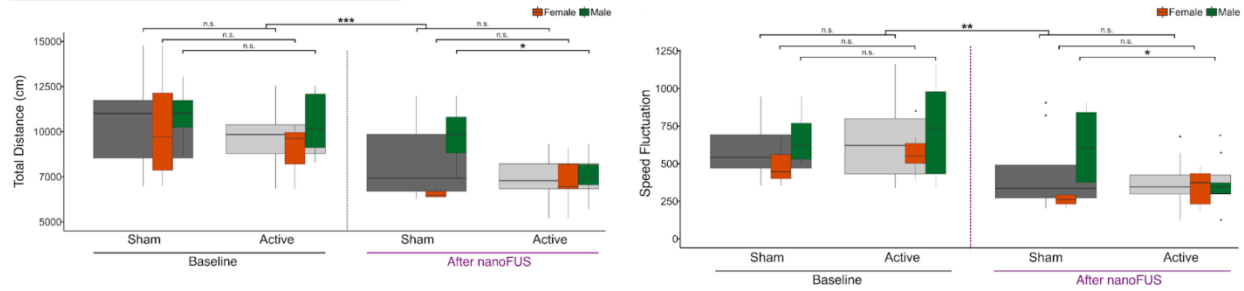
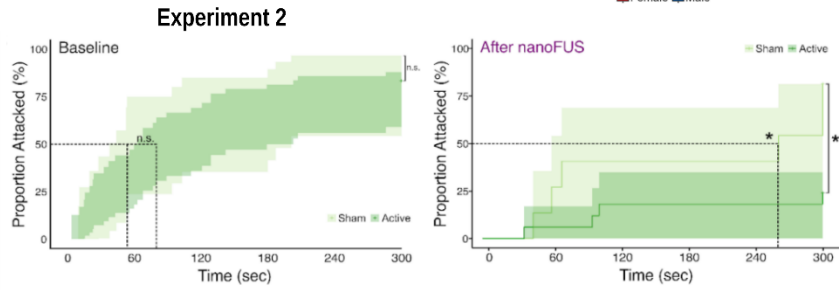
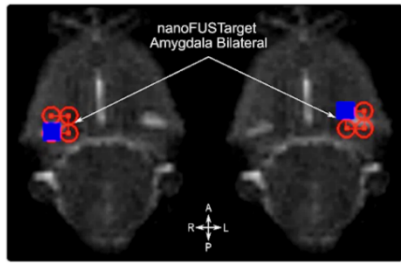
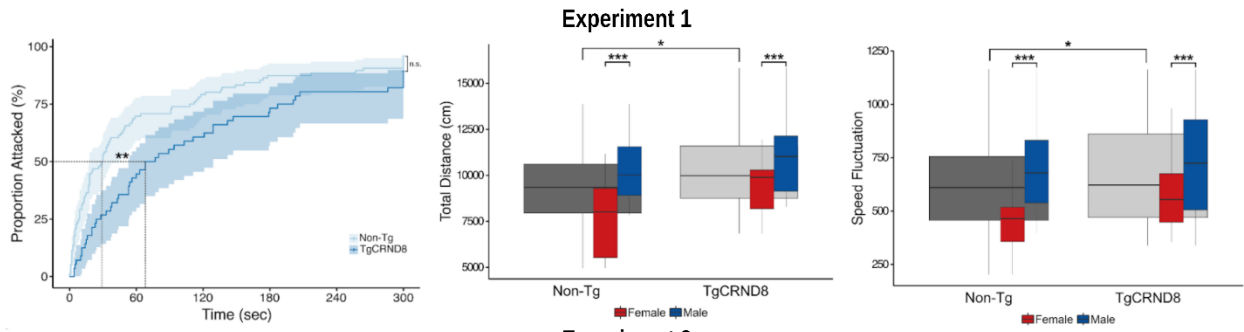
Experiment1: Identify agitation and aggressive phenotype of TgCRND8 mice. Experiment2: Treat agitation and aggressive behaviour with intra-amygdala delivery of ultrasound sensitive nanodroplets loaded with anesthetics.

Male and female 3 months old TgCRND8 mice, and non-transgenic (non-Tg) littermates were used (Experiment1: TgCRND8 n=26, non-Tg n=38, Experiment2: TgCRND8 n=26). The Open Field, Resident-Intruder and Neurological Tests were used for behavioral characterization before and after treatment. T2-weighted images acquired on a 7-Tesla MRI (Bruker,USA) were co-registered to the LP100 system (FUS Instruments, Canada) for targeting, followed by sonication of ultrasound-sensitive nanodroplets loaded with anesthetics (2.5 µg/mL).

Experiment 1: TgCRND8 male mice showed aggressive behaviour and increased socialization. TgCRND8 female mice showed no aggressive behaviour, and reduced socialization. Both male and female TgCRND8 mice have increased motor agitation, as detected by increased total distance travelled and greater speed fluctuation. Experiment 2: Treatment with active-nanoFUS significantly reduced aggressive behaviour in males, as observed by increased latency to attack, and reduced proportion of animals attacking and number of attacks per trial. Active-nanoFUS also reduced motor agitation in males, as detected by significant reduction in total distance travelled and speed fluctuation. No effects of active-nanoFUS treatment were observed in females.

TgCRND8 mice presented agitation and aggressive behaviour, thus being a useful tool for studying novel therapies for neuropsychiatric symptoms of AD. Treatment with active-nanoFUS reduced agitation and aggressive behaviour in male TgCRND8 mice. Further studies are necessary to establish cellular/molecular changes, and investigate chronic treatment and long-term behavioural changes.

The authors would like to thank Shawna Rideout-Gros, Kristina Mikloska, Mustansir Diwan, and Melissa Theodore. Funding was provided by the Harquail Centre for Neuromodulation (Canada).



Agar/Wood-powder Breast Phantom for Focused Ultrasound Applications

Presenter: Christakis Damianou

Authors in order: Antria Filippou, *Cyprus University of Technology*, Marinos Giannakou, *Medsonic Limited*, Nikolas Evripidou, *Cyprus University of Technology*, Anastasia Antoniou, *Cyprus University of Technology*, Christakis Damianou, *Cyprus University of Technology*, Leonidas Georgiou, *German Oncology Center*

The main objective was to develop an agar-based phantom doped with wood-powder capable of mimicking breast tissue in Magnetic Resonance guided Focused Ultrasound (MRgFUS) applications.

A tissue mimicking phantom (TMM) containing 2 % w/v agar and 4 % w/v wood powder was developed with the shape of real breast. A series of experiments were conducted to estimate the acoustic, thermal, and MR properties of the wood-powder doped material. The acoustic attenuation coefficient was measured utilizing a typical transmission through technique in the frequency range of 1–3 MHz, whereas the ultrasonic velocity was investigated utilizing a pulse-echo technique.

The TMM demonstrated tissue like visibility in MRI. The estimated attenuation coefficient was close to 0.5 dB/cm.MHz and nearly proportional to frequency, whereas the acoustic absorption was about 0.35 dB/cm-MHz. It was also proven that the addition of wood-powder enhances acoustic absorption. The estimated propagation speed of 1487 m/s is close to that of soft tissue at room temperature. The thermal conductivity of the material was estimated at 0.5 W/m.K. Regarding MR properties, the T1 and T2 relaxation times were 844 and 66 ms, respectively. These values are within the range of values reported in the literature for soft tissue.

Overall, the TMM matched critical acoustic, thermal, and MR properties of human tissues adequately. Therefore, wood-powder could serve as a cost-effective modifier of critical properties of agar-based phantoms intended for MRgFUS applications. Furthermore, experiments using MR thermometry demonstrated the usefulness of this phantom to evaluate ultrasonic thermal protocols.

Spatially Targeted Sonobiopsy Releases Brain-derived Protein Biomarkers into the Blood Circulation in a Tauopathy Mouse Model

Presenter: Hong Chen

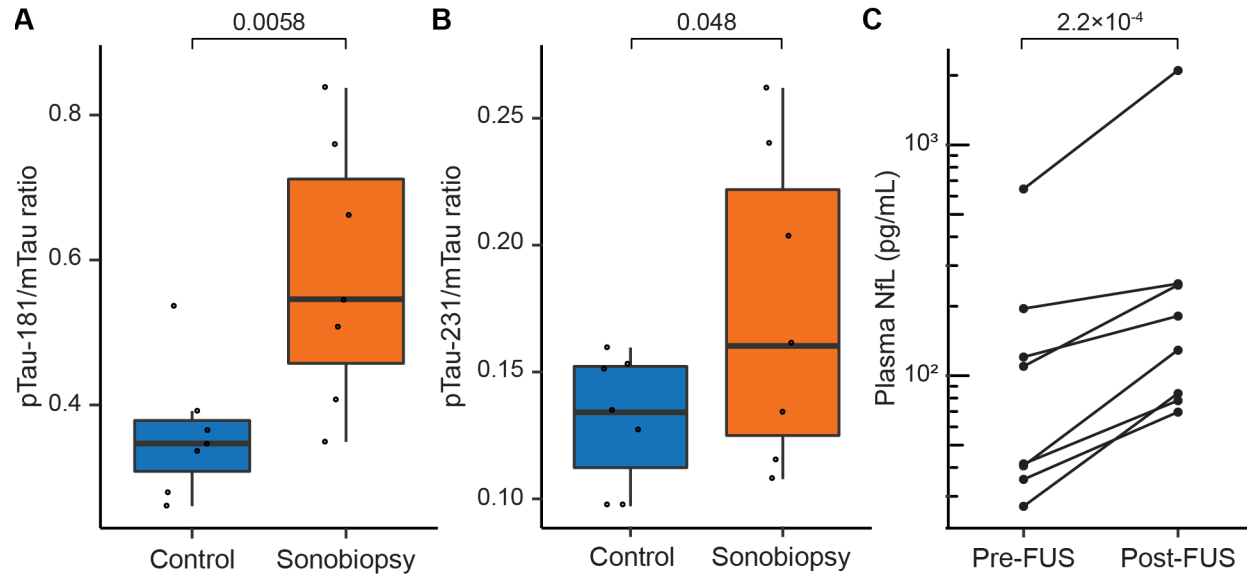
Authors in order: Christopher Pacia, *Washington University in St. Louis*, JINYUN YUAN, *Washington university in st louis*, Yimei Yue, Eric Leuthardt, *Washington University School of Medicine*, Tammie Benzinger, *Washington University School of Medicine*, Arash Nazeri, *Washington University School of Medicine*, Hong Chen, *Washington University in St. Louis*

This study aimed to evaluate the feasibility and safety of sonobiopsy to release brain-derived protein biomarkers for the diagnosis of neurodegenerative disorders.

MRI-guided sonobiopsy was performed on a transgenic mouse model of tauopathy (PS19). Blood was collected via cardiac puncture during non-survival experiments in PS19 and wild-type mice after sonobiopsy or without FUS sonication. During survival experiments, blood was collected from the submandibular vein pre- and post-sonication. Plasma levels of mouse tau (mTau), phosphorylated tau species (pTau-181, pTau-231), and neurofilament light chain (NfL) were analyzed. Histological staining was performed to evaluate the safety of sonobiopsy.

MRI scans confirmed successful FUS-induced BBB disruption. Sonobiopsy significantly increased the normalized level of pTau-181 (Fig A; 1.7-fold increase, $p = 0.0058$) and pTau-231 (Fig B; 1.4-fold increase, $p = 0.048$) in treated PS19 mice compared to the control PS19 mice. There was no significant change in normalized level of pTau species in the wild-type mice. Sonobiopsy significantly increased the plasma NfL levels (Fig C; 2.3-fold increase, $p = 2.2 \times 10^{-4}$). Sonobiopsy was safe and minimal brain damage could be avoided by lowering the FUS pressure without compromising biomarker release.

This study demonstrated the feasibility and safety of sonobiopsy to enhance the detection of brain-derived protein biomarkers of neurodegenerative disorders. This proof-of-principle study is the first to expand the diagnostic capability of sonobiopsy from brain cancer to tauopathies and neurodegenerative disorders.



Acoustic and Thermal Numerical Modelling of Transcranial Ultrasound Thermal Therapy

Presenter: Andrew Drainville

Authors in order: Andrew Drainville, *LabTAU INSERM U1032*, David Moore, *Focused Ultrasound Foundation*, John Snell, *Focused Ultrasound Foundation*, Sylvain Chatillon, *Université Paris-Saclay, CEA, List, F-91120, Palaiseau, France*, Frederic Padilla, *Focused Ultrasound Foundation & University of Virginia*, Cyril Lafon, *INSERM*

This work presents a rapid and accurate numerical model of intra-cranial acoustic and thermal fields, and quantifies the effect of model complexity on clinically relevant parameters.

The CIVA simulation platform provides rapid simulation of acoustic and thermal fields arising from transcranial focused ultrasound therapy using the INSIGHTEC ExAblate clinical system. Acoustic simulations were performed to quantify the effect of mode conversion and internal reflection within a layered skull model on the resultant acoustic field at the focus. Simulated acoustic fields were then combined with the CIVA thermal model to predict temperature rise at the focus, which was compared to experimental temperature rise measured using MR thermometry.

The results quantify the effect of mode conversion and internal reflection as a function of skull heterogeneity within a ray-tracing model of transcranial acoustic propagation. Results demonstrate the necessity of including the effects of shear wave mode conversion within the skull when using ray-tracing models, while the contributions of internal reflection do not significantly alter the position or amplitude of the maximum acoustic field near the focus. The comparison of simulated temperature rise produced using transcranial focused ultrasound demonstrated a high degree of agreement with experimentally measured temperatures across a range of acoustic power levels.

This work quantifies the importance of various acoustic wave behaviour and skull heterogeneity in transcranial focused ultrasound modelling, which may help guide the use and required complexity of numerical models. Comparison of simulated and experimentally measured temperature fields demonstrates that the CIVA Healthcare platform can provide rapid and accurate prediction of temperature rise.

This work was financially supported by the Focused Ultrasound Foundation.

P1-36

Cavitation Quantification Metric for Cross-system Comparison

Presenter: Andrew Drainville

Authors in order: Andrew Drainville, *LabTAU INSERM U1032*, Mehdi Caillon, *LabTAU INSERM U1032*, Jean-Louis Mestas, *Univ Lyon, Université Claude Bernard Lyon 1, Centre Léon Bérard, INSERM, LabTAU UMR1032*, Cyril Lafon, *INSERM*, Maxime Lafond, *LabTAU, Inserm U1032*

This work presents a method of quantifying cavitation activity to allow for translation between different systems, and is compared against chemical cavitation quantification.

Experiments were performed using two different but geometrically similar systems composed of two confocal transducers. Cavitation activity was quantified acoustically using a cavitation index (CI) calculated from the average acoustic amplitude in pascals across multiple frequency windows between 2.475 and 5.775Mhz using calibrated passive cavitation detectors. Chemical dosimetry of cavitation activity was assessed using 650uL samples of 2mM terephthalic acid by measuring the fluorescence intensity following 30 second ultrasound exposures at fixed source voltage levels.

Figures 1a and 1b shows the fluorescence and the CI as a function of driving voltage amplitude, respectively. Figure 1c illustrates the measured fluorescence plotted against the CI for each sample.

Figure 1a illustrates a high level of variability in fluorescence between systems for similar voltage amplitudes. The CI vs voltage amplitude shows significant differences between systems, with differences in the dependence of CI with source voltage. The measured fluorescence as a function of CI demonstrates good agreement between the cavitation index and fluorescence measurements.

This method of quantifying cavitation activity may provide a useful metric of comparison between systems in order to allow for direct comparison of experimental conditions. This metric was able to provide a quantitative measure of cavitation activity that agreed between the two different systems.

Work supported by ITMO Cancer through its PCSI 2020 call.

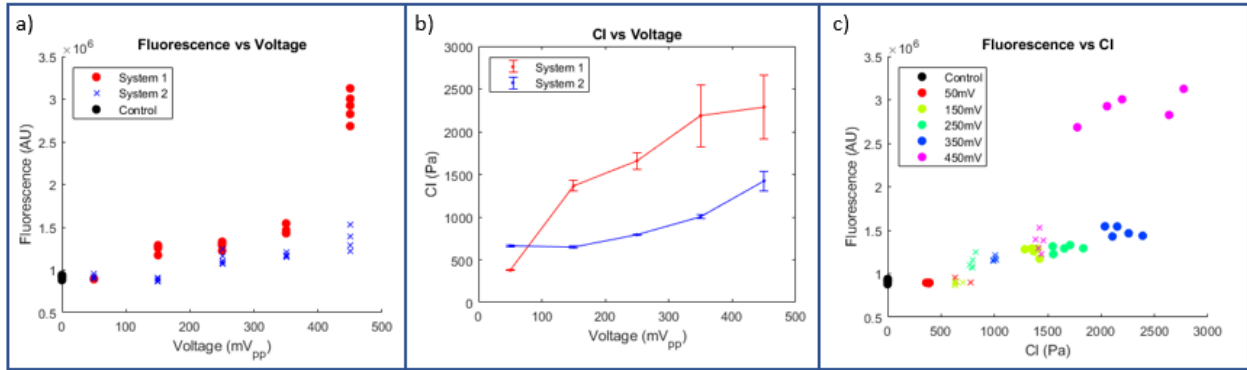


Figure 1: a) Fluorescence vs source voltage. b) Cavitation index (CI) vs source voltage for systems 1 and 2, with corresponding CI error bars across 10 signal measurements. c) Fluorescence vs cavitation index (CI) for system 1 (solid dots) and system 2 (x) for various of source voltage values.

A Low-Cost Method of Cavitation Detection for Developing Histotripsy Transducers

Presenter: Theresa Gu

Authors in order: Theresa Gu, *Dalhousie University*, Jeremy Brown, *Dalhousie University*, Thomas Landry, *Dalhousie University*

To develop a passive system for quickly and accurately measuring cavitation threshold in water for characterizing the sensitivity of newly fabricated histotripsy transducers.

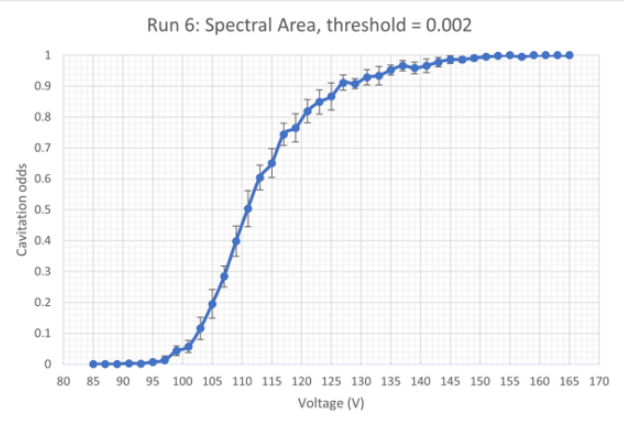
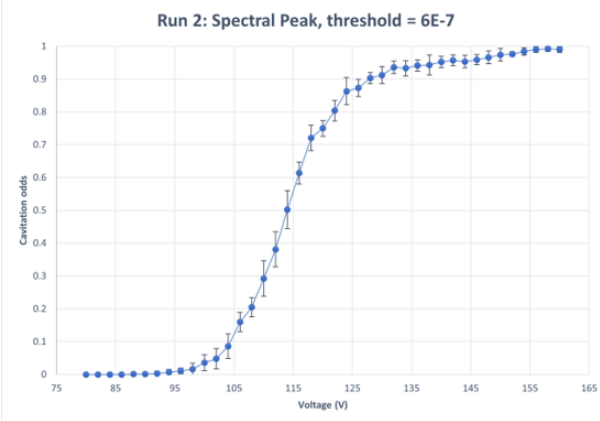
A LabVIEW program was developed to passively monitor the cavitation sensitivity of a lab-fabricated histotripsy devices using a waveform generator, pulser, NI-DAQ, and a low-cost in-lab fabricated piezoelectric hydrophone.

After acoustic signals were captured using the hydrophone-NI-DAQ-LabVIEW signal pathway, true cavitation events were detected using two methods in the software. A true cavitation event was determined if either the spectral peak or the area under the spectral curve exceeded a pre-determined threshold.

Cavitation was continuously monitored in LabView while incrementally increasing the histotripsy drive voltage. A 10 mm diameter histotripsy transducer was tested using 8-cycle pulse bursts at a 1kHz PRF. Multiple trials/sample blocks were taken at each voltage to provide a statistically significant estimate of the probability of a true cavitation event occurring. Graphical data demonstrated a sigmoidal relationship between the driving voltage and cavitation probability where the average voltage required to achieve a 50% cavitation probability was calculated to define a threshold for the transducer tested. Error margins were obtained as standard deviations from each block of trials.

A cavitation detection method was developed using an inexpensive piezo-ceramic disk hydrophone and a data acquisition system. Two methods of cavitation detection by monitoring spectral features were evaluated. Both methods produce highly accurate cavitation detection probability curves, demonstrating a capability to characterize the threshold of newly developed histotripsy transducers.

I would like to express my deepest thanks to Dr. Rob Adamson and Jeffrey Woodacre for their guidance and support in this project.



P1-4

Transcranial Histotripsy Induces Blood Brain Barrier Opening and Repair

Presenter: Sarah Duclos

Authors in order: Sarah Duclos, *University of Michigan*, Sang Won Choi, *University of Michigan*, Anuska Andjelkovic-Zochowska, *University of Michigan*, Sandra Camelo-Piragua, *University of Michigan*, Neeraj Chaudhary, *University of Michigan*, Jonathan Sukovich, *University of Michigan*, Timothy Hall, *University of Michigan*, Zhen Xu, *University of Michigan*

The aim of this study was to observe and quantify blood-brain barrier disruption (BBBD) following murine transcranial histotripsy treatment via MRI and histology.

C57BL/6 mice underwent transcranial histotripsy treatment using a 1 MHz, 8-element histotripsy array (5 Hz PRF, $-p \leq 30$ MPa, 5 mm³ treatment volume). BBBD was monitored via T1-Gadolinium-(Gd) weighted MRI sequences at 0, 2, 7, 14, 21, and 28 days after histotripsy. Brains were processed for H&E staining at each time point (n=3 for each group).

T1-Gd MR images showed Gd leakage through the BBBD in the region surrounding the histotripsy ablation zone in the normal mouse brain. The Gd leakage through the BBBD region peaked at 7 days post histotripsy treatment, and significantly subsided at 21 days, with no to minimal leakage at 28 days (Fig. 1). H&E staining showed increased immune cell activity for all timepoints, indicating wound healing. Histology to evaluate vascular damage and tight junctions is pending.

Our data suggest that histotripsy leads to temporary BBBD at the ablation boundary that reduces ~21 days after treatment, which may be used to combine histotripsy with drug delivery for brain treatment. Future work is needed to quantify the extent and duration of the BBBD in brain tumor models.

This work was funded by the Focused Ultrasound Foundation and the National Science Foundation.

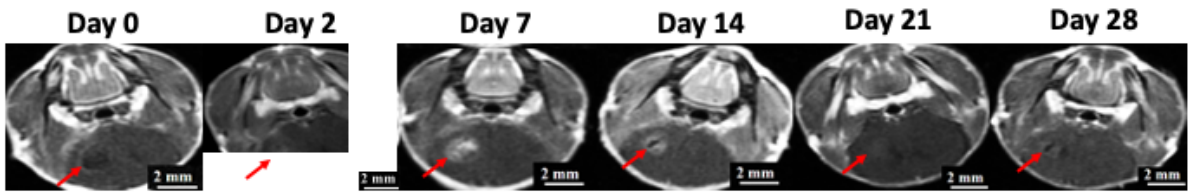


Fig. 1: T1-Gd MRI at different timepoints following histotripsy treatment.

P1-5

Delivery of Mesenchymal Stem Cells using MR-Guided Focused Ultrasound Exerts Therapeutic Effects on Rodent Parkinsonian Model

Presenter: Sheng-Kai Wu

Authors in order: Sheng-Kai Wu, *Sunnybrook Research Institute*, Chia-Lin Tsai, *Tri-Service General Hospital, National Defense Medical Center, Taipei, Taiwan*, Aisha Mir, *Sunnybrook Research Institute, Toronto, ON, Canada*, Kullervo Hynynen, *Sunnybrook Research Institute/ University of Toronto*

To investigate the effects of MR-guided focused ultrasound (MRgFUS) delivery of human mesenchymal stem cells (MSCs) on the 6-OHDA induced Parkinson's disease rat model.

6-OHDA was stereotaxically injected into the right substantia nigra (SN) two weeks before the treatment. Baseline and endpoint behaviour tests were performed, including cylinder test and apomorphine-induced rotations. MRgFUS-induced BBB permeability modulation was conducted using an acoustic controller with the targets at the striatum (ST) and SN. Human MSCs were injected immediately before sonication. Immunohistochemical stains were used to identify the stem cells. Tyrosine hydroxylase (TH) expression was quantified in the ST and SN.

Here we show that we can deliver human mesenchymal stem cells into Parkinsonian rats by MRgFUS-induced BBB modulation using the acoustic controller. The CD90+ and CD105+ labelled cells were identified in the sonicated brain regions, indicating the feasibility of stem cell delivery via MRgFUS. MSCs+FUS treatment significantly improves the behaviour outcomes compared with control, FUS alone, and MSCs alone groups. In the quantification analysis of the TH stain, a significant reservation of dopamine neurons can be seen in the MSCs+FUS group (ST: $33.22 \pm 6.44\%$, $p=0.034$; SN: $40.5 \pm 3.33\%$, $p=0.0005$ to the contralateral side) as compared with MSCs group (ST: $28.24 \pm 2.36\%$; SN: $32.24 \pm 5.2\%$).

Mesenchymal stem cell therapy may be a viable option in treating neurodegenerative diseases such as Parkinson's disease. Transcranial MRgFUS serves as a better method for targeted and minimally-invasive stem cell homing. Further investigations on the optimal conditions, such as an alternate injection route, are necessary.

The authors would like to thank Shawna Rideout-Gros for the help with animal preparation and monitoring during experiments.

P1-6

Pressure Attenuation and Focal Shift Estimation for Therapeutic Ultrasound Applications at Low Frequencies

Presenter: Sua Bae

Authors in order: Omid Yousefian, *Columbia University*, Sua Bae, *Columbia University*, Robin Ji, *Columbia University*, Antonios N. Pouliopoulos, *Columbia University*, Hermes Kamimura, Elisa Konofagou, *Columbia University*

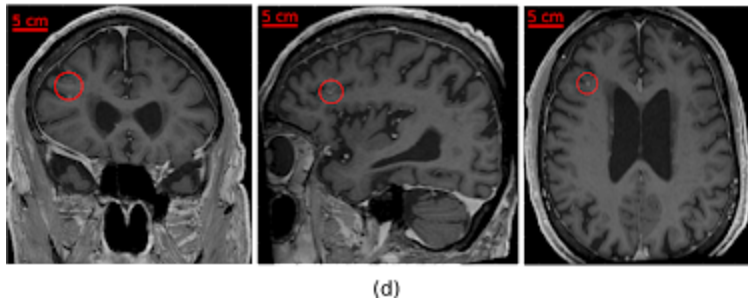
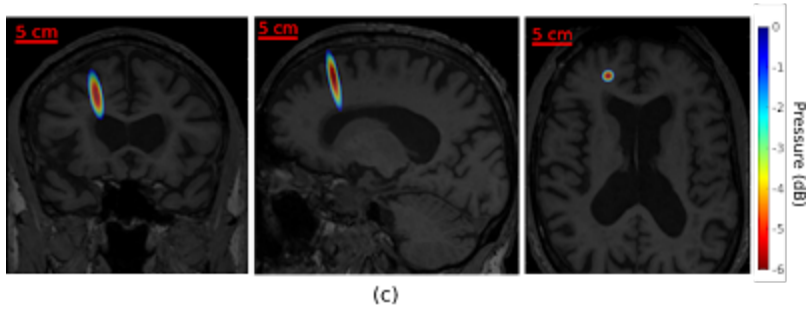
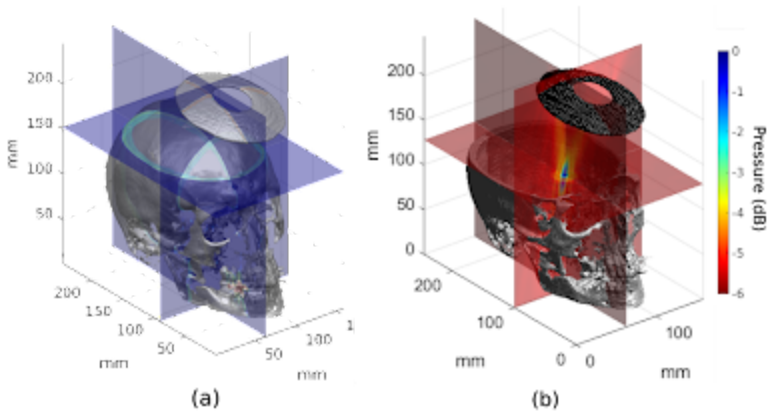
Estimating the pressure attenuation and focal shift in transcranial ex-vivo and in-vivo FUS using numerical simulation at 250 kHz for BBB opening.

Using the clinical CT data to map the variation of acoustical properties in the human skull, we compared the estimated pressure attenuation values and focal shift modeled through k-space pseudospectral numerical (k-wave) frameworks with hydrophone measurements of attenuation through 9 human skull fragments from the parietal bone. We also investigated the feasibility of using the proposed numerical scheme and parameters for pre-planning for opening of the blood-brain barrier (BBB) of a patient with mild Alzheimer's disease.

Our results indicated that using the histogram of skull CT images to map the input acoustical parameters there is no significant different ($p > 0.05$) between the mean values of pressure attenuation measured using hydrophone across ex-vivo skull fragments and those estimated with k-wave numerical simulation. We observed a significant difference ($p < 0.01$) between the mean values of the experimentally measured and numerically estimated axial focal shift. In the in vivo case, we observed that adjusting the peak negative pressure for the estimated pressure attenuation led to opening of the BBB in the prefrontal cortex with a 9.25, 8.75, 10.25mm difference.

Acoustic modeling of transcranial ultrasound propagation using k-space pseudo-spectral numerical scheme to estimate the pressure attenuation and focal shift for in-vivo blood-brain barrier opening in prefrontal cortex at 250kHz was shown reliable both ex vivo and in vivo.

The study was funded in part by National Institutes of Health Under (R01EB027576, R01EB009041 and R01AG038961) and the Focused Ultrasound Foundation.



P1-7

Behavior of Ultrasound Neuromodulation on the Kainic-Acid-induced Epilepsy Models

Presenter: PO-CHUN CHU

Authors in order: PO-CHUN CHU, *National Taiwan University*, Chen-Syuan Huang, *National Taiwan University*, Hao-Li Liu, *National Taiwan University*

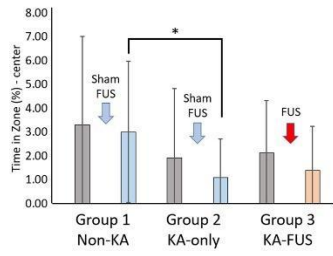
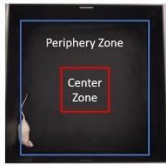
The purpose of this study is to confirm whether FUS modulates epileptic behavior during chronic phase of KA model.

Nineteen Sprague-Dawley rats were separated to 3 groups: group 1 served as non-KA control, group 2 received KA injection to be served as KA-only positive control, and group 3 received KA injection but treated with FUS (ISPTA is 0.5W/cm², three consecutive 10 minutes) in chronic phase of the KA-induced epilepsy. Several behavioral tests have been conducted: the open field test; the cylinder test and water maze test. In addition, the change of hippocampus volume was observed through T2-weighted MRI and quantitated via image J.

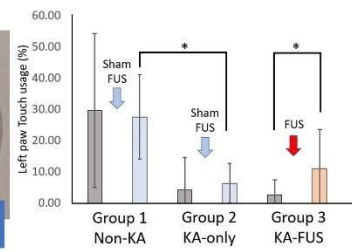
Open field test shows that FUS exposure slightly increased the exploring of KA models (group 3) when compared to the untreated KA animals (group 2; p hippocampus volume decrease toxic by KA can be retarded via FUS treatment (-8.6±15.3% decrease when compared to -13.8±11.4% decrease in KA-only group), showing that FUS has potential to provide hippocampal protection effect.

This study support that consecutive pulsed FUS treatment provides decreased anxiety, improved exploring, limb usage, memory function, as well as hippocampal volume shrinkage, showing that FUS has potential to provide hippocampal protection effect and coincided with the behavioral observation.

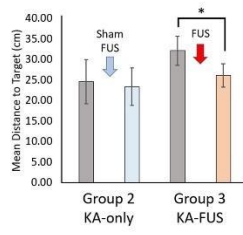
Open field test



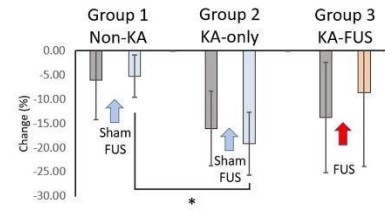
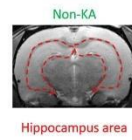
Cylinder test



Water Maze



MRI analysis



P1-8

A Low-intensity Focused Ultrasound (LIFU) Neuromodulation Platform for Human Studies

Presenter: Ali Zadeh

Authors in order: Ali Zadeh, *University of Calgary*, Shirshak Shrestha, Siyun Li, *University of Calgary*, James Wrightson, Roch Comeau, G. Bruce Pike, Samuel Pichardo, *University of Calgary*, Oury Monchi,

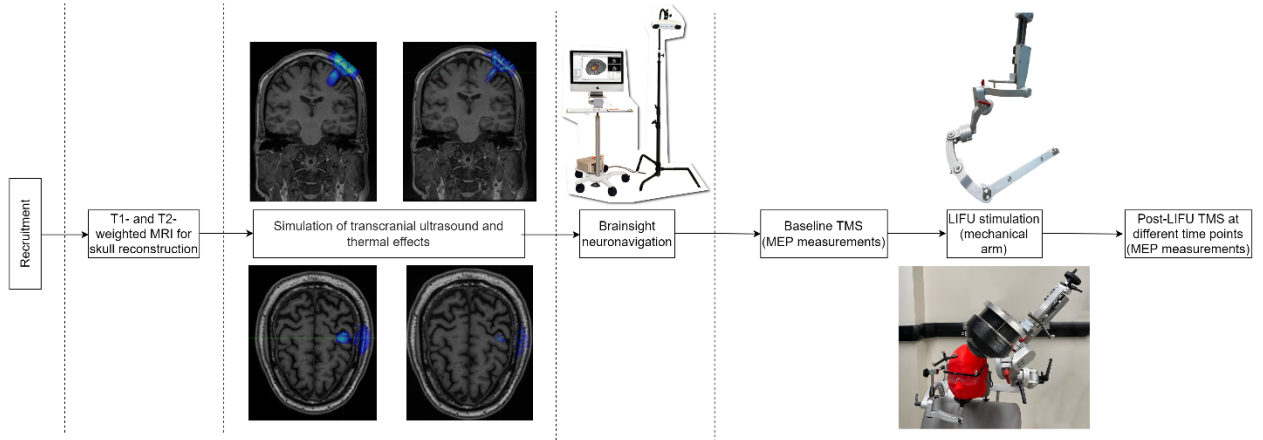
We present a LIFU platform for neuromodulation studies that tightly integrates MRI-based neuronavigation, positioning of actuators, prediction of transcranial ultrasound and control of a phased-array.

T1- and T2-weighted structural magnetic resonance imaging (MRI) scans with 1mm isotropic resolution are acquired to reconstruct the skull and incorporate transcranial ultrasound and thermal modeling (BabelViscoFDTD) in the neuronavigation system (BrainSight, Rogue Research). Transcranial magnetic stimulation (TMS) is applied to the primary motor cortex (M1) to test the effects of LIFU on cortical excitability. A mechanical arm is designed to position the transducer on the target and to quickly remove it during TMS sessions.

We have created a simulation pipeline using numerical modeling and reconstructed MRI data to visualize the propagation of ultrasound and thermal effects on the target for each participant. We have chosen a wide range of pulse repetition frequencies (PRFs) and different focal spot diameters to examine their delayed effects at different time points after LIFU stimulation by measuring the amplitude of the TMS motor evoked potentials. The LIFU mechanical arm with 8 degrees of freedom can navigate to different targets in the Left hemisphere.

This platform enables accurate LIFU-TMS experiments by integrating a phased-array transducer, precise transcranial ultrasound transmission and thermal modeling, a mechanical arm and a neuronavigation system.

Canada Foundation for Innovation Major Science Initiative fund, the Cumming Medical Research Fund, and Natural Sciences and Engineering Research Council of Canada discovery grants.



Rat Brain Stimulation by Shock Wave from Laser-generated Focused Ultrasound Transducer

Presenter: Jooho Lee

Authors in order: Jooho Lee, *Jeju National University*, John Larocco, Dong-Guk Paeng, *Jeju National University*

The purpose of this study is to investigate the feasibility of neurostimulation by shock waves generated from a focused Carbon Nano Tube (fCNT) transducer.

Laser-generated focused ultrasound was irradiated to the rat brain for 10 minutes with laser energy of 350 mJ/pulse and PRF of 5 Hz. The EEG (electroencephalography) signals were measured and compared for three rats before and after sonication in time and frequency domains. The number of EEG peaks over the standard deviation ($\pm 6.7 \mu\text{V}$) in the time domain and power spectrum density (PSD) in theta, alpha, and 1-30 Hz bands were compared before and after sonication.

It was confirmed more EEG peaks after ultrasound sonication than the ones before sonication in all three rats. The PSD of the EEG signal responses in the 1-30 Hz band after sonication were higher to 31.6 ± 4.2 , 14.7 ± 11.0 , and 14.8 ± 4.4 dB in average than those before sonication for three rats. PSD of the theta and alpha frequency bands also showed significant differences before and after sonication.

The possibility of rat brain stimulation by laser-generated focused ultrasound was confirmed by EEG signals in time and frequency domains. This fCNT transducer may stimulate a small area of the brain target in the axial direction, so it can be a means to precisely verify brain function of the rat.

This research was supported by the Focused Ultrasound Foundation and supported by the NRF of Korea grant funded by the Korea government (MSIT, No.2018R1A2B2007997).

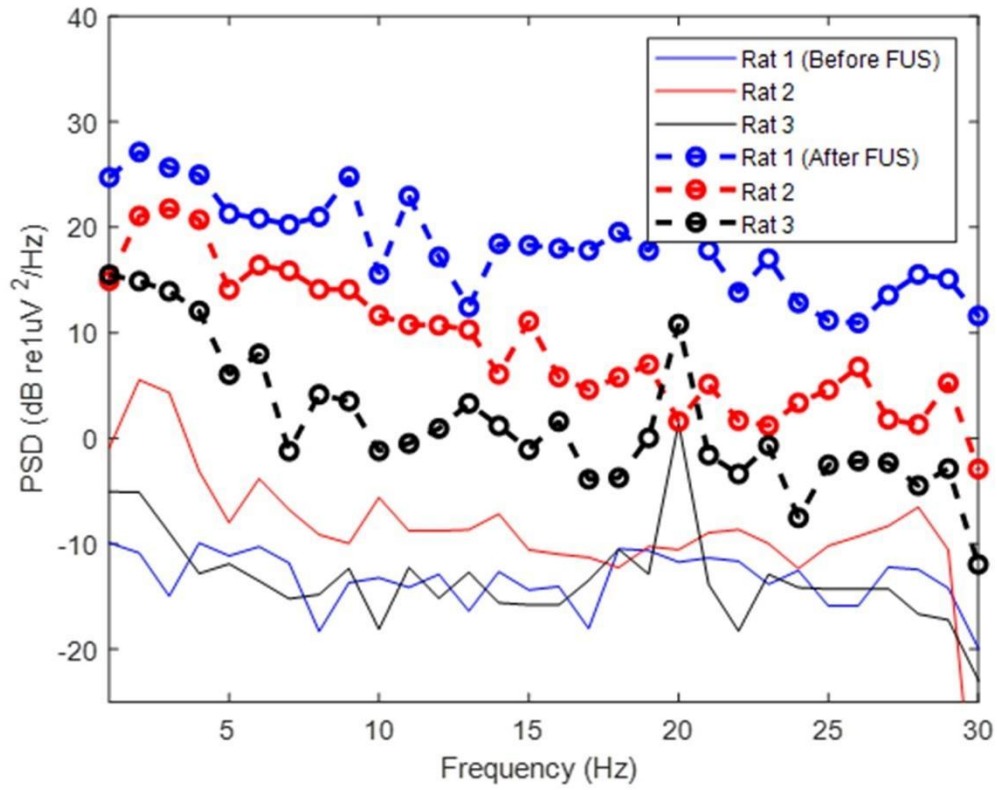


Figure 1 Power Spectrum Density (PSD) of the electroencephalography (EEG) signal responses of three rats in 1-30 Hz band before and after sonication of focused ultrasound (FUS).

P2-1

Microbubble Dynamics in Brain Microvessels at 330 kHz and 1 MHz Ultrasound Frequencies

Presenter: James Bezer

Authors in order: James Bezer, *Imperial College London*, Paul Prentice, *University of Glasgow*, Zheng Jiang, *Imperial College London*, William Lim Kee Chang, *Imperial College London*, Sophie Morse, *Imperial College London*, Kirsten Christensen-Jeffries, *King's College London*, Christopher Rowlands, *Imperial College London*, Andrei Kozlov, James Choi, *Imperial College London*

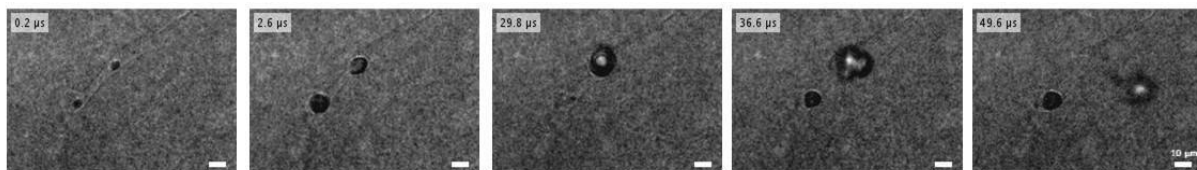
To directly observe behaviours of individual microbubbles within the brain microvasculature when exposed to ultrasound pulses typical in transcranial ultrasound therapy.

Acute brain slices were obtained from juvenile rats that had been transcatheterially perfused post-mortem with SonoVue, heparin, and dye. In each slice, a suitable bubble in a microvessel (5-15 μm diameter) was observed at both microsecond and millisecond time scales during ultrasound exposure. Low centre frequencies of 1 MHz and 330 kHz were used, at mechanical indices of 0.2-1, and pulse lengths up to 10 ms. Probability of microbubble extravasation was compared between parameters.

Oscillating microbubbles cause microvessel walls to distend and invaginate at the ultrasound driving frequency, and can cause micrometre-scale tissue displacements well beyond the endothelial wall. Microbubbles can also be forced out of small microvessels due to the primary radiation force; this occurred at both frequencies tested. The probability of extravasation scales approximately with mechanical index, being rare at low pressures, but much more common at $MI \geq 0.6$, at both 1 MHz and 330 kHz centre frequencies.

Microbubble extravasation due to the primary radiation force may be a mechanism of BBB disruption or of tissue damage during exposure to ultrasound parameters typical of those used in therapy. These results may aid development of safer and more effective therapies.

Funded by EPSRC Grant EP/L015226/1



Estimation of the Acoustic Attenuation Along the Propagation Path of Focused Ultrasound using Reflected Echoes: Ex Vivo Study

Presenter: Tianfeng Zhang

Authors in order: Tianfeng Zhang, *ChongQing Medical University*, Yufeng Zhou, *Chongqing Medical University*

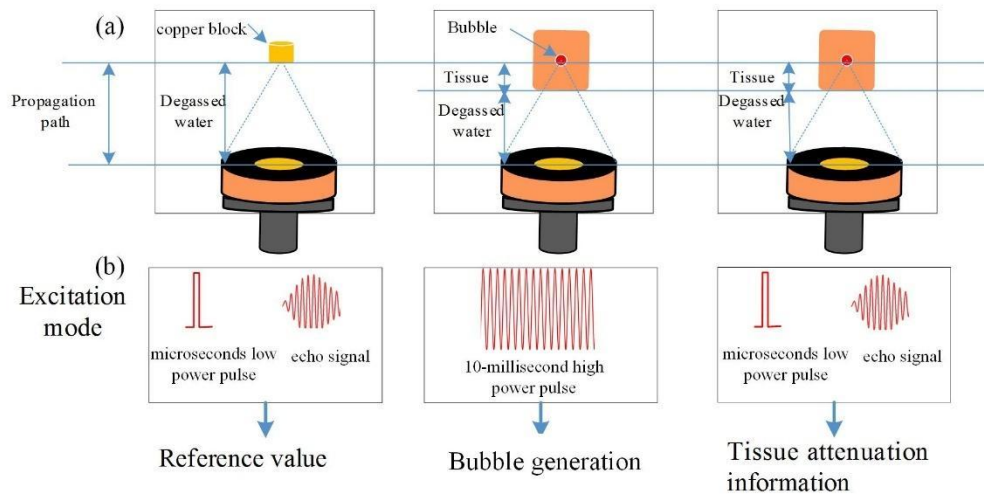
The acoustic attenuation of the tissue is critical for the HIFU ablation, but challenging for measurement in vivo. We propose a new measurement approach.

A big boiling bubble inside the tissue was produced at the focal point of a commercial HIFU device (JC-200, Chongqing Haifu Medical Technology Ltd, China) by a 10-millisecond pulse at the high power output. Then the HIFU transducer was switched to the pulser-receiver mode. Echoes of a few emitted pulses at the duration of microseconds at the low power was received for analysis and acoustic attenuation values were calculated.

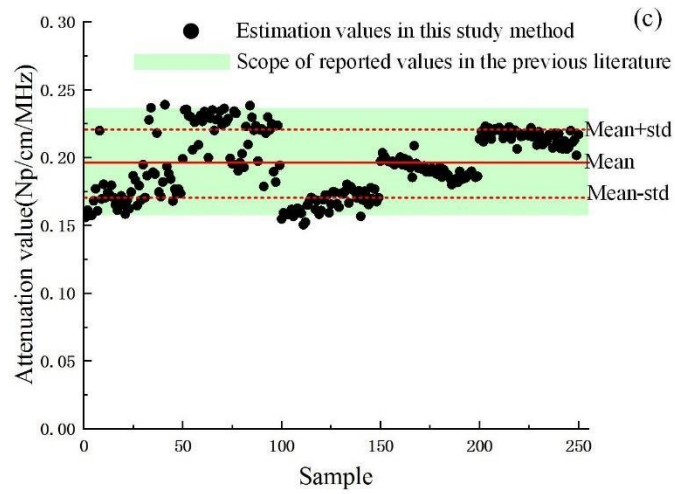
The method was verified via experimental studies of pork tenderloin ex vivo. The experimental results showed that the acoustic attenuation measured at the same depth (i.e., 4 cm) of ex vivo pork tenderloin samples existed differences (0.194 ± 0.023 Np/cm/MHz at 4 centimeters). A statistical attenuation value calculation of pork tenderloin was varied from 0.15 to 0.239 Np/cm/MHz which is within the scope of reported values in the previous literature, from 0.16 to 0.24 Np/cm/MHz.

It suggests that the tissue acoustic attenuation could be accurately determined in situ. Thus, this proposed noninvasive and quantitative approach may be applied in the clinical HIFU ablation to select the appropriate path and make the treatment plan.

Method introduction



Result



Bubble Dynamics on the Potential Therapeutic Ultrasound Contrast Agents with Heterodyne Driving Pulses

Presenter: Xue Song

Authors in order: Xue Song, *Shanghai Jiao Tong University*, Huaxin Lu, *Shanghai Jiao Tong University*, Guofeng Shen, *Shanghai Jiao Tong University*

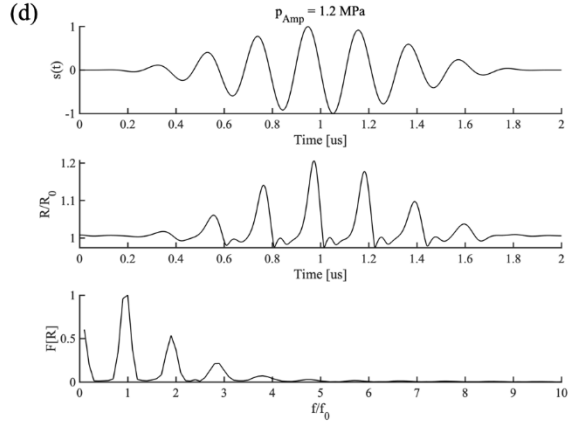
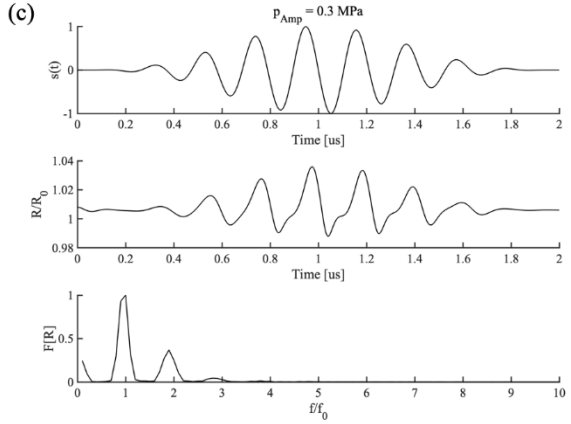
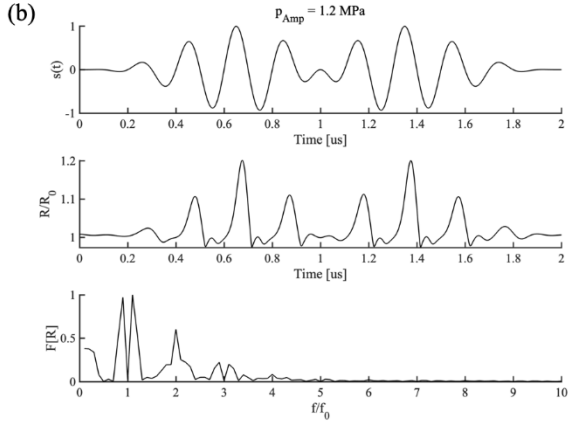
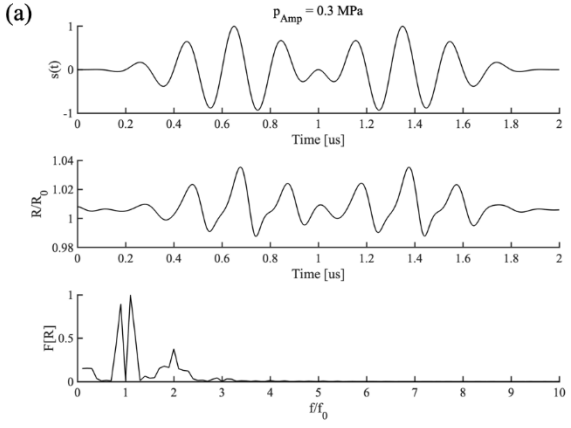
Bubble dynamics simulation can provide basic information for acoustic activities of therapeutic acoustic droplets. This work introduced heterodyne excitation to explore the bubble's simulated behavior.

The simulation was based on a four-phase droplet model derived from the Rayleigh-Plesset like equation. Solutions of the equation were obtained using the ode15s function implemented in the MATLAB. Heterodyne excitation was applied on the model, with shell thickness of 5 nm, the diameter of 2.5 μm . Shear modulus of 200 MPa and shear viscosity of 2 Pa•s were applied in the simulation. Different ultrasound pressures were exploited to explore the dynamics of the droplet.

The bubble's temporal evolution of the radius and their fast Fourier Transform (FFT) of are shown in the Figure. We can see from the figure that higher pressure generates higher oscillation, where the radius can expand to at most 1.2 times than the initial size. However, the radius doesn't change a lot at 0.3 MPa. For the 2-microseconds beating heterodyne signal, the bubble experienced relatively continuous contraction and had higher harmonic component, compared with mixing heterodyne signal. This might be due to the frequency component and envelope of the signal.

The droplet model can be used for predicting the bubble dynamics under different driving pulses and driving pressures. In addition, the heterodyne signal generation can also influence the bubble's oscillating form. It is also important in the future research on other parameters, such as shell property.

The authors would like to acknowledge the financial support from China and Shanghai, No.2017YFC0108900, No. 81727806, No. 11774231, No. 17441906400.



P2-12

USgHIFU for Unresectable Pancreatic Cancer: Survival after Successful Ablation (NPVR \geq 50%)

Presenter: Kun ZHOU

Authors in order: Kun ZHOU, *The Second Affiliated Hospital of Chongqing Medical University*, Jinyun CHENG,, Jun Zhang

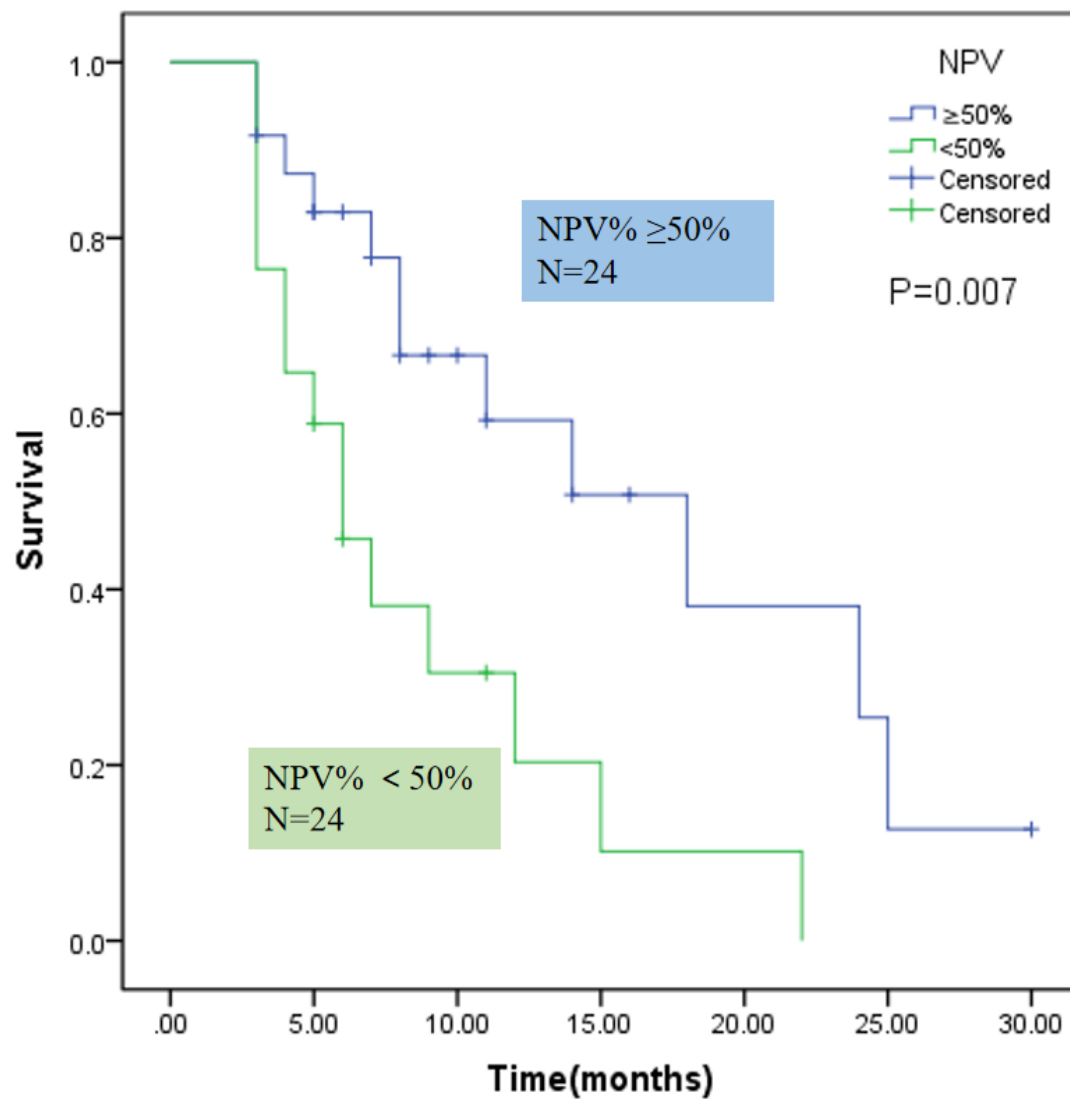
To assess survival benefits of patients with initial diagnosed and unresectable pancreatic cancer who were treated with one session of USgHIFU ablation.

Patients with non-resectable PC disease after MDT discussion who underwent one session of ultrasound-guided HIFU ablation for tumor. Real-time ultrasonographic imaging was used to monitor the procedure. Contrast-enhanced computed tomography (CT) or magnetic resonance imaging (MRI) were performed to measure the lesion size and non-perfusion volume (NPV) pre-HIFU and –one month post-HIFUa.

Forty-one patients were enrolled and all HIFU were performed successfully without severe adverse events . The age was 64.8 ± 9.8 years. The mean size of the PC was 38.1 ± 13.6 mm . 12 were at TNM stage III, and 29 at stage IV. The HIFU procedure time was 109.2 ± 46.1 min. The sonication time was 18.6 ± 8.4 min. The mean acoustic power was 288.5 ± 52.3 W. The NPV% at 1month post-HIFU was $53.3\% \pm 18.4\%$ while the median NPV% was 52.8%. The NPVR were also associated with survival by univariate analysis, the median survival time of patients with NPVR \geq 50% of tumor and NPVR < 50% was 18 and 6 months, respectively (P=0.007).

The NPVR greater than 50% is a sign of successful ablation for patients with non-resectable PC disease, which might be a potential prognostic factor with higher long-term survival.

This research was supported by Kuanren Talents Program of the Second Affiliated Hospital of Chongqing Medical University.



Inertial Cavitation with Low Energy Caused by Focused Ultrasound Thalamotomy for Tremor-dominant Parkinson's Disease

Presenter: Toshio Yamaguchi

Authors in order: Toshio Yamaguchi, *Shin-yurigaoka General Hospital*

We present a rare case of a patient with tremor-dominant Parkinson's disease (TDPD) who had inertial cavitation during focused ultrasound (FUS) thalamotomy.

A 61-year-old man with TDPD has had a 30-year history of resting tremors in the neck and upper and lower extremities, which progressed to rigidity in the upper extremities by the age of 59 years. He was subsequently diagnosed with TDPD and essential tremor and prescribed trihexyphenidyl (Artane). On admission to our institution, left VIM thalamotomy with FUS was performed (skull density ratio = 0.52).

During the third sonication (277 W, 2 S, 691 J), total modulation occurred due to cavitation. He felt "light" in the brain and had slight unconsciousness, dysarthria, and paresthesia, prompting treatment cessation. Simultaneously, tremors and rigidity in the upper and lower extremities improved immediately. MR imaging revealed extensive high-intensity lesions in the thalamus, internal capsule, and partly in the globus pallidum. He was then administered steroid infusion for 3 days, which resolved in adverse events. His tremors and rigidity in the upper extremities also improved in 6 months after FUS treatment without any adverse events.

We should be careful to avoid inertial cavitation even in low energy delivery. Acting as the efficacy standpoint, mechanical bioeffect in the extensive thalamus might work if we could control the cavitation. We will examine the duration of effectiveness for the control of tremors and rigidity in this patient.

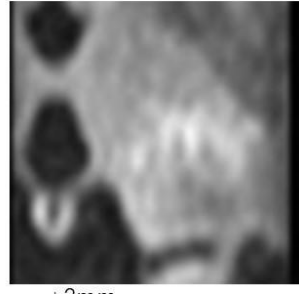
Fan out lesions caused by cavitation

MR on the following day showed extensive high intensity lesions in the thalamus, internal capsule and partly globus pallidum,

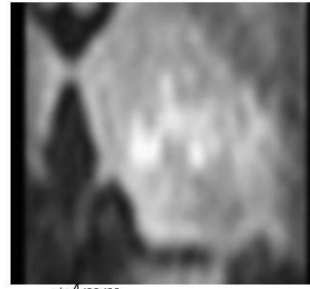
DWI



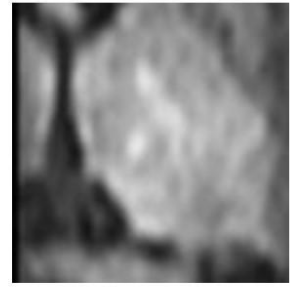
ACPC



+2mm

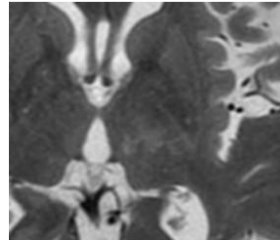
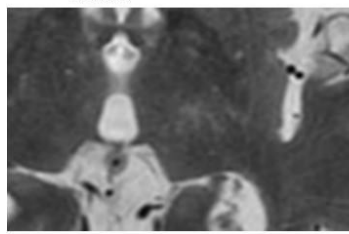


+4mm



+6mm

T2WI



Single Acoustic Hologram for Reconstructing Acoustic Fields of HIFU Arrays

Presenter: Azamat Kaloev

Authors in order: Azamat Kaloev, *Physics Faculty, Lomonosov Moscow State University, Moscow, Russian Federation; Institut Polytechnique, Paris, France*, Dmitry Nikolaev, *Physics Faculty, Lomonosov Moscow State University, Moscow, Russian Federation*, Vera Khokhlova, *Physics Faculty, Lomonosov Moscow State University, Moscow, Russian Federation; Center for Industrial and Medical Ultrasound, University of Washington, Seattle, United States of America*, Oleg Sapozhnikov, *University of Washington*

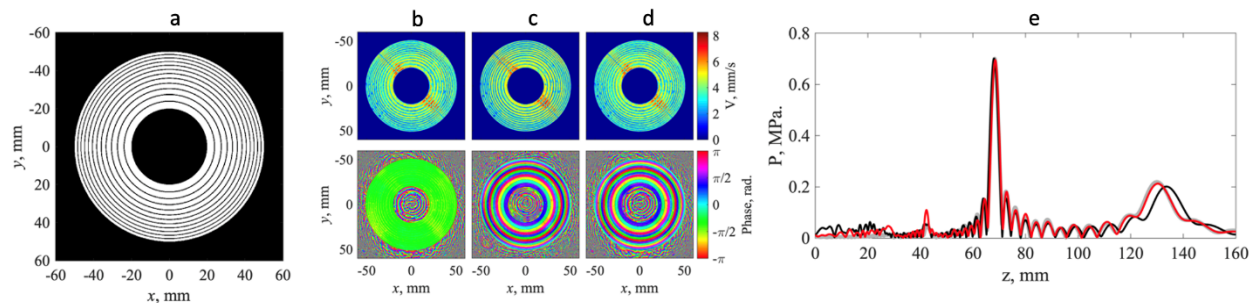
A method based on one measured hologram of a multi-element array, which allows reconstructing the array fields with various electronics steering is proposed and tested.

A hologram of a 12-elements annular phased array (Imasonic, France, Fig. a) was measured when all elements operated in phase, backpropagated to the array's surface, and then each element was spatially separated from the others. The element's acoustic field phases were varied and used for simulating a field with electronically steered focus. The resulting field was compared with the one calculated from a hologram of the array operating with the same electronic focus steering.

Two vibrational velocity patterns of the array were reconstructed from holography measurements: with no focus steering (Fig. b) and with the focus, electronically steered by 12 mm towards the transducer (Fig. c). Individual elements were spatially isolated in the first hologram and their phases were shifted by prior calculated values to steer the focus by 12 mm towards the array (Fig. d). Then, from this boundary condition, pressure distribution on the axis of the array was calculated (Fig. e, red) that is in a good agreement with the one reconstructed from a hologram measured when the focus was shifted electronically (Fig. e, gray).

It was proposed and demonstrated experimentally that under assumption of weak mechanical and electrical cross talk between the elements of a multi-element array, one measured hologram can be used to predict vibrational velocity patterns of the array for arbitrary focus steering conditions and to reconstruct the corresponding ultrasound fields.

Work supported by RSF 20-12-00145 and FUSF Global Internship program.



(a) Phased array; (b-d) array's vibrational pattern; (e) axial pressure distributions

Schlieren-Optical Characterization of Ultrasound Waves: Towards an MRI-compatible Setup

Presenter: Johannes Lindemeyer

Authors in order: Johannes Lindemeyer, *University of Cologne, Faculty of Medicine and University Hospital Cologne*, Luisa Brecht, *University of Cologne, Faculty of Medicine and University Hospital Cologne*, Jörg-Bernd Bonekamp, *Soluxx GmbH*, Florian Steinmeyer, *Technische Hochschule Nürnberg*, Holger Gruell, *University Hospital of Cologne*

To design an MRI-compatible Schlieren-optical system that can characterize the acoustic field of the ultrasound transducer within the clinical setup of a Sonalleve-V2 table.

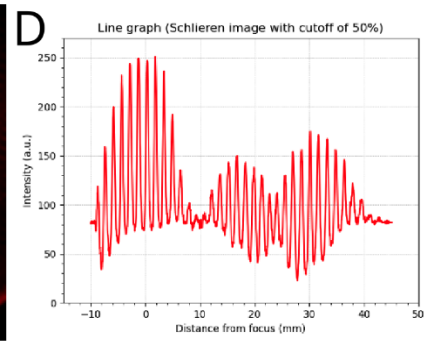
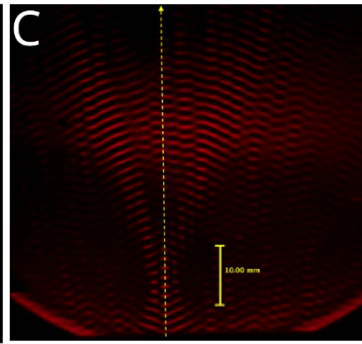
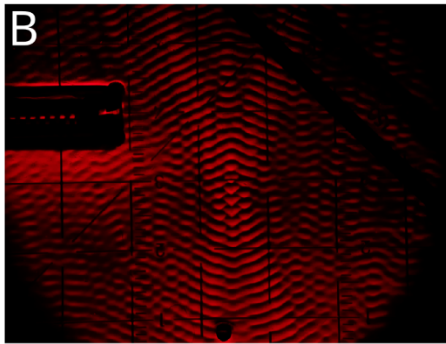
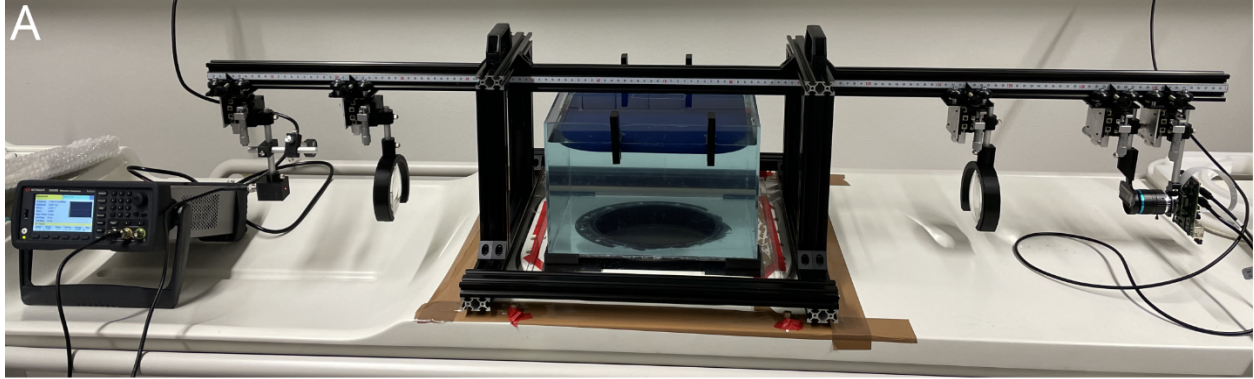
The pressure profile of ultrasound transducer fields alters the refractive index of water. This was visualized by a Toepler-based Schlieren system, consisting of a collimator around a water basin, a stroboscopic light source and a camera behind a Schlieren knife-edge. Custom MRI-compatible components were composed on a Sonalleve V2 table (Fig.A) to fit into a clinical MRI system. Continuous waves at power level 30-100W were recorded with a Raspberry Pi HQ camera at zero field.

With a 16mm lens, a spatial resolution of 0.03mm could be achieved (Fig.B). First measurements of the intensity profile in a 1.2MHz continuous-wave ultrasound field show the wave distribution in the central plane. A line plot through the beam axis exploits the hull curve of the incident wave through the focal region (Figs.C+D).

Compatibility of Raspberry Pi+Camera module powered by a Lithium-Ion power bank, operated by a Wifi-connected notebook outside of the magnet room was validated up to 30cm in front of magnet bore entrance. Optical rail and mounts are being modified to contain a minimum of magnetic materials.

An optical system for the characterization of an MRI-guided HIFU device was established. First acquisitions clearly visualize applied ultrasound fields and allow for studying custom pulse sequences or quality assessment. MR-compatibility was tested for the acquisition electronics. Measurements with the entire setup inside of the magnet are our next objective.

We gratefully acknowledge Raimund Jung and Simo Kustaanheimo (Profound Medical). This work was supported by the German Federal Ministry of Education and Research ("MR-HIFU-Pancreas",FKZ:13GW0364D).



A: Experimental setup, **B:** 1.2MHz@100W continuous-wave, square size 1cm²,
C: 1.2MHz@30W, **D:** Line plot (yellow line in B)

Anti-Cancer Provascular Therapy Using Ultrasound Microbubble Cavitation and Nitrites to Increase Radiotherapy Efficacy

Presenter: Francois Yu

Authors in order: Simon Michon, *Institut de Génie Biomédical, Université de Montréal*, Francis rodier, *Radiologie, radio-oncologie et médecine nucléaire, Faculté de Médecine, Université de Montréal*, Francois Yu, *Université de Montréal*

Hypoxia induces resistance to radiation therapy in solid tumors. We hypothesized that MB cavitation (UTMC) can radiosensitize solid tumors by increasing blood perfusion.

Mice were injected bilaterally with PC3 cancer cells and treated with UTMC unilaterally. A therapeutic transducer (S3 probe, 1.3MHz, SONOS 5500) was used to transmit 60 US pulses (M.I = 1.3) during the injection of MBs (Definity) intravenously (3-5 μ L/min). Nitrites were injected 5 minutes before treatment (4mg/kg). MB perfusion was quantified by US contrast burst replenishment imaging (CPS 7MHz, Sequoia, Siemens). Mice were then treated with radiotherapy (2 and 8 Gy).

Perfusion increased in tumors subjected to UTMC + Nitrites (Figure 1A : up to 3 times the pre-treatment value, and lasted for at least 10-15 minutes. After radiotherapy, there was an improved growth inhibition for the 8 Gy + UTMC + Nitrites group vs. 8 Gy + Nitrites alone (Figure 1B : +++ $p < 0.005$, Mixed-model Analysis). This effect was not significant with mice treated by UTMC + Nitrites and receiving 0 Gy or 2 Gy, and in tumors treated with lower M.I. and without nitrites. The decrease in hypoxia post UTMC was confirmed by histology.

In conclusion, UTMC + Nitrites increased blood flow and reduced hypoxia in our tumor model, which lead to an increase in radiotherapy efficacy at 8 Gy. This locally targeted approach is promising for activating the vascular reserve in hypoxic tumors.

This work was funded by the Cancer Research Society, FRQS, TransmedTech Institute and the Institut du cancer de Montréal Canderel.

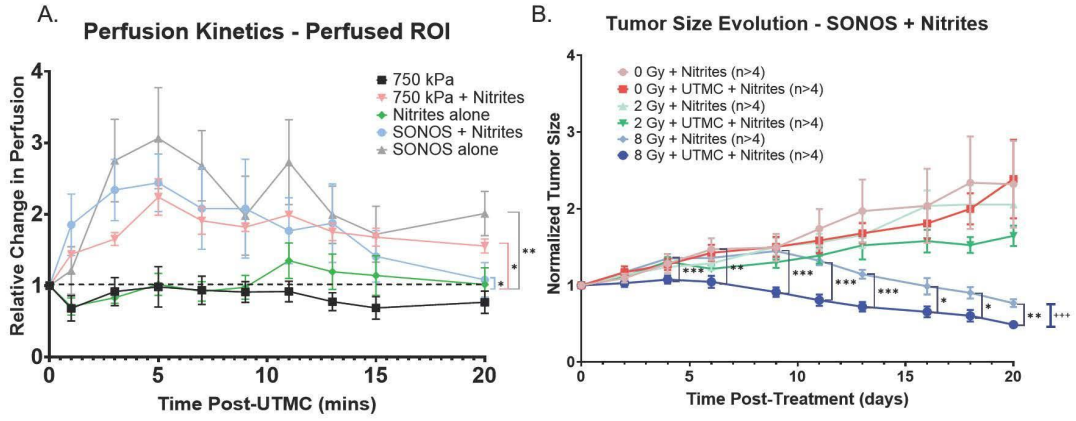


Figure 6 : Effect of UTMC + Nitrites. A. UTMC + nitrites improved perfusion in tumors by 2-3 folds compared to nitrites alone. In particular, the addition of nitrites induced a provascular response with the 750 kPa pulse that was not observed without nitrites. This effect was significant when compared to nitrites alone for SONOS alone (** = $p < 0.01$, T-Test), 750 kPa + nitrites (* = $p < 0.05$, T-Test) and SONOS + nitrites (* = $p < 0.05$, T-Test). B. Tumor size evolution was monitored for 30 and 25 days post-UTMC. Mice were irradiated 10 minutes after the end of the UTMC treatment. This has been shown to be the optimal perfusion increase window. There was a significant difference in the size evolution of tumors between the 8 Gy group (no-treatment) and the 8 Gy + UTMC + nitrites group (+++ = $p < 0.005$, Mixed-Model Analysis).

Ultrasound and Microbubbles Mediated Oncolytic Virotherapy to Treat Cancer

Presenter: KISHAN ITALIYA

Authors in order: KISHAN ITALIYA, *CRCHUM: "Centre Hospitalier de l'Université de Montréal" Research Centre, Montreal, QC, Canada*, Victor Mullins-Dansereau, *Université de Montréal, Bourgeois Daigneault Marie Claude, CRCHUM: "Centre Hospitalier de l'Université de Montréal" Research Centre, Francois Yu, Université de Montréal*

To deliver oncolytic-virus (OV) sensitizing drugs (e.g. Paclitaxel) to tumors by using microbubbles (MB) and ultrasound (US)

PTX-carrying lipid MBs (PTXLPMBs) were developed using a thin-film hydration mechanical vibration method (VIALMIX). MBs size, morphology, count and drug-loading were determined. We assessed MB stability in plasma and culture medium. PTXLPMB cytotoxicity was evaluated on plated 4T1 cells. MB destruction was obtained using burst-mode on Acuson Sequoia (15L8, CPS7, Burst MI=1.9). After US, cells were infected with fluorescent-OV (VSV) for 24h at 0.1 Multiplicity of infection (MOI). OV replication and cell viability were quantified.

For PTXLPMBs, drug loading was 25-30µg of PTX per 10e8 MB with average size $1.57 \pm 0.78 \mu\text{m}$. PTXLPMBs were found to be acoustically active and could be burst by US. PTXLPMBs stability in cell-culture media (> 30min) and plasma (>10 min) are compatible with in vivo delivery. In-vitro cytotoxicity assay for PTXLPMB confirms that PTX can be delivered using MB burst by US. When combined with OV, PTXLPMB + US significantly increased OV replication (3 times at 4 µM) and significantly decreased cell viability with increasing concentration of PTXLPMB.

In this work, we demonstrate that MB can be used to deliver OV sensitizing drugs to cells in vitro. In vivo, targeted delivery of OV sensitizing drugs is expected to enhance OV replication in sonicated tumors, potentially allowing intravenous administration of OV therapy.

This work was funded by the Government of Canada's New Frontiers in Research Fund (NFRF), [NFRFE-2019-01010] and the Institut du Cancer de Montréal.

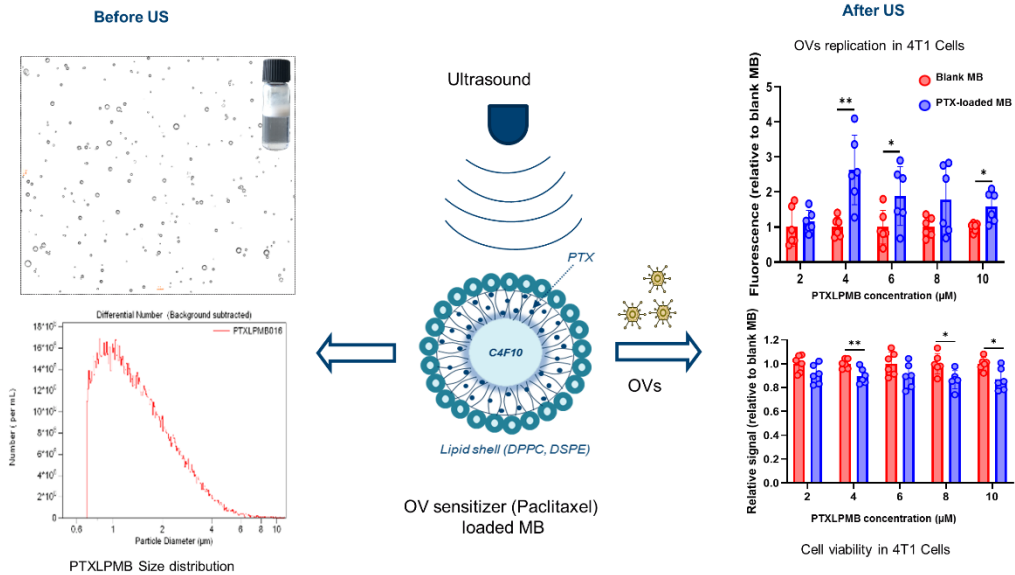


Figure 1: Paclitaxel loaded microbubbles enhanced oncolytic virus (VSV) replication in 4T1 cells

Stable Cavitation Behaviour of Size-isolated Protein-shelled Microbubbles and SonoVue

Presenter: Anuj Kaushik

Authors in order: Anuj Kaushik, *IIT Gandhinagar*, Pratibha ., *Indian Institute of Technology Gandhinagar*, Aaqib Khan, *Indian Institute of Technology Gandhinagar*, Sameer Dalvi, *Indian Institute of Technology Gandhinagar*, Himanshu Shekhar, *Indian Institute of Technology Gandhinagar*

Stable cavitation is implicated in several therapeutic ultrasound applications. We characterised stable cavitation from size-isolated protein-shelled ultrasound contrast agents (UCAs) and SonoVue, a lipid-shelled UCA.

Bovine serum albumin (BSA) microbubbles were prepared and size isolated using differential centrifugation. Size distributions were measured with electrozone sensing and acoustic characterization was performed (Fig. 1(a)). Sinusoidal (2 MHz frequency, 60 cycles) excitation was used to drive a focused transducer (f-number=0.97). A broadband PVDF transducer (20 MHz frequency) was used as a passive cavitation detector. The subharmonic emission data was fitted with a piecewise linear curve to assess the stable cavitation threshold.

Figure 1(b) demonstrates the number-weighted size distributions of SonoVue (mean diameter = 1.69 μm) and bovine serum albumin-shelled agents (BSA1, BSA2, and BSA3), with mean diameters of 1.77 μm , 3.52 μm , and 4.32 μm , respectively. Fig. 1(c-f) illustrates the root mean squared subharmonic emission versus peak rarefactional pressures. The peak rarefactional pressure at the inflection between the first two segments was defined as stable cavitation threshold (SCT). The SCT was determined to be 270, 300, 340, and 850 kPa for SonoVue, BSA1, BSA2, and BSA3, respectively.

The SCT was observed to increase with the mean size diameter of BSA shelled microbubbles. SCT thresholds were higher for protein-shelled microbubbles than SonoVue. The measured SCT for SonoVue was consistent with earlier reports. These findings could help guide the choice of UCAs for therapeutic applications.

The Department of Biotechnology (India) funded this study with Grant No. MIS/IITGN/R&D/HS/202021/049.

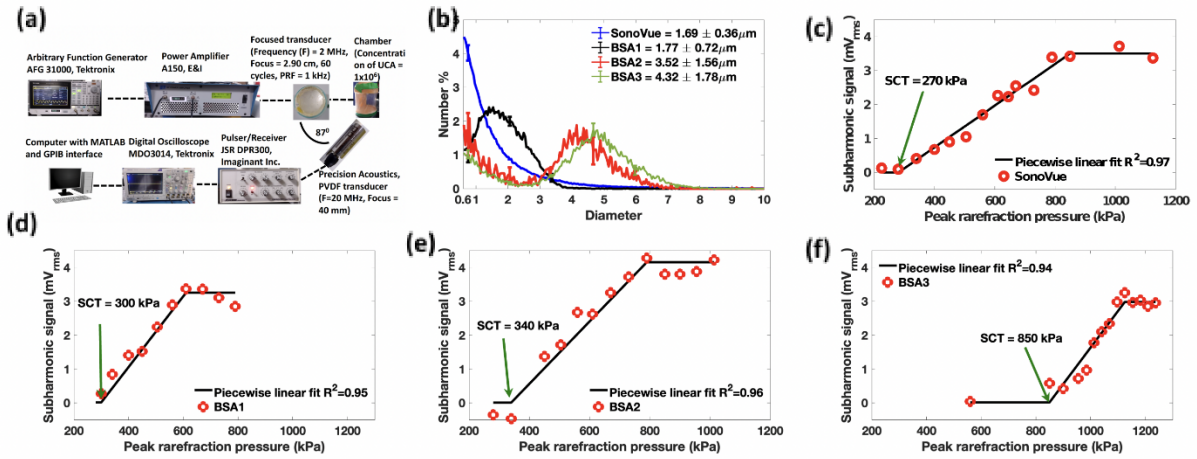


Fig. 1 (a) Experimental setup. (b) Number-Weighted size distribution of SonoVue, BSA1, BSA2, and BSA3. (c-f) Quantification of subharmonic emissions from SonoVue, BSA1, BSA2, and BSA3 as a function of insonation peak rarefactional pressures. The SCT was determined as the first inflection between the segments of a three-segment piecewise linear fit.

Passive Cavitation Detection Using a Fiber Bragg Grating Sensor

Presenter: Kuldeep Jajoria

Authors in order: Kuldeep Jajoria, *Indian Institute Of Technology–Gandhinagar (IIT–Gandhinagar)*, Chandan Jha, *IITGN*, Arup Chakraborty, *IITGN*, Himanshu Shekhar, *Indian Institute of Technology Gandhinagar*

This study demonstrates the feasibility of using an optical fiber Bragg grating sensor for detecting cavitation nucleated by a commercial lipid-shelled contrast agent (SonoVue).

A 2 MHz focused ultrasound transducer was used to generate cavitation from SonoVue. The transducer and a polyvinylidene fluoride (PVDF) receiver were aligned at 90 degrees and the microbubbles were placed in an acoustically transparent chamber (Fig. 1.A.). Cavitation nucleated by the bubbles was first recorded by the PVDF transducer. Next, cavitation was detected by the FBG by measuring the Bragg wavelength shift caused by modulation of the refractive index in response to ultrasound.

Fig.1.B. shows the spectra of time-domain traces obtained using the FBG sensor and a broadband PVDF transducer at a peak negative acoustic pressure of 175 kPa. The presence of subharmonic (1 MHz), ultraharmonic (3 MHz, 5 MHz), and harmonics (4 MHz, 6 MHz, 8 MHz, 10 MHz) in the detected signal indicates the presence of stable cavitation. The differences in the magnitudes of fundamental with the subharmonic and ultraharmonic signal of the sensors are similar, indicating that FBG has comparable sensitivity to that of PVDF transducer.

These results show the feasibility of passive cavitation detection using FBGs. Future work will focus on assessing the potential of using FBGs for PCD in vivo.

We thank IIT Gandhinagar for funding this project. We acknowledge members of MUSE Lab and Photonics Sensors Lab for their suggestions.

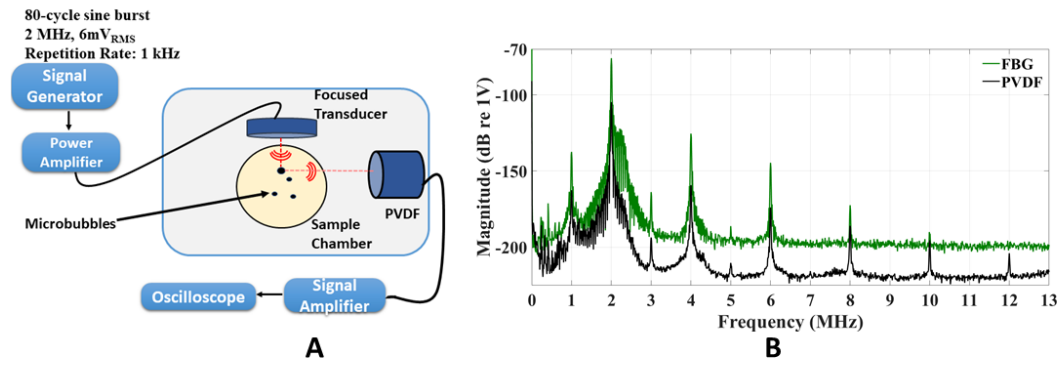


Fig.1 (A) Schematic of cavitation detection setup; (B) Cavitation signal detected by FBG sensor and PVDF transducer.

Ultrasound-triggered Microbubble Destruction Enhances the Radiosensitivity of Glioblastoma by Inhibiting Autophagy

Presenter: Ying He

Authors in order: Ying He, *Xinqiao Hospital, Army Medical University*, Xun-Hu Dong, Qiong Zhu, Ya-Li Xu, Mingliang Chen, *Army medical research*, Zheng Liu,

To delineate the effect of ultrasound-triggered microbubble destruction (UTMD) on the radiosensitivity of glioblastoma and the potential involvement of autophagy.

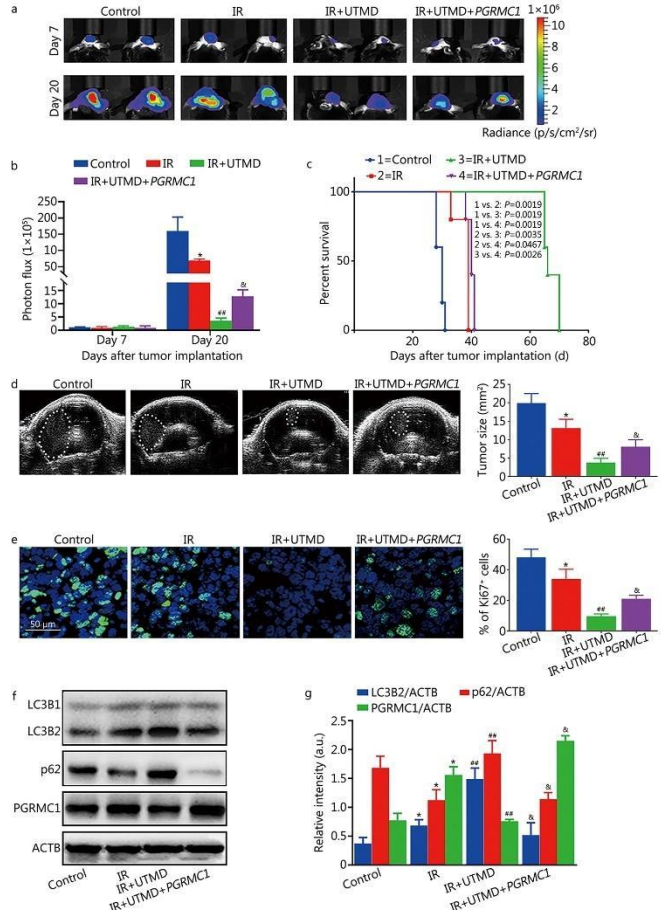
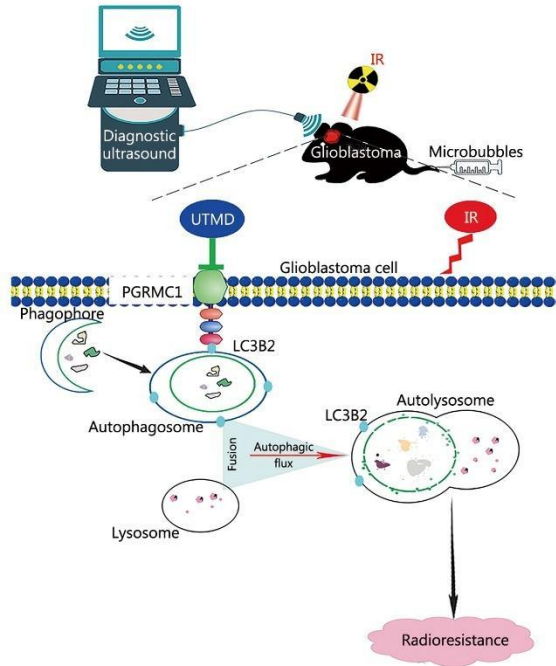
GL261, U251 cells and orthotopic glioblastoma-bearing mice were treated with ionizing radiation (IR) or IR plus UTMD. Autophagy was observed by confocal microscopy and transmission electron microscopy. Western blotting and immunofluorescence analysis were used to detect progesterone receptor membrane component 1 (PGRMC1), light chain 3 beta 2 (LC3B2) and sequestosome 1 (SQSTM1/p62) levels. Lentiviral vectors or siRNAs transfection, and fluorescent probes staining were used to explore the underlying mechanism.

UTMD enhanced the radiosensitivity of glioblastoma in vitro and in vivo. UTMD inhibited autophagic flux by disrupting autophagosome-lysosome fusion without impairing lysosomal function or autophagosome synthesis in IR-treated glioblastoma cells. Suppression or induction of autophagy had no significant effect on UTMD-induced radiosensitization in glioblastoma cells. Furthermore, UTMD inhibited PGRMC1 expression and binding with LC3B2 in IR-exposed glioblastoma cells. PGRMC1 or PGRMC1 siRNA pretreatment enhanced UTMD-induced LC3B2 and p62 accumulation in IR-exposed glioblastoma cells, thereby promoting UTMD-mediated radiosensitization. Moreover, PGRMC1 overexpression abolished UTMD-caused blockade of autophagic degradation, subsequently inhibiting UTMD-induced radiosensitization of glioblastoma in vitro and in vivo.

UTMD enhanced the radiosensitivity of glioblastoma partially by disrupting PGRMC1-mediated autophagy. These results indicate that UTMD would be an effective adjuvant for radiotherapy in glioblastoma and provide new biological evidence for clinical applications of UTMD in tumor therapy.

This work was supported by the National Natural Science Foundation of China (82073544 and 81971774), the Chongqing Talent Project (CQYC2019).

UTMD enhanced the radiosensitivity of glioblastoma by inhibiting PGRMC1-mediated autophagy



Sonodynamic Response of a Water-soluble Porphyrin Derivative to Ultrasound Exposure at 1 MHz

Presenter: Manita Das

Authors in order: Vishwa Patel, *Indian Institute of Technology Gandhinagar*, Manita Das, *Indian Institute of Technology (IIT) Gandhinagar*, Vijayalakshmi Pandey, *Indian Institute of Technology Gandhinagar*, Dhiraj Bhatia, *Indian Institute of Technology Gandhinagar*, Iti Gupta, *Indian Institute of Technology Gandhinagar*, Himanshu Shekhar, *Indian Institute of Technology Gandhinagar*

Sonodynamic therapy (SDT) can achieve site-specific cytotoxic effects mediated by reactive oxygen species (ROS). We assessed ultrasound-mediated ROS generation from a novel porphyrin agent.

A water-soluble thioglycosylated transA2B2-type porphyrin was exposed to ultrasound at 1 MHz, intensities of 0.5 - 2.0 W/cm², at 100 Hz pulse repetition frequency. Exposure times of 0 - 5 minutes were used. ROS generation was quantified by UV-vis spectrophotometry using degradation on 1,3-diphenylisobenzofuran (DPBF) as a chemical trap for singlet oxygen. The quantum yield of ROS generation ($\Phi\Delta$) was calculated at 1.5 W/cm² by using a Rose Bengal standard.

The porphyrin derivative generated ROS for the range of exposure conditions tested at concentrations as low as 12 μ M (figure 1). A DPBF degradation of 1.4 % was observed at 0.5 W/cm² that increased to 36 % at 1.5 W/cm². However, increasing the intensity further to 2.0 W/cm² showed only a marginal increase in ROS generation with only 38 % DPBF degradation. The quantum yield was found to be 0.59 ± 0.05 at 1.5 W/cm².

We characterized a novel agent previously reported to improve cellular uptake over non metallated porphyrins. We found that exposure at 1.5 W/cm² intensity for 2 mins is well-suited to promote ROS generation. Future studies will focus on the therapeutic potential of this agent in ex-vivo and in vivo models.

Science and Engineering Research Board (India) funded this study (Grant No. SRG/2020/001123)

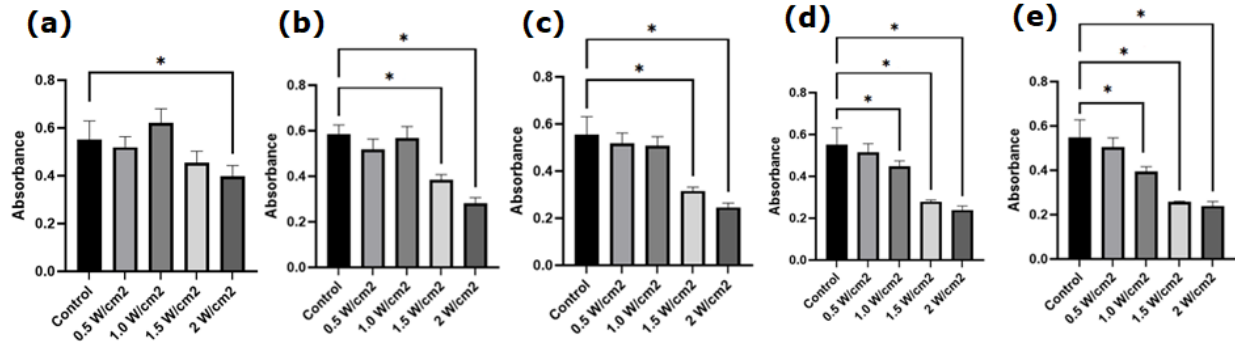


Figure 1. Bar plot showing ROS generation from porphyrin with a range of exposure intensities at (a) 1 (b) 2 (c) 3 (d) 4 and (e) 5 minute/s (mean \pm SD, N=3) * denotes statistical significance, $p < 0.05$.

Histotripsy Bubble Cloud Contrast using Chirp-Coded Excitation and Volterra Filtering

Presenter: Vishwas Trivedi

Authors in order: Vishwas Trivedi, *Indian Institute of Technology Gandhinagar, India*, Emily Wallach, *University of Chicago*, Kenneth Bader, *University of Chicago*, Himanshu Shekhar, *Indian Institute of Technology Gandhinagar*

The detection of histotripsy bubble clouds is difficult in abdominal targets. Here, chirp-coded excitation was combined with Volterra filtering to improve bubble visualization at depth.

Histotripsy bubble clouds were generated in agarose tissue-mimicking phantoms doped with cornstarch scatterers (8 g/l). Bubble clouds were interrogated with a chirped pulse (7-12 MHz, 1.9 μ s) using a plane wave sequence. A subharmonic matched filter was first applied to the received radiofrequency data, followed by a tuned second-order Volterra filter to emphasize bubble-specific signals. The contrast-to-tissue ratio (CTR) was computed to assess performance.

In total, 30 data sets were processed with either standard delay-and-sum, subharmonic chirp-coded excitation, or chirp-coded excitation combined with the Volterra filter. Representative examples of bubble visualization with each method are shown in Figure 1. For still frames, bubble cloud detection is not apparent and users must rely on changes in speckle in cineloops to indicate cavitation location. Bubble signals became apparent with subharmonic chirp-coded excitation (CTR = 6 dB), and quadratic Volterra filtering improved the CTR further by more than 2-fold (CTR = 12 dB).

While conventional nonlinear imaging is effective for microbubbles, other methods may be necessary to provide visualization of the large bubbles generated via histotripsy. Here, we demonstrated the Volterra filter as a means to improve the detection of the nonlinear bubble cloud signal and reject background tissue and noise.

This work was funded by IIT Gandhinagar and the American Cancer Society.

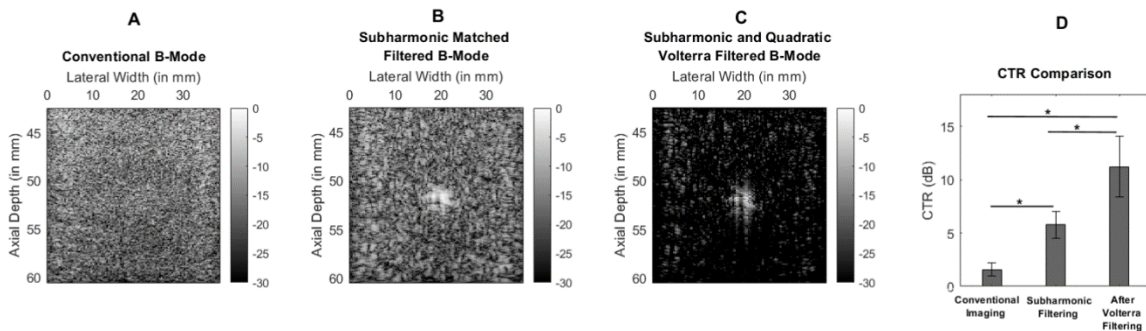


Fig. 1. **A)** Conventional image. **B)** After applying subharmonic matched filter. **C)** After applying quadratic Volterra filter. **D)** Comparison of CTR (mean \pm SD, N=30). (* denotes $p < 0.0001$).

P2-23

Evaluation of 8 mm Diameter Miniature Histotripsy Transducers of Various Operating Frequencies (4, 5 and 6 MHz)

Presenter: Justin Greige

Authors in order: Justin Greige, *Dalhousie University*, Matthew Mally, *Dalhousie University*, Jeremy Brown, *Dalhousie University*

To Evaluate and chracterize the sensitivity and cavitation threshold of Pz39 ceramic transducers of varying operational frequencies

Six transducers were fabricated by bonding Pz39 ceramic to an 8mm diameter lens with 7mm focus.

Two transducers of each thickness were fabricated for frequencies of 4Mhz, 5Mhz and 6MHz.

Transmit sensitivities were measured using a hydrophone and the cavitation thresholds in water were measured using a custom system for acoustic cavitation detection.

Results are extrapolated using HITU Simulator v2.0 data.

Measured transmit sensitivities increased as piezo frequency increases due to higher E-field for a given voltage and higher focal gain. The maximum sensitivity for the 4, 5 and 6 MHz transducers occurred at 5.1, 5.7 and 7.6 MHz respectively, while cavitation thresholds in distilled water were 280, 197 and 180 Vpp when operated at those frequencies. Although cavitation above 7 MHz became less pronounced compared to 5-7MHz. The linearly extrapolated cavitation threshold pressure increased with frequency. Extrapolating the results using non-linear simulations suggested that the peak negative pressure required for cavitation increases with frequency.

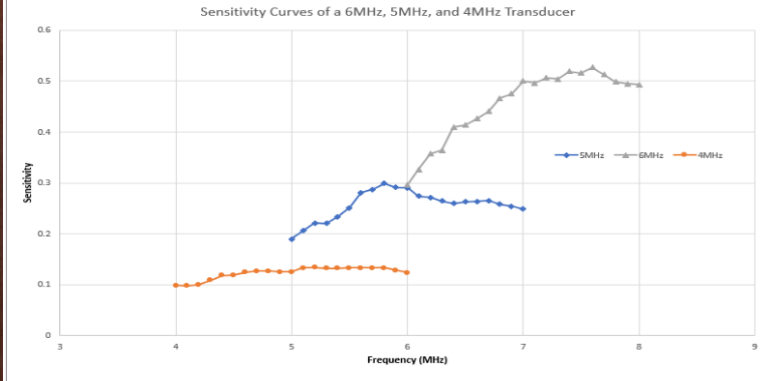
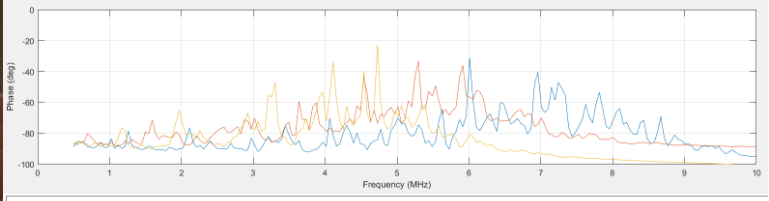
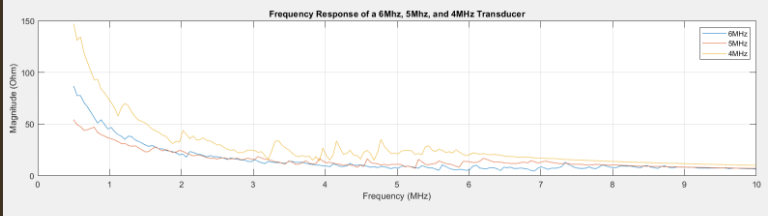
Six 8mm diameter miniature histotripsy transducers were fabricated at three operational frequencies.

Measured sensitivities agreed decently with KLM simulations.

Cavitation threshold measurements suggest that 5MHz had the best performance.

The optimal operating frequency is a balance between sensitivity and cavitation threshold.

Dr. Jeff Woodrace, Dr. Thomas Landry, and my supervisors Mr. Mathew Mally and Dr. Jeremy Brown



Feasibility Assessment of Aerosolized Contrast to Enhance Airway Imaging

Presenter: Phillip Durham

Authors in order: Phillip Durham, *Eshelman School of Pharmacy, University of North Carolina at Chapel Hill*, Paul Dayton, *The University of North Carolina at Chapel Hill*, Phillip Clapp, *The University of North Carolina at Chapel Hill*, Jamie Antinori, *The University of North Carolina at Chapel Hill*, Rachel Walmer, *The University of North Carolina at Chapel Hill*, Jessica Chlebowski, *The University of North Carolina at Chapel Hill*, Melissa Caughey, *The University of North Carolina at Chapel Hill*

A respiratory route of microbubble contrast agent (MCA) administration has not been previously described for the enhancement of airway imaging.

Microbubbles were dispensed into a jet nebulizer which was actuated into a water bath and imaged via contrast pulse sequence. Ultrasound imaging was performed on an agar-embedded ex vivo porcine trachea before, during and after nebulized contrast was delivered through the trachea. Additionally, bronchial epithelial cells cultured at the air-liquid interface were exposed to contrast and characterized for inflammation and viability. An aspiration model was used to visualize contrast in the murine airway.

Contrast microbubbles remained intact following nebulization and were visible in contrast specific imaging modes. Nebulized microbubble solution enhanced sonographic delineation of ex vivo porcine tracheal walls, indicating adherence of the nebulized MCA to the luminal mucosa. No significant cytotoxic or inflammatory effects were observed in cultured hBE cells following exposure to MCA. Delineation of the murine airway was achieved following aspiration of microbubble contrast on dual frequency contrast specific ultrasound imaging in vivo.

We present proof-of-concept for an inhaled MCA for the enhancement of sonographic evaluations of the large airways. Pending further evaluations for safety and effectiveness, inhaled MCA may be feasible for clinical ultrasound applications, such as enhancing ultrasound-guided tracheal intubation, detecting airway bleeds, or monitoring large airway diseases in pediatric populations.

A Spinal “Back-Door” Approach for Gene Delivery into the Brain: An Alternative to Ultrasound BBB Opening Method

Presenter: Hiroshi Kida

Authors in order: Hiroshi Kida, *Fukuoka University*, Yutaro Yamasaki, *Fukuoka University*, Hitomi Endo, *Fukuoka University*, Loreto Feril, *Fukuoka University*, Katsuro Tachibana, *Fukuoka University*

The aim of this study is to establish a novel gene delivery system to the brain by ultrasound and bubble reagent without opening the BBB.

Eight-week-old male BALB/c mice anesthetized were used. One hundred μ L of solution containing albumin-based nanobubbles and 2 μ g pDNA (pNL1.3.CMV [secNluc/CMV]) was intrathecally injected. Five minutes after the injection, ultrasound (US) of 1 MHz, 5 W/cm², 30 sec was irradiated from the midline of the occipital bone toward the brain. After 48 hours, D-luciferin was injected intraperitoneally and 10 minutes later luminescence was measured using IVIS to observe gene delivery to the brain.

Relative luminescence unit (RLU) value of US irradiation area of head was 1.53×10^4 , which was 65.11 folds that of mouse without pDNA+NBs injection. Highly efficient gene transfer to the brain was achieved. Damage to the skin or neurological disorder was not observed.

Intrathecal "Back-Door" approach may become an alternative gene delivery method to the brain replacing BBB Opening.

Influence of Nanobubble Size Distribution on Ultrasound-mediated Plasmid DNA and Messenger RNA Gene Delivery

Presenter: Hiroshi Kida

Authors in order: Hiroshi Kida, *Fukuoka University*, Hitomi Endo, *Fukuoka University*, Loreto Feril, *Fukuoka University*, Yutaka Irie, *Fukuoka University*, Keiji Itaka, *Tokyo Medical and Dental University (TMDU)*, Katsuro Tachibana, *Fukuoka University*

The aim of this study is to optimize nanobubbles (NBs) for future therapies and understanding in more depth the mechanism of sub-micro scale sonoporation.

Various size of albumin-based NBs were examined in an in vitro ultrasound (1 MHz) irradiation or centrifugation (1000G or 5000 G) setup. The particle size and distribution of NBs were measured by Nano Sight. 100ng of carrier-free secreted NanoLuc (secNluc) pDNA or Gaussia luciferase (GLuc) mRNA was transfected into oral squamous carcinoma cell line (HSC-2) by ultrasonic irradiation at 1 MHz, 1-5 W/cm² in the presence of NBs.

NB size distribution measured revealed bubble diameter of 200 nm or more ($200\text{NB} \leq$) decrease with centrifugation or sonication physical stress treatment, while NBs smaller than diameter 200 nm ($< 200\text{NB}$) remained intact. These treated NB of various sizes were used for sonoporation gene transfer experiments. Results with pDNA showed that gene transfer efficiency in the presence of NB size of 254.7 ± 3.8 nm was 2.5 fold greater than those with 187.3 ± 4.8 nm. Similarly, carrier-free mRNA transfer efficiency increased in the same conditions.

It is suggested that NB size greater than 200 nm contributed more to the delivery of genes into the cytoplasm with ultrasound. Although further experiments are needed to understand the underlying mechanism for this phenomenon, the present results offer valuable information in optimizing of NB for future ultrasound-mediate gene therapy.

Ultrasound Modulation of Glymphatic System

Presenter: Ming-Yen Hsiao

Authors in order: Ming-Yen Hsiao, *National Taiwan University Hospital*, Yu-Ling Lin, Wei-Hao Liao, Chueh-Hung Wu, Wen-Shiang Chen ,

To investigate the effect of low-intensity transcranial ultrasound on glymphatic perfusion and possible involving pathways. To investigate the effect of low-intensity transcranial ultrasound on glymphatic perfusion

CSF tracer was injected into cisterna magna of mice to observe glymphatic influx. Intracerebral injection of fluorescence tracer was used to measure glymphatic clearance. Low-intensity transcranial ultrasound was applied to one hemisphere. The coronal brain slices were imaged by fluorescent microscopy before and after stimulation. Fluorescence intensity and distribution territory of CSF tracer were analyzed. Immunohistochemistry and ELISA of brain tissues were performed to measure the expression of receptors related to regulation of glymphatic system.

After ultrasound stimulation the distribution area and fluorescent intensity of CSF tracer in the ipsilateral and contralateral hemisphere significantly increased, and the retained intracerebral tracer was reduced, as compared with control group. The AQP4 and mechanosensitive receptors were upregulated after ultrasound stimulation.

Low-intensity transcranial ultrasound facilitates glymphatic perfusion. The possible mechanisms may include the interaction of ultrasound and mechanosensitive receptors, with upregulated AQP4 receptors.

Effectiveness of 3 MHz Ultrasound in Ex-vivo Scleral Delivery of Macromolecules of Different Sizes

Presenter: Hanaa Almogbil

Authors in order: Hanaa Almogbil, *George Washington Univeristy*, Fadi P. Nasrallah, *Retina Consultants, Washington DC*, Vesna Zderic, *The George Washington University*

Therapeutic ultrasound offers a novel approach for enhancing scleral delivery of macromolecules for treatment of various ocular diseases.

We tested 3 MHz ultrasound in an ex vivo whole eye rabbit model by using fluorescently-labeled FITC-dextran of various sizes (40, 70 & 150 kDa) to mimic the sizes of the current macromolecules drugs for treatment of retinopathies. 3 MHz ultrasound was applied for 5 minutes on the sclera of the eye submersed in a macromolecule solution, and then the eyes were left in the solution for an additional 55 minutes while in the water bath at 34.6°C.

Our previous in vitro diffusion cell studies showed that 3 MHz ultrasound could enhance scleral delivery of Avastin (MW: 149 kDa). The fluorescence intensity of ultrasound-treated group was 1839996 (Mean SD) and 1463503, and the sham-treated group had 1136138 and 1344264 using FITC-150 and FITC-70, respectively. Thermal simulations demonstrated a temperature rise of 4.6 °C, while experimentally the average and the maximum temperatures were 2.2 and 4.4 °C, respectively.

Our preliminary results suggest that ultrasound at 3 MHz and 1 W/cm² may be effective in the delivery of macromolecules through the sclera. These results open the door for the development of a clinical potential approach for minimally invasive treatment of retinopathies and other vision-threatening diseases.

P2-3

Influence of a Dual-frequency Excitation on the Inertial Cavitation Threshold in Various Viscoelastic Mediums

Presenter: Tatiana Filonets

Authors in order: Tatiana Filonets, *National Taiwan University*, Maxim Solovchuk, *National Health Research Institutes*

Simulation study of the inertial cavitation, its dependency from dual-frequency ultrasonic excitation in various viscoelastic mediums, and temperature behavior inside/outside of the collapsed bubble.

For the modeling of bubble dynamics, we used the Gilmore-Akulichev-Zener (GAZ) model. Inertial cavitation threshold behavior was investigated for different values of initial bubble size, frequency, tissue viscosity, and elasticity. The optimal thresholds and the corresponding optimal frequency combinations have been found for all considered initial bubble radii simultaneously. GAZ model was combined with models of inside and outside bubble temperature to investigate the temperature behavior during bubble collapse.

Using optimal dual-frequency signal is able not only to significantly reduce the threshold pressure but keep the same threshold pressure for different initial bubble sizes. Moreover, when using optimal frequencies in the dual-frequency signal, tissue elasticity has a much stronger effect on the threshold than tissue viscosity. Viscoelastic properties of tissue impact the optimal frequency values. For high viscosities frequencies are small and almost the same whereas for minor viscosities the optimal frequencies have different values. An increase in elasticity leads to the enhancement of the optimal frequency values.

This study presents a detailed analysis of the inertial cavitation in the soft tissue under the dual-frequency driving signal and can be helpful for the further development of different applications of biomedical ultrasound.

This work was supported by the National Health Research Institutes, Taiwan [BN-109-PP-08] and the Ministry of Science and Technology, Taiwan [MOST 110-2221-E-400-001-MY2].

Claudin-5 Binder Enhances Focused Ultrasound-Mediated Opening In-vitro

Presenter: LIYU CHEN

Authors in order: LIYU CHEN, *Queensland Brain Institute*, Ratneswary Sutharsan, Jonathan Lee, *Queensland Brain Institute*, Esteban Cruz, Blaise Asnicar, *University of Queensland*, Tishila Palliyaguru, Gerhard Leinenga, *The University of Queensland*, Jürgen Götz, *University of Queensland*

To lower the risk associated with high acoustic pressure focused ultrasound-mediated blood-brain barrier opening, we explored preincubation with a claudin-5 binder to lower this threshold.

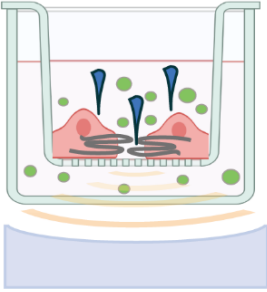
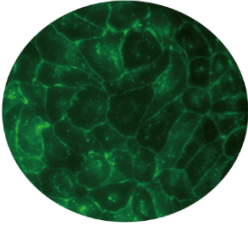
We generated a stable MDCK II cell line (eGFP-hCldn5-MDCK II) that expresses fluorescently tagged human claudin-5. Two claudin-5 binders, mC5C2 (a peptide) and cCPEm (a truncated form of an enterotoxin) were synthesized and assessed for their abilities to enhance the permeability of cellular monolayers. We then performed a comparative analysis of single and combination treatments, measuring transendothelial electrical resistance (TEER) and cargo leakage, combined with confocal image analysis.

The novel cell line formed functional monolayers as validated by an TEER reading and a low (< 0.2%) permeability to sodium fluorescein (376 Da). The two binders exerted a time- and concentration-dependent effect on BBB opening when incubated over an extended period, whereas FUS+MB caused a rapid barrier opening followed by recovery after 12 hours within the tested pressure range. Importantly, preincubation with cCPEm prior to FUS+MB treatment resulted in greater barrier opening compared to either FUS+MB or cCPEm alone as measured by reduced TEER values and an increased permeability to fluorescently labelled 40 kDa dextran. (doi:10.7150/thno.65539)

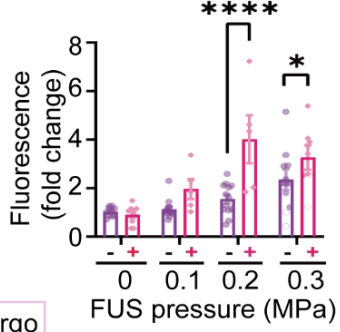
The data suggest that preincubation with clinically suitable binders to BBB tight junction proteins may be a general strategy to facilitate safer and more effective focused ultrasound-mediated BBB opening in cellular and animal systems and potentially also for the treatment of human diseases of the brain.

We thank Drs Lotta Oikara and Anthony White for providing iBECs. We thank the QBI Microscopy facility for assistance with imaging.

hClaudin-5 transfected MDCK II cells



 Claudin-5  GST-cPEM  Ultrasound beam  Cargo



Acoustic Coupling Pads for the Control of Ultrasound Neuromodulation Exposure

Presenter: Samantha Schafer

Authors in order: Samantha Schafer, *Drexel University*, Mark Schafer, *Drexel University*

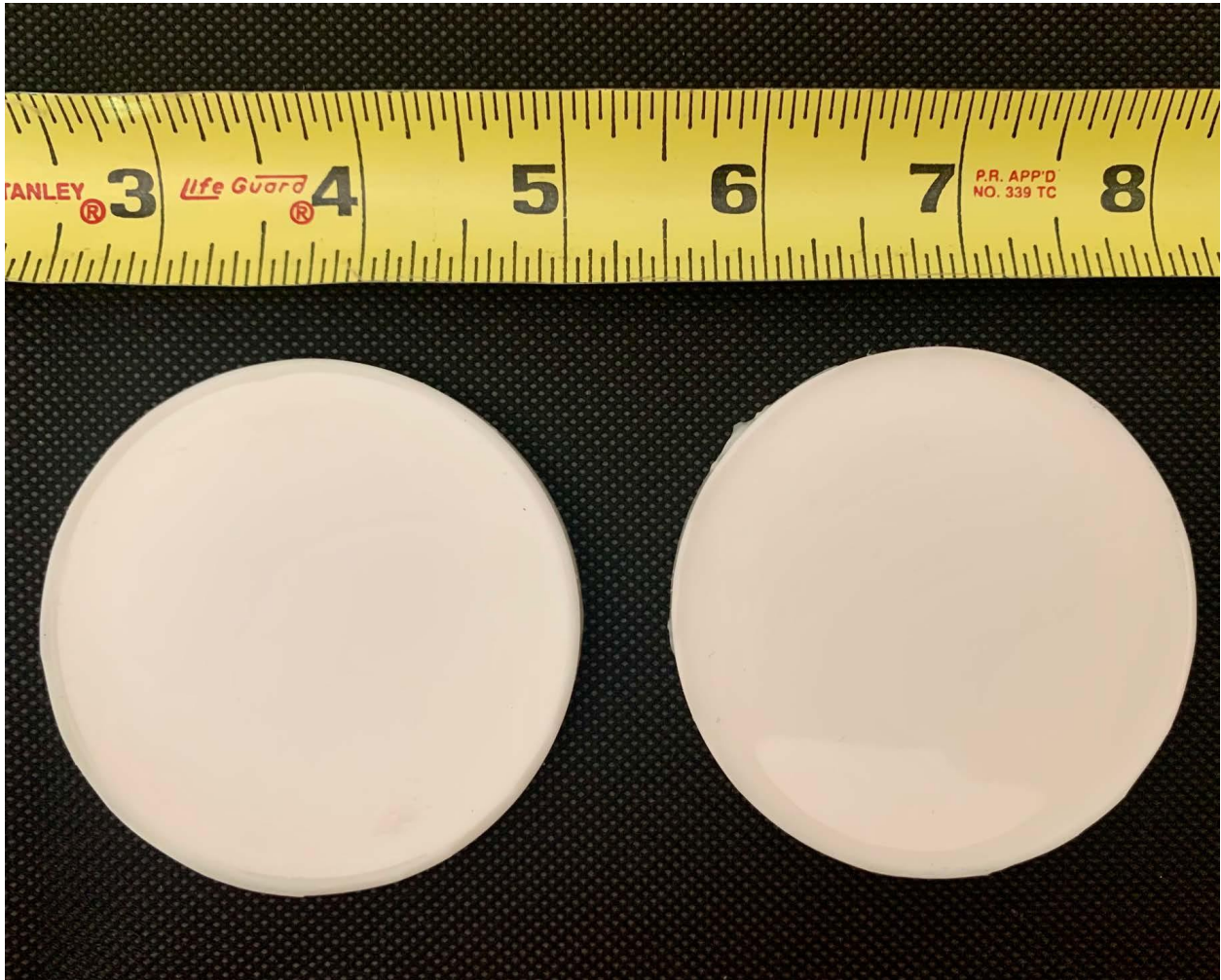
We have developed acoustic coupling pads that facilitate single-blind and double-blind neuromodulation experiments by selectively transmitting ultrasound without affecting the audible sound.

The pads were made from a skin-safe two-part silicone with little to no ultrasonic attenuation, that also provided the necessary acoustic properties, mechanical stability and flexibility. In order to inhibit the transmission of ultrasound, a foam disk was imbedded into the pad during the manufacturing process. The design goal for acoustic attenuation was -40dB (factor of 10,000 in intensity). Pads are assigned individual serial numbers so that testing can be unblinded later.

Ten sets of transmit pads and non-transmit pads (see Figure) were fabricated. Acoustic transmission loss was measured in a water tank with a 60mm diameter, 80mm focus circular disk transducer operated at 650kHz and a standard hydrophone (Reson TC4038). Transmit pads had an average of -0.5dB loss (2% variation); non-transmit pads met the required -40dB loss (average: -46.6dB). An operator experienced with ultrasound treatments was unable to distinguish them by visual inspection or casual physical manipulation. An experienced subject exposed to a typical treatment regimen, once using each type of pad, was not able to distinguish any audible difference.

The acoustic coupling pads create identical testing situations for single-blind and double-blind studies for neuromodulation treatments so that neither the patient nor the operator administering the treatment can distinguish which patient group received the ultrasound treatment and which did not.

Work funded by Brainsonix, Inc. Acoustic coupling pads are patent pending.



Imaging Mechanisms of Therapeutic Ultrasound in Human Islets In-vitro

Presenter: Andrew Chen

Authors in order: Andrew Chen, *The George Washington University*, Aleksandar Jeremic, Vesna Zderic, *The George Washington University*

We aim to explore mechanisms of therapeutic ultrasound (TUS) on the pancreas the physiologically relevant human islet model for potential therapies for type 2 diabetes.

Fluorescence microscopy was performed on live human islets with dyes that can label for intracellular calcium, sodium and reactive oxygen species (ROS). During microscopy TUS was applied at 800 kHz at 0.5 W/cm² with a pulse repetition frequency of 0.166 Hz and a 16.6% duty cycle for 3 minutes. The amount of insulin released from human islets as a result of TUS application was quantified with an enzyme-linked immunoassay (ELISA).

Thus far, we have noticed a trend of increased intracellular sodium and ROS generation due to TUS application however the percent increase in ROS appears to be less than for intracellular sodium. Our initial ELISA results show that TUS does appear to increase insulin release from human islets ($0.55 \pm 0.90 \mu\text{U/ml/min}$) when compared to control ($-0.14 \pm 0.19 \mu\text{U/ml/min}$) however not as much as with high glucose application at 20 mM ($2.47 \pm 3.54 \mu\text{U/ml/min}$).

Ongoing studies aim to increase sample number to improve confidence in our current observations. ELISA results match trends in previous studies on rodent cell lines. It is promising that TUS mobilizes sodium more than ROS generation, we would like to optimize TUS to minimize the amount of ROS generation.

The Cost-Effectiveness of Unilateral MRgFUS Thalamotomy for Medically Refractory Essential Tremor in England, UK

Presenter: Ayesha Jameel

Authors in order: Ayesha Jameel, *Imperial College*, Anne Meiwald, *Aquarius Population Health*, peter bain, *IMPERIAL COLLEGE*, neekhil patel, *Imperial College London NHS Trust*, dipankar dipankar.nandi, *IMPERIAL COLLEGE HEALTHCARE NHS TRUST*, brynmor jones, *IMPERIAL COLLEGE HEALTHCARE NHS TRUST*, georgie weston, *Aquarius Population Health*, Elisabeth Adams, *Aquarius Population Health*, wladyslaw gedroyc, *IMPERIAL COLLEGE HEALTHCARE NHS TRUST*

This study aims to ascertain the cost-effectiveness of unilateral MRgFUS for the treatment of medically refractory Essential Tremor (mrET) in England, United Kingdom (UK)

A Markov model was used to assess two sub-populations of mrET- those eligible and those ineligible for neurosurgery - in a context specific to England's healthcare system. For those eligible for neurosurgery, MRgFUS was compared to deep brain stimulation (DBS), the current standard treatment. For patients ineligible for neurosurgery, MRgFUS was compared to treatment with medication alone. The model calculated the Incremental Cost-Effectiveness Ratio (ICER) with appropriate sensitivity and scenario analyses.

For those eligible for neurosurgery: In the model base case, MRgFUS was economically dominant compared to DBS: MRgFUS was less costly (£19,779 vs £62,348) and more effective, generating 0.03 additional QALYs (3.71 vs 3.68) per patient over the 5-year time horizon.

For those ineligible for neurosurgery: In the model base case, MRgFUS cost over £16,000 more than medication alone (£19,779 vs £3,735) but yielded 0.77 additional QALYs (3.71 vs. 2.95) per patient, producing an ICER of £20,851 per QALY gained. This ICER falls within the National Institute of Clinical Excellence (NICE) willingness to pay threshold (WTP) of £20,000-30,000 per QALY

This study demonstrates the favourable cost-effectiveness profile of MRgFUS treatment for mrET in England in both sub-populations of ET assessed (patients who are suitable and those who are not suitable for DBS). This study, the first in Europe, provides a basis for future brain MRgFUS commissioning in the UK, Europe and globally.

Relation Between In-vitro Microbubbles Cavitation Threshold and In-vivo Blood-Brain Barrier Opening (BBBO)

Presenter: Alexis Vivien

Authors in order: Alexis Vivien, *Bracco Suisse SA*

Highlight size-dependance of microbubble cavitation and therapeutical potential before microbubble collapse by linking in-vitro inertial cavitation thresholds with in-vivo Blood-Brain Barrier Opening (BBBO)

In-silico Matlab simulations were done to modelize the radius evolution of a single microbubble with time, following Marmottant's model, cavitation threshold was defined as Blake critical radius, beyond wich the microbubble enters explosive growth.

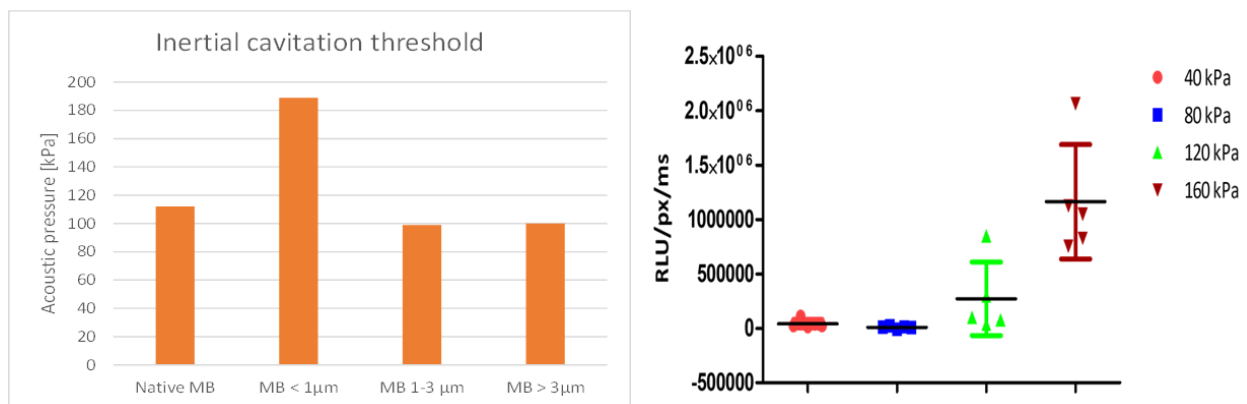
Cavitation thresholds were determined in-vitro on a home-made polydisperse formulation and its monodisperse sub-populations obtained through filtering. Broadband noise was chosen as the metric defining inerial cavitation.

In-vitro thresholds were then verified in-vivo in a rat BBBO model with a fluorescent dye.

Smaller microbubbles (In-vivo fluorescence was detected at acoustic pressures of 120 kPa and beyond, very close to the in-vitro value of 110 kPa and below the Blake threshold, hence potentially indicating safe treatment.

This study highlights the close relation between cavitation and BBBO, despite the differences thajt might exist between in-vitro and in-vivo cavitation onset due to bubble confinement in vessels or fluid viscosity change (water/blood).

Moreover, it supports the use of cavitation detection as a mean to prevent biological damages.



The Role of Boosting based Machine Learning Algorithms in Predicting the Outcome of HIFU Ablation of Uterine Fibroids

Presenter: Emine Akpınar

Authors in order: Emine Akpınar, *Yıldız Technical University*, Onur Bayrak, *Yıldız Technical University/IHIRC*, Bilgin Keserci, *Universiti Sains Malaysia*

To evaluate the role of boosting based ML algorithms for predicting the treatment outcome of HIFU ablation with an NPV ratio of at least 90%.

We, in this study, used multiparametric (mp) MRI features including anatomical characteristics of patients and tissue characteristics of lesion outlining its cellularity, diffusivity, and vascularity. Five ML classifiers—including Adaboost classifier, Gradient boosting (GBM) classifier, XGBOOST classifier, CatBoost classifier, LightGBM Classifier, HistGradientBoosting classifier and ensemble model that consist of the combination of these classifiers were used. For the evaluation of the classifier performance, cross validation score was utilized.

The whole data set of 73 patients was split into 4 groups by performing the 4-fold cross validation to evaluate generalizability and accuracy of the model. The best classifier performance was achieved using ensemble model whose cross-validation score was 0.96. XGBOOST classifier showed the secondary predictive performance with cross validation score 0.95, followed by HistGradientBoosting, Adaboost, CatBoost, LightGBM and GBM classifiers (cross validation score: 0.93, 0.92, 0.92, 0.90 and 0.89), respectively.

This preliminary study indicates that ML algorithms should be considered in assisting physicians to fully evaluate the outcome of the HIFU therapy.

Numerical Approach for Treatment Planning and Aberration Correction for Renal HIFU Ablation Based on Computed Tomography Data

Presenter: George Schade

Authors in order: Pavel Rosnitskiy, *Lomonosov Moscow State University*, Tatiana Khokhlova, *University of Washington*, George Schade, *UNIVERSITY OF WASHINGTON*, Oleg Sapozhnikov, *University of Washington*, Vera Khokhlova, *Physics Faculty, Lomonosov Moscow State University, Moscow, Russian Federation*; *Center for Industrial and Medical Ultrasound, University of Washington, Seattle, United States of America*

The goal of this work was to develop a numerical approach for HIFU treatment planning with aberration correction in kidney using computed tomography (CT).

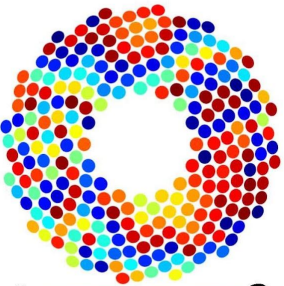
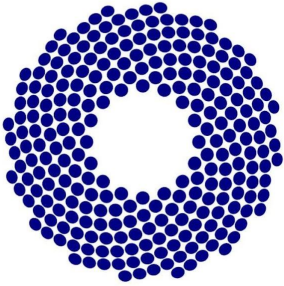
CTs from three anonymous renal cell carcinoma patients were partitioned into segments with different acoustic attenuation. The density and sound speed distributions were determined from the radiodensity. A quantitative strategy was proposed for positioning a 1.5-MHz 256-element spiral array (Fig. A) within an acoustic window to achieve most beneficial incident angle and minimize bone presence (Fig. B). Field simulation and aberration correction were based on combining the pseudospectral (k-Wave) and ordinary least squares (OLS) methods.

The proposed aberration correction method provided tight focusing through the identified optimal acoustic windows. The pressure amplitude at the focus increased by factors of 2.39, 1.81, and 3.02, respectively, for the three patients vs. focusing without correction (Fig. C). The OLS correction method yielded a 8–31% enhancement of the focusing gain vs. conventional backpropagation of the virtual point source field from the focal point to the centers of the array elements. Additional 10–24% amplitude increase was observed when focusing at the field maximum of the initially distorted beam as opposed to the center of the array curvature.

The proposed numerical approach for treatment planning and aberration correction provided tight focusing quality for HIFU-ablation of renal cell carcinoma in models of real patients. The combination of pseudospectral and OLS methods for correcting aberrations shows a threefold improvement in the maximum pressure amplitude in the target area.

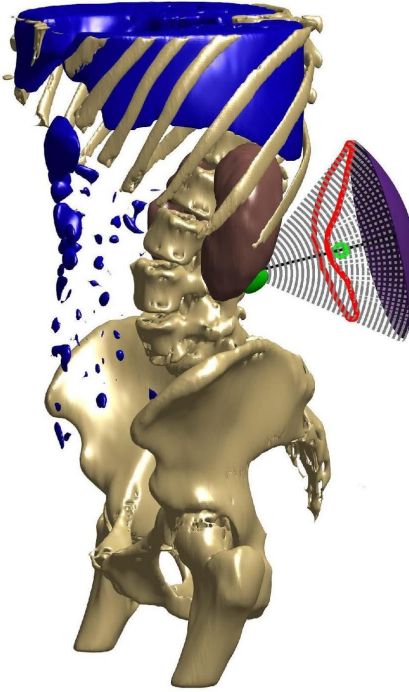
Work supported by RSF 20-12-00145 and NIH R01EB007643.

(A) Phases at the array elements

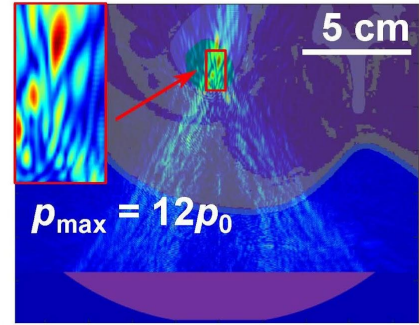


0  2π

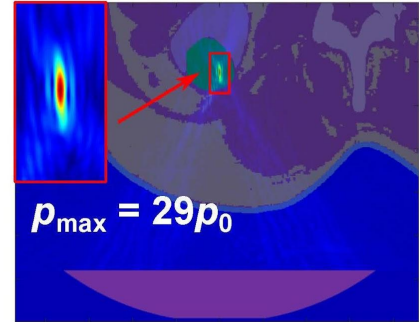
(B) Focusing geometry



(C) No correction



After correction



Volumetric Analysis of Thermal Dose and Vascular Perfusion in MR-HIFU Ablation of Pediatric Osteoid Osteoma

Presenter: Reshma Modi

Authors in order: Reshma Modi, *Children's National Medical Center*, Caitlin Tydings, *Children's National Medical Center*, Ari Partanen, *Profound Medical Corporation*, Haydar Celik, *Children's National Medical Center*, Aerang Kim, *Children's National Medical Center*, Matthew Oetgen, *Children's National Medical Center*, Karun Sharma, *Children's National Medical Center*, Pavel Yarmolenko, *The Sheikh Zayed Institute for Pediatric Surgical Innovation*

To improve guidance of osteoid osteoma ablation with MR-guided high-intensity focused ultrasound (MR-HIFU), we developed software enabling 3D visualization and evaluation of cumulative thermal dose.

Our MATLAB toolkit assembled 2D MRI thermometry datasets from multiple sonication targets into 3D datasets to allow for multi-plane visualization of cumulative thermal dose. The nidus (central zone) of an osteoid osteoma, surrounding bone, and non-perfused treatment volume (NPV) were manually segmented on pre-treatment T1, post-treatment T2w, and post-treatment contrast-enhanced subtraction MRI, respectively. The toolkit calculated spatial overlap between clinically-relevant combinations of nidus, bone, NPV, and 3D thermal dose data (outside the bone).

Retrospective analysis was performed on treatment data from 13 pediatric patients (10M, 3F, median age: 12) from two MR-HIFU clinical trials (NCT02349971, NCT04658771). Perfusion was eliminated in a median of 80.4% (range: 28.9 - 100%) of the nidus volume. A median of 72.6% (42.9 - 98%) of NPV was confined to the bone. Outside the bone, 59.1% (6.3 - 87.9%) of NPV did not overlap with lethal thermal dose and 74.8% (7.3 - 97.6%) of the lethally dosed volume retained perfusion immediately after treatment. Soft tissue NPV and thermal dose had a Dice similarity coefficient of 0.24.

Reconstruction of cumulative 3D thermal dose maps of the entire treatment enabled visualization and quantitative assessment of treatment extent. The analysis reveals that NPV was preferentially confined to the targeted bone, and that lethal thermal dose in soft tissue may not reliably indicate cessation of vascular perfusion.

This work was supported by the Sheikh Zayed Institute for Pediatric Surgical Innovation.

Towards a Mechanistic Understanding of Therapeutic Ultrasound as a Treatment Modality for Alzheimer Disease

Presenter: Jürgen Götz

Authors in order: Jürgen Götz, *University of Queensland*, Gerhard Leinenga, *The University of Queensland*, Jae Hee Song, *University of Queensland*, Dan Blackmore, *University of Queensland*

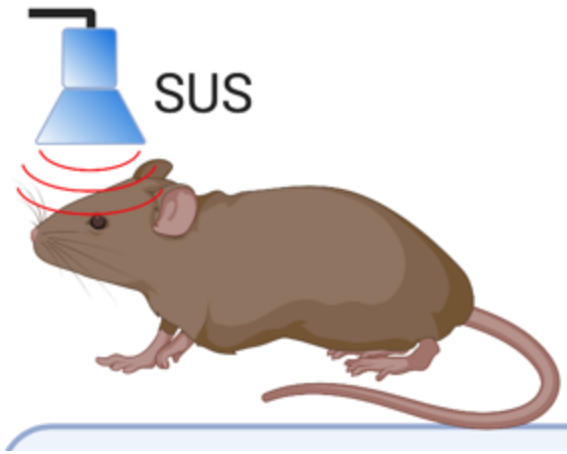
We are interested in understanding the bio-effects of ultrasound used with (BBBO/neuromodulation) and without microbubbles (neuromodulation) in mouse models of senescence and Alzheimer's disease.

We explored two ultrasound strategies, scanning ultrasound with microbubbles (SUS+MB) which achieves blood-brain barrier opening, and scanning ultrasound without microbubbles (SUSonly), over a range of ultrasound parameters in amyloid-depositing APP23 mice and senescent wild-type mice, with several weekly treatment sessions. Analysis tools included an extensive behavioural, electrophysiological, biochemical, histological, proteomics and imaging (MRI) analysis.

We will discuss data that reveal that SUS+MB reduces amyloid pathology and restores cognition (Leinenga & Götz, *ScienceTranslMed* 2015), that BBB opening is required for amyloid clearance (Leinenga et al., *BrainResBull* 2019) and whether SUSonly is sufficient to restore cognition (in progress). We will further discuss work that reveals that both SUS+MB and SUSonly restore LTP deficits and improve cognition in senescent mice via pleiotropic mechanisms including NMDAR-dependent signalling (Blackmore et al., *MolPsych* 2021). Finally, we will discuss the development of a clinical-trial ready device as part of setting up a therapeutic ultrasound platform.

We conclude that therapeutic ultrasound is a non-invasive modality for the treatment for Alzheimer's disease and other brain diseases. We also conclude that this modality has the potential of cognition enhancement in physiological aging.

Supported by Estate of Dr. Clem Jones AO, the National Health and Medical Research Council of Australia [GNT1145580], and the State Government of Queensland (DSITI).



Reflectors for Therapeutic Vortex Beam Generation

Presenter: Noe Jimenez

Authors in order: Noe Jimenez, *Universitat Politècnica de València*, Enrique González Mateo, *Universitat Politècnica de València*, José M. Benlloch, *Universitat Politècnica de València*, Francisco Camarena, *Universitat Politècnica de València*

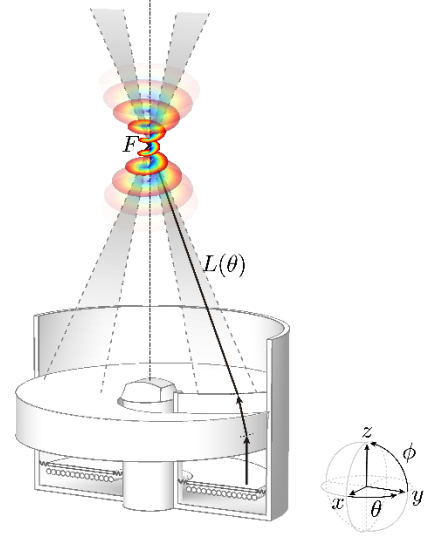
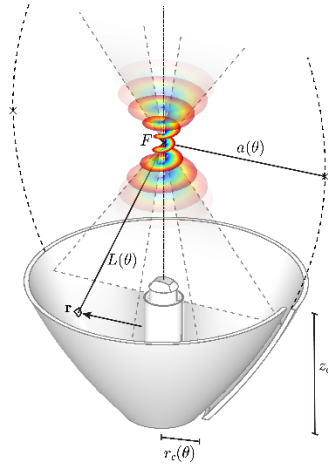
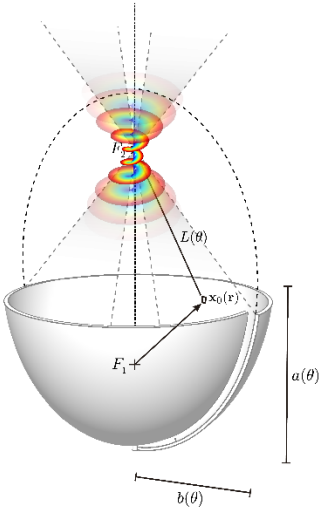
Vortex beams are currently used in many emerging therapeutical ultrasound applications. In this work, we present several reflectors to synthesize focused vortex beams for therapeutical ultrasound.

We present the design equations of several topologies of reflectors to generate focused vortex beams. By using geometrical methods, we derived the parametric surfaces for helico-elliptical vortex reflectors using electrohydraulic sources, helico-parabolic vortex reflectors and convex helicoidal lenses using electromagnetic sources. Using pseudo-spectral time-domain methods, the performance of these topologies is compared with other known vortex generators, such as therapeutical phased array systems or spiral diffraction gratings.

Results show that helico-elliptical reflectors, helico-parabolic reflectors, and helical lenses can generate focused vortex beams containing phase dislocations. The topological charge of the vortices at the design frequency can be tuned by the design equations. We observe that vortices with integer topological charge emerge at the design frequency, while vortices of fractional topological charge are observed at other frequencies. While these structures can focus broadband acoustic vortices, phase dislocations cannot be generated at low frequency and reflected pulses generate vortices of fractional topological charge. The pressure gain of the different vortex generators is compared.

Helico-elliptical and helico-parabolic reflectors efficiently generate focused vortices. While these complex wavefronts can be generated by phased arrays or lenses, the proposed mirrors do not introduce remarkable attenuation and, therefore, they can be used when a large mechanical amplitude is needed, such as in lithotripsy, histotripsy, or particle and tissue manipulation applications.

Research supported by the Spanish Ministry of Science, Innovation and Universities through grants PID2019-111436RB-C22, IJC2018-037897-I. Action co-financed by European Union grant IDIFEDER/2021/004.



Quantitative Assessment of Tissue Susceptibility to Boiling Histotripsy

Presenter: Alisa Krokhmal

Authors in order: Ekaterina Ponomarchuk, *Lomonosov Moscow State University, Physics Faculty*, Alisa Krokhmal, *Lomonosov Moscow State University, Moscow, Russian Federation*, Anastasia Tyurina, *Physics Faculty, Lomonosov Moscow State University, Moscow, Russian Federation*, Minhong Song, *University of Washington, Seattle, United States of America*, Gilles Thomas, *Center for Industrial and Medical Ultrasound, University of Washington, Seattle, United States of America*, Yak-Nam Wang, *Center for Industrial and Medical Ultrasound, University of Washington, Seattle, United States of America*, Vera Khokhlova, *Physics Faculty, Lomonosov Moscow State University, Moscow, Russian Federation; Center for Industrial and Medical Ultrasound, University of Washington, Seattle, United States of America*, Tatiana Khokhlova, *University of Washington*

In the context of boiling histotripsy (BH) dose development, quantitative relationships between the lesion parameters, pulsing protocols, and types of targeted tissue were investigated.

Volumetric BH lesions were produced in ex vivo porcine and canine liver and kidneys and bovine heart at 1% duty cycle with 1.5MHz 256-element BH array with varying exposure parameters: 1–10 ms pulses, 5–15 pulses per sonication point (ppp) (Fig.1A,B). Histological sections were taken throughout each lesion, stained with Masson's Trichrome (Fig.1C) and subjected to a combination of manual and automated segmentation of fully and partially liquefied tissue using neural network ResNet-18 (Fig.1D).

The developed neural network allowed for segmenting fully and partially liquefied tissue within the BH lesion in all considered tissue types with errors, relative to manually segmented images, not exceeding 3% of the analyzed image area. Automated segmentation of serial lesion sections and subsequent 3D-reconstruction provided the estimation of the lesion volume, percentage of the volume of intact tissue fragments within the lesion (Fig.1E), and the ablation rate (Fig.1F) for each tissue type and exposure parameter set. For example, in porcine liver 1-ms pulses with 5ppp provided the highest ablation rate, and the sensitivity was largely independent of exposure parameters.

BH protocols maximizing the ablation rate and the degree of tissue disintegration, were determined for ex vivo hepatic, cardiac and renal tissues.

Supported by Nonprofit Foundation for the Development of Science and Education "Intellect", FUSF Cultivate the Next Generation program and "BASIS" foundation student grant 20-2-10-10-1.

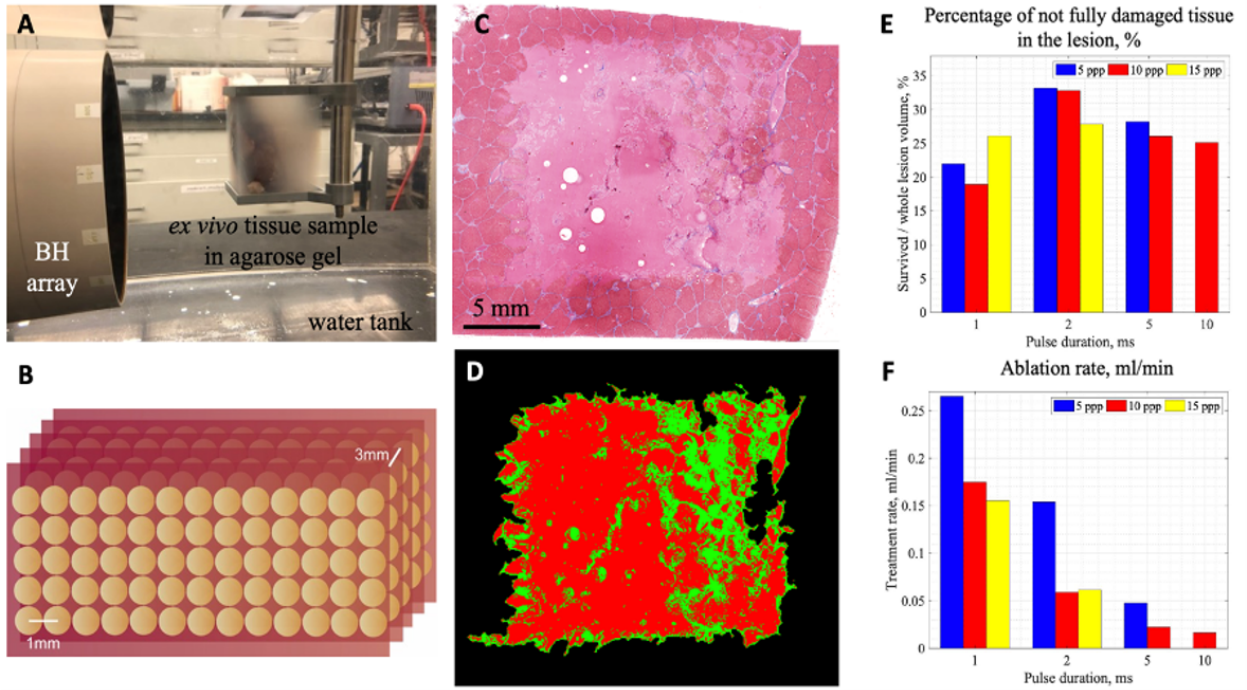


Figure 1. (A) Experimental setup. (B) Sonication geometry. (C) Histological image. (D) Computerized segmentation. (E,F) Results for liver.

Feasibility of the Noninvasive Gene Delivery to Large Brain Areas

Presenter: Shirin Nouraein

Authors in order: Shirin Nouraein, *Rice university*, Jerzy Szablowski, *Rice University*, Huckie Del Mundo,

We use focused ultrasound blood-brain barrier opening (FUS-BBBO) to test the maximum volume of the BBB that can be safely opened for gene delivery.

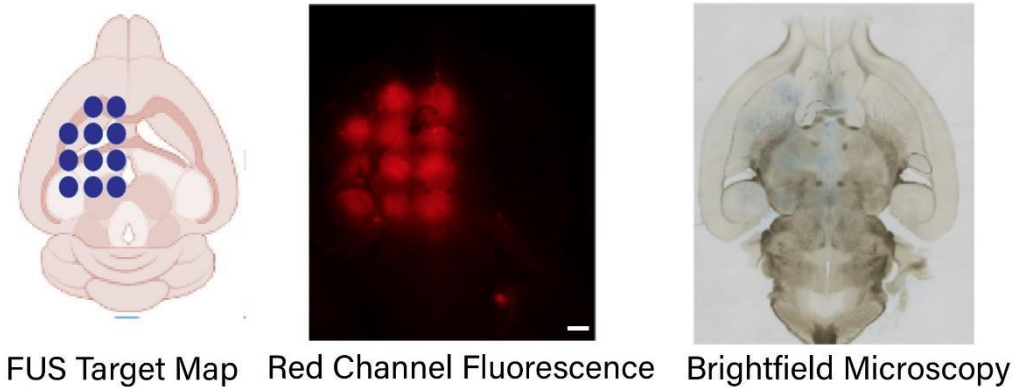
We targeted between 11 sites and 105sites, with latter covering majority of the brain, using various ultrasound parameters (0.27 – 0.36 MPa pressure, 1.5 MHz frequency, 10 ms pulse length, 30 pulses, 1 Hz pulse repetition frequency). During the parameter optimization, we used Evans blue dye [EBD] extravasation as a measure of efficacy, and red blood cell (RBC) extravasation as a measure of safety. Gene delivery was performed using AAV9 carrying GFP under CAG promoter.

We found EBD extravasation across all tested parameters. The pressure of 0.27 MPa was determined to be safe (A), with no RBC extravasation in any of the targeted sites (n=4), and was used for further studies. Delivery of AAVs carrying GFP under CAG promoter via FUS-BBBO (B) leads to 25-fold higher transduction compared to contralateral control (C). Histological analysis of GFP expression for 105-site targeting revealed expression was present in the whole volume of the brain including the cortex and cerebellum area, and transduction efficiency was highest in the Hippocampus (52.23%) followed by Striatum (49.17%), and Midbrain (47.06%) (D).

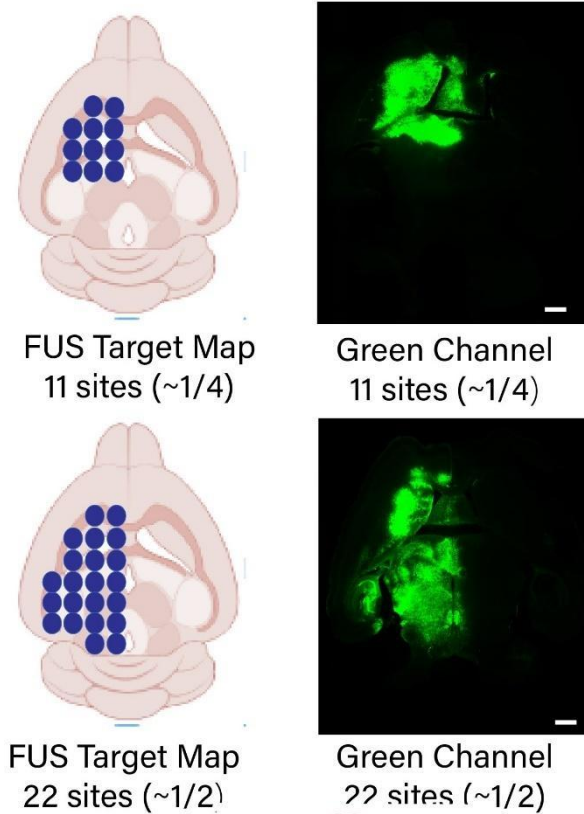
We found that FUS-BBBO can be used to target the majority of the BBB without serious adverse events or hemorrhage. Our data suggest that targeting large brain regions, or nearly entirely of the BBB for gene delivery is feasible with FUS-BBBO, suggesting possible applicability to large animal and clinical studies.

This work was supported by John S. Dunn Foundation.

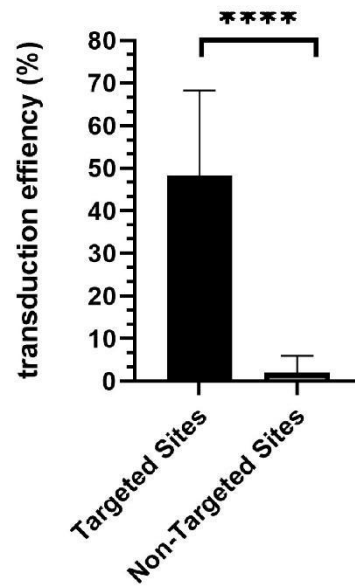
A



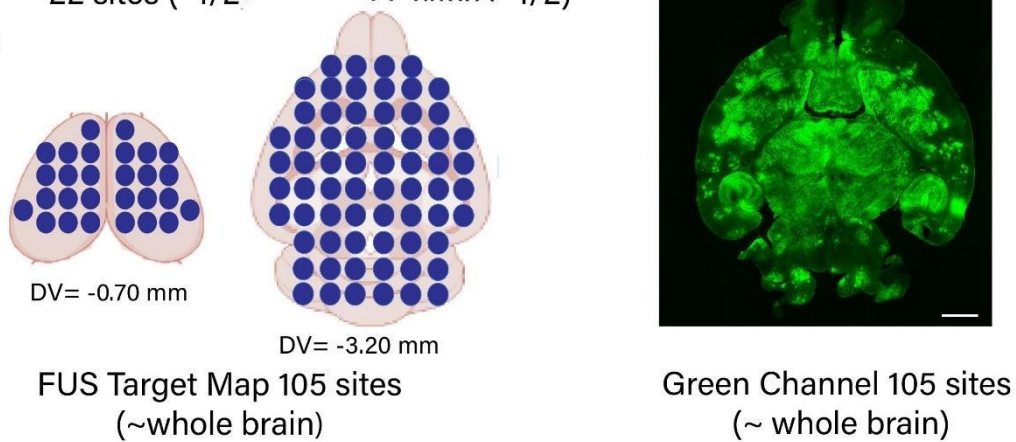
B



C



D



Control of the Extent of Lesion Formation in Pressure-modulated Shockwave Histotripsy (PSH) Approach: An In-vitro Study

Presenter: Jun Hong Park

Authors in order: Jun Hong Park, *Korea Institute of Science and Technology (KIST)*, Jeongmin Heo, *Korea Institute of Science and Technology*, Hyo Jun Kim, *Korea Institute of Science and Technology (KIST)*, Byung Chul Lee, *Korea Institute of Science and Technology (KIST)*, Ki Joo Park, *Kyung Hee University*

To demonstrate the effectiveness of PSH approach, the effects of variation of exposure conditions of PSH on lesion formation are investigated.

Bubble dynamics in liver tissue phantom were observed using a high speed camera and a passive cavitation detection systems under a 10 ms-long 2 MHz PSH pulse ($P_{1,+} = 89.1\text{MPa}$, $P_{1,-} = -14.6\text{MPa}$, $P_{2,+} = 29.9\text{MPa}$, $P_{2,-} = -9.6\text{MPa}$) with varying pressure modulation time interval (4 to 9 ms) and the number of pulses (1 to 50 pulses, PRF of 1 Hz). The extent of a PSH lesion in the phantom was measured and compared with a boiling histotripsy.

In the PSH method, the longer the pressure modulation time interval, the more the shock scattering-induced cavitation clouds formed. The extents of cavitation and PSH lesion size gradually increased with increasing the level of the cavitation clouds generation as well as the number of pulses applied (Fig. 1(a, b)). The PSH lesions were measured to be up to 2.5 times smaller than the BH lesions produced with the same number of pulses (PRF of 1 Hz) (Fig. 1(c)).

Our results showed that PSH approach can control the extent of mechanical damage through modulating the pressure modulation time interval and the number of pulses.

This work was supported by the National Research Foundation of Korea (NRF) and National Research Council of Science & Technology (NST) (No. NRF-2021R1C1C1008240, CAP-18-01-KIST).

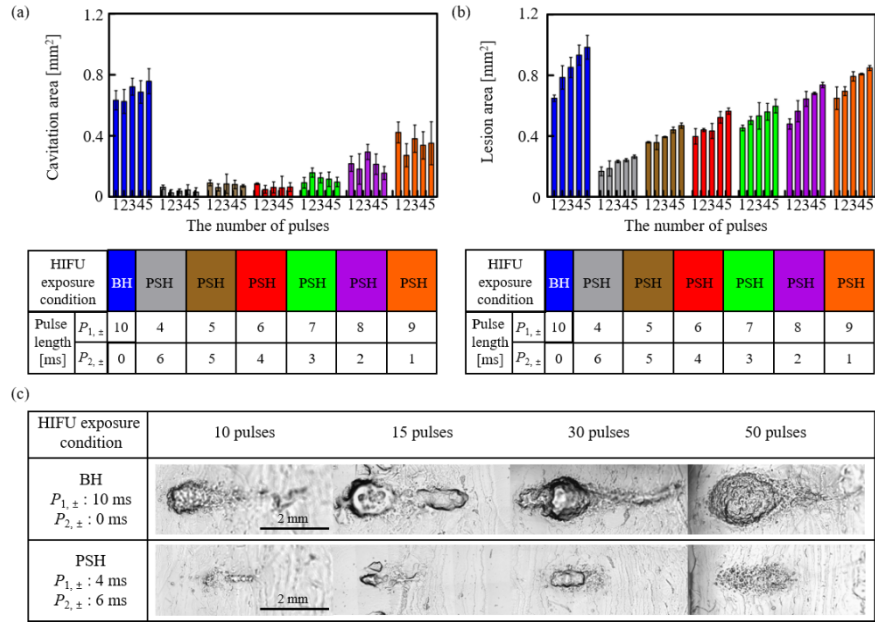


Fig. 1 (a) Cavitation area measured at the end of the exposure during boiling histotripsy (BH) or pressure-modulated shockwave histotripsy (PSH) with varying pressure modulation time interval (for PSH) and the number of pulses (1 to 5 pulses). (b) Measured lesion size produced in the phantom after the BH or PSH treatment (1 to 5 pulses). (c) Microscopic images of the cross-sectioned lesions induced in the tissue phantom after the BH or PSH treatment (10 to 50 pulses).

Recovery of Markers through Insonation: An Alternative to Monitoring Gene Expression in Deep Tissues

Presenter: Joon Pyung Seo

Authors in order: Joon Pyung Seo, *Rice University*, Jerzy Szablowski, *Rice University*, James Trippett, *Rice University*

We developed a method to noninvasively measure transgene expression in the specific brain regions using a blood test.

We use engineered protein reporters that are released from the cells into the brain interstitium. We call these reporters released markers of activity or RMA. We then use focused ultrasound (FUS) to transiently open the blood-brain barrier (BBBO) and release these reporters into the blood. The reporters then can be conveniently sampled. We call this approach REcovery of Markers through InSonation, or REMIS (Fig. 1a).

We show that levels of markers secreted from neurons into the serum correlate with the levels of transgene expression in the brain. We measured up to 5.5-fold increase of marker levels (Fig. 1b, c) in the blood after opening of 8% of the blood-brain barrier (BBB). We show the procedure is well tolerated and avoids significant tissue damage, consistent with other BBB opening studies.

Monitoring gene expression in deep tissues of living animals is critical for in vivo studies and translation of gene therapies. This technology allows for site-specific measurement of gene expression in the brain.

This work was partially supported by the Packard Fellowship for Science and Engineering, and the Michael J. Fox Foundation, grant #020154 to Szablowski JO.

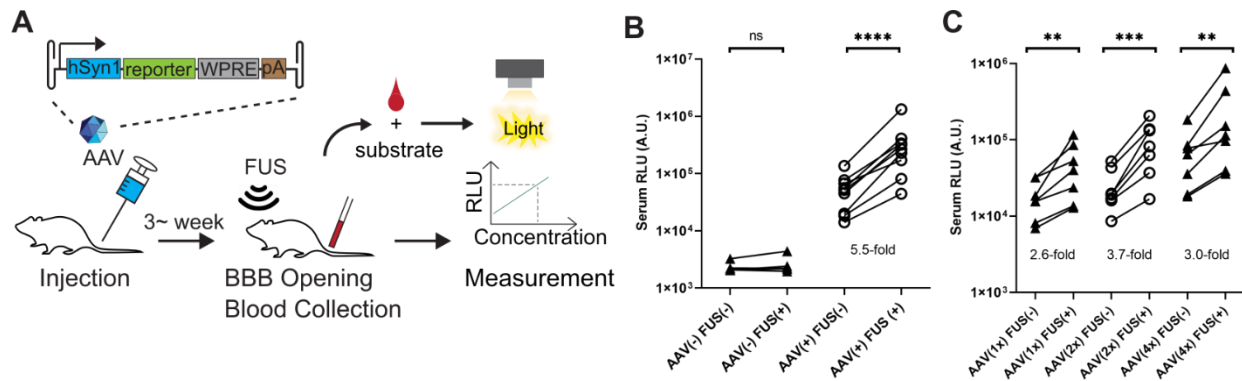


Figure 1 Recovery of RMA schematic (A) and results (B and C)

P3-1

The Effect of Inter-bubble Spacing of the Resonance Response of Phospholipid Encapsulated Ultrasound Contrast Agents

Presenter: Hossein Yusefi

Authors in order: Hossein Yusefi, *Concordia University*, Brandon Helfield, *Concordia University*

The objective of this work is to investigate the resonance response of a two acoustically-driven phospholipid-encapsulated bubble system in close proximity to each other.

We developed a finite element model using COMSOL to study the radial resonance response of microbubbles and nanobubbles within a two-bubble system, with bubble diameters ranging from 0.5-4 μm and bubble center-to-center distances $h=2-24 \mu\text{m}$. Bubbles were driven with a cosine-tapered 10 cycle pulse from 1-8 MHz and peak-negative pressures ranging from 30-200 kPa.

For two identical microbubbles, our results show the frequency of maximum response (f_{MR}) decreases (7-10%) and the amplitude of maximum response (A_{MR}) increases (9-11%) as the microbubbles approach one another. For a two-bubble system of different microbubble sizes, the larger bubble shows no change in f_{MR} and a slight shift of A_{MR} (2-3%). However, the smaller bubble exhibits an increase in f_{MR} (7-11%) and a significant decrease of A_{MR} (38-52%). Furthermore, in very close proximity, smaller bubbles exhibit a secondary resonance peak corresponding to the f_{MR} of the larger bubble, with amplitudes comparable to its primary resonance peak.

Our work highlights that microbubble resonance behaviour is greatly affected by the presence of nearby bubbles, which has implications in imaging and therapy. Furthermore, our work suggests a potential mechanism by which nanobubbles can elicit significant off-resonant vibrations within the clinical frequency range.

This work was funded by NSERC and the FRQNT.

Motion Compensation During MRgHIFU may Improve Thermosensitive Drug Release

Presenter: Suzanne Wong

Authors in order: Suzanne Wong, *University of Toronto*, Claire Wunker, *Luenfeld-Tanenbaum Research Institute*, Ben Keunen, *Hospital for Sick Children*, Karolina Piorkowska, *Hospital for Sick Children*, Maryam Siddiqui, *University of Calgary*, Yael Babichev, *Mount Sinai Hospital*, Warren Foltz, *University Health Network*, Rebecca Gladdy, *Mount Sinai Hospital*, Samuel Pichardo, *University of Calgary*, Adam Waspe, *Hospital for Sick Children*, James Drake, *Hospital for Sick Children*

To investigate the role of motion compensation during magnetic resonance-guided high-intensity focused ultrasound (MRgHIFU) controlled hyperthermia for mediated thermosensitive liposomal doxorubicin (TLD) release in vivo.

Immunocompetent mice (n=6) with hindlimb rhabdomyosarcoma received 20 minutes of MRgHIFU controlled hyperthermia with TLD (Figure 1) where tumour temperature was maintained at 40.5°C during treatment (Figure 2). The small-animal MRgHIFU system consisted of a 7T Bruker MRI (BioSpec, Germany) and Image Guided Therapy HIFU device (LabFUS, France). Retrospective motion compensation used principal component analysis and projection onto dipole fields (PCA-PDF). High performance liquid chromatography quantified the amount of doxorubicin that was delivered to tumours.

The average measured temperature in the sarcoma over the treatment was 40.1°C ± 0.2°C. Average rectal and esophageal temperatures were 36.8°C ± 1.5°C and 30.6°C ± 1.6°C, respectively. Retrospective PCA-PDF motion artifact removal predicted lower the average sarcoma temperature to 36.5°C ± 2.5°C, with some mice having varying degrees of thermometry motion artifacts. If accurate, this temperature discrepancy would be detrimental to drug release efficacy since the liposomal drug release decreases to only 15% when the average temperature falls below 37°C. Figure 3 displays a distinct relationship between average temperature after retrospective PCA-PDF analysis and doxorubicin levels in the sarcoma.

Motion artifacts corrupted the thermometry data from some of the mice leading to an overestimation of tumour temperature. As a result, the tumour may not have been optimally heated for drug release resulting in less doxorubicin delivered. Future experiments may benefit from real-time motion compensation to maximize drug delivery efficacy.

We thank Maria Bisa, the Allen Lab, and the SickKids AFBM for their help with this project. Funding provided by C17 Research Network and NSERC.

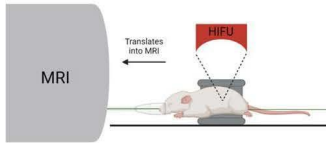


Figure 1: Experimental set-up for controlled hyperthermia administered by a small-animal MRgHIFU.

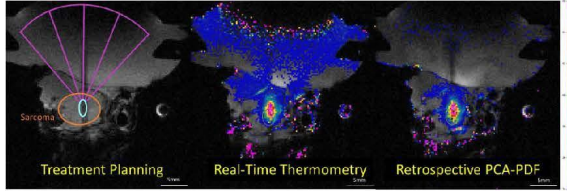


Figure 2: HIFU treatment planning, monitoring and retrospective motion analysis.

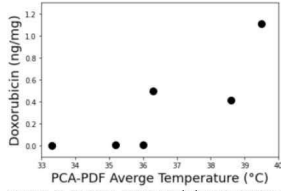


Figure 3: Motion corrected thermometry impact on tumour drug delivery efficacy.

P3-11

An Exposure System for In-vitro 3D Tumour HIFU Studies

Presenter: Ian Rivens

Authors in order: Ian Rivens, *Institute of Cancer Research*, Petros Mouratidis, *The Institute of Cancer Research*, Diana Andres, *Universitat Politècnica de València*, Noe Jimenez, *Universitat Politècnica de València*, Francisco Camarena, *Universitat Politècnica de València*

A system for targeting, delivering and quantifying thermal exposure of 3D tumour spheroids for application in hyperthermia ± radiation studies was developed and tested

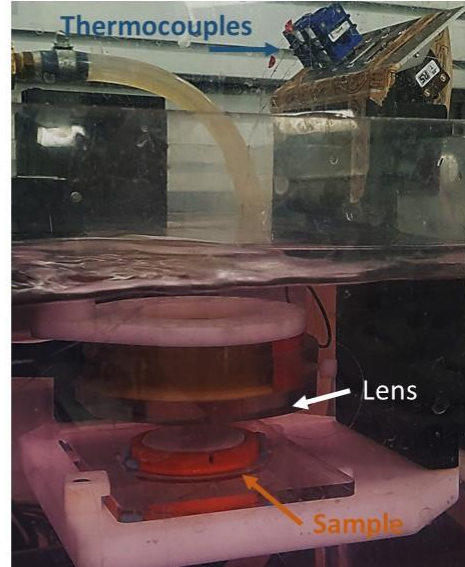
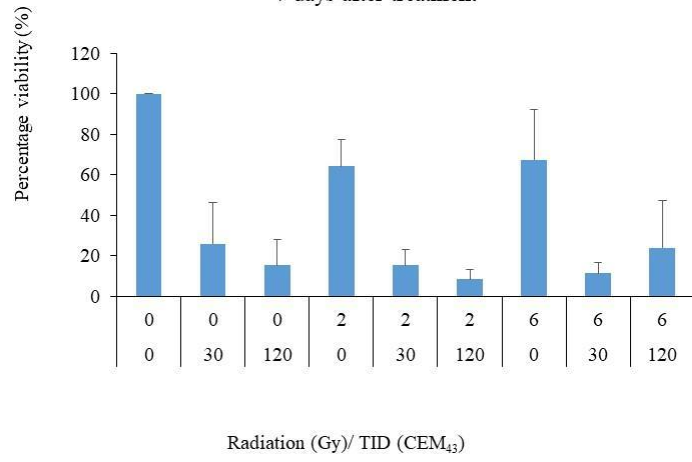
An acoustic holography designed lens was used to broaden a focused ultrasound beam. A gel phantom (IEC standard tissue mimic with 25 mg/100ml of Phenol red to improve visualization of spheroids) was used. One layer had 3 100um diameter T-type thermocouples set 0.5mm below a 0.7mm deep, 1mm diameter well. One spheroid per well was covered with a drop of Matrigel. A flat gel lid was placed on top, with culture medium as acoustic coupling.

The lens design convert a 12 x 1.5mm ellipsoidal focus into a region 10mm long, by 8 and 6mm (6dB) lateral widths. Sham exposed spheroids survived being mounted in the phantom, submerged in degassed tap water (pH neutral) pre-heated to 38oC and removed again. The system allowed ultrasound exposure of 3 spheroids at once e.g. to 35, 120 and 90 CEM43. Real-time logging of temperature and thermal dose allowed alignment to within 0.5 mm and dosimetry control to within 1 CEM43 in one well, and within a range of < 1 5% in 2 other wells.

Preliminary experiments demonstrate the system is fit for purpose. It is being used to compare ultrasound hyperthermia exposed spheroids with water bath heating experiments. Spheroid exposures have been completed (see figure) and the results of viability studies and comparison with water bath heat spheroids will be presented at the meeting.

This project, 18HLT06 RaCHy, has received funding from the EMPIR programme co-financed by the Participating States and from the European Union's Horizon 2020 research and innovation programme.

Hyperthermia (water bath) then irradiation
 3D spheroid viability of U87MG relative to 0 Gy 0 TID cells
 7 days after treatment



P3-12

Tumor Response Monitoring of Ultrasound-Stimulated Microbubbles and Hyperthermia In-vivo

Presenter: Deepa Sharma

Authors in order: Deepa Sharma, *Sunnybrook Health Sciences Centre*, Holliday Cartar, Anoja Giles, Martin Stanisiz, Gregory Czarnota, *Sunnybrook Research Institute*

The study aimed to determine tumor response to ultrasound-stimulated microbubbles (USMB) and hyperthermia (HT).

Experiments were performed using male mice bearing prostate tumor (PC3) and female mice bearing breast tumor (MDA-MB-231) xenografts. Mice received an intravenous injection of 1-3% (v/v) Definity microbubbles which were subsequently stimulated at various peak negative pressures using ultrasound. Five hours after USMB treatment, mice received a HT treatment at 43°C for 10-50 minutes. Tumor response was assessed after 24 hours and longitudinally (multiple weeks) using quantitative ultrasound techniques and histopathological analyses.

The combined USMB and HT groups revealed enhanced cell death and reduced vascularity compared to the control group. The longitudinal studies highlighted that the combined USMB and HT treatment resulted in increased fibrosis, a reduction in the vascular index, and a less proliferative fraction of cells compared to either control or USMB or HT treatment each on their own. Analysis of quantitative ultrasound radiofrequency (RF) data for the combined treatment indicated an increase in ultrasound backscatter parameters such as mid-band fit (MBF), 0-MHz spectral intercept (SI), and average acoustic concentration (AAC) that correlated with changes in the histology findings.

The results from both PC3 and MDA-MB-231 xenograft suggest that a combination of USMB and HT induces increased cell death and reduced vascularity. Ultrasound backscatter parameters tend to increase along with enhanced tissue microstructural changes and cell disruption induced by a combined treatment of USMB and HT.

This work was supported by the Canadian Cancer Society Research Institute (CCSRI) and the National Institutes of Health (NIH).

Effect of Tumor Microvessels on HIFU Thermal Field

Presenter: Farshad Moradi Kashkooli

Authors in order: Farshad Moradi Kashkooli, *Ryerson University*, Michael Kolios, *Ryerson University*, Jahangir (Jahan) Tavakkoli, *Ryerson University*

To simulate the effects of tumor microvascular network on the efficacy of high-intensity focused ultrasound (HIFU) thermal treatments.

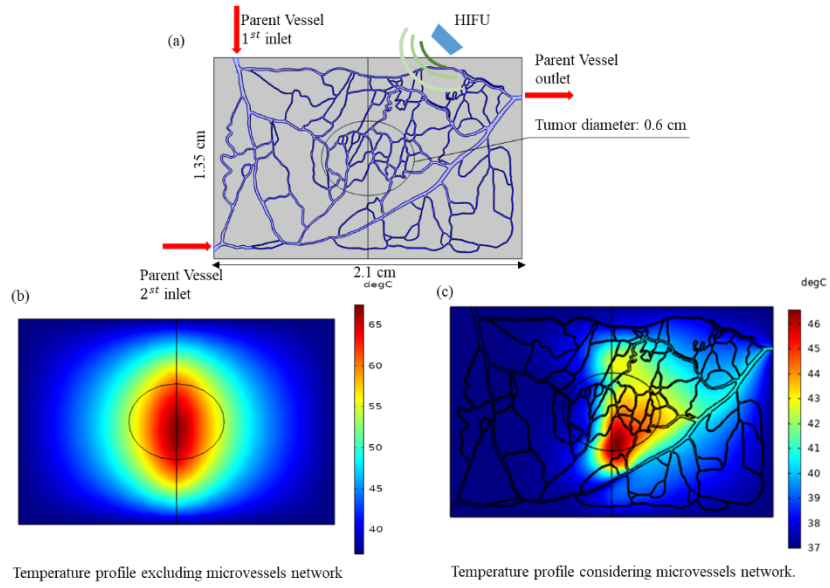
Using computational modeling integrated with image-based vascularized tumor geometry, the effect of the tumor microvessels was assessed by solving fully-coupled equations of acoustic propagation, heat transfer, and fluid flow using finite element based COMSOL software. The Helmholtz equation was first solved to simulate the effects of ultrasound beam propagation and absorption on tissue heating. Subsequently, convective fluid flow in microvessels and heat conduction in both the microvasculature and tissue were solved to predict temperature field.

Comparison between the HIFU induced thermal maps predicted by bio-heat transfer (BHT) equation using the Pennes' approach (excluding microvessels network), and general heat transfer equations (considering microvessels network) shows a considerable difference, demonstrating how microvascular flow causes heterogeneous temperature field in a tumor. Our results illustrate that a part of the vascularized tumor is not adequately heated because of the cooling effects of blood flow and microvascular network structure. Moreover, considering cooling effect of microvasculature, the maximum temperature reduces from 65°C (BHT prediction) to 47°C. Therefore, the inclusion of tumor microvessels is an important parameter in predicting HIFU-induced thermal profiles.

Using a realistic vascularized tumor model, a more accurate assessment of the efficacy of HIFU thermal treatment can be achieved. Our simulations show that excluding blood microvessels network significantly overestimate the HIFU temperature field by about 18°C.

This work was supported by an NSERC Alliance grant (ALLRP 55627-20) and a research contract from Toronto Poly Clinic Inc.

Schematic of a computational domain including tumor microvessels network and normal tissue



P3-14

Cavitation Dynamics and Shockwave Evolutions during Histotripsy Treatment

Presenter: Scott Haskell

Authors in order: Scott Haskell, *University of Michigan*, Jonathan Sukovich, *University of Michigan*, Zhen Xu, *University of Michigan*

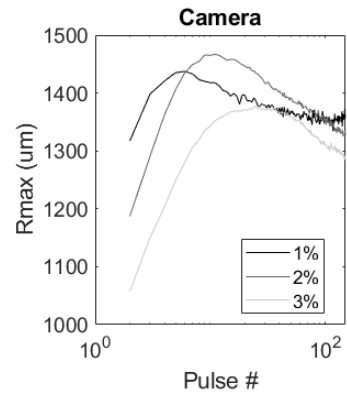
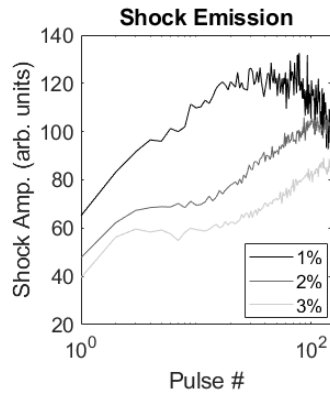
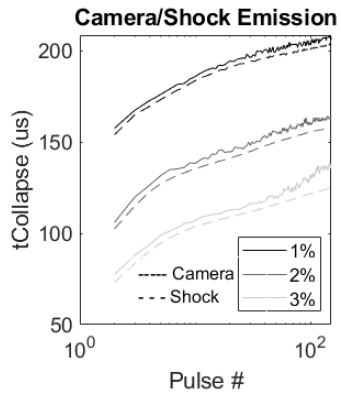
We aim to identify correlations between cavitation dynamics and shockwave emissions in materials repeatedly exposed to cavitation to develop methods for monitoring damage during histotripsy.

Cavitation events were generated in tissue-mimicking hydrogels of different material stiffnesses/structures using a 700kHz, 360 element hemispherical Histotripsy transducer with a focal distance of 15cm. Shockwave emission signals from cavitation were collected using receive-capable acoustic elements of the array. Cavitation dynamics were also monitored via high-speed optical imaging. Features analyzed from the shockwave signals, including cavitation collapse times, amplitudes, and rebound interval timings, were correlated with high-speed images of the bubble dynamics.

Cavitation collapse times and amplitudes increased monotonically with the number of histotripsy pulses applied, which agreed closely with imaged bubble lifespans. Images showed that bubble maximum radii initially increased with exposure-count before reaching a plateau and then decreasing. These trends were seen to be consistent across gels, but evolved at different rates depending on gel stiffness, e.g., bubble maximum radii were observed to plateau at higher exposure-counts in stiffer gels than softer ones. The simultaneous trends in bubble maximum radii and lifespans are suggestive of an elastic-to-viscous transition in the properties of the nucleation media and corresponding bubble responses.

Repeated exposure to cavitation alters properties of the nucleation medium, and corresponding impacts on cavitation dynamics can be detected in emitted shockwaves. Rates of bubble dynamics evolutions varied with medium stiffness. Observed trends in dynamics suggest evolving viscoelastic properties during treatment, which could indicate the damage state of the medium.

This work was funded by the ONR (Dr. Tim Bentley, #N000141712058) and the Focused Ultrasound Foundation.



The Strain and the Flurry: Thrombolysis via Histotripsy and Thrombolytics

Presenter: Kenneth Bader

Authors in order: Kenneth Bader, *University of Chicago*, Sam Hendley

Studies have demonstrated histotripsy-induced thrombus disruption is enhanced with a thrombolytic drug. Here, we quantify markers of clot degradation generated by this combination approach.

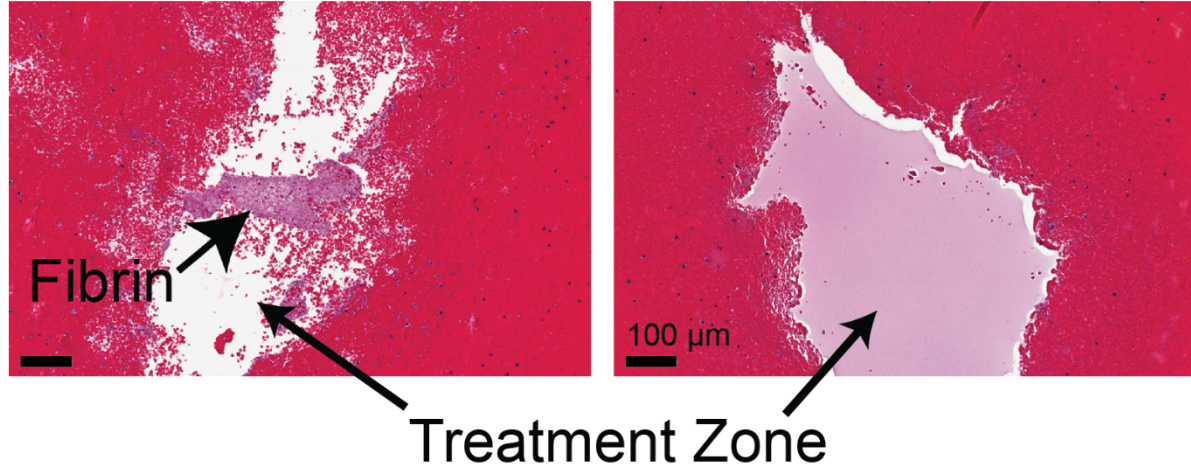
There are two hypothesized mechanisms of clot degradation when histotripsy is fused with thrombolytic: fractionation of erythrocytes (hemolysis) and enhanced drug activity (fibrinolysis). Human whole blood clots were exposure to histotripsy with or without thrombolytic drug in an in vitro venous flow model. Following treatment, assays were conducted on the perfusate to quantify the generation of hemoglobin (metric of hemolysis) and D-dimer (metric of fibrinolysis). The change in clot mass was also tabulated.

Using linear regression analysis, our findings indicated hemolysis and fibrinolysis contributed equally to overall treatment efficacy (clot mass loss) for histotripsy and thrombolytic arms. In contrast, hemolysis was the lone clot degradation marker observed for histotripsy alone. These finding were consistent with histological assessment of clot samples, as there was no observable fibrin structure in targeted regions for the combination approach. Conversely, fibrin was a prominent feature in the treatment zones of histotripsy-alone arms.

This study and others exhibit the capacity of histotripsy to decellularize tissue while preserving its extracellular structures. For thrombus, residual fibrin is prothrombotic and there is a risk of re-occlusion. Our findings demonstrate histotripsy combined with a thrombolytic drug fulfills the niche required to address all components of the thrombus.

These studies were funded in part by the National Institutes of Health, grant R01 HL133334.

Histotripsy Alone Histotripsy +Thrombolytic



P3-16

Feasibility Study for Histotripsy of Soft Tissue Sarcoma Treatment

Presenter: Ryan Hubbard

Authors in order: Ryan Hubbard, *University of Michigan*, Wei Yan, *University of Michigan Rogel Cancer Center*, Geoff Siegel, *University of Michigan*, Zhen Xu, *University of Michigan*, Christina Angeles, *University of Michigan*, Jodi Wilkowski, *University of Michigan*, Reliza McGinnis, Ashley Cornett,

We aim to demonstrate the initial feasibility of histotripsy to treat soft tissue sarcomas (STS) and other soft tissue tumors.

Patients consented to STS biobanking at the University of Michigan. Human sarcoma samples from surgical specimens were embedded in 1.5% agarose phantoms. Additionally, patient-derived xenografts (PDX) were created by subcutaneous engraftment of undifferentiated pleomorphic sarcomas in NSG mice. Each tumor received 1 MHz, ~30MPa p-, 100 Hz PRF, 1-cycle pulses (50 pulses per focal location) with a custom built 8-element histotripsy transducer. Immediately following treatment each sample was harvested and submitted for histology.

A total of 14 ex-vivo human samples of various STS including liposarcoma, desmoid, and benign lipoma and hibernoma, and 3 in-vivo mouse PDX sarcomas were treated with histotripsy. Cellular integrity within both in-vivo and ex-vivo untreated tumor samples remained intact. In comparison, treated ex-vivo human sarcoma samples exhibited little to no cellular structure and few remaining nuclei. In-vivo treated mouse PDX sarcoma samples exhibit multifocal necrosis within the ablated area with nuclei shrinkage and fragmentation. Representative histopathology of the untreated and treated sarcoma samples are shown in Figure 1.

Histotripsy effectively breaks down cellular structure of both ex-vivo human sarcoma samples and in-vivo mouse PDX sarcomas. These results demonstrate the initial feasibility of using histotripsy as an alternative treatment for soft tissue malignancies.

We thank our patients in the Sarcoma Program at the Rogel Cancer Center for participating in research and the diligence of our tumor procurement staff.

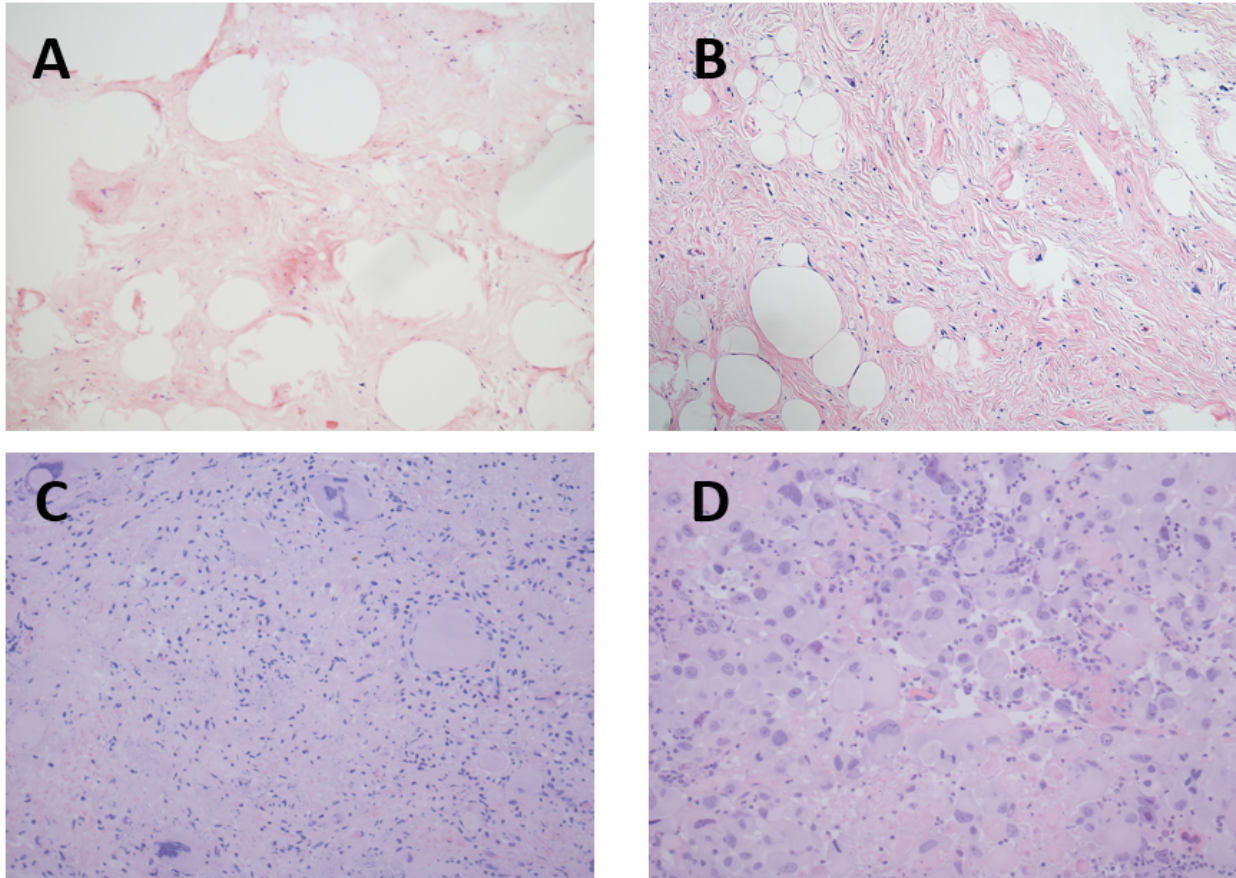


Figure 1. H&E stained tissue sections. Treated (A) and untreated (B) resected liposarcoma samples. Extensive coagulative necrosis without visual nuclei remaining (A). Treated (C) and untreated control (D) in-vivo patient-derived xenograft (PDX) sarcoma mouse model. Histotripsy treated samples exhibit multifocal micro-necrosis with karyopyknosis and karyorrhexis whereas untreated samples maintain intact tumor cellular structure and tumor microenvironment.

Effects of High Frequency Histotripsy Pulse Settings on Brain Ablation Outcomes

Presenter: Thomas Landry

Authors in order: Thomas Landry, *Dalhousie University*, Jeremy Brown, *Dalhousie University*, Eli Vlaisavljevich, *Virginia Tech*, Jessica Gannon, *Virginia Tech - Wake Forest School of Biomedical Engineering and Sciences*

To determine whether high frequency (6.3MHz) histotripsy in the brain is significantly affected by changing pressure, N cycles, N pulses, and pulse repetition frequency (PRF).

Using a novel co-registered precision histotripsy and high-resolution ultrasound imaging system, histotripsy was performed in the brains of anesthetized rats (N=25) with the device rigidly held. The cavitation threshold was measured via ultrasound imaging, then a number of suprathreshold ablations were performed with various settings. The brain tissue was examined in histology and the ablation shape measured by the area as well as the length (axial direction) and width of a fit ellipse.

Several statistically significant relationships were found in regression analyses. The ablation area and width, but not length, significantly increased with increasing N cycles. The ablation length, but not overall area or width, increased with increasing pressure. However, the magnitudes of these differences were small compared to the variances and not likely to be practically manipulable. Area, width, and length each significantly increased with increasing PRF up to 500 Hz, then plateaued. Unlike N cycles and pressure, this effect was likely large enough to be a practical manipulation parameter. There were no differences between N pulses (4000 vs 10000).

Despite some statistically significant effects of N cycles, pulses, and pressure on outcomes, the small ablations (0.5-1 mm) were generally consistent and those parameters are not likely useful for manipulation. Conversely, ablation size may be manipulated at PRFs < 500 Hz. However, real-time ablation monitoring was difficult at PRFs < 200 Hz.

This study was funded by the Atlantic Canada Opportunities Agency (Atlantic Innovation Fund no.207828) and the Natural Sciences and Engineering Research Council of Canada (NSERC).

PRF: 500Hz



200Hz



10Hz



500μm



Ablations from a single brain showing ablation size decreasing with PRF.

Histotripsy Bubble Dynamics in Tendons and Anisotropic Hydrogels

Presenter: Julianna Simon

Authors in order: Jacob Elliott, *The Pennsylvania State University*, Julianna Simon, *The Pennsylvania State University*, Andrea Arguelles,

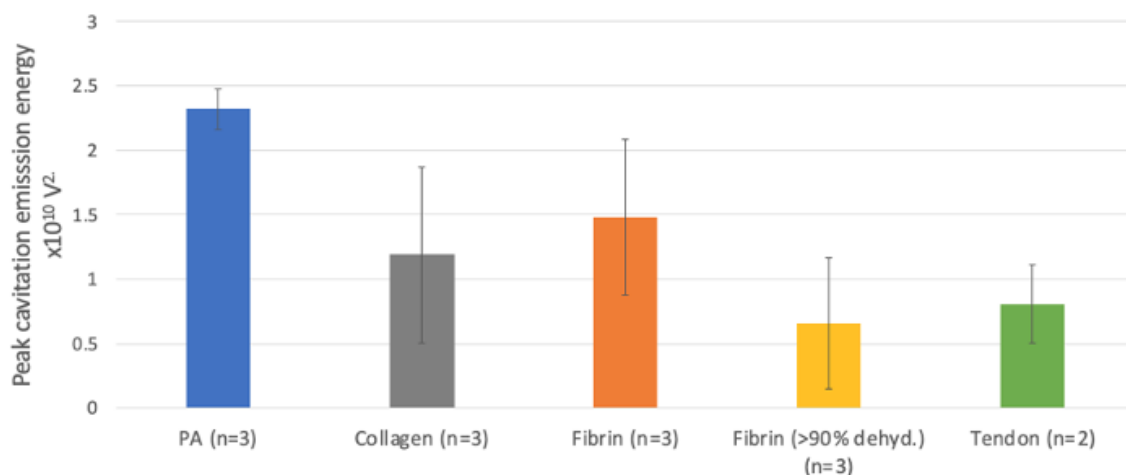
We are evaluating the effects of anisotropy on bubble dynamics in tissue-mimicking hydrogels as we work to understand bubble dynamics in anisotropic tissues like tendon.

Polyacrylamide (PA), fibrin, and collagen hydrogels were fabricated; ex vivo bovine tendons were obtained. Sound speeds were measured in each direction to determine degree of anisotropy as the ratio of axial elastic moduli. Hydrogels and tendons were treated with 1.5-MHz focused ultrasound using 10-ms pulses repeated at 1-Hz with $p_+ = 89$ MPa, $p_- = 26$ MPa. Cavitation activity was monitored with high-speed photography and passive cavitation imaging using a Philips/ATL L7-4 transducer and Vantage® ultrasound system.

As shown in figure 1, violent cavitation activity and fractionation was observed in polyacrylamide, collagen, and fibrin hydrogels with low degrees of anisotropy (90% resulted in a 55% reduction in cavitation emission energy (0.66 ± 0.5 [$\times 10^{10}$ V²])) compared to standard fibrin gel formulations (1.48 ± 0.6 [$\times 10^{10}$ V²]), and a 795% increase in degree of anisotropy (9.54 ± 4.18).

Dehydrated fibrin gels demonstrated similar cavitation emission energies to tendons (within 4%), although anisotropy was approximately 50% lower in dehydrated fibrin compared to tendons. These results suggest dehydrated fibrin may allow for a thorough investigation of bubble dynamics in anisotropic tissues like tendon.

This work is supported by National Institutes of Health (Grant R21EB027886).



Peak cavitation emission energies for hydrogels and bovine tendons

Histotripsy Ablation to Treat Soft Tissue Sarcoma: In-vivo Study in Dogs

Presenter: Lauren Ruger

Authors in order: Lauren Ruger, *Virginia Polytechnic Institute and State University*, Ester Yang, *Virginia-Maryland College of Veterinary Medicine*, Jessica Gannon, *Virginia Tech - Wake Forest School of Biomedical Engineering and Sciences*, Hannah Sheppard, *Virginia Polytechnic Institute and State University*, Sheryl Coutermarsh-Ott, *Virginia Polytechnic Institute and State University*, Irving Allen, *Virginia Polytechnic Institute and State University*, Nikolaos Dervisis, *Virginia-Maryland College of Veterinary Medicine*, Shawna Klahn, *Virginia-Maryland College of Veterinary Medicine*, Eli Vlasisavljevich, *Virginia Tech*

In this study, we investigated histotripsy for the treatment of soft tissue sarcoma (STS) in vivo using spontaneous STS in client-owned dogs.

A 500kHz histotripsy system guided by real-time US imaging was used to treat spherical ablation volumes of 2-3cm in diameter within a portion of STS tumors. Tumors were surgically removed 4-6 days after treatment. The ability to ablate targeted regions was evaluated histologically, and tumor microenvironment gene expression was evaluated with the NanoString Canine IO panel. Multiplex serum cytokine levels were used to evaluate the systemic immune response via a commercial canine-specific bead-based multiplex assay.

Ten STS treatments were completed with bubble clouds generated and maintained throughout treatment at peak negative pressures 22.60 ± 7.21 MPa. All dogs recovered after treatment without immediate adverse events; self-limiting cutaneous injury was sometimes noted following treatment. Histological analysis of treated tissues revealed ablation marked by hemorrhage and destruction of viable tumor cells. Distinct borders were visible between treated and untreated tissues.

Differential gene expression analysis identified 72 genes with >2-fold upregulation between treated and untreated groups. Genes associated with inflammation, immune cell migration, and immune cell interactions were the highest upregulated. There were no differences between pre- and post-treatment cytokine concentrations.

Results suggest histotripsy can safely and effectively ablate tumors in dogs with STS. Changes in the tumor microenvironment reflect increases in the expression of genes associated with inflammation, matrix remodeling, innate immune cell functions, and immune cell interactions. Histotripsy as a therapy for soft tissue sarcoma should be further investigated.

This study was financially supported by the Focused Ultrasound Foundation. Author Lauren Ruger was supported by the VT ICTAS Doctoral Scholars program throughout this work.

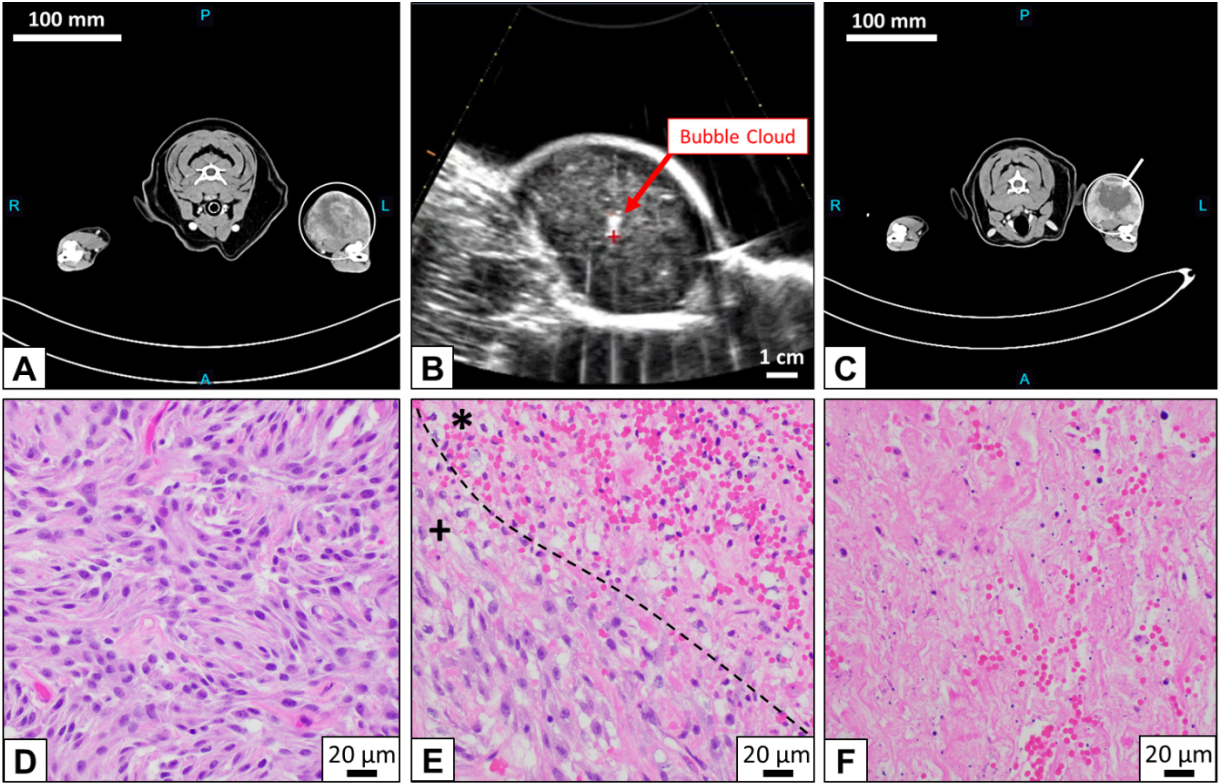


Figure 1: (A) Pre-treatment CT image of a canine STS (circled). (B) Real-time ultrasound image during histotripsy treatment showing cavitation bubble cloud. (C-F) Patient-matched (C) post-treatment CT image with visible ablation zone (arrow), (D) hematoxylin & eosin (H&E) histological stain of untreated STS tumor, (E) H&E tissue stain of the treatment boundary (+ = untreated, * = treated), and (F) treated, stained STS tumor.

Influence of the Medium Salinity and Charges on the Dynamics of Size Isolated Lipid-coat MBs

Presenter: Amin Jafarisojahrood

Authors in order: Amin Jafarisojahrood, *Sunnybrook Health Science Center*, Celina Yang, *Ryerson University*, Claire COUNIL, *Case Western Reserve University*, Pinunta Nittayacharn, *Case Western Reserve University*, Agata Exner, *Case Western Reserve University*, David Goertz, *Sunnybrook Research Insititute*, Michael Kolios, *Ryerson University*

To investigate the influence of the liquid salinity on the dynamics of lipid coated microbubbles (MBs) in order to optimize their biomedical ultrasound applications.

In house made lipid-coated MBs¹ were size isolated into populations with mean diameters of 2.7, 3.4 and 4.8 μ m. The attenuation of each population was measured in the linear regime using a pair of 100% bandwidth 10MHz center frequency transducers at a peak negative pressure of 3kPa. To investigate the influence of the charges of the medium on the MB resonance, the measurements were performed in distilled water (DW) and different salt concentration (PBS-1x-PBS-10x).

The size and volume distribution of the MBs are shown in Figs 1a-b. MB resonance frequency is highly affected by the salinity of the medium. The frequency of the attenuation peak decreases with salinity increase (Fig 1c-f). For instance, the attenuation peak of the 2.7 μ m MBs were 14, 7.2, and 4.2 MHz in DW, PBS-1x and PBS-10x, respectively (fig. 1d). The MB's response to salinity depends on the shell composition and, in particular, on the PEG quantity in the shell. Liquid salinity effects on the MB resonance frequency became negligible at high PEG molar ratios.

The reduction in the MB resonance might be due to the attraction of charged ions by the MB shell. This reduces the surface tension on MBs as the charged layer may act as a secondary stabilizing shell. The interaction between the lipid shell and the medium charges cannot be neglected.

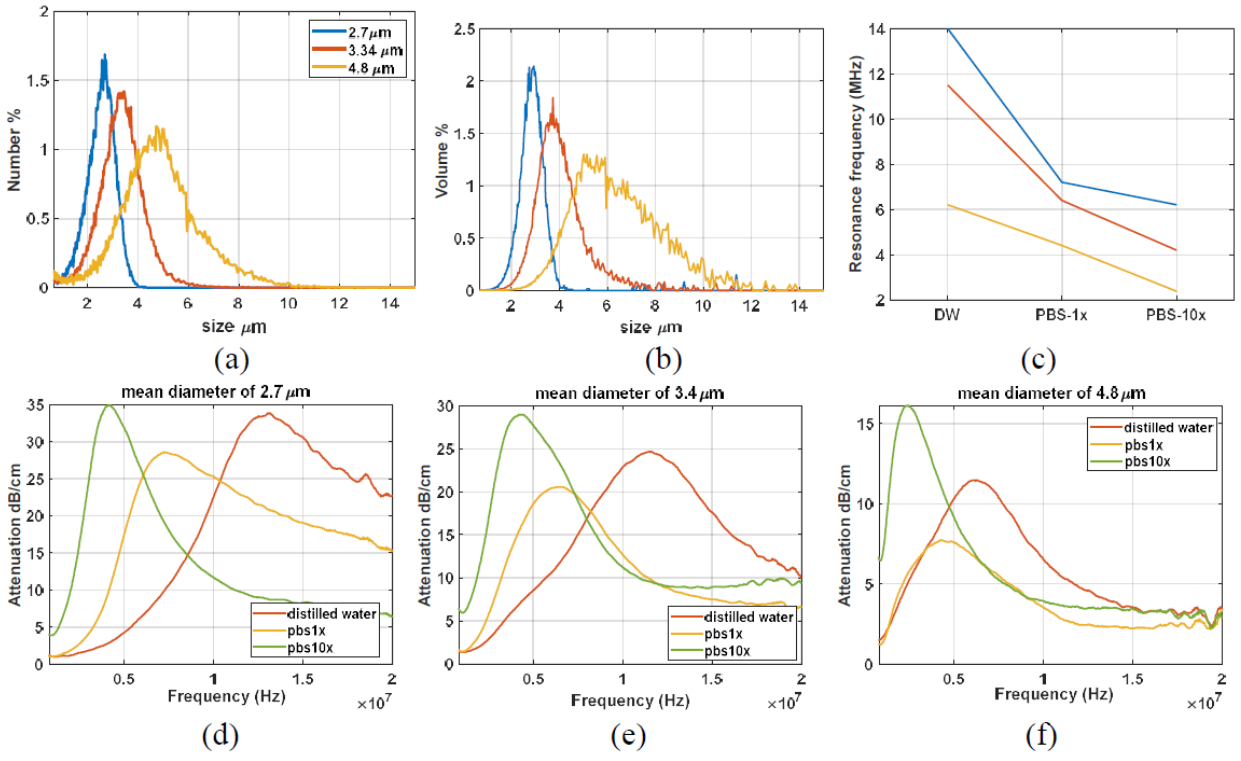


Figure 1. Size (a) and volume (b) distribution of the MBs as measured by the coulter counter. (c)-(f)- Attenuation-frequency curves of the MBs in distilled water, PBS-1x and PBS-10x. A dramatic decrease in the resonant frequency is measured. [1]. A deLeon et al, *Nanoscale*, 11(33), pp.15647-15658.

Effects of Dose and Parameter Selection in Treating Human Benign Prostatic Hyperplasia with Different Histotripsy Modalities

Presenter: Adam Maxwell

Authors in order: Yashwanth Nanda Kumar, *University of Washington*, Zorawar Singh, *University of Washington, School of Medicine*, Yak-Nam Wang, *Center for Industrial and Medical Ultrasound, University of Washington, Seattle, United States of America*, Adam Maxwell, *University of Washington*, Matthew Bruce, *University of Washington*, Rishi Sekar, *University of Washington, School of Medicine*, Eli Vlasisavljevich, *Virginia Tech*, Lawrence True, *University of Washington School of Medicine*, George Schade, *UNIVERSITY OF WASHINGTON*

This study aims to identify the doses required to homogenize tissue in human benign prostatic hyperplasia (BPH) tissue by different histotripsy modalities.

Two transducers operating at 700 kHz and 1.5 MHz were used to treat deidentified BPH tissue *ex-vivo* (n=18). A combination of the three pulsing parameter sets inducing cavitation or boiling histotripsy were applied to each sample. Varying doses between 30–288 seconds per focal point were applied to determine liquefaction time. The efficacy of treatment was evaluated using shear wave elastography (SWE) measuring Young's modulus pre and post-treatment. Additionally, histological analysis was performed using H&E and Masson's Trichrome.

A paired t-test analysis showed a statistically significant reduction in the Young's modulus at 30 seconds for boiling histotripsy (PRF=1 Hz, duration=15000 cycles) with mean difference (MD) (Pre-Post)= 19.07kPa (P < 0.0001*) and at 60 seconds MD= 27.88kPa (P=0.0002*) with histology showing a complete lesion (Figure 1). With cavitation histotripsy (PRF=10 Hz, duration=20 cycles), significant reduction was detected at 30 seconds MD= 7.93kPa (P < 0.05*) and at 86.6 seconds MD= 66.73kPa (P < 0.0001*), histology demonstrated near complete lesion. At a higher PRF (500Hz) and shorter duration (3 cycles) significant reduction was seen at 60 seconds MD= 13.12kPa (P=0.007*) and at 288 seconds MD= 46.60kPa (P < 0.0001*), histology showed complete liquefaction at the highest dose.

Boiling histotripsy rapidly generated a complete volumetric lesion, but cavitation histotripsy was also found to produce complete liquefaction in human BPH tissue. Applying cavitation histotripsy with high PRF and short pulses appeared to be less effective and required higher doses. Further comparisons will better elucidate the effects of different parameters.

The authors would like to thank the National Institutes of Health for the financial support through R01-DK119310 and L30-DK122509 grants.

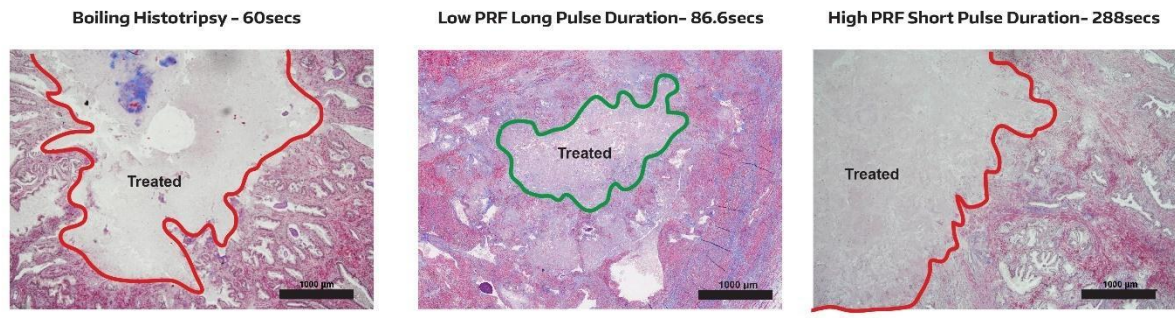


Figure 1. Masson's Trichrome stain showing completely liquified (red outline) and near complete cavity (green outline).

Experimental Passive Directivity Detection with Biaxial Transducers

Presenter: Nathan Meulenbroek

Authors in order: Nathan Meulenbroek, *University of Calgary*, Sagid Delgado, *University of Calgary*, Laura Curiel, *University of Calgary*, Adam Waspe, *Hospital for Sick Children*, Samuel Pichardo, *University of Calgary*

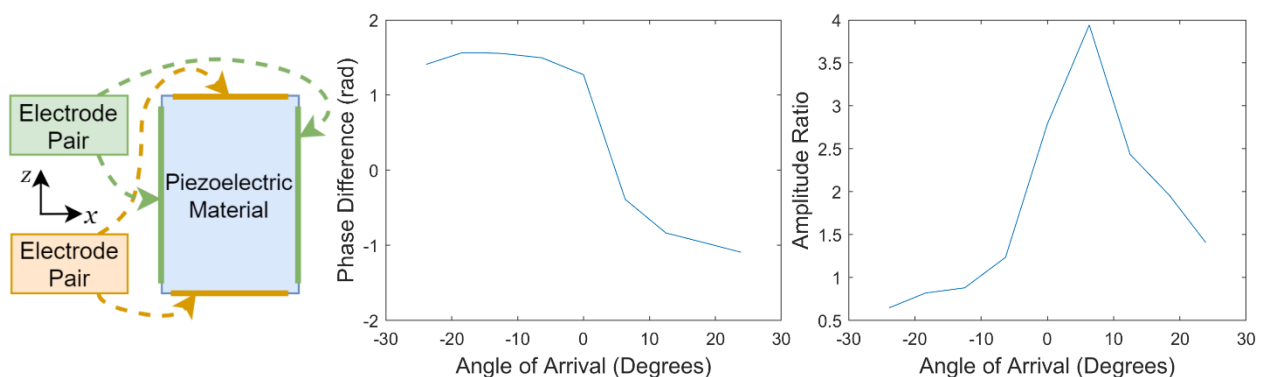
This research seeks to experimentally verify biaxial directivity estimates demonstrated in-silico and establish directivity as an independent parameter detected by biaxial transducers.

Three cuboid piezoceramics with two pairs of orthogonal electrodes (Figure 1, left) are characterized. Impedance is measured for each pair from 5 to 1500 kHz using a vector network analyser. Each transducer is placed in a water tank with a separate hemispherical source operated at 250 kHz and attached to a moveable arm. Voltages are recorded for source positions in an xy-plane parallel to the transducers' front surfaces at a depth of approximately 9 cm.

Three biaxial transducers were manufactured and tested. All transducers are resonant at approximately the same frequency in the directions of the electrode pairs. The phase difference (Figure 1, middle) and amplitude ratio (Figure 1, right) of the voltages demonstrates a dependence on incident sound directivity along the xz-plane formed by the electrodes. Each transducer was capable of detecting incidence angles from approximately -24 degrees to +24 degrees without using time-of-arrival information.

Directivity detection using biaxial transducers has been experimentally demonstrated and verified for three transducers. This ability is independent of any time-of-arrival information. This work contributes to the development of a multiaxial passive ultrasound imaging system for enhanced monitoring of ultrasound therapies. Future work will explore directivity-enhanced passive image reconstruction methods.

This research is supported by funding from: Canada Foundation for Innovation, Natural Sciences and Engineering Research Council of Canada, and Canadian Institutes of Health Research.



Broadband Multiple-focus Synthesis using Orthogonal Frequency Division Multiplexing

Presenter: Collin Smith

Authors in order: Collin Smith, *UMN*, Emad Ebbini, *University of Minnesota*

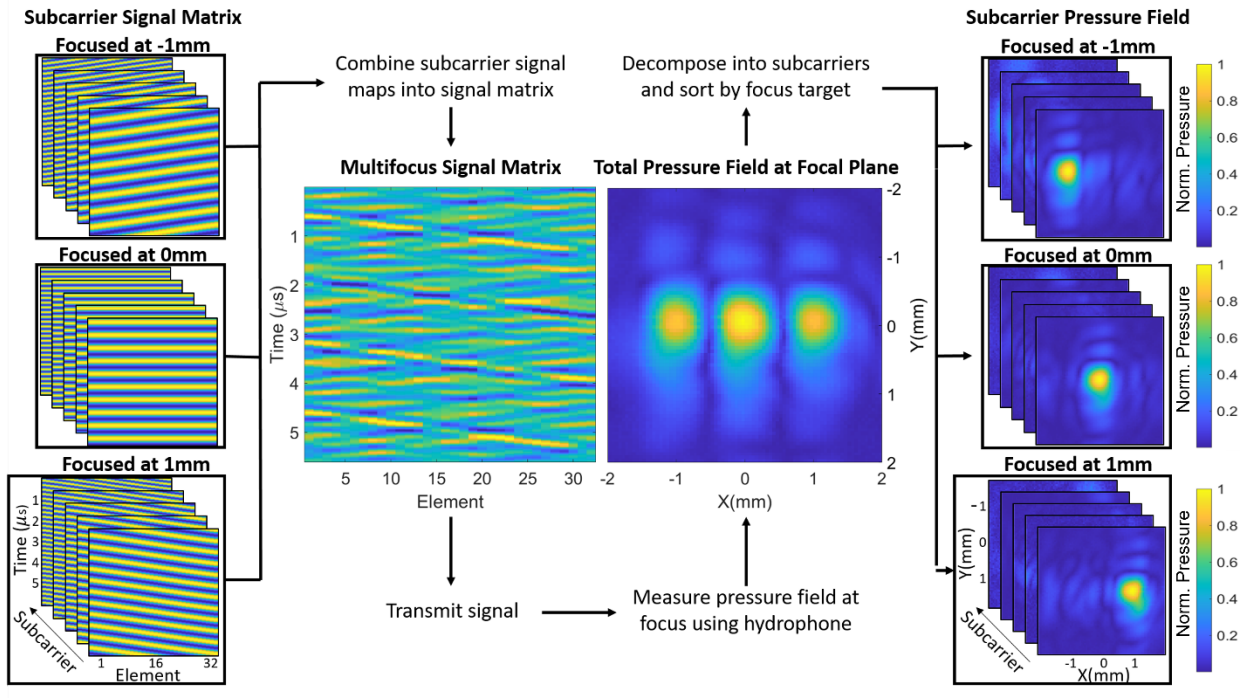
We used orthogonal frequency-division multiplexing (OFDM) to simultaneously perform frequency-specific broadband multifocusing and rapid multispectral pressure field characterization in a dual-mode ultrasound array (DMUA).

A type of signal processing called orthogonal frequency-division multiplexing (OFDM) allows for the generation of long-duration broadband signals capable of being used in FUS. OFDM is used in a multiple focusing algorithm to generate three foci. A hydrophone scan then characterizes the pressure field produced by the DMUA implementing this algorithm. Then, the subcarriers in the OFDM signal are transmitted individually, measuring the pressure field generated by each. The results are then compared.

Three distinct foci are generated using the multiple focusing algorithm, each with a unique spectral characteristic. Due to the orthogonality of the subcarriers, the pressure field measured by the hydrophone itself can be decomposed into its constituent subcarriers. From a single hydrophone scan, it is possible to measure the pressure field generated by all subcarriers simultaneously. The integrity of the multispectral characterization from a single OFDM measurement is validated from the multiple narrowband transmissions. From these subcarrier pressure fields, it is shown that only certain subcarriers contribute energy to predetermined foci.

OFDM signals are shown to provide broadband multiple-focus patterns with distinct spectral characteristics at the desired foci. The orthogonality of the subcarriers allows both for arbitrary control over the frequency characteristics of the broadband signal, and simultaneous multispectral pressure field characterization.

This work is funded by Grant NS118785 from the National Institutes of Health.



P3-23

High-throughput Acoustic Rheometry System Tracks Clotting Blood in Real Time

Presenter: Christina Hendren

Authors in order: Christina Hendren, *University of Michigan*, Eric Hobson, Zhen Xu, *University of Michigan*, Timothy Hall, *University of Michigan*, Cheri Deng, *University of Michigan*

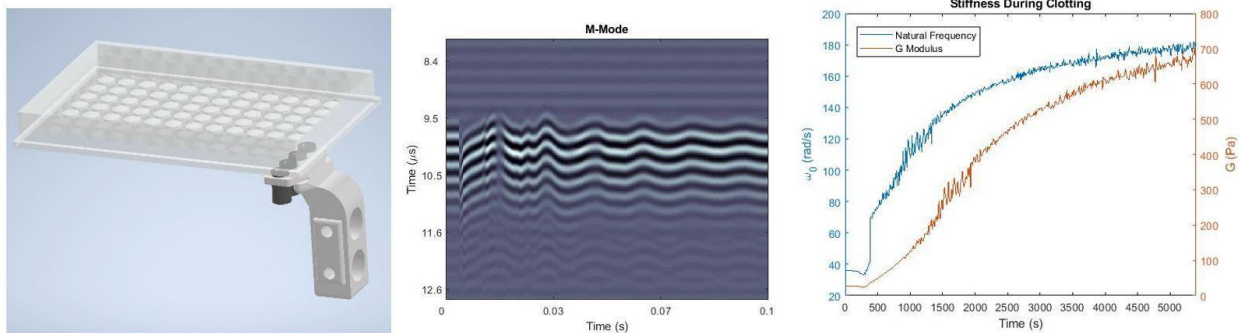
Demonstrate a new ultrasound system for high throughput dynamic mechanical characterization of soft biomaterials to overcome limitations of contact-based approaches.

Acoustic rheometry non-invasively generates and detects oscillation of a soft biomaterial surface. An array of focused 5MHz transducers was fabricated using 3D printing. A custom electrical driver was built to produce acoustic radiation force and imaging pulses. Transducer elements were evaluated using a hydrophone and aligned beneath a microplate at the top of a water bath. Initial tests measured changes in surface displacement dynamics during blood clotting using a cross-correlation algorithm.

Working prototypes of 4 focused transducers were fabricated with focal (sensing) area of μm in the liquid phase and 25-100 μm once clotted. Resonant frequency of the blood changed greater than 100 rad/s and the shear modulus increased greater than 20-fold (assuming Rayleigh waves).

This system demonstrated nearly simultaneous acoustic pushing and imaging used for acoustic rheometry. The transducers deformed the sample surface to a degree that was trackable, allowing derivation of material properties. The system was shown to be capable of tracking blood clotting in real time by monitoring the dynamic phase changes.

Support from the NIH (R01-DE026630) is acknowledged.



Preliminary Study: PSMA Nanobubbles for TUS Treatment/Prevention of Tumor Growth in a Rabbit Orthotopic Prostate Tumor Model

Presenter: Eric Abenojar

Authors in order: Eric Abenojar, *Case Western Reserve University*, Jing Wang, Sidhartha Tavri, Felipe Matsunaga, Pinunta Nittayacharn, *Case Western Reserve University*, Youjoung Kim, *Case Western Reserve University*, Xinning Wang, *Case Western Reserve University*, James Basilion, *Case Western Reserve University*, Agata Exner, *Case Western Reserve University*

This work examined nanobubbles (NBs) targeted to the prostate specific membrane antigen (PSMA) for potential ultrasound (US)-mediated treatment of orthotopic prostate tumor in rabbits.

Orthotopic tumors were instilled into prostates of immunosuppressed rabbits by US-guided injection of PC3 cells transformed to express PSMA.1 PSMA-NBs were prepared by adding DSPE-PEG-PSMA-1 to a solution composed of DBPC, DPPA, DPPE, and mPEG2000-DSPE lipids dissolved in propylene glycol, glycerol, and PBS.2 One week after inoculation, tumors were treated with PSMA-NBs (0.8 mL/kg) injected IV followed by unfocused ultrasound treatment (1 MHz, 2.2 W/cm², 10% duty cycle, 15 min) 30 min after NB injection.

Following 3 to 5 weekly treatments, B-mode US, MRI, and H&E analyses reveal that tumors did not grow in the rabbit prostate region following therapeutic ultrasound (TUS) treatment with PSMA targeted NBs (Figure 1). In one of two rabbits, tumors grew outside the prostate region but not in the prostate gland of the rabbit. This is most likely because the tumor treatment was localized in the prostate gland, thus, any extraprostatic growth is likely a result of cell leakage following injection. In comparison, untreated tumors progressed at a rate of 39 ± 25 mm² per week.

Preliminary results of US-mediated treatment of rabbits following injection of PSMA-NBs show the absence of the tumor progression in the prostate region of the rabbit. The study offers preliminary evidence that a combination of unfocused US and PSMA-NBs has therapeutic potential in a large animal rabbit model.

This work was funded by the Case-Coulter Translational Research Partnership and the National Institute of Biomedical Imaging and Bioengineering Award No. R01-EB025741.

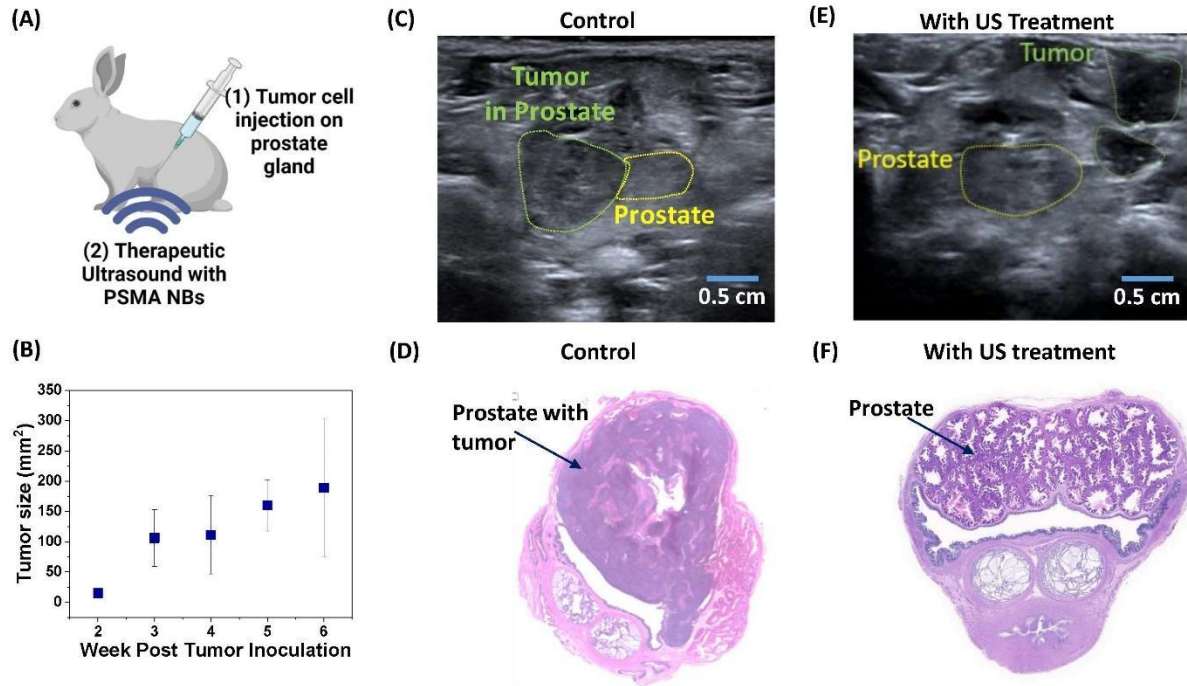


Figure 1. (A) Rabbits were inoculated with PC3pip GFP tumor cells and exposed to therapeutic US treatment with PSMA NBs. (B) Rabbit tumor growth rate at different weeks following tumor cell inoculation measured by US. (C) At 3 weeks post tumor inoculation, a large tumor in the prostate was visible via B-mode US imaging for a representative control rabbit that did not undergo therapeutic US treatment. This is confirmed by the (D) H&E staining done at 4 weeks after tumor inoculation. (E) In contrast, for a representative rabbit that had therapeutic US treatment, at 4 weeks post tumor cell inoculation no tumors were visible in the prostate but tumors grew outside the prostate. Corresponding H&E staining of the (F) prostate is shown at 5 weeks post tumor cell inoculation showing that no tumor was visible in the prostate gland. Figure (A) was created with BioRender.com. References: ¹Wang Y, Abenojar EC, Wang J. et al. *Prostate* 2022, 1-11, DOI: 10.1002/pros.24314. ²de Leon A, Perera R, Hernandez C, et al. *Nanoscale* 2019, 11, 15647–15658.

Algorithm for Path Planning in MRgFUS Therapy

Presenter: Christakis Damianou

Authors in order: Andreas Georgiou, *Cyprus University of Technology*, Nikolas Evripidou, *Cyprus University of Technology*, Anastasia Antoniou, *Cyprus University of Technology*, Ioannis Demetriades, *Cyprus University of Technology*, Christos Messios, *Ministry of Transport, Communications And Works*, Christakis Damianou, *Cyprus University of Technology*

This study concerns the development of a full coverage path planning algorithm for Magnetic Resonance guided Focused Ultrasound (MRgFUS) therapy.

The algorithm implements five basic subprocesses starting from the segmentation stage that requires the indication of initial points by the user to the extraction of the transducer's path for full ablation of two-dimensional regions of interest (ROIs) following a Zig-Zag pathway. The developed algorithm was implemented in the software of an MRgFUS device. Its performance in path planning was evaluated on medical images, whereas the planned sonication paths were executed on acrylic films.

Path planning on MR images was successfully implemented. The output motion vectors were successively sent to and executed by the driving system of the MRgFUS device using a 2.75 MHz single-element transducer. The motion step between adjacent sonications was adjusted by the user resulting in the formation of overlapping lesions on the films. A perfect match was observed between the segmented ROIs and experimental lesions formed on the acrylic films. In this regard, proper communication between software and hardware was also demonstrated.

Plastic films constitute a cheap phantom for quality assurance of FUS equipment. The software as integrated with the MRgFUS system provides accurate planning and execution of ablation for any segmented two-dimensional ROI. The development of a fully automated segmentation procedure would be a key improvement in enhancing the algorithm's reliability.

Multiaxial Driving Method Applied for Concave Phased Arrays

Presenter: Samuel Pichardo

Authors in order: Samuel Pichardo, *University of Calgary*, Sagid Delgado, *University of Calgary*, Laura Curiel, *University of Calgary*

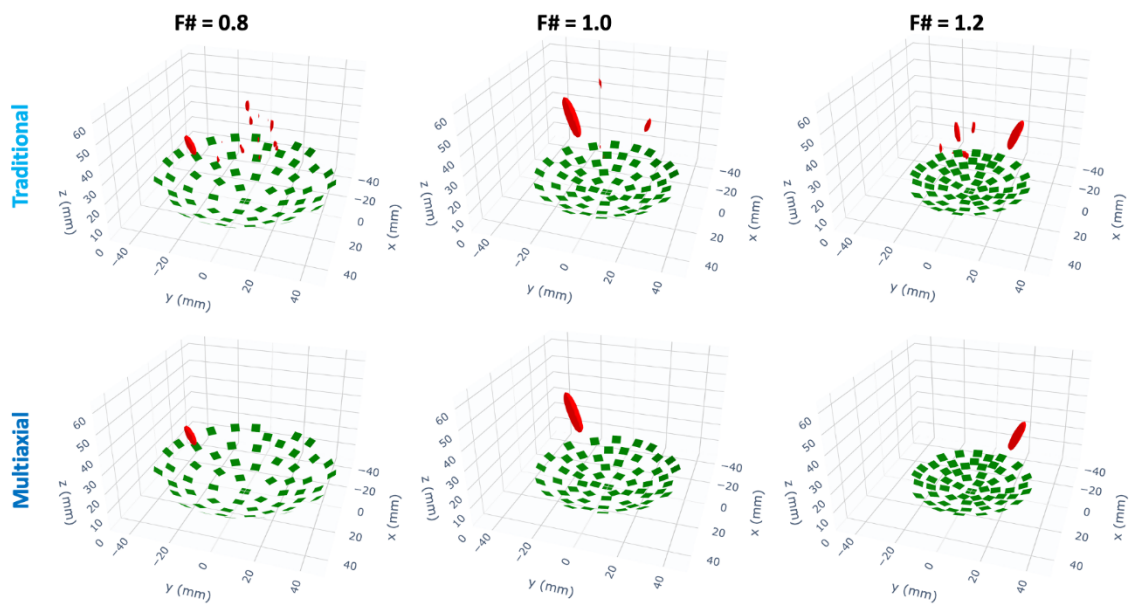
We present an in silico study demonstrating the capabilities of the multiaxial driving method to improve the focusing of ultrasound phased arrays

A dataset of 1728 combinations of multiaxial conditions for a single-element transducer operating at 320 kHz ($W,D=5.2\text{mm}$, $H=3.4\text{mm}$), each producing a different degree of 3D steering, was calculated with finite element analysis software. Fifty-six transducer elements were randomly distributed ($n=3$) in concave shells with $F\#s = 0.8, 1.0$ and 1.2 and focal length of 70 mm. Focusing was evaluated in a volume of $10\text{cm} \times 10\text{cm} \times 9\text{cm}$ (step= 1cm , 900 locations) centred around the natural focal length.

Results of the focal gain ($G = \text{Pressure focal location} / \text{Pressure next main lobe}$) indicated that the multiaxial driving increased the volume of adequate focusing ($G > 2.0$) in 134%, 126% and 37.5% for concave transducers with $F\#$ of 0.8, 1.0 and 1.2, respectively. Calculations of optimal multiaxial driving conditions were accelerated using our multi GPU-backend Rayleigh-Sommerfeld integral code (BabelViscoFDTD), allowing calculations to establish optimal driving conditions for a given focal location in a few ms of computing time. Results indicated that the multiaxial-driven method improves significantly the feasible region of correct focusing in all tested configurations, especially in the less densely-populated arrays.

The multiaxial method to drive transducers offer new opportunities to improve the degree of steering of phased arrays in concave configurations.

Canada Foundation for Innovation. Natural Sciences and Engineering Research Council of Canada. Mathematics of Information Technology and Complex Systems.



Rendering of simulated acoustic fields (isovolume at 50% peak pressure) of traditional and multi-axial phased arrays for different F#s.

Monitoring Focused Ultrasound Therapy of Tendon using Cavitation Detection

Presenter: Imogen den Otter-Moore

Authors in order: Imogen den Otter-Moore, *Hospital for Sick Children, University of Toronto*, Catherine Campbell, *University of Toronto*, William Chu Kwan, *University of Toronto*, Adam Waspe, *Hospital for Sick Children*, James Drake, *Hospital for Sick Children*

We previously demonstrated non-invasive tendon release using a therapy of histotripsy and ablation. This study investigates the measured cavitation activity during tendon histotripsy.

Porcine tendons were embedded in a 2% agar phantom and coupled to the acoustic window of the Sonalleve V1 MR-HIFU system. Tendons received a sonication at a central point along the longitudinal axis with pulse duration of 5, 10 or 20ms and pulse repetition frequency (PRF) of 1, 2 or 10Hz for 60s with n=4 per group. A cavitation detector collected acoustic emissions. Histotripsy was followed by ablation at 20W for 30s.

Two metrics were examined – inertial cavitation dose (root mean square of the subharmonic broadband signal) and cavitation activity (integral over the broadband subharmonic emissions). When PRF was held constant and pulse duration was increased we observed an increase in the inertial cavitation dose. We found that when PRF was increased above 1Hz the cavitation activity decreased over time (Figure 2). This decline was more pronounced for the 10Hz PRF than for the PRF of 2Hz. Visible lesions were present at the focal point in some tendons with lesion area increasing as pulse duration and PRF were increased (Figure 1).

Future work will examine what causes the decline in cavitation activity at high PRF (Figure 2). We will also use ultrasound shear wave elastography to detect any change in tendon stiffness following treatments and compare this change as a function of treatment parameters (total treatment time, pulse duration and PRF).

We thank Meaghan O'Reilly and Ari Partanen for their support. This work is funded by CIHR.

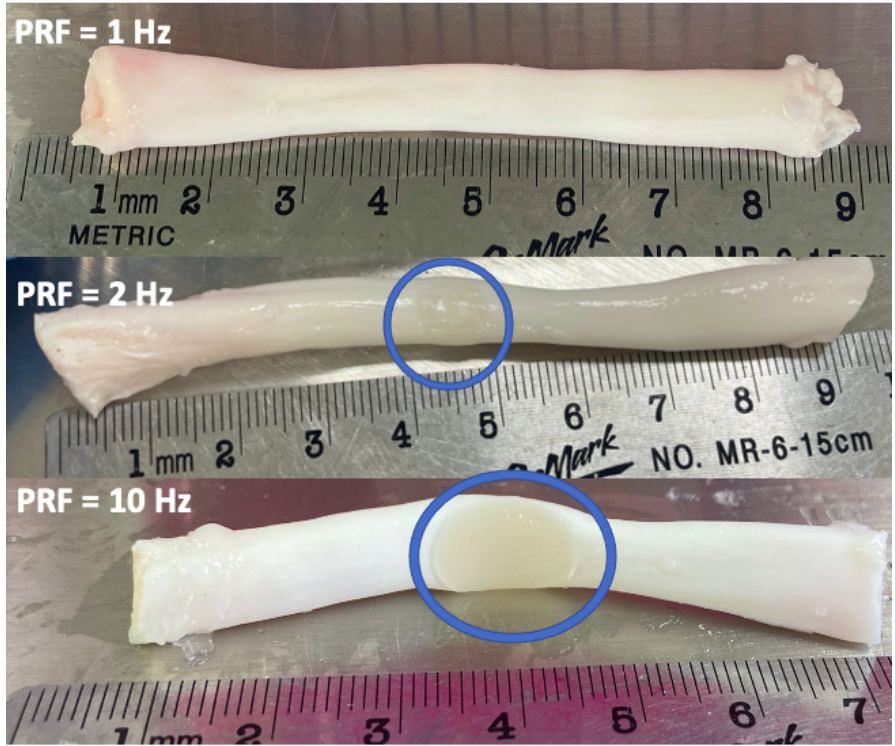


Figure 1: Lesion size as pulse repetition frequency is increased.

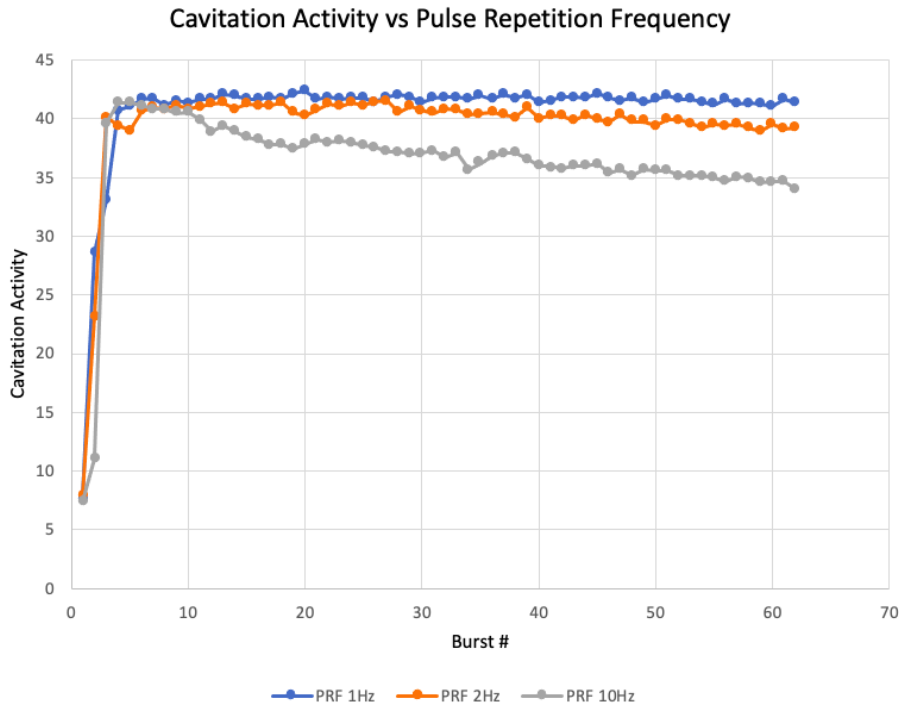


Figure 2: Cavitation activity as pulse repetition frequency is increased.

A Low-cost Driving Circuit for Microbubble-Based Therapeutic Ultrasound Systems

Presenter: Betül İlbelgi Yıldız

Authors in order: Betül İlbelgi Yıldız, *Imperial College London*, Zheng Jiang, *Imperial College London*, Timothy Hall, *University of Michigan*, James Choi, *Imperial College London*

We aimed to build a cost-effective therapeutic ultrasound driver for microbubble-based drug delivery which is scalable to arrays with a very high number of elements.

Most published work on driving engines have been designed for ultrasound imaging and high-intensity focused ultrasound. Here, we designed a low-cost circuit that emits a square wave through a filter to form a sinusoidal waveform. Two digital signals (0-3.3V) were used to control the amplitude and frequency of the signal. We tested our circuit with a 0.5MHz PZT-PVDF stacked transducer in a water-tank. Data were collected with a needle hydrophone and digitized by an oscilloscope.

Our circuit successfully produced 10-cycle pulses ranging from 100 kHz to 1 MHz with an amplitude of 0-150V. The frequency and the number of cycles were controlled by the rise and fall of one digital input (0-3.3V). The voltage amplitude was controlled with the duty cycle of a second digital input. As an example, a 10-cycle square wave pulse at 0.5MHz and with a 75 V amplitude was produced (Fig. 1a) and then filtered. The transducer emitted a sinusoidal pressure waveform (Fig. 1b) with a narrow centre frequency (Fig. 1c).

Here we demonstrate a low-cost, single-channel driving circuit. We are in the process of scaling this circuit up to a multi-channel driving system, enabling steering, and focusing. We estimate that the overall cost of a 128-channel driving circuit, excluding the power supply and control unit, would be less than \$1600.

We thank Paschal Egan for guidance with the circuit design and the Turkish Ministry of National Education for funding Betül's PhD Studentship

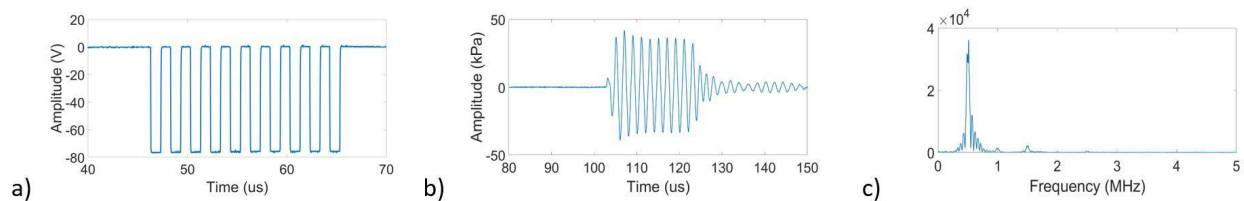


Fig.1. Signals from the (a) circuit and (b, c) the transducer.

Numerical Simulations and Experimental Verification of the Extent of HIFU-induced Necrotic Lesions

Presenter: Lukasz Fura

Authors in order: Lukasz Fura, *Institute of Fundamental Technological Research Polish Academy of Sciences*, Norbert Zolek, *Institute of Fundamental Technological Research Polish Academy of Sciences*, Tamara Kujawska, *Institute of Fundamental Technological Research Polish Academy of Sciences*

Development of a theoretical model to predict the extent of necrosis induced locally in ex vivo tissue exposed to a single or multiple HIFU beam.

The proposed tool was based on the modelling of non-linear acoustic wave propagation and heat transfer in heterogeneous media using the k-wave toolbox. The wave propagation equations were solved for two-layer (water-tissue) media. The distribution of heat sources was determined from the calculated acoustic pressure distribution in the HIFU beam. The obtained temperature distributions during heating and cooling allowed to calculate the thermal dose and predict the extent of the necrotic lesion.

The obtained simulation results were compared with the experimental data from previous studies. The mean difference between the numerically simulated and measured length or diameter of a single necrotic lesion was 1.37 ± 0.64 mm and 0.27 ± 0.25 mm, respectively. The axial and radial cross-sectional area of the larger cylindrical necrotic lesion (formed after multiple exposure to the HIFU beam) measured from the photos and MR images was also compared with the results of numerical simulations. The mean difference between the calculated cross-sectional area of a necrotic lesion planned for treatment, and that determined experimentally was approximately 11.2 %.

Due to the good agreement of the obtained results of numerical simulations with the experimental data, the applied numerical model describes well the thermal field induced locally in the examined tissue. Therefore, it can be used to optimize the planning of the treatment of solid tumors by the HIFU technique.

The work was partially supported by the National Science Centre (Grant 2016/21/B/ST8/02445) and ESF (POWR.03.02.00-00-I028/17-00) grants.

Spatial Filtering for Improved Passive Cavitation Imaging

Presenter: Kevin Haworth

Authors in order: Kevin Haworth, *University of Cincinnati*, Maxime Lafond, *LabTAU, Inserm U1032*, Nuria Salido, Christy Holland, *University of Cincinnati*

Four passive cavitation imaging (PCI) beamforming algorithms for diagnostic imaging arrays were explored to minimize the point-spread function and improve computational efficiency.

Delay, Sum, and Integrate (DSI) beamforming is computationally efficient but suffers from a large point-spread function (PSF). Robust capon beamforming (RCB) has a smaller PSF but is computationally costly. ROC analysis of simulations mirroring experimental PCI data (Lafond et al. 2021, *Ultrasound Med Biol*) obtained from an EkoSonic® catheter insonifying Definity® in an arterial flow phantom was used to identify binary masking thresholds for spatially filtering DSI and RCB PCIs to improve image quality.

Applying thresholding significantly reduced the spread of energy for DSI in both simulated and experimental data sets (Figure 1). Thresholding did not significantly impact RCB images. RCB was superior to DSI with respect to the area under the ROC, sensitivity, specificity, positive predictive value, and F1-score. However the differences between thresholded RCB and thresholded DSI beamforming algorithms were less than 8%. Sources mapped with a low amplitude signal were no longer observed after thresholding was applied. The computation times on a GPU were approximately 2 orders of magnitude smaller for thresholded DSI relative to RCB.

Data adaptive spatial filtering of DSI PCIs enables comparable predictive power, relative to RCB, for identifying cavitation source locations but at a significantly reduced computational cost. However, low amplitude sources were lost due to thresholding, which was observed for experimental data sets.

Funding provided by the U.S. National Institutes of Health (R01HL135092). Boston Scientific supplied the EkoSonic® endovascular system. We thank Curtis Genstler, MD, for helpful discussions.

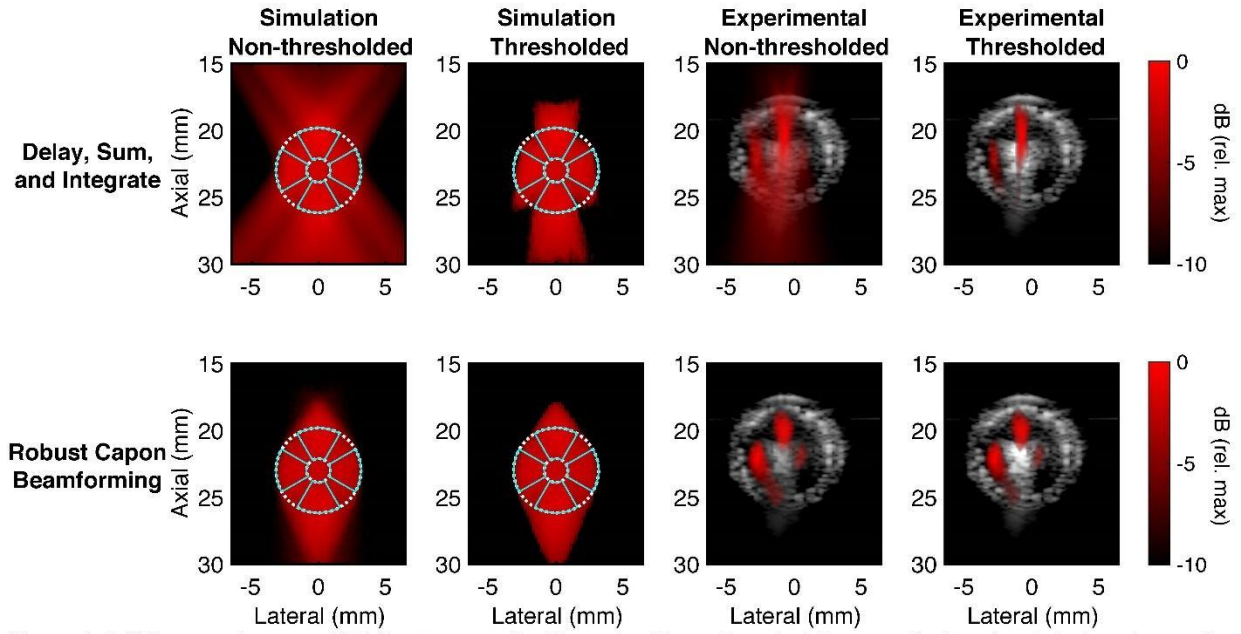


Figure 1: DSI (top row) versus RCB (bottom row) with and without thresholding applied to simulated and experimental data. The location of the simulated bubble clouds are outlined in cyan and are based on the beam pattern of an EkoSonic® catheter.

Gadgetron-based Open Source Thermometry Pipeline for Siemens MRI Platforms

Presenter: Craig Macsemchuk

Authors in order: Craig Macsemchuk, *University of Toronto*, Warren Foltz, *University Health Network*, Christopher Macgowan, *The Hospital for Sick Children*, Samuel Pichardo, *University of Calgary*, Adam Waspe, *Hospital for Sick Children*, James Drake, *Hospital for Sick Children*

To create Gadgetron pipelines to connect Siemens MRI scanners to the Proteus software platform to enable magnetic resonance-guided focused ultrasound (MRgFUS) research with Siemens scanners. Proteus is a software library to facilitate the development of new MRgFUS therapy applications.

Preliminary Siemens support does exist; however, an ideal connection between Proteus and Siemens scanners would allow all required software to run on a single workstation. This imaging pipeline would

need to be easy to deploy, configure and perform online data processing across many Siemens scanner models. Lastly, this online data processing pipeline must be real-time for MRgFUS controlled hyperthermia and ablation.

The Gadgetron open-source reconstructor framework was selected for interfacing with Siemens imaging pipelines. Next, we created a custom Docker-Compose deployment schema to enable streamlined deployment of Gadgetron and Proteus to the same workstation. Custom Gadgetron modules for saving data to Disk and for sending reconstructed images to Proteus for real-time thermometry were implemented. These modules were tested to reconstruct image data on the fly and reliably transmit the data from the Docker container to the host application running Proteus. Lastly, configuration sharing between Proteus and the Gadgetron container was completed to provide feedback to the user about the reconstruction status.

A pipeline was developed to connect the Proteus software library to Siemens MRI scanners for online data processing for MRgFUS thermometry. Integrity verification was done with ISMRM standard data. Deployment was addressed using an automatic container system. Testing with Siemens 1.5T and 3T scanners is underway for final pipeline verification.

Project funding provided by CIHR-NSERC Collaborative Health Research Project and the Focused Ultrasound Foundation's Follow-On Funding Program

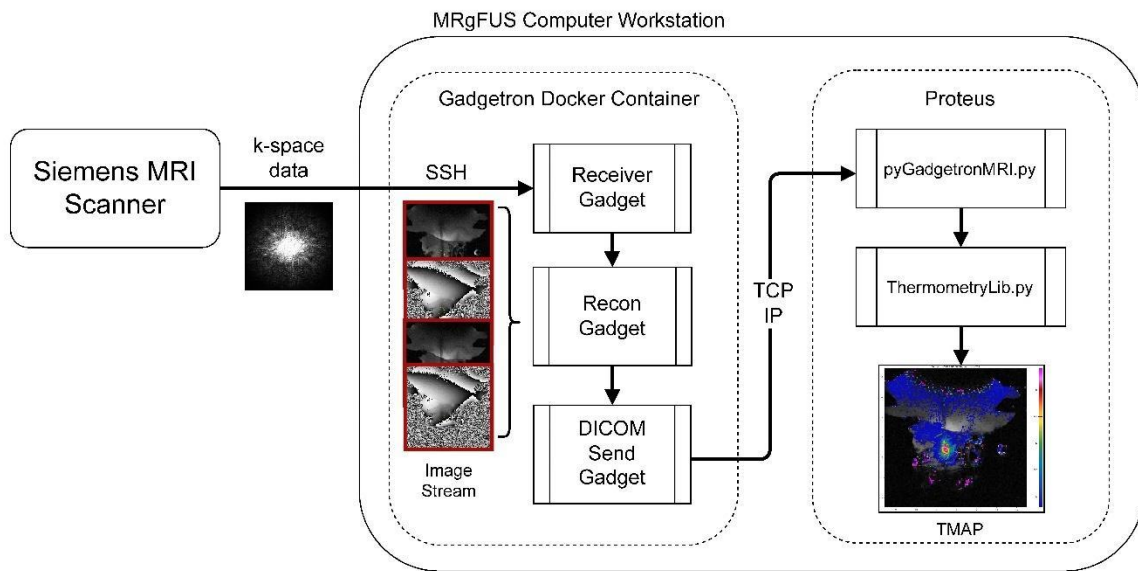


Figure 1: Image data pipeline between Siemens MRI, Gadgetron, and Proteus

Quantitative Acoustic Output Measurement Device for Low Intensity Focused Ultrasound Systems

Presenter: Mark Schafer

Authors in order: Mark Schafer, *Drexel University*, James Gessert, Samantha Schafer, *Drexel University*

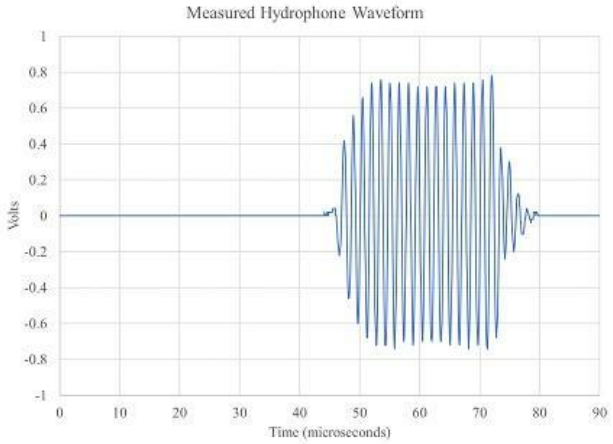
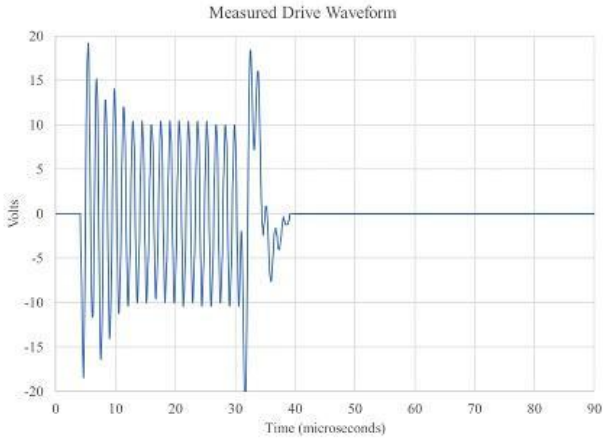
We have developed a hydrophone-based acoustic output measurement system that provides a convenient way to monitor Low Intensity Focused Ultrasound system output over time.

The device mates directly with the ultrasound treatment transducer to lock in the acoustic axis alignment. Acoustical coupling requires less than 20ml of water. A piezopolymer hydrophone located along the acoustic axis is embedded in a low loss castable silicone and sampled at 20MHz. The device interconnects between the transmit electronics and the transducer to measure the transmitter electrical power, frequency, and transducer electrical impedance. Control and analysis software run on a USB connected laptop.

Under program control, the system first disconnected the transducer from the drive electronics and measured the transmitter voltage and drive frequency. It then measured the transducer electrical impedance at that frequency. Finally, it reconnected the transmitter and drive electronics and measured the transmitted ultrasound wave as well as the change in the electrical drive signal when connected to the transducer. Experimental data showed that the system produced stable readings after repeated test cycles. The transducer output was reduced 5% by adding a resistor to the circuit; the shift was detected and the software alerted the operator.

The overall test process was convenient and rapid enough to be used before and after each clinical treatment, assuring exposure consistency over the course of a clinical study. Recorded data are timestamped to assess performance trends. Although optimized for single element transducers, the approach can be broadened to multi-element systems.

Work funded by Brainsonix, Inc.; patent pending



Transducer drive signal (left) and received waveform (right)

First Report on the Persist Time of the Free Radical Produced by Shock Wave Pulses Employed in Clinical ESWL

Presenter: Eun-Joo Park

Authors in order: Eun-Joo Park, *Seoul National University Hospital*, Min Joo Choi, *Jeju National University*, Jae-Young Lee, *Seoul National University Hospital*

This study was for evaluating the harmfulness of FR in the ESWL by measuring the incidence and persist time of FR caused by shock-wave in nanoseconds.

The OH* FR generated by the ESWL shock wave reacts with luminol and emits blue light, which is called sonochemical luminescence (SCL) phenomenon. FR generation and persist time were measured by recording this SCL with a sensitive photomultiplier tube (PMT) that responds in nanoseconds. An electromagnetic (EM) type ESWL device was used as the shock wave generator. A luminol solution was prepared by completely dissolving 0.1 g of luminol in 500 mL of distilled water.

As a result of measurement with the PMT, the amount of light emitted per unit time reached its maximum value within a very short time ($< \sim 600\mu\text{s}$) and then exponentially decreased for a long time (\sim several hundred ms). As the output of the shock wave generator increases, the minimum/average FR persist time increases, but the maximum value does not show a high correlation with the output setting. The amount of generated FR shows a very high correlation with the shock wave setting, and it increases very sensitively, rapidly and non-linearly as the setting changed from low to high.

Based on the generation and persist time of OH* FRs induced by ESWL shock waves observed using a luminol solution, in order to reduce the risk of FR to lithotripsy patients, it is recommended to the interval between the shock wave pulses sufficiently larger than the FR persist time.

This work was supported by a research grant from National Research Foundation of Korea (2017R1A2B3007907) and the Korea medical device development grant (1711134987, KMDF_PR_20200901_0010).

An Experimental Demonstration of the Ultrasonic Rewarming of Frozen Biological Tissue

Presenter: Rui Xu

Authors in order: Rui Xu, *University College London*, Elly Martin, *Department of Medical Physics and Biomedical Engineering, University College London*

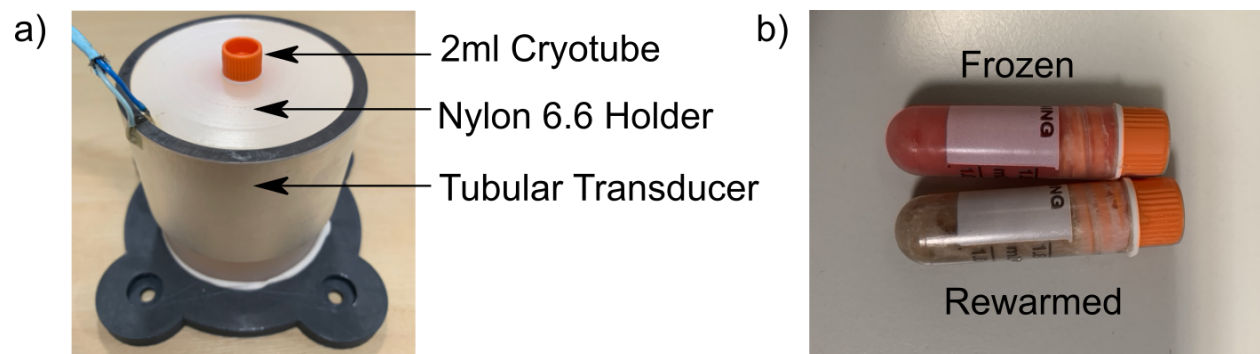
To investigate ultrasound as a new method for rewarming cryogenically preserved tissues and experimentally demonstrate the rewarming of a frozen biological tissue.

An air-backed tubular transducer with a Nylon coupling block (Fig. a) was designed and implemented for rewarming samples stored in 2 ml cryotubes. 5% fat minced beef was homogenized, loaded into 2 ml cryotubes with type T thermocouples embedded, and frozen in a -10°C freezer. Frozen samples were placed into the coupling block and the transducer was driven continuously (444 kHz). Sample temperatures were measured for both thermal conduction and thermal conduction + ultrasound cases.

Thermal conduction alone melted a sample but took 410s to warm from -1°C to 1°C . When ultrasound was applied, the time spent between -1°C to 1°C was reduced by approximately a factor of four. The temperature of the tissue must be increased at rates on the order of $30^{\circ}\text{C}/\text{min}$ to avoid cell-damaging ice crystal formation. Increasing the transducer driving voltage may further reduce the melting time. An initial trial demonstrated the browning of a beef sample within 5 minutes of heating (Fig. b), demonstrating the heating of both frozen and thawed beef.

Ultrasonic rewarming of frozen biological tissue was experimentally demonstrated for the first time in preliminary experiments. Further investigation is needed to optimise the acoustic parameters for faster warming, and to optimise for warming rates for cell survival.

This work was supported by the Wellcome/EPSRC Centre for Interventional and Surgical Sciences (WEISS) (203145Z/16/Z), and by a UKRI Future Leaders Fellowship [MR/T019166/1].



Evaluation of CMUT for Passive Monitoring of Microbubble-assisted Ultrasound Therapies

Presenter: Ambre Dauba

Authors in order: Ambre Dauba, *Université Paris Saclay*, Jordane Goulas, Laurent Colin, *GREMAN*, Laurène Jourdain, *Université Paris-Saclay*, Benoit Larrat, *CEA*, Jean-Luc Gennisson, *Université Paris Saclay - CNRS*, Dominique Certon, *GREMAN*, Anthony Novell, *BioMaps*, *Université Paris Saclay*, *CEA*, *CNRS*, *Inserm*

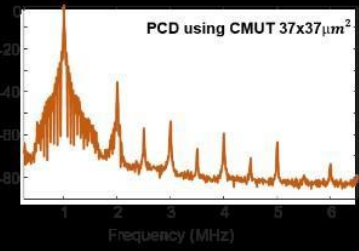
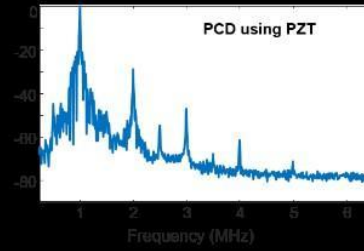
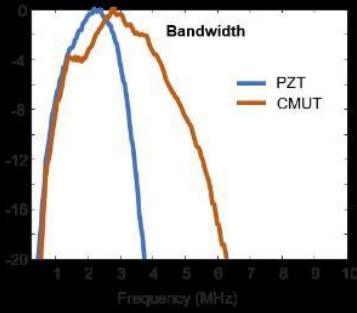
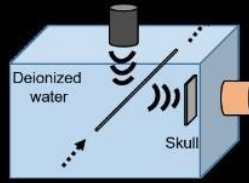
In this study, we exploited the unique properties of CMUT technology to ensure the safety of the ultrasound protocols through wideband passive cavitation detection.

Multiple CMUT single-elements were developed and characterized to determine their bandwidths, operating modes (collapse voltage) and nonlinear behavior when used in receive mode. Their ability to detect the signal from a flow of microbubbles (MB, SonoVue) through ex vivo skulls (rat or macaque) was also evaluated and compared with a standard piezoelectric transducer (V306 Olympus) used as PCD. MB were excited at $f_0=1\text{MHz}$ (PNP: 270kPa, 80 cycles every 100 ms) using an unfocused transducer (Imasonic).

All CMUT configurations were able to operate efficiently between 0.6 and 6.3 MHz. A moderate bias voltage must be applied to avoid intrinsic CMUT nonlinearity and detect the signal from MB. A bias voltage corresponding to 60% collapse is a good tradeoff between SNR and nonlinearity (SNR > 65dB; fundamental/harmonic ratio > 30 dB). Our results show that we were able to detect the MB through the skulls using CMUT. Compared to standard piezoelectric, the ultraharmonic signal from MB is increased by 23.3 dB through the rat skull and 12.1 dB for the macaque.

These results are encouraging for the development of a CMUT-based PCD setup for in vivo validation.

This work was partly funded by ANR DROPMUT (Grant No. ANR-19-CE19-0011) and France Life Imaging (Grant No. ANR-11-INBS-0006).



Modification of Heavily Calcified Lesions with Ultrasound-induced Microbubble Cavitation in PTA

Presenter: YUNG HAN LEE

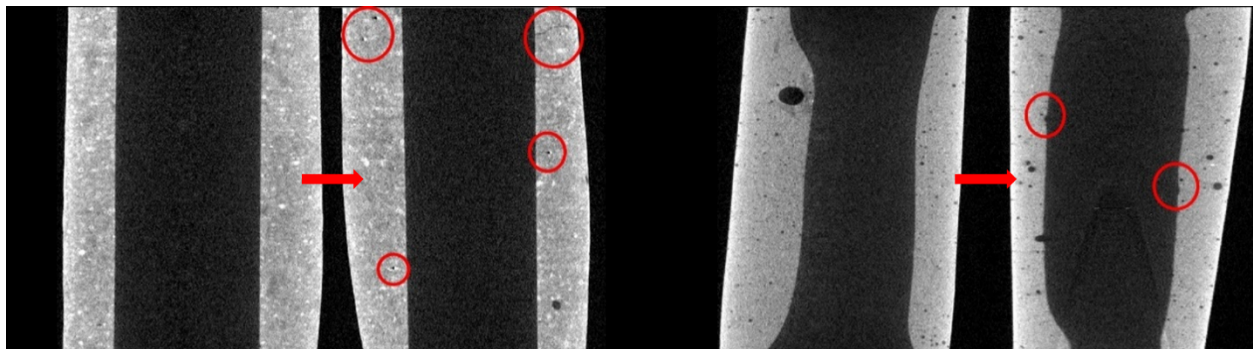
Authors in order: YUNG HAN LEE, *National Tsing Hua University*, Chieh-Yu Tsai, *National Tsing Hua University*, Liou Ya-Fu, *National Tsing Hua University*, Yu-Lin Chui, *National Tsing Hua University*, Chih-Kuang Yeh, *National Tsing Hua University*

This study proposed to use cavitation to disrupt calcified plaques and reduce the pressure required for PTA treatment.

Two different hardness of tubular plaster which corresponded to level 3 and level 4 in Agatston calcification scoring were made to mimic the calcified plaques. A 600 kHz US transducer was replaced in the plaster with an infusion of MBs to generate cavitation. After the treatment, a PTA catheter was inserted into the plaster and measured the pressure threshold for balloon inflation. The sonicated plaster was scanned by micro-CT to investigate the internal structural change.

The balloon inflation threshold of the level 3 plaster and level 4 were reduced from 4 ± 0.8 atm to 3 ± 0.3 atm and 9 ± 1.1 atm to 7.3 ± 0.7 atm, respectively. The CT slice images showed that small cavities and cracks had occurred in level 3, and minor pits had occurred on the inner surface of the phantom in level 4.

This data suggested that the pressure of PTA for disrupting calcified plaques could be reduced by cavitation. Future works include optimizing parameters and exploring in vivo applications.



Small cavities ,cracks and pits occurred after cavitation procedure

Robotic Device for Preclinical and Veterinary Trials of Focused Ultrasound

Presenter: Christakis Damianou

Authors in order: Marinos Giannakou, *Medsonic Limited*, Nikolas Evripidou, *Cyprus University of Technology*, Anastasia Antoniou, *Cyprus University of Technology*, Christakis Damianou, *Cyprus University of Technology*

This study aimed at the development of a Magnetic Resonance guided Focused Ultrasound (MRgFUS) robotic system for preclinical studies and veterinary trials in companion animals.

The performance of the developed robotic system was evaluated in terms of MR compatibility, positioning accuracy, and temperature evolution during high intensity FUS exposures by both benchtop and MRI techniques. The heating effects of the transducer were assessed by sonicating freshly excised tissue with varying sonication parameters. Finally, the in vivo efficacy of the developed system and therapeutic protocol was assessed utilizing a rabbit thigh model.

Sufficient accuracy of motion in three linear and one angular axes was demonstrated through benchtop and MRI techniques. The FUS transducer can be robotically moved with a mean positioning error smaller than 0.1 mm. In addition, the system was proven safe for operation in an MR environment exhibiting minimal effect on the quality of MR thermometry. Discrete and overlapping thermal lesions were successfully inflicted in freshly excised tissue depending on the selected sonication parameters. Regarding in vivo validation, well-defined areas of coagulative necrosis were produced on rabbit tissue. Remarkably, no adverse events compromising animal welfare were reported.

In conclusion, a compact and ergonomic robotic device has been developed and validated through extensive preclinical studies. In vivo FUS ablation in rabbits was proven safe and feasible when performed under proper monitoring. Future actions include validation of the device in pets.

Changes of Mechanical and Ultrastructural Characteristics of In-vitro Human Hematomas Over Time

Presenter: Kseniia Tumanova

Authors in order: Kseniia Tumanova, *Physics Faculty, Lomonosov Moscow State University, Moscow, Russian Federation; Department of Medical Biophysics, Temerty Faculty of Medicine, University of Toronto*, Ekaterina Ponomarchuk, *Lomonosov Moscow State University, Physics Faculty*, Anna Kunturova, *Lomonosov Moscow State University, Physics Faculty*, Anastasia Tyurina, *Physics Faculty, Lomonosov Moscow State University, Moscow, Russian Federation*, Alexey Kadrev, *Medical Research and Educational Centre, Lomonosov Moscow State University*, Sergey Buravkov, *Lomonosov Moscow State University*, Vera Khokhlova, *Physics Faculty, Lomonosov Moscow State University, Moscow, Russian Federation; Center for Industrial and Medical Ultrasound, University of Washington, Seattle, United States of America*

In the context of biological tissue susceptibility to histotripsy liquefaction, stiffness and ultrastructure of large clotted blood volumes in vitro were investigated over time.

Naturally clotted (55mL) and recalcified with 25 mmol/L of CaCl₂ solution at 37°C human blood samples (55mL and 200mL) served as large-volume hematoma models. Shear moduli were measured by shear wave elastography (SWE, Aixplorer Supersonic Imagine, SL7-14 probe) during clotting for 120 min, and then once a day during 8-day storage of the formed clots by SWE and with a custom-built indentometer. Ultrastructural analysis was performed using scanning electron microscopy (SEM, Camscan Series 4).

For recalcified hematomas, the shear modulus reached a stationary value of 0.53 ± 0.17 kPa (averaged across all samples) within 20–25 min after the onset of clotting at 37°C and remained unchanged till the end of observations. Both SWE and indentometer measurements demonstrated that the shear modulus values do not change significantly over 8 days, regardless of the method of blood clotting. Scanning electron microscopy has not revealed any apparent ultrastructural changes of the fibrin fibers over 8 days (Fig. 1).

The results demonstrate that once the large-volume hematoma in vitro model is formed (20–25 min after coagulant is added at 37°C) its shear modulus and ultrastructure of the fibrin network remain unchanged for the next 8 days, which arguably should not directly affect hematoma sensitivity to ultrasound exposure.

Work supported by NIH R01GM122859, RFBR 20-02-00210, FUSF Global Internship Program, “BASIS” Foundation student grants 20-2-10-10-1, 20-2-1-83-1.

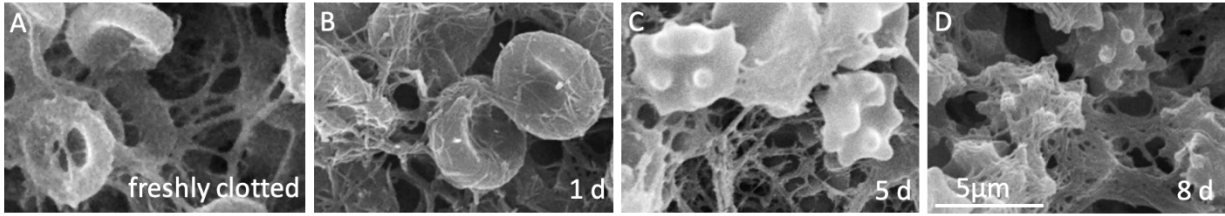


Figure 1: SEM images of the formed hematoma content over time.

In-vitro Evaluation of Single Pulsed vs. Burst Shock Waves

Presenter: Nina Reinhardt

Authors in order: Nina Reinhardt, *Chair of Medical Engineering, RWTH Aachen University,* Matias de la Fuente

The aim of this work is to compare the mechanical effects of single pulsed and short burst high energy shock waves in a stone model.

Two commercial piezoelectric transducers with similar geometries but different numbers of oscillations were examined. Both devices were compared at a setting with the same maximum pressure but different pulse intensity integrals. Sound field measurements, stone fragmentation and B-mode cavitation detection were conducted in an in-vitro test setup in ultrapure degassed water. The fragmentation of stone phantoms was used as an objective measure in order to evaluate the direct mechanical effects of the pressure waves.

In the focal spot, the burst wave device generates a significantly higher energy density than the shock wave device due to the higher number of oscillations. The peak positive and negative pressure are in the same range for both devices. The differences in the sound field characteristics also influence the mechanical effects in vitro. In the stone comminution setup, the fragmentation effect of burst waves was significantly reduced compared to single pulsed shock waves at the same peak maximum pressure. In water, B-mode measurements showed that burst waves generate significantly more and longer lasting cavitation compared to shock waves.

The measurements demonstrated impaired stone fragmentation with burst waves despite higher energy densities compared to shock waves. This can be due to cavitation clouds, which dampen subsequent shocks. The interplay of sound field parameters and the test setup affect the mechanical effects. Next, the transferability into clinical practice is investigated.

Research funding: This work was supported by Richard Wolf GmbH, Knittlingen, Germany.

Sonowell®: A Versatile Ultrasound Platform for Reproducible In-vitro Experiments on Prokaryotic and Eukaryotic Cells

Presenter: Gaetano Barbato

Authors in order: Gaetano Barbato, *Inno-Sol SRL*, Jessica Cornice, Francesca Zazzeroni, Rosanna Papa, Donatella Lucchetti, Alessandro Sgambato,

Set up a versatile instrument platform able to perform different types of experiments on cells using standard well plates while optimizing measures reproducibility.

Several studies have analyzed the problems arising from the interaction of ultrasound (US) waves with the plasticware of common plate-wells [1-4]. Following a strategy of finding different mitigating solutions to the problems we have designed and patented a bench-top US system the SonoWell®; and two new technologies Block-US™, minimizing shear waves and mode conversion waves and Inno-CAP™, minimizing reflections and cavitation. Using the platform on different applications we demonstrate the improvement of measures reproducibility [5-7].

We demonstrate that it is possible to perform reproducible in vitro experiments with cellular studies in different fields (i.e. identification of 4 new potential miRNA biomarkers released from prostate cancer cells [5]; study of LIPUS induced changes in malignant phenotype of CRC cells [6]; influence on inhibitory concentration of antibiotics on multiresistant bacterial cells [7]), sonicating with different frequencies simultaneously on the same plate or keeping constant the relevant physical parameters, for instance acoustic pressure, but varying one at the time frequency, pulse length or duty cycle etc, obtaining very reproducible results, as shown by the SD values.

Using the suitable combination of our platform SonoWell®; + Block-US™; + Inno-CAP™; robust and reproducible results on cellular experiments are obtained using standard 6-96 plate-wells.

Bibliography

Hensel K et al. *Ultrasound Med. Biol.* 2011 Dec;37(12):2105-15

Kinoshita M. et al. *Biochem Biophys Res Commun.* 2007 Aug 10;359(4):860-5

Shear Wave Passive Elastography for Crystalline Lens Elasticity Measurement in the Context of Presbyopia Treatment

Presenter: Alice Ganeau

Authors in order: Alice Ganeau, *INSERM*, Gabrielle Laloy Borgna, *University of Lyon*, Maxime Lafond, *LabTAU, Inserm U1032*, Thibaut Divoux, *ENS of Lyon*, Olfa Ben Moussa, *BiigC, University of Saint Etienne*, Frédéric Mascarelli, *BiigC, University of Saint Etienne*, Cyril Lafon, *INSERM*, Stefan Catheline, *INSERM, University of Lyon*

We propose curvilinear shear wave elastography to monitor the potential softening of the speckle-free crystalline lens, exposed to ultrasonic cavitation for presbyopia treatment.

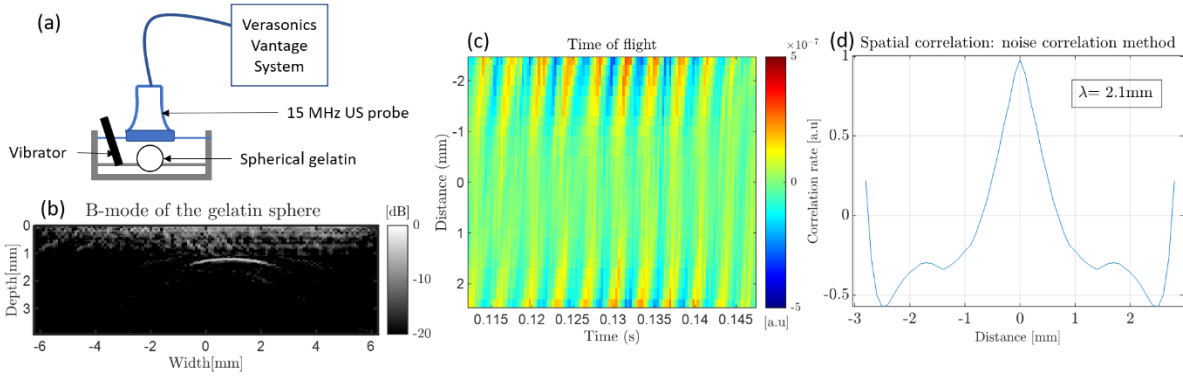
Lens is transparent to ultrasound excepting its interface, rendering classic elastography inapplicable. Gelatin spheres were used to evaluate the feasibility of curvilinear elastography. Vibrations (0.1–3.5 kHz) were induced by vibrators and tracked by ultrafast ultrasound imaging along the capsule. Three methods of elasticity measurements were compared in gelatin spheres and ex vivo porcine whole eyes: time of flight (TOF), noise correlation and indentation (response to a compressive strength, not applicable in the whole eye).

The measured Young moduli in the gelatin spheres was consistent across the three methods: 62 ± 16 kPa, 50 ± 2.9 kPa, and 42 ± 4.6 kPa for the TOF, noise correlation, and indentation, respectively. Spectral analysis indicated only a small dispersive effect. The same acquisitions were performed on pig lenses by vibrating the entire eye. We found elasticity consistent with other studies 0.8 ± 0.1 kPa (0.52 ± 0.03 m/s) using both TOF and noise correlation methods. However, spectral analysis showed a marked dispersion, likely because of the complex inhomogeneous structure of the lens. Further studies are necessary to understand its impact on elasticity.

The experiments implemented on the gelatin spheres validated the curvilinear shear wave elastography method. Spectral analysis in lens highlighted the complexity of this inhomogeneous multilayer medium. Shear waves elastography into the crystalline lens could enable to assess the efficacy of cavitation as a potential treatment for presbyopia.

This work was supported by the Focused Ultrasound Foundation (FUS).

A special thanks to the BiigC lab and the Physics lab of ENS Lyon.



Set-up and methods to measure elasticity by Shear Wave Elastography

Synthetic Focalization using the Correlation Framework

Presenter: Tamara Krpic

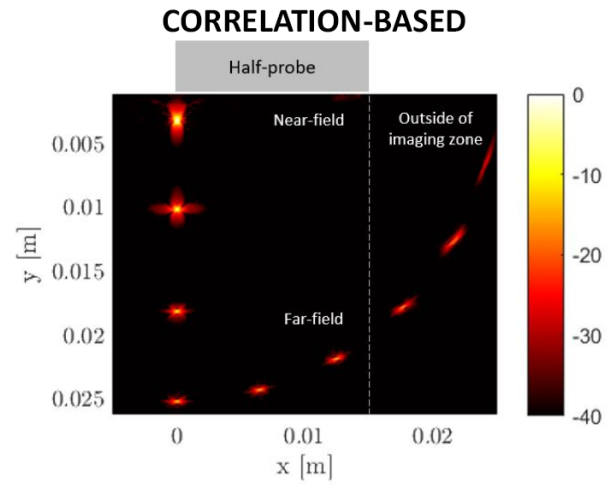
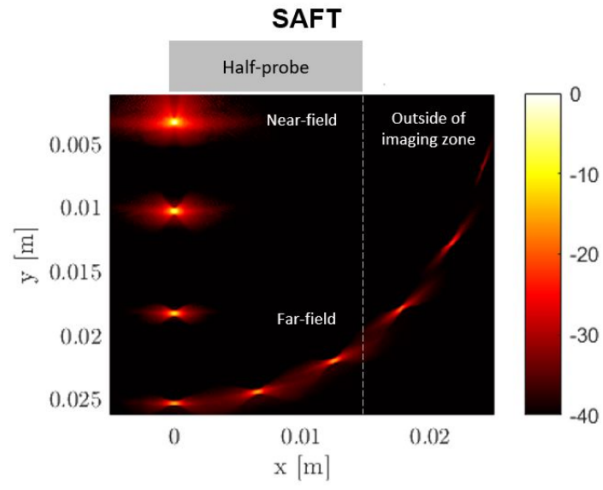
Authors in order: Tamara Krpic, *Universite de Sherbrooke*, Maxime Bilodeau, *GAUS - Université de Sherbrooke*, Patrice Masson, *Université de Sherbrooke*, Nicolas Quaegebeur, *Universite de Sherbrooke*

In this work, the benefits of using the correlation framework for synthetic imaging is presented through the use of analytical, numerical and experimental baselines.

Using a realistic signal database for correlation with measured signals allows considering and correcting the intrinsic properties of the transducers (directivity, dynamics, imperfections, lenses). In this work, different databases (numerical and experimental) are constructed by considering point-like reflectors at different locations. Numerical databases are constructed using Field-II, while experimentally, a robot arm (UR5e) is used to automate the Full Matrix Capture measurement of a 64-element probe over a moving steel wire (0.4 mm diameter).

When compared with the Synthetic Aperture Focusing Technique (SAFT), the use of simulated or experimental signal databases results in improved lateral and axial resolutions and in a reduction of imaging artefacts. Using the experimental database also results in contrasts below -80 dB in the case of point-like reflectors such as contrast agents. This formalism allows retrieving the phase of the identified reflectors, which can be used to determine the nature of the different reflectors. Finally, the observation window can be extended since transducer directivity and sensitivity are compensated through correlation, allowing enhanced near-field imaging and extended angular apertures.

The performance of different signal databases in the correlation framework are compared. For all databases, the formalism enables phase imaging which can be used for feature distinction. By using the experimental database, all classical image quality metrics are improved, and the observation window is increased with respect to SAFT imaging.



P3-6

Design of an Array of Multiaxial Sensors for Usage in Passive Cavitation Imaging

Presenter: Raya Subah

Authors in order: Raya Subah, *University of Calgary*, Nathan Meulenbroek, *University of Calgary*, Adam Waspe, *Hospital for Sick Children*, Samuel Pichardo, *University of Calgary*

This project's objective was to fabricate an attachment to contain piezoelectric sensors using computer-aided design (CAD) and 3-D printing for multi-axial passive cavitation imaging (PCI).

Initial designs were conceptualized through multi-view technical drawings. Models were then created using the CAD software SolidWorks, 3-D printed, then fit tested inside a water-filled cone. Three iterations were created following the same procedure, resulting in modifications to both the transducer cone and sensor casings. An attachment system was contrived to fasten the array to the transducer cone by designing places for tapped holes aligned between the array and the cone on SolidWorks.

Six CAD models were developed to address problems identified during the prototyping process. Final physical models of the array attachment and sensor casings were 3D-printed and fit tested together successfully. The modified cone was also 3-D printed, and fit tested with the array. The sensor casings fit within the array attachment, and in turn, the array fits within the transducer cone. Using nylon screws, an attachment system was implemented to fasten the array and cone together. The sensor casings were affixed to the array using silicone adhesive. The system is ready to be used in preliminary experiments.

A modular array holder for PCI was implemented. This project will be integrated with a focused ultrasound platform being co-developed by The Hospital for Sick Children (Toronto, ON) and the University of Calgary. This project contributes to the development of safe and effective therapeutic ultrasound methods and their clinical translation.

We are grateful for the support received from the Focused Ultrasound Foundation and the Schulich School of Engineering at the University of Calgary.



Array (Left), Modified Casing (Top Right), and Cone (Bottom Right)

The Development of a Graphical User Interface for Passive Cavitation Detection During Boiling Histotripsy Treatments

Presenter: Catherine Campbell

Authors in order: Catherine Campbell, *University of Toronto*, Imogen den Otter-Moore, *Hospital for Sick Children*, Samuel Pichardo, *University of Calgary*, Naomi Matsuura, *University of Toronto*, Adam Waspe, *Hospital for Sick Children*, James Drake, *Hospital for Sick Children*

A custom cavitation detection software was developed and employed to assess the effects of varied sonication powers, treatment durations, and focal depths on cavitation.

A Python-based, multithreaded application compatible with existing lab software was developed using a Qt GUI framework. The software was used to collect data during histotripsy treatments on agar phantoms and bovine liver at 1.2MHz, 10ms pulse duration, 1% duty cycle, 100-900W power, and 60-300s treatment duration. Inertial cavitation dose (RMS amplitude of the filtered voltage signal) and cavitation activity (integral over the broadband subharmonic frequency emissions) were calculated, and lesions were measured using MR imaging.

Generally, higher acoustic power resulted in higher cavitation activity. Cavitation consistently peaked early in the treatment and then decreased over time, indicating a diminishing effect of continued sonication after a certain time (Figure 1). Greater cavitation signal and larger lesion area were measured in foci closer to the transducer in agar phantoms (Figure 1), whereas no such conclusion could be made in liver due to high variability between replicates. Cavitation signal was detectable at up to 7.5cm in liver, the deepest focal length tested. Liquified lesions were visible throughout the liver (Figure 2), consistent with successful histotripsy.

The presence of cavitation signal from deep within the liver tissue suggests that histotripsy may be effective at depths of up to 7.5 cm. The software developed provides real-time monitoring and quantitative measurement of cavitation, both of which are valuable tools for enhancing the clinical feasibility of histotripsy therapies.

We acknowledge funding from the FUS Foundation Global Intern program and CIHR. We also thank Ari Partanen and Craig Macsemchuk for their technical support.

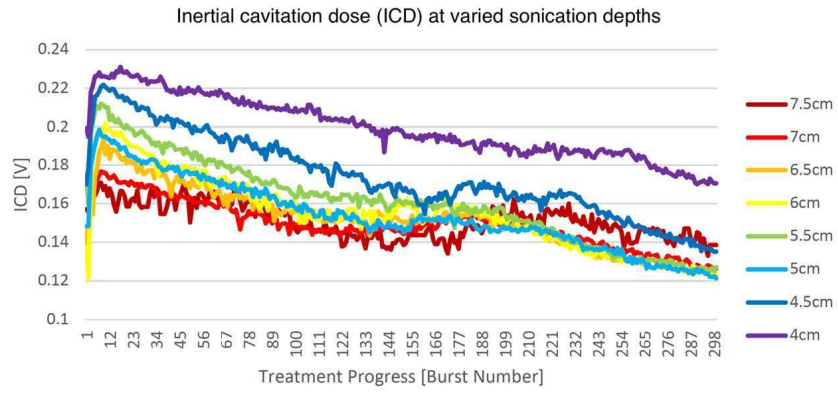


Figure 1. ICD voltage signal at varied sonication depths in phantom

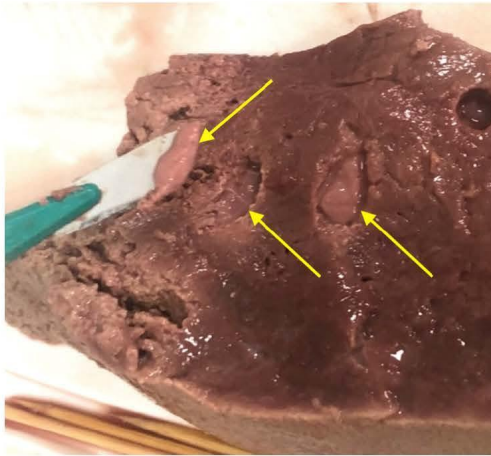


Figure 2. Sonicated liver with liquified tissue lesions

Increase of the Ablated Volume in Liver Tissue using a Cross-shaped Toroidal Transducer

Presenter: Sophie CAMBRONERO

Authors in order: Sophie CAMBRONERO, *LabTAU, INSERM, Centre Léon Bérard, Université Lyon 1, Univ Lyon, F-69003, Lyon, France*, David Melodelima, *INSERM*

A cross-shaped HIFU toroidal transducer has been developed for the treatment of liver tumor. The treated volume can be significantly increased using shifted focalization.

The radius of curvature, diameter and frequency of the cross-shaped toroidal HIFU transducer respectively were 130mm, 120mm and 1.1MHz. A 6MHz US-imaging probe was placed at the center of the transducer. The transducer surface was divided into two rectilinear bands forming a cross. The optimal surface of each band for using shifted focalization was found to be 33% of the total transducer surface. In vitro experiments were performed using one band of the cross-shaped transducer.

The active surface ratio of 33% was optimum to maximize the pressure at the shifted focus while reducing side lobes. HIFU lesions were created using shifted focusing 9mm away to the right and then left of the emission axis. Each HIFU exposure lasted 34 seconds using an acoustic power of 105W. HIFU lesions were created in the liver at a depth of 32mm from the hepatic capsule. The shortest and longest axes of the HIFU lesions were 25 mm and 33 mm respectively (Figure 1).

A cross-shaped toroidal transducer allows for maximization of the pressure at the focal zone shifted 9mm from the emission axis while minimizing the undesirable pressure on the axis and the number of elements composing the transducer. Such device can result in an increase of the treated volume without resorting to

This work was partly funded by the French National Research Agency (ANR-19-CE19-0027-01) and by the FUS Foundation (N° RC17129CC).

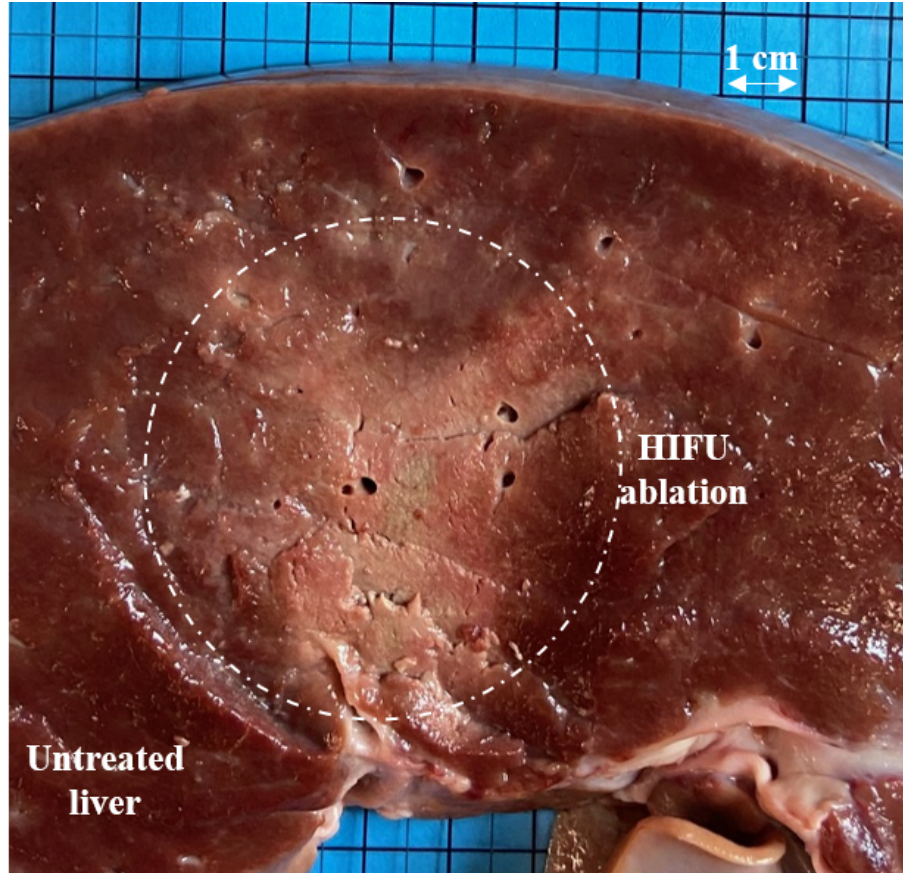


Fig. 1. HIFU ablation created in the liver with a cross-shaped toroidal transducer

P3-9

Development of 3T Head Coil to Improve MRgFUS Planning and Therapy

Presenter: Giulia Frazzetta

Authors in order: Giulia Frazzetta, *Insightec*, Ryan Clanton, *Insightec*, Kevin Tsai, *Insightec*, Paul Wragg, *InSightec LTD*, Itay Rachmilevitch, *Insightec Ltd*.

Insightec's newly developed 3T head-coil aims to improve the imaging used for planning and real-time thermal monitoring;Magnetic Resonance;guided Focused Ultrasound (MRgFUS) therapy.

MRgFUS;therapy relies;on precise planning images for targeting and thermal images for heat monitoring. We developed a customized;3T coil to be used in treatment to improve both. The new coil;was validated and approved by FDA and CE. As part of the validation we performed testing and volunteers sessions to assess the benefit of the new 3T coil from both a;quantitative and qualitative standpoint compared to the current 3T imaging standard.

;The thermal imaging validation results are:

Current Standard

3T Head Coil

Single Echo -TMAP

Phase Time

3.45

2.3

SNR / SD

13 / 1.4

46 / 0.9

Multi Echo-TMAP

Phase Time

3.65

2.6

SNR / SD

9 / 1.2

18 / 0.8

Multi Slice Multi Echo TMAP (MMM)

Phase Time

5.7

3.9

SNR / SD

Not usable

23 / 0.8

We improved nominal planning sequences in terms of SNR and acquisition time (example in Figure 1), and we developed new high resolution sequences that were previously not possible due to existing hardware limitations (example in Figure 2).

Figure 1

Figure 2. 3D T1 FSPGR. Whole head acquisition, scan time 2:50

The introduction of the 3T coil is expected to significantly improve the current imaging standard for 3T MRgFUS imaging and positively impact the therapy flow. The improvement of live thermometry will allow for more precise thermal monitoring; the new planning sequences will allow for better image based targeting and lesion evaluation.

SA-1

The Evolution of Ventral Intermediate Nucleus (VIM) Targeting in MRgFUS Thalamotomy for Tremor: An International Perspective

Presenter: Ayesha Jameel

Authors in order: Ayesha Jameel, *Imperial College*, Sena Akgun, *La Sapienza University*, joely smith, *Imperial College London NHS Trust*, Nada Yousif, *University of Hertfordshire*, brynmor jones, *IMPERIAL COLLEGE HEALTHCARE NHS TRUST*, dipankar dipankar.nandi, *IMPERIAL COLLEGE HEALTHCARE NHS TRUST*, peter bain, *IMPERIAL COLLEGE*, wladyslaw gedroyc, *IMPERIAL COLLEGE HEALTHCARE NHS TRUST*

To ascertain the various international approaches to targeting the VIM in MRgFUS thalamotomy for tremor, and consider how targeting has evolved internationally as experience develops.

All 39 MRgFUS centres from Insightec's international database who perform thalamotomies for tremor were invited to participate by sharing their VIM targeting approach (VIM-TA) in 2019 and 2021. Each centre was contacted at least 3 times.

Results were analysed with regard to anatomical landmarks and use of tractography; and change in approach. Each VIM-TA was mapped in relation to the mid-commissural point (MCP) onto a 3D model of the thalamus based on the Schaltenbrand-Wahren Atlas.

30 centres participated across the study period; 26 centers reported 2019 VIM-TA, 22 centers provided 2021 VIM-TA and 20 centers shared both.

In 2019, 92.3% centres (n=24) and in 2021, 95.7% centres (n=21) based targeting on anatomical landmarks rather than tractography. Although in 2021, 30.4% centres (n=7) incorporated tractography as a targeting adjunct, citing reliability as a challenge.

In 2019, 37.5% VIM-TAs were level with the MCP, however, in 2021 there was a notable superior trend with 43.5% targeting 2mm above MCP (previously 11.5% in 2019). In contrast, the VIM-TA medial-lateral and anterior-posterior positions remained stable across the study period.

In the 2-year interval from 2019 to 2021, many MRgFUS centers have evolved their VIM-TA with a notable move superiorly within the VIM (2mm above the MCP) and the introduction of tractography to aid VIM localisation. This pattern has been demonstrated internationally and independently across the participating MRgFUS tremor centres.

We would like to thank the Focused Ultrasound Foundation and all MRgFUS centres that participated, all of whom cannot be listed here due to word count restrictions.

SA-10

In-situ Encapsulation of Free DNA with Microbubbles (MBs) and Focused Ultrasound (FUS)

Presenter: Matthew Chen

Authors in order: Matthew Chen, *University of Toronto*, Catherine Campbell, *University of Toronto*, James Drake, *Hospital for Sick Children*, Adam Waspe, *Hospital for Sick Children*, Naomi Matsuura, *University of Toronto*, Sean McGrath, *University of Toronto*, Matthew Di Carlo, *University of Toronto*

To assess the encapsulation efficacy of surrogate circulating tumour DNA (ctDNA) in liposomes with MBs and FUS for liquid biopsy applications.

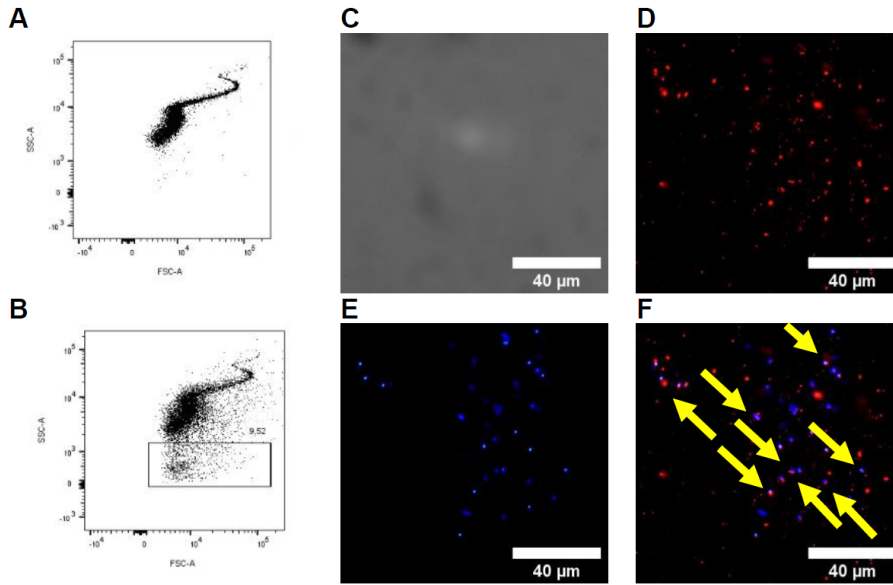
Definity™ MBs ($\sim 2 \times 10^7$ /mL), DAPI-stained free DNA, and calcein (0.001 mM) were insonated under flow (10mm/s) in a polyimide tube (ϕ : 1.1mm) with FUS (1 MHz, 5% duty cycle, 550 kPa) to encapsulate salmon sperm DNA as ctDNA surrogate; and calcein as a fluorescent marker. MB size and concentration were measured using for size and concentration; DNA and calcein encapsulation were assessed with fluorescence microscopy and flow cytometry. 5×10^4 events were counted for flow cytometry measurements.

Flow and insonation of MBs with DAPI-stained DNA and calcein each resulted in the formation of a secondary population of particles; $2.3 \pm 0.9 \times 10^2$ particles (flow alone) and $5.1 \pm 0.6 \times 10^3$ (flow+FUS). Under both conditions, this secondary population contained $1.5 \pm 0.6 \times 10^2$ (58.7 \pm 4.8%, flow) and $1.6 \pm 0.1 \times 10^3$ (31.8 \pm 2.5%, flow+FUS) calcein-positive particles. Significantly ($p < 0.001$) more calcein-positive particles were present with flow+FUS. Among this population, FUS also significantly ($p < 0.01$) increased the number of DAPI-positive particles from 67 ± 25 (flow) to $5.0 \pm 0.9 \times 10^2$ (flow+FUS). This demonstrated the increased number of particles containing both DNA and calcein due to FUS.

FUS-cavitated MBs create particles that can encapsulate nearby free DNA and fluorescent molecules. This system may be an avenue to identify and isolate tumour DNA released in the bloodstream at low concentrations (e.g., for liquid biopsies in the brain). Future work will evaluate the capability of ctDNA capture in vivo.

This work was funded by CIHR, NSERC, ORF, Government of Ontario, EMHSeed, The Hospital for Sick Children, OCE, CCSRI, PCC, NFRF.

Figure. (A) Microbubbles flowed without ultrasound resulted in a single population with flow cytometry in a forward scatter (FSC) -side scatter (SSC) dot plot. (B) However, when exposed to focused ultrasound a secondary group of particles were consistently created. (C) Under optical microscopy (D) Lipophilic stain (red) was used to visualize the co-localization of lipids with (E) DAPI-stained DNA, as (F) overlaid in a composite image and indicated in yellow.



MRI-Targeted Focused Ultrasound Blood-Brain Barrier Opening for Drug Delivery to Cerebral Cavernous Malformations

Presenter: Delaney Fisher

Authors in order: Delaney Fisher, *University of Virginia*, Khadijeh Sharifi, *University of Virginia*, Anna Debski, *University of Virginia*, Catherine Gorick, *University of Virginia*, Jeyan Kumar, *University of Virginia*, Rene Roy, *University of Virginia*, G. Miller, *University of Virginia*, Petr Tvrdik, *University of Virginia*, Richard Price, *University of Virginia*

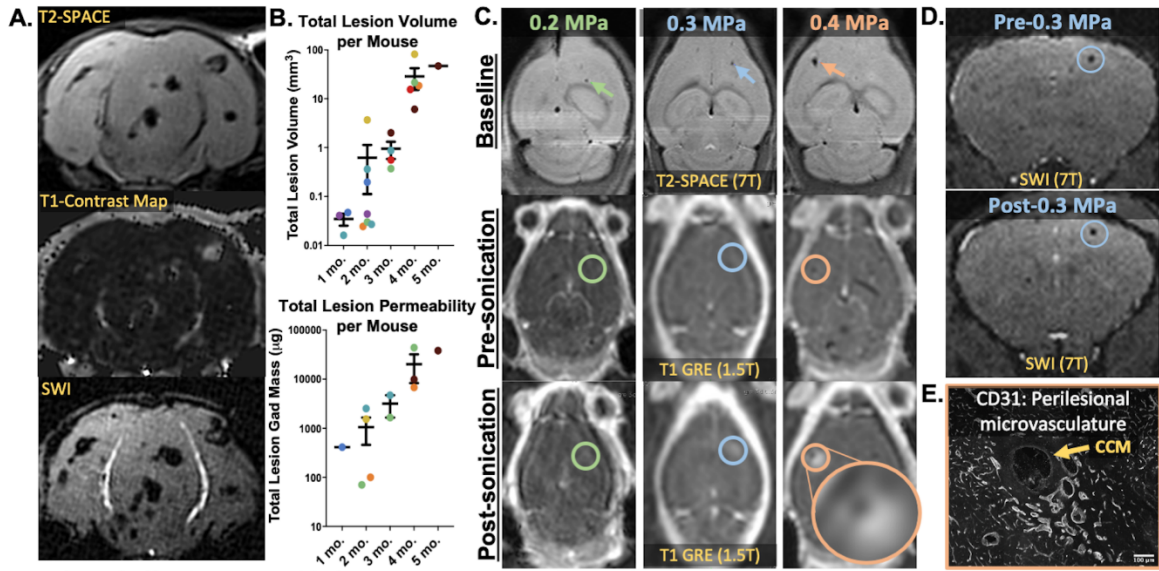
Develop optimized MRI protocols for targeting and monitoring murine cerebral cavernous malformations (CCMs) and demonstrate safe, effective FUS blood-brain barrier opening (BBBO) to CCM microenvironment.

CCMs—hemorrhagic lesions of the cerebral vasculature—were induced in mice by postnatal, endothelial-specific (PdgfbCreER or Cdh5CreER) Krit1 ablation. MRI protocols (T2-SPACE, T1-contrast-mapping, and susceptibility-weighted imaging [SWI]) were optimized at 7T MRI to monitor CCMs in the absence of, prior to, and following FUS BBBO. CCM mice were sonicated (i.v. microbubbles; 1.1-MHz; 10-ms bursts; 0.5-Hz PRF; 2-min) at either 0.2-, 0.3-, or 0.4-MPa peak-negative pressure.

Our MRI protocols enabled long-term monitoring of lesion volume (T2-SPACE), permeability (T1-contrast mapping), and iron deposition (SWI; Fig. 1A), which established baseline CCM burden over our model's lifespan (Fig. 1B). FUS-mediated BBBO delivered gadolinium contrast agent to the CCM microenvironment at 0.2-, 0.3-, and 0.4-MPa as a function of peak-negative pressure (Fig. 1C). SWI pre- and post-treatment revealed no increases in iron deposition, indicating lack of hemorrhage and thus safe BBBO parameters (Fig. 1D). The pattern of contrast enhancement suggests that access to the CCM microenvironment is via the perilesional microvasculature rather than the lesion itself (Fig. 1C, E).

To our knowledge, this is the first-ever application of FUS-augmented drug delivery to CCMs. Despite the abnormal endothelium associated with this disease, our results indicate that FUS BBBO can be a safe, effective approach in this context, laying the foundation for much-needed improvement of therapeutic options for this debilitating disease.

Supported by NIH R01EB030744 and R01NS111102 to RJP and AHA 830909 to DGF.



Safe and Effective MRI-guided FUS BBBO to CCM Microenvironment

Histotripsy for the Treatment of Primary Bone Tumors: In-vivo Canine Study

Presenter: Lauren Ruger

Authors in order: Lauren Ruger, *Virginia Polytechnic Institute and State University*, Alayna Hay, *Virginia-Maryland College of Veterinary Medicine*, Jessica Gannon, *Virginia Tech - Wake Forest School of Biomedical Engineering and Sciences*, Hannah Sheppard, *Virginia Polytechnic Institute and State University*, Haleigh Hixson, *Virginia-Maryland College of Veterinary Medicine*, Sheryl Coutermarsh-Ott, *Virginia Polytechnic Institute and State University*, Katharine Kierski, *Virginia-Maryland College of Veterinary Medicine*, Brittany Ciepluch, *Virginia-Maryland College of Veterinary Medicine*, Joanne Tuohy, *Virginia-Maryland College of Veterinary Medicine*, Eli Vlasisavljevich, *Virginia Tech*

In this study, we investigated the ablative and early immunological effects of histotripsy in vivo in dogs with spontaneous primary canine bone tumors.

Spherical ablation volumes were treated within a portion of primary bone tumors using a 500kHz histotripsy system guided by real-time US imaging. Standard-of-care limb amputations were performed 1 day after treatment. Treated tumors were evaluated grossly and histologically to determine histotripsy's ablative efficacy. Peripheral blood samples were collected pre-, 24 hours post-, and 2 weeks post-treatment for immune cell phenotyping. Immune cell populations within the tumor microenvironment were assessed via immunohistochemistry and gene expression arrays.

Fifteen primary bone tumors (n=13 osteosarcoma, n=2 chondrosarcoma) were treated with histotripsy. Visible bubble clouds on US imaging were generated in 7 of 15 treatments at peak negative pressures 27.57 ± 5.53 MPa. Cavitation activity was monitored for all treatments using passive cavitation detection. Gross analysis revealed ablated tissue characterized by hemorrhage and/or necrosis in targeted regions. Histological evaluation microscopically confirmed the loss of viable tumor cells.

Flow cytometry results indicated changes in T-lymphocyte populations and expression of monocyte and T-lymphocyte cell surface receptors. Grouped analysis of gene expression arrays revealed gene upregulation related to immune cell infiltration, inflammation, and immunogenic cell death.

Results demonstrate histotripsy's ability to ablate primary bone tumors and suggest histotripsy stimulates systemic and local immune responses. Challenges remain to accurately track and monitor cavitation bubble clouds during bone tumor treatments. Future studies are warranted to continue developing histotripsy as an ablation technique and immunotherapeutic for primary bone tumors.

The authors thank the American Kennel Club Canine Health Foundation, the Focused Ultrasound Foundation, and the National Institutes of Health for their financial support.

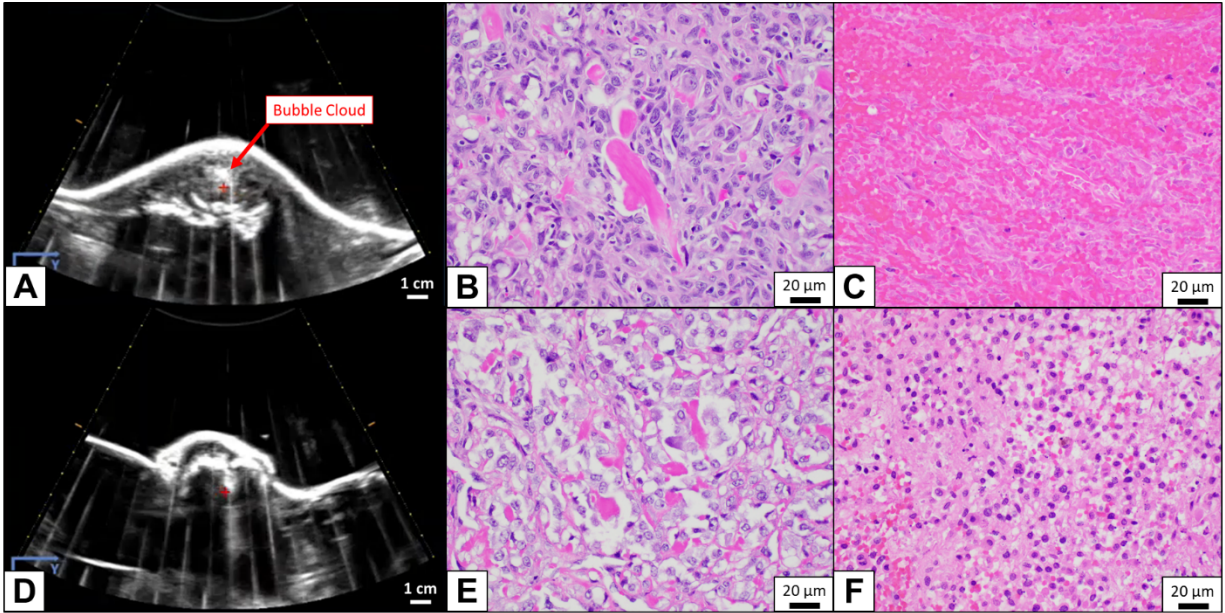


Figure 1: (A-F) Histotripsy ablation of primary bone tumors with (A-C) and without (D-F) bubble cloud visibility during treatment. (A,D) Real-time ultrasound imaging during histotripsy treatment. (B,E) Hematoxylin & eosin stains of untreated OS tumors. (C,F) Hematoxylin & eosin stains of treated OS tumors.

SA-4

Effective Drug Release from Safe Ultrasound-triggered Nanocarriers

Presenter: Matthew Wilson

Authors in order: Matthew Wilson, *University of Utah*, Jan Kubanek, *University of Utah*

Our objective is to optimize safe and effective targeted drug delivery in the brain. We characterized the drug release and safety of stable nanocarriers.

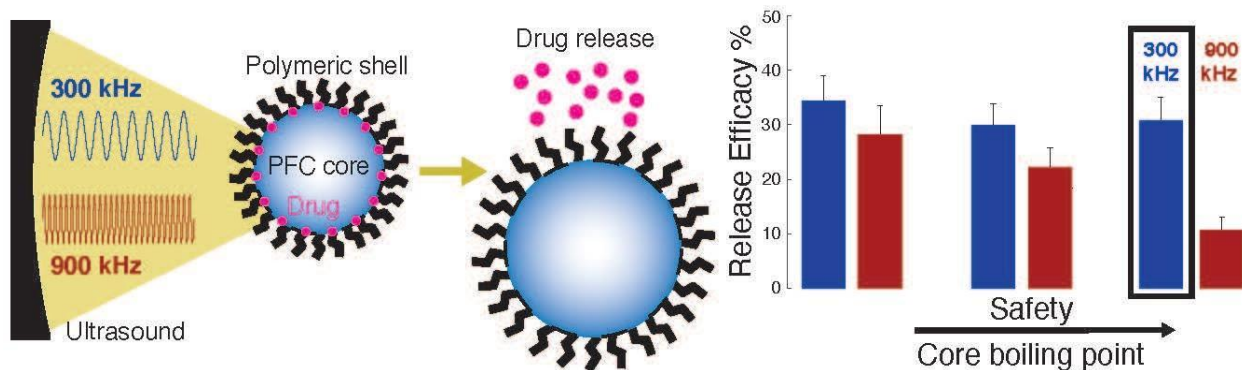
Propofol loaded perfluorocarbon (PFC) nanocarriers were formed using PFCs with boiling points of 29°C, 55°C, and 142°C. Drug release was assessed in vitro in response to 300 kHz and 900 kHz ultrasound to study mechanical and thermal effects. The same transducer was operated at both frequencies and focused on a vial containing the nanocarrier solution and hexane to extract the released propofol.

Infrared dye-doped nanocarriers were administered to 3 rats and 3 primates to quantify pharmacokinetics and biodistribution.

Low frequency ultrasound triggered more drug release than high frequency across the PFC cores tested (31.7% and 20.3% drug released, respectively. $t(130) = 3.3$, $p = 0.0013$, two-sample two-tailed t-test). At the higher frequency, the release effectiveness strongly depends on the boiling point of the PFC - the lower the boiling point of the PFC, the higher the release effectiveness. However, core boiling point did not strongly influence drug release at low frequency.

High boiling point PFC nanocarriers elicited no adverse reactions in acute administrations, showing a 32-minute half-life in the bloodstream. The nanocarriers primarily accumulated in the liver.

High-boiling point PFCs were effectively activated by low frequency ultrasound (300 kHz), consistent with a mechanical mechanism of release. We additionally found that such nanoparticles can be safely administered to primates. This informs the selection of PFC-based nanoparticles and ultrasound parameters for effective, safe, and targeted drug release in humans.



Modulation of Cytoplasmic Diffusion by Low-intensity Pulsed Ultrasound and Its Biological Effects

Presenter: Hyo Jun Kim

Authors in order: Hyo Jun Kim, *Korea Institute of Science and Technology (KIST)*, Hyungmin Kim, *Korea Institute of Science and Technology (KIST)*, So Yeon Kim, *Korea Institute of Science and Technology (KIST)*, Yeonho Choi, *Korea University*, Ki Joo Pahk, *Kyung Hee University*

The change of cytoplasmic molecular diffusivity by low-intensity pulsed ultrasound (LIPUS) and its biological effects are investigated at the single-cell level (Fig 1a).

SaOS-2 and HeLa cells were exposed to LIPUS, and the exposure conditions were varied as follows: 0.5 to 3-MHz frequency and 200 to 400-kPa acoustic pressure. Tracers of various hydrodynamic radii were introduced to the cytoplasmic area via glass bead loading and biosynthesis upon transfection. During insonation, cytoplasmic diffusivity and nuclear translocation rate were measured by fluorescence recovery after photobleaching (FRAP). The activation of ERK kinase was quantified using Förster resonance energy transfer (FRET) imaging.

We observed that the diffusivity of various sizes of biomolecules floating in the cytoplasm increased with acoustic pressure (i.e., increased by 33.7% at 400-kPa, 3-MHz, Fig. 1b). This ultrasound-enhanced cytoplasmic diffusion can directly affect many cellular processes coupled with protein transport over the whole cellular volume. LIPUS stimulation increased the nuclear translocation rate of EGFP by 20.4%, which is a small protein that can translocate between nucleus and cytoplasm by passive diffusion (Fig. 1c). The activation of ERK, a signal transduction protein transmitting mitogen signals by diffusion, was significantly accelerated during the sonication (Fig. 1d).

This is the first study reporting that molecular dynamics inside a cell (i.e., cytoplasmic diffusivity) can be altered by LIPUS. Ultrasound-enhanced diffusivity can therefore modulate cellular physiology, raising the rate of passive nucleus translocation and mitogen cell signaling process.

This work was supported by the National Research Foundation of Korea (NRF) and National Research Council of Science & Technology (NST) (No. NRF-2021R1C1C1008240, CAP-18-01-KIST).

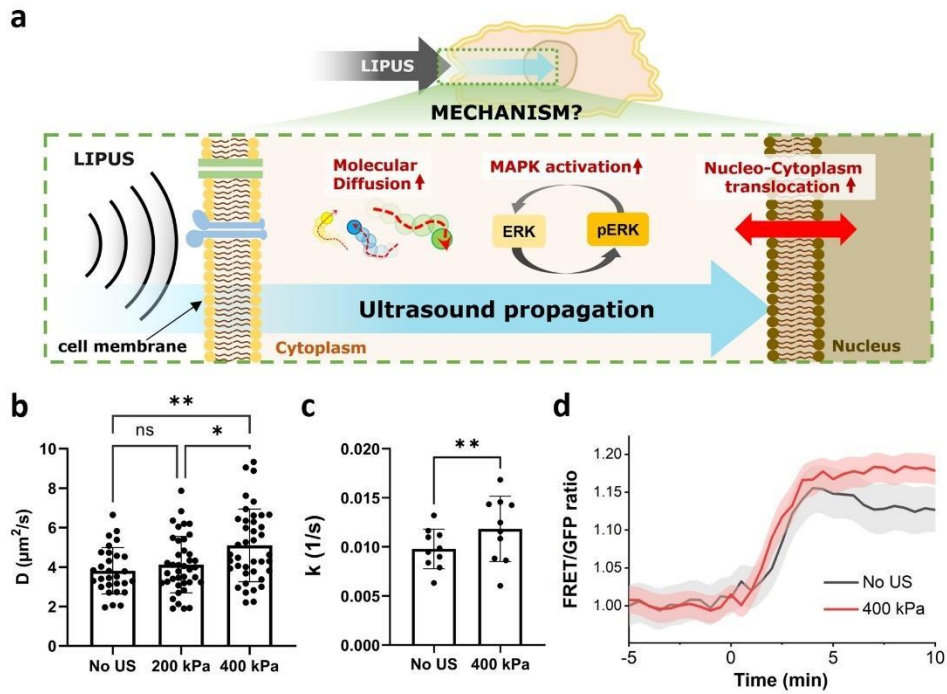


Fig. 1 (a) Proposed biophysical mechanism of LIPUS. LIPUS modulates cytoplasmic molecular diffusion and its related cell physiology. (b) Enhanced diffusivity of 500-kDa FITC-Dextran in response to LIPUS. (c, d) Accelerated nucleus translocation rate of EGFP and ERK activation by LIPUS.

SA-6

Temperature Sensitive State Switches for Focused Ultrasound Control of Macrophage Immunotherapy

Presenter: Abdullah Farooq

Authors in order: Abdullah Farooq, *California Institute of Technology*, Mohamad Abedi, *University of Washington*, Margaret Swift, Mikhail Shapiro, *Caltech*

We seek to develop the capability to spatially localize the activity of immunotherapeutics to reduce the potential for adverse side effects associated with systemic activation.

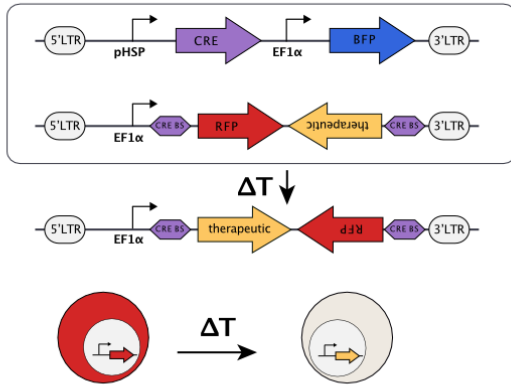
We are developing temperature-sensitive genetic circuits to remotely control engineered macrophages deep within the body using high-precision non-invasive techniques such as focused ultrasound hyperthermia. We take advantage of the ability of macrophages to be recruited into solid tumors to serve as “Trojan horses” for therapeutics. Using focused ultrasound hyperthermia (FUS-H), we can induce local hyperthermia in 100 mm³ Raji tumors following systemic injection of engineered macrophages. The recombinase-mediated inversion enables stable, long-term gene activation.

Reporter circuits display low baseline activity in vitro at room temperature (1.4 ± 0.4% of cells activated), and high induction after stimulation (49.9 ± 2% of cells activated, n=3, ± SEM). In vivo, we have observed low baseline activity of the circuit in the absence of FUS-H (3.0 ± 0.2% of cells activated, n=3, ± SEM) and activation following application of FUS-H (18.8 ± 4.2% of cells activated, n=3, ± SEM). We are also characterizing therapeutic gene secretion of BiTE following thermal stimulation in vitro. Baseline BiTE remains low (1.49 ± 0.49 ng/mL, n=3, ± SEM) while cells treated with thermal stimulation secrete significantly more BiTE (11.0 ± 2.2 ng/mL).

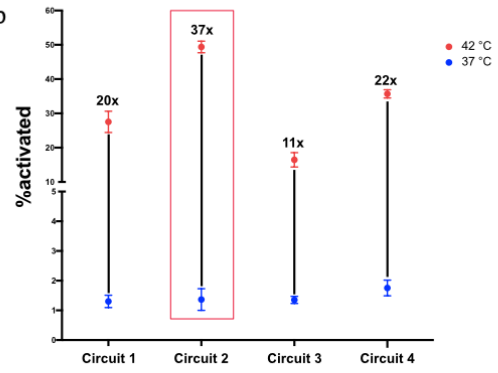
Our results demonstrate the ability to activate gene expression in macrophages with temperature-sensitive state switches. These switches can be controlled using FUS-H in vivo. We are working to control secretion of BiTE using FUS-H in a murine tumor model.

A.F. was supported by NSERC-PGS-D. M.H.A. was supported by NSF GRFP and the Soros Fellowship. The Packard Foundation and US Army funded this work.

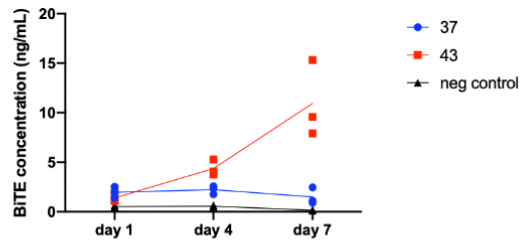
a



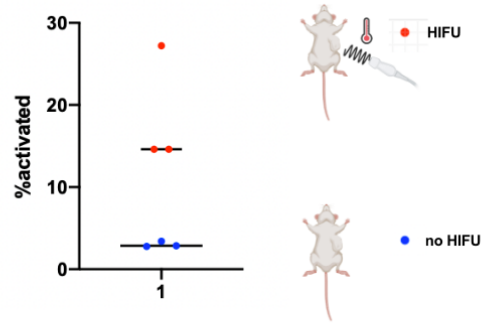
b



c



d



FUS Lowers Pain Perception in Neuropathic Pain Patients

Presenter: Stephen Lee

Authors in order: Stephen Lee, *Columbia University*, Erica McCune, *Columbia University*, Hermes Kamimura, Christopher Winfree, Elisa Konofagou, *Columbia University*

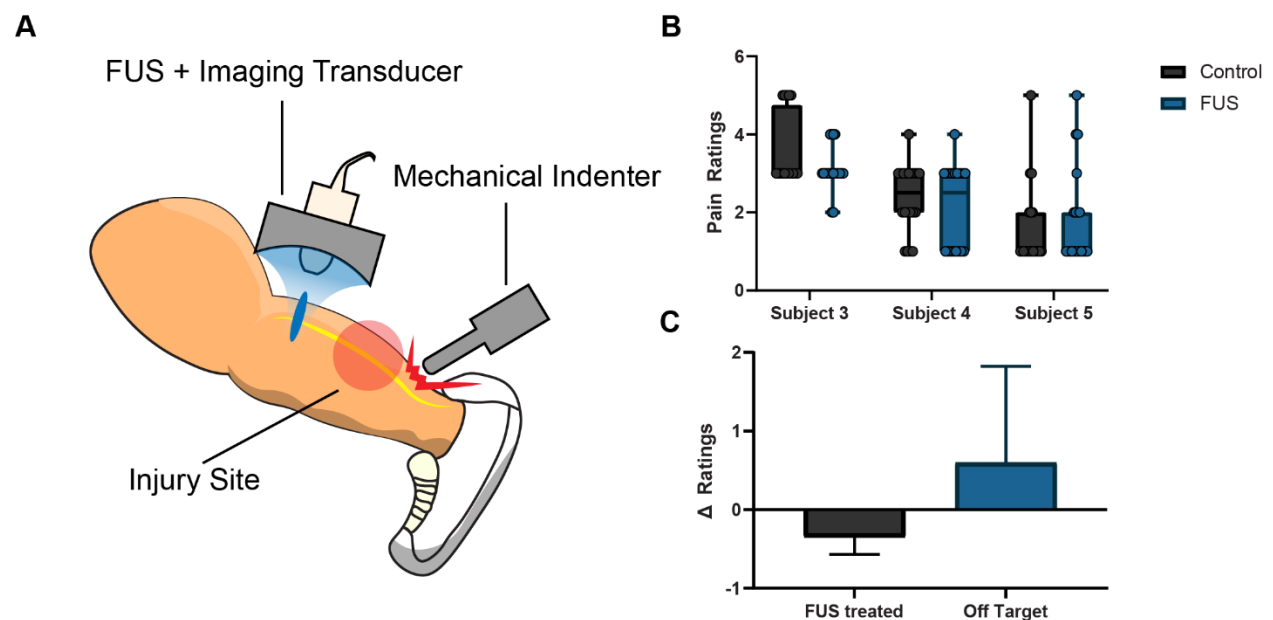
To understand the clinical viability and characterize pain control properties of focused ultrasound (FUS) peripheral nerve neuromodulation in patients with neuropathic pain.

Human neuropathic pain patients ($n = 6$) with sural nerve biopsies, nerve tumors, or nerve entrapments received FUS with displacement targeting (Lee et al. 2020) to the relative nerve bundle. Patients subjectively rated pain for 40 mechanical stimulations, through an indenter, with randomized FUS/Sham pulse trains (> 5 MPa, 10 s at 7.5% duty cycle) in a double blinded fashion (Fig 1A). Half of subjects ($n=3$) received either off-target or on-target stimulations.

Intra-subject analysis indicated that pain ratings were lower after FUS vs sham pulses when accurately targeting the associated nerve (sural, common peroneal or radial) (Fig 1B). Two patients verbally relayed immediate pain relief following the procedure and, in one subject, relief persisted for three days post-FUS. Across subjects, pain ratings either decreased or remained unchanged in patients receiving on-target FUS nerve stimulation (Fig 1C). By comparison, the control group either experienced pain increase or not change.

This initial clinical feasibility study demonstrated short- and long-term pain-relief in patients with acute or chronic neuropathic pain. Further investigation in a larger patient study will determine efficacy of the technique for post-surgical pain relief.

The authors would like to thank our funding sources, FUS foundation and Google X, as well as Dr. Tony Wang and Maria Olofernes for their help.



SA-8

Monitoring Thermal Lesions using Decorrelated Compounded Ultrasound Imaging

Presenter: Michael Nguyen

Authors in order: Michael Nguyen, *Ryerson University*, Jahangir (Jahan) Tavakkoli, *Ryerson University*, Yuan Xu, *Ryerson*

Decorrelated Compounding (DC) for synthetic aperture ultrasound can reduce speckle variation in images, suggesting enhanced detectability of low-contrast thermal lesions produced by Focused Ultrasound (FUS).

Low-contrast cyst targets (+/-3 dB) of a tissue mimicking phantom were imaged using various ultrasound imaging methods, including B-mode imaging. Synthetic aperture RF echo data was processed using the delay-and-sum (DAS), a combination of spatial and frequency compounding referred to as Traditional Compounding (TC), and the proposed DC method. Image quality was assessed using the Signal-to-Noise Ratio (SNR) and Contrast-to-Noise Ratio (CNR) of the cyst targets, and the speckle SNR (sSNR) of the background region.

The DC method significantly improved image quality in comparison to other imaging methods. In comparison to B-mode imaging, CNR was shown to improve by a factor of 6 and 3 for the -3 dB and +3 dB cyst targets, respectively. The corresponding SNR improved by a factor of 6 and 10 for the -3 dB and +3 dB cyst targets, respectively, and sSNR by a factor of 7 in the background region, in comparison to B-mode imaging. The study on low-contrast FUS thermal lesions is ongoing with anticipation of achieving comparable results.

Early results suggest that the despeckling performance of the DC method allows for more effective detection of low-contrast structures. This suggests that the proposed method can detect low-contrast thermal lesions induced by FUS therapy that are not detectable using standard B-mode imaging. The study to monitor FUS treatments is ongoing.

We thank Dr. Graham Ferrier, Dr. Elyas Shaswary, and Na Zhao for their technical assistance in this project.

Adaptive Refocusing of Broadband Wavefronts

Presenter: Collin Smith

Authors in order: Collin Smith, *UMN*, Emad Ebbini, *University of Minnesota*

Refocusing is performed to optimize the coherence of all spectral components of a broadband wavefront after propagating through a dispersive medium such as the skull.

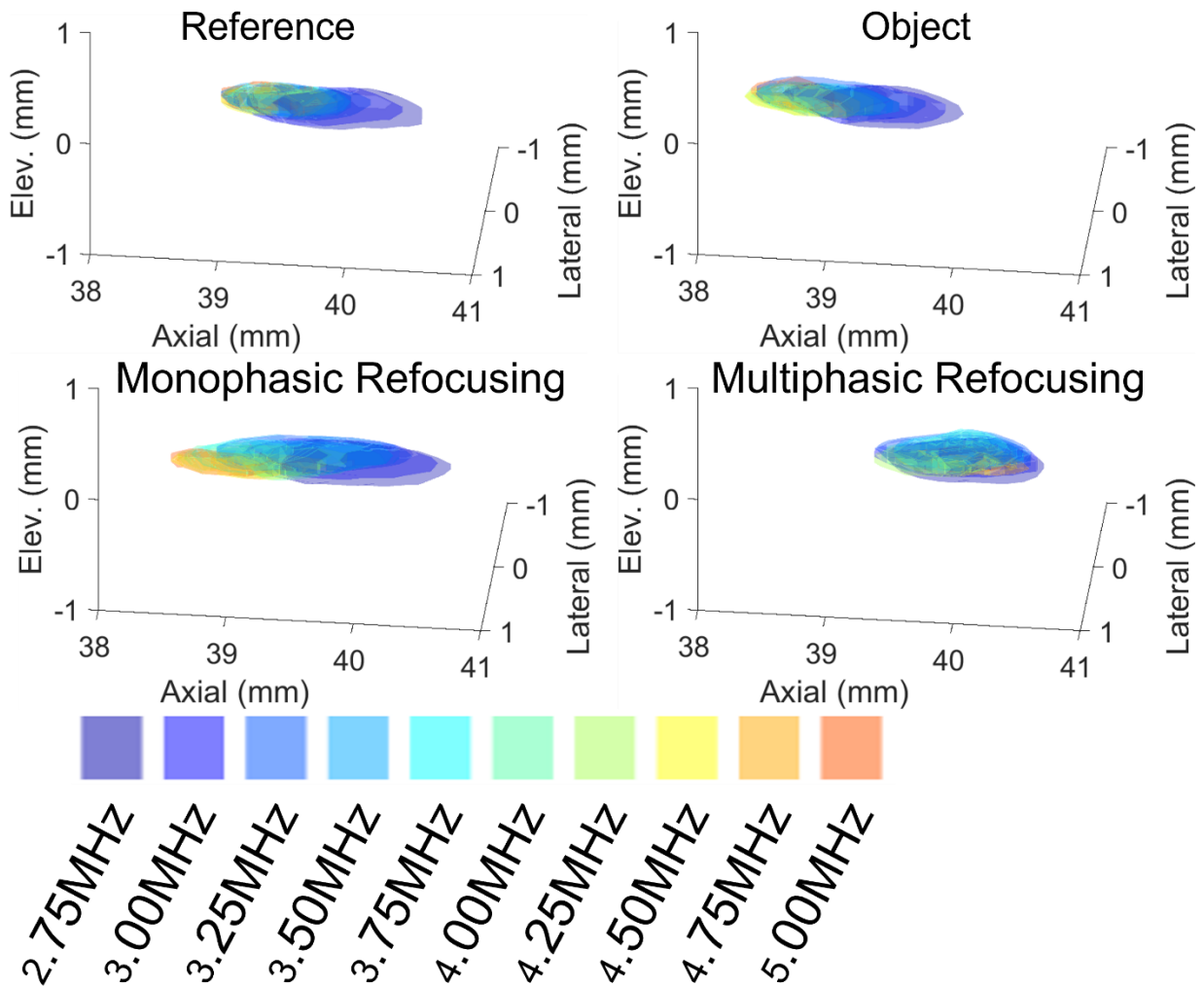
Using orthogonal frequency-division multiplexing (OFDM), a refocusing technique that was previously limited to single-frequency corrections was generalized to perform broadband refocusing. A dual-mode ultrasound array (DMUA) transmits an OFDM signal through a rat skull in a degassed water bath. A hydrophone is used to measure the coherence of the wavefront in the target focal plane. A combination of a hydrophone scan and the angular spectrum method then characterizes the pressure field produced after refocusing.

The average coherence of the broadband wavefront is increased to 0.98 using broadband refocusing, as compared with narrowband refocusing, which was only 0.93. Post-analysis showed that the broadband algorithms not only corrected for the dispersive media, but differences in the frequency-responses of transducer elements as well. The hydrophone scans revealed that the broadband refocusing causes the focal volumes generated by each subcarrier to focus at the same location, producing not only an improvement in pressure at the target location but concentrating the energy in a smaller volume as well. This leads to an increase of 16% in focal volume intensity.

The arbitrary control of subcarriers in orthogonal frequency-division multiplexing is shown to be able to correct for the frequency-specific distortive effects of dispersive media. This highlights the flexibility and advantages of using broadband waveforms for FUS applications in conjunction with broadband waveform synthesis.

This work is funded by grant NS118785 from the National Institutes of Health.

Subcarrier Focal Volumes



SP1

Neuronavigation-guided Transcranial Histotripsy on Human Cadavers: A Feasibility Study

Presenter: Sang Won Choi

Authors in order: Sang Won Choi, *University of Michigan*, Mahmoud Komaiha, *University of Michigan*, Timothy Hall, *University of Michigan*, Zhen Xu, *University of Michigan*, Jonathan Sukovich, *University of Michigan*, Dave Choi, *University of Michigan*, Ning Lu, *University of Michigan*, Aditya Pandey, *University of Michigan*, Sandra Camelo-Piragua, *University of Michigan*, Neeraj Chaudhary, *University of Michigan*, Badih Junior Daou, *University of Michigan*

We aim to demonstrate the feasibility of transcranial histotripsy for non-invasive brain treatment by treating whole-body cadavers (< 96 hours postmortem) guided by a neuronavigation system.

Approximately 1cm³ of the brains of two whole-body cadavers were treated by electronically steering the focus with a 1.1 mm spacing using a 700kHz, 360-element, 15cm focal distance, hemispherical array. 1-cycle pulses, 200Hz PRF, p- of >28 MPa, and 50 pulses per focal location were used. Aberration correction was done with Kranion and pre-treatment CT scans. Prescribed ablation locations on pre-treatment MRI and post-treatment MRI were compared to evaluate the treatment accuracy.

Three lesions were successfully generated in the septum, thalamus, corpus callosum, and identified by the post-treatment MR images. Representative pre and post-treatment MRI images of one of the cadavers treated are shown (Figure 1). Apparent Diffusion Coefficient (ADC) images best showed the histotripsy homogenized region. The targeting accuracy was 4.1, 8.0, and 6.5 mm for the septum, corpus callosum, and thalamus respectively. The low targeting accuracy is attributed to the imperfect co-registration between the cadaver head and the array and the suboptimal setup. On-going improvements to the experimental setup and workflow are expected to increase the targeting accuracy.

The feasibility of neuronavigation-guided transcranial histotripsy was demonstrated on human cadavers. Future improvements to the system are needed to increase accuracy to a clinically acceptable level. We plan to study the full extent of transcranial histotripsy treatment location profile and efficacy in human cadaver brains.

This work was funded by NIH grants (R01 - EB028309, R01 - NS - 108042) and Focused Ultrasound Foundation

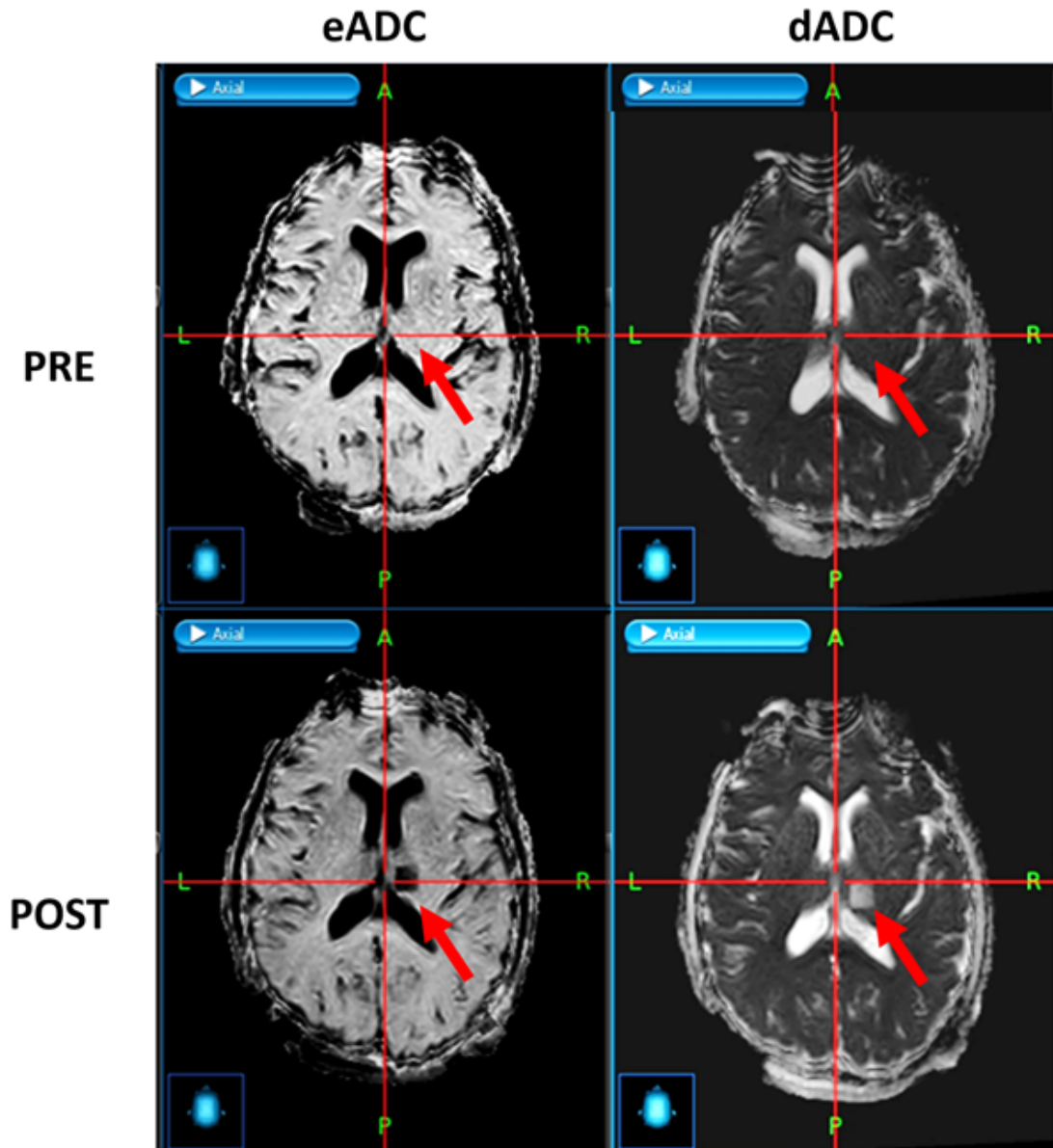


Figure 1. Apparent Diffusion Coefficient (ADC) images of one of the cadavers.

SP10

Sonoporation-mediated DNA Vaccination Against Hepatitis B

Presenter: Yuanchao Shi

Authors in order: Yaxin Hu, *Shenzhen University*, Yuanchao Shi, *Shenzhen University*, Mengting Chen, *Shenzhen University*

To increase the antigen expression efficiency of a hepatitis B DNA vaccine, we employed ultrasound and microbubble-mediated sonoporation to facilitate the intracellular delivery of DNA.

Cationic microbubbles loaded with DNA and Polyethylenimine (PEI) complex were first injected into the tibialis muscle of the mouse hind leg. Then, pulsed ultrasound (frequency: 0.5 MHz, pulse duration: 100 cycles, pulse repetition frequency: 1 kHz) of different pressures (0.16, 0.33, 0.52 and 0.70 MPa) and durations (5 seconds and 2 minutes) was applied to trigger sonoporation and to facilitate plasmid delivery. The status of the microbubbles was imaged using high-frequency (40 MHz) ultrasound.

We found that the transfection efficiency of sonoporation in muscle decreased with the increasing N:P ratio of DNA-PEI complex. Obvious cytotoxicity of PEI on muscle cells was found at the N:P ratio of 7. We also found that the highest transfection efficiency was achieved using ultrasound pressure of 0.7 MPa and duration of 2 minutes. Using immunofluorescence labelling, we found that the number of antigen-presenting immune cells increased in muscle treated with sonoporation. Using a plasmid encoding small surface antigen of the hepatitis B virus (HBsAg) as DNA vaccine, we detected anti-HBsAg antibody in mouse serum 4 weeks after sonoporation.

After the optimization of sonoporation parameters for muscle transfection, antigen expression efficiency as well as immune responses of the HBsAg DNA vaccine were improved.

This work was funded by the National Natural Science Foundation of China (Grant No.: 82071947) and the Shenzhen Science and Technology Programme (Grant No.: 20200813152218001).

SP11

Cavitation Bubble Cloud Behavior and Tissue Ablation from a 6.3 MHz High Frequency Endoscopic Histotripsy System

Presenter: Jessica Gannon

Authors in order: Jessica Gannon, *Virginia Tech - Wake Forest School of Biomedical Engineering and Sciences*, Thomas Landry, *Dalhousie University*, Jeremy Brown, *Dalhousie University*, Jeffrey Woodacre, *Dalhousie University*, Eli Vlaisavljevich, *Virginia Tech*

This study investigates the cavitation bubble cloud dynamics and ablation capabilities of a 6.3MHz endoscopic histotripsy transducer recently developed for high precision histotripsy ablation.

High-speed optical imaging captured bubble cloud images generated by the high-frequency transducer inside 1% agarose phantoms. Bubble cloud features were characterized for 1-12 cycle pulses applied at pressures ranging from 26-44MPa at 1kHz pulse repetition frequency. Histotripsy was applied to red blood cell (RBC) phantoms to evaluate ablation efficiency, comparing ablation area as a function of pulse number for each pulsing parameter. Results for all experiments were compared to previous histotripsy studies at lower frequencies.

Results showed that the 6.3MHz histotripsy transducer was capable of generating precise, well-defined bubble clouds (< 1 mm in maximum dimension), with no off-target cavitation observed outside the focus. The cavitation threshold decreased as a function of applied cycles, ranging from ~ 34 and ~ 26 MPa for 1 and 12 cycle pulses, respectively. Cloud size increased with cycles, with maximum cloud dimension ranging from $\sim 0.35 \pm 0.08$ mm and $\sim 0.83 \pm 0.24$ mm for 3 and 12 cycle pulses, respectively. Compared with lower frequency histotripsy systems, the 6.3MHz cloud was significantly smaller and well-defined, suggesting this system is ideal for high-precision treatments. Ablation efficiency characterization in RBC phantoms is ongoing.

This study demonstrates the high-precision capabilities of a 6.3MHz endoscopic histotripsy transducer in development for the treatment of brain tumors and other disorders. Results further show the bubble cloud dimensions can be finely tuned by adjusting acoustic parameters, allowing for the generation of sub-millimeter bubble clouds and precise tissue ablation.

This work is supported by a National Science Foundation Graduate Research Fellowship and the Atlantic Canada Opportunities Agency (Atlantic Innovation Fund no.207828).

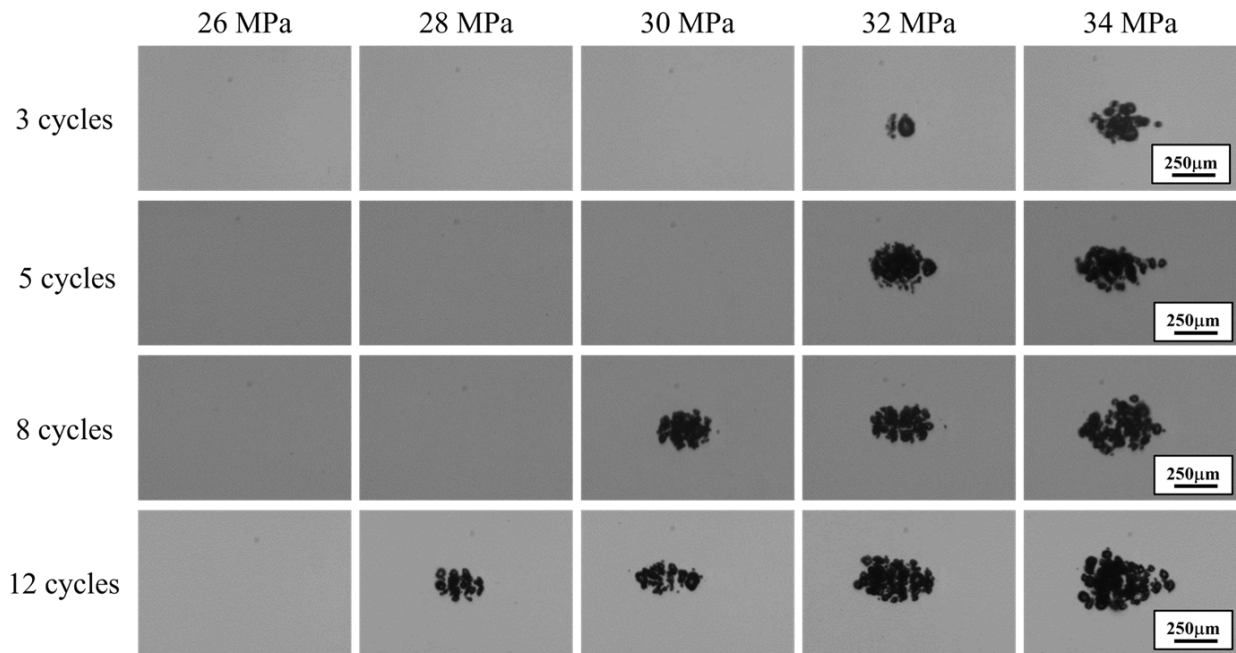


Figure 1. 6.3MHz bubble cloud images in 1% agarose phantoms.

SP12

Small Focal Volume Blood Brain Barrier Opening in the Non-human Primate through Intact Skull

Presenter: Thomas Manuel

Authors in order: Thomas Manuel, *Vanderbilt University*, M. Phipps, *Vanderbilt University Medical Center*, Huiwen Luo, *Vanderbilt University*, Jiro Kusunose, *Vanderbilt University Medical Center*, Pai-Feng Yang, *Vanderbilt University Medical Center*, Jamie Reed, *Vanderbilt University Medical Center*, Michelle Sigona, *Vanderbilt University*, Allen Newton, *Vanderbilt University Medical Center*, William Grissom, *Vanderbilt University*, Li Min Chen, *Vanderbilt University Medical Center*, Charles Caskey, *Vanderbilt University Medical Center*

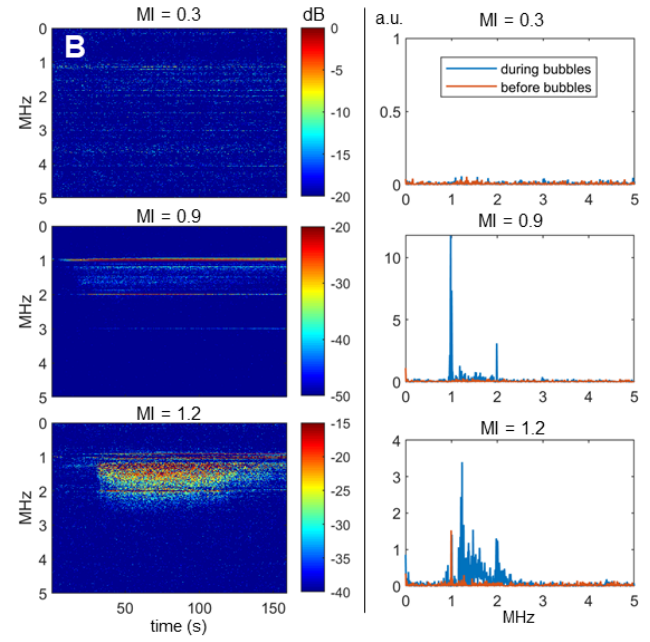
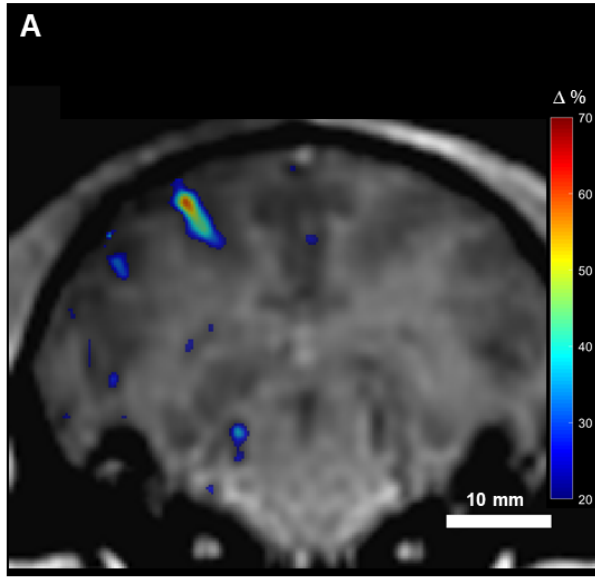
Develop a transducer and cavitation monitoring system for millimeter-scale blood brain barrier opening (BBBO) in non-human primates (NHPS) through the intact skull under image guidance.

Transducer design was performed in k-Wave (81 transcranial simulations in four NHPs varying transducer frequency and geometry). We integrated the transducer into an image-guidance system and developed a custom python application to process cavitation signals and guide transducer output during therapy. The system was validated in the macaque by first targeting the cortex and then performing BBBO on 2 macaques using Gadolinium-based contrast enhancement to quantify BBBO volume and susceptibility-weighted imaging (SWI) to assess safety.

A 1 MHz, 128-element transducer ($f=53.2$ mm, $D=58$ mm) with one central receive element (2 MHz) was identified as the optimal design based on spot size and footprint. When steering inward 10 mm through skull simulations showed an ellipsoidal focus with lateral size of 2.9 ± 0.5 mm by 3.1 ± 0.8 mm and axial 11.6 ± 3.4 mm and transmission of $13 \pm 3.1\%$ ($n=4$ NHPs). In vivo BBBO was demonstrated with a FWHM (evaluated with contrast enhancement) of $3 \times 3 \times 11$ mm. Therapy with stable cavitation showed no hemorrhage signature in SWI, and therapy with inertial cavitation showed hemorrhage.

We designed and evaluated a small footprint transducer capable of BBBO at volumes comparable to functional brain regions in monkeys. The transducer generated a smaller focus steered inward than when steered to the geometric focus. The system will be used to facilitate precise BBBO for neuromodulation via acoustically targeted chemogenetics.

NIH UG3 MH120102 for funding. Vanderbilt University Institute of Imaging Science.



A) T1-weighted subtraction image following BBBO overlaid on t1-weighted image. B) Spectrograms and spectra for three cavitation scenarios (baseline subtracted).

A 32-element PZT-PVDF Stacked Transducer Array for Transcranial Focusing and Reception using Short Ultrasound Pulses

Presenter: Zheng Jiang

Authors in order: Zheng Jiang, *Imperial College London*, Javier Cudeiro-Blanco, *Imperial College London*, Betul Ilbilgi Yildiz, *Imperial College London*, Robert Dickinson, *Imperial College London*, Lluís Guasch, *Imperial College London*, MengXing Tang, *Imperial College London*, Timothy Hall, *University of Michigan*, James Choi, *Imperial College London*

We aimed to build a multi-element ultrasound array that could stimulate and monitor microbubble activity across the human skull efficiently and with highly sensitivity.

Many array systems place emitters and receivers at separate locations, creating a trade-off between efficient transmission and reception. Here, we built a 32-element array (radius: 150 mm, F-number: 1.06) with each element composed of a PZT-PVDF stack [PZT for narrowband (500 kHz) emission, PVDF for broadband reception as a front layer]. We evaluated the array's ability to focus, steer, and monitor microbubble activity in water alone and across an ex vivo human skull.

The array was shown to focus ultrasound and receive microbubble signals across the skull. In water alone, the focal dimensions were 4.5*4.5*32 mm and the peak-rarefactional pressure could reach 1.95 MPa. The focus could be steered 30-40 mm and greater than 30 mm in lateral and axial directions, respectively. With aberration correction, ultrasound was focused through the skull with a pressure of 28.8%. The array received acoustic emissions from microbubbles flowing through a 0.6-mm-in-diameter channel exposed to a 3.5-cycle, 0.45-MPa pulse. Microbubble signals were detected with the PVDF and microbubble location was accurately defined using passive acoustic mapping.

By stacking the emitters and receivers, we have overcome the traditional trade-off of efficient transmission and sensitive reception. Such an array design may improve our ability to stimulate and monitor ultrasound methods for delivering drugs across the blood-brain barrier, providing safer and more robust clinical methods.

The authors would like to thank Dr. Matthieu Toulemonde and Dr. Carlos Cueto for their help with the Verasonics. Funding source: Alzheimer's Research U.K (ARUK-IRG2017A-7).

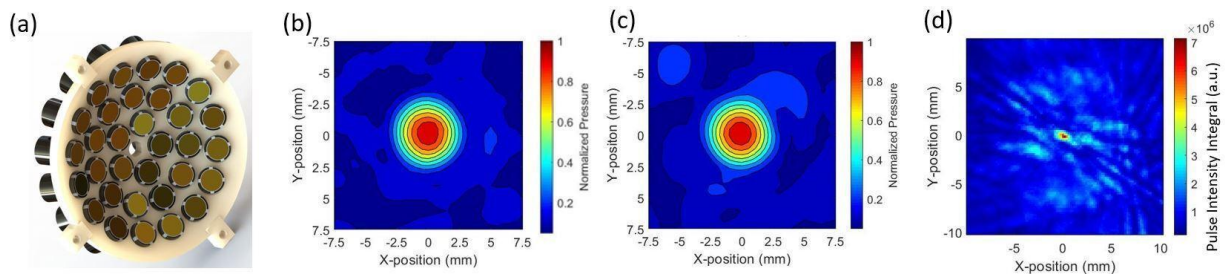


Fig.1. (a)The array. Beam profile (b) in water and (c) through the skull. (d)Transcranial passive acoustic mapping.

SP14

Sonogenetics for Locomotor Behavior Modulation in Freely Moving Mice

Presenter: Kevin Xu

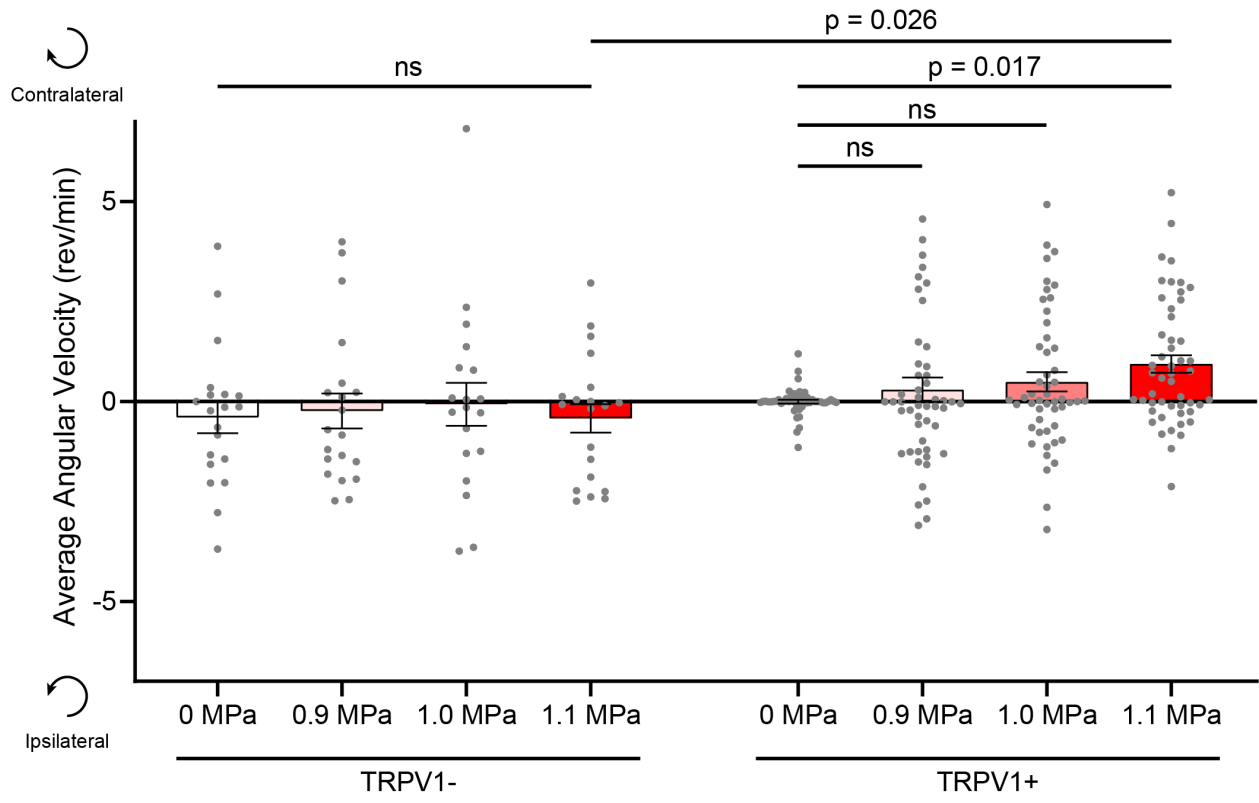
Authors in order: Kevin Xu, *Washington University in St. Louis*, Yaoheng Yang, *Washington University in St. Louis*, Yimei Yue, Hong Chen, *Washington University in St. Louis*

We evaluated the feasibility and safety of TRPV1-mediated sonogenetics to modulate the locomotor behavior of freely moving mice by targeting the motor cortex.

Adeno-associated virus was delivered to the mouse motor cortex via intracranial injection to express TRPV1 (TRPV1+) in excitatory neurons. After a month, a wearable focused ultrasound (FUS) transducer targeting the motor cortex was installed to control neuronal activity by activating TRPV1 through FUS sonication at different pressures. The mouse motor behavior was quantified using angular velocities to characterize the efficacy of sonogenetics. Control mice were injected with TRPV1- virus. Immunohistochemistry was performed for safety evaluation.

Sonogenetic stimulation of TRPV1+ mice at different acoustic pressures evoked rotational behavior in the direction contralateral to the stimulation site. The average angular velocities of TRPV1+ mice increased as acoustic pressure increased, while those of TRPV1- mice did not show such a trend (see figure). At 1.1 MPa, the average angular velocity of TRPV1+ mice was significantly higher compared to that of the sham (0 MPa), indicating that this is the minimum pressure needed for sonogenetic control of motor cortex. Sonogenetics did not induce significant changes in inflammatory or apoptotic markers (GFAP, Iba1, Caspase-3, and TUNEL).

This study demonstrated the feasibility and safety of sonogenetics to modulate locomotor behaviors by targeting the motor cortex.



SP15

Partial Thermal Ablation of Melanoma Augments Intratumoral IL-1b Expression, Implicating Pyroptosis as Pro-tumorigenic

Presenter: Mark Schwartz

Authors in order: Eric Thim, *University Of Virginia*, Lydia Petricca, *University of Virginia*, Alexander Mathew, Mark Schwartz, *University of Virginia*, Timothy Bullock, Richard Price, *University of Virginia*

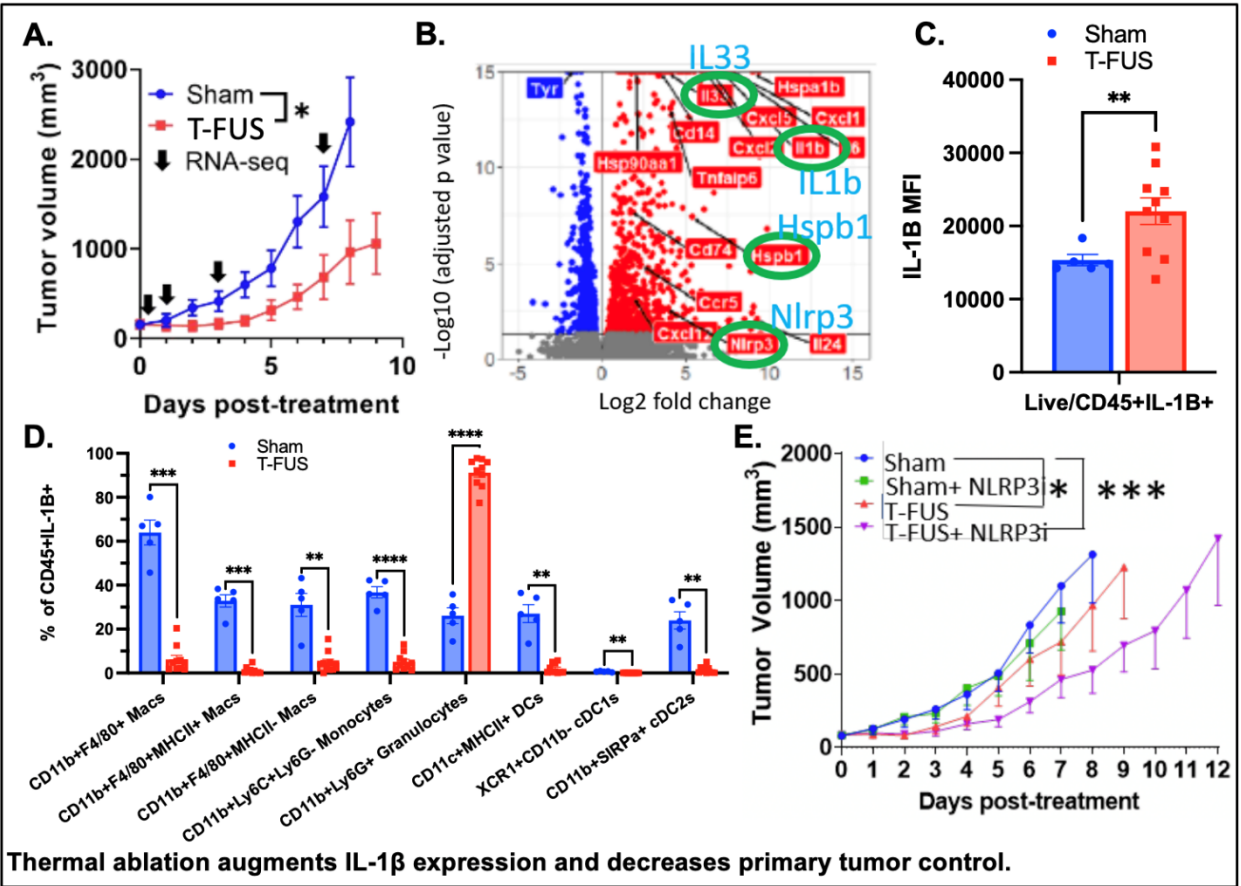
Investigate IL-1b upregulation in partial thermally ablated (TA) B16 melanoma tumors and determine efficacy of blocking NLRP3, an upstream regulator of IL-1b

C57/Bl6J mice were subcutaneously inoculated with 5×10^4 or 2×10^5 B16F10 cells in the right flank and TA ($f_0 = 3.28$ MHz, PNP = -12 MPa, 10 seconds/treatment point, 2 mm spacing between treatment points) was applied 13 days post inoculation. Post-treatment tumor harvests were performed for RNA sequencing and flow cytometry at 8, 24, 72 and 168 hrs and 24 hrs, respectively. MCC950, an NLRP3 inhibitor, was delivered 1 hr prior to thermal ablation.

TA transiently controlled primary B16F10 melanoma tumor growth (Figure 1A). Bulk RNA sequencing revealed upregulation of IL-1b and NLRP3 transcripts 8 hrs post TA but returns to baseline after 24 hrs (Figure 1B). Pro-IL-1b protein level on a per cell basis increased in the CD45+ cell compartment 24 hrs post TA (Figure 1C), with a striking pro-IL-1b expression redistribution to a predominantly granulocytic myeloid cell population (Figure 1D). Systemically inhibiting NLRP3 (upstream upstream regulator of IL-1b) in combination with TA increased tumor growth control beyond either monotherapy (Figure 1E).

TA shifts IL-1b expression levels and cell sources in the tumor microenvironment. By inhibiting NLRP3 in combination with TA to increase growth control, we have implicated pyroptosis as a pro-tumorigenic mechanism through the NLRP3-IL-1b pathway.

Supported by NIH R01EB030007 to RJP and TNJB



Thermal ablation augments IL-1β expression and decreases primary tumor control.

SP16

Characterisation of Cavitation Threshold Properties of Selected Hydrogels as Tissue Mimics for Therapeutic Ultrasound

Presenter: Lisa Braunstein

Authors in order: Lisa Braunstein, *The Institute of Cancer Research*, Sarah Brüningk, *ETH Zurich*, Ian Rivens, *Institute of Cancer Research*, John Civale, *The Institute of Cancer Research*, Gail ter Haar, *The Institute of Cancer Research*

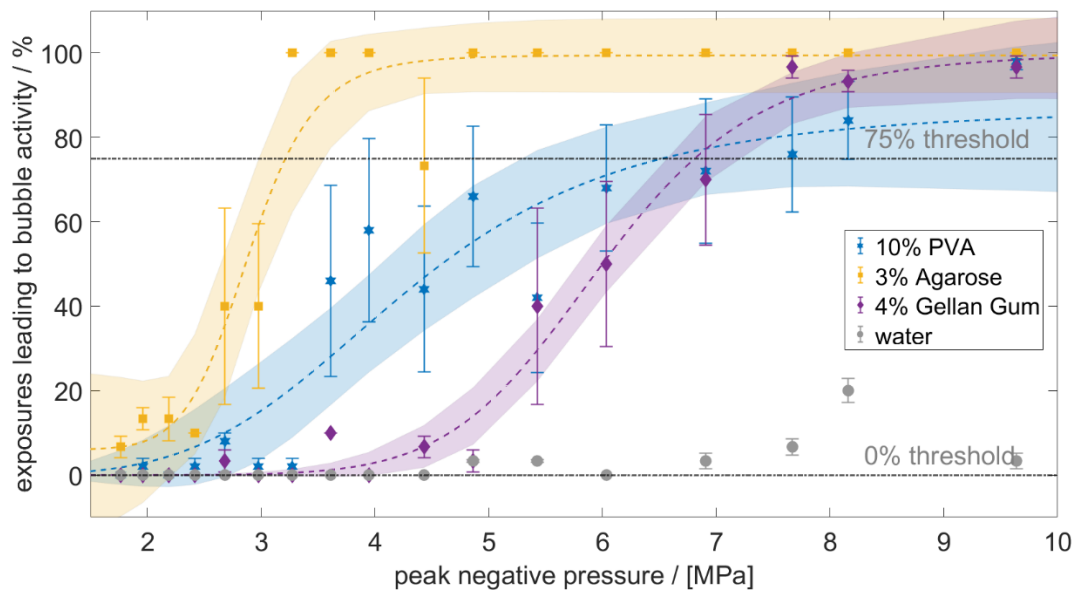
Mechanical effects of ultrasound traversing tissue, specifically ultrasonic cavitation, can be exploited for therapeutic applications. To evaluate its potential, tissue mimicking materials have been characterised.

10% w/w poly(vinyl alcohol) (PVA) hydrogels, with or without cellulose scatterers (5-10% w/w), agarose hydrogels (concentrations 1.25 and 3% w/w \pm 3% cellulose) and gellan gum gels (concentration 4% w/w \pm 2% silicone oxide scatterer) were studied. All hydrogels were acoustically characterised (sound speed (cs), attenuation coefficient (α)), using the finite amplitude insertion substitution method (frequency range 1.8-3MHz). The cavitation thresholds were investigated at peak negative pressures of 1.76-9.64MPa, using a passive cavitation detector.

The measured acoustic parameters were higher in PVA (cs:1532-1590m/s, α :0.08-0.37dB/cmMHz) than in agarose hydrogels (cs:1484-1492m/s, α :0.03-0.05dB/cmMHz). Acoustic gellan gum data will be presented. Cavitation thresholds for all materials followed a sigmoidal trend in probability of occurrence as a function of negative acoustic pressure, with agarose showing the lowest (2.9-3.5MPa for 75% probability). While gellan gum showed cavitation later than the other gels (6.6-7.2MPa), the increase in cavitation was steeper (slope: 8.7 ± 2.9 , Figure 1). Addition of cellulose scatterers lowered the 75% probability cavitation threshold in PVA gels from 5.4-8.2MPa (no cellulose) to 3.8-4.3MPa (10% cellulose w/w).

The acoustic properties of PVA hydrogels were close to those of published tissue data. Cavitation thresholds of gellan gum and PVA gels appear more suitable than agarose gels for mimicking tissues for these applications.

This project has received funding from the European Union's Horizon 2020 research and innovation programme under the Marie Skłodowska-Curie grant agreement No. 813766.



SP18

A Neuronavigation-guided Sonobiopsy Device for the Noninvasive Diagnosis of Brain Diseases

Presenter: Lu Xu

Authors in order: Lu Xu, *Washington University in St. Louis*, Chih-Yen Chien, *Washington University in St. Louis*, Christopher Pacia, *Washington University in St. Louis*, H. Gach, *Washington University School of Medicine*, Yao Hao, *Washington University in St. Louis*, Eric Leuthardt, *Washington University School of Medicine*, Hong Chen, *Washington University in St. Louis*

Develop a neuronavigation-guided sonobiopsy device for noninvasive diagnosis of brain diseases by enhancing the release of disease-specific biomarkers from the brain into the blood circulation.

The sonobiopsy device integrated a neuronavigation system with a single-element, focused-ultrasound (FUS) transducer. The accuracy in targeting specific brain location was characterized in a water tank without and with human skull. It was verified with in vivo pig studies by measuring the offsets between the intended and the actual locations of blood-brain barrier opening. Blood samples were collected post-FUS to analyze the plasma concentration of brain-specific biomarkers (glial fibrillary acidic protein and neurofilament light chain protein).

The targeting accuracy of the neuronavigation-guided sonobiopsy device as measured in the water tank was $1.40\text{mm} \pm 0.70\text{mm}$ without skull (A). It was $11.32\text{mm} \pm 3.42\text{mm}$ with the human skull and the offset was mainly along the FUS beam axis and towards the skull due to the skull aberration (B). This skull aberration caused error can potentially be mitigated with repositioning the transducer deeper. The targeting accuracy evaluated based on in vivo pig study was $0.89\text{mm} \pm 2.24\text{mm}$ (C). The sonobiopsy device successfully enhanced the release of brain-specific protein markers post-sonication compared with pre-sonication.

This study showed that the developed neuronavigation-guided sonobiopsy device had a high spatial targeting accuracy and achieved effective biomarker release in the pig model, paving the foundation for its translation to clinical use.

SP19

Engineering Viral Vectors for Acoustically Targeted Gene Delivery

Presenter: Hongyi Li

Authors in order: Hongyi Li, *California Institute of Technology*, Mikhail Shapiro, *Caltech*

We aim to apply high-throughput in vivo selection to engineer novel AAV vectors specifically for local neuronal transduction at the sites of focused ultrasound blood-brain-barrier opening (FUS-BBBO).

We employ an in vivo viral evolution method: a library of AAVs with mutated capsids based on AAV9 (Fig. 1a) is injected intravenously into hSyn1-Cre mouse and delivered via FUS-BBBO to one hemisphere. When a particular AAV variant transduces Cre-expressing neurons, its viral genome is modified, becomes detectable by a Cre-dependent PCR and Next-generation Sequencing (NGS) (Fig. 1b). Repeated rounds of selection for vectors uniquely appear in the targeted hemisphere lead to desired novel AAV vectors for objectives.

Histological analysis revealed higher efficiency of transduction in the brain for all final 5 viral variants (AAV.FUS.1-5) (Fig. 2a,b; up to 130% improvement over AAV9). Each serotype transduced the liver less strongly (Fig. 2c,d; up to 6.8-fold reduction compared to AAV9). The top AAV.FUS variant (AAV.FUS.3) showed 12.1-fold improvement in overall tissue specificity (Fig. 2e). All candidates show improved neuronal tropism as well: AAV.FUS.3 has a 69.8% likelihood of transducing a neuron, compared to 44.7% for AAV9 (Fig. 2f,g,h). Our screen yielded AAV.FUS.3, the first viral vector expressly engineered to work in conjunction with ultrasound-mediated gene delivery to the brain.

Overall, this study shows that the molecular engineering of AAV capsids can lead to improved noninvasive, site-specific ultrasound-mediated gene delivery to the brain. Our screen yielded AAV.FUS.3, the first viral vector expressly engineered to work in conjunction with the specific physical delivery method (FUS-BBBO).

The authors thank Viviana Gradinaru lab, and the CLOVER center at Caltech for helpful discussions. Thanks to Prof. Mikhail Shapiro and Jerzy Szablowski for extraordinary mentorship.

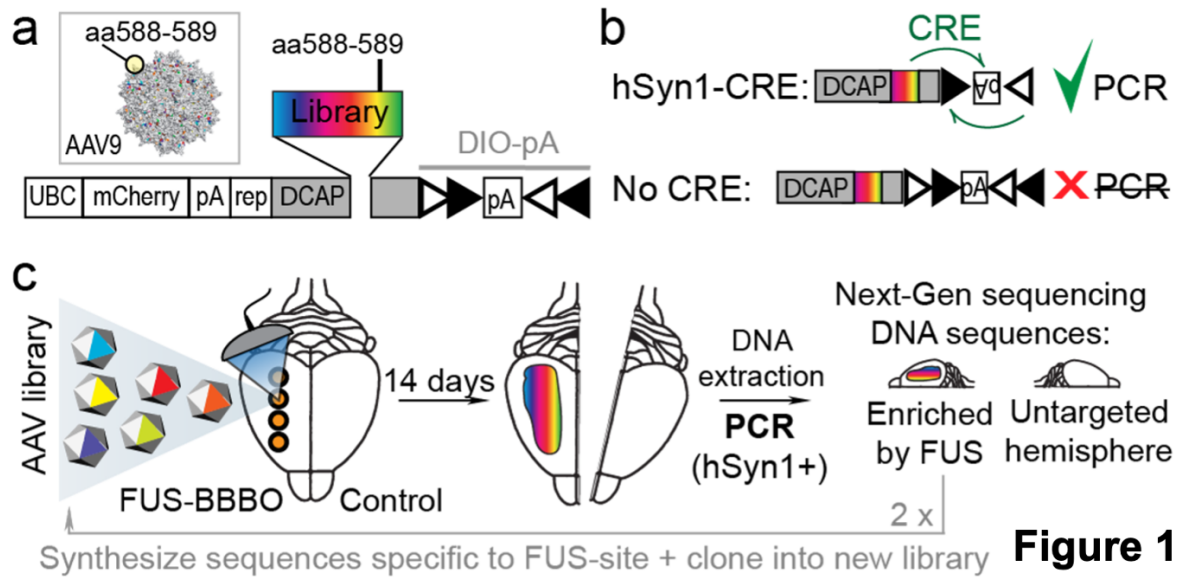


Figure 1

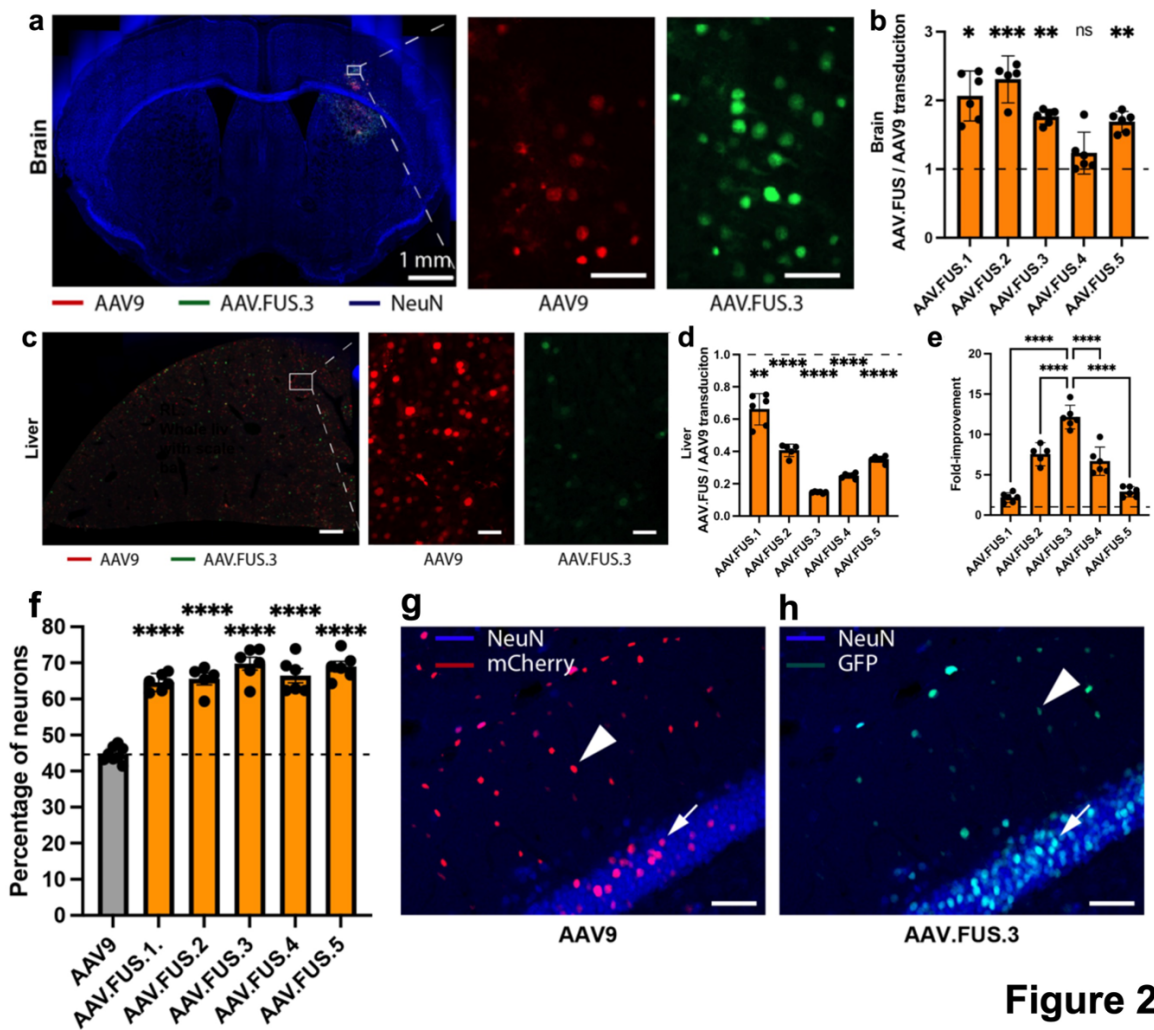


Figure 2

SP2

High-speed Microscopy of Microbubble-vessel Interactions in an In-vivo Chorioallantoic Membrane Model

Presenter: Rojin Anbarafshan

Authors in order: Rojin Anbarafshan, *University of Toronto, Sunnybrook Research Institute*, Carly Pellow, *Sunnybrook Research Institute*, Alex Wright, *Sunnybrook Research Institute*, Sara Mar, *University of Toronto*, Hon Leong, *Sunnybrook Research Institute*, David Goertz, *Sunnybrook Research Insititute*

To investigate microbubble-microvessel interactions in an in-vivo chorioallantoic membrane (CAM) model using high-speed microscopy and cavitation monitoring at high pressures relevant to mechanical ablation.

A novel high-speed microscopy system (10kfps, 2 μ s shutter speed) was developed to directly visualize the interaction of ultrasound-stimulated microbubbles and vasculature in-vivo in the chorioallantoic membrane of a duck embryo. This enables co-aligned simultaneous optical monitoring (single vessel: 40x, 100 μ s timescale; vascular network: 10x, 0.3ms timescale) and sonication (custom PZT 'ring' transducer) of the CAM with passive cavitation detection during high pressures and therapeutically relevant long exposures (1MHz, 5ms pulse length, 1-4MPa).

Insonated microbubbles were observed to interact with and deform microvessel walls, leading to blood flow alterations and eventual extravasation of intact microbubbles in some cases. At 1MPa, wall deformations were minor (2MPa), local deformations reached as high as 88% and led to vessel wall rupture and erythrocyte leakage, with sustained damage in 48% of cases. Smaller vessels () were preferentially affected whereas larger vessels (>75 μ m) mostly remained intact. Acoustic emissions at higher pressures exhibited broadband noise levels, in addition to distinct 1/3 and 1/2 order sub- and ultraharmonics.

These observations provide the first direct in-vivo evidence of microbubble extravasation along with new insights into the mechanisms of microbubble-microvessel interactions under conditions relevant to mechanical ablation (vascular disruption therapy). Results suggest that the induced effects are highly dependent on vessel size, with smaller vessels being more susceptible to damage.

This work was funded by the Canadian Institutes of Health Research.

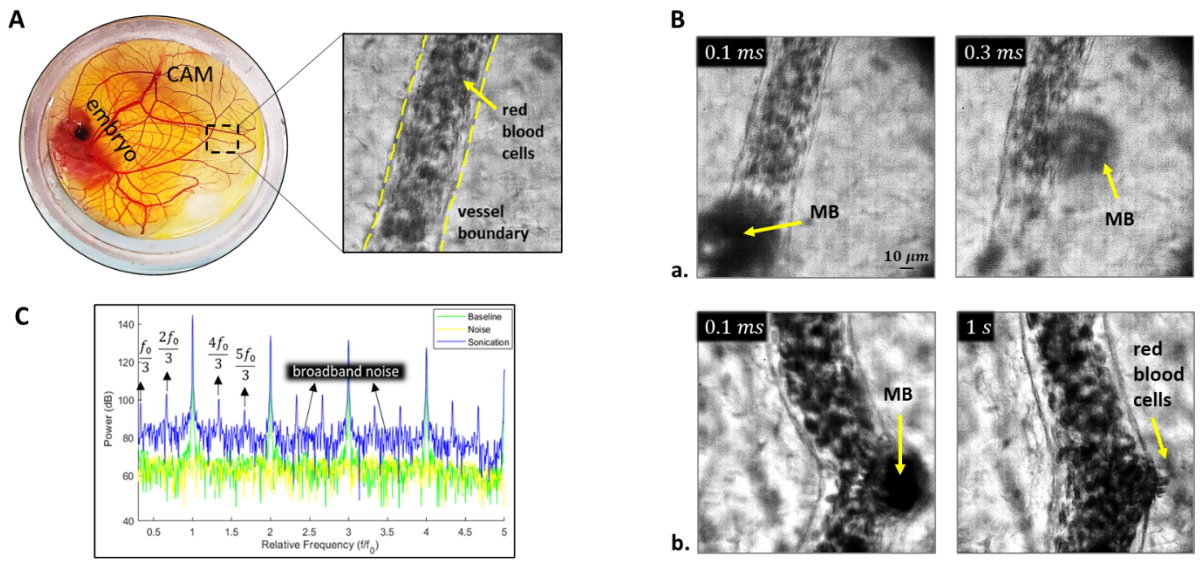


Fig. 1. (A) Duck embryo in custom dish with example image of CAM. **(B)** Microbubble activity and vascular effects (a. MB extravasation b. Blood leakage) **(C)** Frequency spectrum of the acoustic signal associated with bubble activity.

SP20

Non Invasive Liver Treatment with a Toroidal HIFU Transducer In-vivo Study

Presenter: Sophie CAMBRONERO

Authors in order: Sophie CAMBRONERO, *LabTAU, INSERM, Centre Léon Bérard, Université Lyon 1, Univ Lyon, F-69003, Lyon, France*, Aurélien DUPRE, Charles MASTIER, David Melodelima, *INSERM*

A toroidal transducer was developed and clinically used to treat liver metastases intraoperatively. We aim to use this transducer noninvasively on an in vivo porcine

The diameter and the radius of curvature of the toroidal transducer were 70mm. The operating frequency was 2.5MHz. An ultrasound imaging probe operating at 7.5MHz was placed in the center of the HIFU transducer.

In vivo experiments were conducted in eight animals that were followed over 7 days after HIFU exposure. Animals were placed in reverse Trendelenburg supine position to have access to about 50% of the hepatic volume without facing the rib cage.

The toroidal device was hand-held during the procedure. The thickness of intervening tissues was measured before each HIFU sonication and was on average 14.9 ± 2.0 mm. HIFU exposure lasted between 30s and 50s at an acoustic power of 140W; corresponding to a delivered acoustic energy ranging from 4200 to 7000J. The dimensions of the HIFU ablations were 21.2 ± 6.0 mm long by 14.7 ± 5.3 mm large. HIFU ablations were visible in ultrasound images transcutaneously and intra-operatively. Ultrasound imaging measurements at day 7 of the HIFU ablations were significantly correlated to macroscopic measurements. No skin burns were observed. The treatment was well tolerated over 7 days.

Treatment parameters resulted to be strongly dependent to the thickness and attenuation of intervening tissues. A noninvasive HIFU treatment of the liver is safe, feasible and well tolerated using a toroidal transducer. The hand-held toroidal device allowed for large volumes of ablation obtained in 40s without resorting to mechanical scanning.

This project was partly funded by SIRIC LyriCAN grant INCa_INSERM_DGOS_12563, the French National Research Agency (ANR-19-CE19-0027-01) and the FUS foundation (RC17121CC).

SP3

MR-Thermometry Pre-treatment Targeting for MR-guided Histotripsy

Presenter: Dinank Gupta

Authors in order: Dinank Gupta, *University of Michigan*, Dave Choi, *University of Michigan*, Ning Lu, *University of Michigan*, Steven Allen, *Brigham Young University*, Timothy Hall, *University of Michigan*, Douglas Noll, *University of Michigan*, Zhen Xu, *University of Michigan*

The aim of this study is to evaluate the use of MR-thermometry for pre-treatment targeting of MR-guided histotripsy treatments in ex-vivo brain.

A 15-element 750-kHz MR-compatible transducer with specialized drivers was used for both histotripsy and low-temperature heating. The tissues were first heated to 1-2°C using continuous-waves at ~4MPa p- for 15 seconds during simultaneous MR-thermometry acquisition. Target location was estimated by fitting a Gaussian over the heated region. Then histotripsy was delivered with 1-cycle pulses, 54MPa p-, 50Hz PRF, and 100-pulses. Post-treatment MRI of histotripsy lesion was compared with pre-treatment MR-thermometry to evaluate the targeting accuracy.

For targeting accuracy evaluation, the mean/standard-deviation of the difference between the target location estimated by pre-treatment MR-thermometry and the histotripsy lesion location from post-treatment diffusion-weighted MR images was 0.64/0.49 mm and 1.21/0.91 mm in transverse and longitudinal direction, respectively. Targeting error was also estimated by comparing histotripsy lesion location with array geometrical focus estimated using fiducials placed on the array (mean/std difference: 0.24/0.20 and 0.93/0.48 mm in transverse and longitudinal directions). Since the image resolution was 0.5mm, the error accounts for a few voxels.

There is a concern regarding the accuracy of using low-temperature heating and MR-thermometry for histotripsy targeting, because low-temperature heating is a linear process while histotripsy depends on non-linear ultrasound propagation at a high pressure. This is the first study demonstrating good accuracy of MR-thermometry for pre-treatment targeting of MR-guided histotripsy.

This work was funded by NIH grant R01 - EB028309.

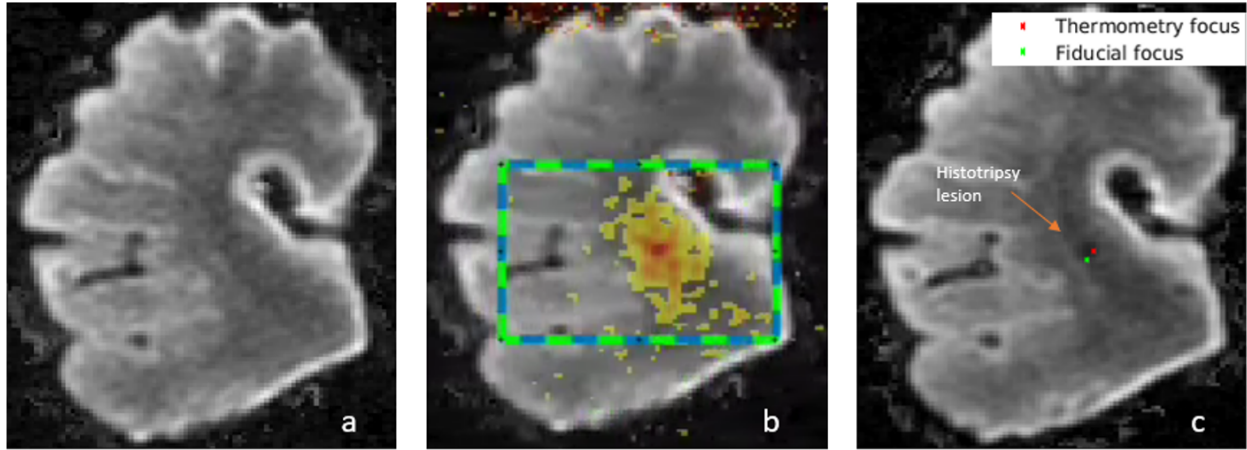


Figure 1: DWI ($b=1000$) for a tissue. a) Pre-treatment. b) MR-thermometry and ROI to fit Gaussian. c) Histotripsy lesion along with estimated foci for thermometry and fiducials

SP4

Simulation of Transvertebral Passive Acoustic Mapping for Bubble Based Therapy in the Spinal Cord

Presenter: Andrew Frizado

Authors in order: Andrew Frizado, *Sunnybrook Research Institute/University of Toronto*, Meaghan O'Reilly, *Sunnybrook Research Institute*

Passive Acoustic Mapping (PAM) through the intact spine, for BSCB disruption, is required as a means of treatment monitoring during microbubble mediated FUS.

Using CT-derived acoustic property maps of ex-vivo stacked human vertebra, time-domain FUS (forward) and cavitation (inverse) emission simulations were performed using the kWave toolbox in MATLAB. A spine-specific phased array was used in receive mode for trans-vertebral signal detection, Signals were then beamformed using the passive Time Exposure Acoustics (TEA) algorithm and its "gated" or "synchronous" alternative. Considerations for unwanted, pre-focal cavitation and associated acoustic interference were also interrogated.

To investigate the transvertebral detection of intra-canal sources (microbubbles), acoustic emissions from short burst sonications were simulated as single point source locations along the axial, lateral and vertical directions, then sampled across over these 150 locations in 10 vertebrae. Using TEA beamforming, source localization error was 1.3 ± 1.1 mm, with peak side-lobe ratio of 0.43 ± 0.14 which were improved via phase-correction methods to 0.4 ± 0.5 mm and 0.36 ± 0.7 , respectively. In the presence of pre-focal sources, localization of intra-canal sources was disrupted when using TEA and its gated form algorithms.

With the spine-optimized aperture, beamforming through the vertebra presents to be feasible when isolating point sources, though with the introduction of significant pre-focal source interference, TEA and its gated form, proved insufficient for cavitation site localization. Further work regarding pre-focal and focal source interactions, and their suppression, will be required.

This work was supported by the Canadian Institutes of Health Research and the QEII-GSST Scholarship.

SP5

Decorrelation Time Mapping for Analysis of Nanobubble Dynamics in Tumours

Presenter: Dana Wegierak

Authors in order: Dana Wegierak, *Case Western Reserve University*, Michaela Cooley, *Case Western Reserve University*, Reshani Perera, *Case Western Reaserve University*, Michael Kolios, *Ryerson University*, Agata Exner, *Case Western Reserve University*

Nanobubbles (NBs) show potential as an extravascular and therapeutic contrast agent. Here, we propose decorrelation mapping to quantify NB targeting and accumulation in tumours.

NBs and prostate-specific membrane antigen targeted NBs (PSMA-NBs) were formulated as previously described¹. Bubbles were infused via tail vein into mice bearing PSMA-expressing flank tumours and were imaged using nonlinear contrast mode (VisualSonics Vevo 3100, 18 MHz, 5 fps, 4% power). Wash-in and wash-out dynamics were captured for NBs, PSMA-NBs and microbubbles (MB, Lumason). Using intensity data, the 50% decorrelation time (DT) was calculated at each spatial location using MATLAB and decorrelation maps were created.

As shown in Figure 1, DT mapping showed a high degree of sensitivity to tumour versus normal tissue. The average DT in tumour regions was significantly longer (NBs-11.9s; PSMA-NBs-14.5s) than surrounding normal tissue (NBs-1.3s; PSMA-NBs-2.0s). DT was longer for targeted vs. plain NBs, while MBs showed a rapid DT in both regions. Longest DT appears to coincide with NB entrapment in tumours and shortest with areas of flow (blood vessels). NB targeting further extends DT and is linked with greater PSMA-NB retention in tumours. MBs, which typically show a rapid wash-in and wash-out, had the shortest DT without tumour specificity.

Decorrelation mapping of in vivo NBs dynamics presents a sensitive assessment of tumour tissue and may be useful for quantifying extravascular NB kinetics. A comparison of DT mapping vs. mapping of time-intensity curve parameters (time to peak, slope to peak, area under curve) is ongoing.

This work was funded by the National Institutes of Health grants R01EB025741 and R01EB028144 . We thank Dr. James Basilion and group for their contributions.

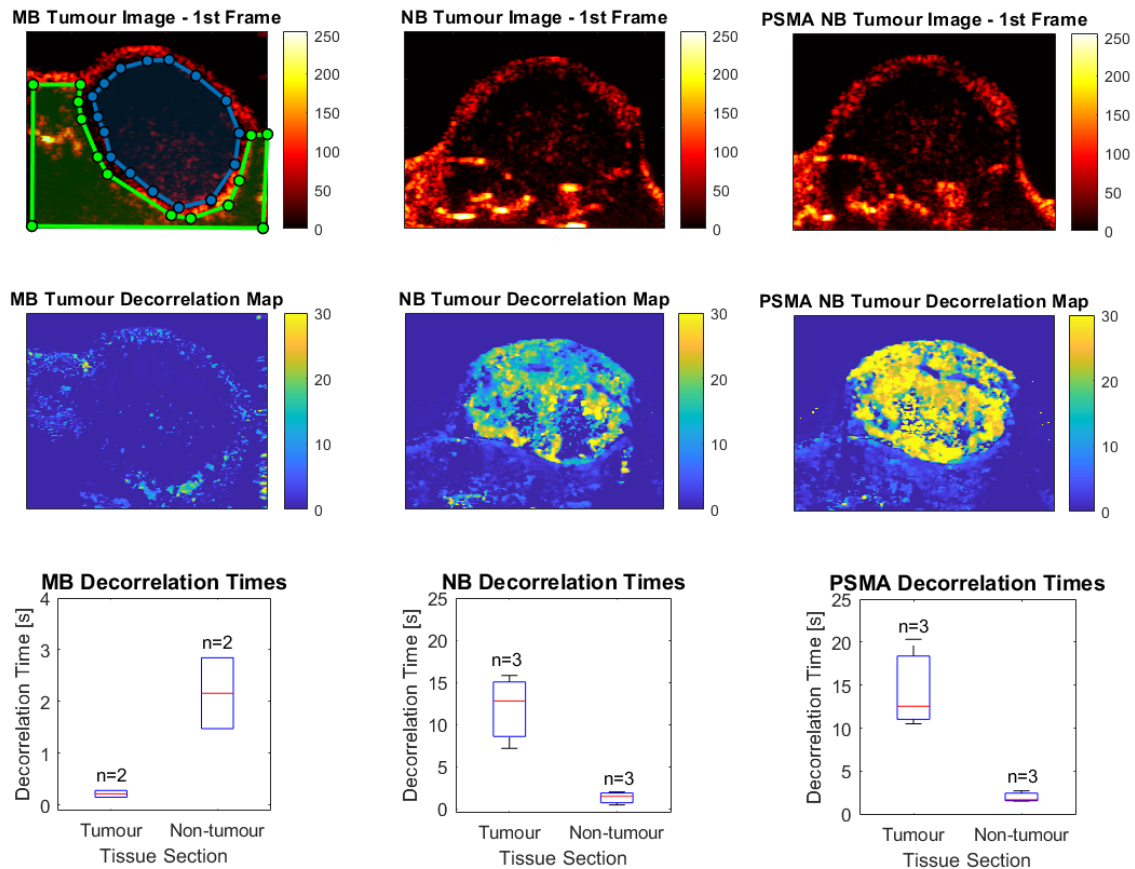


Figure 1. *Top row:* First frame of 1000 frame greyscale wash-in-video collected in nonlinear contrast mode of MBs, NBs or PSMA-targeted NBs. The blue and green polygons represent sectioning of tumour tissue and normal tissue respectively. *Center row:* sample decorrelation maps of tumours after the wash in of MBs, NBs or PSMA-targeted NBs. *Bottom row:* Correlation time comparisons from sectioned ROIs of decorrelation maps after the wash in of MBs, NBs or PSMA-targeted NBs. On each box, the central mark indicates the median, and the bottom and top edges of the box indicate the 25th and 75th percentiles, respectively. The whiskers extend to the most extreme data points not considered outliers, and the outliers are plotted individually using the '+' symbol.¹Perera R et al., *Nanomedicine NBM*, 2020

SP6

Comparing Focused Ultrasound and Dry Needling Therapies on Healing of Rat Tendinopathy

Presenter: Molly Smallcomb

Authors in order: Molly Smallcomb, *The Pennsylvania State University*, Sujata Khandare, *The Pennsylvania State University*, Jacob Elliott, *The Pennsylvania State University*, Meghan Vidt, *The Pennsylvania State University*, Julianna Simon, *The Pennsylvania State University*

The objective of this study is to compare healing after focused ultrasound (fUS) or dry needling (DN) treatments in a murine tendinopathy model.

Twenty-six rats were subjected to Achilles tenotomy. One week post-surgery, tendons were treated with fUS (1.5MHz, 1-ms pulses @10Hz for 60s, p+ = 89MPa, p- = 26MPa) or DN (30G needle, 5 fenestrations over 20s) and survived for 1 additional week. Blood was collected from the tail vein immediately before and after treatment and before euthanasia. Plasma was assayed for IGF-1, VEGF-A, and TGF- β healing factors. Tendons were harvested for histology or mechanical testing.

No significant differences were found between fUS and DN in the release of IGF-1 and TGF- β healing factors (Fig.1a); VEGF-A concentrations were too low to be detected. For both fUS and DN, IGF-1 concentrations decreased immediately after intervention and increased 1 week post-intervention. Conversely, TGF- β concentrations for both treatments increased after intervention and decreased 1 week after intervention. No differences were found between fUS- or DN-treated tendons and controls in H&E-stained histology (Fig.1b). Stiffness and percent relaxation of DN-treated tendons were lower than controls (p=0.0041, p=0.0441, respectively), whereas stiffness and percent relaxation of fUS-treated tendons were similar to controls.

fUS performed similar to DN in the release of healing factors with no differences noted upon histological analysis. However, fUS better preserved the mechanical integrity of the tendon compared to DN, which suggests fUS may be a viable alternative to DN in the treatment of tendinopathies.

This work was funded by NIH – National Institute of Biomedical Imaging and Bioengineering (R21EB027886), and NSF Graduate Research Fellowship (Smallcomb; DGE1255832).

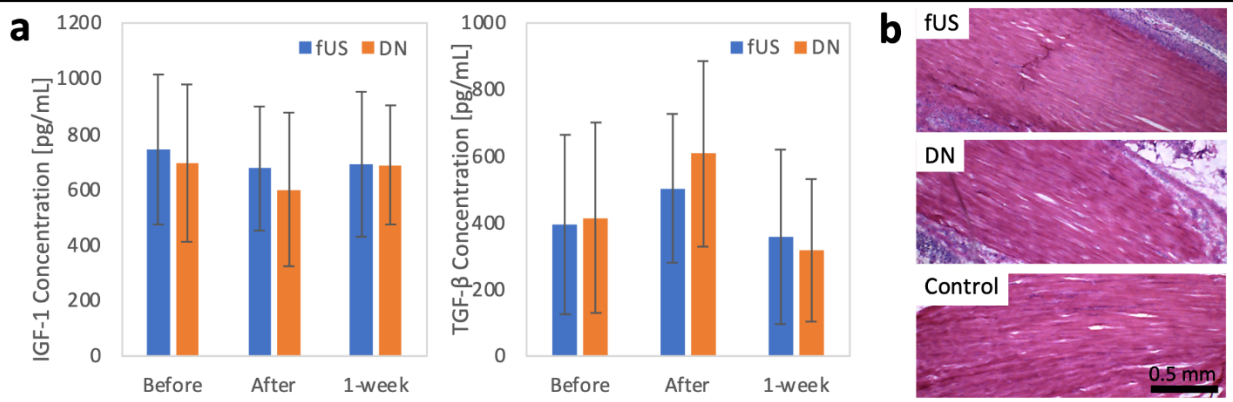


Fig.1 a) Healing factor concentrations for treatments. b) H&E-stained histology for treatments.

SP7

Array Based Focusing to the Human Vertebral Canal using Non-invasive Phase Correction

Presenter: David Martin

Authors in order: David Martin, *University of Toronto*, Rui Xu, *University College London*, Meaghan O'Reilly, *Sunnybrook Research Institute*

The fidelity of two simulation-based phase correction methods for transvertebral focusing applications was explored in ex vivo benchtop experiments.

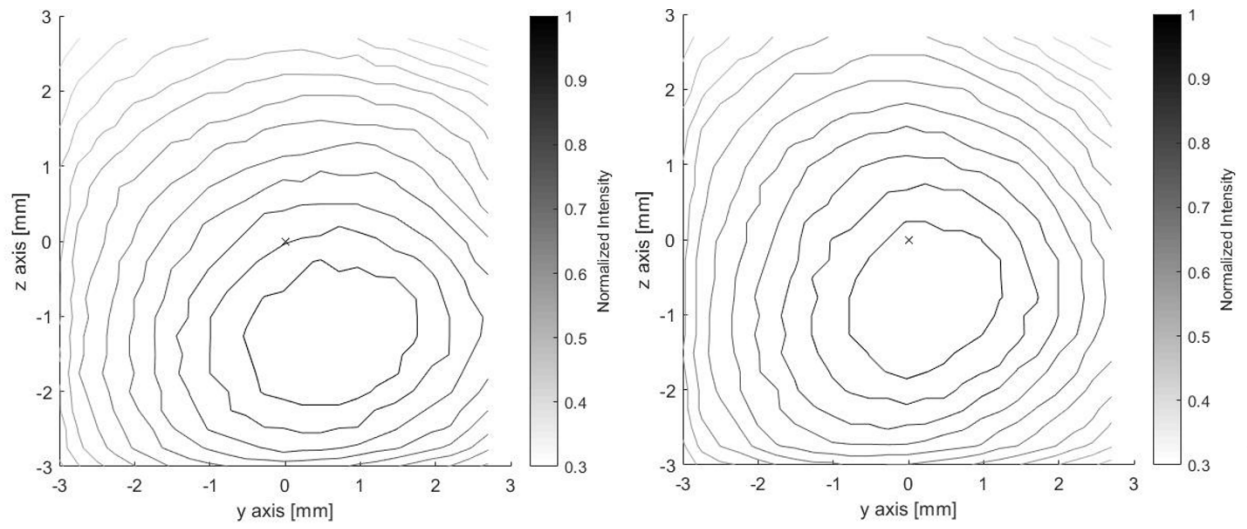
Two simulation models were tested for transvertebral focusing: steady-state ray acoustics (in-house) and a pseudospectral time domain model (kWave). Sound (400 kHz) was propagated in silico from a target location in the vertebral canal to the transducer surfaces of a custom, 64-element phased array. Phase corrections were extracted and applied experimentally for transvertebral focusing in a segment (T7 to T9) of ex vivo human thoracic spine at eight vertical locations (2 mm spacing).

Hydrophone measurements of the focus in the spinal canal were recorded in the transverse and sagittal planes (0.25 mm step size). Geometric (i.e. no correction for bone distortion) focusing and gold-standard hydrophone-based correction were performed for comparison.

Geometric focusing produced mean focal shifts of 1.2 ± 0.4 mm (transverse) and 1.5 ± 0.6 mm (sagittal), while hydrophone correction produced focal shifts of 0.6 ± 0.3 mm (transverse) and 0.7 ± 0.4 mm (sagittal). Simulation-based focusing performed better than geometric but worse than hydrophone correction. Ray acoustics produced foci shifted by 1.1 ± 0.4 mm (transverse) and 1.2 ± 0.5 mm (sagittal), and kWave produced shifts of 1.0 ± 0.5 mm (transverse) and 1.1 ± 0.5 mm (sagittal).

Steady-state ray acoustics and the kWave time domain model produce a comparable partial correction of bone-induced focal shifts in the human vertebral canal. Additional benchtop and in vivo experiments are needed to assess the viability of these methods in therapeutic treatment planning applications.

This work was supported by the Terry Fox Research Institute and NSERC.



Transverse plane of a geometric (left) and kWave-corrected (right) focus.

SP8

Motor Responses Induced by LIFU Neuromodulation and Piezoelectric Vibration in Mice

Presenter: Jake Hesselink

Authors in order: Jake Hesselink, *University of Calgary*, Siyun Li, *University of Calgary*, Zelma Kiss, *University of Calgary*, Samuel Pichardo, *University of Calgary*

We aimed to compare the motor responses produced by low intensity focused ultrasound (LIFU) neuromodulation to those caused by piezoelectric-induced skull vibrations.

C57Bl/6 mice were stimulated with 477 kHz LIFU with 1.5 kHz pulse repetition frequency (PRF). To obtain motor responses, isoflurane concentration was reduced below 0.5%. Motor activity was recorded via video and electromyography. A piezoelectric actuator was used to produce skull vibrations at the PRF, the parameter that is associated with indirect auditory activation, and a higher-frequency PRF harmonic. Response rates were compared between fixed and random PRF LIFU, sham, piezoelectric vibration, and air-puff stimulations.

Results from 10 mice suggest LIFU treatment with fixed PRF ($68.33 \pm 19.26\%$) and random PRF ($68.33 \pm 26.16\%$) both produced consistent motor responses at rates comparable to a physical air-puff stimulus ($83.19 \pm 21.14\%$). These rates were significantly higher than response rates to piezoelectric-induced skull vibrations and sham treatments ($p < 0.01$). While response rates to 4.5 kHz skull vibrations ($26.11 \pm 24.86\%$) were greater than 1.5 kHz vibrations ($5.05 \pm 5.51\%$), both piezoelectric vibration treatments yielded motor responses comparable to movement during sham treatment ($9.67 \pm 9.87\%$; Figure 1).

The high rate of motor responses to air-puff stimuli showed that arousing physical stimuli can induce motor activity under LIFU neuromodulation experimental conditions. However, as neither piezoelectric vibration treatment produced significant motor response rates, these results suggest that skull vibrations do not contribute significantly to motor responses in LIFU neuromodulation.

I would like to acknowledge the support of Dr. Pichardo and the NeuroFUS Lab, the University of Calgary, NSERC and the Brain Create program.

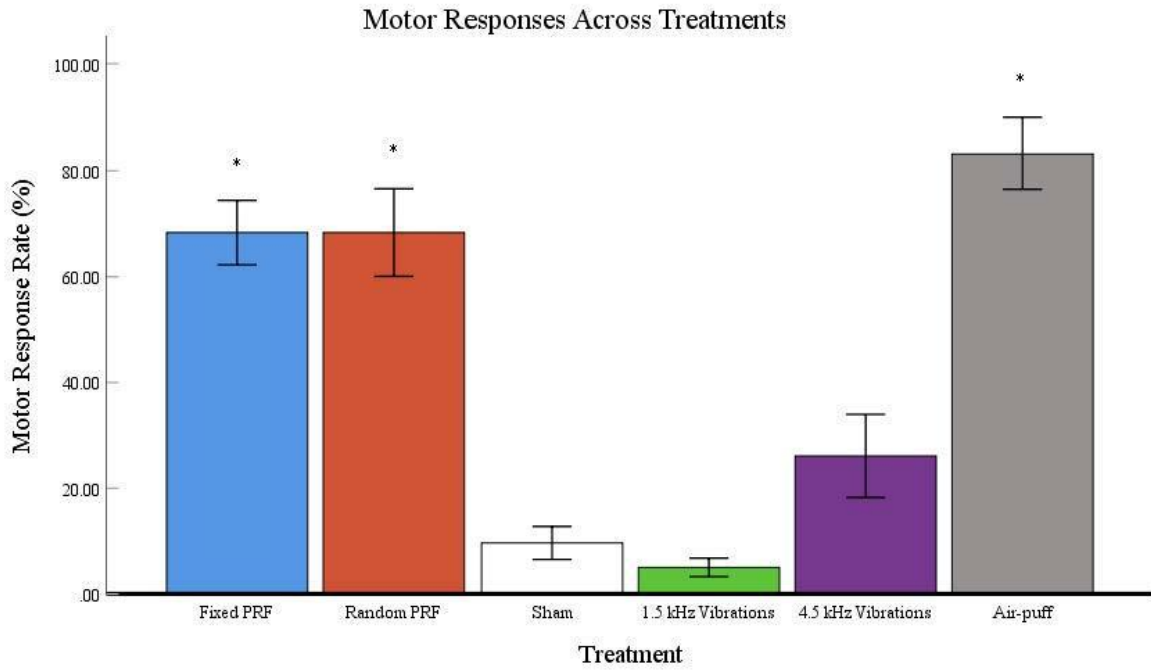


Figure 1. Motor response rates to various treatments including LIFU neuromodulation and piezoelectric-induced skull vibrations. n=10

SP9

Simulation-guided Navigation System for Transcranial Focused Ultrasound

Presenter: TaeYoung Park

Authors in order: TaeYoung Park, *Bio-Medical Science and Technology, KIST School, Korea Institute of Science and Technology*, Heekyung Koh, *Korea Institute of Science and Technology (KIST)*, Hyungmin Kim, *Korea Institute of Science and Technology (KIST)*

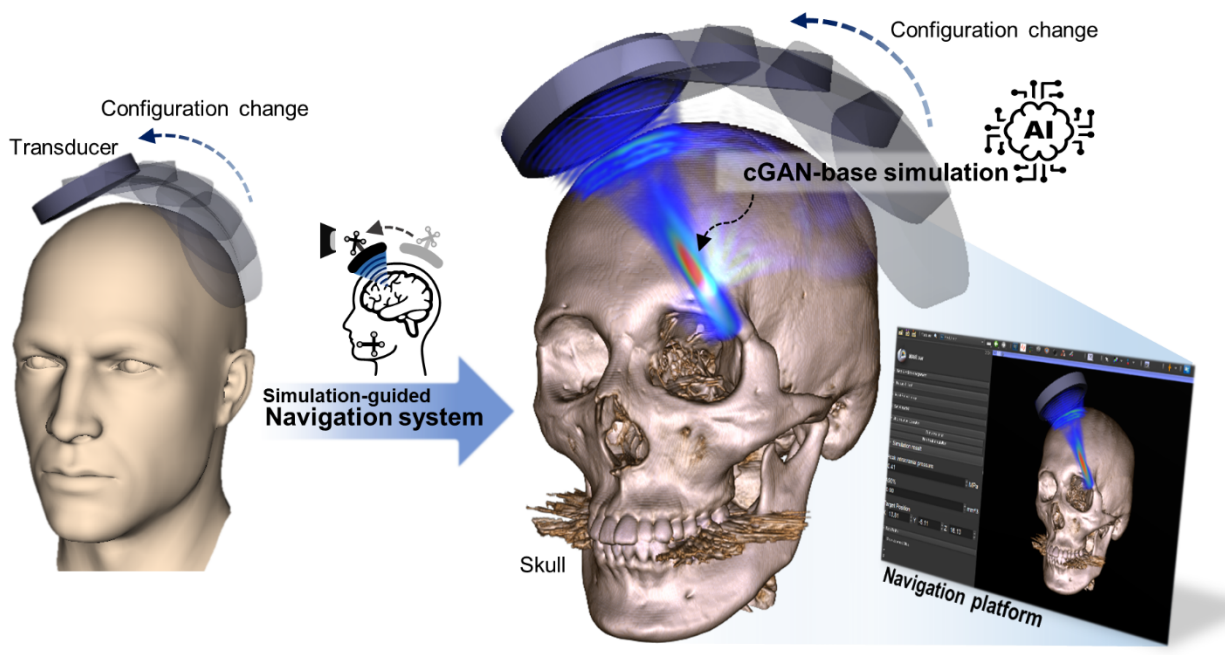
We proposed a simulation-guided navigation system, which can provide an online simulation of the intracranial acoustic field based on a neural network.

For real-time acoustic simulation, the 3D conditional generative adversarial network (cGAN) model featuring residual blocks and multiple loss functions was suggested. The acoustic simulation result, pre-calculated by the conventional numerical solver, was used as training data for the cGAN model. We implemented a simulation-guided navigation system based on 3D Slicer (<https://www.slicer.org/>) by integrating the real-time acoustic simulation. We also validated the accuracy of the simulation-guided navigation system numerically and experimentally.

The figure below shows the overview of the simulation-guided navigation system. The cGAN-based real-time acoustic simulation was performed at the transducer configuration provided by the navigation system. The simulation result was updated with a sampling rate of 4 Hz, including all pre/post-processing time (computed in Intel Core i9-10900K, NVIDIA GeForce RTX 3090, 128 GB RAM). In numerical and experimental validation of cGAN-based acoustic simulation, the intracranial peak pressure error was less than 5.7 %, and the positional error of the acoustic focus was less than 4.2 mm.

We proposed the simulation-guided navigation system using the cGAN-based real-time acoustic simulation. The proposed system can predict intracranial acoustic fields in real-time depending on the transducer's configuration.

This work was supported by the University of Science and Technology (UST) Young Scientist Program and the National Research Council of Science and Technology (NST).





ISTU 2022

21st Annual International Symposium
on Therapeutic Ultrasound

Toronto, Canada

Thank you to our
sponsors!

INSIGHTTEC

 **ARRAYUS**
Technologies

 **FOCUSED
ULTRASOUND
FOUNDATION**

 **ISTU**

Presented by:

 **Sunnybrook**
RESEARCH INSTITUTE